Exploiting the Properties and Reactivity of Thiazoles in the Design of Conjugated Materials

by

Geoffrey Scott Sinclair

A thesis

presented to the University of Waterloo

in fulfillment of the

thesis requirement for the degree of

Doctor of Philosophy

in

Chemistry

Waterloo, Ontario, Canada, 2020

Examining Committee Membership

The following served on the Examining Committee for this thesis. The decision of the Examining Committee is by majority vote.

External Examiner: Dwight Seferos, Professor, University of Toronto

Supervisor: Derek Schipper, Associate Professor, University of Waterloo

Internal Member: Graham Murphy, Associate Professor, University of Waterloo

Internal Member: Eric Fillion, Professor, University of Waterloo

Internal-External Member: Yuning Li, Professor, University of Waterloo (Chemical Eng.)

Author’s Declaration

I hereby declare that I am the sole author of this thesis. This is a true copy of the thesis including any required final revisions, as accepted by my examiners.

I understand that this thesis may be made electronically available to the public.

Abstract

Of fundamental importance to the advancement of next-generation technologies using organic electronic materials is the development of new synthetic methodologies and the investigation of novel material properties. Thiazoles have been reported in conjugated organic molecules and polymers for well over two decades; however, various aspects of these distinct heterocycles have thus far been overlooked and undervalued. This thesis will report our efforts to exploit both the reactivity and properties of thiazole in order to develop new methods for the synthesis of conjugated materials, and to produce conjugated small molecules and polymers with unique properties.

First, our work towards the development of a new transition metal-free condensation reaction for the synthesis of poly(hetero)arenes will be discussed. This reaction utilizes a protecting group strategy, and the unique reactivity of readily accessible thiazole-*N*-oxides, in order to realize a wide range of bithiazole-*N*-oxide conjugated small molecules and polymers. In the following section, these bithiazole-*N*-oxides are explored as a new class of conjugated materials in an extensive joint experimental and computational study. This study revealed a notably strong non-covalent S – O interaction found in the bithiazole-*N*-oxide core, the effects of which are examined on the optical, electrochemical, and physical properties of the conjugated materials.

Next, the inclusion of alkoxy substituents to the backbone of the conjugated polymer chain, a strategy well-known for poly(thiophene)s, is investigated in bithiazole-containing conjugated polymers. These strong electron-donating groups have been shown to largely decrease the electronic band gaps of the bithiazole polymers, and additionally have allowed for the facile preparation of these polymers through promoting the monomer's propensity for direct arylation polymerization.

Finally, the reactivity of thiazole-*N*-oxides is revisited in an attempt to facilitate cross-coupling with electron-rich arenes. Preliminary investigations are described in which a triflic anhydride activation strategy has allowed for the formation of 2-arylthiazoles through the nucleophilic addition of these arenes to thiazole-*N*-oxide.

Acknowledgements

Throughout my ten-year university career, I have first and foremost had the support of my parents Karin and Gordon, my sister Alex, and my grandmother Margarete. Thank you for never questioning my choice to pursue this goal, and for always being interested in my work despite it seeming like hieroglyphics to you.

Derek, thank you for bringing me into your lab and instilling your trust in my chemistry, my writings, my presentations, and my general duties within the group. I will always be thankful for all the skills – chemistry and life – I have gained as this group has grown from its early days until now, as well as your knowledge of organic chemistry that you have shared with me through group meetings and one-on-one chats.

I have had the pleasure to work in this group alongside a wild cast of characters who I am sure will continue to be friends wherever we end up next. To the graduate line-up: Tianyu – my first friend in the lab, thanks for training me and being a great role model of a hard worker. Rob and Luke – I don't think I ever had quite as much fun in the lab as when you guys were at your prime goofiness. Serxho – It has been awesome to grow a lasting friendship with you and I have always been grateful to have you as a mentor. Sara – thanks for helping to establish the awesome workplace environment we had, and for being such a supportive friend. Raf and Jianan - it has been great to see you grow as people and as chemists, and I'm glad that you are there to usher in the next era. Sarah, Wayne and Javan – while you joined later, you all had a major impact on my time in the group, and I'm glad I had plenty of time to get to know you and develop our friendships.

Many undergraduates passed through the lab during my time in the Schipper group, a lot of whom remain friends while some have even become colleagues. I had the great opportunity to learn how to be a supervisor to Jacky, Kevin, Lubna, Andrew, and Josh – thank you all for the work you put in and for helping me grow (and putting up with me) in this role.

I am grateful to have had all my committee members have an impact on my organic chemistry career. Prof. Barra and Prof. Fillion, without your excellence in teaching and engagement in undergraduate organic chemistry I very well may not have found my way

into this field. Prof. Murphy, I will always be thankful for being given my first organic laboratory opportunity, and how you personally took the time to build the foundations of the chemist I am today.

Finally, I would like to thank all of my awesome friends in Waterloo, Toronto, and elsewhere, that have been by my side along the way. I’m looking forward to joining you in the real world shortly! A big thank you to Richard Tran and Serxho Selmani for dedicating their time to editing major sections of my thesis.

Table of Contents

List of Figures

List of Tables

List of Schemes

List of Abbreviations

2MT	2-Methylthiophene
Abs	Absorbance
Ac	Acetyl
AG	Activating group
AIM	Atoms in Molecules, Quantum Theory of
Ar	Aryl
ATR	Attenuated total reflectance
B3LYP	Becke, 3-parameter, Lee–Yang–Parr hybrid functional
BCP	Bond critical point
BD*	Anti-bonding orbital
BLA	Bond length alternation
br	Broad (signal pattern)
Bu	Butyl
CCSD(T)	Coupled cluster single-double-triple
CMD	Concerted metalation-deprotonation
CNT	Carbon nanotubes
CRT	Cathode ray tube
CV	Cyclic voltammetry
Cy	Cyclohexyl
d	Doublet (signal pattern)
DAr	Direct arylation
DArP	Direct arylation polymerization
dba	Dibenzylideneacetone
DCE	1,2-Dichloroethane
Dec	Decyl
DFT	Density Functional theory
DMA	*N,N*-Dimethylacetamide
DPP	Diketopyrrolopyrrole
DSC	Differential scanning calorimetry
DSSC	Dye-sensitized solar cells
E	Electrophile
e^-	Electron
EDG	Electron donating group
E_{dist}	Energy of distortion
EDOT	3,4-Ethylenedioxythiophene
Eg(ec)	Electrochemical band gap
Eg(opt)	Optical band gap
EH	2-Ethylhexyl
E_{int}	Energy of interaction
Em	Emission
Equiv	Equivalents (stoichiometric)
Et	Ethyl
EWG	Electron withdrawing group
GPC	Gel-permeation chromatography
h^+	Electron hole
Hex	Hexyl
HH	Head-to-head
HOMO	Highest occupied molecular orbital
HR-MS	High-resolution mass spectrometry
HT	Head-to-tail
i	Iso (prefix)
IR	Infrared
KIE	Kinetic isotope effect
LCD	Liquid crystal display
LED	Light-emitting diode
LG	Leaving group
LP	Lone pair
LR-MS	Low-resolution mass spectrometry
LSV	Linear sweep voltammetry
LUMO	Lowest unoccupied molecular orbital
M	Metal
m	Meta (prefix)
***m*-CPBA**	meta-Chloroperoxybenzoic acid
Me	Methyl
Mn	Number-average molecular weight
mp	Melting point
MP2	Moller-Plesset perturbation theory
MS	Mass spectrometry
MW	Microwave heating
Mw	Weight-average molecular weight
n	normal (prefix)
Naph	Naphthyl
NBO	Natural Bonding Order
NMR	Nuclear magnetic resonance
Nu	Nucleophile
o	Ortho (prefix)
Oct	Octyl
OFET	Organic field-effect transistors
OLEDs	Organic light-emitting diodes
OPV	Organic photovoltaics

OSC	Organic solar cells
p	Para (prefix)
P3MT	Poly(3-methylthiophene)
P3HT	Poly(3-hexylthiophene)
PCBM	[6,6]-Phenyl-C_{61}-butyric acid methyl ester
PDI	Polydispersity index
PEDOT	Poly(3,4-ethylenedioxythiophene)
PET	Polyethylene terephthalate
PF	Polyfluorene
Ph	Phenyl
PLED	Organic polymer light-emitting diode
PPP	Poly(*para*-phenylene)
PPV	Poly(*para*-phenylene vinylene)
Pr	Propyl
PT	Polythiophene
PTz	Polythiazole
PyBroP	Bromotripyrrolidinophosphonium hexafluorophosphate
q	Quartet (signal pattern)
quint	Quintet (signal pattern)
QTAIM	Quantum Theory of Atoms in Molecules
R_f	Retention factor
RFID	Radio-frequency identification
rt	Room temperature
s	Singlet (signal pattern)
S_EAr	Electrophilic aromatic substitution
SM	Starting material
SM-OLED	Organic small molecule light-emitting diode
t	Triplet (signal pattern)
t	Tert (prefix)
TD-DFT	Time-dependent density functional theory
Tf	Trifluoromethanesulfonyl
TFAA	Trifluoroacetic anhydride
TGA	Thermogravimetric analysis
THF	Tetrahydrofuran
TLC	Thin-layer chromatography
Tol	Tolyl
TS	Transition state
Ts	Toluenesulfonyl
TT	Tail-to-tail
USD	United States dollars
UV	Ultraviolet
UV-Vis	Ultraviolet-to-visible
V_d	Source drain voltage
V_g	Gate voltage
xp	Crystallization point
Φ_F	Quantum yield

1

Introduction to Organic Electronic Materials

1.1 Conjugated organic materials

Organic electronic materials constitute a class of semiconducting molecules and polymers that are primarily composed of carbon. The chemical structure of these materials must possess uninterrupted chains of linked unsaturated units in the form of alkenes and/or aromatic rings. The alternating double and single bonds throughout the backbones of these molecules results in a highly conjugated system with p-orbital overlap extended throughout.[1] Electron delocalization through the conjugated backbone of a molecule, as well as from molecule to molecule, allows for charge transport and ultimately gives rise to the semiconducting capability of the material (Figure 1.1).[2]

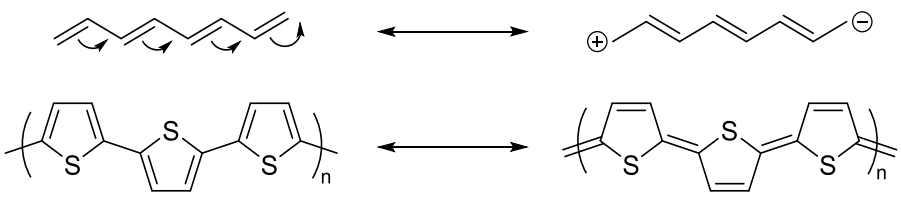

Figure 1.1 – Electron delocalization in organic molecules through π-bond conjugation.

Organic semiconductors have been identified as low charge mobility materials since as early as the mid 1900's, however, interest did not spike until the 1977 discovery by Alan J. Heeger, Alan G. MacDiarmid and Hideki Shirakawa, that polyacetylene could be made highly conducting through doping with I_2.[3] These individuals went on to receive the 2000 Nobel Prize in Chemistry "for the discovery and development of conductive polymers".[4]

Organic electronic materials are under investigation primarily due to the growing desire to substitute inorganic silicon-based technology for device applications in which they are not suitable, or in instances where the fabrication expenses remain high. Organic materials possess several advantages compared to their inorganic counterparts that make them particularly suitable in specific applications. These advantages include: light weight, mechanical flexibility, potential low material cost, and the ease of processing with cost-effective fabrication technologies.[5] Device fabrication methods for organic electronic materials include direct printing, ink-jet and other low temperature solution-based techniques, which offer fast, cheap, and large-area production that can be costly to replicate with inorganic silicon-based materials.[5] The charge carrier mobility of conjugated organic materials has increased six orders of magnitude over the past 30 years, achieving mobilities higher than 1 cm^2/Vs with the latest advances in conjugated polymers. While this has been able to match and even, in some cases, exceed the charge carrier mobility

of amorphous silicon, charge transport is still insufficiently understood to reach the order of polycrystalline and crystalline silicon.[6–8]

Perhaps the most important advantage that organic semiconductors possess over their inorganic counterparts is the infinite variation in achievable structures.[9] While inorganic semiconductors, such as crystalline silicon, possess static properties that are only slightly modifiable through doping, the molecular structure of both conjugated organic molecules and polymers can be modified by any number of organic transformations. This molecular structure has a huge effect on both the electronic properties of the material, such as the electronic band gap, as well as the physical properties, such as crystal packing in the solid state. The development of new reaction methodologies to produce conjugated small molecules and, more importantly, conjugated polymers, is essential towards the development of high-performance organic electronics. New reactions allow for the progress of materials with precisely designed chemical structures that can afford specific desired physical and electronic properties.

1.1.1 Band gap

Inorganic and organic materials can broadly be classified into conductors, semiconductors, and insulators, based on their electronic band structure (Figure 1.2). Electronic bands are used to describe the energy level of closely spaced orbitals in a material in relationship to the Fermi level, that is the energy level at which one could expect 50% electron occupancy. The filled band closest to the Fermi level is known as the valence band while the closest unoccupied band is known as the conduction band.[10] The difference in eV between the energy level of the valence band and the energy level of the conduction band is known as the band gap (E_g). If the Fermi level falls within a

band (seen as the overlap of the valence and conduction band) the material therefore possesses no band gap and is referred to as a conductor. Conductors, also sometimes referred to simply as metals, have free movement of charge throughout the material as there is no barrier to overcome between the conduction and valence band. Insulators are classified as materials that possess band gaps of around 3 - 4 eV or higher, which results in no charge transfer since electrons cannot be promoted from the valence band to the conduction band in the material.

The band gap of semiconducting materials falls in between those of insulators and conductors, and are generally between 0.5 eV and 3 eV. In the electronic band structure of a semiconductor, if the Fermi level energy is closer to the conduction band, the material is considered n-type and acts best as a transporter of electrons. Alternatively, if the Fermi level is closer in energy to the valence band, the material is considered a p-type and is

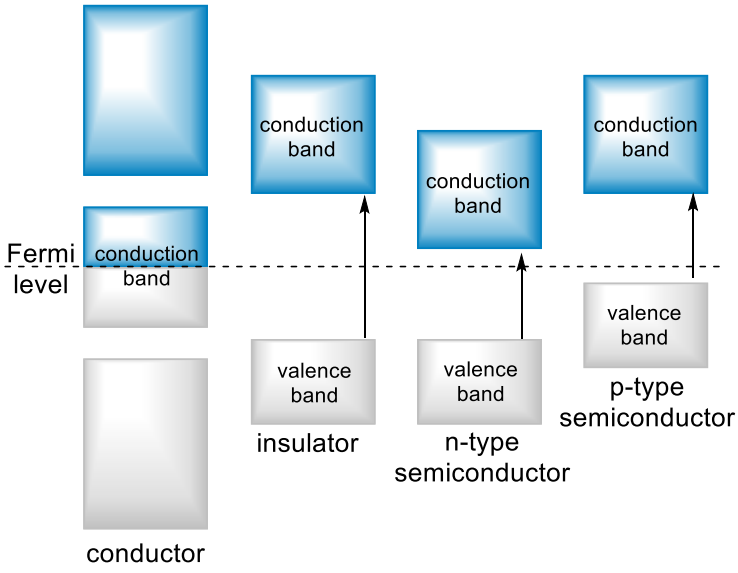

Figure 1.2 – 2D-Band structure diagram for conductor, insulator and both p-type and n-type semiconductors.

proficient for the transportation of holes. Holes are a quasi-particle used to denote the absence of an electron.

The p-orbital overlap found in conjugated organic molecules gives rise to their intrinsic charge carrier mobility and therefore semiconducting abilities. Important to this ability are the energy levels of the organic material's frontier molecular orbitals: the highest occupied molecular orbital (HOMO) and the lowest unoccupied molecular orbital (LUMO). When an organic material is deposited as a crystal or film, the energies of the molecular orbitals in individual molecules overlap to give rise to an electronic band structure. The HOMO of an organic molecule, therefore, has an electronic structure representative of that of the valence band of a material, while the LUMO is similarly representative of a materials conduction band. Thus, the energy difference between the HOMO and LUMO energy levels, known as the HOMO-LUMO gap, is proportional to the solid-state material's band gap. Understanding a conjugated molecule's HOMO-LUMO gap can be used to predict the semiconducting abilities of the material and target bulk electronic properties.

1.1.2 Band gap determination

Determination of the band gap of a material is an important aspect of predicting its applicability in electronic devices. The band gaps of conjugated organic materials are traditionally approximated either optically or electrochemically. However, since these methods are not a direct measurement of the band gap itself, it is important to note the band gap measurement as either $E_{g(opt)}$ or $E_{g(EC)}$, dependent on the which measurement method is used.

Optical band gap ($E_{g(opt)}$) measurement involves absorption-based spectrophotometric techniques (such as UV-Vis) of either thin films or a substrate in solution. Absorbance of light at a required wavelength results in the excitation of an electron from a molecule's HOMO to its LUMO. The longest wavelength of light to be absorbed (onset of absorbance) indicates the minimum energy required to perform this excitation and, therefore, is a good estimate of the HOMO-LUMO gap.[11] . In general, the higher the level of conjugation present in a molecule, the lower the HOMO-LUMO gap and longer wavelength of light able to be absorbed (Figure 1.3). Approximately eight conjugated double bonds are required for a molecule to absorb into the visible light absorbance region.[1] The optical band gap generally approximates a value lower than the actual HOMO-LUMO gap, as upon single photon absorption, an electron is promoted to the first excited state but remains electrostatically bound to the hole.[12] This binding energy, on the order of 10^{-1} eV, results in the transition to the lowest excited state being of lower energy than that of the actual HOMO-LUMO gap, however, it remains a good estimate.[12]

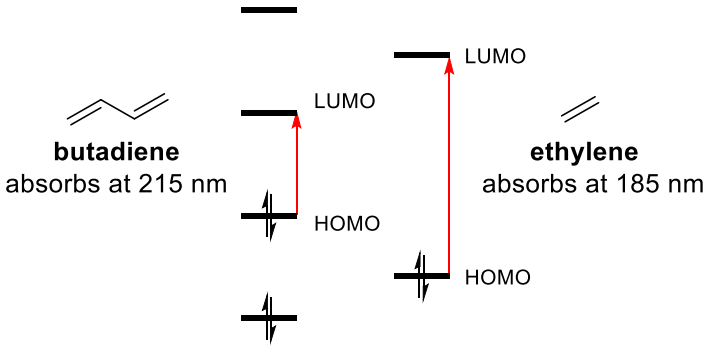

Figure 1.3 – Energy diagram comparing increased conjugation between ethylene and butadiene and the corresponding decrease in HOMO-LUMO gap

Alternatively, the band gap of a conjugated organic molecule can be approximated electrochemically using cyclic voltammetry (CV). CV is used to determine the oxidation and reduction potentials of an analyte in solution by sweeping the potential between two electrodes and observing the voltage requirement for electron flow (current).[13,14] The analyte can undergo a reduction when the electrode's potential energy is raised higher (negative voltage) than that of that of the analyte's LUMO. Equally, if the electrode potential energy is decreased lower (positive voltage) than the analyte's HOMO, the analyte can undergo oxidation. This can be used to approximate the ionization potential (oxidation) and electron affinity (reduction) of a conjugated material, which together can

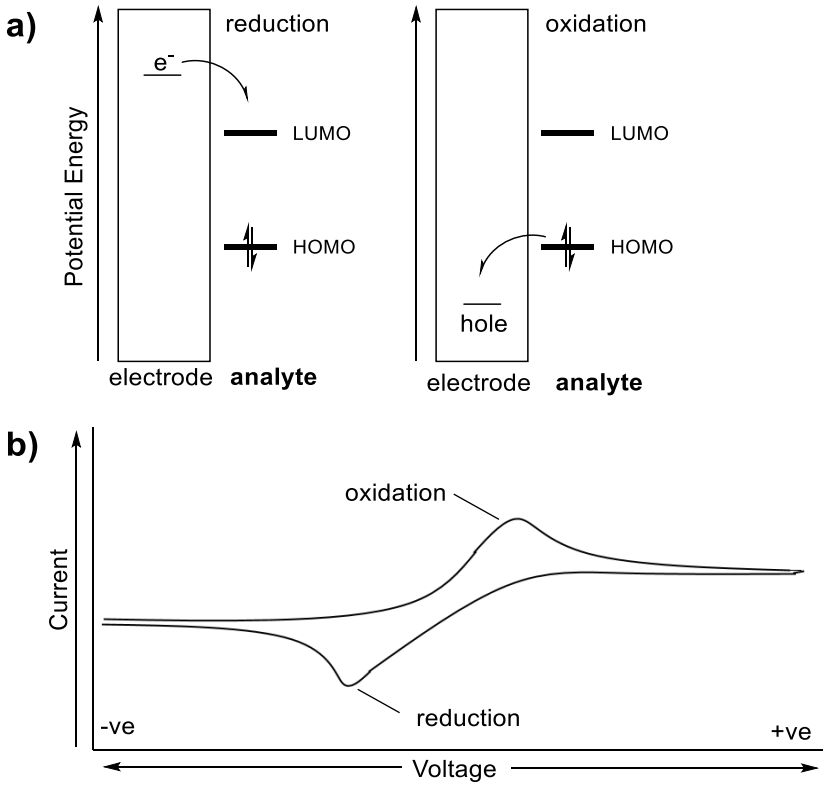

Figure 1.4 – a) Electron transfer to/from electrodes for the reduction/oxidation of the analyte b) Example CV.

be used to calculate the electrochemical band gap ($E_{g(EC)}$) (Figure 1.4).[12] The oxidation and reduction potentials obtained through CV can also be used to determine the absolute values of the HOMO and LUMO energy levels of a conjugated organic material through the inclusion of a reference standard in solution such as ferrocene.

1.2 Categories of semiconducting organic materials

Semiconducting organic materials are generally categorized into three main groups based on their structural similarities. Since their discovery, conjugated polymers have remained perhaps the most heavily studied type of organic material used in electronic devices, though conjugated small molecules and molecularly-defined oligomers have also found a niche role. Finally, another category of materials broadly classified as carbon nanomaterials have made their way to the forefront of organic semiconducting materials in the last 20 years.

1.2.1 Conjugated polymers

Conjugated polymers include all manner of organic polymers possessing an extended π-system through repeat units of unsaturation. The most commonly investigated classes of conjugated polymers are those based on alternating alkenes (pol-

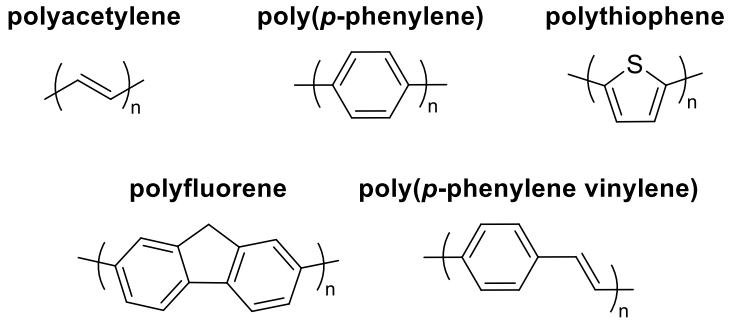

Figure 1.5 – Common classes of conjugated polymers.

yacetylene derivatives), those based on alternating aromatic units (poly(*p*-phenylene) (PPP) derivatives, polythiophene (PT) derivatives, polyfluorene (PF) derivatives, etc.), and those based on a combination of the two (ie: poly(*p*-phenylene vinylene) (PPV) derivatives) (Figure 1.5).[15] Conjugated polymers possess several features that present them as desirable candidates for deployment in device applications. Polymers with high molecular weights and long unbranched chains possess the commonly desired properties of plastics such as a high level of mechanical flexibility. Additionally, solution-processable conjugated polymers can be designed to easily form films, facilitating large scale industrial device production through cost-effective means.

Important to the deployment of conjugated polymers in electronic applications are the number average molecular weight (Mn), weight average molecular weight (Mw), and polydispersity index (PDI). While Mn is simply the statistical average molecular weight of all polymer chains, Mw considers the molecular weights of the polymers in contribution to the average. PDI is simply a measure of molecular weight distribution broadness by comparison of Mw to Mn. These properties are important aspects that can affect the polymer's solubility, aggregation in solution, thin film morphology, and mechanical strength.[16] It is important to optimize the fabrication of a conjugated polymer to a specific Mw and PDI such that consistent properties are obtained batch-to-batch. For polythiophenes, an Mn of 20 - 30 kDa and PDI of 1.2-1.8 are generally sought after for the physical and electronic properties desired for use in device applications.[17] Unfortunately, however, even low PDI polymers still remain a statistical mixture of molecular weights which can have an impact on both the physical and electronic behavior of the material.[18]

The molecular weight distribution of a conjugated polymer is highly dependent on both the repeating unit structure as well as the synthetic route. Fundamentally, polymerization methods for conjugated polymers can be either chain-growth or step-growth. In a chain-growth mechanism, an initiation step creates a reactive intermediate that further propagates through repeat unit addition to yield the polymer. More commonly, conjugated polymers are synthesized by step-growth polymerization, wherein the molecular weight of the polymer builds as a function of the extent of monomer conversion. In order to achieve high molecular weights by step-wise polymerization, a high degree of monomer purity and an equal stoichiometry of monomers are required.[19] Specific methods for the synthesis of conjugated polymers and the structural considerations will be discussed in further detail *vide infra*.

1.2.2 Conjugated small molecules

Conjugated small molecules and conjugated oligomers make up a class of materials commonly referred to as molecular semiconducting materials. Compared to their polymer counterparts, small molecules and oligomers have attracted considerable attention due to some fundamental advantages. Firstly, molecular semiconductors have definite molecular structures and distinct, monodisperse molecular weights, which allows for a better structure-to-property correlation when observing the physical and optical properties of a material.[20] Small molecules are also significantly easier to achieve at high purity through standard chromatographic methods and do not possess the batch-to-batch variation observed due to the varied lengths produced in the synthesis of conjugated polymers.[21] Finally, in conjugated polymers the effective conjugation length has been shown to be approximately 10 repeating units.[22,23] Therefore, conjugated oligomers can

be synthesized to possess similar electronic properties, such as band gaps, to their polymer counterparts, without having a dispersity in molecular weights.

Small molecules have been employed as both p-type and n-type materials in a variety of organic electronic device applications including liquid crystalline semiconductors, light-emitting diodes and organic solar cells - where they are arguably most prevalent.[20,24,25] As p-type materials, molecular semiconductors fall into several categories that include dye-based small molecules, fused acenes, triphenylamine derivatives and oligothiophenes.[21,26,27] N-type conjugated small molecules are scarce in scope compared to p-type materials, and include perylene diimide-based molecules as well as other molecular systems incorporating electron-withdrawing groups such as -CN or -F substituents into the π-conjugated backbone (Figure 1.6).[21] With oligothiophenes being one of the most heavily investigated molecular semiconductors, and the inclusion of other (hetero)arenes common, approaches to the synthesis of this class of materials

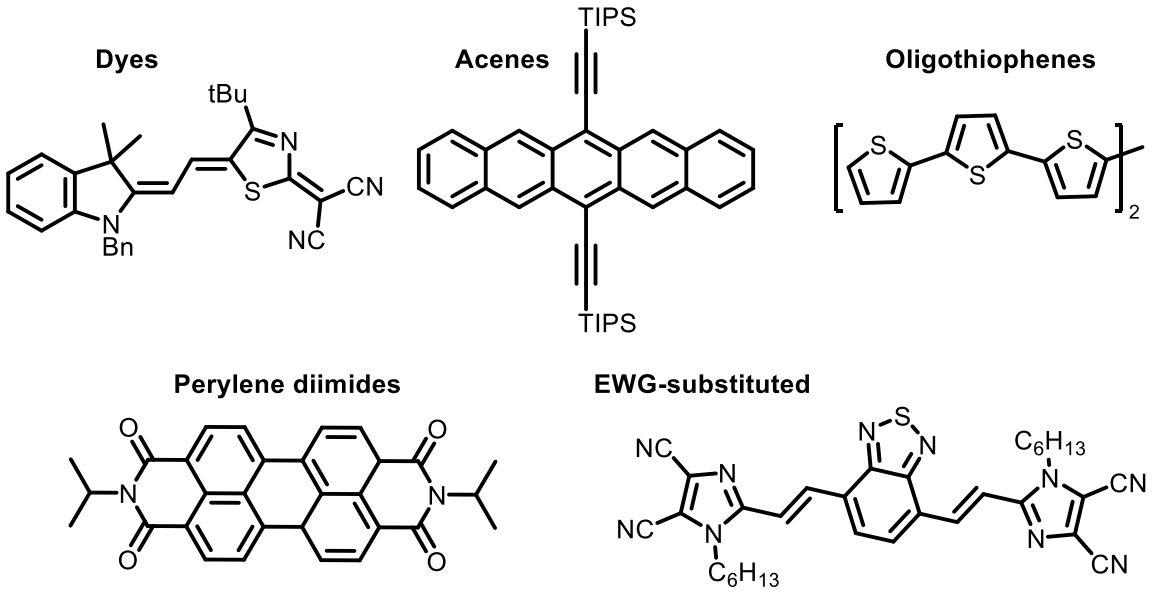

Figure 1.6 – Examples of molecular organic semiconductors.

are highly dependent on C_{sp2}-C_{sp2} cross-coupling reactions.[25]

Another major difference between the deployment of conjugated polymers and small molecules/oligomers is in the area of morphology and processability. Small molecules are notably easier to crystallize; however, this can cause difficulty in the preparation of thin films. In the case of poor solubility that does not allow for solution processability, conjugated small molecule layers are often formed through vacuum sublimation.[27] This requires thermal stability of the small molecule as it is sublimed onto a surface usually held above the source (in what is known as bottom-up fabrication).[28] Using this approach, several layers of differing materials can be deposited to complete the device structure. Processing in this manner can, however, be wasteful of material and difficult to maintain a uniform rate of deposition.[28]

1.2.3 Carbon nanomaterials

Carbon nanomaterials conclude the major categories of conjugated organic materials that are under investigation for their physical and electronic properties. This category consists of carbon allotropes that possess mainly C_{sp2}-C_{sp2} bonds; the most notable of which are carbon nanotubes (CNTs), fullerenes and graphene, as well as their derivatives (Figure 1.7).[29,30] While these materials will not be a focus throughout this work, the contributions and prevalence of these materials in the field of conjugated organic materials warrants introduction.

The buckminsterfullerene C_{60} was first identified as a soccer ball-like structure possessing 12 pentagons and 20 hexagons made up in sp^2 carbons in 1985 by Kroto et al.[31] Since then, the larger 70-carbon fullerene C_{70} and a handful of higher order fullerenes

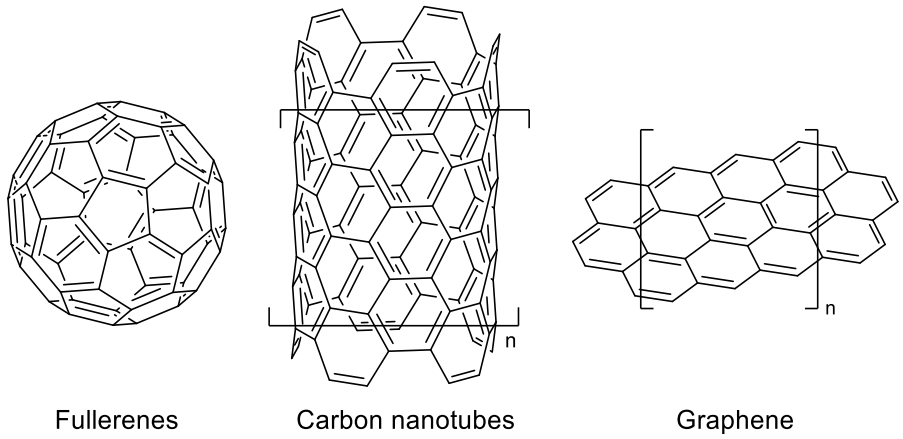

Figure 1.7 – Fundamental types of carbon nanomaterials used in organic electronic devices.

have been identified. While fullerenes do not present the same mechanical properties as other carbon allotropes, they have proven to be useful from a materials perspective due to their high electron affinity which has been exploited in organic photovoltaic devices as n-type acceptor materials. Additionally, fullerenes have found use as radical scavengers in organic transformations as well as in biomedical applications as antioxidants.[32]

In 1991, CNTs were identified by Iijima et al. as products generated by arc-discharge, a popular method for the formation of mixed carbon allotropes from graphite rods.[33] CNTs are sheets of graphene rolled up into a tube and can either be single-walled or multi-walled. The diameter of CNTs ranges from a few angstroms to tens of nanometers and their length can range from several micrometers to a few centimeters. CNTs have a notably high charge transports ability and can exhibit semiconducting or metallic behavior depending on the diameter and chirality.[29] Due the high strength of covalent C=C bonds, mechanically, CNTs are some of the strongest known materials and show high flexibility and unprecedented ability to stretch before breaking.[32]

A planar, one-atom-thick sheet of sp^2 carbons, graphene was not identified until 2004 by Geim and Novoselov who obtained the single atom sheets from graphite crystals by repeated removal of layers through mechanical exfoliation.[34] Graphene possesses properties similar to or better than CNTs in many areas including electrical and thermal conductivity as well as charge mobility and fracture strength.[29] Along with CNTs and fullerenes, graphene has proven to be an attractive new material for device applications.

1.3 Applications of organic materials in electronic devices

Organic semiconducting materials, whether they are small molecules, polymers, or carbon nanomaterials, have been exploited for use in a multitude of devices depending on the physical and electronic properties of the material. The devices for which organic semiconducting materials seem highly suited to replace inorganic semiconductors are in field-effect transistors, light-emitting diodes and solar cells.

1.3.1 Organic field-effect transistors

Organic field-effect transistors (OFETs) are a type of electronic architecture that has found application in next-generation flexible devices such as radio frequency identification (RFID) tags, displays, electronic papers and chemical sensors.[8,35,36] OFETs are generally fabricated to possess five components: an organic semiconducting layer, insulating dielectric layer, gate electrode, as well as source and drain electrodes. These components can be organized in one of several geometries, with the “bottom gate – top contact” configuration often used for best performance (Figure 1.8).[37] When a gate voltage (V_G) is applied, charge travels from the source electrode to the gate and accumulates at this electrode along the insulating layer. This bias on the gate electrode

induces a field-effect in the semiconducting film, allowing it to act as a conductor between the source and drain. Application of a source-drain voltage (V_D) allows for a current, directly dependent on the charge induced by V_G, to flow through the organic semiconducting layer, and the transistor is now considered in its "on" state. When no V_G is applied, the organic semiconducting layer will act as an insulator, and the transistor is considered in its "off" state.[37]

Through the induced field effect, an applied negative V_G raises the HOMO and LUMO levels of the semiconducting material such that the HOMO becomes resonant with the Fermi levels of the source/drain. Electron transfer out of the HOMO leaves holes in the semiconducting layer which allows for hole transport induced by the V_D potential

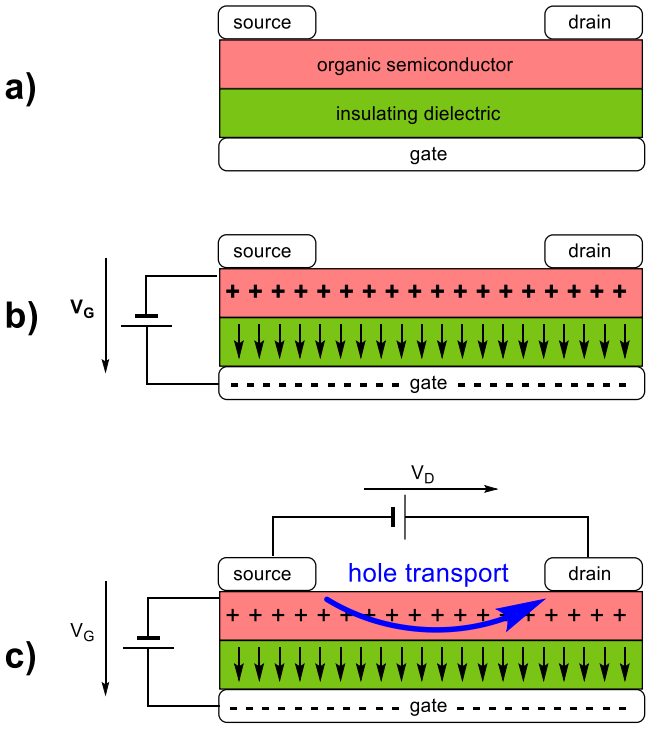

Figure 1.8 – Bottom gate – top contact field-effect transistor a) general architecture b) field-effect on organic semiconducting material upon application of a negative gate voltage (V_G) c) hole transport through organic semiconducting material on application of a source-drain voltage (V_D).

difference. Likewise, a positive V_G field effect lowers the HOMO and LUMO of the semiconducting material such that the LUMO is resonant with the Fermi levels of the source/drain and able to accumulate electrons through these contacts. Application of the V_D potential difference then allows for electron transport through the semiconducting material.[37] The organic semiconductors employed in this operation are generally either hole conductors (p-channel) or electron conductors (n-channel) depending on whether they become more conductive through application of a negative or positive V_G, respectively.

1.3.2 Organic light-emitting diodes

In the last five years, current generation flat panel display technologies have begun to transition to organic light-emitting diodes (OLEDs), replacing the light-emitting diode (LED), liquid crystal displays (LCD) and cathode ray tube (CRT) technologies that reigned before.[38] OLEDs possess a number of desirable properties including their high luminous efficiency, full colour capability, self-emitting property, low power consumption, light weight and high flexibility.[39] These types of devices were first reported in the late 1980s using vapour-deposited organic small molecules, and then in the early 1990s using conjugated polymers.[40] These initial investigations lead to the understanding of the basic processes involved for electroluminescence in organic semiconducting materials.

The general architecture of an OLED consists of one or more films of organic conjugated material inserted between two electrodes (Figure 1.9). Light is produced by recombination of electrons and holes as excitons in the organic semiconducting material. A potential difference (V) between the electrodes injects charges into the organic material. Holes are injected at the anode while electrons are injected at the cathode. Charge

mobility is dependent on the properties of the organic semiconducting material to allow for either electron or hole movement. Upon recombination of the electron and hole in the emissive organic layer, a photon of light is emitted. The wavelength of light emitted is dependent on the HOMO-LUMO gap of the emitting conjugated organic material.[41]

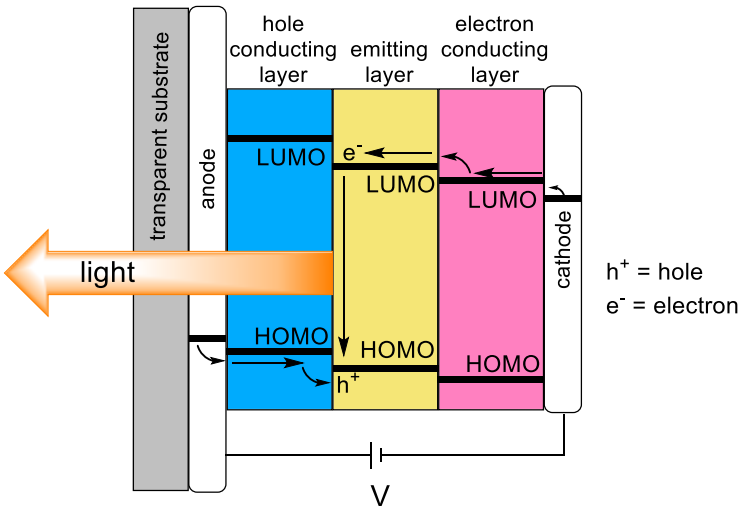

Figure 1.9 – OLED device structure with energy levels for a three-layer (hole conducting, emitting, electron conducting) heterojunction diode.

In order to control the rate of hole and electron injection from the electrodes, and the mobility of the charges towards recombination, multi-layer structures have been deployed in most current OLED devices.[41] These layers include organic semiconducting materials employed for either their hole or electron conducting properties. At the interface between these layers and the emitting layer, there is sizable offset between the energy levels of the HOMOs (as well as the LUMOs) of the two materials. In Figure 1.9, the holes injected from the anode are contained in the hole conducting layer until they can overcome the barrier for transport into the emissive layer. Once the barriers for charge transport have been passed, the hole can recombine with an electron that has proceeded

through the electron conducting layer to the emitting layer and release electroluminescence.[39]

Conjugated materials used in OLED emissive layers and conducting layers generally composed of either small molecules (SM-OLEDs) or polymers (PLEDs) (Figure 1.10). While device performance can be very similar between types of device, fabrication of the film can be quite different depending on the morphology being semi-crystalline or amorphous. SM-OLEDs are generally deposited as films through evaporation under vacuum, while PLEDs are solution cast.[41]

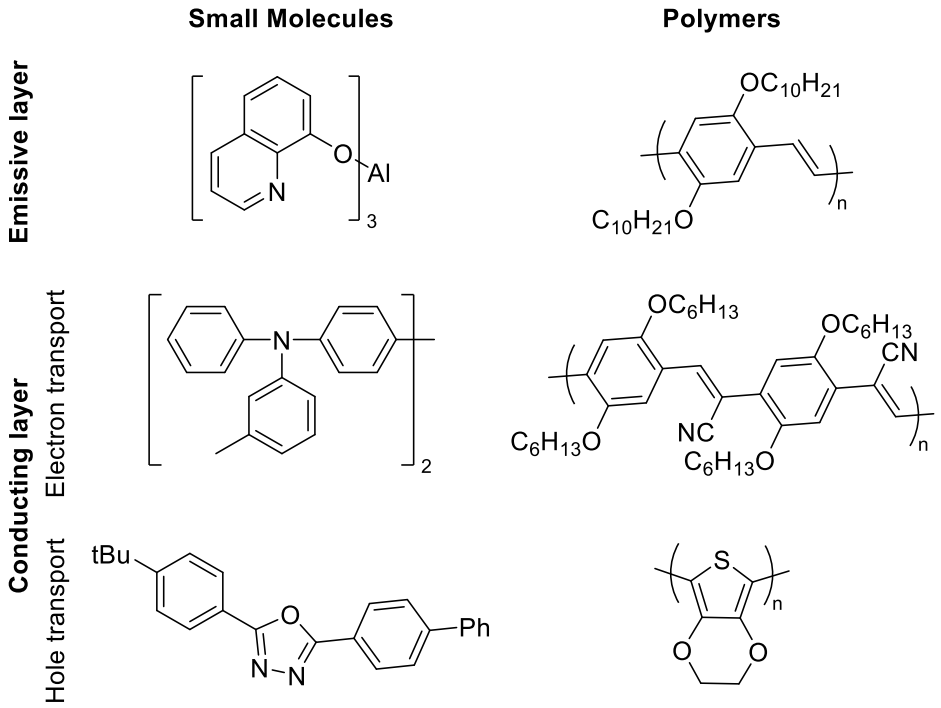

Figure 1.10 – Example conjugated small molecules and polymers used in OLED devices.

1.3.3 Organic photovoltaics

Organic solar cells (OSCs) broadly consist of organic thin film photovoltaics (OPVs), dye-sensitized solar cells (DSSCs) and perovskite solar cells, though only OPVs

will be discussed in further detail. OPVs generally possess a combination of organic n-type semiconductors (acceptor) and p-type semiconductors (donor), where usually the donor acts as a light absorbing layer (Figure 1.11a).[42] Photoexcitation of this donor material results in the formation of an exciton (hole and electron pair). The exciton diffuses along the donor layer to the intersection between the p- and n-type materials whereupon charge separation can occur. Electrons collected into the lower lying LUMO of the n-type layer proceed towards the cathode while holes collected in the p-type material HOMO proceed towards the anode (Figure 1.11b).[41]

While OPV device architecture generally consists of heterojunction layers of p- and n-type organic semiconducting materials inserted between two electrodes, excitons can only diffuse a short distance (5 - 14 nm) before decaying to the ground state. Therefore, when the organic semiconducting material is prepared as planar heterojunction, wherein the two materials are simply processed as separate adjacent films, excitons formed may not reach the charge-generating interface between materials. Instead, a bulk heterojunction can be used in which the two materials are blended in solution to make a homogenous mixture prior to deposition.[43] This results in formation of a film with irregular domains of p- and n-type material, increasing the area of p/n junction and leading to enhanced efficiency of charge separation. Bulk heterojunction configurations also simplify device fabrication as a single layer of solution processed organic material can be deposited. In addition to the donor and acceptor materials, a hole-blocking layer is often employed to prevent the holes from recombining with electrons at the cathode while an electron-blocking layer accomplishes the opposite.[36]

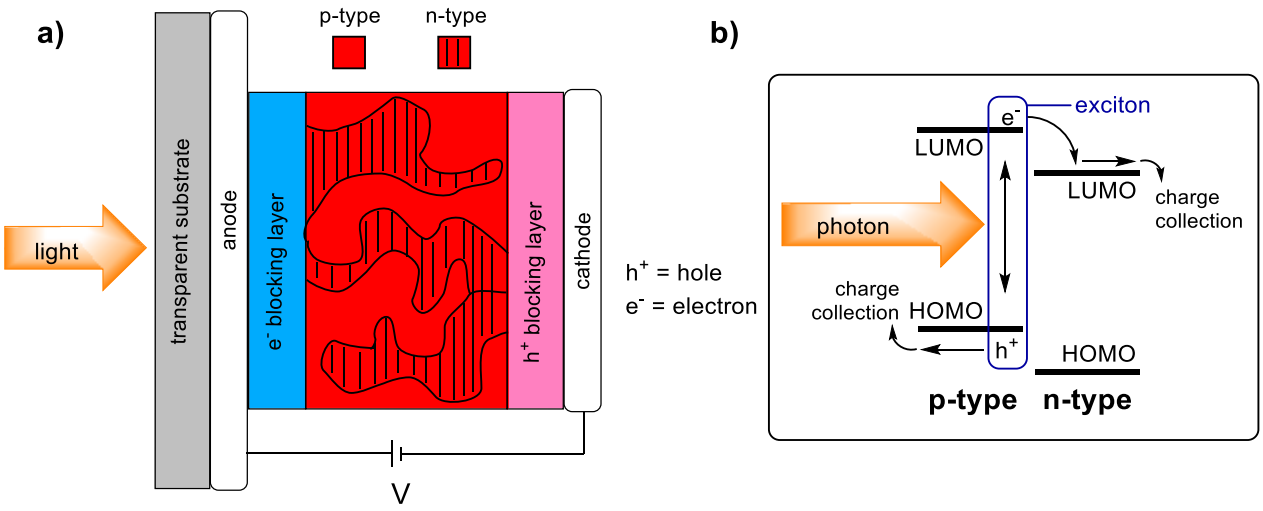

Figure 1.11– a) General device structure of a bulk-heterojunction OPV b) energy level diagram of exciton formation and dissociation.

Ideal n-type materials for bulk heterojunction solar cells have been generally focused around fullerenes (C_{60}, C_{70}) and their derivatives.[44] The advantage of using fullerenes in this application is that they possess relatively low-lying LUMOs that are easily able to act as electron-transport materials upon accepting an electron from the excited p-type material. Additionally, electron charge transfer from the conjugated polymer to fullerene C_{60} occurs several orders of magnitude faster than decay of the exciton, limiting the loss of efficiency due to this pathway. Unfortunately, due to its poor solubility in organic solvent and tendency to crystalize, C_{60} itself is difficult to employ in bulk heterojunction processing. Therefore, functionalized fullerenes such as [6,6]-phenyl-C_{61}-butyric acid methyl ester (PCBM) have been used for increased solubility, but at the cost of having a lower absorption in the visible region (Figure 1.12).[45]

Conjugated polymers are the most commonly used p-type material and have been explored extensively in the last few decades for this application.[46] To act as an ideal p-type material, the conjugated polymer must be highly soluble to allow for solution

processability as bulk heterojunction with an n-type material. Secondly, the deployment of conjugated polymers that possess a small band gap allows for a broad absorption spectrum and increased capture of solar energy. Charge transport also needs to be facilitated by high hole mobility to increase charge collection and decrease charge decay/ recombination. Finally, it is also important to consider the HOMO and LUMO energy levels between p- and n-type material pair to allow for adequate downhill energy offset for exciton dissociation, as well as the physical properties of the material to allow for appropriate morphology of the bulk heterojunction layer.[46]

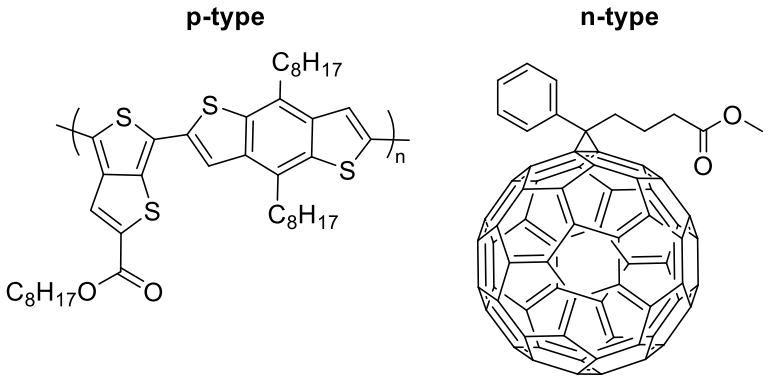

Figure 1.12 – An example conjugated polymer used as p-type material and fullerene-derivative used as n-type material in OPV devices.

In all applications of organic electronic materials, slight changes in the chemical structure of the conjugated small molecule or polymer can have large effects on the material's electronic and physical properties. Fortunately, due to their nature as organic molecules, there exists a diverse set of tools to facilitate these transformations.

1.4 Engineering of the molecular structure

Of the many potential advantages that are associated with the commercialization of conjugated organic materials as alternatives to inorganic materials, arguably the most notable and most important towards realization is the infinite variation of structures. The structural variety of organic small molecules and polymers and the wide array of organic transformations employable on these substrates allows for a unique control both the material's physical properties, as well as its electronic band gap, a feature not observed in inorganic semiconducting materials. The ability to modify the band gap of corresponding materials by adjusting the HOMO and LUMO levels of the conjugated organic molecule or polymer is known as band gap tuning and remains at the center of many investigations into organic materials. As such, several approaches to tuning the HOMO-LUMO gap that rely on transformations to the molecular structure of the conjugated π-system have been established. These include bond length alternation (BLA) adjustments through modification of aromaticity in individual aromatic units, employing the electronic effects of substituents, as well as the establishment planarity or increasing molecular rigidity (Figure 1.13).[46–48] Additionally, enabling positive interchain interactions (such as π-π stacking) can affect both the band gap of the material, as well as its physical properties. Since most simple conjugated organic molecules and polymers have large band gaps, these strategies are often used to decrease the HOMO-LUMO gap into the semi-conducting range, though it is also of importance to manage the absolute HOMO and LUMO energy levels for device stability, and specific band gaps may be targeted for device application (such as light absorption in OPVs).

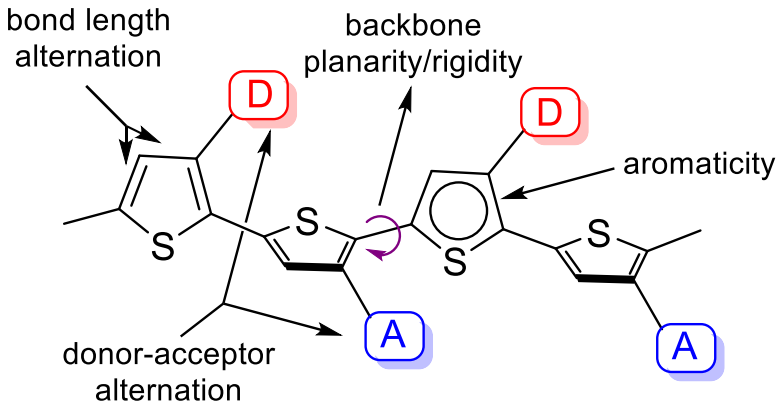

Figure 1.13 – Molecular considerations for engineering conjugated organic materials.

1.4.1 Bond length alternation

When developing conjugated materials with linked arene units, is it important to consider the BLA, that is the average difference in bond lengths of the alternating carbon-carbon bonds in an aromatic conjugated system.[49] This is due to the two possible resonance structures of the ground state – the aromatic and the quinoid forms, being not energetically equivalent (as they would be in polyacetylene). In the aromatic resonance form, each arene in the conjugated system maintains aromaticity with the confined π-electrons of the ring. Delocalization of these π-electrons outside of the aromatic ring results in transformation of the single bonds to double bonds and vice versa. This quinoid resonance form is energetically less favourable compared to the aromatic form due to the loss of aromatic stabilization, and possesses a lower HOMO-LUMO gap.[48,50] If an aromatic form is preferred over the quinoidal form in the ground state, the molecule is considered to have a high bond length alternation degree, contributes to a higher HOMO-LUMO gap. The more the quinoidal resonance form is able to contribute to the ground state, the single bonds connecting adjacent aromatic units will adopt a higher double bond character and the BLA is considered to be lower.

In general, there are two approaches towards decreasing the BLA of a conjugated system. The first method is to decrease the aromatic stabilization energy of the conjugated arenes. This allows the conjugated system to more easily adopt the quinoid form through π-electron delocalization. One unique example of this is the oxidation of thiophene units in a conjugated system to thiophene-S,S-dioxides.[51,52] This oxidation results in a loss of aromaticity in the thiophene ring, greatly reducing the stabilization energy of this resonance form. The carbon-carbon double bonds present in the thiophene ring are therefore energetically more similar to that of a tethered S-cis-butadiene, and can easily delocalize to the quinoidal state. The second method for decreasing the BLA is to stabilize the quinoidal form. The most well-known example of this is in the employment of benzothiophene moieties in conjugated polymers.[53] The quinoidal form of a poly(benzoth-

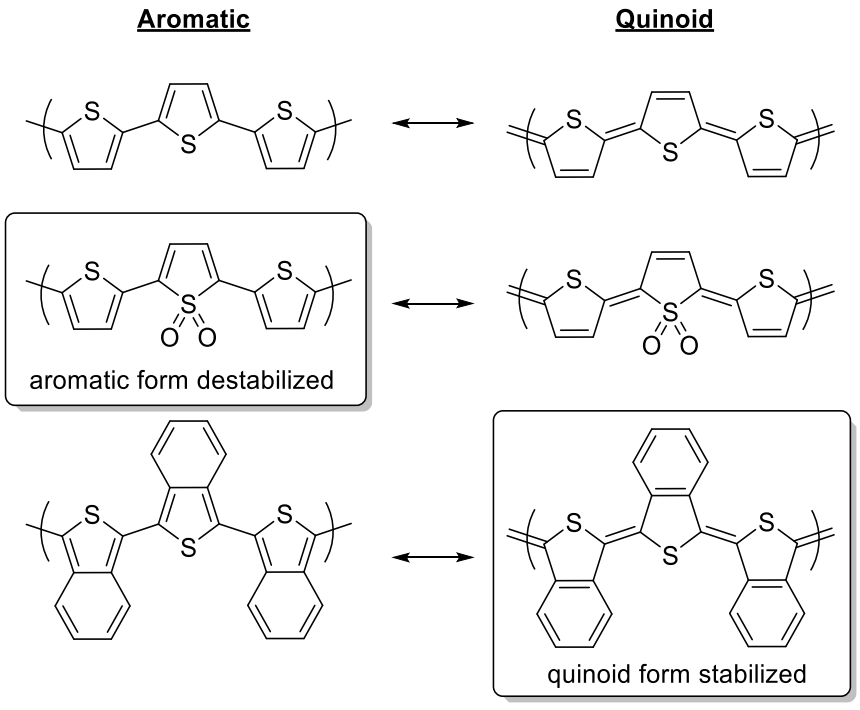

Figure 1.14 – Methods for decreasing the BLA and increasing conjugation in a polythiophene system.

iophene) establishes a Clar's sextet in the benzene ring which stabilizes the quinoid form and reduces the energy difference between the two resonance forms. Benzothiophene, along with thieno[3,4b]pyrazine and thieno[3,4b]thiophene are all commonly employed motifs in conjugated polymers for this purpose (Figure 1.14).

1.4.2 Electronic effects

Another common method for tuning of the band gap in conjugated organic materials is by adjusting the absolute HOMO and LUMO levels through mesomeric or inductive electronic effects. Introduction of electron-donating groups (EDGs) ranging from simple alkyl groups to alkoxy groups generally result in a large increase in the HOMO level and a notable but smaller effect on the LUMO, resulting in a reduction in the HOMO-LUMO gap. The most well-known and perhaps most extensively studied conjugated small molecule or polymer with strong electron-donating groups is poly(3,4-ethylenedioxythiophene) (PEDOT) which possesses a HOMO-LUMO gap of about 0.5 eV less than polythiophene (PT).[54] Likewise, introduction of electron-withdrawing groups (EWGs) such as nitro or cyano substituents on a conjugated small molecule or polymer can decrease the LUMO energy level, while minimally affecting the HOMO, decreasing the HOMO-LUMO gap (Figure 1.15).[55,56]

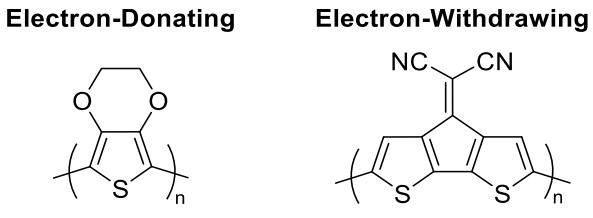

Figure 1.15 – Common electron-donating and electron-withdrawing motifs used in conjugated polymers

1.4.3 Donor-acceptor alternating copolymers

The introduction of EDGs and EWGs into conjugated polymers have been combined into what is known as the alternating donor-acceptor strategy. These conjugated systems possess alternating electron-rich motifs and electron poor motifs. The electron-rich “donor” possesses a raised HOMO level while the electron-poor “acceptor” possesses a lowered LUMO level.[57,58] The HOMO and LUMO energy levels of the material are therefore largely determined by the donor and acceptor moiety respectively. Inclusion of these alternating units results in a smaller HOMO-LUMO gap as well as easier electron delocalization from the donor unit to the acceptor unit and therefore a lower barrier to the quinoid state. The HOMO-LUMO gap of an donor-acceptor conjugated polymer can be visualized as an orbital hybridization of the individual donor molecular orbitals with the individual acceptor molecular orbitals, yielding two new HOMOs (one of which is high lying), as well as two new LUMOs (one of which is low lying) (Figure 1.16).

The development of this strategy has had a profound effect on accessing low band gap conjugated materials and has also allowed for the unprecedented tuning of the individual HOMO and LUMO of the material. Since the HOMO is largely localized on the donor moiety, transformations to this arene will have little to no effect on the LUMO and vice-versa. The specific tuning of energy levels and band gap has been especially useful in the preparation of OPVs to achieve high conversion efficiencies.[59]

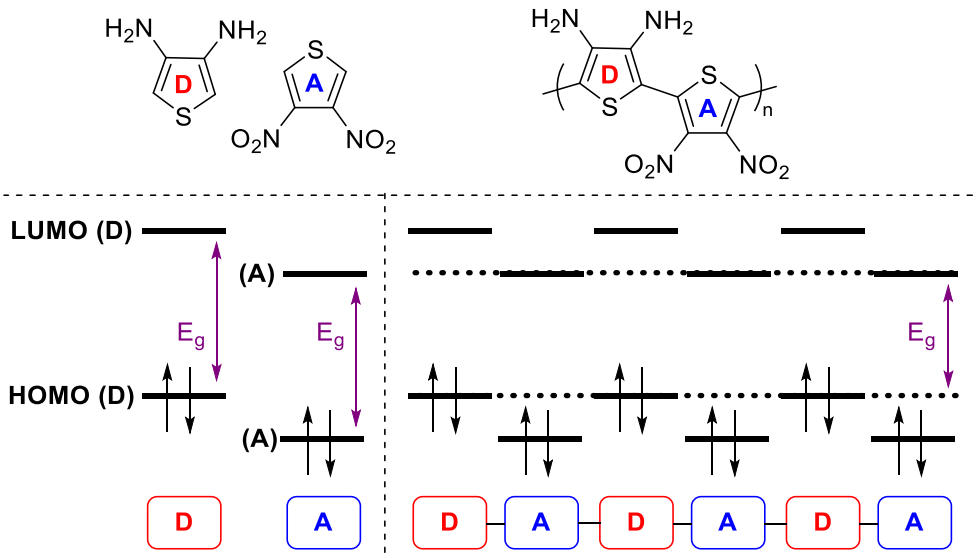

Figure 1.16 – Molecular orbital interactions of donor and acceptor units resulting in a smaller HOMO-LUMO gap.

1.4.4 Planarization and rigidification

Substituents used to induce electronic-effects, solubilizing chains, and even simply protons can result in steric interactions between neighbouring aromatic units which imposes a negative effect on the HOMO-LUMO gap. These steric interactions can cause twisting along the connecting carbon-carbon bond between arene units, leading to de-planarization of the extended conjugated system. Loss of planarity results in a decrease in the p-orbital overlap from one aromatic ring to another and, in turn, results in an increase in both the BLA, as well as the HOMO-LUMO gap. In order to avoid these negative steric interactions between adjacent rings, rotational freedom along this connecting carbon-carbon bond can be reduced through rigidification of the conjugated system. The conceptually most simple way to achieve this is to conformationally lock the adjacent aromatic units through the tethering of a covalently bound bridge. Covalent bridges consist of tethers such as ketals, ethylenes, and even methylenes, installed

between adjacent aromatic rings, and have long been shown to result in a lower HOMO-LUMO gap compared to the equivalent conjugated system with free rotation (Figure 1.17).[60–62] This increase in the number of rings locked by a covalent bridge results increased p-orbital overlap and a higher extent of conjugation. While this is a good method for decreasing the BLA and HOMO-LUMO gap of a conjugated polymer, these types of conjugated polymers with locked aromatic units can often be complex to synthesize and require substantial changes in synthetic planning.

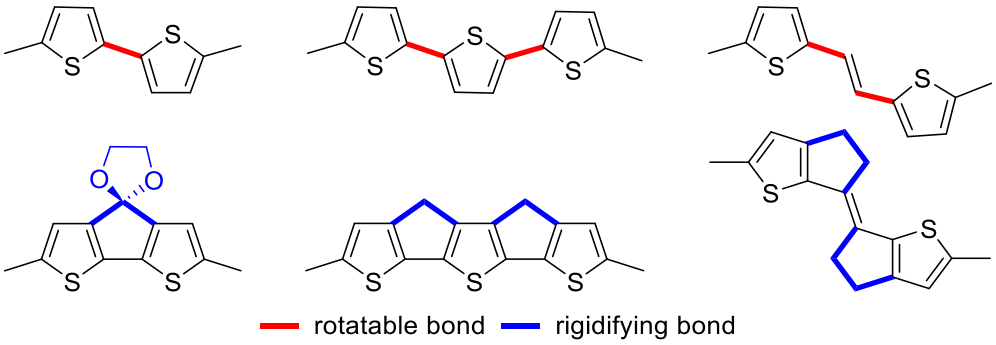

Figure 1.17 – Covalent planarization of polythiophene-based polymers.

As an alternative, non-covalent interactions have been shown to act as conformational locks for the induction of planarity between adjacent arenes.[63] These non-covalent interactions include chalcogen bonding (S – O, S – N, S – F) and hydrogen bonding (O – H, N – H) (Figure 1.18). This will be revisited as a major topic of discussion in Chapter 3.

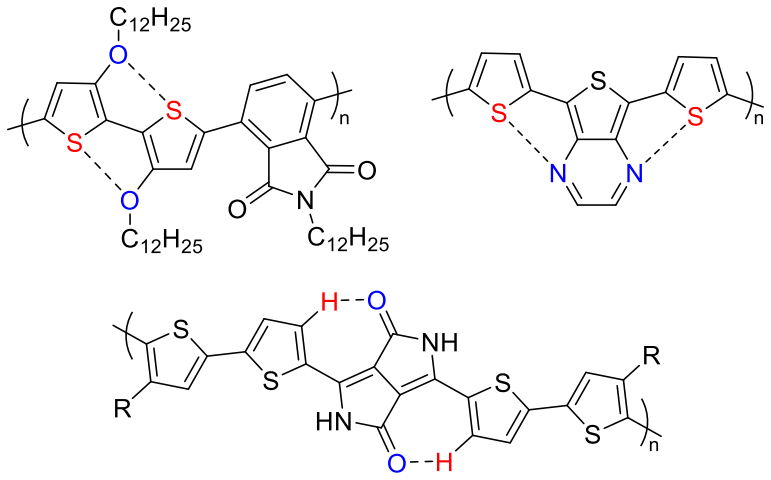

Figure 1.18 – Non-covalent methods for planarization/locking of the π-system.

1.4.5 Interchain interactions

The design strategies for conjugated materials discussed so far have either had a mechanical or electronic effect on intramolecular charge transfer along the π-system of the conjugated backbone. In addition to this, one must consider the two-dimensional structure of conjugated small molecules and polymers and the effect it has on both the electronic band gap of the material, as well as the physical properties essential for device fabrication. This two-dimensional packing is generally facilitated by strong intermolecular interactions between aromatic rings in the conjugated systems backbone (π-π stacking interactions),[64,65] or through organization of side chains.[66] This ordering phenomenon affects the intermolecular charge transfer that occurs through chain-to-chain electron hopping by enhancing the overlap of π-electron orbitals between chains, effecting the band gap of the material.[66] Conjugated polymers that are synthesized to possess stereoregular structures with extended planar sections of conjugation lead to enhanced π-π stacking interactions.[67] Additionally, planarization of a twisted conjugated molecule

or polymer also usually results in a more rigid molecular system which can lead to decreased π-stacking distances and stronger interactions.[68]

In addition to the charge transfer, strong interchain interactions can affect the physical properties of a material; such as its aggregation in solution, film-morphology, and thermal stability.[66,69,70] While a high degree of planarity along the conjugated backbone and two-dimensional packing is advantageous for reducing a materials band gap and facilitating charge transfer, the physical properties imparted by these factors can also have undesired effects. Strong intermolecular interactions enabled by π-π stacking are often the major contributor towards rendering conjugated materials insoluble, though conjugated polymer solubility is also governed by the degree of polymerization and polymer regioregularity. It is important to ensure the solubility of conjugated organic small molecules and polymers in organic solvent such that the desired physical properties of the material are maintained including crystallinity, morphology, phase behavior, and important for device fabrication: the solution-processability.

In order to overcome this lack of solubility caused by intermolecular π-π stacking, the interaction can be reduced between planar conjugated units by employing aliphatic chains. Long aliphatic chains covalently attached to the conjugated backbone generally possess between 8 and 12 carbons in order to create enough steric bulk to disrupt the π-π interactions (Figure 1.19).[71,72] Branching along the aliphatic chains further increases the steric volume between conjugated units and therefore is generally found to further increase solubility.[73,74] While increasing solubility through the inclusion of these sidechains is often necessary, it is deleterious towards the conjugated material's band gap and intermolecular charge transfer. Therefore, when designing and synthesizing new

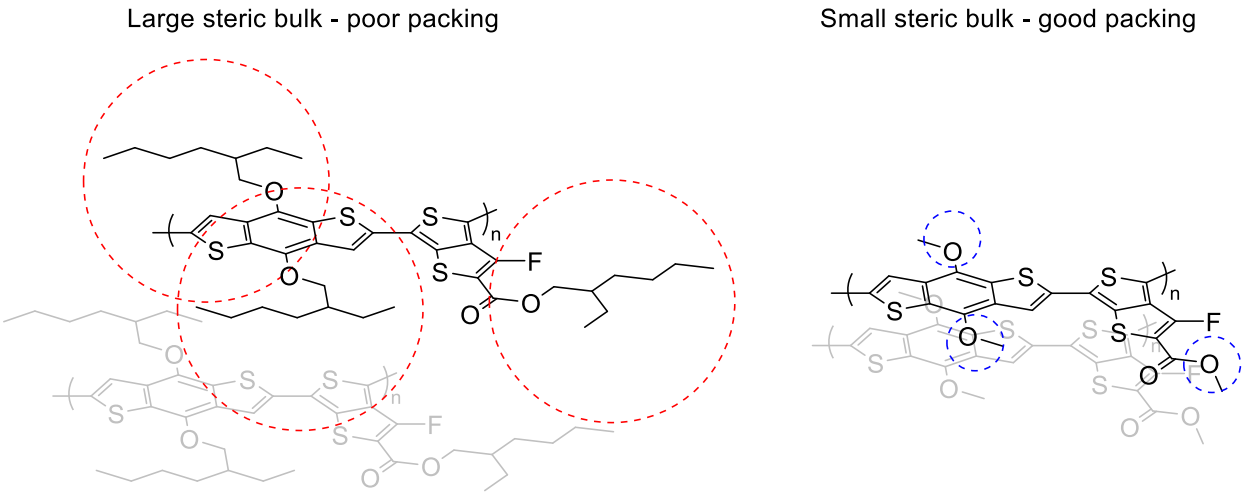

Figure 1.19 – Example packing of polymers with large and small steric bulk with dashed circles representing the steric volume of the alkyl chain.

conjugated materials, a balance between the two factors must be achieved.[75]

The design strategies summarized in this section must all be considered when developing new conjugated small molecules and polymers, and are often used in combination to achieve conjugated materials with precise electronic and physical properties. It is, therefore, important that a wide variety of synthetic methods exist to allow for facile implementation of these design parameters.

1.5 Synthesis of conjugated materials

Poly(hetero)arenes dominate modern conjugated polymers while conjugated small molecules also often consist of biaryl motifs. Modern synthetic chemists are therefore dependent on reactions used to establish new C_{sp2}-C_{sp2} bonds between arenes.[76] The synthesis of small molecules possessing aryl-ene motifs and conjugated polymers such as PPVs employ a wider range of transformations (including Heck coupling[77], the Wittig

reaction[78], Knoevenagel condensation[79] and hydroarylation[80,81]), however, these will not be discussed herein.

The currently employed methods for C_{sp2}-C_{sp2} bond formation between arenes are almost exclusively limited to transition metal-catalyzed cross-couplings. Cross-coupling of arenes allow for not only access to biaryls but also access to regioregular conjugated polymers, which has an important impact on the physical and electronic properties of the material. Before these methods became commonplace, less selective methods such as electrochemical and chemical oxidative couplings for the synthesis of conjugated polymers were employed, and in some cases, are continued to be used today.

1.5.1 Electrochemical and chemical oxidative coupling

For the first few decades after the discovery of conjugated polymers, polypyrrole found its spot as one of the most comprehensively studied semiconducting materials. The most efficient method for the synthesis of polypyrrole at that time was through electropolymerization, wherein a pyrrole monomer is dissolved in solvent with an anionic doping salt.[82] The pyrrole is then oxidized at the surface of an electrode through application of an anodic potential. The pyrrole radical cation can then react by coupling with another pyrrole radical cation to form an intermediate dihydro-dimer dication. The loss of two protons allows for the formation of the neutral dimer that can continue to propagate in the same manner to form a polymer chain (Scheme 1.1).[83] Pyrrole became an attractive substrate for this due to its low oxidation potential relative to other heteroarenes which allows it to undergo electropolymerization in aqueous electrolytes.[83]

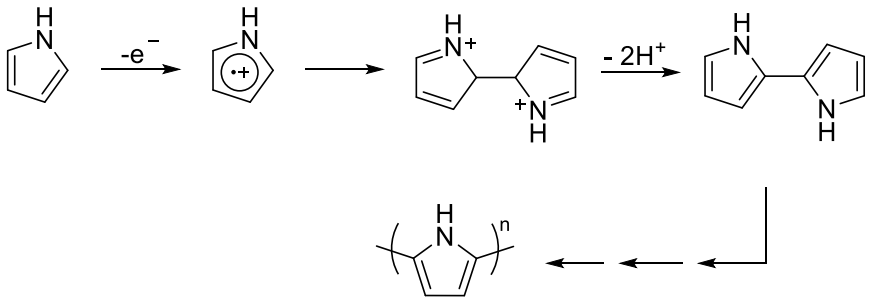

Scheme 1.1 – Electrochemical oxidative polymerization method.

While this is a generally facile method for the synthesis of conjugated polymers, electropolymerization yields polymers that are prone to defects. The electrochemical oxidation of the initial pyrrole creates a delocalized radical cation which has the potential to react at the α (2-position) or β (3-position) (Scheme 1.2a).[82] Since the unpaired electron density is highest at the α-positions, the radical coupling reaction is most likely to occur at this position. The oxidation potential of the pyrrole dimer formed from the first coupling is lower than that of the pyrrole monomer and therefore more easily oxidized to the dimer radical cation. With this radical, the unpaired electron density is distributed over the two pyrrole units leading to an increase in density at the β-positions. Coupling at this position leads to branching of the polymer which yields a material that possesses poor crystallinity due to its non-uniformity and poor stacking ability. It is suspected that at least one in every three pyrrole rings in polypyrrole synthesized by electropolymerization is affected by structural disorder in this manner.[83] Accordingly, it is notable that the electropolymerization of 3,4-dimethylpyrrole yields a more crystalline polymer due to the lack of branching ability at the β-position.[82] This methodology has been extended beyond pyrrole to include other heteroarenes such as for the synthesis of polythiophene (PT).

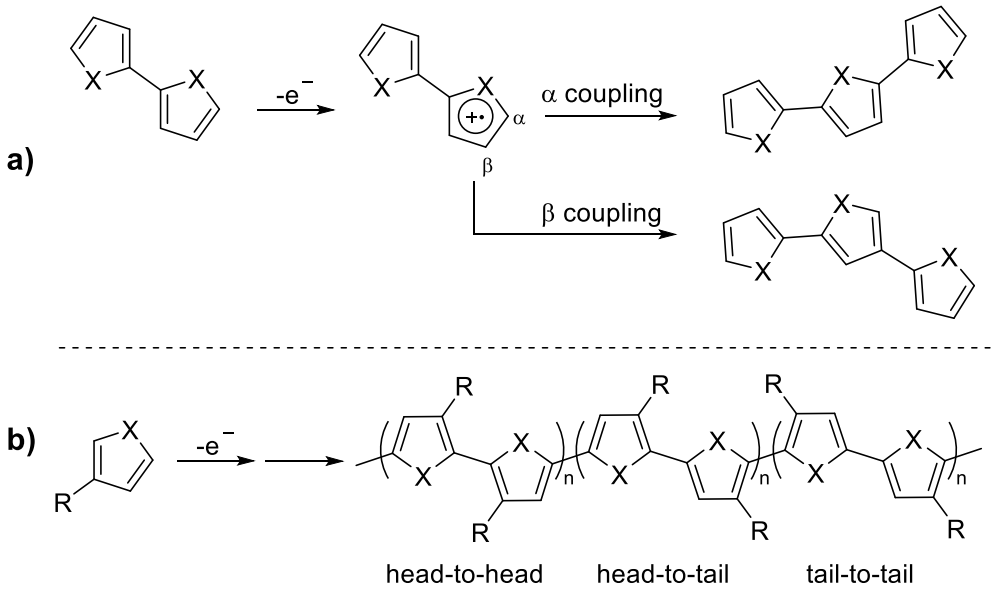

Scheme 1.2 – Regiochemical considerations for the synthesis of conjugated polymers by electropolymerization a) branching b) asymmetric arenes.

Substituents on the heteroarene are also tolerated by the electropolymerization method, although the sterics and electronics can have a dramatic effect. Strong EWGs destabilize the radical cation intermediate and increase reactivity which can result in the formation of side-products being favoured over polymerization. Likewise, while sterics do not generally affect the oxidation of the monomer arene, it can affect the ability of the radical cation to couple which can also lead instead to other side-products.[84] Nevertheless, flexible alkyl sidechains are attractive for increasing solubility and are therefore often included at a less-reactive 3-position (β), for example, in the synthesis of poly(3-alkylthiophenes). Despite the higher molecular weights achievable and increase in solubility, this comes with the added issue of polymer regioregularity. Due to the asymmetrical nature of a 3-alkylthiophene, the radical cation intermediate generated by electrochemical oxidation can react at the 2-α or 5-α position (Scheme 1.2b). This leads to the formation of a dimer in which the thiophenes can be bonded at either their sterically

congested 2-position (head), or at the 5-position (tail). The dimer can form one of three regioisomers; denoted as either head-to-head (HH), head-to-tail (HT), or tail-to-tail (TT). Subsequent coupling continues in such a manner to yield conjugated polymers with a high percentage of regioirregularity. This non-specific control over polymerization can once again have a negative effect on both polymer morphology, and crystallinity, as batch-to-batch variation also influences the conjugated polymers electronic properties. Particularly, steric hinderance occurring in HH orientations can cause a twisting of the conjugated backbone leading to reduced planarity and altering the π-π stacking.[84]

As with electrochemical oxidative polymerization, arenes such as pyrrole and thiophene can by polymerized to their corresponding conjugated polymer through means of chemical oxidation. A common chemical oxidant used in this manner is iron (III) chloride. Chemical oxidation to synthesize conjugated polymers is generally less utilized than electrochemical methods, despite producing polymers in higher yields and with less regioirregularity.[85,86] Though these methods present a facile way to access conjugated materials, oxidative polymerizations remain lacking for the development of regioregular conjugated polymers with high crystallinity suitable electronic properties for device use. The ultimate vision of accessing regioregular conjugated polymers was only finally achieved following the rise of transition metal cross-couplings.

1.5.2 Organometallic cross-coupling reactions

The rapid development and growth of transition metal-catalyzed cross-couplings greatly simplified the synthetic routes to biaryl species found in pharmaceuticals, natural products, and organic electronics. Through these methods, biaryls can now be synthesized routinely in high yields, under mild conditions and with robust functional

group tolerance.[76] Furthermore, these cross-coupling reactions allowed, for the first time, access to regioregular conjugated polymers with wide-ranging structural variations. This is due to the unparalleled ability of these reactions to regioselectivity form C_{sp2}-C_{sp2} bonds between two activated arenes: generally, an aryl halide (Ar-X) and an organometallic arene (Ar-M = Ar-MgX, Ar-SnR_3, Ar-$B(OR)_2$, Ar-SiR_3) (Scheme 1.3). While several transition metals, including nickel and platinum, have been shown to facilitate these

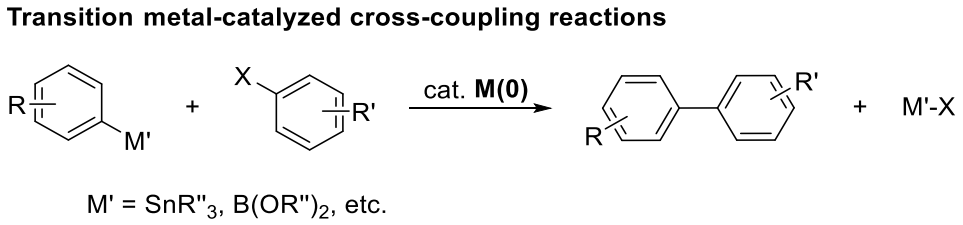

Scheme 1.3 – Conceptual scheme for the synthesis of biaryls through traditional transition metal-catalyzed cross-coupling reactions.

transformations, palladium-catalyzed cross-couplings are most prominent.

Most of these transition metal-catalyzed cross-couplings proceed through a three-step process to facilitate construction of a new aryl-aryl bond. First, the transition metal catalyst undergoes oxidative addition into the C_{sp2}-X bond of an aryl halide (or pseudo halide). Following this, the metal-arene complex proceeds through a transmetallation step with the organometallic arene. Finally, reductive elimination of the biaryl-metal complex facilitates formation of the new carbon-carbon bond and returns the transition metal catalyst to its original reduced state (Figure 1.20).[87]

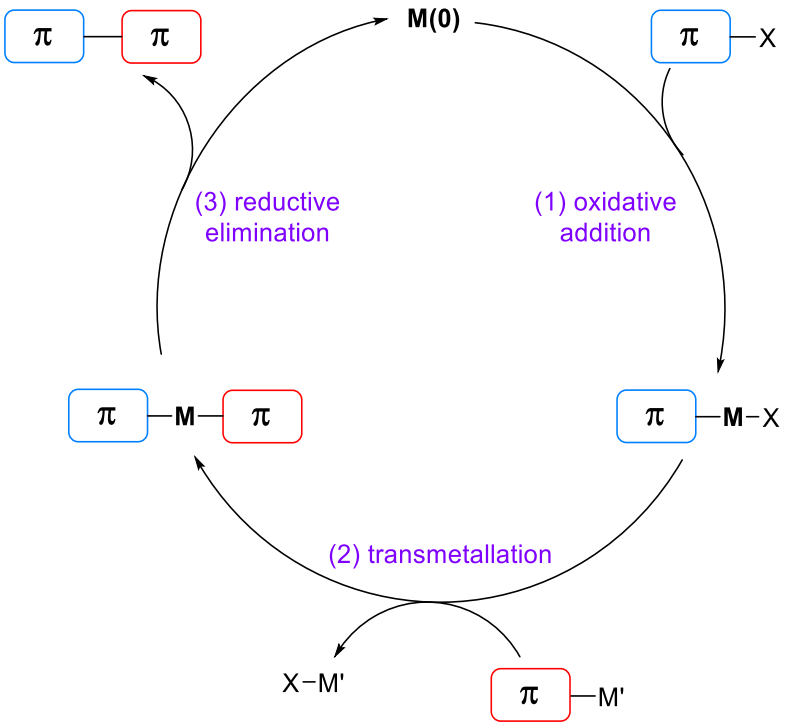

Figure 1.20 – Catalytic cycle of a transition-metal catalyzed cross-coupling.

Organometallic cross-couplings have been employed to generate conjugated polymers in the same manner used to synthesize biaryls. To achieve this, one of two differing strategies can be used to prepare the monomers for cross-coupling polymerization (Figure 1.21). The first strategy is to prepare an arene monomer that possesses both an aryl halide functionality as well as an organometallic functionality. This di-functionalized monomer can then proceed through homocoupling in order to generate a polymer in what is known as AB-polymerization. Alternatively, the second strategy is to synthesize a monomer possessing two aryl halide functionalities which can be cross coupled with a monomer possessing two organometallic functionalities in what is known as AA/BB-polymerization.

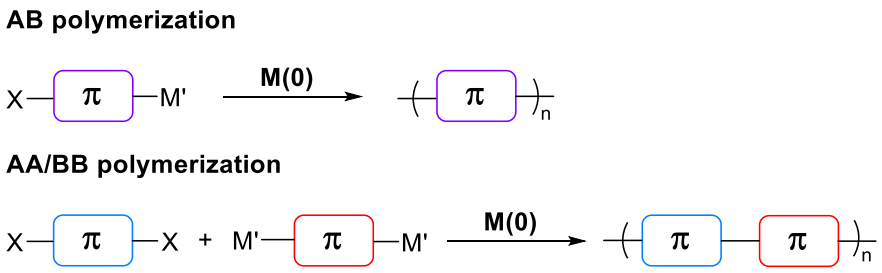

Figure 1.21 – Two approaches to synthesize conjugated polymers through transition metal-catalyzed cross-coupling.

Among the cross-coupling methods employed for the synthesis of conjugated small molecules and polymers, the most prevalent are the Stille and Suzuki-Miyaura couplings. The Stille coupling reaction was discovered in the late 1970s and employs a palladium catalyst to facilitate aryl-aryl bond formations between an aryl halide and an organotin reagent.[88] This method remains popular due to the generally mild reaction conditions and the robust tolerance of a broad array of functional groups.[89] When developing conjugated small molecules and polymers, this allows for the arene coupling partners to be extensively functionalized towards desired properties prior to the reaction. Organotin reagents can conveniently be synthesized through lithiation of the aromatic compound followed by reaction with a trialkyltin chloride. The organotin monomers for Stille-based polymerization are easily purified through recrystallization which is important in ensuring accurate stoichiometry and rendering precise molecular weight control over the polymerization.[90] Unfortunately, the toxicity of stannylated arenes, as well as the stoichiometric amount of organotin byproduct produced from Stille coupling, remain an inherent concern for the practicality of use, especially for commercial scale syntheses.[91,92] A typical example of an AA/BB-type Stille polycondensation towards a conjugated polymer is showcased in Scheme 1.4.

Stille polycondensation

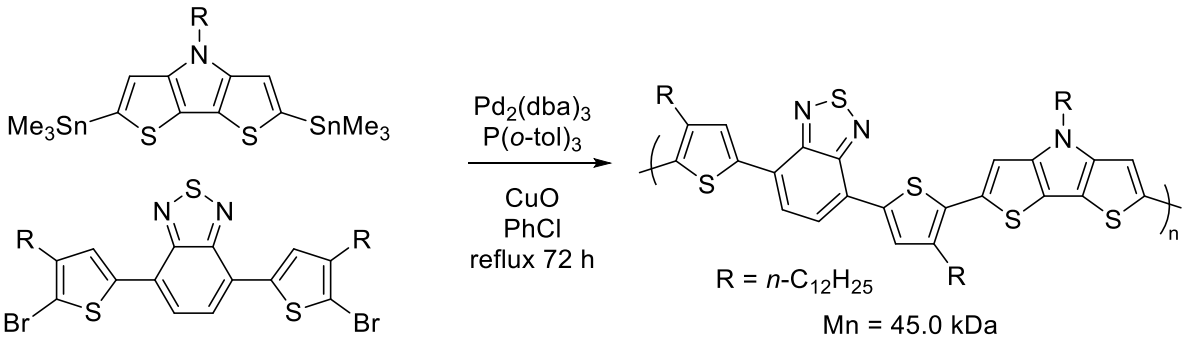

Scheme 1.4 – Example Stille polymerization towards a typical conjugated polymer.[93]

Likewise, Suzuki-Miyaura coupling was developed in 1979 and has expanded to become one of the most attractive methods for the synthesis of aryl-aryl bonds found in organic molecules and conjugated polymers.[94] Suzuki coupling proceeds along a similar catalytic cycle to Stille coupling in which a palladium catalyst is used to form the new C_{sp2}-C_{sp2} bond between an aryl halide and an aryl boronic acid. The boronic acid reagent can be prepared through reaction of an aryl lithium with a diboronyl acid/ester. Like Stille coupling, Suzuki coupling has been advanced through the years to be tolerant of a wide variety of functional groups. The major advantage of Suzuki coupling over its organotin cross-coupling counterpart is the generally low toxicity of the organoborane reagents and byproducts. However, aryl boronic acid reagents tend to be less stable than aryl stannanes due to their propensity for dehydration. Degradation of the boronic acid monomer in a Suzuki polymerization can easily upset the stoichiometric balance.[95] A typical example of an AA/BB-type Suzuki polycondensation towards a conjugated polymer is showcased in Scheme 1.5.[96]

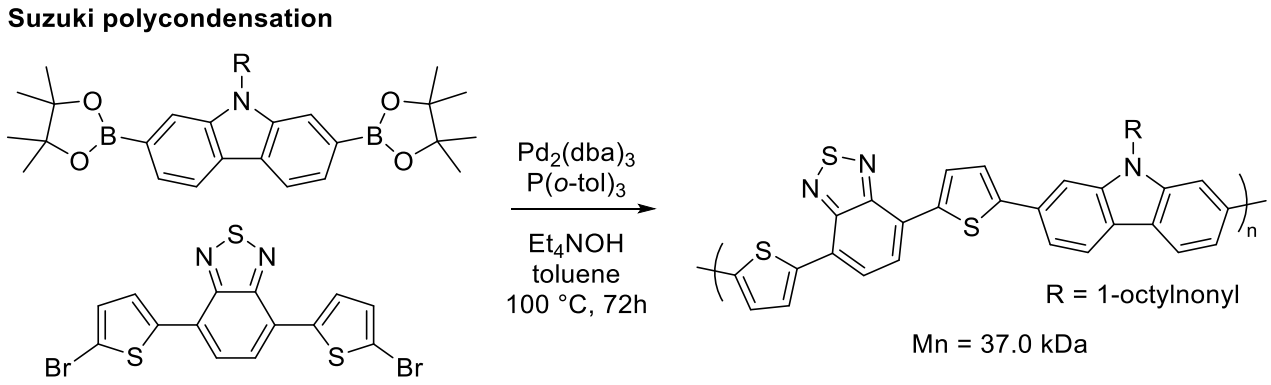

Scheme 1.5 – Example Suzuki polymerization towards a typical conjugated polymer.[96]

Other transition metal-catalyzed coupling reactions are also routinely employed for the synthesis of conjugated small molecules and polymers. Kumada-Corriu coupling reactions use catalytic nickel to form new C-C bonds between aryl Grignards (Ar-MgX).[97] A stoichiometric amount of nickel(0) is utilized in Yamamoto coupling reactions wherein a dihalogenated arene (ArX_2) is homocoupled to yield conjugated polymers.[98] Palladium-catalyzed Sonogashira coupling reactions are a useful tool towards the synthesis of poly(arylethynylene)-type polymers through the formation of C_{sp}-C_{sp2} bonds.[99]

With transition metal-catalyzed cross-coupling reactions in the synthetic toolbox, forming C-C bonds between arene units has become a routine transformation, however, this does not mean that they are without drawbacks. As noted previously, Stille coupling remains arguably the most popular method for the synthesis of biaryls and conjugated polymers despite the toxicity of its reagents and byproducts being a growing concern. The use of expensive transition metal catalysts such as palladium is also antagonistic towards the deployment of these transformations on a commercial scale. Additionally, trace palladium impurities embedded in the 3D structure of a conjugated material can have detrimental effects on the performance of the resulting organic electronic device.[100–102]

Finally, these methods have inherent inefficiencies in the fact that they generally require two “pre-activated” or “pre-functionalized” components – the aryl halide and the organometallic arene. The functionalization to organometallic reagents can often take several steps to prepare, all while generating a stoichiometric amount of metal waste, and requiring the use of expensive or difficult to handle reagents. Therefore, there exists a growing interest in developing new cross-coupling strategies from pre-functionalized materials through processes such as C-H activation.

1.5.3 Direct arylation

In order to eliminate the need for pre-functionalization, cross-coupling reactions in which the organometallic arene is replaced by an unfunctionalized arene became highly sought after. This led to the emergence and development of direct arylation as an attractive alternative to palladium-catalyzed cross-couplings such as the Stille and Suzuki coupling reactions. Direct arylation enables the formation of a new carbon-carbon bond between an aryl halide and a simple unfunctionalized arene, eliminating the need for pre-functionalization, and resulting in only acid as a stoichiometric byproduct (Scheme 1.6).[103–105]

Mechanistically, direct arylation occurs in a similar manner to other palladium-catalyzed cross-couplings. The catalytic cycle begins with oxidative insertion of Pd (0) into the aryl halide (Ar-X) bond. Instead of transmetallation, the next key step is C-H bond activation of the unfunctionalized arene. Finally, reductive elimination yields the biaryl product and regenerates the palladium catalyst (Figure 1.22). While oxidative addition

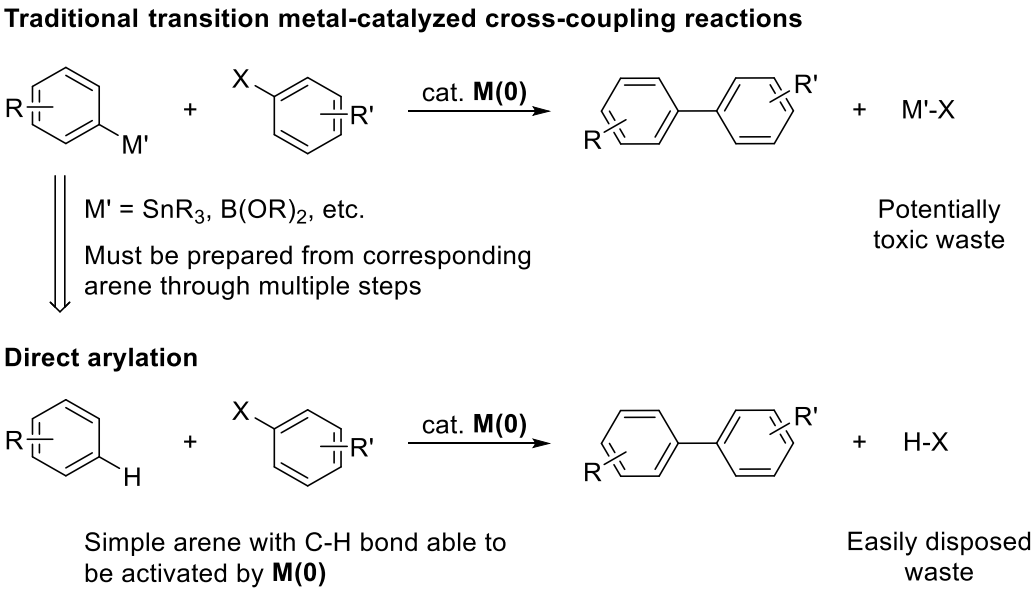

Scheme 1.6 – Conceptual scheme for the synthesis of biaryls through direct arylation as it compares to transition metal-catalyzed cross-couplings.

and reductive elimination are well understood, the process in which the C-H activation step occurs was the subject of much investigation. This step was initialy predicted to proceed through one of several mechanistic pathways including: electrophilic palladation, carbo-palladation (Heck-type), or concerted metalation-deprotonation (CMD). Although the method of C-H activation occurring in the direct arylation catalytic cycle is suspected to be somewhat dependent on both the substrate and catalytic system, a (base-assisted) CMD mechanism has generally been validated for direct arylation by the observed experimental outcomes.[106]

Concerted metalation-deprotonation occurs through simultaneous cleavage of the arene C-H bond and formation of the new C-Pd bond. The deprotonation component of the CMD step can be promoted by a catalytic amount of a carboxylate (usually a pivalate or acetate) base that undergoes a ligand exchange with the anionic halide or pseudo-halide ligand on the palladium, prior to the CMD step. A stoichiometric amount of

carbonate base (K_2CO_3, Cs_2CO_3) is generally included in the direct arylation conditions in order to regenerate the carboxylate co-catalyst from the acid produced through abstraction of the proton in the CMD process.[106]

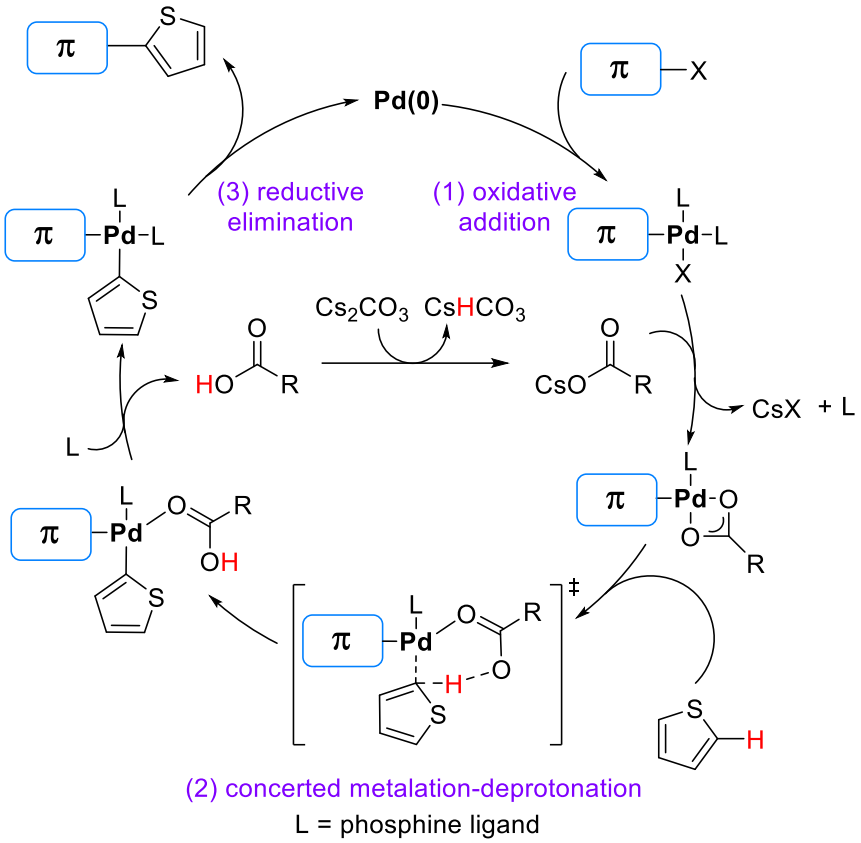

Figure 1.22 – Proposed catalytic cycle for the direct arylation of thiophene with an aryl halide via a concerted metalation-deprotonation step.

Computational evaluation of the CMD step through density functional theory (DFT) calculations has revealed the transition state energy required is dependent on two factors.[107] The first factor is the energy required to break the aryl C-H bond which generally correlates to the acidity of the C-H bond that is being activated. Thus, C-H activation of electron-poor arenes in direct arylation largely proceeds well as the energy to distort the C-H bond remains low. The second factor is the energy to be overcome

when the distorted arene interacts with the palladium center. This generally corresponds to the nucleophilicity of the arene, and therefore electron-rich arenes also are found to proceed well through the C-H activation step.[108]

While direct arylation eliminates the need for pre-functionalization of a single arene, a functionalized aryl halide is still required for the oxidative addition step. Reaction conditions for direct arylation are also notably harsher than those developed for equivalent Stille and Suzuki couplings, often requiring temperature greater than 100 °C under inert atmosphere. The catalytic Pd(0) required for the transformation is generally delivered as a Pd(II) pre-catalyst such as $Pd(OAc)_2$ or the Hermann-Beller catalyst.[109]

Direct arylation has more recently been applied to the synthesis of conjugated polymers in what has been termed direct arylation polymerization (DArP).[110] The earliest demonstration of a DAr-type polymerization was in the synthesis of poly(3-hexyl)thiophene in the late 90's from monohalogenated thiophenes.[111] While initial investigations only produced polymers with number average molecular weights (M_n) of around 3 kDa, fine tuning of direct arylation reaction conditions and catalytic systems over the last two decades has rendered DArP into a useful tool for conjugated polymer synthesis.[112–115] Electron-rich monomers such as those based on thiophene and 3,4-ethylenedioxythiophene (EDOT) are ubiquitous with conjugated materials and are prime candidates for C-H activation. DArP is also a useful technique for the development of acceptor-donor structured conjugated polymers with electron-poor monomers as they often do not polymerize well under Stille or Suzuki coupling conditions.[115] In addition to the advantages that exist for small molecule direct arylation, DArP monomers are significantly more stable than organometallic monomers, and can give rise to conjugated

polymers with higher molecular weights than previously achievable.[114] Where DArP begins to falter, however, is in the control of polymerization. Monomers that possess more than one C-H bond can undergo C-H activation at multiple sites leading to branching and cross-linked polymer products.[116] Blocking of C-H activation sites with alkyl chains or fluorine substituents can diminish this issue, however, this adds to the synthetic complexity of the monomers and can have disruptive effects on the morphology/ crystallinity. Since the CMD step is very substrate-dependent, careful choice of monomer, catalytic system, and optimization of conditions are required to achieve control over polymerization.[117]

1.5.4 Oxidative cross-coupling reactions

Building upon the success of direct arylation, the next natural step towards eliminating the need for pre-functionalization is to proceed in the direction of cross-coupling from unfunctionalized arenes. Unlike transition metal-catalyzed cross-coupling reactions and direct arylation wherein an aryl halide acts as the “electrophilic” arene, the cross-coupling of unfunctionalized arenes would have to proceed through a 2-fold C-H activation of “nucleophilic” arenes. This type of reaction, therefore, requires the employment of an oxidant, in addition to the transition-metal catalyst, in order to return the catalyst to its active state following reductive elimination (Scheme 1.7).[118]

As with direct arylation, C-H activation of an unfunctionalized arene is not a simple process due to the general inertness of an aryl C-H bond. This process can proceed via one of several general modes including: electrophilic aromatic substitution (S_EAr), sigma-bond metathesis, or CMD (previously discussed for direct arylation).[119,120] Additionally, specific strategies must be employed in order to achieve the desired regioselectivity of C-

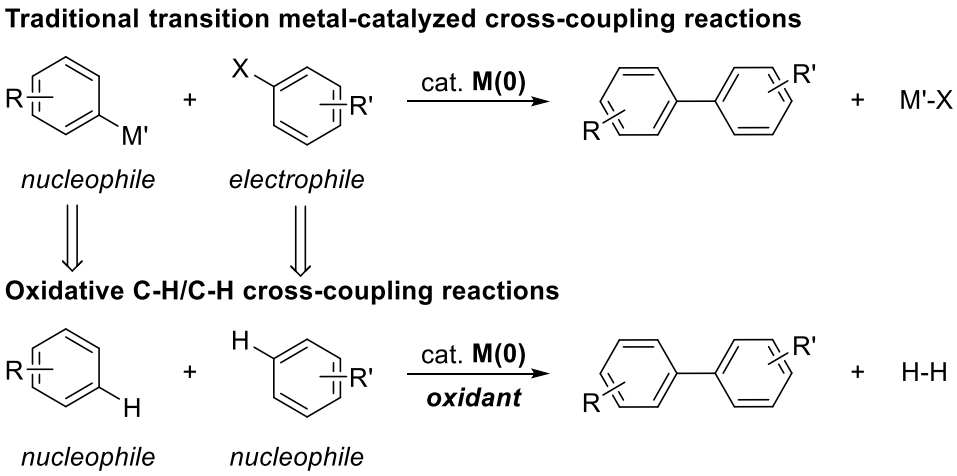

Scheme 1.7 – Conceptual scheme for the synthesis of biaryls through oxidative cross-coupling reactions.

H activation on an aromatic compound that contains multiple C-H bonds, such as the introduction of directing groups to coordinate the metal center at a proximal location to the desired C-H bond, exploiting the electronics of the arene substrate to favor specific C-H activation methods, and manipulating steric effects to disfavor certain C-H bonds (Figure 1.8). Furthermore, a catalytic system (metal and ligands) can be selected to that

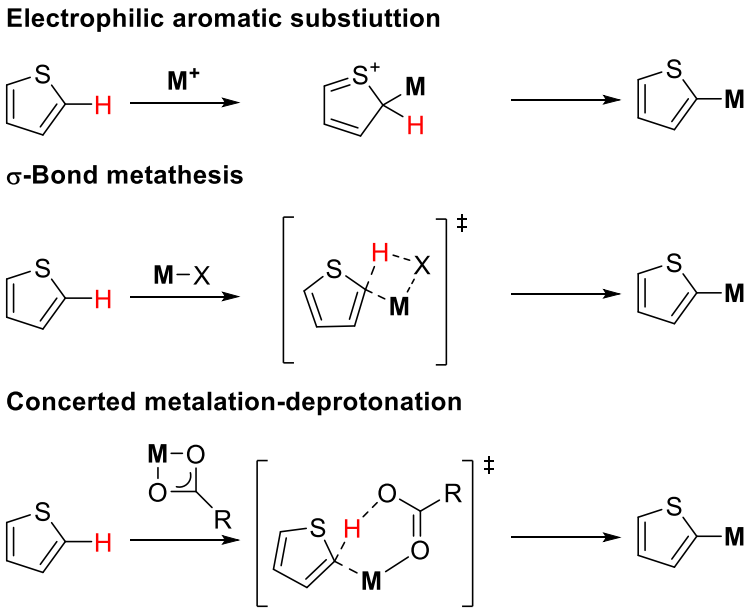

Scheme 1.8 – C-H activation pathways.

is able to influence the regioselectivity of C-H activation.[118]

Beyond the control of C-H regioselectivity, cross-coupling presents several additional new challenges when compared to oxidative homocoupling strategies. With C-H activation having to occur on two separate arenes in the same reaction mixture, there is the potential for three different products to be formed: one cross-coupled product, and the two products as a result of homocoupling.[118] Therefore, the major requirement for oxidative cross-coupling to occur is to have an inversion of reactivity between the two C-H activation steps, such that only the cross-coupled product is formed. A general catalytic cycle for an oxidative cross-coupling reaction begins with an oxidized metal catalyst (such as palladium) which must then proceed through the two back-to-back C-H activation steps in which anionic ligands on the transition metal are exchanged for aryl substituents. Reductive elimination then yields the biaryl species as well as the reduced catalyst which must be regenerated through the inclusion of a stoichiometric oxidant for the catalyst to

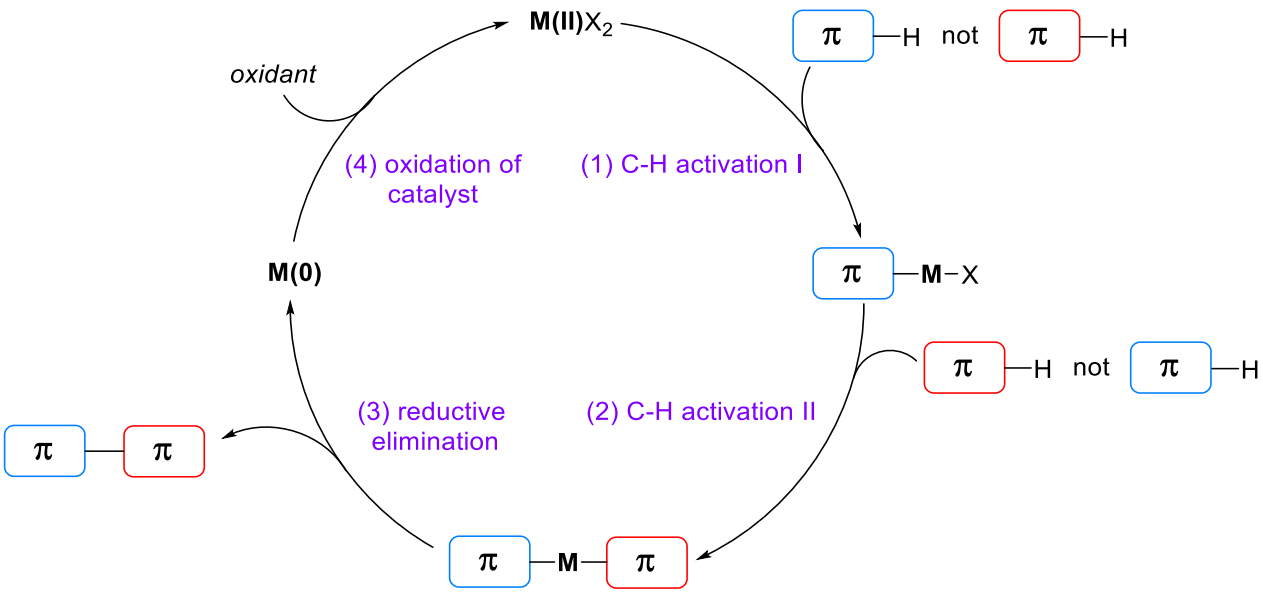

Figure 1.23 – Proposed catalytic cycle for the oxidative coupling of two unfunctionalized arenes

repeat the cycle (Figure 1.23).[118]

Due to the nature of oxidative cross-coupling reactions being highly substrate dependent for the C-H activation steps, no generalized catalytic system exists. Instead, two seminal examples will briefly be discussed. The first example, from 2010, is the oxidative cross-coupling developed by Wei and Su.[121] This coupling reaction employs catalytic $Pd(OAc)_2$ with $Cu(OAc)_2$ as the stoichiometric oxidant, and utilizes the distinct electronic differences between the polyfluoroarenes and benzene (as well as other substituted derivatives) to allow for cross-coupling to take place. A PivOH additive was found to be beneficial towards this transformation and supported the proposal of base-facilitated CMD of the benzene derivative based on kinetic isotope effect (KIE) experiments. Regioselectivity of C-H activation on the substituted benzene derivatives were speculated to be substituent-based as a mixture of products was collected (Scheme 1.9a).

Another notable report was the oxidative cross-coupling of a heteroarene (indole) with benzene derivatives by Stuart and Fagnou in 2007, also employing a catalytic-oxidant system of $Pd(OAc)_2$ and $Cu(OAc)_2$.[122] No homocoupling products were observed from this oxidative coupling which was proposed to proceed through a single catalytic cycle in which C-H activation of the indole occurred through S_EAr, and through PivOH promoted CMD of the secondary unfunctionalized arene. Interestingly, regioselective control over C-H activation at the C2- or C3-position of the indole was found by employing different oxidants (Scheme 1.9b).

Su and co-workers, 2010

(a)

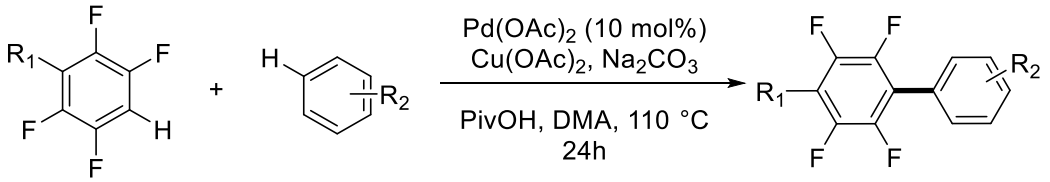

R_1 = F, OMe, styryl

R_2 = H, CH_3, CF_3

Fagnou and co-workers, 2007

(b)

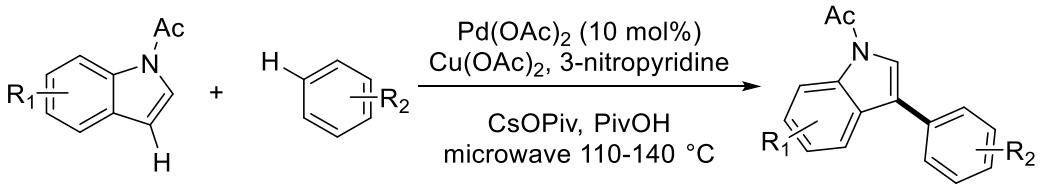

Scheme 1.9 – Examples of oxidative cross-coupling reactions.

While these examples present significant progress towards the development of C-H/C-H cross-coupling reactions, examples of this transformation are few, and remain limited to biaryl small molecules. Regioselectivity remains an important aspect of C-H activation, although the development of new strategies continues to resolve this issue. Furthermore, the generally high reaction temperatures, requirement of an expensive transition metal catalyst and need for stoichiometric amount of metal oxidant leaves much potential for improving the efficiency of this route towards the synthesis of biaryl carbon-carbon bonds.

2

Transition Metal-Free *ipso*-Arylative Condensation

2.1 Background

The rise of direct arylation and the dawn of oxidative C-H/C-H coupling methods over the last decade have systematically begun to eliminate the need for pre-functionalization in the coupling of arenes. However, the fact remains that both of these methods still require a transition metal catalyst that can be both cost-prohibitive towards the commercialization of a synthesis, and result in the deposition of trace impurities which can greatly diminish the electronic abilities of a conjugated material. Instead, our focus as a research group has been to develop methodologies for the synthesis of poly(hetero)arene conjugated polymers that do not rely on transition metal coupling and would not possess the inherent issues associated with them.

Non-conjugated polymers, such as the plastics used in our everyday life, are produced at the millions-of-tons scale yearly.[123] This is achievable due to the ease of synthesis and lack of byproducts. Polycondensations are one of the most common method for the synthesis of plastics and are used in the production of polymers such as Nylon [6,6] and polyethylene terephthalate (PET). Nylon polymers are synthesized through amide formation, while PET is produced by esterification, both of which only produce water as the condensation byproduct (Scheme 2.1). A dehydrative polycondensation route towards poly(hetero)arenes that does not require a transition metal is not as conceptually simple a task, and for that reason, has remained virtually unexplored. We have, therefore, looked towards the unique reactivity of the thiazole heterocycle in our efforts to achieve this goal.

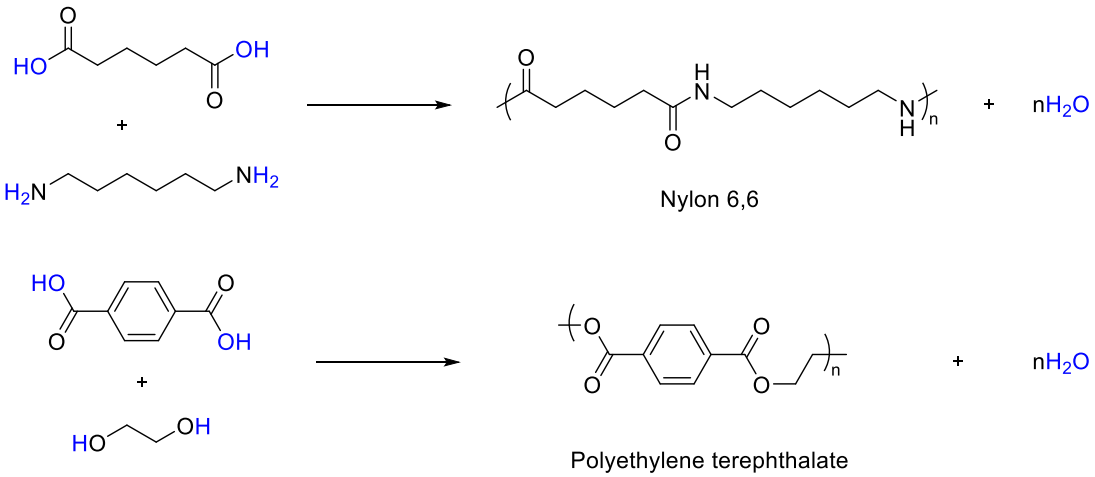

Scheme 2.1 – Commercial polymers synthesized through dehydration polymerization.

2.1.1 Thiazole-containing polymers

Thiazole-containing conjugated polymers are increasingly being explored as an alternative to the heavily present thiophene-containing conjugated polymers. Compared to thiophene, thiazole is a more electron-deficient heterocycle which corresponds to lower

lying HOMO and greater transistor air stability.[124] While this results in thiazole-containing polymers having poorer hole-transport abilities, these materials do possess some advantages: notably the lack of proton at the 3-position of thiazole reduces steric interactions with adjacent aromatic units and therefore increases p-orbital overlap when compared to thiophene.[125–127] Thiazoles are generally employed in conjugated polymers as either as a 2,2'-bithiazole (HH), or 5,5'-bithiazole (TT) motif, although polythiazoles (HT) have also been studied (Figure 2.1).

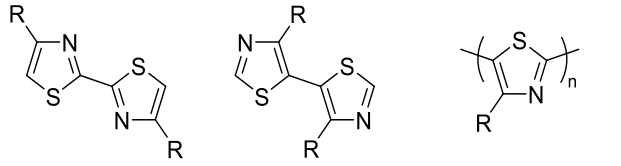

Figure 2.1 – Thiazole motifs in conjugated polymers.

Yamamoto and co-workers reported the first poly(bithiazole)s in 1995,[128] which were synthesized via the homopolymerization of 5,5'-dibromo-2,2'-bithiazoles using nickel-mediated Yamamoto coupling (Scheme 2.2).[129] The reduction potential obtained through CV for the 4,4'-dimethyl polymer was lower than that of poly(3-methylthiophene) (P3MT), indicative of a lower level LUMO. This was expected due to the electron-withdrawing inductive nature of the thiazole nitrogen which makes thiazole a more electron-poor heterocycle than thiophene. Polybithiazole was unable to be oxidized electrochemically in the same voltage range that oxidation of P3MT occurs, indicating a lower energy HOMO. Solubility in chloroform was also found to be poor for the methyl and *n*-butyl substituted bithiazole polymers which is indicative of good planarity and strong π-π stacking interactions.[128]

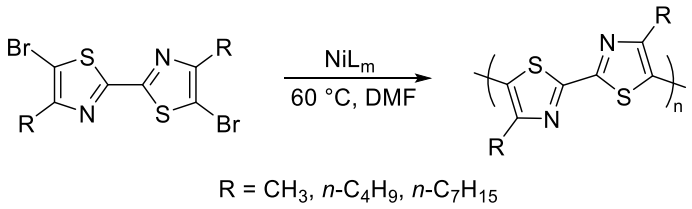

Scheme 2.2 – Yamamoto coupling of 5,5'-dibromo-2,2'-bithiazole.

Thiazoles have been continually explored over the past 25 years, being incorporated into both small molecules and polymers for device applications such as OFETs and OLEDs.[130–137] In order to further expand their potential for use in electronic applications, modern bithiazole-containing polymers are typically coupled with other π-conjugated spacers such as 9,9-dialkylfluorene.[138] These types of polymers have typically been synthesized through AA/BB-type polymerizations utilizing Stille or Suzuki coupling reactions (Scheme 2.3a).[139] In 2014, Kanbara and co-workers found alkyl-substituted 2,2-bithiazole a prime candidate for direct arylation polymerization and prepared a number of conjugated polymers in this manner, using various π-spacers (Scheme 2.3b).[140] Direct arylation polymerization has since been used for the synthesis of

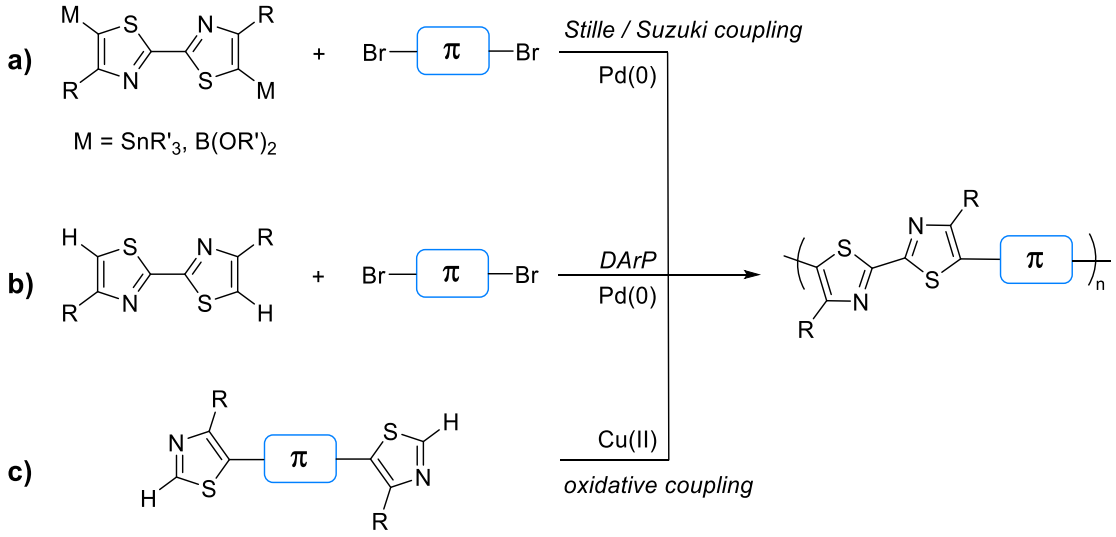

Scheme 2.3 – Modern synthetic routes towards 2,2'-bithiazole-containing conjugated polymers.

bithiazole-containing conjugated polymers in several other notable examples.[141,142] Finally, 2,2'-bithiazole-containing conjugated polymers have most recently been synthesized through formation of the bithiazole C-C bond via copper-catalyzed oxidative homocoupling (Scheme 2.3c).[143,144] While this presents itself as a clever method to reduce pre-functionalization of the monomer and reduce the expensive transition metal requirements, metal impurities can still remain an issue in device performance.

2.1.2 Dehydrative aryl-aryl bond formation

In early 2018, our group reported the first example of a transition metal-free dehydrative polycondensation towards poly(hetero)arenes – specifically, bithiazole-containing conjugated polymers.[145] This reaction, initially developed for the synthesis of small molecules, utilizes the unique reactivity of the 2-unsubstituted thiazole-*N*-oxide starting materials. Upon simple treatment with a *tert*-butoxide base at room temperature, these thiazole *N*-oxides dimerize to the 2,2'-bithiazole-*N*-oxide with the stoichiometric loss of water in only 5 minutes.

The dehydration reaction is believed to proceed via 2-deprotonation of the thiazole-*N*-oxide by the alkoxide base. The anionic thiazole can then perform a nucleophilic attack at the electrophilic 2-position of another equivalent of thiazole-*N*-oxide to form the new aryl-aryl carbon bond. Protonation of this thiazole's anionic oxygen, followed by elimination to restore aromaticity, yields the new 2,2'-bithiazole product with a single *N*-oxide functional group remaining (Scheme 2.4). This dehydration reaction was shown to be tolerant to a wide number of arene functional groups (both electron-rich and electron-poor) as well as heteroarenes at the 5-position, leading to extended conjugation throughout the small molecules.

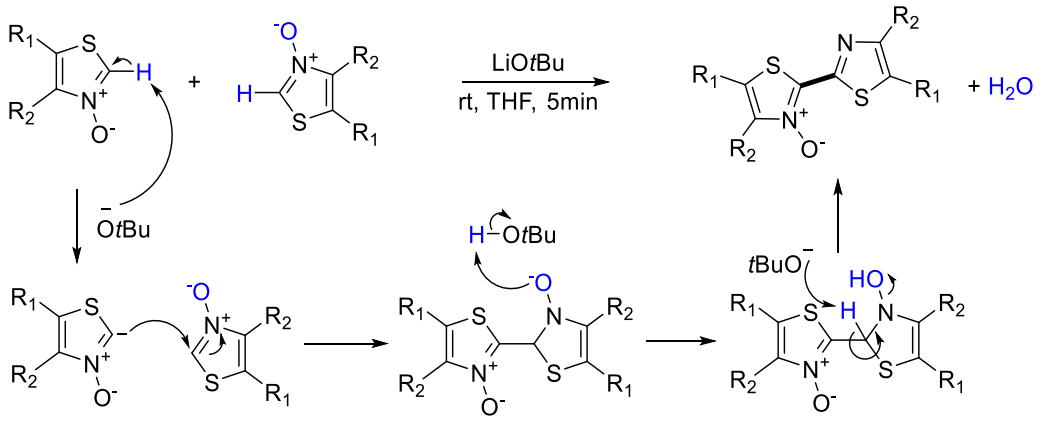

Scheme 2.4 – Proposed mechanism for the dehydrative coupling of thiazole-*N*-oxides.[145]

This dehydrative coupling of thiazole-*N*-oxides was further validated by expanding the scope of the reaction to include the synthesis of poly(hetero)arene conjugated polymers. Monomers were prepared possessing two thiazole-*N*-oxide functionalities connected by varying π-conjugated spacers. These monomers were then subjected to similar conditions as performed for the small molecules albeit with an extension of reaction time. Upon isolation by precipitation, a handful of bithiazole-*N*-oxide-containing polymers were prepared in this manner. Analysis by gel permeation chromatography (GPC) revealed respectable Mn's ranging up to 43 kDa with PDI's of around 2 (Scheme 2.5).

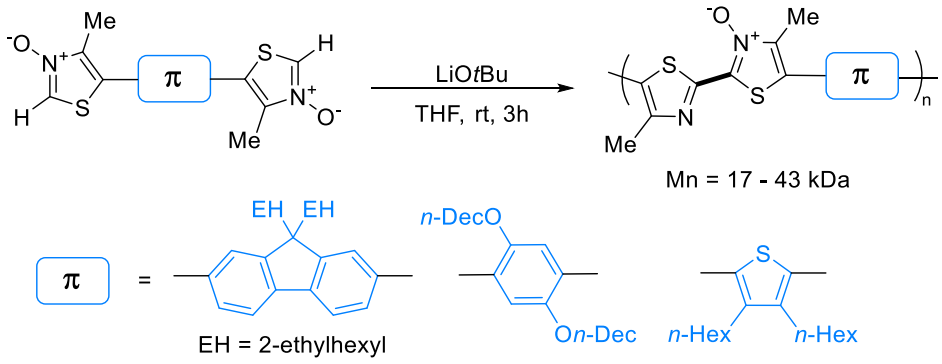

Scheme 2.5 – Scope of the thiazole-*N*-oxide dehydration polymerization.[145]

While this proved to be a facile method to access poly(heteroarene) conjugated polymers, the reaction was mostly limited by the difficulty in accessing thiazole-*N*-oxidesubstrates (and monomers). Oxidation of thiazoles to their *N*-oxide counterparts was completed using *meta*-chloroperoxybenzoic acid (*m*-CPBA), a mild reagent for the oxygen transfer reaction, however, the reactivity was inadequate for thiazole substrates not possessing 4-alkyl substituents. Additionally, the 2-unsubstiuted thiazole-*N*-oxide substrates are thermally unstable at heightened temperatures rendering isolation difficult.

Following our report, in 2018, Voll and Swager described another seminal example of extended π-conjugated structures synthesized through transition metal-free dehydrative aryl-aryl coupling.[146] This reaction proceeds by the nucleophilic addition of electron-rich arenes to readily accessible diols (produced from 9,10-anthraquinone), and requires only a Brønsted acid with mild heating in toluene (Scheme 2.6). The arene nucleophile scope of this reaction include electron-rich arenes such as thiophenes, furan, indole, *N,N*-dimethylaniline, among others.

Though this method is an elegant route for the construction of new C-C bonds between arenes, several factors limit its utility. The substrates scope of nucleophilic arenes is limited to those that possess strong electron-donating groups, with benzene or naphthalene nucleophiles only furnishing trace amounts of product. The reaction is also limited to the construction of conjugated systems which possess anthracene cores, an uncommon motif compared to heteroarenes in extended conjugated systems. Finally, the reaction was unable to lead to polymerization even under forcing conditions, with the closest simply being the difunctionalization of the extremely electron-rich nucleophile EDOT.

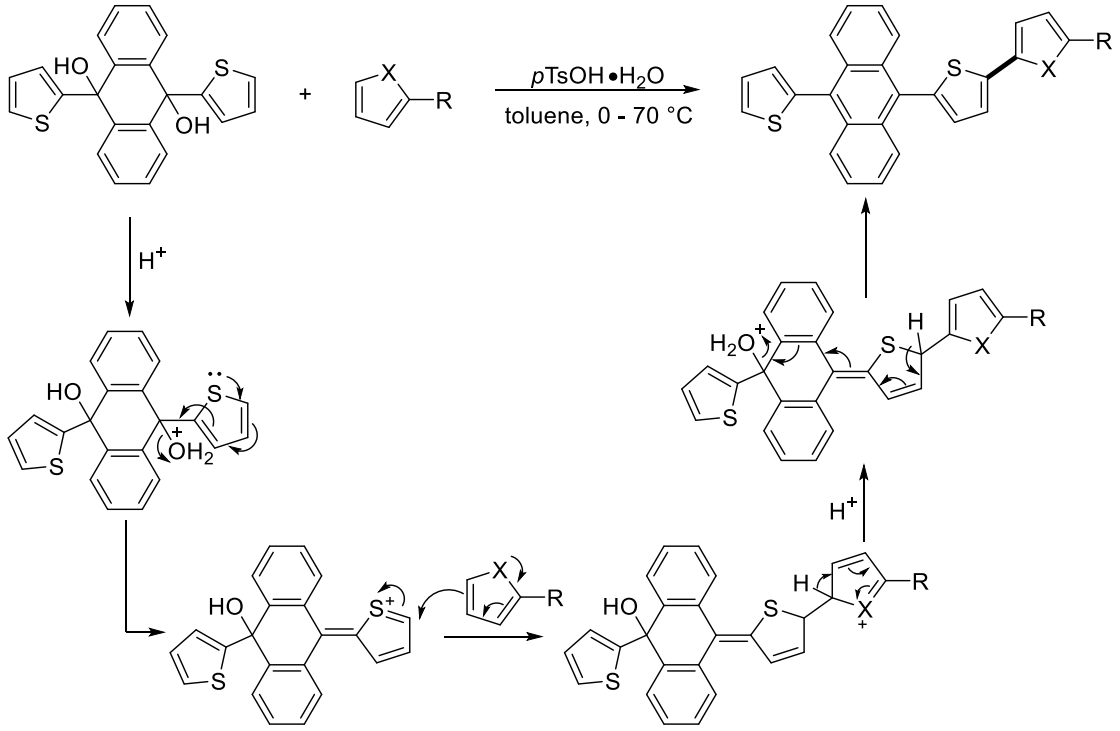

Scheme 2.6 – Proposed mechanism for Swager's dehydrative arene coupling.[146]

Despite the differences between the dehydration of thiazole-*N*-oxides reported by our group and this dehydrative coupling, several fundamental similarities do exist in the mechanism: namely, the loss water (or hydroxide) while establishing aromaticity after nucleophilic attack. Analysis of what has been learned from the reactivity showcased in these methods should prove instrumental towards the realization of other transition metal-free aryl-aryl couplings in the future.

2.1.3 *ipso*-Arylation

An alternative to the traditional palladium-catalyzed cross-coupling reactions (ie: Stille, Suzuki) that has seldom been explored are the coupling reactions that can broadly be classified as *ipso*-arylations. Compared to direct arylation in which a C-H bond is activated to form a new C-Pd bond, *ipso*-arylations form an aryl C-Pd bond through the loss of an organic functionality such as CO_2 or a ketone. While this may seem like a

reversal of the desire to reduce prefunctionalization of aromatics, *ipso*-arylation addresses some issues associated with direct arylation such as the lack of regioselectivity between multiple C-H bonds, as well and the inherent need for an activatable C-H bond (Scheme 2.7).

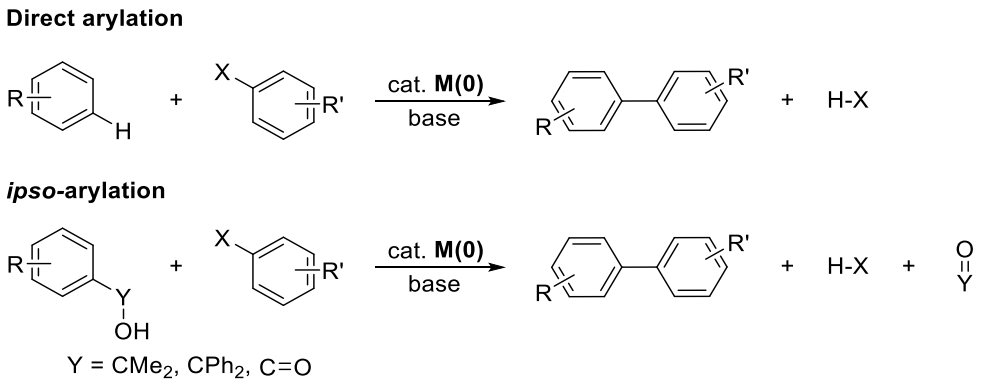

Scheme 2.7 – Conceptual *ipso*-arylation as it compares to direct arylation.

Miura and co-workers first reported the palladium-catalyzed cross-couplings of α,α-disubstituted arylmethanols with aryl bromides in 2001.[147] This *ipso*-arylation product was observed as a side product when attempting *ortho*-arylation using palladium (II) acetate and a carbonate base. With a methyl substituent blocking a single *ortho*-position, only the *ipso*-arylation product was produced (Scheme 2.8). It was suggested that this reaction proceeded through a β-arene elimination of the palladium-oxygen coordinated species to expel a ketone and form a relatively stable palladium intermediate. Subsequent investigations indicated that the reaction was enforced by bulky phosphine ligands, and, in the case of triaryl methanols, steric and electronic factors dictate group elimination.[148,149] The *ipso*-arylation of 2-hydroxymethyl thiophenes was further investigated by Bíró and Kotschy. Unfortunately, these reaction did not proceed as well as on benzene substrates, as the nucleophilicity of the heteroarene increases, so does

the propensity for direct arylation at unsubstituted positions, leading to a mixture of products.[150]

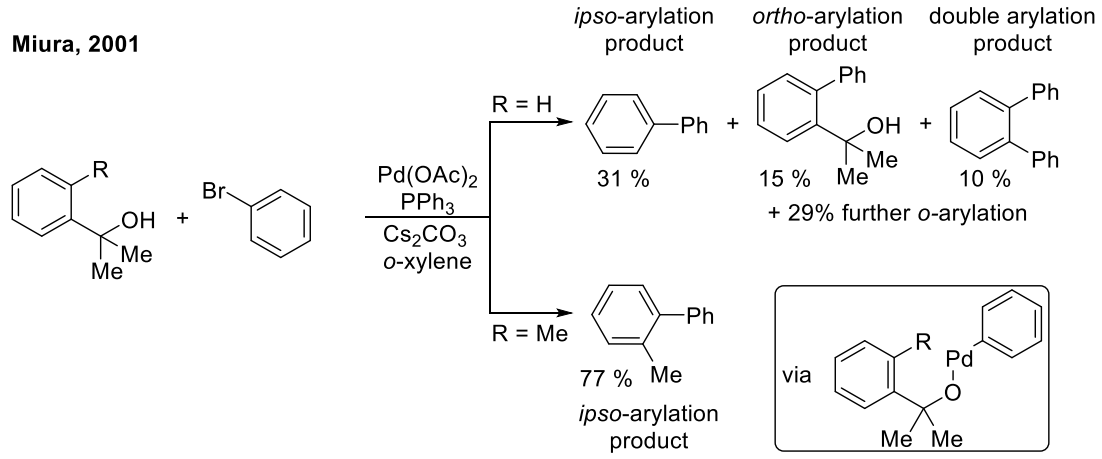

Scheme 2.8 – *ipso*-Arylation using (dimethyl)carbinol activating groups reported by Miura et al.[147]

The mechanism of *ipso*-arylation remained mostly speculation until the investigation of Johnson and co-workers in 2013 to better understand the β-aryl elimination process.[151] Johnson conducted a series of competition reactions between triaryl methanols and aryl halides. These experiments supported the steric effects of *ortho*-substituents contributing to the elimination as previously observed by Miura. Additionally, phenylene substrates possessing either strong EWGs and EDGs both showed a preference compared to unsubstituted phenyl rings. From their experiments, a catalytic cycle involving a β-carbon elimination step was proposed. As with many Pd(0) cross-coupling reactions, this cycle begins by oxidative addition of the palladium into the aryl halide bond. Following ligand exchange of the anionic halide for the deprotonated aryl alcohol, the β-carbon elimination occurs yielding a ketone and a diaryl palladium species. Finally, reductive elimination then affords the biaryl product (Figure 2.2).

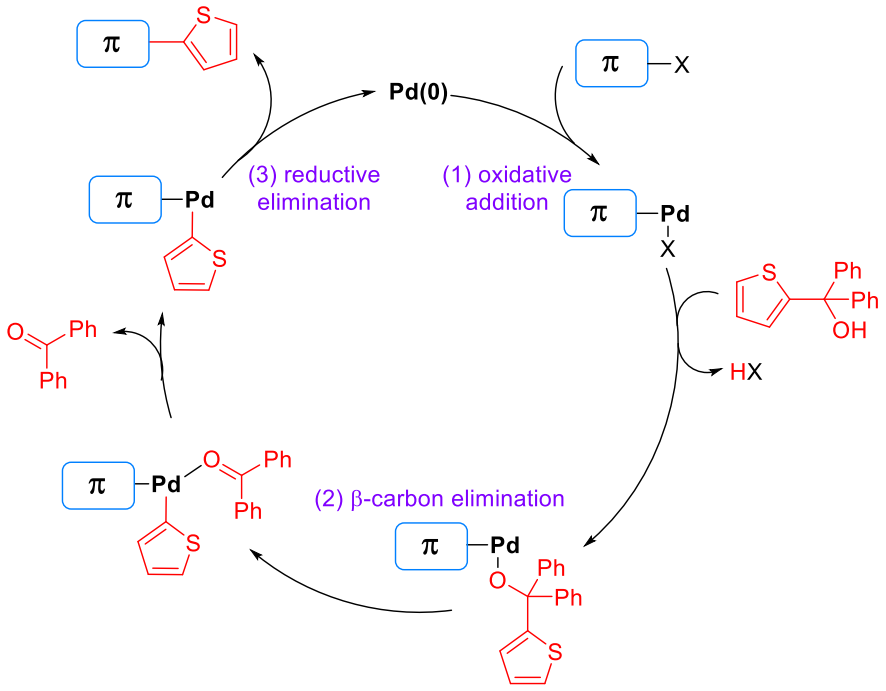

Figure 2.2 – Proposed *ipso*-arylation catalytic cycle.

Another prime example of an *ipso*-arylation was reported by Goossen and co-workers in 2006 which utilized the loss of CO_2 from aryl carboxylic acids to establish the new aryl-metal bond.[152] While this reaction required a palladium catalyst to furnish the new C-C bond, a copper co-catalyst seemed to be essential and was proposed to be responsible for the β-carbon elimination of CO_2.[153] Synchronously, Forgione and Bilodeau reported a decarboxylative cross-coupling of heteroaromatics including pyrroles, furans, thiophenes, thiazoles and oxazoles (Scheme 2.9).[154] Initially, a mixture of *ipso*-arylation at the C4-carboxylic acid position and direct arylation at the C5-H position was observed. Based on the success found in similar transformations, tetrabutyl ammonium chloride hydrate additive was included and resulted in the clean production of the decarboxylation product.[155] As usual, this reaction was proposed to proceed first by oxidative addition of the aryl halide. Electrophilic palladation of the arene 3-position would then be followed by

a C3-C2 palladium migration to expel the CO_2. Finally, reductive elimination would net the biaryl product and regenerate Pd(0). This C3-C2 migration was postulated as to explain the presence of the direct 3-arylation product.[154] Although a universal catalytic system has not been developed and the mechanism remains uncertain, these reactions have found some niche use in the development of biaryls.[156,157]

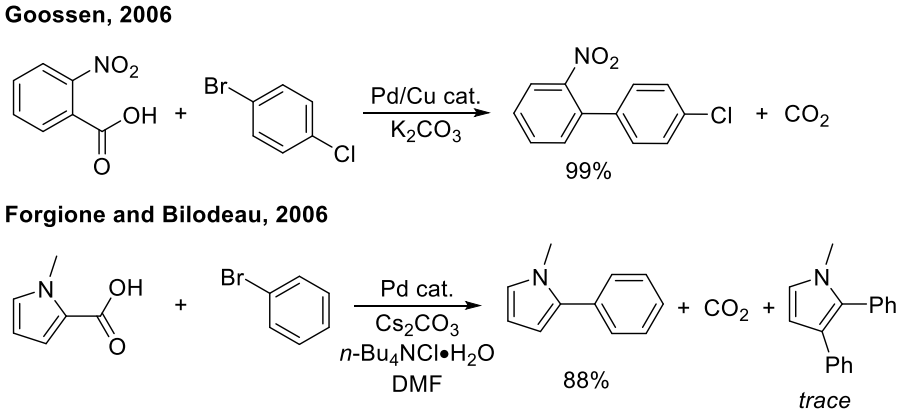

Scheme 2.9 – *ipso*-Arylation using carboxylic acid activating groups reported concurrently by Goossen and Forgione/Bilodeau.[152,154]

ipso-Arylations have only more recently resurfaced in the synthesis of conjugated small molecules as well as the for the first time, conjugated polymers. In 2014, Robert B. Grubbs and co-workers reported the use of *ipso*-arylation for the development of tellurium heterocycle-containing small molecules for photovoltaics.[158] In fact, synthesis of the small molecule semiconductor of interest, a benzotellurophene-capped diketopyrrolopyrrole was first attempted by Stille coupling, however, only trace yields were obtained. Instead, the group turned their attention to using *ipso*-arylation by installation of diphenylcarbinol-substituents on the benzotellurophene, which afforded the desired product in a 42% yield.[158] This work was followed up with complementary synthesis of a tellurophene-containing conjugated polymer in the same manner, the first of its kind.[159]

Recognizing the potential of *ipso*-arylation towards the synthesis of conjugated polymers, Grubbs and co-workers turned their attention towards the synthesis of regioregular poly(3-hexylthiophene), one of the most heavily studied conjugated polymers.[160] This AB polymerization was approached using a single thiophene monomer possessing both the aryl-bromine functionality as well as either a diphenylcarbinol or dimethylcarbinol substituent required for arylation (Scheme 2.10). While only oligomers were obtained using the dimethylcarbinol, *ipso*-arylation using the diphenyl equivalent yielded poly(3-hexylthiophene) with a respectable molecular weight of around 20 kDa. This is notably lower than the molecular weights obtained for the same polymer via Stille coupling, however, this is an important early step in understanding *ipso*-arylation polymerization and could prove useful in situations where monomer stability or lack of tin-by-products are required.

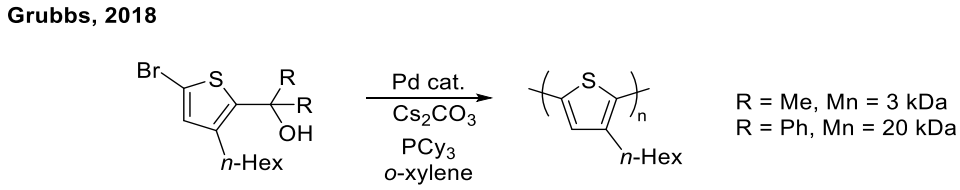

Scheme 2.10 – Poly(3-hexyl)thiophene synthesized through *ipso*-arylative polymerization by Grubbs.[160]

2.2 Proposal[161]

The dehydration polymerization of thiazole-*N*-oxides by our group was a pivotal step towards the development of transition metal-free syntheses of conjugated poly(hetero)arenes. Unfortunately, as previously mentioned, several drawbacks limited the feasibility of the polymerization reaction and must be overcome for wide-scale

deployment. These drawbacks mainly concern the preparation of thiazole-*N*-oxide substrates using practical oxidation conditions, as well as their stability (Figure 2.3).

We sought to continue the preparation of thiazole-*N*-oxides from their corresponding thiazoles using the commercially available *m*-CPBA as an oxygen transfer reagent. The reaction with *m*-CPBA is mild, cheap and far more feasible than other thiazole oxidation reagents such as Rozen's reagent.[162] Unfortunately, when using *m*-CPBA, generally only low yields were ever obtained for thiazole oxidation. Additionally, *N*-oxide substrates synthesized were almost exclusively limited to 4-methyl-substituted thiazoles.[145] Having a substituent at this position instills a negative steric interaction with the adjacent 5-aryl groups which causes a disruption of planarity and therefore has a negative effect on the electronic properties of the molecules and polymers. Finally, it has long been reported that 2-unsubstituted thiazole-*N*-oxides are thermally unstable and have the potential for ring opening, further restricting their use.[163] We therefore sought to

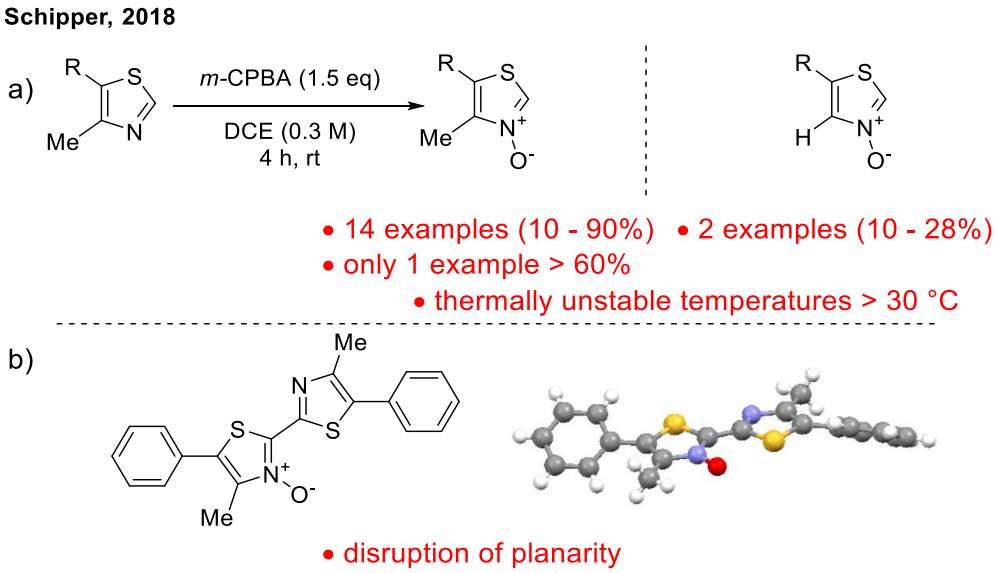

Figure 2.3 – Drawbacks of thiazole oxidation a) low oxidation yields of thermally unstable thiazole-*N*-oxide products b) disruption in planarity caused by steric interactions between 4-methyl groups and 5-aryl groups.

develop a strategy that would enhance the dehydrative coupling reaction while addressing each of these issues and still allowing for the synthesis of conjugated polymers.

Since the instability of the thiazole-*N*-oxide substrates was attributed to be due to the lack of substitution at the 2-position, we speculated this could be remedied through installation of a protecting group. A carbinol group, similar to what has been employed for *ipso*-arylation reactions, was thought to have potential as this protecting group for two primary reasons. Firstly, the carbinol hydroxy group could potentially act as a directing group for thiazole oxidation through hydrogen bonding with the oxygen transfer reagent, *m*-CPBA. Secondly, the conditions required for removal of the carbinol group are the same conditions that facilitated the thiazole-N-oxide dehydration reaction. Therefore, we speculated that the carbinol-substituted thiazole-*N*-oxides would be able to undergo removal of the protecting group – and dehydration reaction in a single ipso-arylative condensation step, simply upon the addition of base (Scheme 2.11).

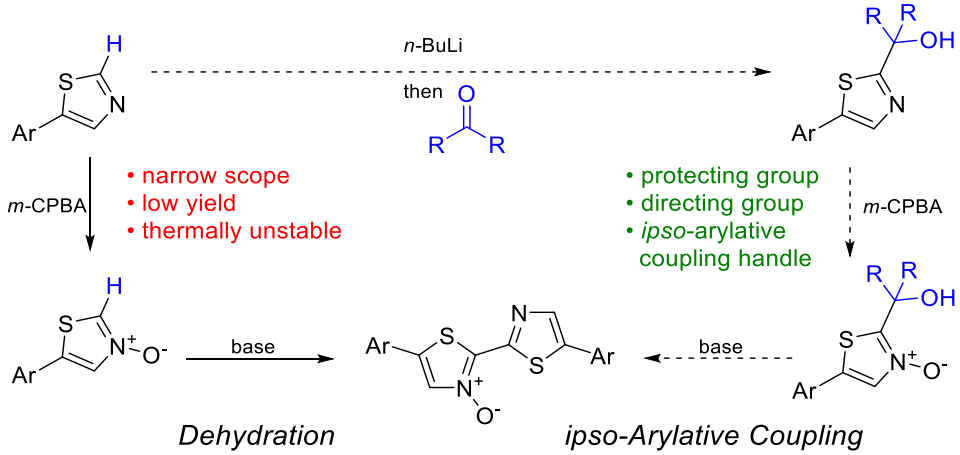

Scheme 2.11 – Proposed route towards bithiazole-containing conjugated materials through transition-metal-free *ipso*-arylative coupling.

2.3 Results and Discussion

In order to begin the reaction development, it was first required that the carbinol substituent be installed at the thiazole 2-position. 4,5-Dimethylthiazole was chosen as our initial model thiazole, primarily due to its commercial availability. Additionally, we chose to pursue the dimethylcarbinol-substituted thiazole due to the ease and availability of using acetone as the electrophilic reactant. 4,5-Dimethylthiazole was deprotonated using *n*-butyllithium (*n*-BuLi) in anhydrous tetrahydrofuran (THF) at -78 °C under an inert atmosphere. After stirring for 30 min, excess acetone was added, and the reaction was allowed to continue stirring for 30 min before quenching. Initial tests using this thiazole showed almost complete conversion to substituted thiazole **2.1**, requiring no purification post work-up. Our mild oxidation conditions using *m*-CPBA in 1,2-dichloroethane (DCE), previously used to oxidized 2-unsubstiuted thiazoles, were then applied to this substrate. The resulting *N*-oxide **2.2** was isolated in a 79% yield. This *N*-oxide product was pointedly easier to isolate by column chromatography due to its decrease in polarity, however; the yield of *N*-oxide product obtained was lower than the previously reported 90% yield obtained for the oxidation of unfunctionalized 4,5-dimethylthiazole (Scheme 2.12).[145]

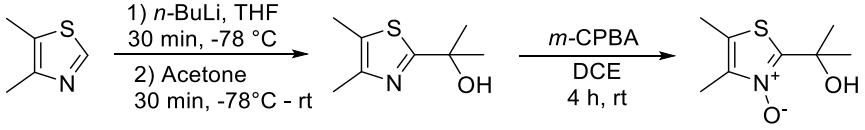

Scheme 2.12 – Installation of carbinol group on 4,5-dimethylthiazole, and subsequent oxidation with *m*-CPBA.

Instead of focusing on a thiazole substrate that had previously shown to oxidize well to its corresponding *N*-oxide, we turned our attention towards two commercially

available substrates in which the oxidation using *m*-CPBA had not proceeded at all – thiazole and benzothiazole. The oxidation of thiazole to thiazole-*N*-oxide has been reported, however, the high polarity of the product results in isolation being extremely difficult through normal-phase column chromatography.[164] To our knowledge, benzothiazole-*N*-oxide has not been reported through the *m*-CPBA oxidation, likely due to its susceptibility for ring-opening at the 2-position.[163] Installation of the dimethylcarbinol at the 2-position of thiazole yielded **2.3** in a 79% yield. To our satisfaction, oxidation of this substrate using *m*-CPBA also proceeded well as *N*-Oxide **2.4** was prepared in a 68% yield, and proved significantly easier to isolate by column chromatography using a mobile phase of 1:9 MeOH:EtOAc. Likewise, substituted 2-(dimethylcarbinol)-substituted benzothiazole **2.5** was prepared in a 62% yield and oxidized with *m*-CPBA to *N*-oxide product **2.6** in a 74% yield with no sign of ring-opening. This represents an unprecedented method to access this class of compounds using mild oxygen-transfer reagents (Scheme 2.13).

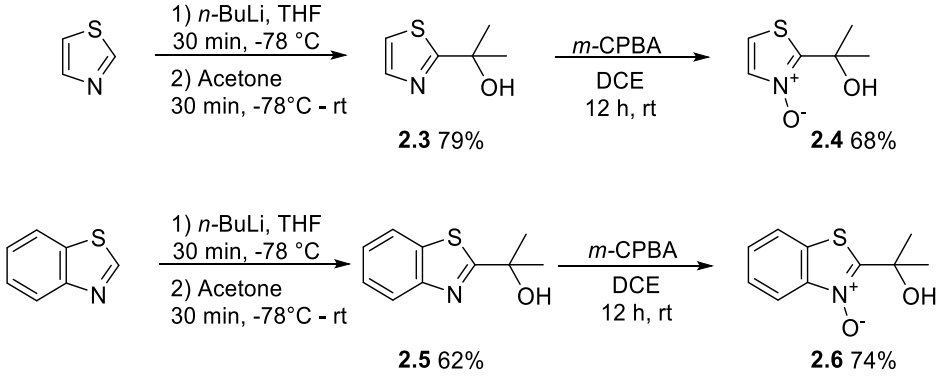

Scheme 2.13 – Synthetic route towards thiazole substrate **2.4** and benzothiazole substrate **2.6**.

2.3.1 Reaction development

Having observed that these 2-substituted thiazoles clearly allowed access to new thiazole-*N*-oxide starting materials, the next step was to develop optimal conditions such that these substrates could undergo an *ipso*-arylative condensation through the loss of acetone and formation of a new bithiazole C-C bond. To begin the investigation, we chose to use the optimal conditions determined for the dehydration of thiazole-*N*-oxides. Unfortunately, performing the reaction with lithium *tert*-butoxide (LiO*t*-Bu) in THF for 10 min on **2.2** did not yield any of the coupled product **2.7** (Table 2.1, Entry 1). We instead pivoted to assess different bases, beginning with other *tert*-butoxide bases. KO*t*-Bu showed our first hint of the *ipso*-arylative coupling product, however, only a trace amount was observable through comparison by thin-layer chromatography (TLC) (Table 2.1, Entry 2). Once again, substituting the base to NaO*t*-Bu delivered our first viable amount of product **2.7** in a 25% yield in 5 min (Table 2.1, Entry 3). Other bases screened yielded no reaction to product **2.7** except for sodium hydride which produced a 15% yield (Table 2.1, Entry 4). We speculated that the sodium counterion may be important to either the loss of acetone following deprotonation or the nucleophilicity of the 2-deprotonated thiazole generated. Proceeding with NaO*t*-Bu, major increases in yield were observed upon increasing the reaction duration to 1 h (Table 2.1, Entry 5) and increasing the temperature to 60 °C (Table 2.1, Entry 6). At temperatures higher than 60 °C, no increase in yield was observed (Table 2.1, Entry 7).

Based on our suspected mechanism of the reaction, we expected that the *ipso*-arylative condensation should proceed with only a catalytic amount of base, as either hydroxide would be produced or *tert*-butoxide would be regenerated. Reducing to 0.5

equiv of base, however, saw a slight decrease in yield to 45% (Table 2.1, Entry 8). It was speculated that NaOH generated in the reaction may precipitate from the THF solvent, causing the lower yield, and not allowing for the catalytic use of base. Nevertheless, using only 1.1 equiv of base produced yields the same as previously obtained using 1.5 equiv (Table 2.1, Entry 9). Re-evaluating the reaction duration, a slight increase in yield to 62% of **2.7** was obtained upon allowing the reaction to proceed for 2h (Table 2.1, Entry 10), but no further increase in yield was found upon extension of this time (Table 2.1, Entry 11). The reaction proved to be robust to solvent choice (Table 2.1, Entry 12-13), though we continued to utilize THF. Isolation of **2.7** throughout these experiments required only a simple NH_4Cl work-up followed by concentration *in vacuo* to yield the pure bithiazole product. The notable lack of starting material recovered was, at this time, presumed to be due to its loss to the aqueous layer, or degradation, following expulsion of acetone.

With what seemed to be the optimal conditions in hand for the *ipso*-arylative coupling of *N*-oxide **2.2**, we sought to apply the same conditions to *N*-oxides **2.4** and **2.6**. Contrary to what was expected, *N*-oxide **2.4** proceeded poorly in the *ipso*-arylative condensation conditions, yielding only a small 14% yield of bithiazole-*N*-oxide (**2.8**) product. Even more displeasingly, benzothiazole substrate **2.6** did not produce any of the bithiazole product **2.9**, with most of the starting material being recovered from the reaction. In this case, the retrieval of starting material indicated that, even upon deprotonation with *tert*-butoxide, the dimethylcarbinol did not eliminate to produce acetone and the benzothiazole-*N*-oxide anion to allow for the coupling to occur (Scheme 2.14).

Table 2.1 – Optimization of reaction conditions around *N*-oxide **2.2**.[a]

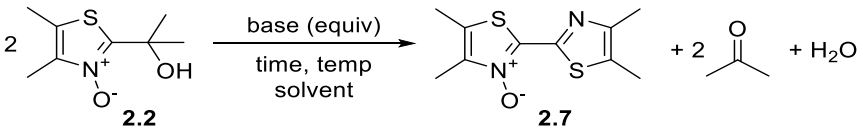

Entry	base	equiv	time	temp[b]	solvent	% yield[c]
1	LiO*t*-Bu	1.5	5 min	rt	THF	--
2	KO*t*-Bu	1.5	5 min	rt	THF	trace
3	NaO*t*-Bu	1.5	5 min	rt	THF	25
4	NaH	1.5	5 min	rt	THF	15
5	NaO*t*-Bu	1.5	1 h	rt	THF	42
6	NaO*t*-Bu	1.5	1 h	60 °C	THF	53
7	NaO*t*-Bu	1.5	1 h	80 °C	THF	53
8	NaO*t*-Bu	0.5	1 h	60 °C	THF	45
9	NaO*t*-Bu	1.1	1 h	60 °C	THF	55
10	**NaO*t*-Bu**	**1.1**	**2 h**	**60 °C**	**THF**	**62**
11	NaO*t*-Bu	1.1	12 h	60 °C	THF	60
12	NaO*t*-Bu	1.1	2 h	60 °C	DMA	45
13	NaO*t*-Bu	1.1	2 h	60 °C	PhCl	60

[a]Conditions: **2.2**, base (equiv), dissolved in solvent (0.3 M), and heated to(temp) while stirring for (time). [b]Heated in sealed pressure vial to prevent solvent loss [c]Isolated yields.

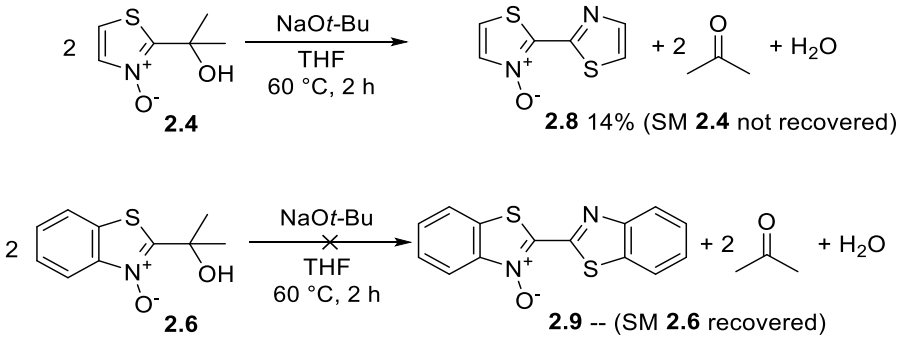

Scheme 2.14 – *ipso*-Arylative coupling reaction on thiazole substrate **2.4** and benzothiazole substrate **2.6**. Conditions: NaO*t*-Bu (1.5 equiv), THF (0.3 M), and heated to 60 °C for 2h.

Slightly disheartened by these results, we pivoted towards the preparation of substrates with extended conjugated systems, as the synthesis of these types of small molecules, along with polymers, remained the goal of the project. The simple phenylthiazole **2.10a** was selected as the model thiazole with extended conjugation for investigation of this reaction. Substrate **2.10a** was synthesized through direct arylation of thiazole with bromobenzene under standard conditions for this type of transformation. We were interested in how our new approach towards thiazole oxidation would compare between substrates with and without a 4-methyl substituent; 4-methyl-5-phenylthiazole (**2.10b**) was also synthesized in the same manner. Installation of the carbinol at the 2-position was once again achieved using *n*-BuLi followed by quenching with acetone in order to yield products **2.11a** and **2.11b**. In our previous work, the oxidation of **2.10a** and **2.10b** using *m*-CPBA had only afforded yields of 10% and 60% of the corresponding thiazole-*N*-oxide, respectively.[145] Utilizing these very same conditions for the oxidation of 2-substituted thiazoles **2.11a** and **2.11b**, we were able to obtain significantly higher yields of the corresponding *N*-oxide. *N*-Oxide **2.12a** possessing no 4-substituent was prepared in a 78% yield from **2.11a**, considerably higher than previously observed for 4-unsubstitut-

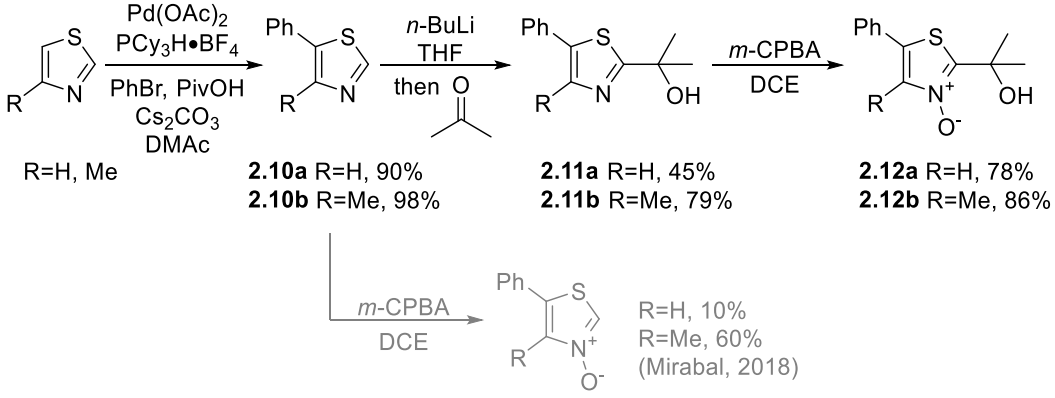

Scheme 2.15 – Synthetic route towards 5-phenyl-substituted thiazole-*N*-oxides **2.12a** and **2.12b**.

ed substrates. Additionally, the oxidation of **2.11b** to **2.12b** provided an 86% yield of product, higher than what was previously reported for the oxidation of the 2-unsubstitued equivalent **2.10b**. Curiously, even among the carbinol-substituted thiazoles, oxidation using *m*-CPBA continue to proceed better on the thiazole possessing a 4-methyl substituent (**2.11b**) than that without (**2.11a**, Scheme 2.15).

With the *N*-oxidation reactions proceeding well on these substrates, the next step was to ensure these thiazoles with extended conjugation could undergo the *ipso*-arylative condensation reaction. *N*-oxides **2.12a** and **2.12b** were both subjected to our determined optimal conditions of NaO*t*-Bu in THF at 60 °C for 2h. Unlike with bithiazoles **2.7** and **2.8**, products **2.15a** and **2.15b** were impure post aqueous work-up, although the presence of each of the products was identifiable by crude ^{1}H NMR and TLC comparison to pure product. Attempts to purify by trituration or column chromatography did not yield either **2.15a**/**b** product pure by NMR – the latter method faltering due to the generally poor solubility of these molecules in organic solvents (Scheme 2.16).

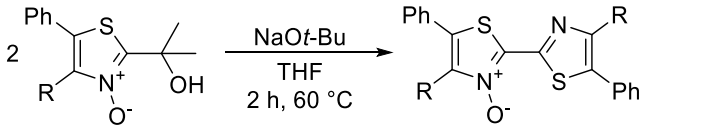

2.12a R=H
2.12b R=Me

2.15a R=H, unisolatable
2.15b R=Me, unisolatable

Scheme 2.16 – *ipso*-Arylative coupling reaction of **2.12a/b** using conditions optimized for **2.2**.

At this point, attempts were made in order to re-optimize the reaction conditions for the transformation of **2.12a** in order to yield and isolatable amount of product **2.15a** without inseparable by-products. Changes to reaction conditions included altering the base, decreasing the reaction temperature, differing the solvent, etc., however, no change

in purity was observed and **2.15a** remained unisolatable. Since the impurities present in the crude product mainly existed in the alkyl region of the ^{1}H NMR, we speculated that this could be due to enolization of the produced acetone byproduct which could be further reacting in an undesired manner. We therefore turned our sights towards using an alternate group to allow for *ipso*-arylative condensation that did not possess enolizable protons upon expulsion by base.

We next chose to explore the use of benzophenone as an activating unit and a replacement for acetone. The diphenylcarbinol-substituent would potentially allow for the same directing effect on the oxygen-transfer reagent, *m*-CPBA, while lacking the enolizable protons thought to cause unwanted side reactions. Diphenylcarbinol-substituted thiazole **2.13a** was prepared in much the same way as previously described: deprotonation of **2.10a** using *n*-BuLi, followed by the addition of benzophenone to yield the desired product in an 84% yield. Substrate **2.13a** was then oxidized using *m*-CPBA to deliver the corresponding thiazole-*N*-oxide **2.14a** in an 89% yield (Scheme 2.17). We were pleased with not only how this compares to the 10% yield reported for the oxidation of **2.10a**, but also that the yield was higher than that of **2.12a** prepared from dimethylcarbinol-substituted **2.11a**. The additional phenyl substituents also contributed to further reducing the polarity of the *N*-oxide product (**2.14a**), enabling isolation by column chromatography using EtOAc and hexanes.

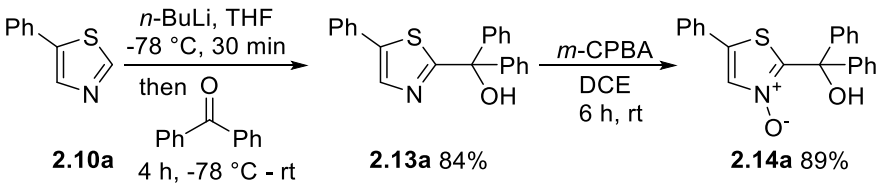

Scheme 2.17 – Preparation of (diphenyl)carbinol-substrate **2.14a**.

While we were investigating additional directing/protecting groups, we speculated that the installation of a carboxylic acid group at the 2-position could achieve the same desired directing effect as observed with the carbinols. This carboxylic acid substituent would then be easily removed as CO_2 by the addition of base during the *ipso*-arylative condensation. The synthesis of thiazole-2-carboxylates have been previously reported in the literature, however, facile decarboxylation upon protonation required the substrate to be isolated as the lithium carboxylate salt.[165] Carboxylate **2.16** was prepared from **2.10a** using *n*-BuLi, followed by the addition of solid CO_2, in a 64% yield. Intermediate **2.16** was then subjected to *m*-CPBA oxidation conditions for conversion to the *N*-oxide, however, due to poor solubility of the lithium salt in DCE, methanol was required as the solvent. Unfortunately, upon the addition of *m*-CPBA, rapid decarboxylation was observed, and *N*-oxide **2.17** was not obtained (Scheme 2.18). We instead returned our focus to the diphenylcarbinol-substituted *N*-oxide **2.14a** which had shown to proceed well through the thiazole oxidation and pursued its use in the *ipso*-arylative condensation.

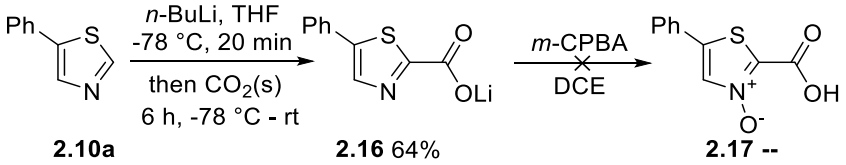

2.10a **2.16** 64% **2.17** --

Scheme 2.18 – Attempted preparation of carboxylic acid substrate **2.17**.

2.3.2 Optimization of reaction conditions

To test the effectiveness of *N*-oxide **2.14a** towards the *ipso*-arylative coupling reaction, we first returned to conditions similar to those we had previously found optimal for *N*-oxide **2.2**. Sodium *tert*-butoxide in THF for 1 h at room temperature yielded the bithiazole product **2.15a** in only a 33% yield (Table 2.2, Entry 1). While this initial yield

was low, we were pleased to observe that the crude ^{1}H NMR contained only peaks corresponding to **2.15a**, starting material **2.14a**, and benzophenone, with no sign of other byproducts. We next re-examined KO*t*-Bu and LiO*t*-Bu as alternative bases. While once again KO*t*-Bu was unable to generate anything other than trace amounts of product (Table 2.2, Entry 2), to our surprise, LiO*t*-Bu produced product **2.15a** at a slightly higher yield than that of NaO*t*-Bu (Table 2.2, Entry 3). Proceeding with LiO*t*-Bu, we then attempted to reduce the reaction time to 10 min as to replicate conditions similar to our previously reported dehydration reaction, however, a decrease in yield to 24% was observed (Table 2.2, Entry 4).

Mechanistically, we had been working under the assumption that the reaction would proceed through generation of the thiazole-*N*-oxide anion via the loss of benzophenone. We therefore speculated that to further increase the reaction yield, the addition of a protic source may facilitate generation of the protonated thiazole which acts as the electrophile. A solvent mixture of 20:1 THF: H_2O was employed in order to observe the effects of a protic source, however, almost no product was produced (Table 2.2, Entry 5). This is presumed to be due to NaOH being produced from the NaO*t*-Bu and H_2O which likely precipitates out of solution and is unable to facilitate the *ipso*-arylative condensation. Pleasingly, an increase of yield to 56% of product **2.15a** was obtained using a solvent

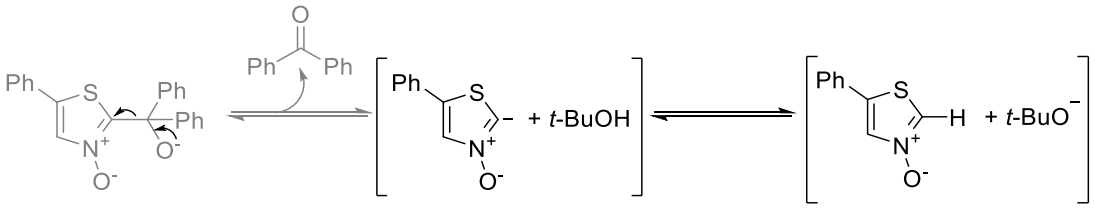

Scheme 2.19 – Proposed equilibrium formed between 2-deprotonated thiazole-*N*-oxide and *tert*-butanol.

ratio of 20:1 THF:*t*-BuOH (Table 2.2, Entry 6), with the *t*-BuOH presumably acting as the protic source in equilibrium with the deprotected thiazole-*N*-oxide (Scheme 2.19).

Increasing the temperature to 60 °C resulted in an additional surge in yield of **2.15a** to 73% (Table 2.2, Entry 7), however further increasing the reaction temperature only saw a negative effect on the yield (Table 2.2, Entry 8). Shifting from thermal heating to microwave irradiation saw another small, but significant rise in yield to 83% (Table 2.2, Entry 9). Finally, the concentration of substrate **2.14a** in THF was reduced, as the increase in product yield observed to have a negative effect on the homogeneity of the

Table 2.2 – Optimization of reaction conditions around *N*-oxide **2.14a.**[a]

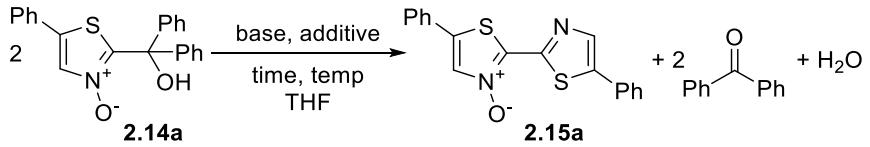

2.14a **2.15a**

Entry	base	conc. (M)	time	temp[b]	additive	% yield[c]	% SM[c]
1	NaO*t*-Bu	0.1	1 h	rt	--	33	27
2	KO*t*-Bu	0.1	1 h	rt	--	trace	95
3	LiO*t*-Bu	0.1	1 h	rt	--	36	37
4	LiO*t*-Bu	0.1	10 min	rt	--	24	60
5	LiO*t*-Bu	0.1	1 h	rt	H_2O	<10	90
6	LiO*t*-Bu	0.1	1 h	rt	*t*-BuOH	56	16
7	LiO*t*-Bu	0.1	1 h	60 °C	*t*-BuOH	73	7
8	LiO*t*-Bu	0.1	1 h	80 °C	*t*-BuOH	62	3
9	LiO*t*-Bu	0.1	1 h	60 °C[d]	*t*-BuOH	83	0
10	**LiO*t*-Bu**	**0.05**	**1 h**	**60 °C[d]**	***t*-BuOH**	**95**	**0**

[a]Conditions: **2.14a**, base (1.5 equiv), in THF (conc.) with additive (5% v/v) while heated thermally and stirred for (time). [b]Heated in sealed pressure vial to prevent solvent loss. [c]^{1}H NMR yields using internal standard of 1,3,5-trimethoxybenzene. [d]Heated by microwave irradiation.

reaction mixture. This alteration in concentration resulted in a 95% yield of **2.15a** with no sign of remaining starting material (Table 2.2, Entry 10).

The optimal conditions determined for substrate **2.14a** were also applied to dimethylcarbinol **2.12a**. From this substrate, a record high yield of 81% of **2.15a** was obtained, and the ^{1}H NMR of the crude reaction mixture showed a reduced presence of byproducts than previously observed, however, the yield remained still lower than the *ipso*-arylative condensation of **2.14a**. Combined with the increased oxidation yield observed in the synthesis of **2.14a**, this solidified diphenylcarbinol as the optimal 2-substituent to facilitate this transformation.

2.3.3 Improved *N*-oxidation of thiazoles

With our optimal carbinol group selected, we continued our investigation into the functional group tolerance of the oxidation reaction. In addition to the previously prepared **2.10a**, an array of thiazoles possessing various 5-aryl substituents (**2.10b** – **2.10o**) were prepared through direct arylation of either thiazole or 4-methylthiazole. Installation of the diphenylcarbinol substituent at the 2-position of the 5-arylthiazoles (**2.10**) was achieved using *n*-BuLi followed by quenching with benzophenone in order to yield substrates **2.13b** – **2.13o** (Scheme 2.20). These conditions only proved to be difficult for substrates

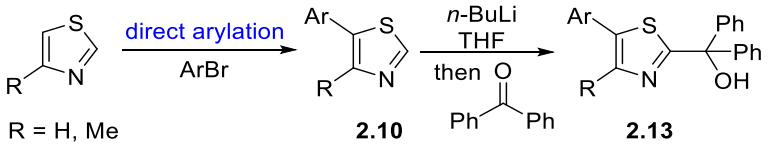

Scheme 2.20 – General route towards 5-arylthiazol-2-yl(diphenyl)methanols.

possessing electrophilic substituents such as **2.10j** and **2.10k**, as nucleophilic attack by deprotonated thiazoles resulted in a mixture of by-products and generally low yields (Scheme 2.21).

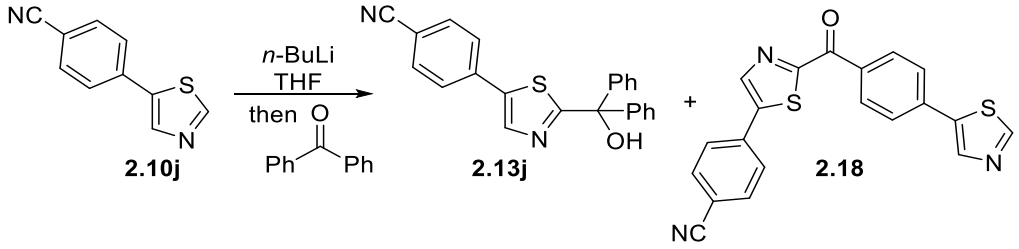

Scheme 2.21 – Side reaction of **2.10j** during installation of diphenylcarbinol substituent.

2-Substituted thiazoles (**2.13**) were then were then subject to *m*-CPBA oxidation conditions to yield *N*-oxides **2.14b** – **2.14o** in moderate to high yields (Figure 2.4). We were pleased to observe that the oxidation proceeded well on thiazoles possessing electron-neutral (**2.14a** – **2.14f**), electron-donating (**2.14g** – **2.14i**) and electron-withdrawing arene substituents (**2.14j** – **2.14o**). All oxidations proceeded in considerably higher yields than for their 2-unsubstituted counterparts previously reported by our group. Additionally, the diphenylcarbinol thiazole-*N*-oxides (**2.14**) are significantly more thermally stable, allowing easier isolation of products using heat-dependent concentration techniques such as rotary evaporation. Due to the decrease in polarity caused by the installation of the diphenylcarbinol substituent, these *N*-oxides were pointedly easier to isolate via column chromatography with most cases only requiring gradients of up 30% EtOAc in hexanes to elute. No side-reaction products, such as those resulting from sulfur oxidation, were observed using *m*-CPBA.

4,5-Dimethylthiazole, thiazole and benzothiazole were also revisited as substrates for *N*-oxidation using the diphenylcarbinol protecting group (Scheme 2.22). In all cases, installation of the carbinol at the thiazole 2-position proceeded well to yield **2.19a-c**, and

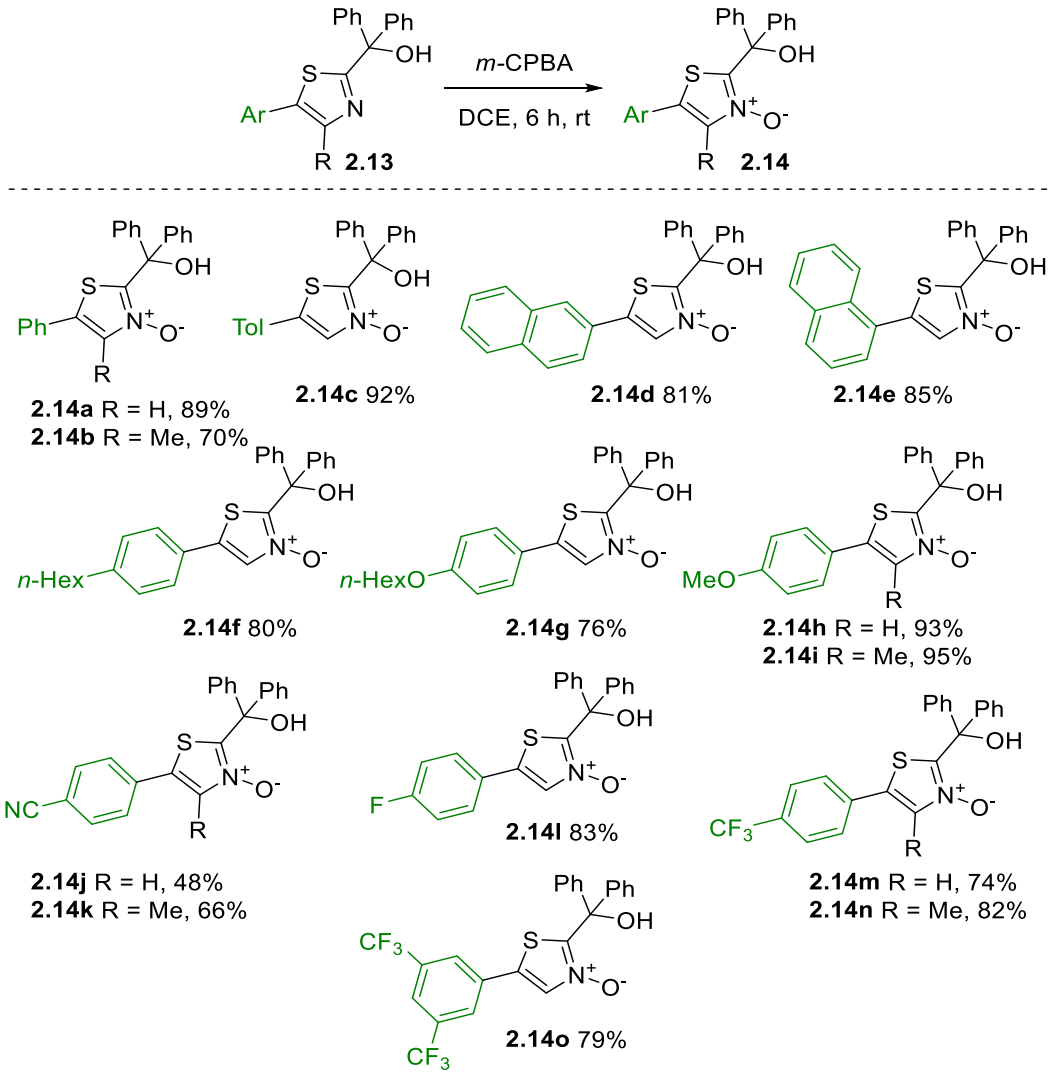

Figure 2.4 – Scope of the m-CPBA oxidation of diphenyl(thiazol-2-yl)methanols (**2.13**) to corresponding *N*-oxides (**2.14**). Conditions: **2.13** (1.0 equiv), *m*-CPBA (1.5 equiv), in DCE (0.3 M) at rt for 8 h. Isolated yields.

in similar or better yields than to the dimethylcarbinol variants. Oxidation of these compounds using *m*-CPBA afforded the desired 2-substituted thiazole-*N*-oxides **2.20a-c**. While **2.20a** and **b** were both produced in a high 86% yield, the oxidation of benzothiazole **2.19c** to **2.20c** was difficult due to the similar polarity of the product to *m*-CPBA (and its by-products). Column chromatography yielded an impure product, though following a wash with sat. $NaHCO_3$ solution, the clean *N*-oxide **2.20c** was afforded in a 37% yield.

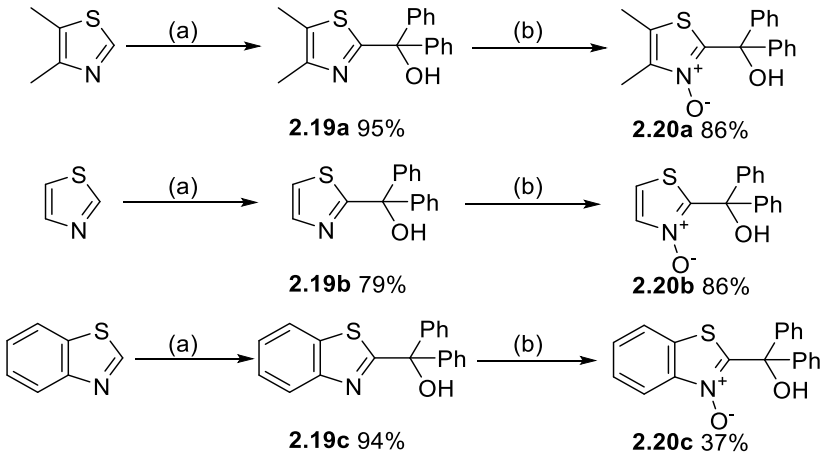

Scheme 2.22 – Preparation of *N*-oxides (**2.20a-c**). Conditions: (a) thiazole (1.0 equiv), *n*-BuLi (1.2 equiv) in THF (0.1 M) at -78 °C for 30 min, followed by benzophenone (1.5 equiv) for 4 h. (b) **2.19** (1.0 equiv), *m*-CPBA (1.5 equiv) in DCE (0.3 M) at rt for 6 h.

In order to obtain a better understanding of the effects of the carbinol substituent on the *N*-oxidation using *m*-CPBA, we designed a handful of mechanistic experiments in an attempt to gain key insight into the proposed directing-group effect. First, dithiazole-containing compound **2.21,** in which only a single thiazole is 2-substituted with the diphenylcarbinol group, was prepared and oxidized with a single equivalent of *m*-CPBA (Scheme 2.23). We had hoped to observe regioselective oxidation of the 2-substituted thiazole, demonstrating the groups' effect as a directing group. Surprisingly, the products **2.22a** and **2.22b,** though inseparable by column chromatography, were determined to exist in a 1:1 ratio by comparative integration of the isolated mixture's ^{1}H NMR spectrum. This did not assist in determining why there exists a disparity between oxidizing a 2-unsubstituted and a 2-hydroxymethyl substituted thiazole.

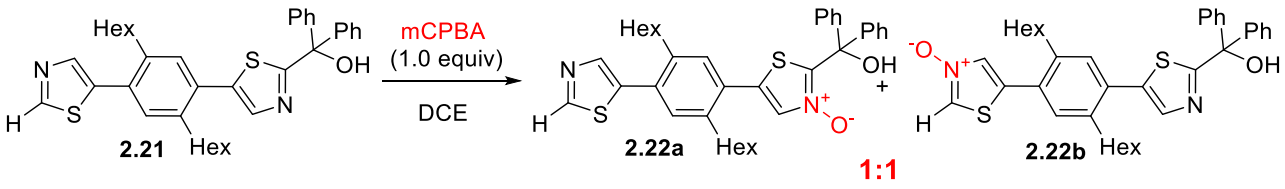

Scheme 2.23 – *N*-Oxidation regioselectivity experiment.

As an alternative experiment, a competitive oxidation was performed in which 5-tolylthiazole (**2.10c**) and equivalent 2-diphenylcarbinol substrate (**2.13c**) were oxidized in a single pot using *m*-CPBA (0.7 equiv) and the ratio of products was observed (Scheme 2.24a). From this trial a 1.25:1 ratio of **2.14c** to **2.23** was obtained, indicating that there was a slight preference for the *N*-oxidation of the thiazole possessing a carbinol substituent (**2.13c**) over the 2-unsubstituted thiazole (**2.10c**), however, again this did not explain the large disparity in yield seen between the individual oxidations. To solely investigate the potential effect of hydrogen bonding in directing *m*-CPBA oxidation, we performed a competition oxidation between **2.13c** and methyl carbinol **2.24**. On methyl carbinol **2.24**, the hydrogen bond donor of the alcohol has been eliminated through methylation, while the steric bulk has remained relatively the same (Scheme 2.24b). From this competition experiment, a ratio of 6:1 favoring the alcohol product **2.14c** versus *N*-oxide **2.25**, indicating that the hydrogen bond is likely of importance for the directing of *m*-CPBA for oxidation.

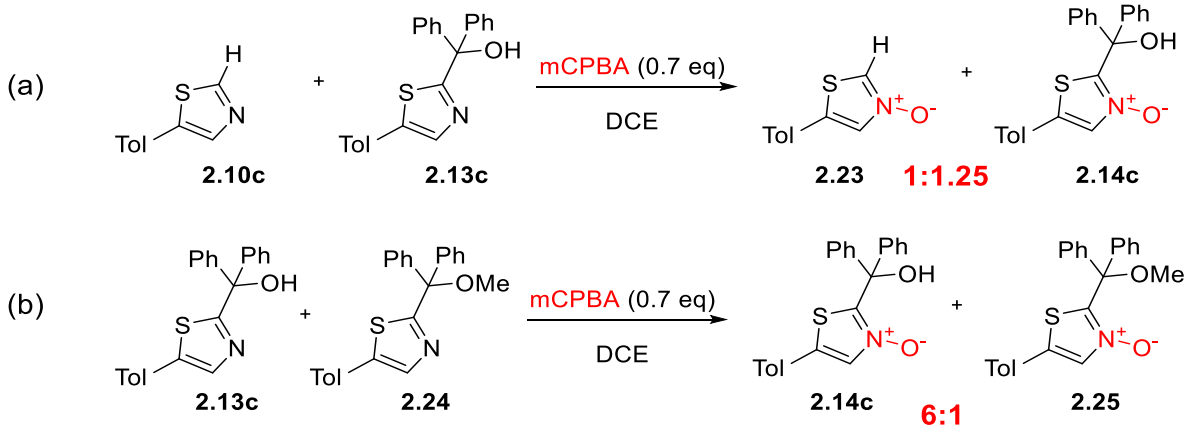

Scheme 2.24 – *N*-Oxidation competition experiments a) unsubstituted v. carbinol-substituted b) carbinol v. methylcarbinol.

While overall pleased with the scope and capability of the *m*-CPBA oxidation of 2-dphenylcarbinol-substituted thiazoles, there are some notable challenges presented by

this method. These mainly concern thiazoles with substituents possessing atoms such as nitrogen or sulfur which can alternatively be susceptible to oxidation (Scheme 2.25). 5-Thiophen-2-ylthiazole (**2.10p**) was prepared via direct arylation, and functionalized at the 2-position using the general conditions of *n*-BuLi followed by benzophenone, to obtain substrate **2.13p**. Oxidation of this compound with *m*-CPBA, however, did not yield an appreciable amount of the *N*-oxide **2.14p**, though the mass was detectable by TLC-MS. The poor yield was likely to be due to oxidation of the thiophene sulfur atom resulting in a mixture of undesired by-products. Similarly, the reaction of 4-(dimethylamino)phenyl-substrate **2.13q** with *m*-CPBA delivered an indecipherable mixture of products. Again, this was presumably due to side reactions occurring between the oxygen transfer reagent and the amine. Thus, the *m*-CPBA *N*-oxidation of thiazoles was primarily limited to arene substituents without sulfur or nitrogen atoms (other than the previously discussed nitrile-containing **2.13j**/**k**).

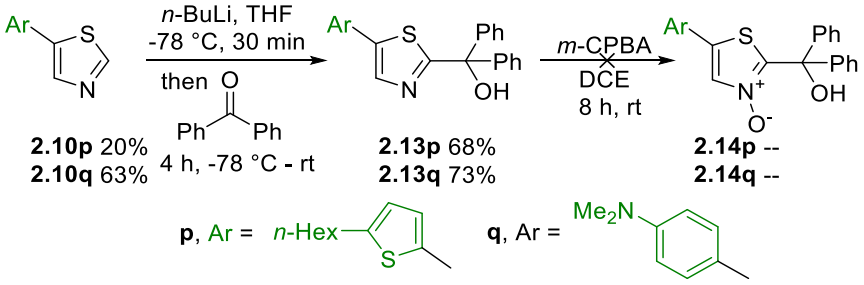

Scheme 2.25 – Attempted preparation of *N*-oxides **2.14p** and **q**. Conditions: (a) **2.10p**/**q** (1.0 equiv), *n*-BuLi (1.2 equiv) in THF (0.1 M) at -78 °C for 30 min, followed by benzophenone (1.5 equiv) for 4 h. (b) **2.13p**/**q** (1.0 equiv), *m*-CPBA (1.5 equiv) in DCE (0.3 M) at rt for 8 h.

2.3.4 *ipso*-Arylative condensation small molecules

With our optimal conditions for the formation of **2.15a** through *ipso*-arylative condensation, and a handful of 2-(hydroxydiphenylmethyl)thiazole-*N*-oxides (**2.14a** –

2.14o) synthesized, we proceeded to test the functional group tolerance of the reaction of interest (Figure 2.5). With the reaction being optimized on phenyl-substrate **2.14a**, we were unsurprised to find that other electron-neutral substrates including those with 4-tolyl (**2.14c**) and 4-hexylphenyl (**2.14f**) substituents, as well as 2-(**2.14d**) and 1-naphthyl (**2.14e**) substituents proceeded to the corresponding bithiazoles (**2.15c** – **2.15f**) without issue. Likewise, EDG-substituted thiazoles such as alkoxyarenes **2.14g** and **2.14h** also proceeded well to give high yields of 4-hexyloxyphenyl product **2.15g** and 4-methoxyphenyl product **2.15h**. EWG-possessing arenes, including 4-cyanophenyl (**2.14j**), 4-fluorophenyl (**2.14l**), as well as 4-trifluoromethylphenyl (**2.14m**) and 3,5-di(trifluoromethyl)phenyl (**2.14o**) were shown to proceed smoothly as well to the corresponding condensation product.

As the test of functional group tolerance proceeded, it was evident that a poor solubility in organic solvents was a factor for many substrates. This was speculated to be dependant on the degree of π-π stacking, as the lack of a substituent at the 4-position would reduces the twisting along the conjugated backbone and increase the overall planarity of the system. This poor solubility was particularly noticeable in bithiazole products **2.15d**, **2.15e**, **2.15h**, **2.15j**, **2.15m**, and **2.15o**. Given that this poor solubility made full characterization of a number of these small molecules difficult, bithiazoles **2.15b, 2.15i**, **2.15k**, and **2.15n** possessing the same functional groups (Ph, 4-MeOPh, 4-NCPh, and 4-CF_3Ph, respectively) were prepared from the 4-methylthiazole-*N*-oxides **2.14b**, **2.14i**, **2.14k**, and **2.14n**. The 4-methyl substituent assists with disruption of planarity due to unfavourable steric interactions between the methyl and the arene, which ultimately decreases the π-π stacking and increases the solubility. Using these

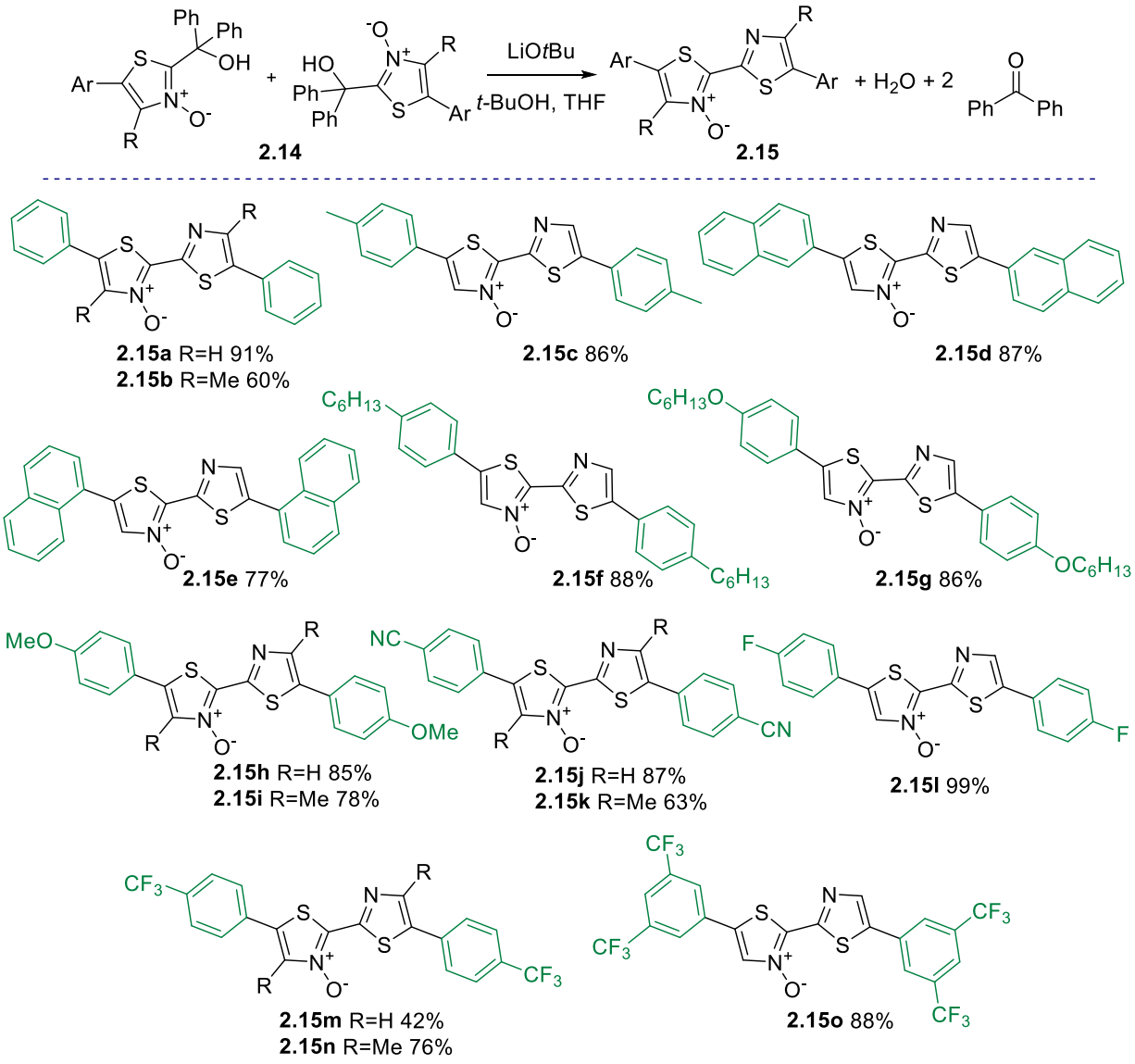

Figure 2.5 – Scope of the *ipso*-arylative condensation of thiazole *N*-oxides (**2.14**). Conditions: **2.14** (1.0 equiv), LiO*t*-Bu (1.5 equiv), in THF (0.05 M) with *t*-BuOH heated under microwave irradiation at 60 °C for 1 h. Isolated yields.

substrates, we were able to confirm the functional group tolerance of the ipso-arylative condensation while still being able to fully characterize the products. Interestingly, while nitrile-substituent possessing bithiazole **2.15k** was significantly more soluble than its non-methylated (and completely insoluble) counterpart **2.15j**, it remained only partially soluble in any organic solvents.

The preparation of bithiazole small molecules not possessing 5-aryl substituents was also achieved applying the optimal *ipso*-arylative condensation conditions to diphenylcarbinol substrates **2.20a**-**c** (Scheme 2.26). 4,5-Dimethylthiazole product **2.7** was obtained in a 79% yield while a 56% yield bithiazole **2.8** was obtained. Although these yields are notably lower than many of the 5-arylthiazoles, both products were produced in higher yields than when prepared from dimethylcarbinols **2.2** and **2.4**. We were also pleased to find that benzothiazole **2.20b** also proceeded to the ipso-arylative condensation product **2.9**, despite the product being previously unobtainable form the dimethylcarbinol **2.6**. Benzothiazole product **2.9** was also notably insoluble compared to **2.7** and **2.8**, rendering characterization difficult.

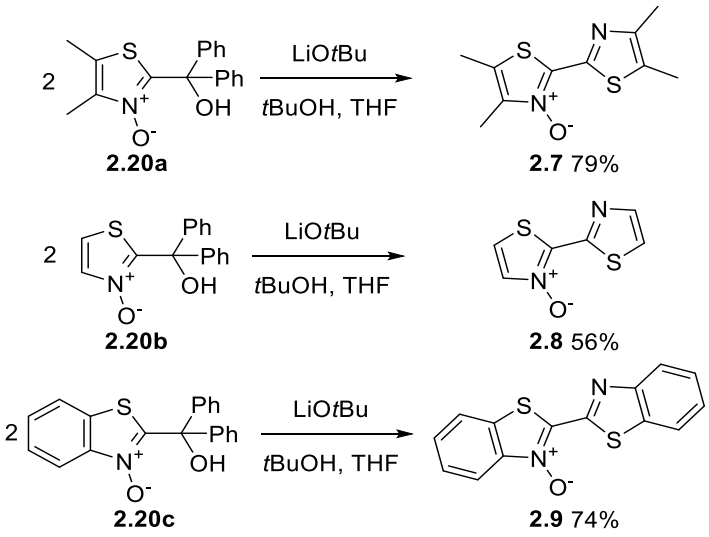

Scheme 2.26 – Revisiting the preparation of bithiazoles **2.7** – **2.9**. Conditions: **2.20** (1.0 equiv), LiO*t*-Bu (1.5 equiv), in THF (0.05 M) with *t*-BuOH heated under microwave irradiation at 60 °C for 1 h.

2.3.5 Optical properties of small molecules

With our array of bithiazole-*N*-oxides small molecules synthesized, we next sought to investigate the effects of substituents on the optical properties of the molecules. Of

particular interest to us was to determine if the 4,4'-unsubstituted bithiazole-*N*-oxides possess a difference in their HOMO-LUMO gap compared to their 4,4'-dimethyl bithiazoles counterparts to which we had previously been limited. Based on the hypothesized increase in planarity, a decrease in the HOMO-LUMO was expected. Pleasingly, in the UV-Vis absorbance spectra of bithiazoles **2.15a/b**,

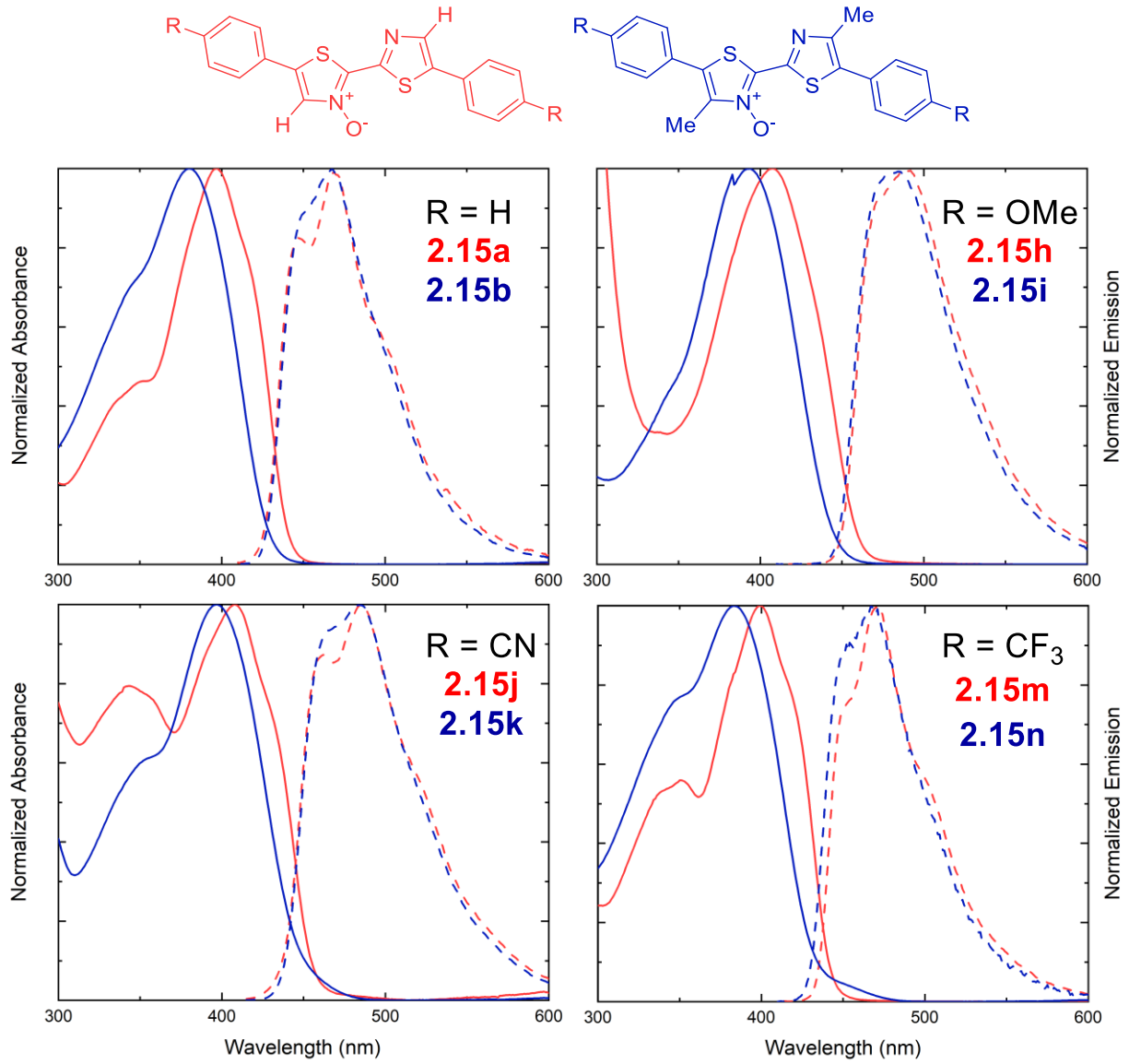

Figure 2.6 – UV-Vis absorption (solid) and emission (dashed) spectra for 4,4'-unsubstituted (red) and 4,4'-dimethyl (blue) bithiazoles. Absorption spectra recorded in $CHCl_3$. Emission spectra recorded in CH_2Cl_2.

2.15h/i, **2.15j/k**, and **2.15m/n**, we observed a notable bathochromic shift in the bithiazoles possessing no methyl substituents at the 4-positions (Figure 2.6). This red-shift corresponds to a decrease in the HOMO-LUMO gap that can likely be attributed to the increased planarity of the molecule, as no other electronic effects should be modified. Interestingly, *ipso*-arylative condensation products possessing either a strong EDG (**2.15g/h/i**) or strong EWG (**2.15j/k**) were observed to possess the lowest optical band gaps of around 2.70 eV. This is perhaps indicative of a push-pull effect present in these molecules where the bithiazole core can act as the acceptor unit in the

Table 2.3 – Optical properties of bithiazole-*N*-oxide small molecules (**2.15**). 4-H/Me pairs denoted in red/blue respectively.

Entry	Ar	Eg_{Opt} (eV)	Abs_{Max} (nm)	Em_{Max} (nm)	Φ_F
2.15a	Ph	2.80	396	467	0.09
2.15b	Ph	2.88	381	468	0.14
2.15c	Tol	2.77	402	477	0.12
2.15d	2-Naph	2.68	414	497	0.21
2.15e	1-Naph	2.85	380	489	0.09
2.15f	4-HexPh	2.75	403	479	0.13
2.15g	4-HexOPh	2.68	411	492	0.47
2.15h	4-MeOPh	2.70	407	491	0.23
2.15i	4-MeOPh	2.79	394	485	0.48
2.15j	4-NCPh	2.68	409	486	0.09
2.15k	4-NCPh	2.79	398	483	0.12
2.15l	4-FPh	2.82	396	466	0.09
2.15m	4-CF_3Ph	2.80	399	471	0.05
2.15n	4-CF_3Ph	2.86	383	467	0.12
2.15o	3,5-CF_3Ph	2.81	398	470	0.05

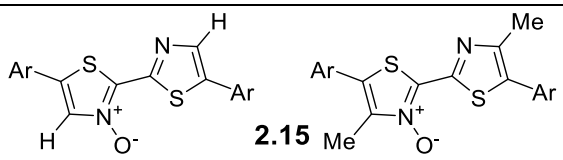

case of EDG-substituents, or the donor unit in the case of EWG-substituents. The optical properties of the bithiazole-*N*-oxide small molecules (**2.15**) are compiled in Table 2.3.

The difference in planarization between **2.15a** and **2.15b** was further confirmed by obtaining the single crystal x-ray structure of compound **2.15b**. We had previously determined and reported the crystal structure of **2.15a** which was found to be a highly planar system (Figure 2.7a). On the other hand, the structure of **2.15b** shows a visible twisting of the π-system compared to the completely planar **2.15a**, clearly illustrating the disruptive effects of the 4-methyl substituent on the system's planarity (Figure 2.7b).

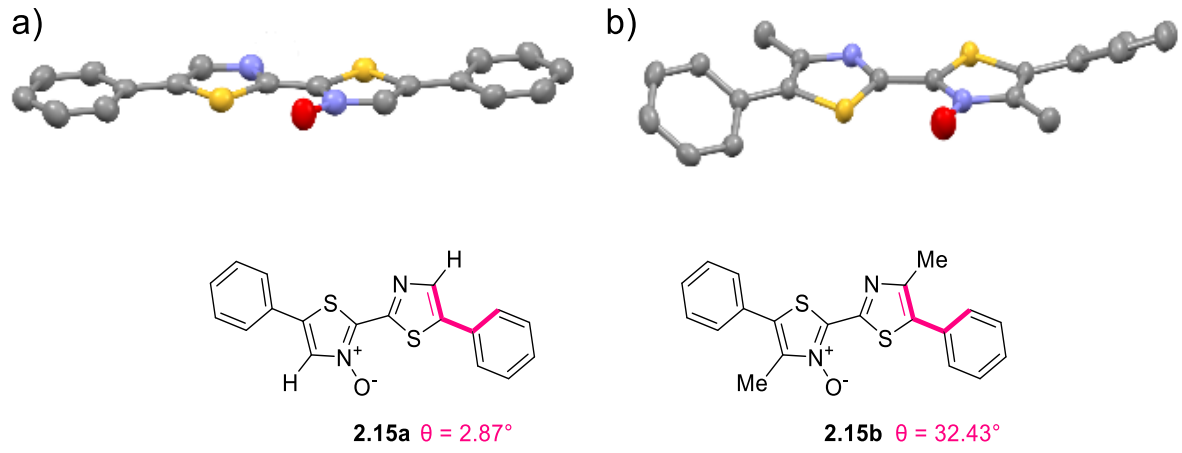

Figure 2.7 – Single crystal x-ray structures of bithiazoles a) **2.15a** and b) **2.15b**.

2.3.6 *ipso*-Arylative polycondensation scope

To fully realize the potential of the developed *ipso*-arylative condensation, we sought to use this method towards the synthesis of conjugated polymers. The *ipso*-arylative polycondensation was proposed to proceed from a single monomer possessing two carbinol-substituted thiazole-*N*-oxide moieties in an AB-type polymerization. These monomers were prepared first through the double direct arylation of a dibromo-π-spacer using either thiazole or 4-methylthiazole to yield di(thiazolyl)-substrates **2.26**. The π-

spacers investigated for this reaction include fluorenes (**2.26a** – **2.26d**), phenylenes (**2.26e** and **2.26f**), and thiophene (**2.26g**). Among the dithiazole substrates prepared possessing a fluorene unit, linear (**2.26a** and **2.26b**) and branched (**22.6c** and **22.6d**) alkyl chains were employed in order to observe the effects of chain branching on polymer solubility. Di(thiazolyl)-substrates **2.26** were dually substituted through double-deprotonation with *n*-BuLi, followed by the addition of excess benzophenone to yield compounds **2.27**. Subsequent oxidation of these species with 3.0 equiv of *m*-CPBA yielded di-*N*-oxide monomers **2.28** in good yields (Scheme 2.27).

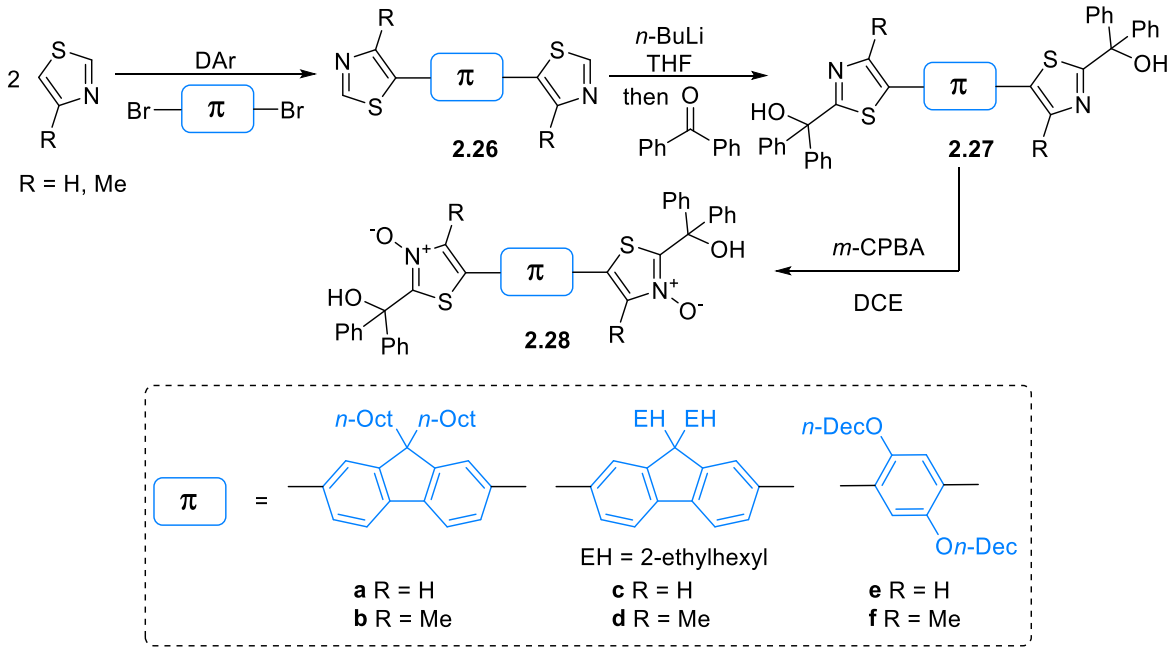

Scheme 2.27 – Synthetic route towards monomers for *ipso*-arylative polycondensation.

With our di-*N*-oxide monomers **2.28a** – **2.28f** in hand, we then subjected them to the same optimal conditions as previously reported for our small molecule substrates, albeit for a slightly longer duration of 2 h and at a higher dilution. To our delight, we were able to achieve bithiazole-*N*-oxide polymers **P1** – **P6** through *ipso*-arylative polycondensation following precipitation in MeOH and gravity filtration (Scheme 2.28).

The molecular weights of these polymers were determined by gel-permeation chromatography (GPC) in THF versus a polystyrene standard curve. The polymerization towards fluorene spacer-containing polymer (**P1** – **P4**) proceeded exceptionally well, and yielded Mw's between 23 and 46 kDa. It is notable that a slight increase in the extent of polymerization was observed for the branched 2-ethylhexyl-substituted fluorene polymers (**P3**, **P4**) compared to the linear chain *n*-octyl-substituted fluorene polymers (**P1**, **P2**). This indicates that the solubility (enhanced by the branching) was likely the cause of polymerization termination. The polymerization of phenylene monomers **2.28e** and **2.28f,** to polymers **P5** and **P6** respectively, produced extremely insoluble material despite the

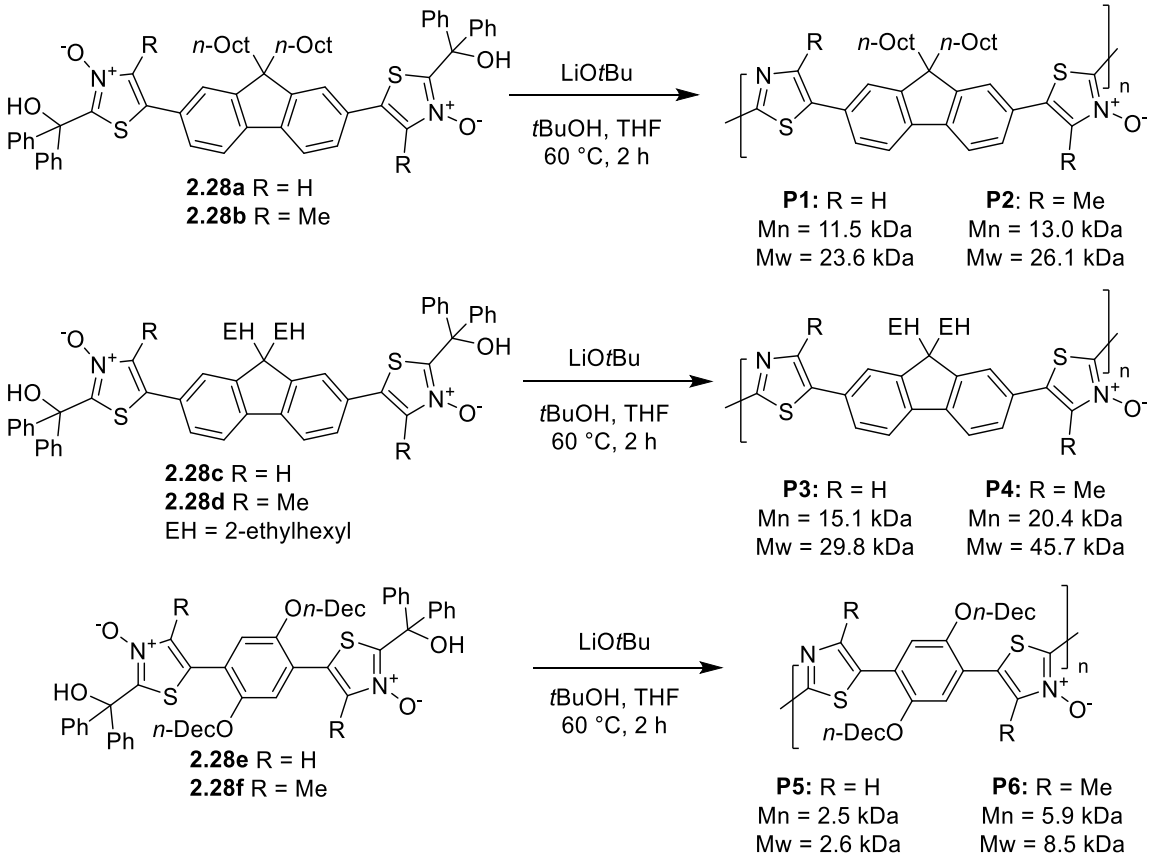

Scheme 2.28 – *ipso*-Arylative polycondensation scope. Conditions: **2.28** (1.0 equiv), LiO*t*-Bu (3.0 equiv), in THF (0.05 M) with *t*-BuOH heated under microwave irradiation at 60 °C for 2 h.

substantial alkyl chains. GPC analysis of the soluble material determined the polymer's Mw to be around 8.5 kDa for **P6** while only oligomers of ~ n = 5 being observed for **P5**.

Having prepared both polymers possessing 4-methyl-substituted thiazoles (**P2**, **P4**, **P6**) and 4-unsubstituted thiazoles (**P1**, **P3**, **P5**), we were interested to see how this affected the extent of polymerization. As expected, in all cases, the presence of the 4-methyl substituents resulted in an increase in molecular weights, once again likely due to the steric effects of the methyl group disrupting planarity and decreasing π-π interactions. This decrease in π-π stacking would result in improved solubility which would increase the extent of polymerization. Thus, it seems that the extent of polymerization was not limited by the capabilities of the *ipso*-arylative polycondensation, but rather simply due to the solubility of the resulting polymers.

In addition to the fluorene (**P1** – **P4**) and phenylene (**P5**, **P6**) π-spacers, additional conjugated polymer motifs should be capable of incorporation so long as they possess the suitable solubilizing chains for polymerization. To completely replicate the polymers that we had previously produced through our dehydration of thiazole-*N*-oxides, we sought to develop a polymer with a 3,4-dihexylthiophene π-spacer. Unfortunately, upon *m*-CPBA oxidation of **2.27g**, the di-*N*-oxide monomer **2.28g** was not obtained. Unlike what was observed for the thiophene-containing small molecule, the products from this oxidation were determined to be a mixture of the thiophene-*S,S*-dioxide **2.29a,** and the mono-*N*-oxide **2.29b** (Scheme 2.29). Oddly, further subjecting either of **2.29a**/**2.29b** to further oxidation with *m*-CPBA resulted in no reaction, indicating that perhaps a stronger oxygen-transfer reagent would be required to achieved monomer **2.28g**.

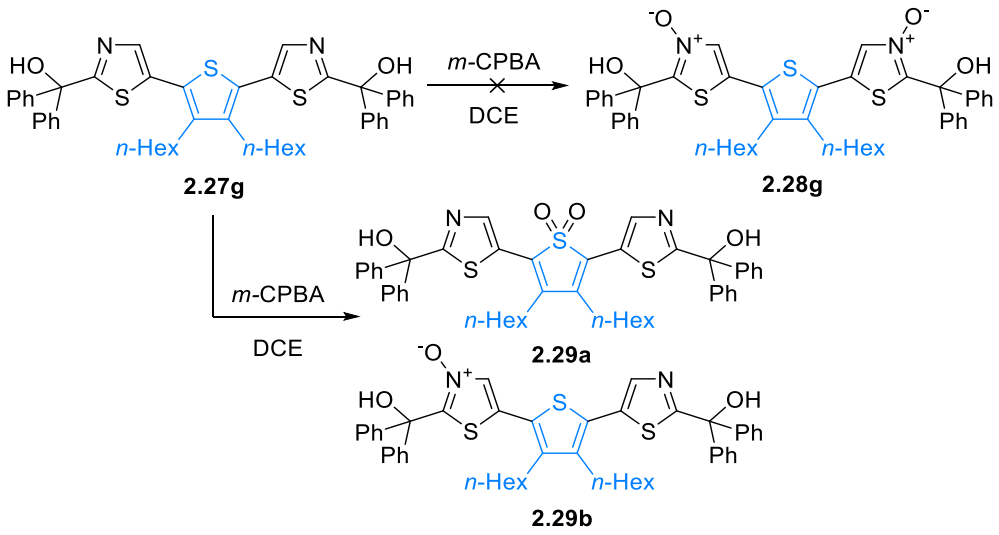

Scheme 2.29 – Attempted preparation of bis(*N*-oxide) monomer with a 3,4-dihexylthiophene conjugated spacer.

2.3.7 Optical properties of polymers

Having synthesized a handful of polymers through *ipso*-arylative polycondensation, we next determined their optical properties through UV-Vis absorbance spectroscopy and fluorescence (Figure 2.8). Most importantly, we were curious to learn if the 4-unsubstituted polymers (**P1**, **P3**, **P5**) displayed the same decrease in band gap compared to their 4-methyl equivalents (**P2**, **P4**, **P6**), which would support the idea of increased planarization. Agreeably, these polymers followed the same trend observed in the extended small molecules, as the 4-unsubstituted conjugated polymers were indeed found to have a decreased optical band gap. Between fluorene polymers **P1** and **P2**, the removal of the 4-methyl group resulted in a decrease in HOMO-LUMO gap of ~ 0.11 eV, which was also consistently observed from polymers **P3** and **P4**. An even larger difference of 0.3 eV was observed between the HOMO-LUMO gaps of phenylene polymers **P5** and **P6**. It is also worth noting that the band gap of polymers **P1** and **P3** as well as **P2** and **P4**, in which the only difference are the alkyl chains, are almost identical.

This was expected as the alkyl chains should only affect the solubility of the polymer without influencing the band gap.

The observed decrease in the optical band gap is accompanied with a decrease in the Stokes shift, that is, the difference between absorbance and emission maxima. This is also indicative of a more planar π-system with increased rigidification and better π-orbital overlap. The photophysical properties of the bithiazole-*N*-oxide small polymers (**P1** – **P6**) are compiled in Table 2.4.

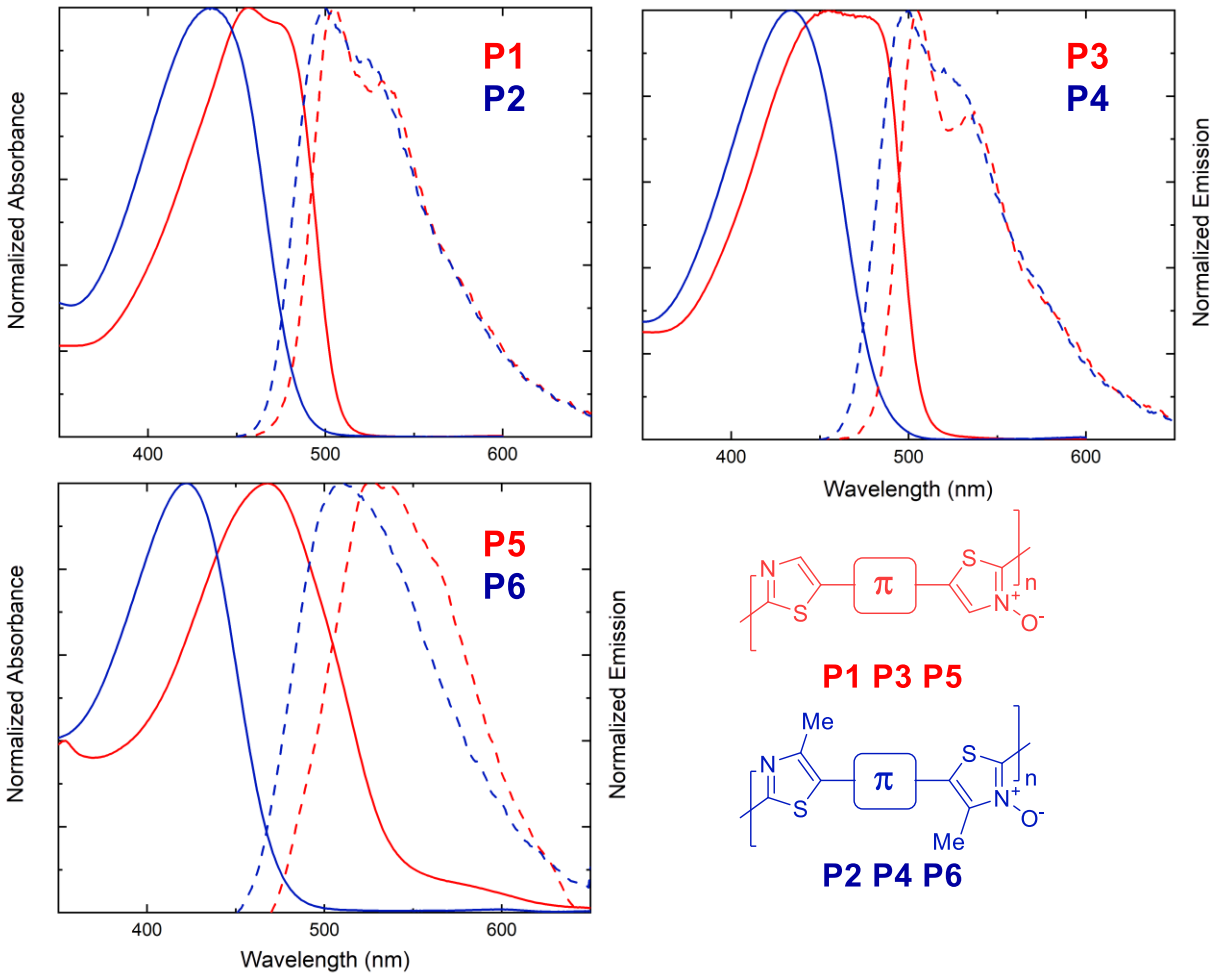

Figure 2.8 – UV-Vis absorbance (solid) and emission (dashed) spectra for 4,4'-unsubstituted (red) and 4,4'-dimethyl (blue) bithiazole polymers.

Table 2.4 – Optical properties of bithiazole-*N*-oxide polymers (**P1 – P6**).

Entry	Eg_{Opt} (eV)	Abs_{Max} (nm)	Em_{Max} (nm)	Stokes Shift (eV)	Φ_F
P1	2.44	456	505	0.26	0.57
P2	2.55	436	500	0.36	0.46
P3	2.44	455	506	0.27	0.72
P4	2.56	434	500	0.38	0.37
P5	2.28	468	542	0.36	0.26
P6	2.63	422	512	0.52	0.27

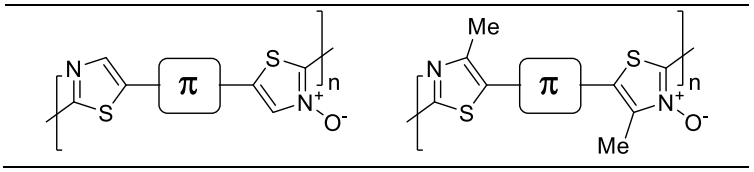

2.4 Conclusions and Outlook

In conclusion, we have developed and investigated a new *ipso*-arylative condensation that has yielded a wide range of highly conjugated bithiazole-containing small molecules and polymers. This arene coupling reaction proceeds without the use of transition metals and only produces water and a simple ketone as by-products. The reaction has been shown to be tolerant to many different electron-poor and electron-rich functional groups, proceeding in yields of up to 99% for the synthesis of bithiazole-*N*-oxide small molecules.

This methodology has also allowed for easy access to a wider range of bithiazole-*N*-oxide products, doubling the scope previously obtained using our thiazole-*N*-oxide dehydration strategy, due to the change in approach to accessing *N*-oxide starting materials. This in turn has facilitated the synthesis of some highly planar small molecules as determined by both the UV-Vis absorbance spectroscopy and single crystal x-ray structures. The *ipso*-arylative condensation is also robust enough to yield bithiazole-

containing conjugated polymers with molecular weights that are chiefly limited by the solubility of the polymer. This is one of only very few developed methods for the synthesis of poly(hetero)arenes that does not require the deployment of transition metal catalysts or reagents.

This *ipso*-arylative polycondensation has potential for use as a tool for the development of bithiazole-containing polymers that possess properties more suited for device applications through modification of the π-spacer. More importantly, however, we envision that this methodology, along with the dehydration reactions reported by our group and Swager's group, will act as a foundation to spur the development of conjugated polymers through related strategies.

3

N-Oxide Chalcogen Bonding in Conjugated Materials

3.1 Background

Non-covalent bonding interactions are ubiquitous in many current generation-conjugated organic small molecules and polymers. These interactions are most commonly discussed as a strategy for band gap engineering; and are used to induce planarity between, or otherwise conformationally lock, adjacent conjugated units. As with covalent tethers, planarity induced by non-covalent interactions results in an enhanced level of p-orbital overlap, and extends the effective conjugation length of the system.[60–62] An increase in effective conjugation length manifests itself in the electronic properties as a decrease in the band gap, while molecular rigidification of the system can lead to stronger interchain interactions which can affect the physical and thermal properties of a

material. Non-covalent interactions are often exploited for this purpose as the synthetic considerations for enabling these interactions are often less than that of using covalent tethers. The most commonly observed non-covalent interactions in conjugated materials are various modes of chalcogen bonding (O – S, N – S, F – S), and hydrogen bonding (O – H, N – H).[63]

3.1.1 Chalcogen bonding interactions

Chalcogen-bonding interactions are favourable non-covalent interactions between electron-rich donors and electrophilic chalcogen atoms. Whether the nature of this interaction stemmed from electrostatic interactions between partially charged atoms, or perhaps van der Waals dispersion forces, remained unclear for some time. More recently, it has been established that chalcogen bonding originates from orbital delocalization of a lone pair ($n \rightarrow \sigma^*$) to antibonding orbital.[166] In addition to being present in conjugated materials, these contacts have long been observed in and applied to catalysis, biological processes, and medicinal chemistry.[167] In organic materials, these non-covalent interactions are specifically observed most commonly between oxygen (O – S), nitrogen (N – S), and fluorine (F – S) donors and thiophene acceptors. Molecular stabilization is achieved through orbital delocalization between one, or multiple, lone pairs on the donor (O, N, F) and the antibonding σ* orbitals of the accepting sulfur (Figure 3.1).[166] Localizati-

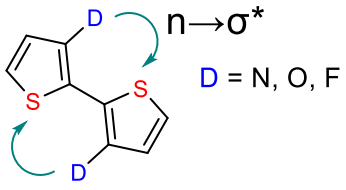

Figure 3.1 – Chalcogen bonding from donor (D = N, O, F) to acceptor (S).

on of the donor atom's lone pairs at the backside of the S – C bond (in the σ* direction) is therefore imperative for the chalcogen bonding interaction.[168]

Early investigations into sulfur-oxygen interactions in conjugated small molecules and polymers surfaced as ethylenedioxythiophene (EDOT) became prevalent as a building block. In 2005, Roncali and co-workers reported several EDOT-containing small molecule systems that were shown by x-ray crystal to adopt fully planar geometries.[169] The bond distances between thiophene sulfur and oxygen substituents in adjacent aromatic units were shown to be markedly smaller than the van der Waals radii of the two atoms. This interaction, and resulting planarity, was speculated to be the cause for the observed reduction in HOMO-LUMO gap upon installation of the ethylenedioxy moeity, in addition to the increase in absolute HOMO and LUMO energy levels caused by the electron-rich donating groups.

Roncali and co-workers also investigated the x-ray crystal structures of two hybrid quarterthiophenes, one possessing two external EDOT groups, and one possessing two internal EDOT groups (Figure 3.2). The thiophene oligomer possessing two external EDOT groups formed no manner of conformational locking between the innermost bithiophene single bond, resulting in a distortion angle of 13° from a planar *syn*

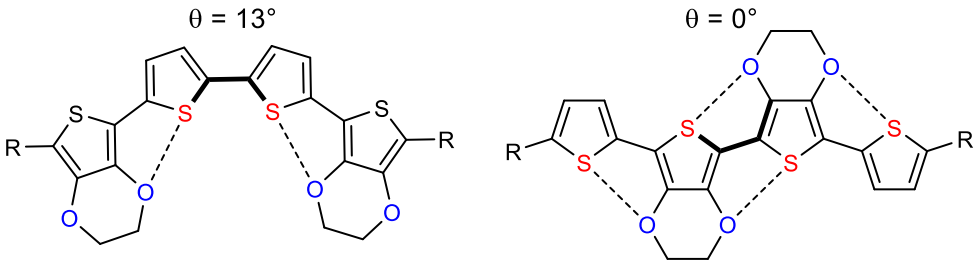

Figure 3.2 – EDOT-containing quarterthiophene small molecules showing donor (blue) – acceptor (red) interactions of chalcogen bonding.

conformation. Conversely, the oligomer possessing two internal EDOT groups adopted fully planar (0°) *anti* conformation stabilized through intramolecular S-O interactions. Additionally, they found that increasing the number of EDOTs in a thiophene pentamer lead to a bathochromic shift in the UV-Vis absorption spectra – indicative of a smaller HOMO-LUMO gap. The absorption spectra also displayed the presence of vibronic fine structures, an effect indicative of a rigid structure.[170]

Most commonly, non-covalent S – O interactions used in conjugated organic materials are observed between thiophene acceptors and either alkoxy or carbonyl oxygen donors. Long aliphatic chains often incorporated into oligothiophenes and PTs for solubility net unfavourable steric interactions which result in twisting of the backbone, and often have a negative effect on the band gap. Therefore, replacing these alkyl chains with alkoxy substituents can allow for the desired solubilizing effects while still resulting in a planar conjugated system (Figure 3.3).

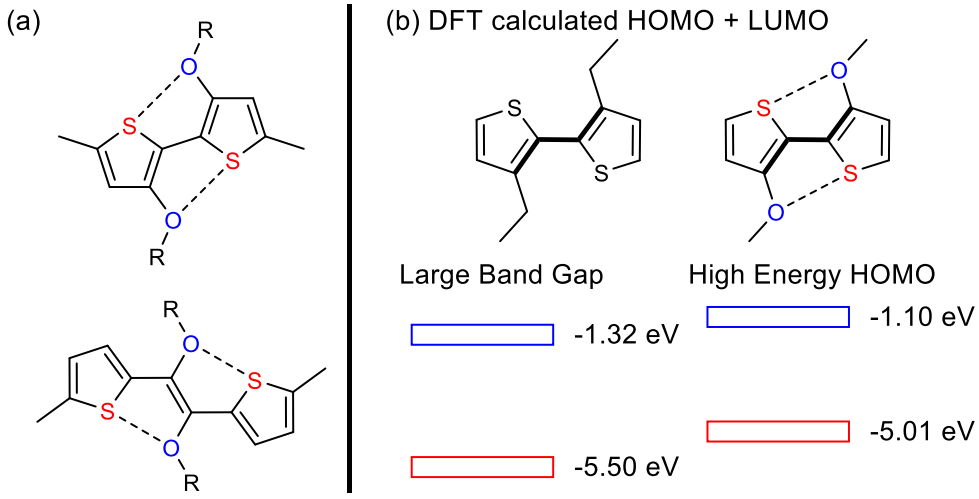

Figure 3.3 – a) example substructures in conjugated materials with conformational locking through S – O interactions b) DFT/B3LYP/6-311+g(d,p) calculated HOMO and LUMO energy levels for 3-alkyl and 3-alkoxythiophene biaryls.

Similarly, chalcogen bonding can occur between nitrogen donor lone pairs and sulfur σ* acceptors, and has been explored in conjugated materials as a method of conformational locking. Both nitrogen- and sulfur-containing heterocycles are both highly prevalent in these types of materials which makes stabilizing S – N interactions highly beneficial to achieving molecular rigidification without additional synthetic effort. Many examples of conjugated polymers in the literature, including as those prepared by Pei and co-workers (Figure 3.4), propose the presence of S – N interactions resulting in a lower band gap when compared to an equivalent polymer possessing a C_{sp2}-H in place of the N_{sp2}.[171] Incorporation of a nitrogen also reduces the steric bulk of the arene which also contributes towards planarization. Prior to further analysis, it was therefore difficult to determine how much of a planarization effect the S – N interactions really contribute compared to simply reducing the steric load of the arene through nitrogen incorporation.

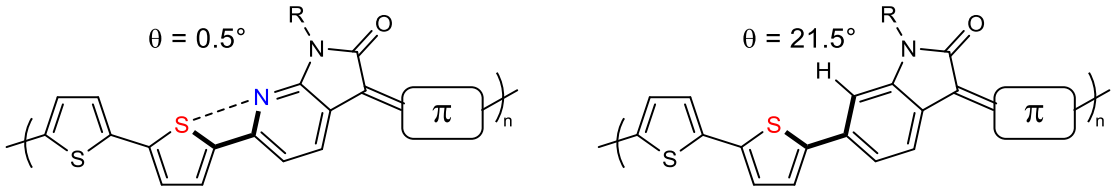

Figure 3.4 – Conjugated polymers with and without proposed S – N interactions based on DFT (B3LYP/6-311g(d,p)) calculations.

Bazan and co-workers also investigated these types of interactions by evaluating the effect of pyridyl-nitrogen placement relative to a silylene-2,2'-bithiophene core (Figure 3.5a).[68,172] Presumably due to similar planarity between the molecules, little difference in the absorption profiles was observed. However, the molecule with the pyridyl-nitrogen proximal to the thiophene-sulfur showed a more stable crystalline lattice with a significant increase in thermal transition temperatures, a higher level of insolubility, and larger

presence of crystallites in the thin-films. This indicated that the S – N interactions are likely resulting in a more rigid molecule that possesses more and/or stronger intermolecular interactions in the solid state.[68] In a subsequent study by Bazan, computational analysis was used to further investigate the degree of interaction between S and N in conjugated small molecules.[173] Several model substrates possessing thiadiazolopyridines were examined for signs of *N*-lone pair donation into adjacent thiophene σ-holes. These calculations revealed that a substantial N – S stabilization energy of 2 – 2.25 kcal/mol did, in fact, contribute to the rigidification of the biaryl bonds (Figure 3.5b).[173]

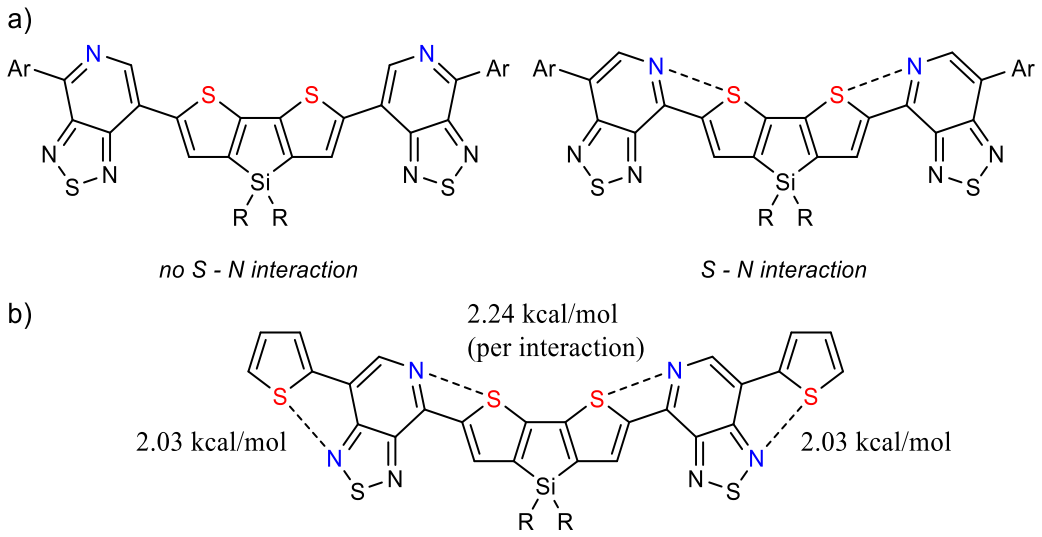

Figure 3.5 –S – N interactions investigated a) experimentally and b) computationally investigated by Bazan and co-workers.

The final chalcogen bonding interaction commonly observed in conjugated materials is that between fluorine and sulfur. Fluorine atoms are often incorporated for their inductive electronic properties. When fixed to the conjugated backbone, fluorine's high electronegativity typically lowers the HOMO and LUMO of the system with little effect on the actual band gap. The reduction of a high-level HOMO in this manner can enhance

the chemical and air stability of the material.[174] In many of these cases, fluorine is also able to develop non-covalent interactions with heteroatoms, such as thiophene sulfurs, favourably resulting in planarization between aryl units. These interactions have been the subject of a computational investigation by Chen and co-workers in 2016, wherein optimization of various fluorinated biaryl structures suggested that F – S interactions are strong enough to overcome repulsive interactions and conformationally lock neighbouring aromatic rings (Figure 3.6).[174]

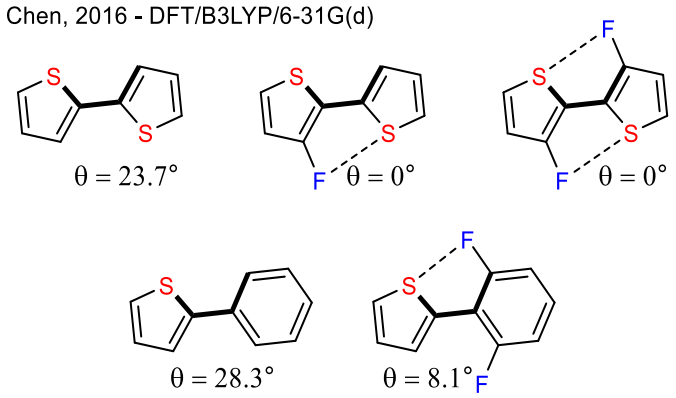

Figure 3.6 – F – S interactions computationally investigated by Chen and co-workers on DFT optimized structure.

The conformational locking of F – S interactions has also observed experimentally in synthesized small molecules and polymers which display high degree of planarity.[175] To showcase these effects, 3,3'-difluoro-2,2'-bithiophene was employed as a building

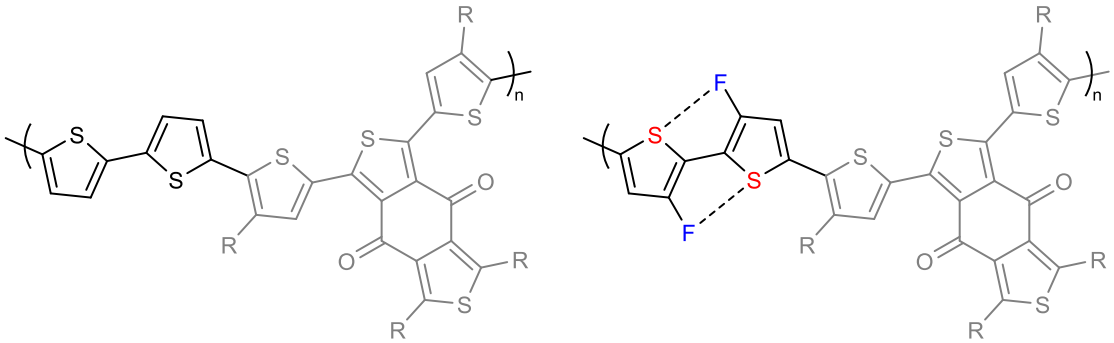

Figure 3.7 – Conjugated polymers with and without proposed S – F interactions prepared by Hou and co-workers.

block in several p-type conjugated polymers (Figure 3.7). The fluorinated bithiophene was shown to possess a planar backbone configuration with a 1.3 kcal/mol higher torsional compared to equivalent simple bithiophene structure. This increased rigidity along the bithiophene manifested as stronger, and more compact, π-π stacking effects, as well as increased solution aggregation in the fluorinated polymers.[175]

3.1.4 Hydrogen bonding interactions

Hydrogen bonding between hydrogen and electronegative atoms (H – X) has been recognized as a non-covalent interaction in numerous biological systems such as proteins, polynucleotides, dyes, and pigments.[176] It is, therefore, unsurprising that these effects are also present in conjugated organic materials and can have a large effect on the material's properties. Conventionally, hydrogen bonding is observed between an electronegative heteroatom (O, N, F), and a hydrogen atom that is polarized through bonding to an electronegative atom itself (OH – X). While this is observed in some molecular conjugated motifs, such as that of indigo, it is not the principal H-bonding interaction present in many conjugated organic materials (Figure 3.8a). What is sometimes deemed "non-traditional" hydrogen bonding occurs between electronegative heteroatoms and hydrogens bonded to carbon (CH – X).[177] A notable example of this is found in the deployment of diketopyrrolopyrrole (DPP) motifs, wherein non-conventional hydrogen bonding (CH – O) is found to instill planarity between the DPP and adjacent thiophene rings (Figure 3.8b).[178,179] Not only is this interaction favoured over interaction of the carbonyl with the thiophene sulfur (O – S), a generally unfavoured s-cis conformation between the two aromatic rings is found in the crystal structure.[180] The strength of non-traditional hydrogen bonding interactions in these types of materials was

the subject of investigation in an extensive computational study by Ratner and co-workers.[181] Confirming what had been observed, they reported that CH – O and CH – N interactions provide a sufficient torsional barrier, leading to an increase in backbone planarity (with CH – F interactions contributing to a lesser degree).

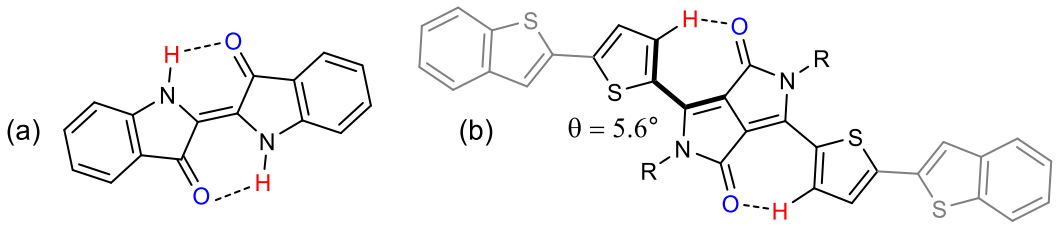

Figure 3.8 – Hydrogen bonding: a) traditional H-bonding in indigo b) non-traditional H-bonding in a DPP organic semiconductor. Dihedral angle from x-ray single crystal structures.

3.1.5 Computational evaluation of non-covalent interactions

To confirm the non-covalent interactions that are predicted to be responsible for the planarization observed in the structure and properties of conjugated organic materials, there exist several computational stratagems. One framework for computational analysis is to predict conformational preferences through the assessment of torsional potential of the dihedral angle between two aromatic units.[181,182] In the computational study by Ratner and co-workers, biaryl geometries were first optimized using Density Functional Theory (DFT) with a fixed dihedral between 0° and 180° in 10° intervals. The resulting optimized structures could then be used as inputs for single-point energy calculations using Moller-Plesset perturbation theory (MP2/cc-pVTZ).[181] A torsional potential energy surface was then constructed by plotting the relative energy (kcal/mol) of each optimized structure against the dihedral angle (°). This analysis can be indicative of conformational locking mechanisms such as non-covalent interactions in instances in which there are large

barriers of rotation from conformations that would otherwise be sterically hindered. For example, in the torsional analysis of 3-methoxy-2,2'-bithiophene, a planar, 180° geometry along the biaryl dihedral is found to be the lowest energy conformer (Figure 3.9).

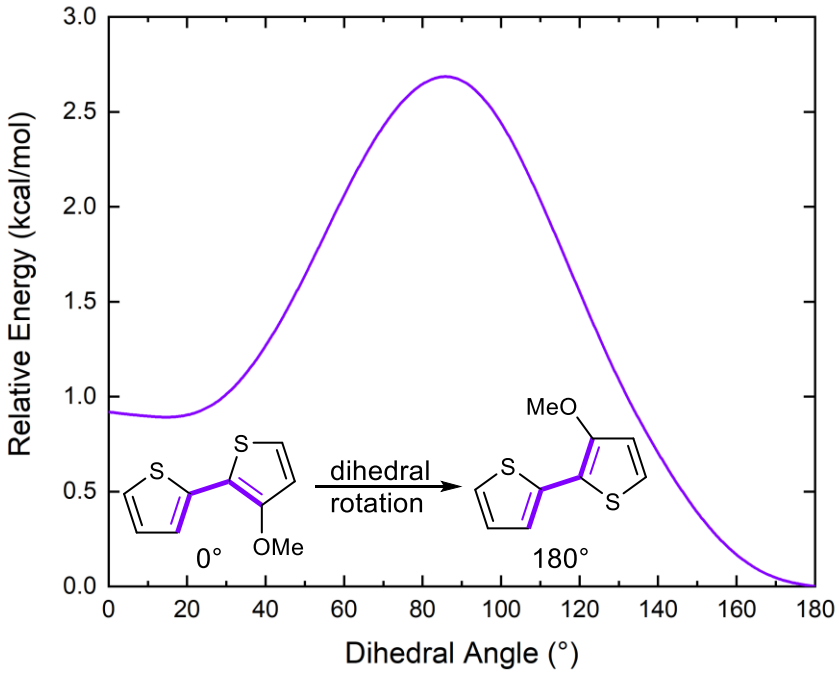

Figure 3.9 – Torsional potential analysis of bithiophene dihedral calculated on optimized structures using DFT/B3LYP/6-311++g(d,p)

Another computational tool that has been employed for the examination of non-covalent conformational locks is Natural Bonding Orbital (NBO) analysis.[183] NBO calculations can be used to determine the major interactions that dominate the energetics in a molecular system. When analyzing by NBO, second-order perturbation energies are considered to evaluate the delocalization of electrons from a filled donor orbital (σ bond, π bond, lone pair) into a nearby empty orbital acceptor (σ*, π*). This tool was first employed towards this subject by Bazan and Tretiak in 2012 to examine the interactions between two π-conjugated heterocycles with the intention of determining which

interactions give rise to conformational preference.[173] NBO analysis revealed that near-bridge bonds dominate the energetics which results in the double bonds of the π-system favouring the s-trans configuration. Additionally, several close-contact interactions were identified which varied in strength. NBO revealed that the strongest of these donor-acceptor interactions involve the delocalization of lone pairs on heteroatoms into nearby σ*-orbitals.

While reported examples of its use for the study of conformational locking in organic materials remain limited, the Quantum Theory of Atoms in Molecules (QTAIM, also abbreviated as simply AIM) is a popular method for the analysis of non-covalent-binding interactions, and especially σ-hole interactions.[184,185] AIM analysis provides some key details used to quantify non-covalent interactions, specifically; the interaction's electron density (ρ), its gradient (∇ρ) as well as the Laplacian ($\nabla^2\rho$). The electron density (ρ) found at bond critical points (BCPs), identified for interactions between two atoms, can act as a meaningful measurement of bond strength, and therefore be used to determine the nature of the bonding interaction (covalent, H-bonding, etc.).[186]

3.2 Proposal[187]

Considering the presence of thiazoles in conjugated small molecules and polymers, it is surprising that the deployment of thiazole-*N*-oxides in these materials, so far, has been entirely overlooked. The bithiazole-*N*-oxide polymers synthesized through both our dehydration polymerization and *ipso*-arylative polycondensation represent the first reported examples of these types of materials.[145,161] A natural assumption would be that the bithiazole-*N*-oxide functionality in these molecules could simply be reduced in

order to deliver the corresponding bithiazole material (like those synthesized by transition metal cross-couplings). This reduction was attempted by our group using Zn metal in a 1:1 THF:$NH_4Cl_{(sat.)}$ solution, and shown to proceed on bithiazole-*N*-oxide small molecules to yield reduced bithiazoles in high yields (Scheme 3.1.)[145] The same conditions were applied to the reduction of the bithiazole-*N*-oxide polymers; however, we found it difficult to quantify the extent of reduction.

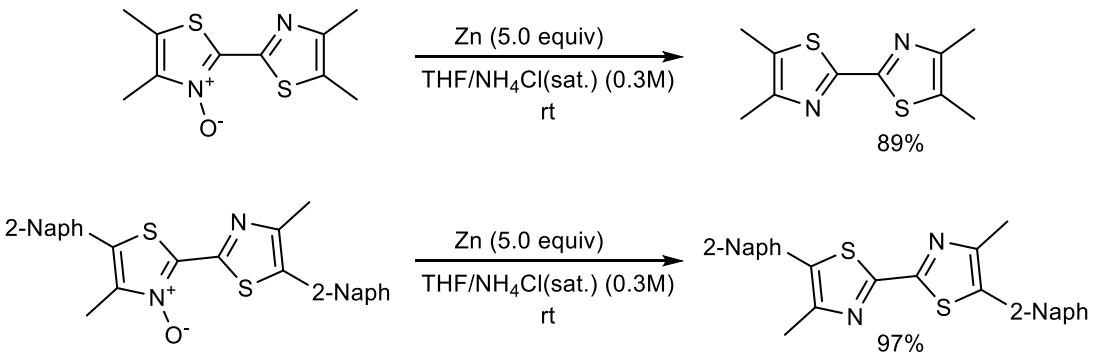

Scheme 3.1 – Reported reduction procedure for bithiazole-*N*-oxides with Zn in THF:NH_4Cl(sat.).

Instead of focusing on this polymer reduction, we instead were interested in developing these *N*-oxide-containing polymers as a new class of conjugated materials. As these materials had been completely unexplored, there is potential for unique physical and electronic material properties. Of most interest to us was the potential for the thiazole-*N*-oxide functionality to establish non-covalent chalcogen bonding interactions with the sulfur of the adjacent thiazole ring due to its proximity and proper directionality (Scheme 3.2). Although the 2,2'-bithiazole core itself is planar due to the lack of steric interactions, we speculated that non-covalent bonding from the *N*-oxide could lead to a higher barrier of rotation along the bithiazole C-C bond, enforcing a conformational lock. This more rigid, planar bithiazole core could then manifest as a decrease in the electronic band gap,

and in the supramolecular assembly of the material via increased π-π stacking. *N*-oxidation could, therefore, present itself as an impactful new method for the conformational locking of thiazole-containing conjugated materials, in a manner that is synthetically simple compared other functionalities required for non-covalent interactions.

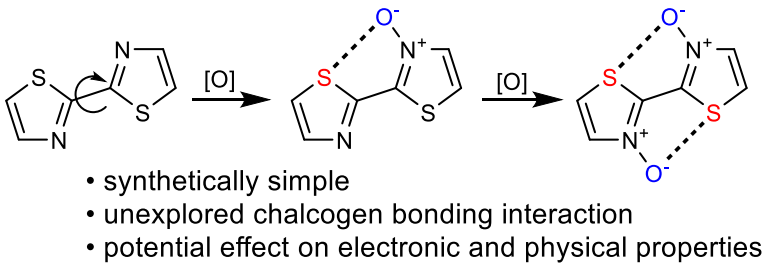

Scheme 3.2 – Proposed conformational locking of bithiazoles through *N*-oxide chalcogen bonding interactions.

3.3 Results and Discussion

To determine the effects of *N*-oxidation on bithiazole conjugated systems, we began our investigation by examining the properties of the most simple of bithiazole systems: 2,2-bithiazole (**3.1a**), as well as its *N*-oxide (**3.1b**) and *N,N'*-dioxide (**3.1c**) forms. Bithiazole **3.1a** was synthesized through the oxidative homocoupling of thiazole in a 64% yield, following a literature report of a $Cu(OAc)_2$/air-mediated C-H activation method (Scheme 3.3a).[188] Single *N*-oxide-containing substrate **3.1b** was synthesized in a 56% yield by *ipso*-arylative coupling as previously described in *Chapter 2* (Scheme 3.3b). The obtained bithiazole-*N*-oxide (**3.1b**) was then further oxidized using standard *m*-CPBA oxidation conditions to deliver bithiazole-*N,N'*-dioxide (**3.1c**) (Scheme 3.3c). A large excess of *m*-CPBA (6.0 equiv) was deployed over an extended reaction duration in an attempt to force conversion to **3.1c**; resulting in a 50% yield of product with the majority of the remaining mass balance recovered as starting material. Though significantly more

polar, isolation of **3.1c** by column chromatography, and separation from remaining **3.1b** and *m*-CPBA by-products, was achievable using a gradient of EtOAc and MeOH.

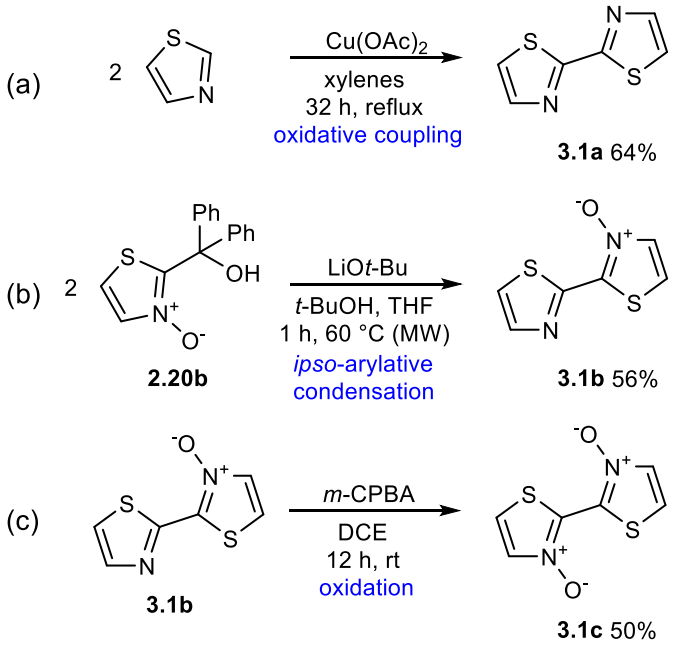

Scheme 3.3 – Synthetic route to a) bithiazole **3.1a**, b) bithiazole-*N*-oxide **3.1b**, and c) bithiazole-*N,N'*-dioxide **3.1c**.

With our three bithiazoles **3.1a-c**, we sought to determine if the incorporation of the *N*-oxide functionality would influence the band gap. The UV-Vis absorption spectrum of each compound was determined in $CHCl_3$ wherein a bathochromic (red) shift of around 50 nm was observed in the onset of absorption upon subsequent *N*-oxidation, corresponding to decreased HOMO-LUMO gap for the oxidized bithiazoles (Figure 3.10). If planarization is enforced through *N*-oxide (S – O) interaction with the adjacent thiazole sulfur, a decrease in the HOMO-LUMO gap upon successive oxidation from bithiazole **3.1a** to *N*-oxide **3.1b,** and again to *N,N'*-dioxide **3.1c** is expected. Additionally, it was observed that with an increased number of *N*-oxide functional groups, there is a notable presence of vibrational fine structures in the absorbance spectra of **3.1b** and **3.1c** when

compared to the broad absorbance peak observed for the non-oxidized compound **3.1a**. These fine structures have previously been shown to be indicative of rigid conjugated systems, and in this case, was suspected to be due to locking of the bithiazole N-C-C-N dihedral. In addition to this bithiazole series, 4,4'-dimethyl-2,2'-bithiazole (**3.2a**), as well as its singly (**3.2b**) and doubly (**3.2c**) oxidized forms were synthesized in much the same manner. The same trend displayed in the UV-Vis absorption spectra of series **3.1** was seen in the spectra of **3.2**, as well as the emergence of vibrational fine structures in **3.2b** and **3.2c** (see Chapter 6: Figure 6.2).

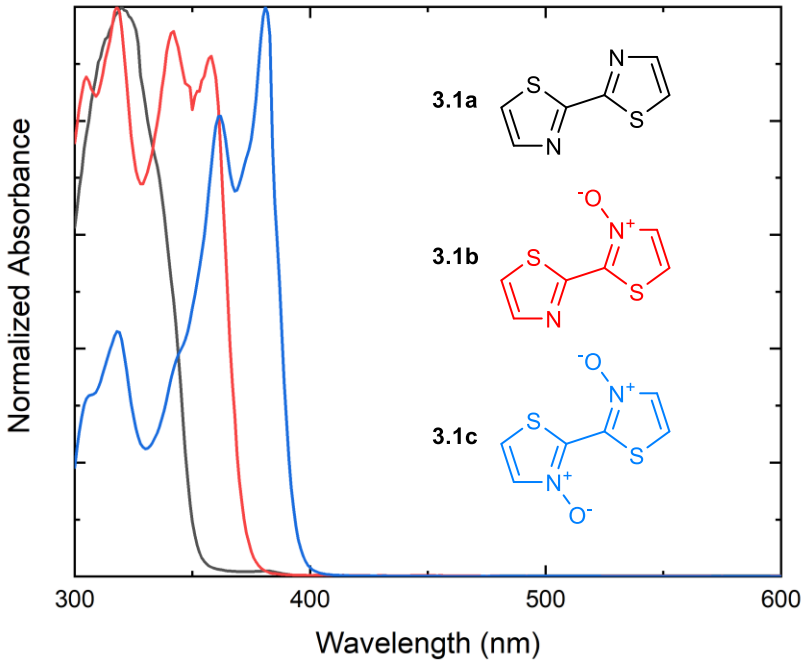

Figure 3.10 – UV-Vis absorption spectra of bithiazoles **3.1a** (black), **3.1b** (red), and **3.1c** (blue) in $CHCl_3$.

3.3.1 *N*-Oxides in extended conjugated systems

Having observed a clear bathochromic shift upon increasing *N*-oxidation in 2,2'-bithiazoles **3.1a-c**, we next sought to explore the effect on extended conjugated systems.

We speculated that with a larger π-system, the effect of *N*-oxidation may not have as noticeable an effect on the optical band gap of bithiazole-containing conjugated materials.

This investigation commenced with the synthesis of extended π-conjugated bis(4-hexylphenyl) bithiazole derivative **3.3a,** as well as its *N*-oxide (**3.3b**), and *N,N'*-dioxide (**3.3c**) variants. These 2,2'-bithiazole derivatives were selected for several reasons. Firstly, this phenylene-thiazole represents a common motif found in conjugated small molecules and would therefore be representative of these compounds. Additionally, 4,4'-unsubstituted bithiazoles were targeted over their 4,4'-dimethyl equivalents in order to reduce steric interactions between the arene units and yield an overall more planar molecule. Finally, to ensure solubility of the bithiazoles, solubilizing hexyl chains were also included.

Bithiazole-*N*-oxide **3.3b** had previously been synthesized in our substrate scope of the *ipso*-arylative condensation (Chapter 2, also Scheme 3.4a). Using the same material **2.14f** from this reaction, access to the bithiazole-*N,N'*-dioxide **3.3c** was achieved in a 66% yield through an unprecedented *ipso*-aryl-oxidative coupling with $Cu(OAc)_2$ and K_2CO_3 (Scheme 3.4b). This reaction presumably proceeds via the loss of benzophenone, followed by the Cu-mediated oxidative coupling. The unoxidized bithiazole **3.3a** was then obtained by employing standard Zn reductive conditions on *N,N'*-dioxide **3.3c**, yielding a respectable 80% yield of the unoxidized product (Scheme 3.4c). We were interested in further exploring this unreported *ipso*-aryl-oxidative coupling as a method to access other bithiazole-*N,N'*-dioxide small molecules from diphenylcarbinol-starting materials (**2.14**), however; little success was found when applying the conditions on substrates other than **2.14f**. This seemed to be due to the incredibly poor solubility of the *N,N'*-dioxide products,

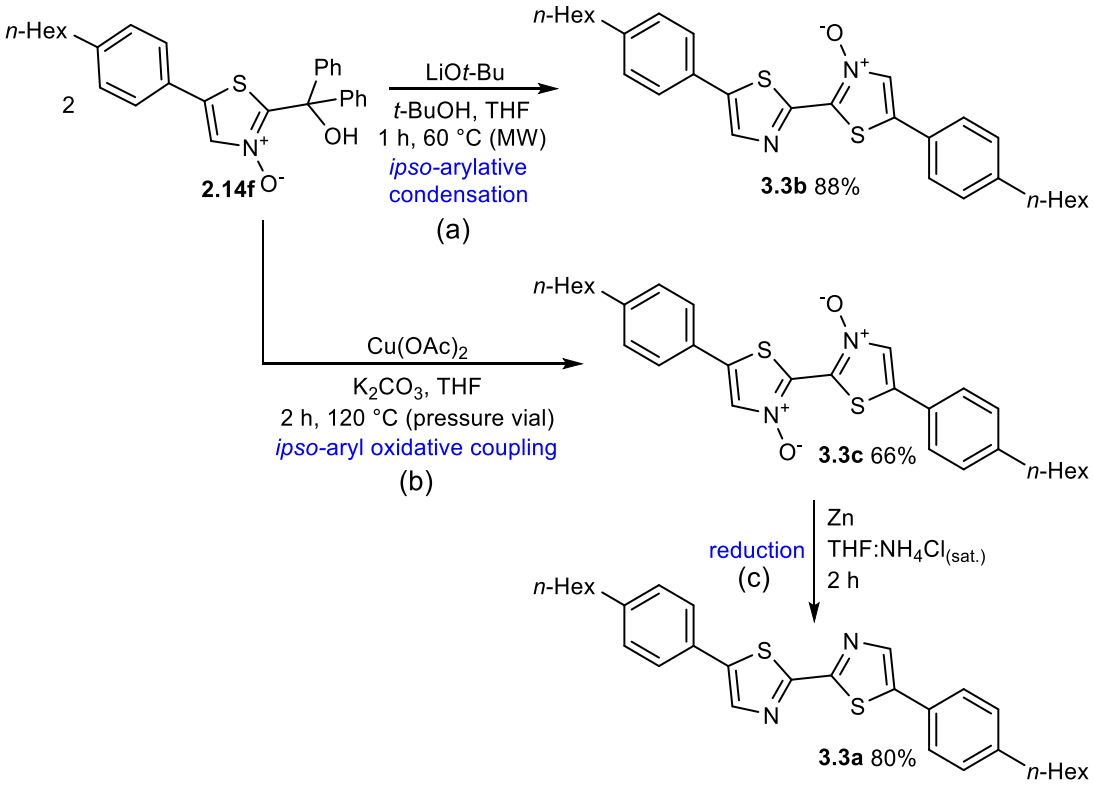

Scheme 3.4 – Synthetic route to bis(4-hexylphenyl)bithiazole series **3.3**.

rendering isolation and characterization extremely difficult (such as in the attempted conversion of **2.14a** to **3.4**, Scheme 3.5). Interestingly, although the synthesis of **3.3c** also proceeded under basic conditions (like those conditions used to furnish **3.3b**), only trace amounts of *ipso*-arylative condensation were ever observed employing K_2CO_3 with $Cu(OAc)_2$.

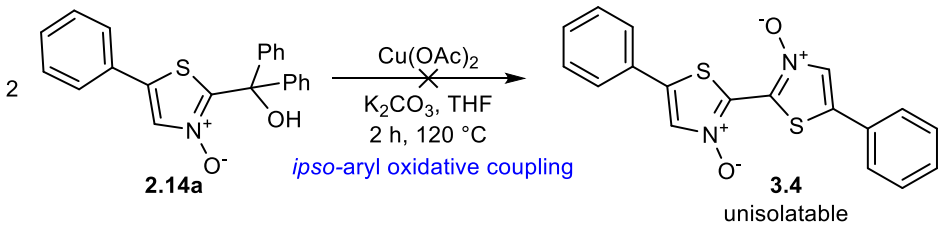

Scheme 3.5 – *ipso*-Aryl-oxidative coupling to produced bithiazole-*N,N'*-dioxides.

With our series of phenylene bithiazoles **3.3a-c** synthesized, we next determined their optical characteristics through analysis by UV-Vis absorption spectroscopy and fluorescence emission. To our delight, the same bathochromic shift upon increasing the number of *N*-oxides, previously observed in bithiazoles **3.1a-c,** was also observed in the UV-Vis spectra of extended π-conjugated molecules **3.3a-c** (Figure 3.11). Although the presence of the sharp vibrational fine structures in the spectra had diminished significantly compared to what had previously noted, a slight shouldering in the spectra of **3.3b** and pronounced shoulder in the spectra of **3.3c** are visible. This observation was expected as the conformational locking of the *N*-oxides is contained to the bithiazole core, and while the molecule may be planar in the solid state, the bond between the phenyl substituent and the thiazole is still freely rotating in solution.

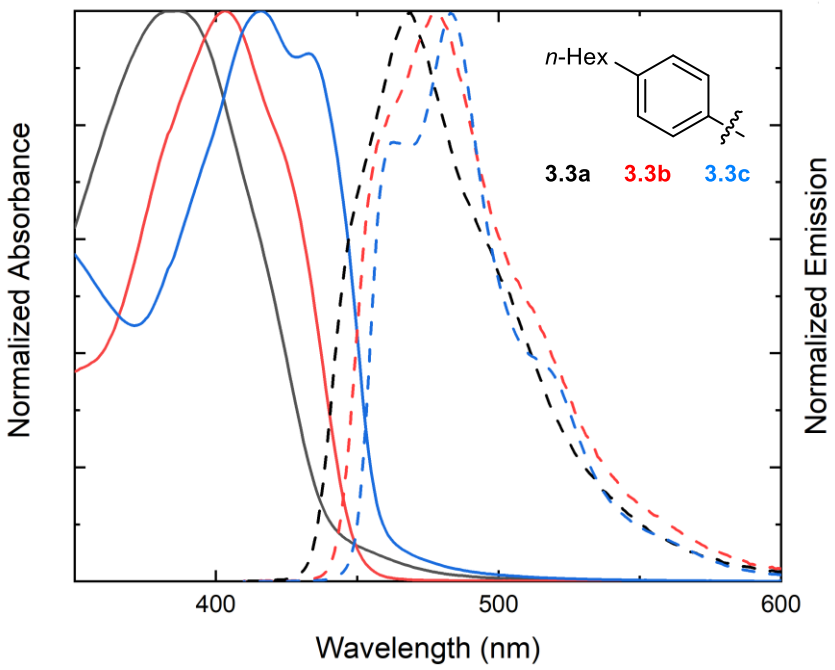

Figure 3.11 – UV-Vis absorption spectra (solid) and steady-state fluorescence spectra (dashed) of 4-hexylphenyl series **3.3a-c** in $CHCl_3$.

Following this, we focused our attention on the synthesis of a bis(5-hexylthiophen-2-yl) series of extended π-conjugated systems (**3.5**), as a model of thiophenyl-thiazole-type small molecules. In this series, 4,4'-dimethyl bithiazoles were targeted over their unsubstituted equivalents, as this simplified our synthetic efforts, and the steric interactions between the 4-methyl and a five-membered arene are less significant compared to the bulk of a phenyl substituent. Once again, to ensure solubility, a thiophene possessing a 5-hexyl substituent was selected.

Although bithiazole-*N*-oxide **3.5b** had previously been synthesized by our group by *N*-dehydration of the *N*-oxide, the moderate 56% yield combined with difficulty in starting material preparation (direct arylation and *N*-oxidation) meant that it was impractical to approach **3.5a** and **3.5c** through the simple reduction/oxidation of **3.5b**.[145] Likewise, difficulties had previously been faced when adapting the *ipso*-arylative conden-

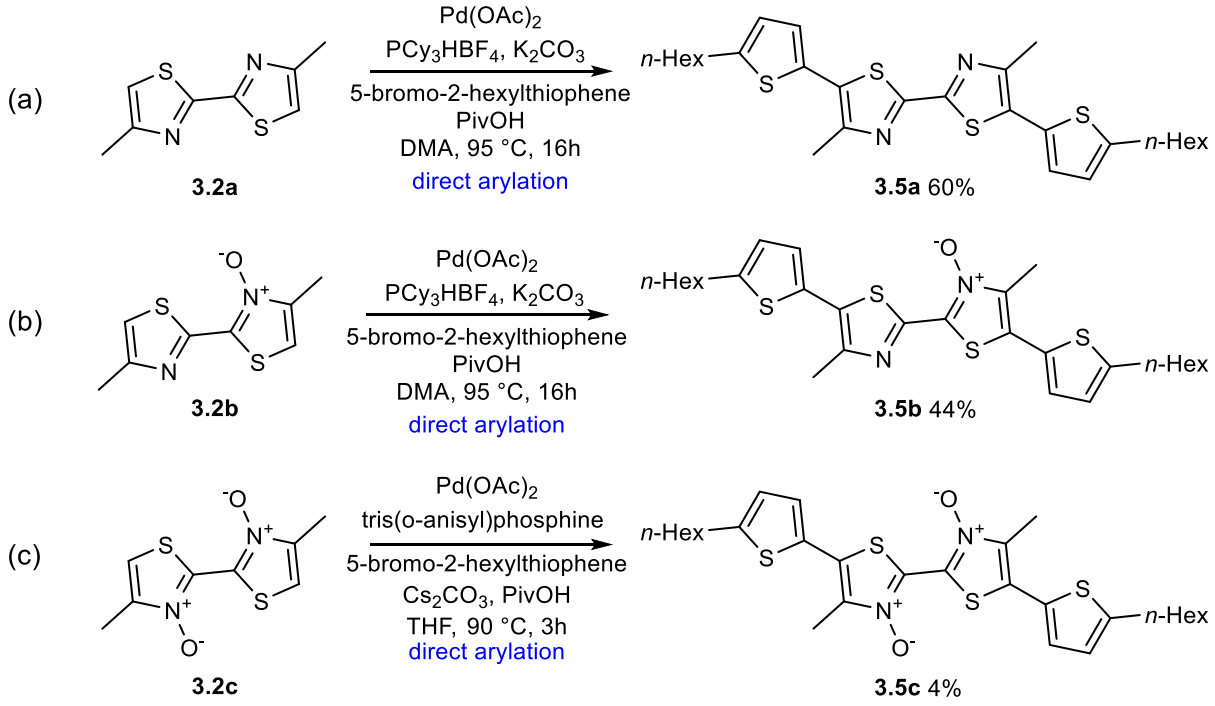

Scheme 3.6 – Synthetic route to bis(5-hexylthiophen-2-yl)bithiazole series **3.5**.

sation to heterocycle-substituted thiazoles. Therefore, in a departure from previous procedures used to produced **3.3a-c**, bithiazole **3.5a**, *N*-oxide **3.5b** and *N*,*N'*-dioxide **3.5c** were instead all prepared by the double direct arylation of 4,4'-dimethylbithiazole **3.2a** (Scheme 3.6a), **3.2b** (Scheme 3.6b) and **3.2c** (Scheme 3.6c), respectively. Although electron rich 2-bromothiophenes do not generally proceed well as substrates for oxidative addition, the direct arylations reactions were able to afford **3.5a** in a 60% yield, and **3.5b** in a 44% yield. Unfortunately, the double direct arylation to **3.5c** did not proceed in nearly as a high a yield (4%), however, this netted enough for analysis.

As with bis(4-hexylphenyl) series **3.3**, a bathochromic shift upon increasing *N*-oxidation was observed in the UV-Vis absorption spectra of bis(5-hexylthiophen-2-yl) **3.5a** and **3.5b** (Figure 3.12). Interestingly, only a small red shift was observed in the onset of absorption between the single *N*-oxide **3.5b** and *N,N'*-dioxide **3.5c**. The presence of vibrational fine structures in the absorbance trace of **3.5c** was almost undectable compared to **3.1c,** or even **3.3c**. However, as previously mentioned, another notable indicator of increased molecular rigidification determinable from optical spectra is a decrease in the Stokes shifts; that is, the difference between the λ_{max} of absorbance and the λ_{max} of fluorescence. In conjugated polymers and small molecules, this phenomenon in the Stokes shift arises from the intramolecular reorganization energy in changing geometries between the ground and excited states.[189] If a conjugated molecule possesses torsional disorder about the σ-bonds in the ground state, emission will occur at a higher wavelength as energy is lost achieving planarization in the excited state.[189] A decrease in the Stokes shift of approximately 0.15 eV was observed in both extended

small molecule series **3.3** and **3.5**, upon incorporation of two *N*-oxides, indicating that the *N*-oxide-containing structures are more planar in the ground state.

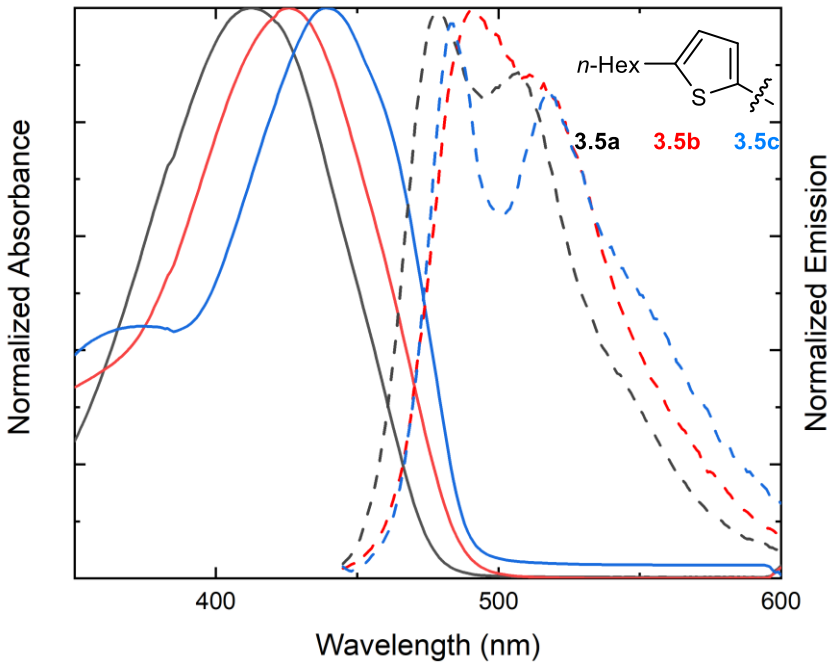

Figure 3.12 – UV-Vis absorption spectra (solid) and steady-state fluorescence spectra (dashed) of 5-hexylthiophen-2-yl series **3.5a-c**.

While preparing these small molecules for analysis, a clear decrease in solubility was observed with increasing level of bithiazole *N*-oxidation, despite the inclusion of solubilizing *n*-hexyl chains. The poor solubility of the *N*,*N*'-dioxide compounds **3.3c** and **3.5c** is speculated to be due to increased π-stacking interactions between molecules as a result of the molecular rigidification. We postulated that the increase in π-stacking upon *N*-oxidation would be observable in the thermal properties of the small molecule series **3.3** and **3.5**. Differential scanning calorimetry (DSC) experiments were, therefore, performed on **3.3a**-**c** and **3.5a**-**c** to determined melting (mp) and crystallization points (xp) (Figure 3.13). Noticeably, upon increasing the level of bithiazole *N*-oxidation from **3.3a** to

3.3b in the 4-hexylphenyl series, an increase is observed in both the melting temperature and crystallization temperature of 57 °C and 61 °C, respectively. Likewise, in the DSC traces of series **3.5**, possessing 5-hexylthiophenes, an increase in both thermal transitions of 28 °C (melting) and 45 °C (crystallization) is observed for **3.5a** and **3.5b**. Thermal transitions were unable to be determined for *N*,*N'*-dioxide molecules **3.3c** and **3.5c**, as decomposition of the material (determined by thermogravimetric analysis (TGA)) occurred prior to any melting transition. Interestingly, the DSC trace of 4-hexylphenyl small molecule **3.3a** showed that the material proceeds to a liquid crystalline state before transitioning to a fully isotropic liquid upon heating. Given the similarities between the molecular structure of **3.3a** and other well-studied liquid crystals, this result was not totally unexpected.

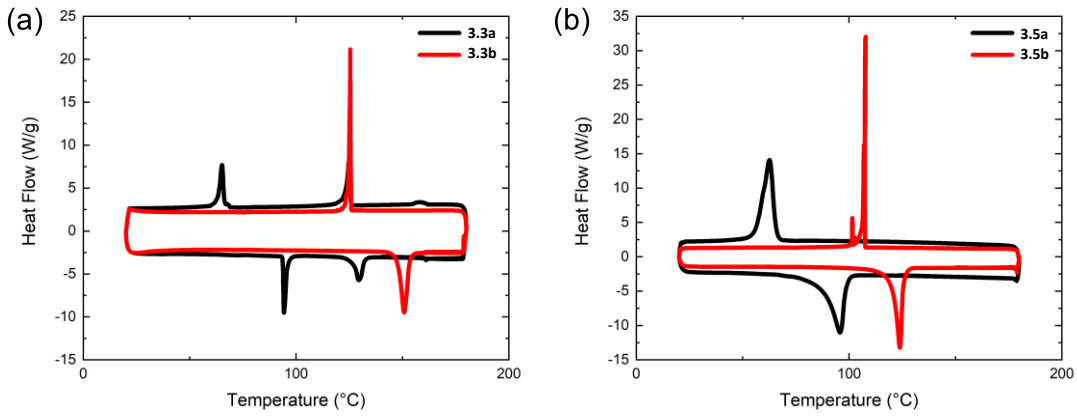

Figure 3.13 – Differential scanning calorimetry traces for a) **3.3a** (black) and **3.3b** (red) and b) **3.5a** (black) and **3.5b** (red).

The same trend of decreasing band gap upon successive oxidation observed in the UV-vis absorption spectra was also observed electrochemically by CV. It is interesting to note that the HOMO-LUMO gap decrease in both series **3.3** and **3.5** appears to be due to both an increase in the HOMO as well as a decrease in the LUMO. Counter-intuitive to

what one may rationalize, a higher HOMO energy level indicates that with increasing *N*-oxidation the bithiazoles are easier to oxidize. The fully compiled thermal, optical and electrochemical properties of the extended π-conjugated small molecule series **3.3** and **3.5** can be found in Table 3.1.

Table 3.1 – Summary of electronic and physical properties for small molecule series **3.3** and **3.5**.

Entry	mp (°C)	xp (°C)	HOMO (eV)	LUMO (eV)	Eg_{EC} (eV)	Eg_{Opt} (eV)	Abs_{Max} (nm)	Em_{Max} (nm)	Stokes Shift (eV)
3.3a	94	65	-5.82	-2.87	2.95	2.80	387	468	0.55
3.3b	151	126	--5.74	-2.96	2.78	2.75	403	479	0.49
3.3c	--	--	-5.68	-3.06	2.62	2.70	416	483	0.41
3.5a	96	63	-5.75	-2.80	2.95	2.60	413	480	0.42
3.5b	124	108	-5.69	-2.86	2.83	2.54	426	491	0.39
3.5c	--	--	-5.65	-2.95	2.70	2.52	439	483	0.26

3.3.2 *N*-Oxides in conjugated polymers

Having observed a clear trend in the electronic/optical band gap, as well as the physical properties of the extended π-conjugated small molecules, we endeavoured to synthesize a series of bithiazole-containing conjugated polymers with varying levels of *N*-oxidation. Model bithiazole polymers possessing π-spacers of either fluorene or thiophene were targeted, once again, due to the popularity of these motifs in conjugated polymers.

Initially pursued was the synthesis of a 9,9-di(2-ethylhexyl)fluorene polymer series (**P7**); possessing a 4,4'-unsubstiuted bithiazole core. **P7b**, containing a bithiazole-*N*-oxide repeating unit, had previously been synthesized with an Mn of 15.1 kDA and a PDI of 2.0,

via the *ipso*-arylative polycondensation of monomer **2.28c** (Scheme 3.7b). In a recent literature report by Kanbara and co-workers, **P7a** was synthesized with an Mn of 19.8 kDa and a PDI of 3.7 through the Cu-catalyzed aerobic oxidative coupling of a single bis(thiazolyl)fluorene monomer.[144] Having already synthesized this monomer (**2.26c**) en route to our *ipso*-arylative polycondensation monomer, we applied the same conditions of $Cu(OAc)_2$ in *p*-xylene at 140 °C (in a sealed pressure vessel) for 24h. Pleasingly, this method yielded **P7a** with an Mn of 50.0 kDa and a PDI of 3.2 (Scheme 3.7a).

Realizing that the di-*N*-oxide equivalent of **2.26c** would not likely stand up to the harsh thermal conditions of Kanbara's oxidative polymerization, an alternative route to polymer **P7c** was required. Direct arylation polymerization conditions were used to couple bithiazole-*N*,*N*'-dioxide (**3.1c**) with the dibromofluorene monomer. Unfortunately, this

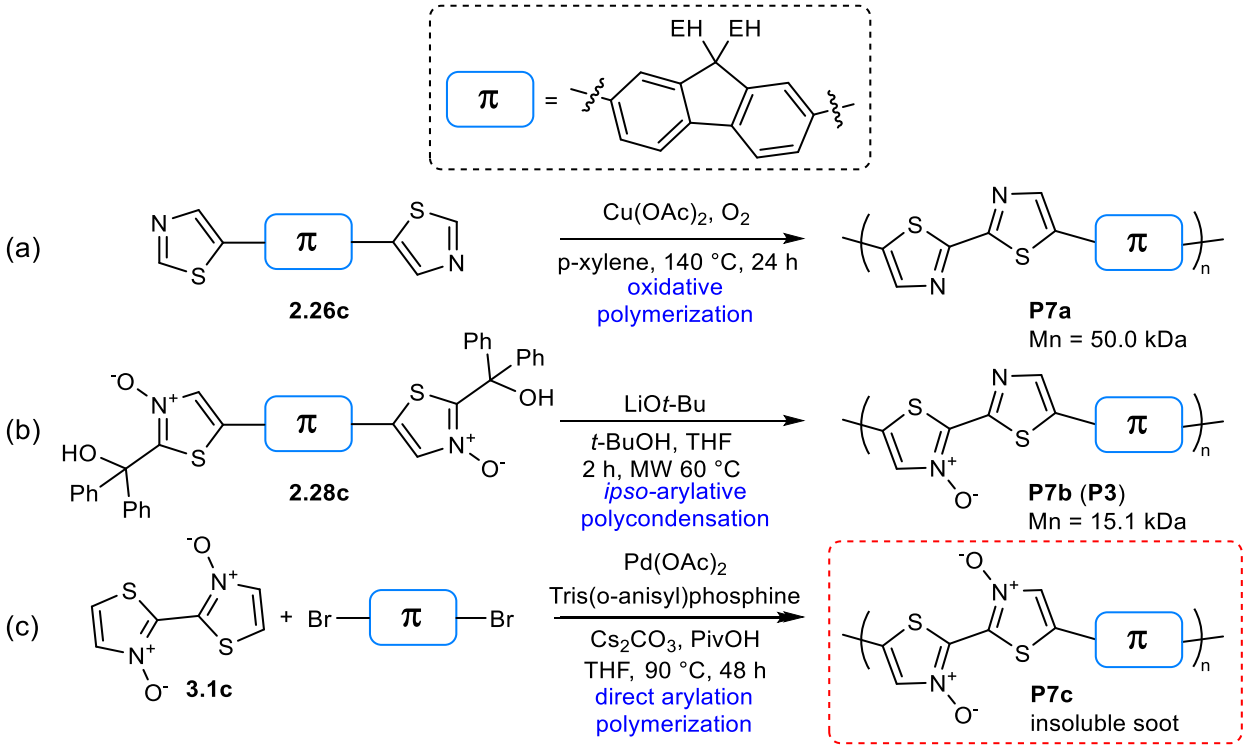

Scheme 3.7 – Synthetic route to fluorene polymer series **P7**.

polymerization yielded what was presumably polymer **P7c** as an insoluble soot, which was unable to be characterized by GPC or by UV-Vis absorption (Scheme 3.7c). The insolubility of this polymer may simply be due to a major increase in planarity of the bithiazole unit caused by the *N*-oxidation, combined with minimal steric interactions of the 4-H with the fluorene unit, leading to a high level of intermolecular π-stacking. Alternatively, the DArP route may have resulted in an insoluble cross-linked polymer as bithiazole monomer **3.1c** has potential for C-H activation at the thiazole 4-position. The route was simultaneously attempted with a 9,9-dioctylfluorene spaced, however, again only the unoxidized bithiazole polymer (**P7d**) and single *N*-oxide polymer (**P7e**) were achievable. The absorption spectra of polymers **P7a** and **P7b** (as well as **P7d** and **P7e**) were, nevertheless, evaluated, and they displayed the expected bathochromic shift in the onset of absorption upon incorporation of an *N*-oxide (Figure 3.14). While it was pleasing to see that the trend continued in the absorption spectra of our bithiazole polymers, we remained determined to develop a series that included a polymer possessing a bithiazole-*N,N'*-dioxide motif.

As solubility seemed to the be the major factor inhibiting our access to *N,N'*-dioxide polymer **P7c**, we turned our attention towards the synthesis of the equivalent polymers possessing a 4,4'-dimethylbithiazole core (**P8a-c**). The methyl substituents would disrupt the planarity between the bithiazole and fluorene units and enable solubility, meanwhile allowing for analysis of the effects of the *N*-oxide integration in the bithiazole core. Bithiazole-*N*-oxide polymer **P8b** had previously been synthesized through the *ipso*-arylative polycondensation of monomer **2.28d** with Mn of 20.4 kDa and PDI of 2.2 (Scheme 3.8b). In this series, we instead chose to approach both polymers **P8a** and

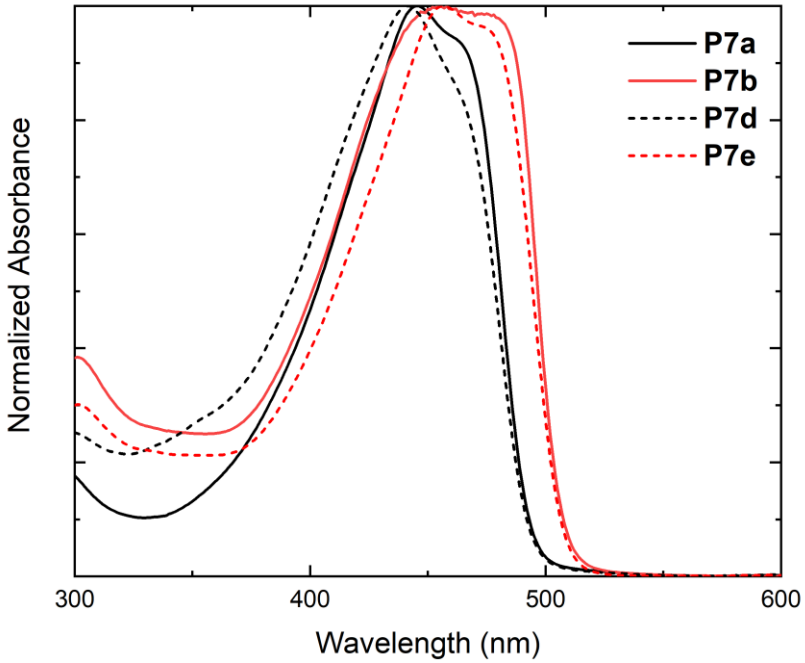

Figure 3.14 – UV-Vis absorption spectra of 9,9-bis(2-ethylhexyl)fluorene polymer series **P7a-b** (solid) and 9,9-dioctylfluorene **P7d-e** (dashed).

P8c, possessing unoxidized bithiazole and *N,N'*-dioxide bithiazole repeating units respectively, through direct arylation polymerization. We suspected this would proceed better than in the preparation of **P7c** as the bithiazole monomers **3.2a** and **3.2c** only possess a single location for C-H activation on each thiazole. Through DArP, **P8a** was obtained with an Mn of 18.2 kDa and a PDI of 2.3 (Scheme 3.8a), while **P8c** was obtained with an Mn of 14.0 kDa and a PDI of 2.3 (Scheme 3.8c).

Having successfully synthesized polymer series **P8** possessing bithiazoles with 0 - 2 *N*-oxides, we proceeded to examine their optical and electrochemical properties through UV-Vis absorption spectroscopy, fluorescence emission and

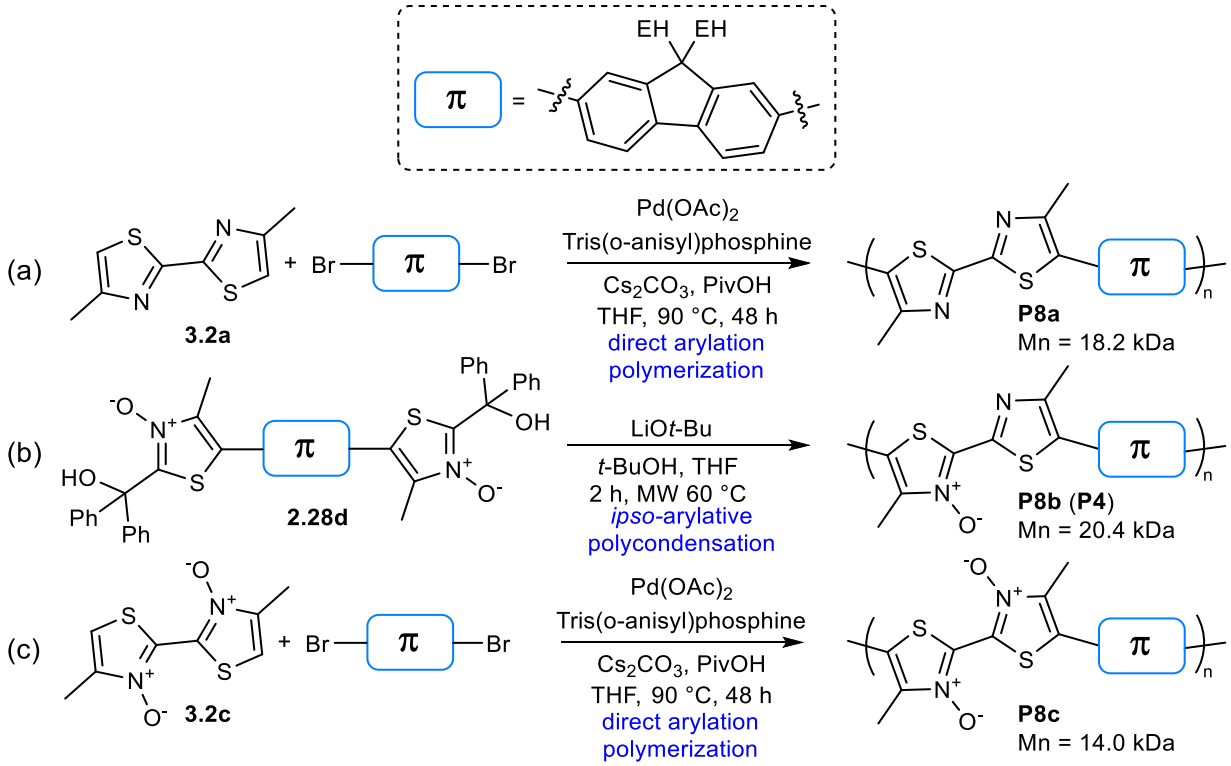

Scheme 3.8 – Synthetic route to fluorene polymer series **P8**.

voltammetry. From the absorbance and emission data of polymer series **P8**, we observed that the optical trends previously recorded in the bithiazole small molecules generally continue to hold consistent. In the UV/Vis absorption spectra, a bathochromic shift was observed upon increased *N*-oxidation, with onsets of absorbance at 475 nm, 495 nm and 520 nm for **P8a**, **P8b** and **P8c**, respectively (Figure 3.15). This corresponds to a decrease in 0.10 eV in the optical band gap per *N*-oxide functionality. From the absorbance and fluorescence measurements of polymers **P8a-c**, a definitive decrease in the Stokes shift is also present upon increased level of *N*-oxidation, once again indicative of polymer rigidification.

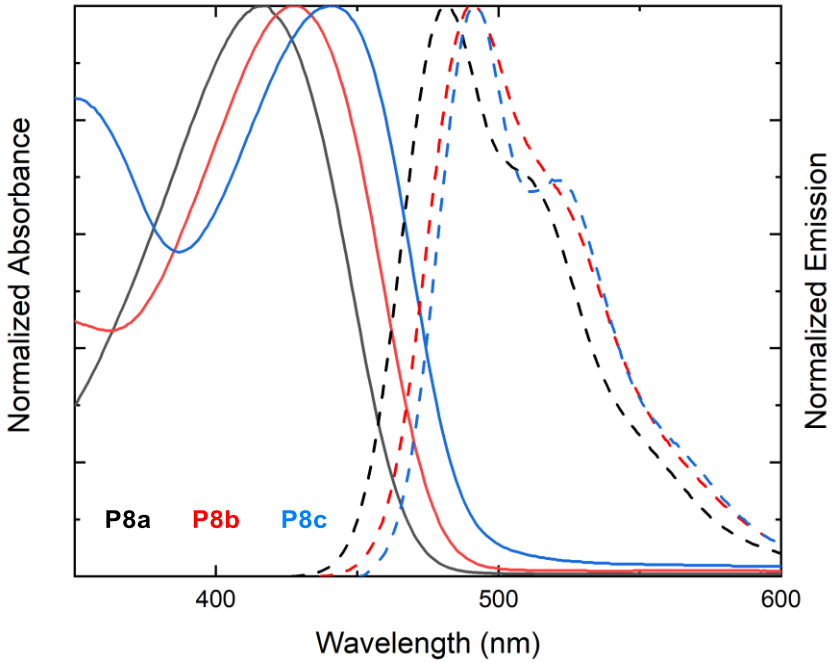

Figure 3.15 – UV-Vis absorption spectra (solid) and steady-state fluorescence spectra (dashed) of fluorene polymer series **P8a-c**.

To complete our analysis of bithiazole-containing conjugated polymers, thiophene polymer series **P9** was approached in much the same way as was done previously for **P8**. Direct arylation polymerization of bithiazole **3.2a** with 2,5-dibromo-3,4-dihexylthiophene yielded polymer **P9a** having an Mn of 20.6 kDa and PDI of 2.2 (Scheme 3.9a). **P9c** was also prepared by direct arylation polymerization, with **3.2c** as a monomer, although significantly shorter polymers were obtained; possessing an Mn of 6.0 kDa and PDI of 2.0 (Scheme 3.9c). This was not unexpected after continually observing that the extent of polymerization being limited by the decreased solubility of highly planar materials. The final bithiazole-*N*-oxide polymer **P9b** had been previously prepared by our group from bis(thiazole-*N*-oxide) monomer **3.6** via dehydration polymerization (Scheme 3.9b).

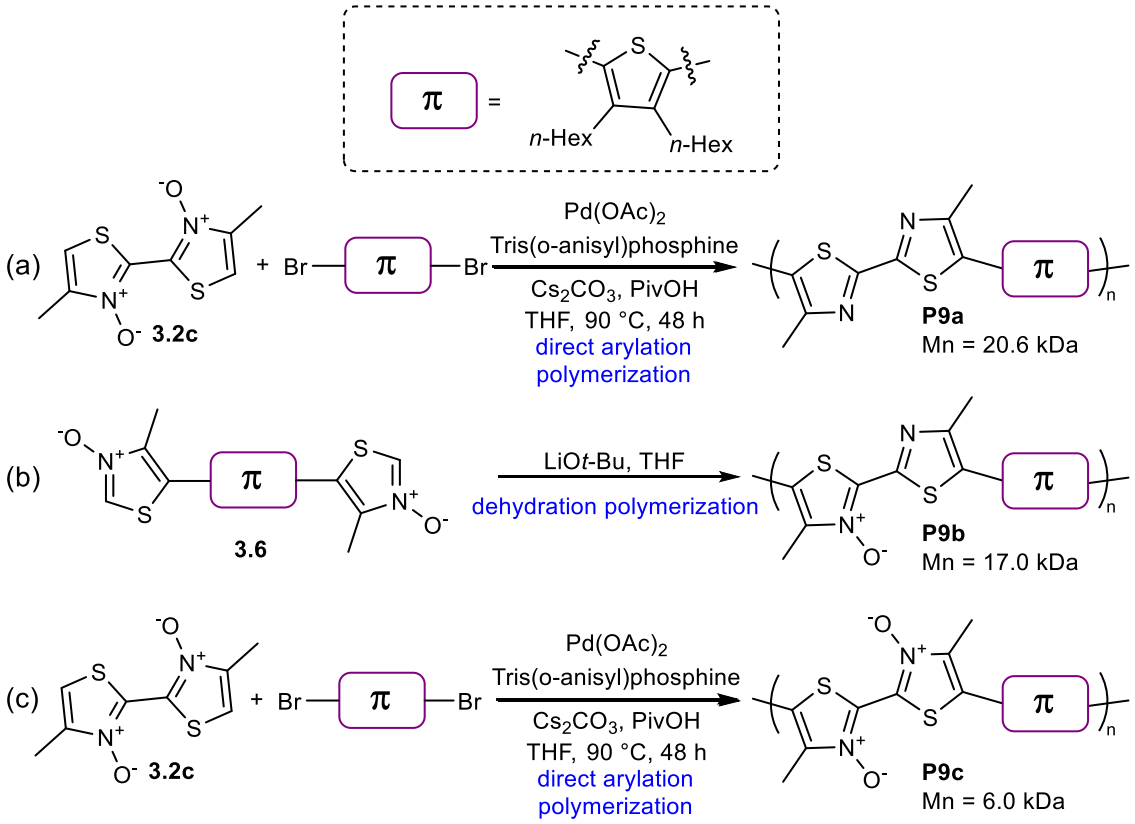

Scheme 3.9 – Synthetic route to thiophene polymer series **P9**.

Thiophene polymer series **P9** also showcased a bathochromic shift in the UV-vis absorption spectra upon increasing *N*-oxidation level of the bithiazole repeat unit (Figure 3.16). An increase in absorbance onset from 475 nm to 485 nm to 515 nm for **P9a**, **P9b** and **P9c**, respectively, corresponds to a decrease in the optical band gap of 0.5 eV and 0.15 eV. It is notable that in series **P9**, there is a significantly larger red shift observed between conjugated polymers **P9b** and **P9c** compared that between the **P9a** and **P9b**. This is uncharacteristic to what has been observed thus far in series **P8**, as well as the small molecule series. This is speculated to be due to the thiophene spacer having a larger contribution towards the frontier molecular orbitals in **P9a** and **P9b**, resulting in similar HOMO-LUMO gaps. Installation of the second *N*-oxide motif could then potentially

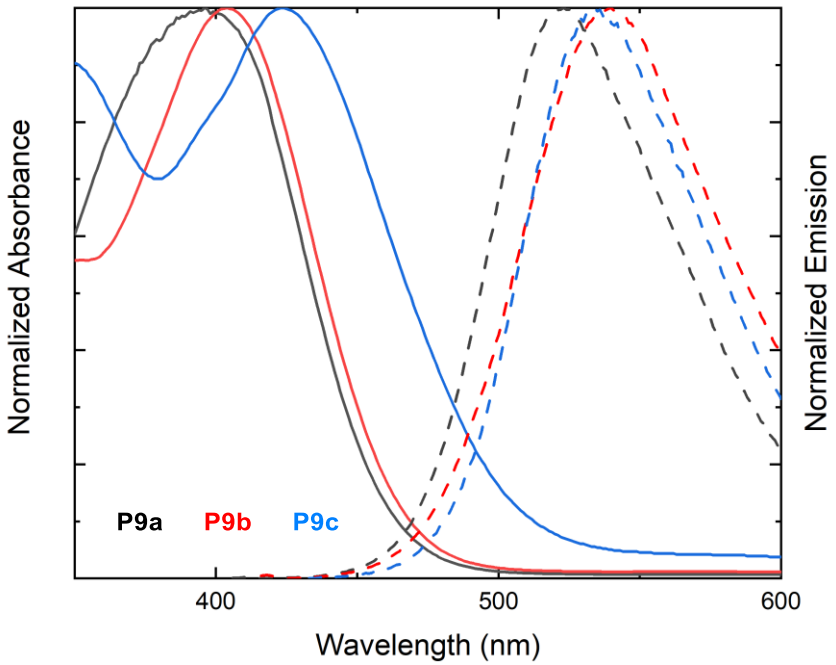

Figure 3.16 – UV-Vis absorption spectra (solid) and steady-state fluorescence spectra (dashed) of fluorene polymer series **P9a-c**.

shift the FMO's to the bithiazole, leading to the large shift observed in the absorbance onset. Coinciding with this discrepancy, the Stokes shift for polymer series **P9** does not decrease following the first *N*-oxidation; however, **P9c**, possessing a *N,N'*-dioxide repeating unit, does possesses the lowest Stokes shift.

Electrochemical band gap determination was attempted for the bithiazole-containing conjugated polymers using cyclic voltammetry; however, difficulty obtaining these measurements led us to use linear sweep voltammetry (LSV) instead. LSV was performed in the solid state after drop casting a solution of the polymer onto the platinum working electrode. As expected, voltammetry measurements of both polymer series **P8** and **P9** displayed a reduced HOMO-LUMO gap upon increased level of bithiazole *N*-oxidation. As seen previously in the voltammetry data of the small molecule series, the

decrease in the HOMO-LUMO gap from *N*-oxidation occurs through both a lowering of the LUMO and a raising of the HOMO. In the polymer set **P8**, the voltammetry determined HOMO was raised roughly 0.05 eV with each successive oxidation. This raising of the HOMO was accompanied by a slight lowering of the LUMO by 0.06 and 0.09 eV following each respective oxidation. In set **P9**, the lowering of the LUMO between the **P9a** and **P9b** was much more drastic at 0.25 eV. While the lowering of the LUMO energy level upon increasing *N*-oxidation of the system was expected, it was a surprise to discover that conversion the bithiazoles to *N*-oxides (or *N,N'*-dioxides) resulted in an increase in the energy of the HOMO as well, indicating that the polymers become easier to oxidize. This trend is unlike that observed upon the addition of alkoxy substituents to poly(heteroarenes) (such as PEDOT), in which HOMO-LUMO gap is reduced through planarization, however, it is accompanied by an increase in both the HOMO and LUMO due to the large electron-donating effects of these substituents. The physical, optical and electrochemical properties of polymer series P7 through P9 are tabulated in Table 3.2.

Table 3.2 – Summary of electronic and physical properties for polymer series **P7-P9**.

Entry	Mn (kDa)	PDI	HOMO (eV)	LUMO (eV)	Eg_{EC} (eV)	Eg_{Opt} (eV)	Abs_{Max} (nm)	Em_{Max} (nm)	Stokes Shift (nm)
P7a	50.0	3.2				2.51	445		
P7b	15.1	2.0				2.44	455		
P7d	13.2	2.2				2.50	441		
P7e	11.5	2.1				2.44	456		
P8a	18.2	2.3	-5.75	-2.80	2.95	2.61	417	482	0.41
P8b	37.0	2.2	-5.69	-2.86	2.83	2.51	427	491	0.38
P8c	14.0	2.3	-5.65	-2.95	2.70	2.41	441	491	0.29
P9a	20.6	2.2	-5.67	-2.71	2.86	2.61	396	523	0.76
P9b	17.0	2.7	-5.57	-2.96	2.61	2.56	404	540	0.77
P9c	6.0	2.0	-5.53	-3.02	2.51	2.41	423	533	0.61

3.3.3 Electronic effect of *N*-oxidation

Due the planar nature of 2,2'-bithiazoles, it remained unclear whether this observed bathochromic shift upon successive oxidation was, in fact, occurring due to the rigidification of planarity in the conjugated system, or rather if *N*-oxide incorporation simply instilled an electronic effect. This electronic effect could be a result of the *N*-oxide functional group acting as both an electron-donating and electron withdrawing group, forming a push-pull system by reduction in the LUMO and increase in the HOMO. To untangle this, we first sought the absorption spectra thiazole-*N*-oxides in non-bithiazole systems, as they would be incapable of possessing any S – O chalcogen bonding interactions. Any change in the optical band gap upon *N*-oxidation would therefore be solely due to incorporation of the *N*-oxide and the electronic effects it instills on the molecule. Phenylthiazole (**3.7a**) and thiophenylthiazole (**3.8a**) were synthesized via direct arylation prior to being oxidized to the corresponding *N*-oxides **3.7b** and **3.8b**. Oxidation using *m*-CPBA proceeded poorly on these 2-unsubstituted thiazoles (as discussed in *Chapter 2*), though enough product for analysis was obtained. The UV-Vis absorption spectra for both the thiazole (**3.7a**/**3.8a**) and thiazole-*N*-oxides (**3.7a**/**3.8a**) were obtained in $CHCl_3$. To our surprise, a slight bathochromic shift was present in the onset of absorption between **3.7a** and **3.7b**, however, the absorption maximum (Abs_{max}) remains relatively constant. This indicates that *N*-oxidation does in fact have some electronic effect on the band gap, even without the ability for chalcogen bonding, though the bathochromic shift was less than that observed for a single *N*-oxidation in the bithiazole small molecules (Figure 3.17). The same observation was made for **3.8a** and

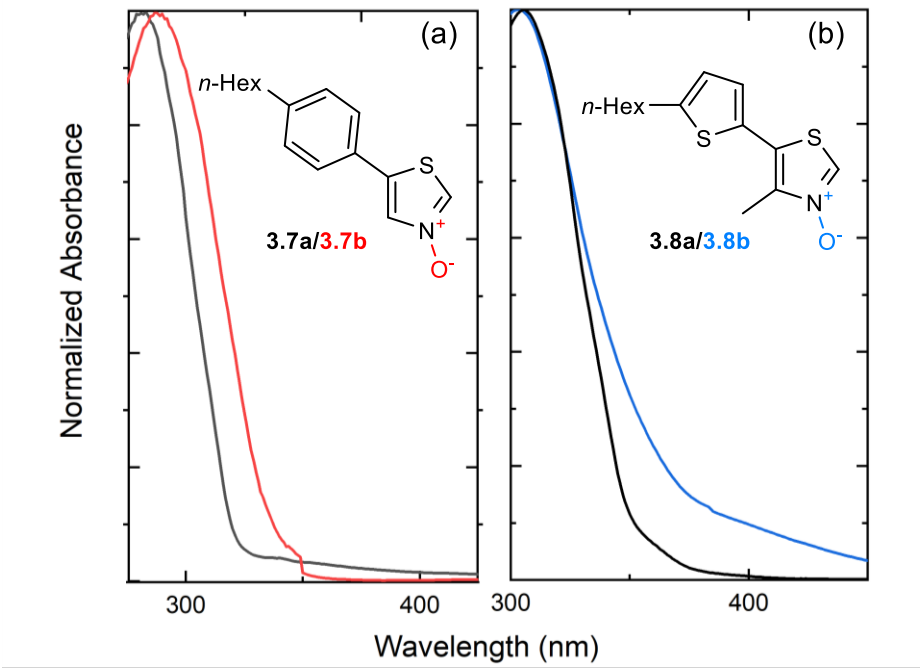

Figure 3.17 – UV-Vis absorption spectra of a) thiazoles **3.7a** (black) and **3.7b** (red) b) thiazoles **3.8a** (black) and **3.8b** (blue).

3.8b, although, to an even smaller degree. As this experiment did not completely clarify the origin of the HOMO-LUMO gap decrease, we instead turned our attention to employing computational methods to further our understanding of *N*-oxide incorporation in bithiazoles.

3.3.4 Computational analysis

To begin our computational investigation into the effects of *N*-oxidation on bithiazole systems, Density Functional Theory (DFT) optimized structures of bithiazoles **3.1a**-**c** were calculated (Figure 3.18a). As expected, the optimal geometry for 2,2'-bithiazole (**3.1a**) possessed a completely planar N-C-C-N dihedral angle, as did the single *N*-oxide **3.1b** and *N*,*N'*-dioxide **3.1c**. If no favourable interaction were occurring between *N*-oxide oxygen and adjacent thiazole sulfur, a slight disruption of planarity to reduce steric interactions would have been expected. On the computed optimized structures,

time-dependant (TD)-DFT calculations were performed in order to generate theoretical UV-Vis absorption spectra based on calculated HOMO and LUMO energies. Somewhat to our surprise, despite the constant 180° N-C-C-N dihedral across molecules **3.1a-c**, a significant bathochromic shift (and reduction in the optical band gap) is suggested upon increasing *N*-oxidation level (Figure 3.18b). Although 2,2'-bithiazoles were known to be planar, we expected that an increased rigidity through conformational locking by S-O interactions could still enable enhanced p-orbital overlap and be responsible for the bathochromic shift observed in our experimental absorption spectra. However, based on

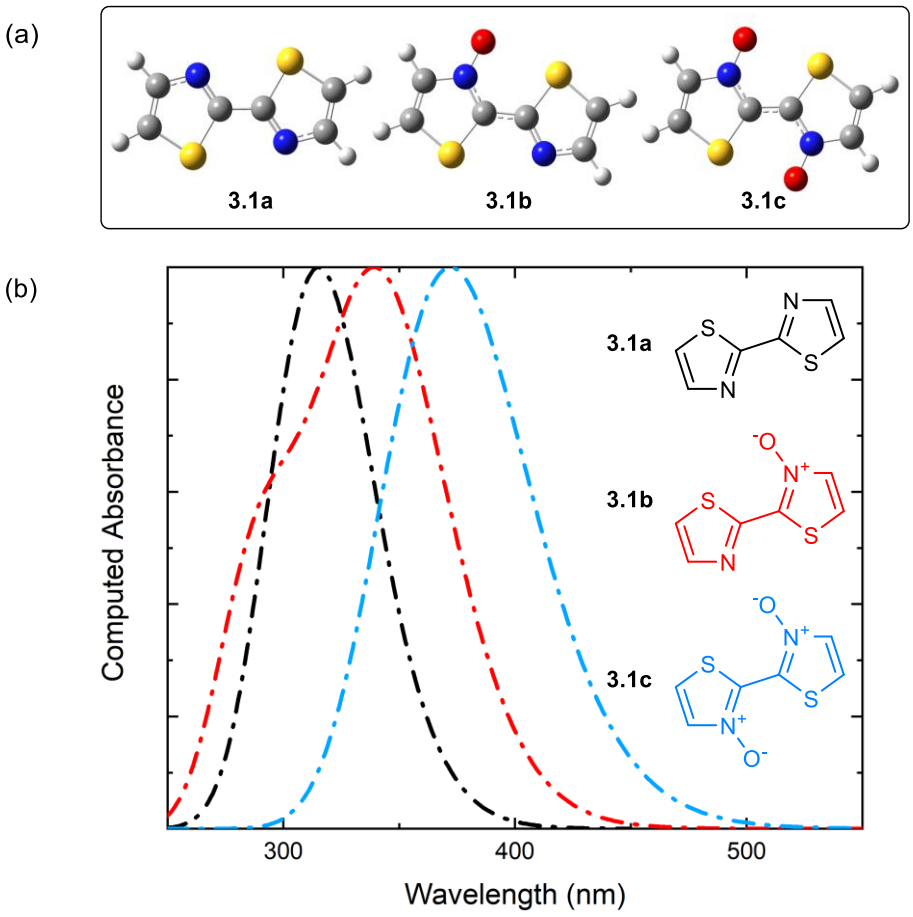

Figure 3.18 – a) DFT optimized structures of bithiazoles **3.1a**, **3.1b**, and **3.1c** b) Computed UV-Vis absorbance spectra from TD-DFT calculations

these TD-DFT calculations, it appears that this is not the case. The decrease in optical band gap observed experimentally for our explored bithiazole series is, therefore, assumed to be due to simply the electronic effects of *N*-oxide incorporation.

To confirm that the bathochromic shift was not a result of S-O chalcogen bonding interactions, the same TD-DFT analysis was performed on the DFT optimized structures of 2,2'-bioxazole (**3.9a**), as well as its singly (**3.9b**) and doubly oxidized (**3.9c**) derivatives. The optimal structures of these bioxazoles also possess an N-C-C-N dihedral of 180°, however, there exists no opportunity for S-O chalcogen bonding interactions. Despite this, the TD-DFT calculations continue show a similar bathochromic shift upon each successive *N*-oxidation of 2,2'-bioxazole, further suggesting that it is simply the electronic effects of *N*-oxide incorporation that is leading to a decrease in the HOMO-LUMO gap (Figure 3.19).

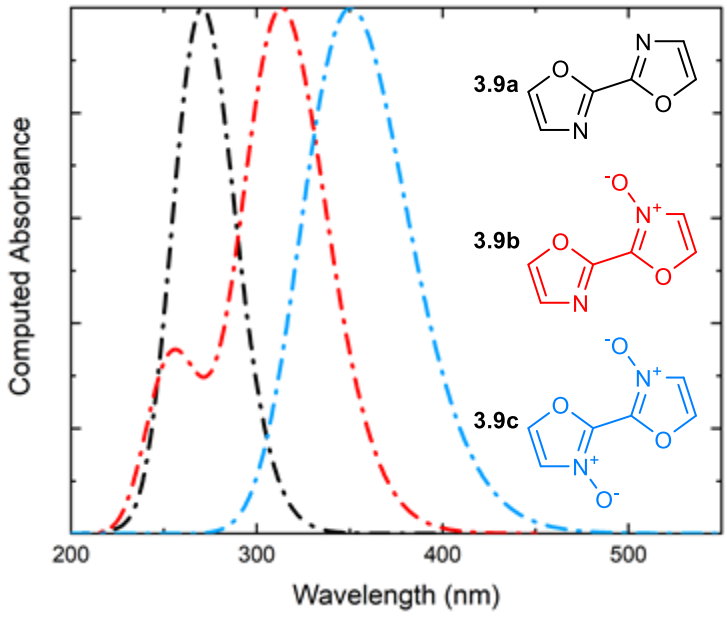

Figure 3.19 – Computed UV-Vis absorbance spectra of bioxazoles **3.9a**, **3.9b**, and **3.9c** from TD-DFT calculations.

The relatively large effect of *N*-oxidation on the optical band gap in the bithiazoles series (**3.1**, **3.2**, **3.3**, **3.5**) in comparison to the monomeric thiazoles (**3.7** and **3.8**) is attributed to establishment of a push-pull polarization through the bithiazole structure (Figure 3.20a). An analogous example of this is in the comparison of the highly coloured indigo to its monomeric form: 3-indolinone, which is uncoloured. The observed optical properties of indigo are attributed to the presence of the diketo-diamino-ethylene molecular centre and push-pull effects therein (Figure 3.20b).[190]

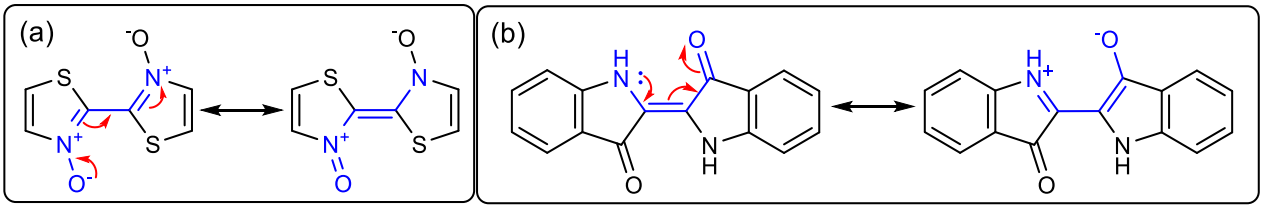

Figure 3.20 – Push-pull effect in a) bithiazole-*N,N'*-dioxide b) indigo.

Although the decrease in HOMO-LUMO gap upon successive *N*-oxidation (determined by optical and electrochemical analyses) could be concluded to be independent of any potential chalcogen bonding interactions, we still suspected these interactions to be responsible for the observed decrease in Stokes shift and presence of vibrational fine structures in the absorption spectra which are often attributed to molecular rigidity. Additionally, this molecular rigidity would likely also explain the thermal properties observed in the DSC of bithiazole series **3.3** and **3.5,** as well as the decreased solubility of *N*-oxide-containing small molecules and polymers, as these attributes are often due to a high level of supramolecular interactions (such as π-stacking).

To analyze the rigidity of bithiazole-*N*-oxide systems, we first looked to the extensive computational analysis of conformational locks by Ratner and coworkers in which the torsional potential of a biaryl is determined through rotation of the biaryl

dihedral.[181] To determine the energy of rotation about the N-C-C-N dihedral angle, the same torsional barrier analysis was conducted on bithiazoles **3.1a-c**. Coupled cluster (CCSD(T)) single point energy calculations were executed on the DFT optimized structures of compounds **3.1a-c**, with the dihedral angle of interest scanned from 90° < θ < 180° in 10° intervals (Figure 3.21). From these calculations, we were able to determine that the energy barrier to break bithiazole planarity (that is, to rotate from a N-C-C-N dihedral angle of 180° to 90°) increased with successive *N*-oxidation from 7.5 to 10.4 to 14.5 kcal/mol for **3.1a**, **3.1b**, and **3.1c**, respectively. The dihedral angles from 0° to 90° were omitted from this analysis due to the high steric barrier caused by the oxygen atoms becoming eclipsed in the *N,N*'-dioxide **3.1c**. This computed rotational barrier of compound **3.11c** from an N-C-C-N dihedral angle of 180° to 90° is notably high when compared to the torsional barrier of approximately 6 kcal/mol reported by Ratner and co-workers for biaryls possessing S-O interactions.[181] Ratner also suggested that non-covalent interactions are minor factors in most cases wherein steric bulk contributes to the high torsional barrier; however, the limited steric bulk of bithiazoles **3.1a-c** clearly indicates that the S-O interactions in this case are likely the cause of the increased stability upon planarization.

Once again, in comparison with the bithiazoles, the torsional barrier of the equivalent bioxazole series **3.9** was also computed by CCSD(T) energy calculations on the DFT optimized structures (scanned from 90° < θ < 180° in 10° intervals) (Figure 3.22). Not only is the torsional barrier for all bioxazoles (**3.9**) significantly less than those computed for bithiazoles (**3.1**), the torsional barrier decreases with incorporation of *N*-oxides. This is likely due to the addition of the *N*-oxide functionality, without the ability to

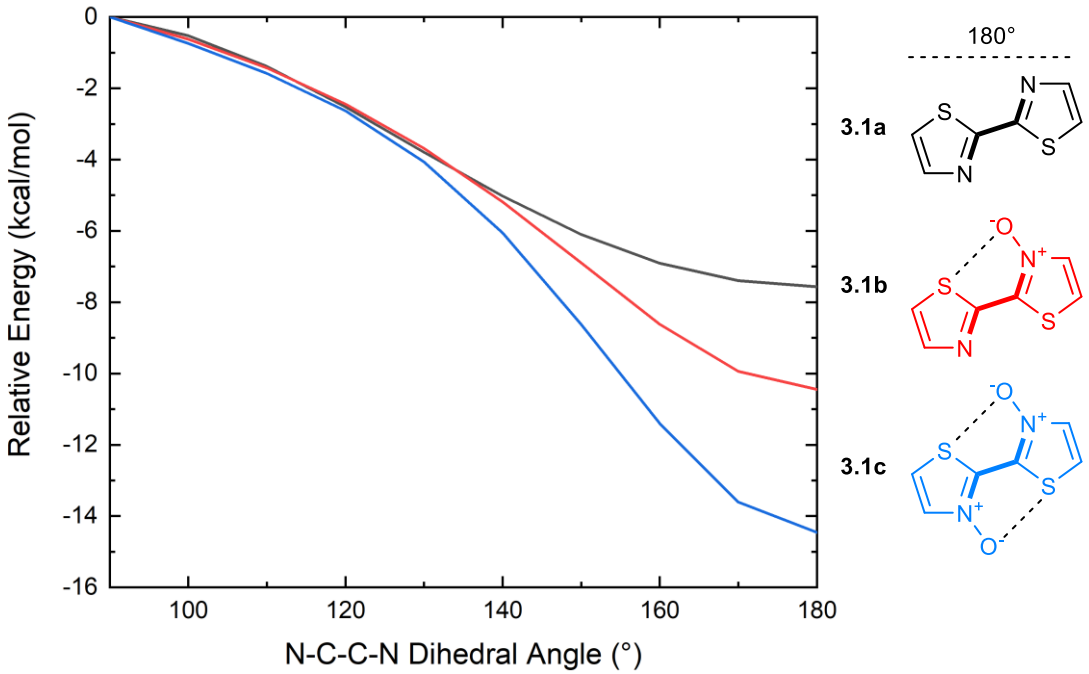

Figure 3.21 – Relative single-point energies of **3.1a-c** for N-C-C-N dihedral of 90° to 180° in 10° increments (dihedral bonds denoted in bold).

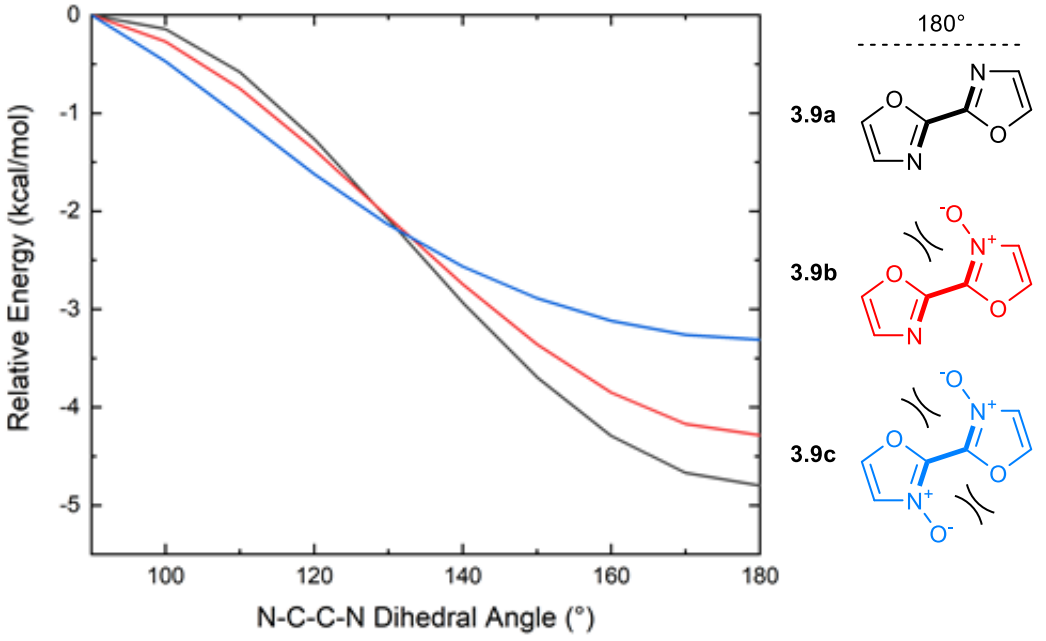

Figure 3.22 – Relative single-point energies of **3.9a-c** for N-C-C-N dihedral of 90° to 180° in 10° increments (dihedral bonds denoted in bold).

chalcogen bond, only leading to negative steric repulsion with the eclipsed oxazole ring in the 180° conformation.

To deconvolute the important intramolecular interactions that contribute to geometric and conformational preferences, we next pursued the use of NBO analysis on our bithiazoles. NBO calculations were performed on the DFT optimized structures of bithiazoles **3.1b** and **3.1c** in order to determine if a donation of electron density from the *N*-oxide oxygen to the adjacent thiazole sulfur is present. When analyzing the second order perturbation energies between the oxygen lone pairs (donor, LP) and sulfur-carbon antibonding orbital (acceptor, BD*), it was calculated that there is a 3.34 kcal/mol stabilization energy provided by this interaction in **3.1b**. Furthermore, NBO analysis of

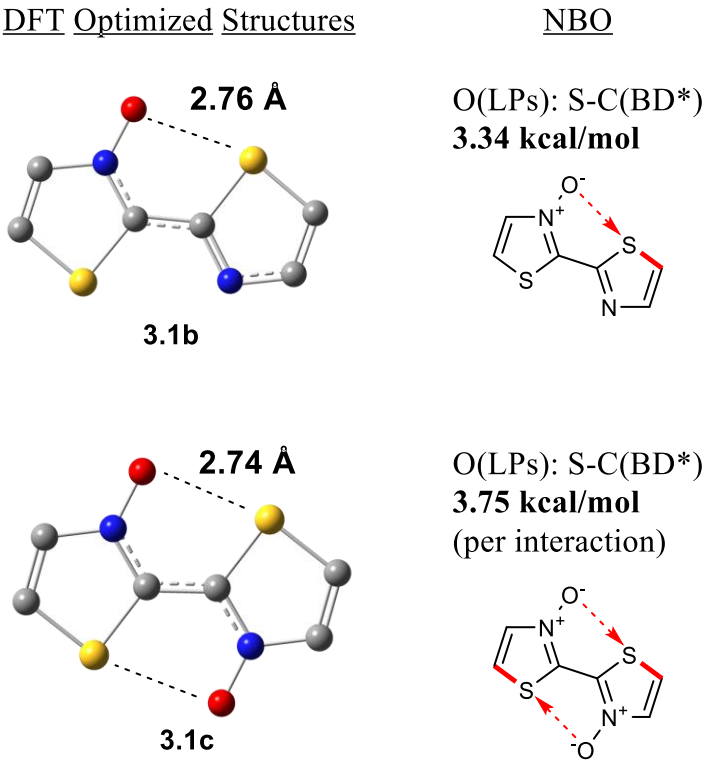

Figure 3.23 – S – O stabilization interactions determined through natural bonding orbital (NBO) calculations on the DFT optimized structures of **3.1b** and **3.1c**.

3.1c concluded that there exists a total of 7.49 kcal/mol increase in stabilization energy from the two S-O interactions (Figure 3.23). These values correspond well to the stabilization energy predicted from comparing the relative energies of **3.1a** to **3.1b** and **3.1c** at an N-C-C-N dihedral of 180°.

Although not necessarily the cause for interaction between *N*-oxide-O and thiazole-S, it is worth nothing that the computed bond distance between the two atoms in the DFT optimized structures of **3.1b** and **3.1c** are ~ 2.75 Å, well less than the combined van der Waals radii of the two atoms (3.25 Å), and consistent with previously calculated S-O chalcogen bond distances.[63] These computed bond distances are also consistent with the 2.74 Å S-O bond distance previously reported for our single crystal x-ray structure of **2.7**.[145]

Additional support for the presence and strength of chalcogen bonding in bithiazoles **3.1b** and **3.1c** was provided using AIM analyses.[184] AIM analysis of the bithiazoles denoted a bond critical point (BCP) (symbolised by a green dot in Figure 3.24a) between the *N*-oxide oxygen and thiazole sulfurs of both **3.1b** and **3.1c**. The charge densities (ρ) of 0.0199 and 0.0210 a.u. at the BCPs of this interaction, for **3.1b** and **3.1c** respectively, indicate incipient chemical bonding in between the range of that expected for hydrogen-bonding ($\rho \approx 10^{-3}$–10^{-2} a.u.) and to covalent bonding ($\rho > 10^{-1}$ a.u.). The positive Laplacians ($\nabla^2\rho$) of +0.0622 (**3.1b**) and +0.0642 a.u. (**3.1c**) at the BCPs are also indicative of electron density donation, like that found in hydrogen-bonding (whereas Laplacians of< 0 are more indicative of the electron sharing found in covalent bonds).[191] This S – O interaction contributes to some of the populated, molecular orbitals observable in Figure 3.24b.

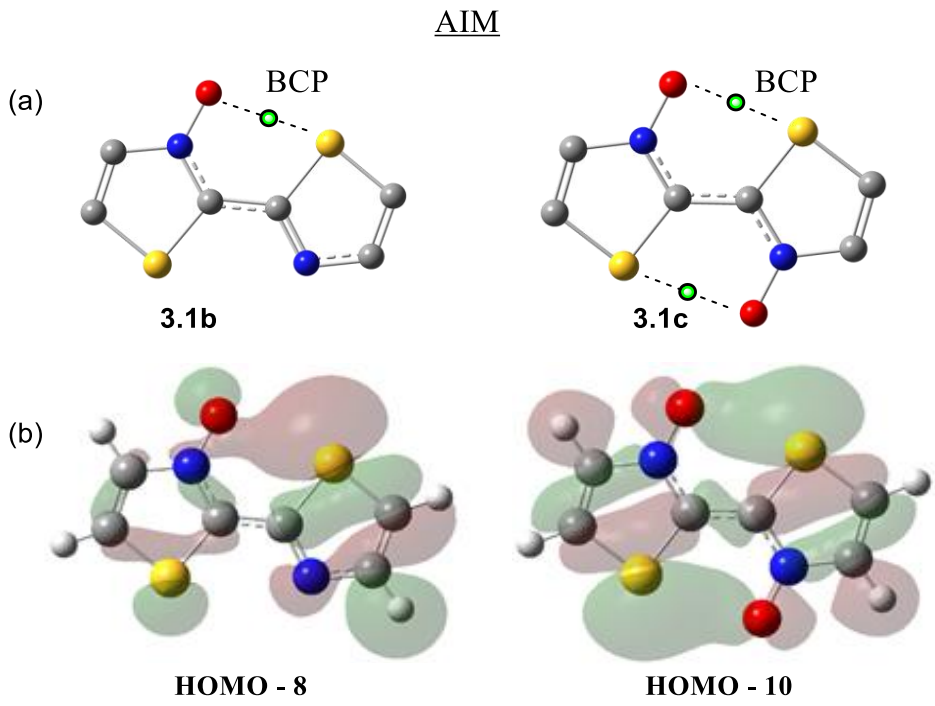

Figure 3.24 – a) Bond critical points (BCP) computed by AIM calculations (green dot) b) high lying populated molecular orbitals showing donation from the oxygen lone pair to the S-C antibonding orbital.

Having obtained the results of the NBO and AIM computational study on *N*-oxides **3.1b** and **3.1c**, we were interested as to how these values compared to other previously studied non-covalent interactions for conformational locking, including: F – S and ether O – S interactions. We, therefore, performed NBO and AIM analysis on a model bithiophene possessing a 3-F substituent (**3.10**) as well as a bithiophene possessing a 3-OMe substituent (**3.11**) in order to probe these two interactions. For consistency, analysis was also performed on 2-(thiophen-2-yl)thiazole-*N*-oxide (**3.12**) such that the sulfur acceptor is in the same thiophene environment (Figure 3.25). The AIM analyses for all model compounds did, indeed, display BCPs between the F/O donor and thiophene S acceptor, with, the expected positive Laplacian values indicative of electron density donation rather than shared electrons. The AIM charge densities of the F- (ρ = 0.0105 a.u.) and MeO-substituted (ρ = 0.0133 a.u.) compounds were significantly lower than the thiazole-*N*-

oxide-containing compound (ρ = 0.0209 a.u.) indicating a weaker interaction between the donor and the sulfur and more along the lines of a hydrogen bond.

NBO analysis was once again used to observe the nature of the non-covalent interactions in the model substrates **3.10** – **3.12**. The second order perturbation energies showed some stabilization from electron donation of the donor lone pairs into the S – C antibonding orbital of the adjacent thiophene. However, the stabilization energy provided by this interaction in substrates **3.10** and **3.11** equated to only 0.57 kcal/mol (-F) and 1.14 kcal/mol (-OMe), respectively. The model *N*-oxide **3.12**, on the other hand, contributed

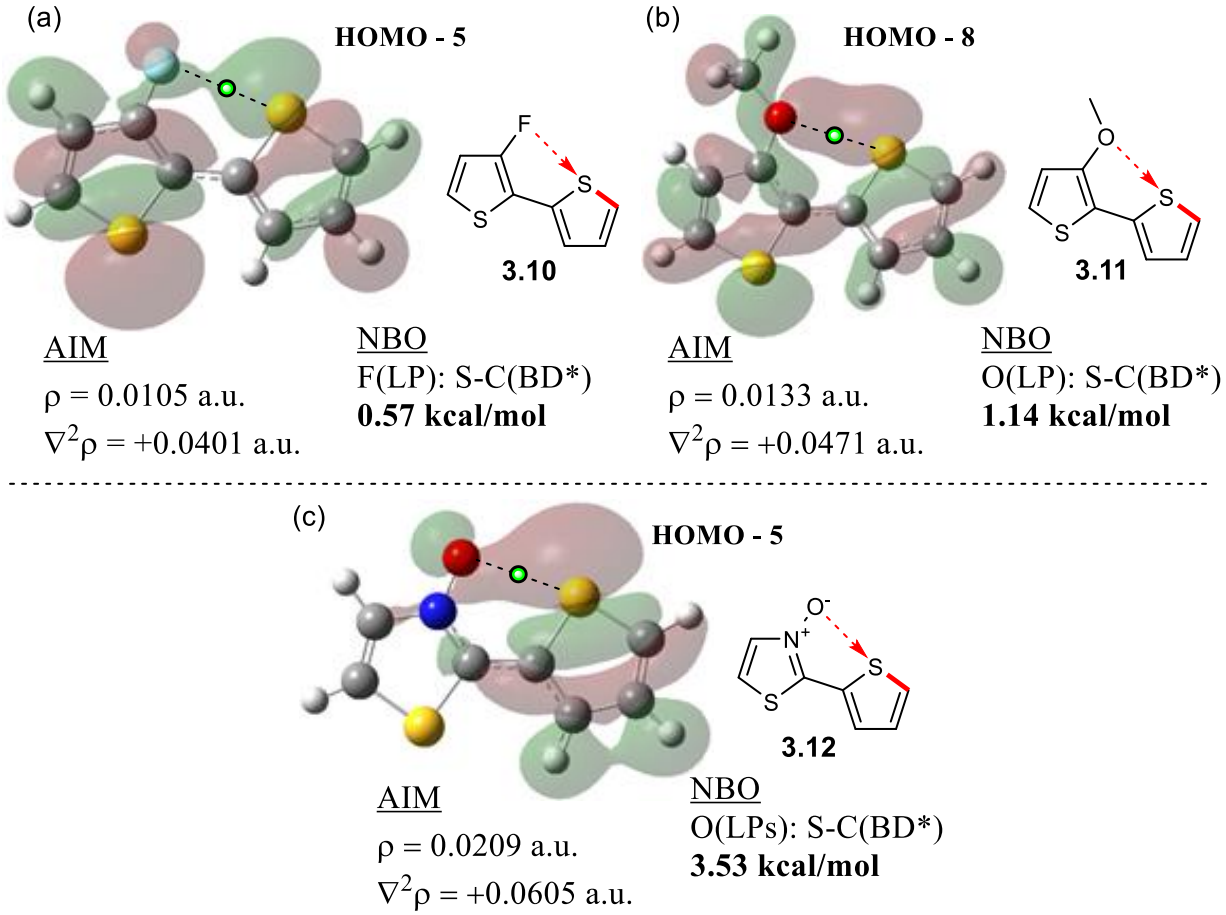

Figure 3.25 – Results of AIM and NBO analyses showing a) F – S (**3.10**) b) ether O – S (**3.11**) and c) *N*-oxide O – S (**3.12**) non-covalent interactions. BCP denoted with green circle.

3.53 kcal/mol in stabilization energy, in line what was had been observed for bithiazoles **3.1b** and **3.1c**, indicating that the nature of the S-acceptor, whether it be thiophene or thiazole, does not play a large part. This extensive computational analysis confirms that these chalcogen bonding S – O interactions found in bithiazole-*N*-oxides and *N,N'*-dioxides are substantial non-covalent interactions that can contribute towards rigidity of the bithiazole system. These interactions are also far greater in bond strength to other previously reported non-covalent interactions exploited to induced conformational locking in conjugated polymers.

3.4 Conclusions and Outlook

Developing new strategies to modify the electronic and physical properties of conjugated polymers remains an imperative task for their widescale deployment in next-gen electronics. Exploiting phenomena such as chalcogen bonding and other non-covalent interactions to induce planarity or affect the supramolecular interactions of conjugated small molecules and polymers has become commonplace. We have identified a new type of chalcogen bonding in conjugated small molecules and polymers possessing bithiazole-*N*-oxide and *N,N*'-dioxide motifs. While *N*-oxidation does instil what we believe is an acceptor-donor electronic effect on the conjugated system, analysis of the band gaps of model compounds has shown this effect to be minimal. The presence of vibronic fine structures in the absorption spectra, decrease in the Stokes shift upon bithiazole N-oxidation, as well as a decrease in solubility and increase in thermal stability, are indicative of rigid molecular system. This rigidity has been attributed to strong chalcogen bonding S − O interactions occurring between the N-oxide and adjacent thiazole sulfur. An extensive computational investigation carried out on these systems has revealed an

increase in torsional barrier about the bithiazole bond by an average of 3-4 kcal/mol per oxygen installed, resulting in the more rigid conjugated system. Furthermore, NBO and AIM analysis were used to evaluate the strength of the N-oxide – sulfur interaction, which was found to be far greater in bond strength than other commonly employed S – O or S – F chalcogen bonding interactions. The ease of oxygen transfer for the formation of thiazole N-oxides compared to the synthetic difficulty of installing alkoxy or fluorine substituents makes this an attractive method to induce rigidity in conjugated materials for organic electronic applications.

4

Direct Arylation Polymerization of 4,4’-Dialkoxybithiazoles

4.1 Background

Throughout our exploration into the use of thiazoles in conjugated small molecules and polymers, it became apparent that one facet of these materials that has yet to be thoroughly explored is the inclusion of 4-alkoxy substituents. As previously touched-on, alkoxy-substituents have long been employed in polythiophenes, such as poly(3,4-ethylenedioxythiophene) (PEDOT), and often induce planarity through O – S, or even O – H, interactions. In many instances, this allows for the inclusion of solubilizing chains into the conjugated materials backbone, without suffering from the undesirable torsional effects caused by negative steric interactions. Unfortunately, equipping already-electron rich thiophene conjugated materials with strong electron-donating groups leads to a

raising of the HOMO and LUMO by around 0.3-0.5 eV.[192] Instead, if alkoxy chains were to be incorporated into a more electron-poor aromatic ring such as thiazole, the electron-donating effects of the alkoxy groups may not have as detrimental an effect on the HOMO energy compared with thiophenes, all while still imparting the desired conformational locking and solubilizing effects (Figure 4.1).

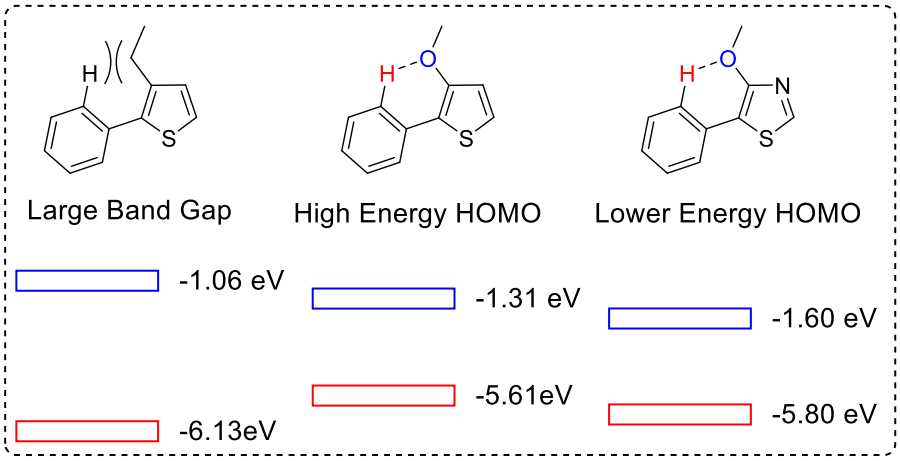

Figure 4.1 – DFT calculated HOMO and LUMO energy levels for phenylthiophene and phenylthiazole possessing alkyl or alkoxy substituents (B3LYP/6-311++g(d,p)).

4.1.1 Alkoxythiazoles in conjugated materials

The first instance of the dialkoxybithiazole motif appearing in the literature for use in conjugated materials was in the development of fluorophore switches by Beckert in 2011 (Scheme 4.1).[193] Proceeding via a double Hantzsch thiazole synthesis, 5,5'-diphenyl-[2,2'-bithiazole]-4,4'-diol was obtained from two equivalents of ethyl 2-bromo-2-phenylacetate and dithiooxamide in pyridine at 100 °C. The resulting diol was then alkylated with ethyl iodide to yield the dialkoxy product. Interestingly, upon solving the single crystal x-ray structure of this product, Beckert and co-workers discovered that the conjugated small molecule was almost completely planar.[193] The torsion angle along the bithiazole bond was determined to be only 0.2° and the phenyl-thiazole torsion angle was

found to be 6.1°. This is significantly smaller than the phenyl-thiazole torsional angle of 32.6° found in the x-ray crystal structure of substrate **2.15b** (possessing 4-methyl substituents). Thus, it seems the alkoxy substituents are instilling planarity, likely through non-traditional hydrogen bonding with the adjacent phenyl substituents.

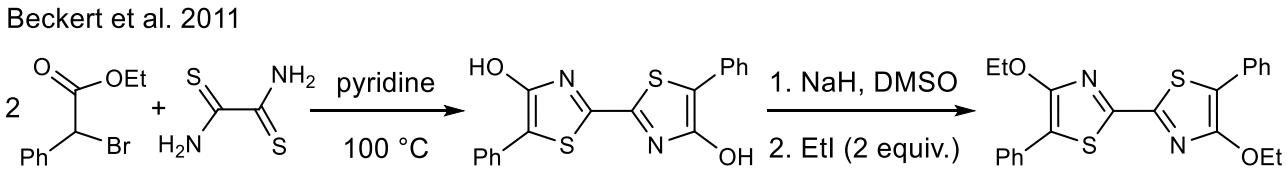

Scheme 4.1 – Synthetic route to 4,4'-dialkoxy bithiazole small molecules by Beckert and co-workers.[193]

In a seminal example by Marks and coworkers, several 5,5'-bithiazole-containing polymers were synthesized possessing either 2-ethylhexyloxy or *n*-dodecyloxy chains at the 4- and 4'-positions (Scheme 4.2).[194] These polymers indeed displayed promising properties including good solubilities from the inclusion of the long alkyl solubilizing chains and low band gaps. Computational modelling of the 5,5-bithiazole core revealed a high degree of planarity which was proposed to occur through S – O chalcogen bonding interactions. Additionally, the reduced steric interactions of the thiazole nitrogen were suggested to allow for planarization with the large neighboring arene units. As expected, the bithiazole conjugated polymers possessed a lower HOMO level (determined by CV) than those observed for equivalent 3-alkoxythiophene-containing polymers, due to the electron-deficient thiazole offsetting the electron-donating nature of the alkoxy chains. While the preparation of these 5,5'-bithiazoles clearly showcased new useful building block for the synthesis of conjugated polymers, synthesis of the bithiazole-monomer functionalized with organotin substituents for Stille coupling required a lengthy seven-step synthetic route from a commercially available 4-halothiazole.

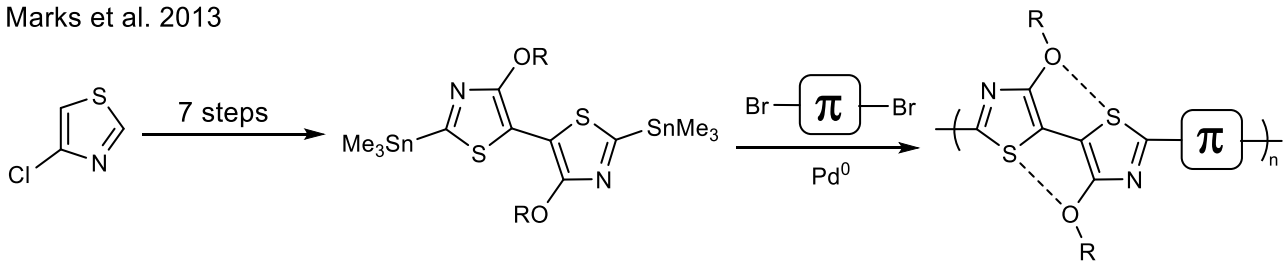

Scheme 4.2 – Synthetic route to 4,4'-dialkoxy-5,5'-bithiazole polymers by Marks and co-workers.[194]

The following year, Tajima and co-workers reported the synthesis of poly(4-hexyloxythiazole), a head-to-tail (2,5'-bithiazole) polymer, and its use in organic electronic device applications.[195] As expected, this polymer possessed a lower band gap than that of poly(3-hexyloxythiophene) due to the more electron-poor nature of the thiazole rings, while maintaining a high degree of crystallinity and packing similar to that of poly(3-hexylthiophene). The HOMO-LUMO gap of the HT polymer was computationally evaluated, as well as that of the 4,4'-dihexyloxy-2,2'-bithiazole polymer equivalent. While only the HT polymer was synthesized, these calculations revealed that the 2,2'-bithiazole equivalent polymer should possess a smaller HOMO-LUMO gap than that of the HT polymer.

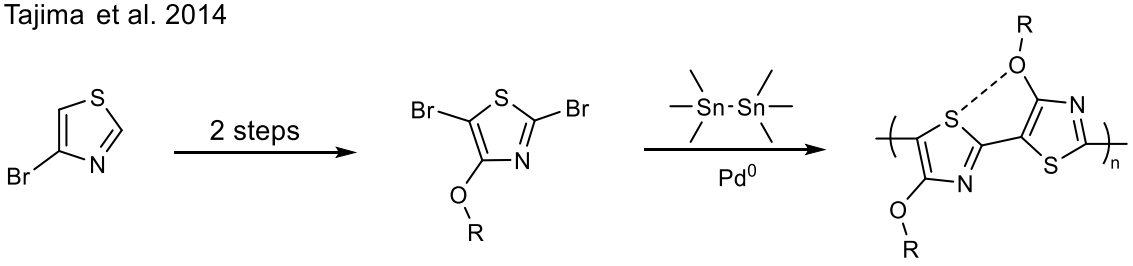

Scheme 4.3 – Synthetic route to a HT-4-alkoxythiazole polymer by Tajima and co-workers.[195]

4.1.2 C-H activation of electron-rich arenes

As previously discussed, direct arylation polymerization is naturally an attractive alternative to palladium-catalyzed polymerizations that require pre-functionalization of starting materials. Unfortunately, direct arylation is still not able to completely replace other cross-coupling methods as the success of DArP is dependent on the substrate being able to undergo C-H activation. Additionally, multiple C-H activation sites can lead to regioselectivity issues that can result in a loss of control over the polymerization. The C-H activation step in direct arylation proceeds through a concerted metalation-deprotonation (CMD) step in which the C-H activatable proton on the arene is deprotonated at the same time in which the aryl-palladium bond is formed.[103]

Our understanding of how the CMD mechanism is applicable to certain heterocycles, and what makes an arene able to undergo C-H activation, is gained through a computational distortion-interaction analysis of the transition state (TS). This analysis predicts the transition state barrier (E_a) as the sum of the distortion energies for the ground state palladium complex and the arene, subtracting the energetic favourability of interaction of the distorted fragments to form the transition state (Figure 4.2).[107] Distortion-interaction analysis of the direct arylation transition state has revealed several factors that influence the ability for C-H activation of an arene C-H. This has enabled one to predict an arene's ability to undergo C-H activation.[196] The first factor for undergoing C-H activation by CMD is to have a low energy of distortion for the arene C-H bond (E_{dist}(ArH)). While not a governing influence, a low distortion energy for the C-H bond is generally paralleled with having a high Brønsted acidity. Thus, arenes that are electron poor often possess C-H bonds capable of direct arylation due to the low energy of distortion. The

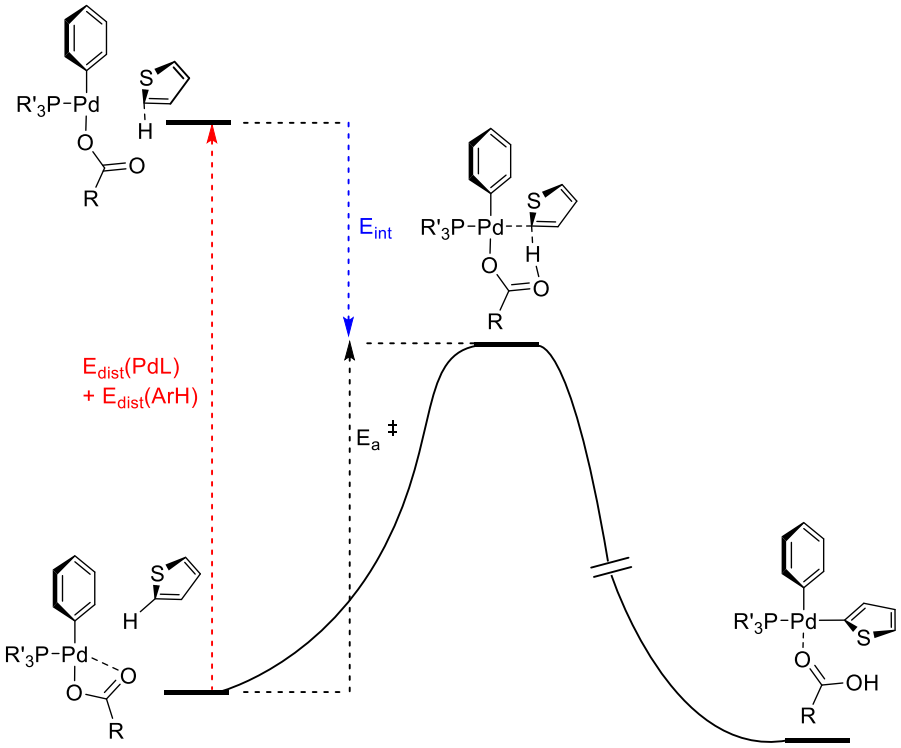

Figure 4.2 – Example distortion-interaction analysis for thiophene in the CMD transition state.

second factor for C-H activation ability is that the arene possesses a strong interaction with the palladium (E_{int}) in formation of the C-Pd bond, which reduces the TS energy. Generally, arenes which are electron rich at the C-H carbon, and therefore more nucleophilic, allow for strong C-Pd bonding interactions. In many instances of direct arylation both E_{dist}(ArH) and E_{int} are crucial to influencing the CMD transition state energy.[108] Thiazole, like many π-excessive 5-membered heterocycles, is a prime candidate for direct arylation, and undergoes C-H activation at the most nucleophilic position due to the high E_{int} between the 5-C and Pd.[197] Increased electron density at the thiazole 5-position should, therefore, increase the E_{int}, and result in a lower TS energy, increasing its propensity for C-H activation and direct arylation reactions [198]

4.2 Proposal[199]

Having explored a number of 2,2’-bithiazole-containing conjugated polymers previously, it became apparent that solubility of the polymers was a hurdle to reaching high molecular weights. The presence of solubilizing chains on the bithiazole unit in addition to those included on the conjugated spacer would assist in remedying this issue, however, the limited locations for installation of these chains (the thiazole 4-position) would without-a-doubt result in a loss in planarity of the π-system. It has become clear that instead of utilizing solubilizing alkyl chains, alkoxy chains on the bithiazole should allow for the desired increase in solubility, while also instilling planarity in the conjugated backbone. 4,4’-Dialkoxy-5,5’-bithiazole conjugated polymers had previously been well explored by Marks and co-workers, wherein S-O interactions allowed for planarization of the core bithiazole unit.[194] We instead hypothesized that a 2,2’-bithiazole-containing conjugated polymer with alkoxy chains at the 4- and 4’-position could allow for the desired increase in solubility, while also enabling planarizing non-covalent interactions. Based on the crystal structure produced by Beckert and co-workers,[193] we speculated that planarization of the conjugated system would be achieved through O – H or O – S interactions between the alkoxy sidechains with the π-spacer. This planarity would be in conjunction with the already planar geometry of the 2,2’-bithiazole due to the lack of repulsive C-H interactions at the 3-position (Figure 4.3). The effect of these alkoxy chains would, therefore, manifest in both the extent of polymerization (from increased polymer solubility), as well as in a decreased in the optical and electrochemical band gap (from planarity of the conjugated system).

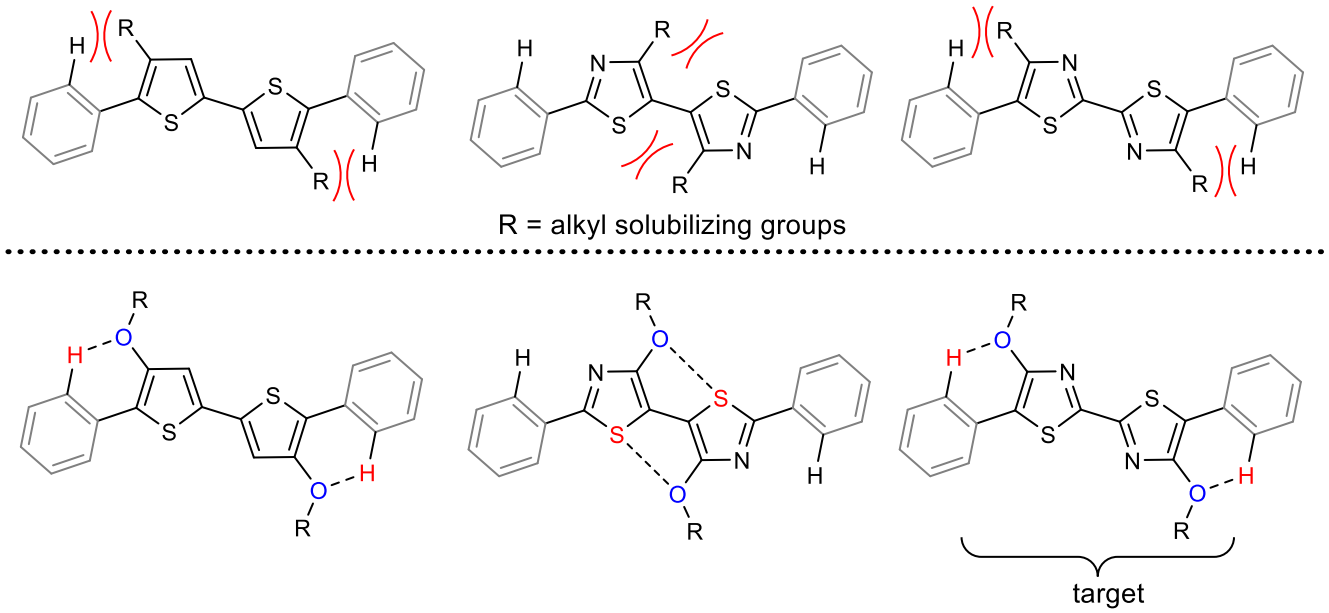

Figure 4.3 – Model bithiophene and bithiazole cores showing interaction with adjacent π-units (example: Ph).

Finally, in order to construct this polymer, a cross-coupling between various π-conjugated spacers and the dialkoxybithiazole monomers was envisioned. We speculated that the 2,2'-bithiazole monomers required for this polymerization, possessing two strongly electron-donating groups, would be prime candidates for direct arylation polymerization. The electron-donation of the 4-alkoxy substituents contributes to the nucleophilicity at the bithiazole's 5- and 5'-positions, increasing the E_{int} (relative to 4-unsubstitued thiazole), and increasing the rate of reaction (Scheme 4.4). Employing direct

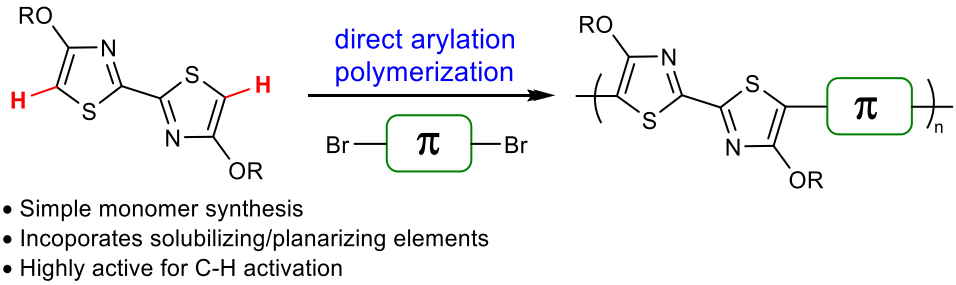

Scheme 4.4 – Proposed direct arylation polymerization using a 4,4'-dialkoxybithiazole monomer.

arylation polymerization for this reaction would represent a far simpler approach toward dialkoxybithiazole-containing polymers, compared to the 8-step route outlined by Marks and co-workers via Stille polycondensation.[194]

4.3 Results and Discussion

To determine if our substrates would indeed proceed well under direct arylation conditions, we first performed a computational disruption-interaction analysis of 4-methoxythiazole in the CMD transition state. Density functional theory optimized structures were elucidated for the two ground state species (the palladium complex and 4-methoxythiazole), as well as the CMD transition state, and the final thiazole-bound palladium complex (Figure 4.4). Additionally, the Gibbs free energies were calculated for the individual components of the transition state in order to determine the E_{dist}(PdL) and E_{dist}(ArH). The same analysis was performed for the CMD at the 5-position of unsubstituted thiazole, in order to compare the effects of the alkoxy-substituent on the energy of activation. The free energy of distortion (E_{dist}(ArH)) was not affected much by the addition of the methoxy-substituent; however, the energy of interaction (E_{int}) for the C-Pd bond formation was computed to be 1.7 kcal/mol larger for 4-methoxy thiazole compared to simply thiazole. This results in a transition state energy for the concerted-metalation deprotonation of 4-methoxythiazole that is lower relative to the ground state than the E_a for the CMD of thiazole. Therefore, as was predicted, C-H activation at the more electron rich (and more nucleophilic) 4-methoxythiazole 5-position, should more easily undergo the direct arylation C-H activation step than thiazole. As thiazole is already a heterocycle that is proven to proceed well in direct arylation reactions, because of its

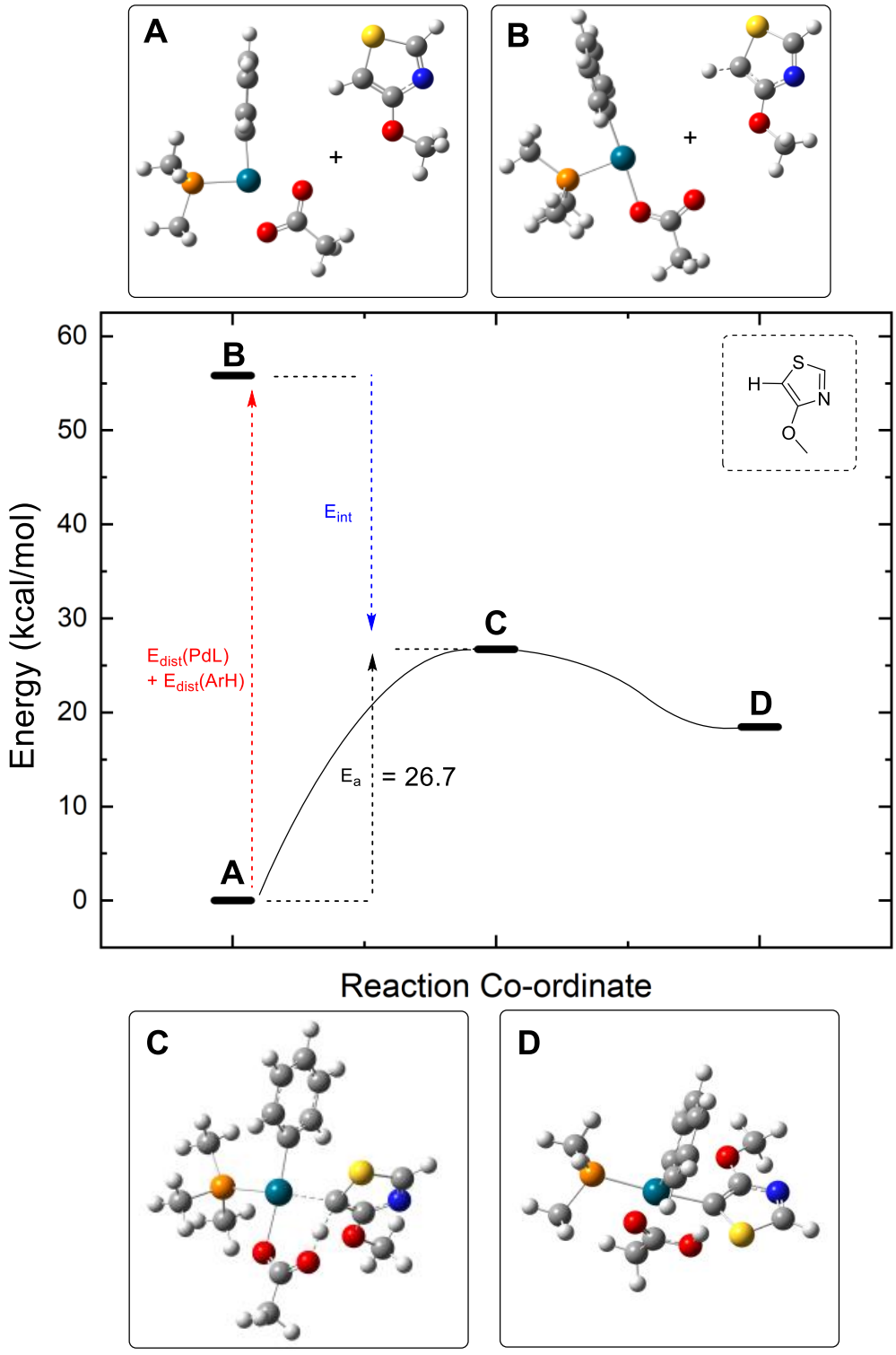

Figure 4.4 – Distortion-interaction analysis for model 4-methoxythiazole in the CMD transition state with DFT optimized structures.

ability to undergo CMD, we expect 4,4'-dialkoxy-2,2'-bithiazoles to proceed well as a substrate for direct arylation polymerization.

4.3.1 Monomer synthesis

Our retrosynthetic approach for the synthesis of the 2,2'-bithiazole monomer began with the bithiazole connection, thought to be achievable through homocoupling of 4-alkoxythiazoles by copper-mediated oxidative coupling (Scheme 4.5). The oxidative coupling of thiazoles had previously been reported in the literature to give the desired 2,2'-bithiazole connection, and had been previously used for the synthesis of **3.1a** and **3.2a**.[188] The required 4-alkoxythiazoles could, in-turn, be prepared through an Ullman-type coupling from the corresponding alcohol and 4-bromothiazole – a commercially available starting material. This route would produce our monomer for direct arylation in only two synthetic steps, as opposed to the six steps (from an equivalent starting material) completed my Marks and coworkers to reach their unfunctionalized 5,5'-bithiazole monomers.[194]

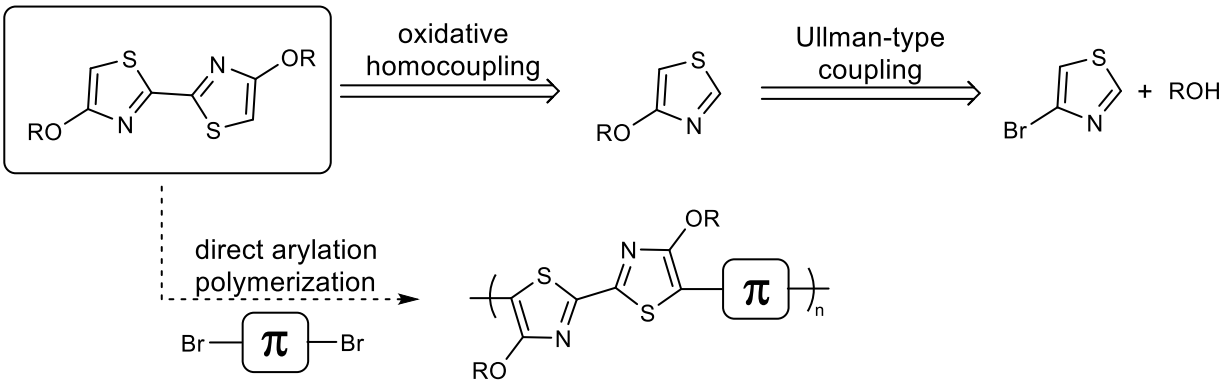

Scheme 4.5 – Retrosynthetic route to 4,4'-dialkoxybithiazole monomers.

Though 4-bromothiazole (23USD/g, Oakwood Chemical) is commercially available, we instead chose to begin our synthesis with the significantly more affordable

2,4-dibromothiazole (30USD/25g, Oakwood Chemical). 2,4-Dibromothiazole was converted to 4-bromothiazole (**4.1**) following a literature procedure in which *n*-BuLi was added to the starting material in anhydrous THF at -78 °C. [200] Lithium-halogen exchange occurs at the more active 2-bromine and the lithiated thiazole is then quenched with MeOH to yield the product **4.1** in upwards of 97% yield.

Next, the synthesized 4-bromothiazole (**4.1**) could then be converted to the 4-alkoxythiazole via Ullman-type coupling with the corresponding alcohol. 2-Ethylhexanol was chosen in order to deliver the solubilizing sidechains desired on the bithiazole monomer. Excess 2-ethylhexanol was deprotonated with NaH in dry THF to form the corresponding alkoxide over a 2 h reaction time. To this mixture was then added the CuI and **4.1,** and the reaction was heated at 80 °C in a sealed pressure vial. Upon purification by column chromatography, the desired 4-(2-ethylhexyloxy)thiazole (**4.2**) was obtained in a 47% yield (Scheme 4.6). If 2-ethylhexanol was used in gross excess, removal through chromatography proved a nuisance due to its similar polarity to the product and lack of UV fluorescence. Unfortunately, although some unidentifiable compounds did elute from the column, unreacted 4-bromothiazole (**4.1**) was never obtained, despite the mediocre yield. The yield of **4.2** from this reaction also seemed inconsistent upon further repetitions, with yields ranging from as low as 30% and as high as 60% being obtained.

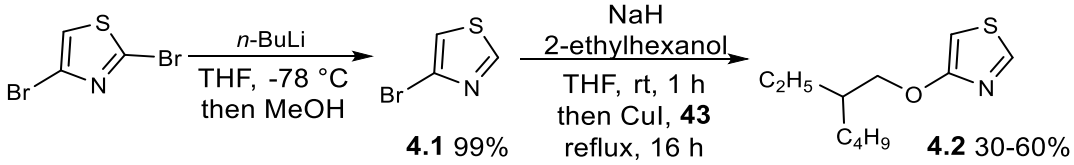

Scheme 4.6 – Debromination and Ullman-type coupling to yield 4-alkoxythiazole **4.2**.

The use of a stoichiometric amount of CuI, or switching the copper salt to CuBr, did not remedy this inconsistency.

With our alkoxythiazole in hand, the next step was to oxidatively homocouple **4.2** at the 2-position through the use of copper (II) acetate in xylenes. The conditions used previously for the synthesis of 2,2'-bithiazole **3.1a** were applied to this coupling. After 40 h at reflux, up to 96% of the desired monomer **4.3** was obtained following chromatography (Scheme 4.7). If starting material **4.2** was used impure in the oxidative coupling (ie: with 2-ethylhexanol), the impurities became even more difficult to remove from product **4.3**, rendering telescoping of the two reactions impractical. Monomer purity for direct arylation is key to ensuring a proper 1:1 stoichiometric ratio as excess of a single monomer can lead to many polymer chains possessing low molecular weights.

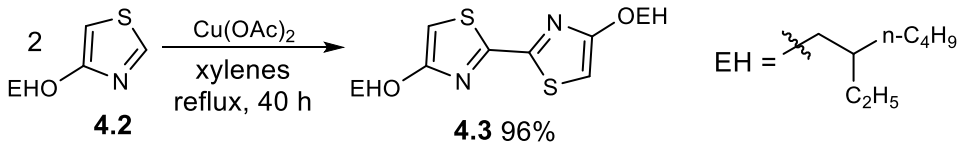

Scheme 4.7 – Oxidative homocoupling to yield dialkoxybithiazole **4.3**.

Due to the low yield in the preparation of **4.2**, and purification issues with this route, we attempted several alternate routes to synthesize the direct arylation monomer **4.3**. Having purchased 2,4-bromothiazole, we were interested to see if we could proceed to the 4,4'-dibromo bithiazole **4.4** via a classical Ullman coupling. We would then simply be able to exchange the two bromines for the alkoxy groups using CuI and the alcohol, and yield product **4.3**. In addition to this being a shorter route to our desired monomer, this would allow for an easier screening of various alkoxy chains on the bithiazole core for their effect on the degree of polymerization and electronic properties. To our surprise, this exact transformation had been reported in the literature using *n*-BuLi, followed by $CuCl_2$

to deliver product **4.4** in a 69% yield.[201] Unfortunately, following this literature precedent, the starting material was converted to a mixture of indeterminable product, none of which corresponding to the desired product **4.4** by ^{1}H NMR or MS (Scheme 4.8a).

Our final approach was to utilize a Hantzsch thiazole synthesis in order to build the 4,4'-dihydroxybithiazole **4.5** from dithiooxamide.[202,203] This method had been used to build similar compounds in the previously discussed work of Beckert and co-workers, although possessing phenyls in the 5- and 5'-positions.[193] Production of **4.5** would allow conversion to monomer **4.3** through simple deprotonation of the hydroxy groups, followed by alkylation. Following the literature precedent, we attempted the reaction with ethyl bromoacetate and dithiooxamide in pyridine at 110 °C, followed by the addition of ethanol and continued stirring at room temperature for 30 min (Scheme 4.8b). Unfortunately, the only identifiable product obtained from this reaction was the product of pyridine alkylation with ethyl bromo acetate. Attempts were made using less nucleophilic bases or no base, as well as varying the solvent and temperature; however, no product **4.5** was ever obtained. Thus, we remained committed to our initial route to monomer **4.3**.

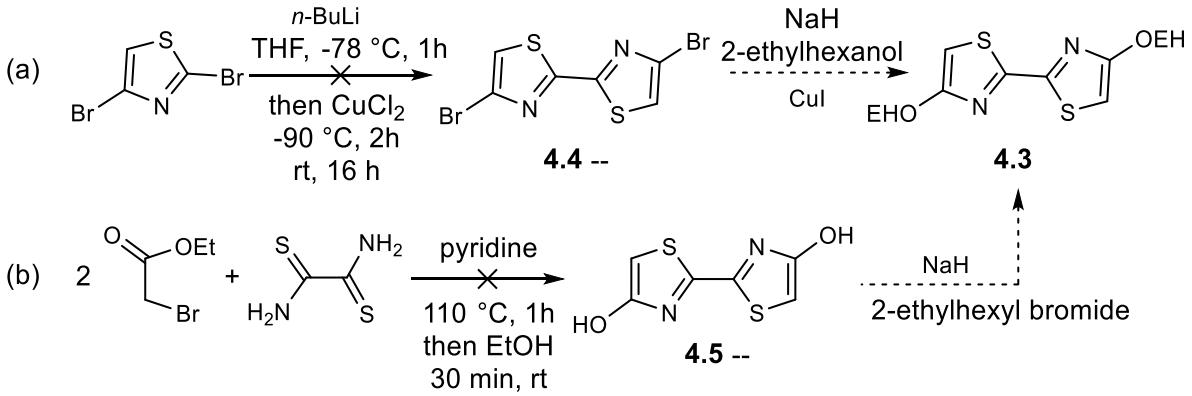

Scheme 4.8 – Alternate routes to dialkoxybithiazole **4.3**.

4.3.2 Polymer synthesis

With our monomer in hand, we proceeded with the use of the 4,4'-dialkoxy-2,2'-bithiazole in direct arylation polymerization. The polymerization was first attempted with 9,9-dioctyl-2,7-dibromofluorene using common DArP conditions (previously employed for the synthesis of **P8a** and **P9a**). As previously mentioned, ensuring an accurate ratio of monomers is important in AABB-type polymerizations for yielding high molecular weights polymers with a low PDI. Pure monomer **4.3** exists as a viscous liquid, and as such, a solution of the material in toluene was made and delivered to the reaction mixture. Bithiazole polymer **P10** was precipitated following the reaction and was characterized by GPC to have an Mw of 31.5 kDa, with a PDI of 2.7 (Scheme 4.9).

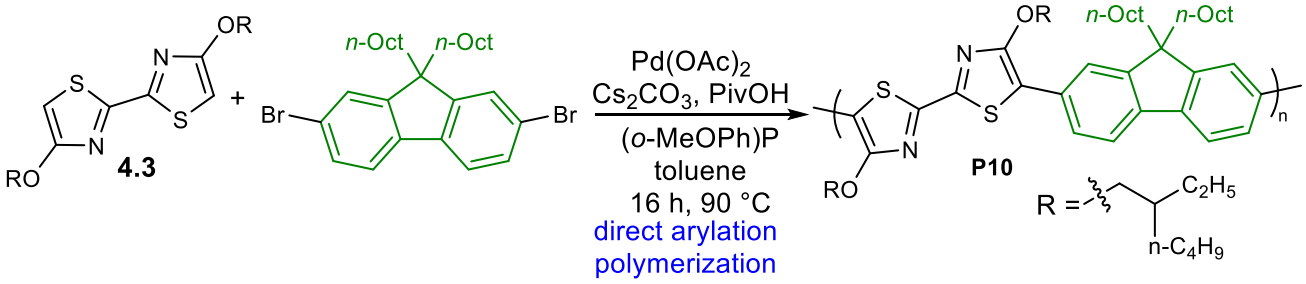

Scheme 4.9 – Direct arylation polymerization of a 4,4'-dialkoxy-2,2'-bithiazole monomer.

Of utmost importance was how the band gap of **P10** would compare to an equivalent bithiazole polymer which possesses only alkyl substituents, to gain insight into the electronic and planarization effects on the system. The 9,9-dioctylfluorene conjugated spacer had been selected for this comparison as the equivalent 4,4'-dinonyl-2,2'-bithiazole polymer equivalent (**P11**) had previously been prepared in our group by direct arylation polymerization (and been long reported in the literature), allowing for a direct comparison to **P10**.[204] The optical band gap of dialkoxy polymer **P10** was determined by

UV-Vis absorption spectroscopy in $CHCl_3$. To our delight, compared to **P11** which possesses alkyl substituents at the thiazole 4-positions, a large bathochromic shift is observed in onset of absorption of **P10**, resulting in a decrease in the optical band gap of 0.58 eV (Figure 4.5). This decrease in the optical band gap is far greater than the 0.12 eV decrease observed for simply increasing planarization from 4,4'-dimethylbithiazole polymer **P8a** and 4,4'-unsubstiuted polymer **P7a** (in Chapter 3). Likewise, the decrease in optical band gap is far greater than the 0.3 eV decrease

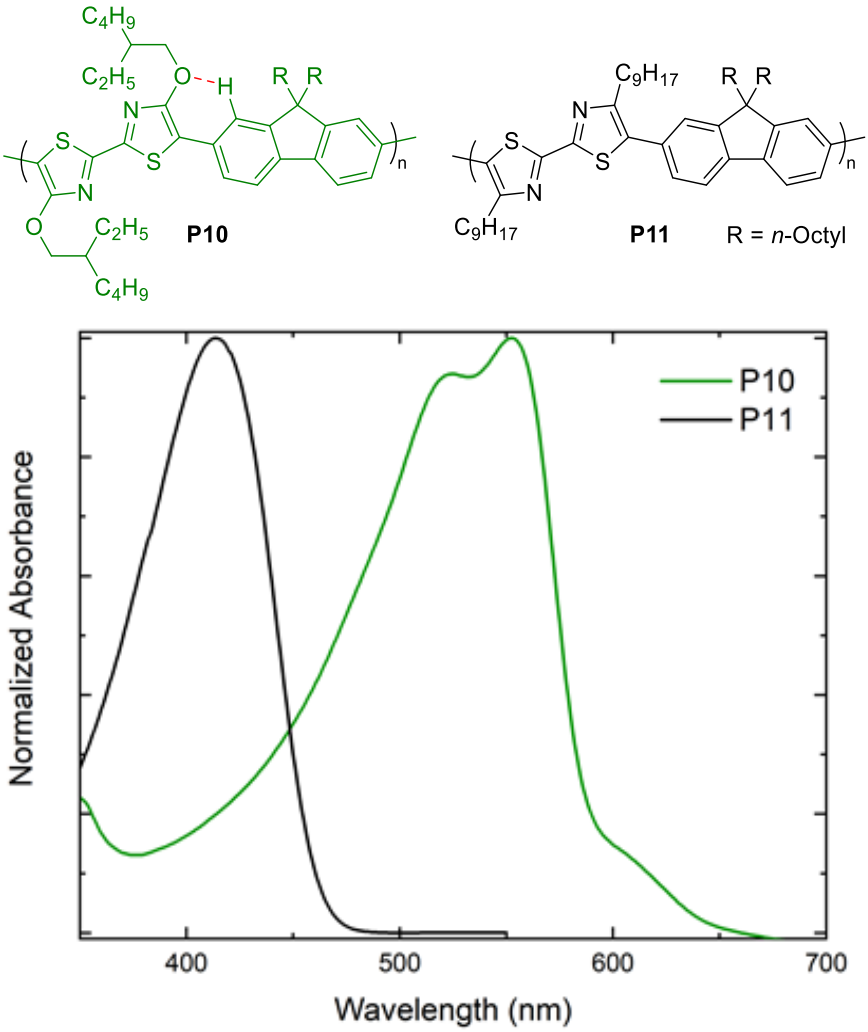

Figure 4.5 – UV-Vis absorption spectra for alkoxy polymer **P10** and equivalent alkyl polymer **P11**.

reported for poly(3-alkyoxythiophene)s (E_g = 1.6 eV) relative to poly(3-alkylthiophene)s (E_g = 1.9 eV).[192] It is likely that some combination of both O – H interactions with the fluorene unit, and the electron-donating effects of the oxygens, are resulting in the large bathochromic shift observed for the absorption of **P10**.

4.3.3 Polymer scope and properties

Having synthesized monomer **4.3** and confirmed its validity for direct arylation polymerization, we sought to investigate the scope of polymerization with various conjugated π-spacer units (Figure 4.6). In addition to the 9,9-dioctylfluorene polymer **P10**, dialkoxybithiazole monomer **4.3** was used to prepare polymers **P12** and **P13,** through DArP with 4-dibromo-2,5-bis(decyloxy)benzene and 2,5-dibromo-3,4-dihexylthiophene, respectively. Polymer **P12** was synthesized possessing an M_n of 14.7 kDa, while **P13** possessed an M_n of 8.6 kDa. The PDI's of both polymerizations were approximately 2.0, an expected polydispersity for conjugated polymers synthesized by direct arylation polymerization. We had anticipated that these polymerizations would proceed well as the polymer chain length would not be limited by solubility owing to the presence of solubilizing chains both on the bithiazole monomer and π-conjugated spacer.

With the inclusion of solubilizing chains on the bithiazole monomer, we were now able to attempt the polymerization of **4.3** with π-conjugated spacers possessing no additional solubilizing chains. Perhaps the simplest coupling partner, 1,4-dibromobenzene was employed in the polymerization with **4.3** to yield phenylene polymer **P14**. Although the bithiazole possesses the required solubilizing chains, **P14** was produced with a notably smaller Mw of 5.6 kDa, a stark contrast compared to phenylene polymer **P12**. This decrease in polymer weights could also potentially be due to an

increased error associated with delivering the monomers in a 1:1 stoichiometric ratio when using lower molecular weight π-spacers. If the reaction were to be performed at a larger scale this error could be reduced, and a potentially higher Mw obtained.

Another conjugated coupling partner possessing no solubilizing chains: 4,7-dibromobenzo[c][1,2,5]thiadiazole was used to produce **P15**. The benzothiadiazole was chosen as a coupling partner due to its strong electron-accepting properties which would complement the electron-richness of the dialkoxybithiazole monomer to form a polymer with an acceptor-donor structure. Additionally, the analogous polymer possessing a dinonylbithiazole motif had been previously prepared by Kanbara and co-workers in 2014.[140] Unfortunately, **P15** was only produced in with a Mw of 4.5 kDa and PDI of 2.0, far smaller than the Mn of 24.3 kDa achieved by Kanbara for the nonyl equivalent polymer, despite there being no major difference in the solubilizing chains of these polymers.

Our final coupling partner employed in the direct arylation polymerization with **4.3** was 2,5-dibromothiophene. Not only was this π-spacer of interest for possessing no solubilizing alkyl chains, the unsubstituted thiophene has 3- and 4-positions capable of undergoing CMD for direct arylation, and for this reason, is not commonly used in DArP. Polymerization of **4.3** with this monomer would, therefore, assess the propensity for the dialkoxybithiazole to undergo C-H activation over the thiophene spacer. Polymer **P16** was produced from this reaction with a fairly small Mw of 5.0 kDa and PDI of 2.1. Although polymerization did not proceed to the extent of some other examples (such as thiophene polymer **P13**), direct arylation of the thiophene C-H bonds did not seem to be prevalent issue, as there was no noticeable sign of insoluble cross-linked material present upon precipitation.

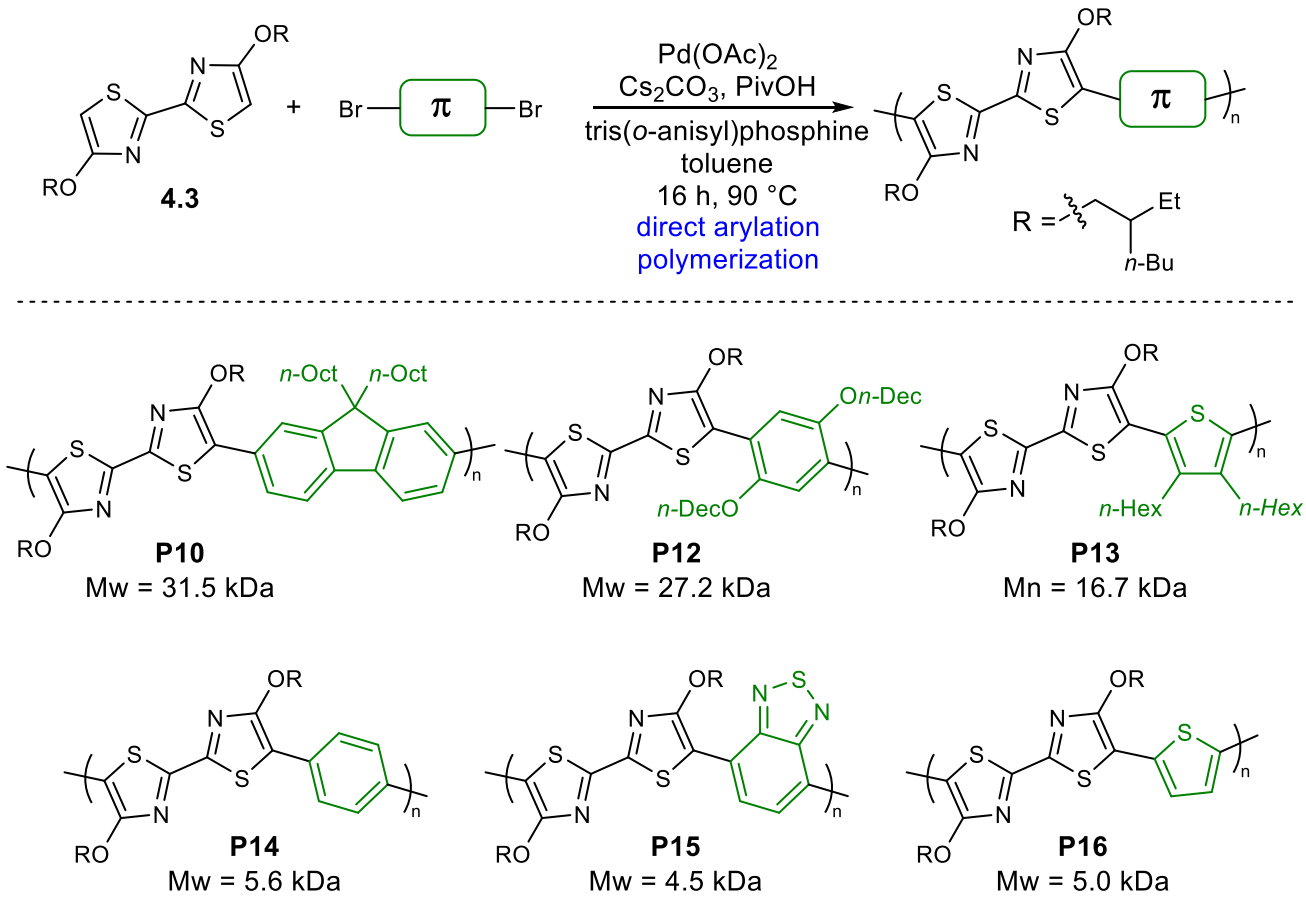

Figure 4.6 – Direct arylation polymerization scope using monomer **4.3**.

To determine the optical band gaps, we next examined our newly synthesized dialkoxybithiazole polymers **P12**-**P16** by absorption spectroscopy (Figure 4.7). As with **P10**, the absorption maxima for all polymers were found in the high visible light-absorbing range of 550 - 675 nm. The onset of absorption for benzothiadiazole polymer **P15** and thiophene polymer **P16** were shifted well into the near-IR region, corresponding to band gaps of 1.43 eV and 1.62 eV, respectively. The low band gap of benzothiadiazole polymer **P15** corresponded well with the suspected formation of an acceptor-donor structure between the electron-rich bithiazole and electron-poor spacer. The optical band gap for **P15** is also 0.56 eV lower than the 1.99 eV band gap reported by Kanbara and co-workers in 2014 for the equivalent polymer with a 4,4'-dinonyl-2,2'-bithiazole motif.[140] On the other

hand, the difference in the band gap of 0.15 eV between 3,4-dihexylthiophene polymer **P13** and unsubstituted thiophene **P16** was not expected, seeing as there is no obvious change to the conjugated system. This difference in band gap could be due to how the thiophene orients relative to the dialkoxybithiazole motif in order to favour either S – O or H – O interactions. The physical and optical properties of **P10** and **P12**-**P16** are compiled in Table 4.1.

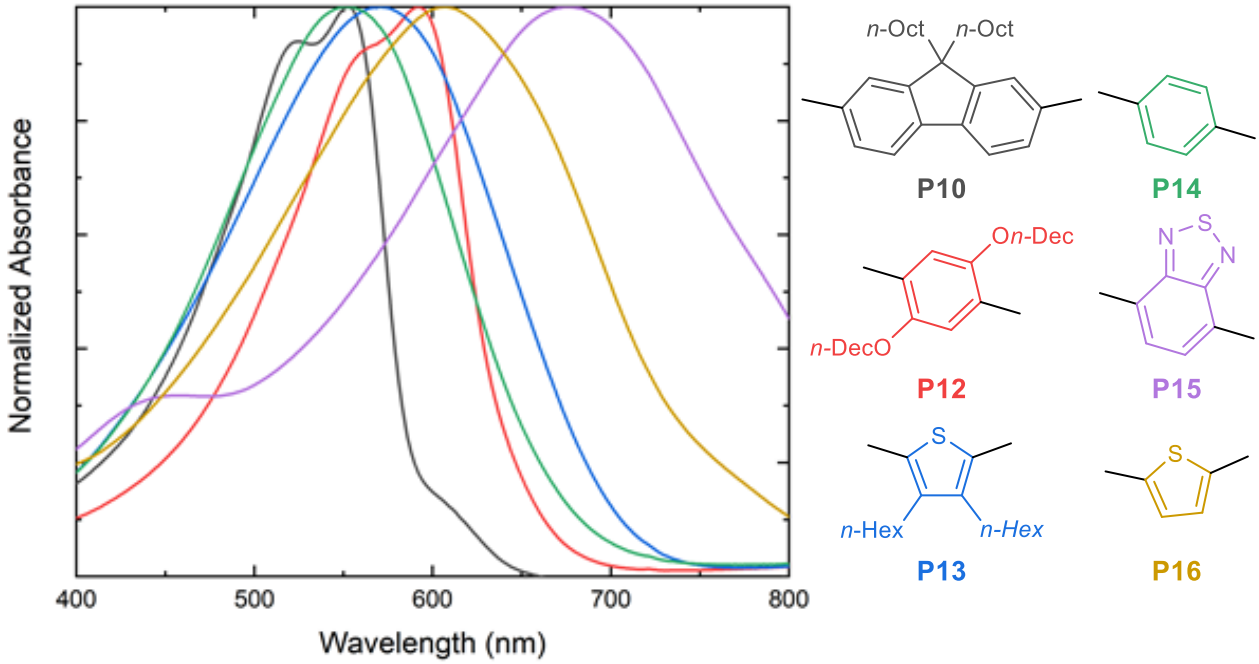

Figure 4.7 – UV-Vis absorption spectra for 4,4'-bis(2-ethylhexyloxy)-2,2'-bithiazole polymers in $CHCl_3$.

Table 4.1 – Summary of optical and physical data of polymers **P10**, **P12**-**P16**.

Entry	Mn (kDa)	Mw (kDa)	PDI	Eg_{Opt} (eV)	Abs_{Max} (nm)
P10	11.9	31.5	2.7	2.09	553
P12	13.6	27.2	2.0	1.90	592
P13	8.7	16.7	1.9	1.77	571
P14	3.2	5.6	1.8	1.85	551
P15	2.3	4.5	2.0	1.43	675
P16	2.4	5.0	2.1	1.62	606

4.4 Conclusions and Outlook

In summary, we have presented an unexplored and overlooked conjugated polymer motif. 4,4’-Dialkoxybithiazole-containing conjugated polymers allow for all the benefits that have popularized 3-alkoxythiophene polymers, mainly the ability to incorporate solubilizing chains without disrupting backbone planarity. Additionally, the electron-donating effects of the alkoxy side chains, often detrimental to the air stability of polythiophenes, are diminished by the decreased electron-richness of the thiazole ring. Finally, the lack of 3-proton on the thiazole ring allows for a planarity throughout the bithiazole unit.

These 4,4’-dialkoxy-2,2’-bithiazoles were also identified by disruption-interaction analysis as prime monomer candidates for direct arylation polymerization due to their propensity to undergo the required concerted-metalation-deprotonation step. DArP was used with 4,4’-bis(2-ethylhexyloxy)-2,2’-bithiazole to yield six new polymers with various electron-rich, and electron-poor, conjugated motifs. Additionally, a 3,4-unsubstiuted thiophene spacer was able to be used as a coupling partner, despite its own ability to undergo direct arylation, without forming a noticeable amount of insoluble cross-linked products.

The route we have presented to 4,4’-dialkoxy-2,2’-bithiazole monomers proceeds in only two steps from commercially available starting materials. Compared to the structurally similar 5,5’-bithiazole polymers presented by Marks and co-workers; our pathway represents a significant decrease in the synthetic effort required to achieve these types of materials. Further optimization of the direct arylation polymerization conditions

will likely result in higher molecular weights obtained for the polymer products and allow them to be explored in device applications.

5

Transition Metal-Free Cross-Coupling of Thiazole-*N*-Oxides

5.1 Background

Much of our synthetic work thus far has revolved around 2,2'-bithiazole-containing small molecules and polymers, and our methods to form the bithiazole C-C bond via dehydration or *ipso*-arylative condensation of thiazole-*N*-oxides. We have, however, been limited to such a motif due to the homocoupling nature of the developed methods. These synthetic methods would be far more powerful if they were to enable the cross-coupling of thiazole-*N*-oxides with alternate arenes, to form a new C-C bond in a 2-arylthiazole product. This would allow for the development of new thiazole-containing conjugated materials that are not strictly limited to those possessing a bithiazole motif. In addition to the materials prospects, 2-arylthiazoles are widespread in other aspects of synthetic

chemistry such as natural products and pharmaceuticals (Figure 5.1).[205,206] Although this chemistry has only minimally been explored with thiazoles, C-C bond formation to other *N*-heterocycles, such as pyridine and quinoline, has long been achieved by exploiting the unique reactivity of the *N*-oxide functional group.

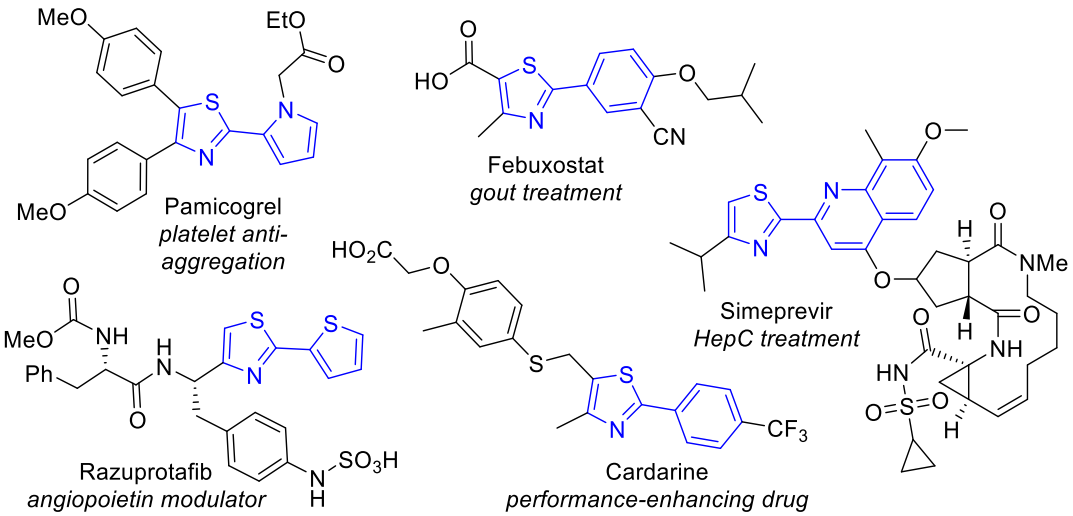

Figure 5.1 – Pharmaceuticals possessing 2-arylthiazole motifs.

5.1.1 Nucleophilic addition to pyridine/quinoline *N*-oxides

The activation of *N*-heterocycles for nucleophilic attack is a concept that dates back to the early 1900's work of Arnold Reissert with quinoline derivatives.[207] Reissert found that the *N*-acylation of quinoline to the quinolinium salt enhanced the electrophilicity of the 2-position and facilitated attack by a cyanide nucleophile. The dehydroquinolines, dubbed Reissert compounds, were then found to undergo subsequent elimination of the acetyl group to restore aromaticity and yield substituted quinolines. Over the following century, Reissert-type chemistry has been extensively used to synthesized 2-substituted quinolines and further expanded to other *N*-heterocycles such as isoquinolines and pyridines.[208]

In a similar fashion, nucleophilic addition to pyridines is facilitated through oxidation to pyridine-*N*-oxides. Pyridine derivatives can be oxidized to the *N*-oxides by various oxygen-transfer reagents including peroxide, peracids, and dimethyldioxirane. Like the formation of Reissert compounds, addition of oxygen to the pyridine nitrogen increases electrophilicity at the 2-position, and lowers the LUMO of the heterocycle.[208] One of the preliminary examples of carbon nucleophile addition to pyridine-*N*-oxide was reported in 1959 by Feely.[209] 2-Cyanation was accomplished from pyridine-*N*-oxide through methylation of the *N*-oxide with dimethylsulfate. Methylation allowed for increased susceptibility to nucleophilic attack at the 2-position and converted the oxygen into a good leaving group. Nucleophilic addition of cyanide from aqueous KCN could then proceed, which is followed by elimination of the methoxide in order to restore aromaticity to the heterocycle (Scheme 5.1).

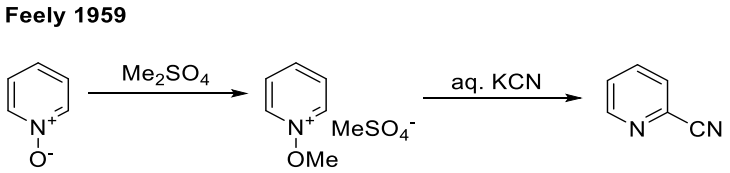

Scheme 5.1 – Nucleophilic addition of cyanide to methylated pyridine-*N*-oxide.

Alternatively, if a strong nucleophile such as a Grignard is deployed, nucleophilic addition to the pyridine-*N*-oxide can be achieved prior to O-activation, due to the electron poor nature of the pyridine ring.[210] The nitrone oxygen of this dearomatized intermediate can then be converted into a good leaving group (ie: through acylation), whereupon subsequent elimination can occur to yield the 2-substituted pyridine with a new carbon-carbon bond (Scheme 5.2).[211,212] This contrasts with the previous cyanation strategies as

it does not proceed through conversion of the *N*-oxide to the pyridinium salt prior to nucleophilic attack.

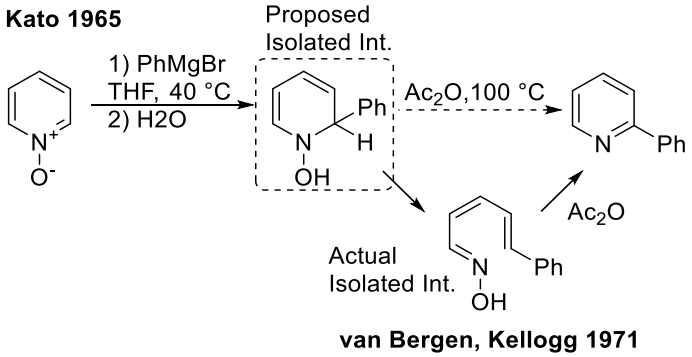

Scheme 5.2 – Grignard addition to pyridine-*N*-oxide followed by re-aromatization.

5.1.2 Nucleophilic addition to thiazole N-oxides

The addition of nucleophiles to the thiazole 2-position presents several challenges compared to pyridine or quinoline derivatives. Unlike these *N*-heterocycles, thiazole is an electron-excessive heterocycle with a high-lying LUMO that, in general, is poorly electrophilic at the 2-position. However, upon oxidation of thiazole to thiazole-*N*-oxide, electrophilicity at the 2-position increases such that nucleophilic addition becomes possible. In a seminal report by Begtrup and Hansen in 1992, it was reported that the reaction of 4,5-dimethylthiazole-*N*-oxide in acetyl chloride at room temperature yielded 2-chloro-4,5-dimethylthiazole (Scheme 5.3).[213] This was proposed to occur through acetylation of the *N*-oxide oxygen to form the chloride salt, followed by attack of the chloride counterion at the 2-position. Elimination of the acetate to re-establish aromaticity yielded the chlorinated, deoxygenated product. While this presents a useful method of functionalizing a heterocycle that is often found in natural products and drug candidates,

this chemistry has remained largely dormant likely due to the difficulty of thiazole-*N*-oxide preparation, as well as their general instability.

Begtrup and Hansen 1992

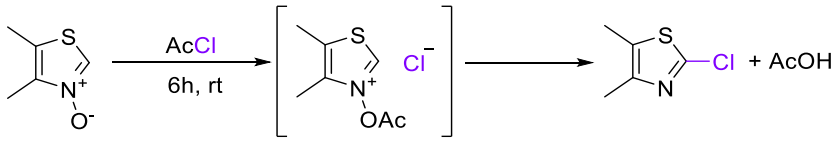

Scheme 5.3 – 2-Chlorination of thiazole-*N*-oxide through loss of acetate.

Not dissimilar to Begtrup and Hansen's work, our initial report on the dehydrative coupling of thiazole-*N*-oxides showcased that if a strong enough nucleophile was generated (through the 2-deprotonation of a thiazole-*N*-oxide with strong base), thiazole-*N*-oxide is also electrophilic enough to undergo nucleophilic attack at the 2-position. This nucleophilic attack under basic conditions forms the new C-C bond and results in the loss of the *N*-oxide oxygen, presumably through protonation and elimination as hydroxide, in order to restore aromaticity (Scheme 5.4).[145] Thus, this reaction occurs in the same manner, although in an alternate step order (nucleophilic addition followed by conversion of oxygen to a good leaving group) as that presented in the work of Begtrup and Hansen.

Schipper 2018

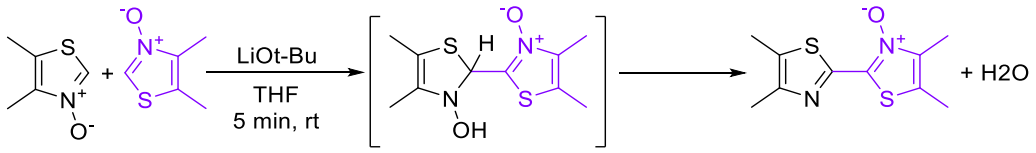

Scheme 5.4 – Nucleophilic addition and subsequent elimination/re-aromatization in the dehydration coupling of thiazole-*N*-oxides.

5.2 Proposal

Previous attempts to cross-couple two differing thiazole-*N*-oxides through our base-mediated dehydration coupling have shown minimal success. Limited control over which thiazole-*N*-oxide acted as the nucleophile and which acted as the electrophile resulted in a mixture of cross-dehydration products as well as the typical dimer products (Scheme 5.5).[145] Instead, we looked to establish an entirely new approach to coupling thiazole-*N*-oxides to alternate arenes while still employing the unique reactivity of these compounds.

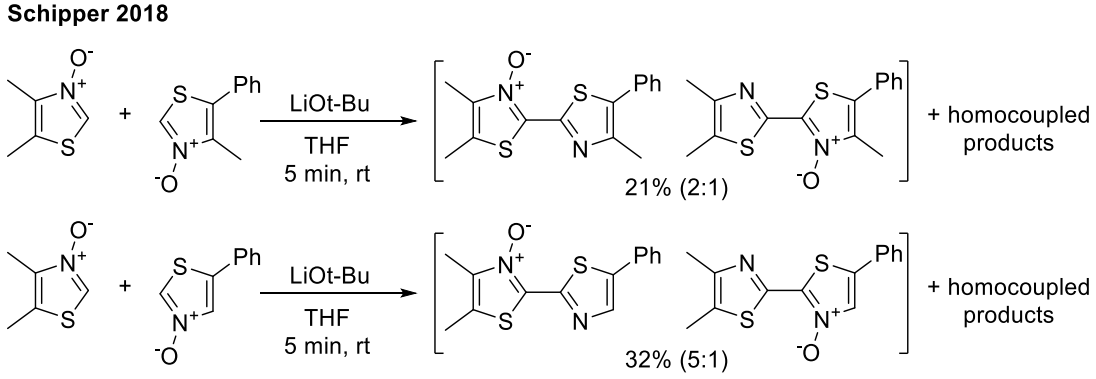

Scheme 5.5 – Cross-dehydrations of thiazole-*N*-oxides.

The dehydration of thiazole-*N*-oxides facilitates C-C bond formation via increasing the nucleophilicity of the *N*-oxide nucleophile through deprotonation of the 2-position with strong base. This deprotonated thiazole can, in turn, perform a nucleophilic attack on an additional molecule of thiazole-*N*-oxide at the electrophilic 2-position. We hypothesized that, if the thiazole-*N*-oxide electrophile could instead be activated towards an increased rate of nucleophilic attack, via conversion of the *N*-oxide oxygen to a good leaving group, we may be able to facilitate the addition of alternative nucleophiles (Scheme 5.6). Specifically, if electron-rich arenes are employed as nucleophiles, we will be able to yield

2-arylthiazole products simply through the loss of a stoichiometric amount of H_2O. This would present a first-of-its-kind, transition metal-free coupling method for the synthesis of thiazole-containing biaryls. Since this proposed pathway to crossed-biaryl species shares many similarities to the addition of nucleophiles to other *N*-heterocycles, such as quinoline and pyridine, we looked to these established methods as inspiration towards our goal.

The proposed a mechanistic pathway for this transformation that would begin with activation of the thiazole-*N*-oxide with an activating group (AG), which would increase both the electrophilicity of the 2-position as well as the leaving group capability of the oxygen. Next, an electron-rich arene would be able to undergo S_EAr on the 2-position of the activated thiazole N-oxide to form the new C-C bond. Finally, elimination of the activated oxygen would rearomatize the thiazole and deliver the new 2-aryl thiazole.

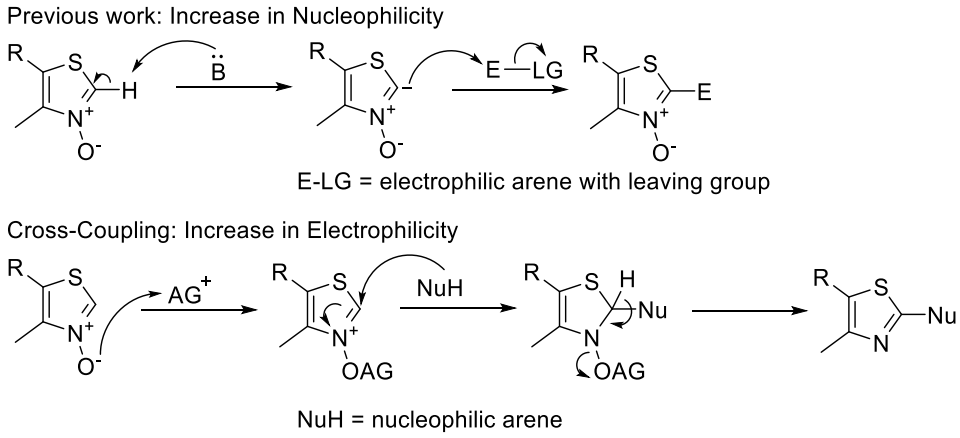

Scheme 5.6 – Conceptual comparison between the dehydration of thiazole-*N*-oxides and the proposed arene addition to an "activated" thiazole-*N*-oxide.

5.3 Results and Discussion

To begin our exploration into the nucleophilic addition of electron-rich arenes to thiazole-*N*-oxides we first had to choose an activating group for which to convert the *N*-oxide oxygen into a good leaving group. With the dehydrative C-C bond formation

between electron rich arenes with quinones reported by Swager in mind (Scheme 5.7a), we speculated we may also be able to use a strong acid such as *para*-toluenesulfonic acid to activate the *N*-oxide into a hydroxide leaving group. Based on this report, we also chose 2-methylthiophene (2MT) as the electron-rich arene to undergo electrophilic aromatic substitution. Thiophene's general prevalence in conjugated small molecules and polymers makes it of great interest for cross-coupling, while the methyl substituent would prevent the thiophene from reacting twice and avoid forming a mixture of products. Due to the affordability of the thiazole starting material, 4,5-dimethylthiazole-*N*-oxide (**5.1**) was a prepared (using *m*-CPBA) for use as the *N*-oxide substrate of interest. Unfortunately, our initial attempts at stirring **5.1** with excess *p*-TsOH and 2MT in toluene showed no sign of the desired product **5.2** by TLC (Scheme 5.7b)

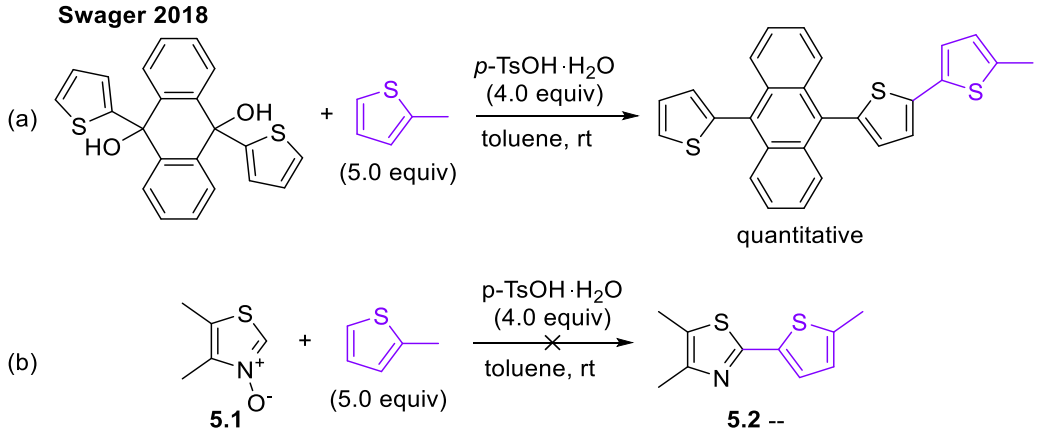

Scheme 5.7 – Acid promoted addition of 2MT to an electrophilic aromatic system a) reported coupling by Swager and Voll[146] b) application of Swager's conditions to **5.1**.

Instead of protonating the thiazole-*N*-oxide, we instead attempted to produce results similar to those observed by Begtrup and Hansen by stirring **5.1** in AcCl, as well as in Ac_2O, for 6h at room temperature. Oddly, 2-chlorothiazole, as reported in the literature from the reaction with AcCl, was not observed from the reaction. However,

through LR-MS and crude ^{1}H NMR, it appeared that the deoxygenated 2-acetoxythiazole product had formed from the reaction with Ac_2O (Scheme 5.8a). Thus, the *N*-oxide must have proceeded through acetylation of the oxygen followed by subsequent nucleophilic attack of the acetoxy counter-ion.

With this in mind, we next wanted to trap the acetylated *N*-oxide intermediate salt with an arene nucleophile. The reaction was performed using substrate **5.1** with 1.5 equiv of Ac_2O, and with 2MT as the solvent. We hoped that having the desired nucleophile in gross excess would allow it to outcompete the acetoxy anion for nucleophilic attack on the 2-position of the activated thiazole. Unfortunately, the product yielded from this reaction remained the acetoxy addition product (Scheme 5.8b). Therefore, we required a new activating group that would release a less nucleophilic leaving group upon attack by the *N*-oxide oxygen.

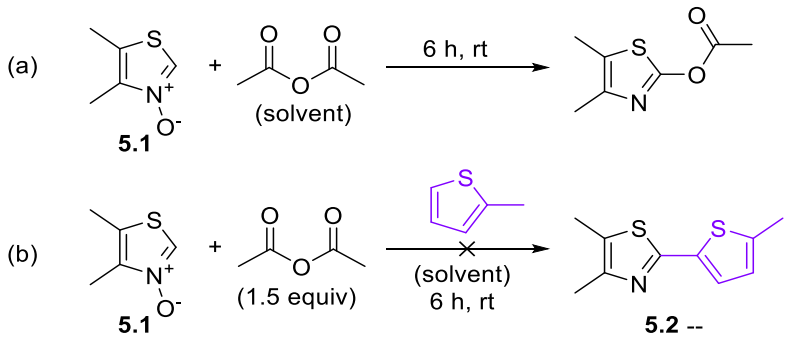

Scheme 5.8 – Activation of thiazole-*N*-oxide with Ac_2O a) with no additional nucleophile b) with 2MT as the nucleophile (products not isolated).

5.3.1 Reaction optimization

As an alternative activating reagent, we selected trifluoroacetic anhydride (TFAA) with the hope that the trifluoroacetate leaving group would be less nucleophilic than the arene. The transformation was attempted on **5.1** with similar equivalents of TFAA and

reduced the 2MT nucleophile from acting as the solvent to 10.0 equiv. To our delight, the desired product **5.2** was visible by crude LR-MS and no sign of trifluoroacetate addition product was visible. Unfortunately, chromatography of this reaction mixture only yielded trace amounts of **5.2** along with unidentifiable side products (Table 5.1, Entry 1).

Continuing to test new activating reagents, we employed *para*-toluenesulfonic anhydride (Ts_2O), and bromotripyrrolidinophosphonium hexafluorophosphate (PyBroP) in place of TFAA. Unfortunately, with these activating reagents, no product **5.2** was produced (Table 5.1, Entry 2 – 3). This changed when the reaction was attempted under identical conditions with trifluoromethanesulfonic anhydride (Tf_2O). Stirring **5.1** with Tf_2O and 10.0 equiv. of 2MT for 16 h at room temperature yielded a significant 46% yield of product **5.2** (Table 5.1, Entry 4). This product was characterized following chromatography; however, the reaction also yielded a substantial amount of a new side product. This side product was inexplicably difficult to identify by ^{1}H and ^{13}C NMR, though we suspected that the side product was likely the result of triflation of the thiophene nucleophile (**5.3**) (Scheme 5.9).

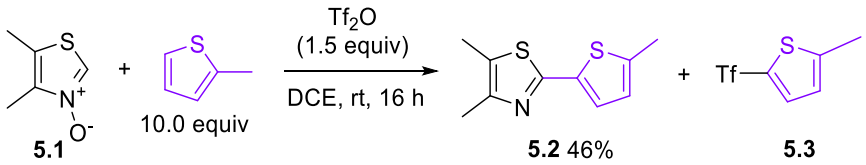

Scheme 5.9 – Products resulting from the addition of 2MT to **5.1** with Tf_2O.

We next sought to reduce the equivalents of 2MT used in the reaction. Halving the amount of 2MT to 5.0 equivalents unfortunately resulted in a decrease in the production of **5.2** to a yield of 31% (Table 5.1, Entry 5). We chose to continue optimizing the reaction

using 5.0 equivalents as we inevitably would have to reduce the equivalents of 2MT in order to increase the appeal of the reaction.

To reduce the presence of the proposed side product **5.3**, we speculated that if substrate **5.1** is pre-activated with Tf_2O, we may be able to force conversion of the *N*-oxide to the *N*-triflate. Introduction of 2MT to the fully *N*-triflated thiazole would then hopefully allow for formation of **5.2** and reduced formation of **5.3**. This process would also be dependant on the *N*-triflated thiazole not being susceptible to nucleophilic attack by the triflate counterion, though this had not been observed thus far and was not expected to occur. Pre-stirring substrate **5.1** with Tf_2O for 1 h (Table 5.1, Entry 6), 6 h (Table 5.1, Entry 7) or longer, unfortunately, did not seem to have a major effect, as the yield of **5.1** remained in the same ballpark as those without the pre-activation step.

Based on our working hypothesis of how the reaction would proceed, using Tf_2O as our activating reagent would generate 2 equivalents of TfOH upon formation of product **5.2**. This could be having a negative effect on our desired transformation and be reducing the yield of product. Therefore, we attempted the reaction with the inclusion of various non-nucleophilic bases. Ultimately, the deployment of an organic base (Table 5.1, Entries 8 – 10) or an inorganic base (Table 5.1, Entry 11) only seemed to have a neutral or negative effect on the yield of product **5.2** obtained.

Altering the reaction solvent from DCE to chlorobenzene (Table 5.1, Entry 12) or toluene (Table 5.1, Entry 13) saw no major change in the yield of product **5.2**. Additionally, increasing the temperature of the reaction to 100 °C did not yield any more product (Table 5.1, Entry 14); however, it allowed for the reduction of the reaction time to 1 h while maintaining yields in the ~30% range (Table 5.1, Entry 15). Not for the lack of trying, our

initial conditions, wherein 10.0 equivalents of 2MT was deployed, were found to be optimal in yielding product **5.2** from *N*-oxide **5.1**.

Table 5.1 – Optimization of reaction conditions around *N*-oxide **5.1**[a]

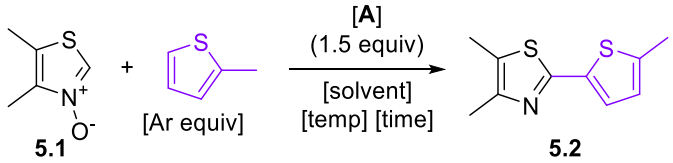

Entry	Ar equiv.	**A**	additive	pre-act[c]	temp	solvent	rxn time	% yield
1	10.0	TFAA	--	--	rt	DCE	16 h	trace
2	10.0	Ts_2O	--	--	rt	DCE	16 h	--
3	10.0	PyBroP	--	--	rt	DCE	16h	--
4	**10.0**	**Tf_2O**	**--**	**--**	**rt**	**DCE**	**16 h**	**46[b]**
5	5.0	Tf_2O	--	--	rt	DCE	16 h	31[b]
6	5.0	Tf_2O	--	1h	rt	DCE	16 h	26[b]
7	5.0	Tf_2O	--	6h	rt	DCE	16 h	27[b]
8	5.0	Tf_2O	2,6-lutidine	--	rt	DCE	16 h	21[b]
9	5.0	Tf_2O	DIPEA	--	rt	DCE	16 h	17[b]
10	5.0	Tf_2O	DBU	--	rt	DCE	16 h	25[b]
11	5.0	Tf_2O	K_2CO_3	--	rt	DCE	16 h	16[b]
12	5.0	Tf_2O	--	--	rt	PhCl	16 h	27[b]
13	5.0	Tf_2O	--	--	rt	toluene	16 h	26[b]
14	5.0	Tf_2O	--	--	100 °C	DCE	16 h	28[d]
15	5.0	Tf_2O	--	--	100 °C	DCE	1 h	30[b]

[a]Conditions: **5.1**, 2MT [equiv], in [solvent] (0.25 M) with [**A**] (1.5 equiv); stirred for [time] at [temp]. [b]Isolated yields. [c]**5.1** was stirred with reagent **A** in DCE prior to addition of 2MT. [d]NMR yield using internal 1,3,5-trimethoxybenzene standard.

5.3.2 Reaction scope

An important aspect for the general applicability of this reaction was to ensure that it would proceed with a multitude of arene nucleophiles (Figure 5.2). Product **5.2** had been synthesized at best in a 46% yield from 2-methylthiophene and *N*-oxide **5.1** employing the optimal conditions. Further nucleophiles consisted of electron-rich arenes which were selected based on approximate nucleophilicities presented by Mayr's database.[214,215] Biaryl **5.4** was produced in a 54% yield from *N*-oxide **5.1** and guaiazulene while 1,3,5-trimethoxybenzene yielded biaryl **5.5** in a 34% yield. While these yields were ultimately poor, it was refreshing to see that the reaction did indeed continue with other arene nucleophiles, and in synthetically useful yields. Isolation of these products by column chromatography proceeded similarly to **5.2,** in that a large amount of side product was present (in addition to remaining starting material). This was again thought to be the result of nucleophilic attack on the Tf_2O by the guaiazulene or 1,3,5-trimethoxybenzene.

Curious as to whether we would be able to observe di-functionalization, the next arene nucleophile we investigated in this reaction was the 2,5-unfunctionalized EDOT. To achieve this, the reaction was performed with only 0.5 equivalents of EDOT relative to *N*-oxide **5.1**, contrary to the previous reactions in which the arene nucleophile was delivered in major excess. Unexpectedly, only the mono-functionalized product **5.6** was obtained from this reaction, and in a low yield of 20%. This yield could most definitely be improved by performing the reaction with the standard 10.0 equivalent excess of EDOT to favour formation of product **5.6**.

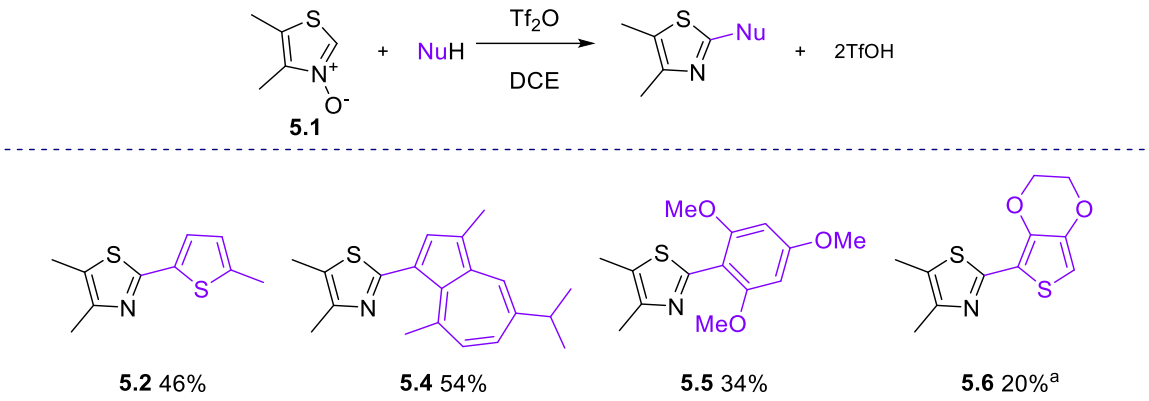

Figure 5.2 – Arene nucleophile scope for coupling with thiazole-*N*-oxide **5.1**. Conditions: *N*-oxide (1.0 equiv), Tf_2O (1.5 equiv), and arene (10.0 equiv) in DCE (0.25 M) at room temperature for 16 h. Isolated yields. [a]Arene (0.5 equiv).

5.3.3 Mechanism insights

To have any hope of improving the practicality of this reaction as a method for coupling arenes to thiazole, we attempted to decipher some mechanistic insights into how the reaction proceeds. Using trifluoromethanesulfonic anhydride as our activating reagent, we were granted the unique ability to survey the transformations in the reaction mixture by ^{19}F NMR.

Our first goal was to confirm the identity of **5.3** as the major side product of the reaction, and potential cause for low yields of **5.2**. *N*-oxide **5.1** was subject to optimal conditions with 2MT and Tf_2O and the resulting crude reaction mixture was quenched with a basic work-up of aqueous $NaHCO_3$. Following concentration of the mixture, ^{19}F NMR analysis revealed the presence of two signals at -46.2 and -78.5 ppm (Figure 5.3a). The peak at -46.2 ppm resides in the range of triflyl substituents and was attributed to the suspected side product **5.3**, while the -78.5 peak was attributed to a triflate salt (such as sodium triflate generated from work-up). Following separation of the major side product through column chromatography, the same -46.2 ppm signal was still observed in the ^{19}F

NMR (Figure 5.3b). To further confirm the presence of **5.3**, 2MT was stirred with Tf_2O in DCE for 1 h, followed by an aqueous $NaHCO_3$ quench. The same signals previously observed were once again present in the ^{19}F NMR of this crude mixture (Figure 5.3c). Although not a complete characterization of **5.3**, it could be concluded that the major side product possesses a triflyl substituent appearing at -46.2ppm in the ^{19}F NMR, and is a result of the 2MT reacting with Tf_2O.

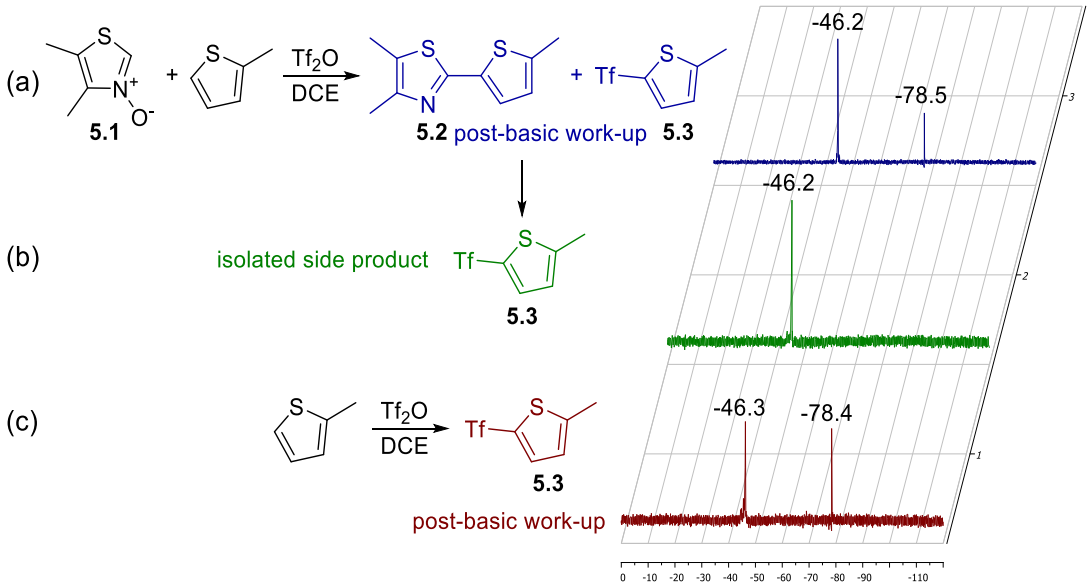

Figure 5.3 – ^{19}F NMR identification of side product **5.3** a) standard reaction conditions with *N*-oxide **5.1** b) isolated side product c) reaction of 2MT with Tf_2O.

We next endeavoured to observe by ^{19}F NMR what occurs between *N*-oxide **5.1** and Tf_2O in the absence of the nucleophilic arene. The *N*-oxide was stirred with 1.5 equivalents of Tf_2O in DCE for 1 h before an aliquot was taken and added to $CDCl_3$ for analysis, without basic quenching (Figure 5.4). An expected signal was observed for the excess Tf_2O at -72.0 ppm, corresponding to the literature. Another large signal was present at the familiar shift of -78.7 ppm, once again thought to belong to a triflate anion. It was expected that this signal corresponded to the triflate counterion of the thiazolium

salt (**5.7**) generated by *N*-oxide triflation. If this was the case, however, we would then expect a 1:1 integration ratio of this signal at -78.7 ppm with another signal corresponding to the thiazolium-*N*-triflate (**5.7**), yet neither new signal at -68.5 or -79.2 ppm are equal in integration (nor is the sum of both integrals). Upon aqueous $NaHCO_3$ work-up of this reaction mixture, only the signal at -78.7 ppm and, surprisingly, the Tf_2O signal at -72.0 ppm remained.

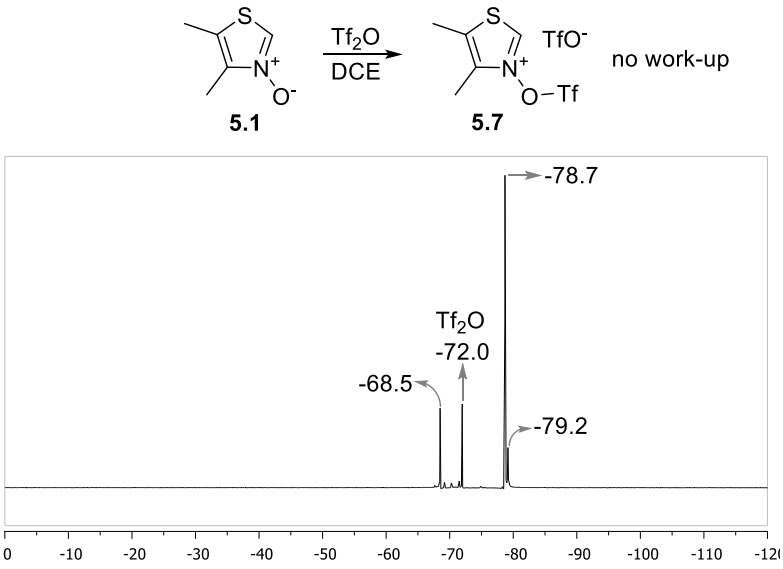

Figure 5.4 – ^{19}F NMR analysis of intermediate generated from *N*-oxide **5.1** and Tf_2O.

The same reaction on thiazole **5.1** was performed using only 0.5 equivalents of Tf_2O. This was carried out in order to determine if complete consumption of the anhydride could be achieved in the formation of the *N*-triflate (**5.7**). Even with the reduced stoichiometry, a significant ^{19}F NMR signal was still observed at -72.0 ppm correlating to residual Tf_2O, albeit, the signal was less intense relative to the other signals compared to when Tf_2O was in excess. If complete consumption of Tf_2O could be achieved, it would be extremely valuable for furthering this methodology to determine if formation of side

product **5.3** can still occur through nucleophilic attack at the *N*-triflate of **5.7**, rather than the 2-position.

5.4 Conclusions and Outlook

The work discussed in this chapter presents a new method for the transition metal-free formation of new C_{sp2}-C_{sp2} bonds between arenes, once again employing the unique reactivity of thiazole-*N*-oxides. At the current stage of development for this reaction, multiple different 2-arylthiazoles have been shown to be accessible in synthetically significant yields from 4,5-dimethylthiazole-*N*-oxide (**5.1**) and a variety of electron-rich arenes. This is achieved simply through the addition of trifluoromethanesulfonic anhydride, followed by stirring at room temperature for 16 hours.

Preliminary mechanistic investigations have shown that eliminating the side products that result from the arene nucleophilic attack on Tf_2O will be key to achieving higher yields of desired products and reducing the required equivalents of arene starting material. We speculate that the use of an activating reagent such as Meerwein's salt instead of Tf_2O may abolish the present side reaction issues; however, we believe this would present a decrease in the accessibility and feasibility of this reaction. Access to thiazole-*N*-oxide starting materials will once again present itself as an important facet of expanding the scope of this work beyond the use of *N*-oxide **5.1**.

6

Supporting Information

6.1 General Considerations

Reactions were performed under an ambient air atmosphere unless otherwise specified in the procedure. Reaction solvents deployed were either reagent grade and/or HPLC grade. Anhydrous tetrahydrofuran, toluene and dichloromethane were obtained from a JC Meyer solvent-purification system (SPS). Chemical reagents used were those primarily purchased from Millipore-Sigma, Oakwood Chemical, Combiblocks or TCI. Reaction monitoring was performed by thin-layer chromatography (TLC) using aluminum-backed silica TLC plates (Kieselgel 60 F_{254}, Merck). Developed TLC plates were then examined under UV lighting (254 nm/ 365 nm). Flash chromatography was performed using 230–400 mesh silica gel (SiliCycle) and primarily using a Teledyne-isco Combiflash Rf+ system.

^{1}H-NMR spectra were recorded on a Brüker AVANCE300 (300 MHz) δ or Brüker AC300 (300 MHz) δ NMR spectrometers. ^{13}C-NMR spectra were broad band decoupled and recorded on a Brüker AVANCE300 (75.5 MHz) δ or Brüker AC300 (75.5 MHz) δ NMR spectrometers. ^{19}F-NMR spectra were recorded on a Brüker AVANCE300 (300 MHz). Chemical shifts are reported in parts per million (ppm) relative to either chloroform (δ 7.28) for ^{1}H-NMR, and (δ 77.0) for ^{13}C-NMR.. The following abbreviations are used for NMR peak multiplicities: s, singlet; d, doublet; t, triplet; q, quartet; quitn ,quintet; dd, doublet of doublets; dt, doublet of triplets; m, multiplet; br, broad. High resolution mass spectra (HRMS) were obtained via electrospray ionization (ESI) which was measured on a Thermo Scientific Q Exactive™ Plus Hybrid Quadrupole-Orbitrap™ at the University of Waterloo Mass Spectrometry Facility. Infrared spectra were recorded on a Perkin Elmer FT-IR Spectrum Two with ATR Two. X-ray crystal structures have been determined by Dr. Jalil Assoud and figures of X-ray crystal structures were generated using the Mercury software package. Fluorescence spectra were measured on a Horiba QuantMaster 8000 using right-angle detection. Ultraviolet-visible (UV-Vis) absorption spectra were measured with a Cary-4000 spectrophotometer and corrected for background signal with a solvent filled cuvette. Fluorescence quantum yields in CH_2Cl_2 were determined relative to quinine sulfate in 1N H_2SO_4 and are corrected for solvent refractive index and absorption differences at the excitation wavelength.

6.2 Synthetic Procedures

Chapter 2

2-(4,5-dimethylthiazol-2-yl)propan-2-ol (**2.1**)

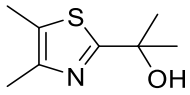

To a round-bottom flask charged with 4,5-dimethylthiazole (935 µL, 8.8 mmol, 1.0 equiv), purged with argon and sealed was added THF (8.8 mL, 1.0 M) and allowed to stir in a -78 °C bath of dry ice and acetone. *n*-BuLi (4.2 mL, 2.5 M, 1.2 equiv) was added and the mixture was stirred at this temperature for 30 min. Acetone (970 µL, 13.2 mmol, 1.5 equiv) was then added, the vessel purged with argon, and continued to stir at this temperature for 30 min. The reaction mixture was then quenched with NH_4Cl (30 mL) and extracted with diethyl ether (3 x 30 mL). The organic layer was then dried with $MgSO_4$ and concentrated. No further purification was required to yield **2.1** (1.35 g, 89%); R_f = 0.12 (EtOAc : Hexane = 1 : 4); ^1H NMR ($CDCl_3$, 300 MHz) δ 2.26 (s, 3H), 2.23 (s, 3H), 1.57 (s, 6H); ^{13}C NMR ($CDCl_3$, 75 MHz) δ 173.9, 147.2, 125.8, 72.6, 30.9, 14.5, 11.1; HRMS calculated for $C_8H_{14}ONS$ (M+H): 172.07906; Found: 172.07845.

2-(2-hydroxypropan-2-yl)-4,5-dimethylthiazole 3-oxide (**2.2**)

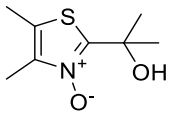

In a round-bottom flask, **2.1** (500 mg, 2.9 mmol, 1.0 equiv) was dissolved in 1,2-dichloroethane (6 mL, 0.5M) allowed to stir at room temperature. *m*-CPBA (982 mg, 77%

pure, 4.4 mmol, 1.5 equiv) was then added and the mixture was continued stirring at this temperature for 4 h. The reaction mixture was then diluted with dichloromethane (30 mL) and then purified by column chromatography (0 % – 10 % gradient MeOH in EtOAc) to afford white solid **2.2** (428 mg, 89%); R_f = 0.14 (EtOAc); ^{1}H NMR ($CDCl_3$, 300 MHz) δ 2.33 (s, 3H), 2.24 (s, 3H), 1.60 (s, 6H); ^{13}C NMR ($CDCl_3$, 75 MHz) δ 149.1, 141.6, 121.9, 70.5, 28.0, 12.7, 10.6; HRMS calculated for $C_8H_{14}NO_2S$ (M+H): 188.07398; Found: 188.07338 m/z.

2-(thiazol-2-yl)propan-2-ol (**2.3**)

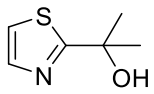

To a round-bottom flask charged with thiazole (1.7 mL, 23.5 mmol, 1.0 equiv), purged with argon and sealed was added THF (24 mL, 1.0 M) and allowed to stir in a -78 °C bath of dry ice and acetone. *n*-BuLi (11.2 mL, 2.5 M, 1.2 equiv) was added and the mixture was stirred at this temperature for 30 min. Acetone (2.05 mL, 35.2 mmol, 1.5 equiv) was then added, the vessel purged with argon, and continued to stir at this temperature for 30 min. The reaction mixture was then quenched with NH_4Cl (50 mL) and extracted with diethyl ether (3 x 50 mL). The organic layer was then dried with $MgSO_4$ and concentrated. No further purification was required to yield **2.3** (2.66 g, 79%); R_f = 0.13 (EtOAc : Hexane = 1 : 4); ^{1}H NMR ($CDCl_3$, 300 MHz) δ 7.59 (d, *J* = 3.3 Hz, 1H), 7.16 (d, *J* = 3.3 Hz, 1H), 1.62 (s, 6H); ^{13}C NMR ($CDCl_3$, 75 MHz) δ 180.3, 142.0, 118.7, 73.1, 30.9; HRMS calculated for $C_6H_{10}NOS$ (M+H): 144.04776; Found: 144.04726 m/z.

2-(2-hydroxypropan-2-yl)thiazole 3-oxide (**2.4**)

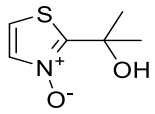

In a round-bottom flask, **2.3** (500 mg, 3.5 mmol, 1.0 equiv) was dissolved in 1,2-dichloroethane (7 mL, 0.5 M) allowed to stir at room temperature. *m*-CPBA (1.18g, 77% pure, 5.25 mmol, 1.5 equiv) was then added and the mixture was continued stirring at this temperature for 12 h. The reaction mixture was then diluted with dichloromethane (30 mL) and then purified by column chromatography (0 % – 10 % gradient MeOH in EtOAc) to afford white solid **2.4** (333 mg, 60%); R_f = 0.06 (EtOAc); ^{1}H NMR ($CDCl_3$, 300 MHz) δ 7.64 (d, *J* = 4.0 Hz, 1H), 7.26 (d, *J* = 4.0 Hz, 1H), 1.69 (s, 6H); ^{13}C NMR ($CDCl_3$, 75 MHz) δ 152.3, 137.8, 115.0, 70.6, 27.7; HRMS calculated for $C_6H_{10}NO_2S$ (M+H): 160.04268; Found: 160.04255 m/z.

2-(benzo[d]thiazol-2-yl)propan-2-ol (**2.5**)

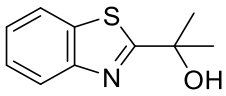

To a round-bottom flask charged with benzothiazole (1.0 g, 7.4 mmol, 1.0 equiv), purged with argon and sealed was added THF (7.4 mL, 1.0 M) and allowed to stir in a -78 °C bath of dry ice and acetone. *n*BuLi (3.6 mL, 2.5 M, 1.2 equiv) was added and the mixture was stirred at this temperature for 30 min. Acetone (646 µL, 11.1 mmol, 1.5 equiv) was then added, the vessel purged with argon, and continued to stir at this temperature for 30 min. The reaction mixture was then quenched with NH_4Cl (30 mL) and extracted with diethyl ether (3 x 30 mL). The organic layer was then dried with $MgSO_4$ and concentrated. The

crude product was then purified by column chromatography (0 % – 20 % gradient EtOAc in hexanes) to yield **2.5** (887 mg, 62%); R_f = 0.47 (EtOAc : Hexane = 3 : 7); ^{1}H NMR ($CDCl_3$, 300 MHz) δ 8.01 (d, *J* = 8.2 Hz, 1H), 7.91 (d, *J* = 8.0 Hz, 1H), 7.50 (t, *J* = 7.7 Hz, 1H), 7.39 (t, *J* = 7.6 Hz, 1H), 3.09 (br s, 1H), 1.77 (s, 6H); ^{13}C NMR ($CDCl_3$, 75 MHz) δ 179.8, 153.0, 135.3, 125.9, 124.8, 122.8, 121.7, 73.5, 30.7; HRMS calculated for $C_{10}H_{12}ONS$ (M+H): 194.06341; Found:194.06299.

2-(2-hydroxypropan-2-yl)benzo[d]thiazole 3-oxide (**2.6**)

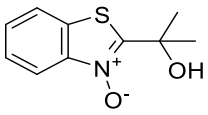

In a round-bottom flask, **2.5** (500 mg, 2.6 mmol, 1.0 equiv) was dissolved in 1,2-dichloroethane (5 mL, 0.5 M) and allowed to stir at room temperature. *m*-CPBA (874 mg, 77% pure, 3.9 mmol, 1.5 equiv) was then added and the mixture was continued stirring at this temperature for 12 h. The reaction mixture was then diluted with dichloromethane (30 mL) and purified by column chromatography (0 % – 10 % gradient MeOH in EtOAc) to afford beige solid **2.6** (402 mg, 77%); R_f = 0.02 (EtOAc); ^{1}H NMR (DMSO-d_6, 300 MHz) δ 8.35 (d, *J* = 8.2 Hz, 1H), 7.69 (d, *J* = 7.7 Hz, 1H), 7.28 (d, *J* = 7.8 Hz, 1H), 7.01 (d, *J* = 7.5 Hz, 1H), 5.61 (s, 1H), 1.33 (s, 6H); ^{13}C NMR ($CDCl_3$, 75 MHz) δ 176.1, 136.3, 135.7, 129.8, 127.4, 122.5, 120.3, 72.8, 28.2; HRMS calculated for $C_{10}H_{12}NO_2S$ (M+H): 210.05833; Found: 210.05879 m/z.

4,4',5,5'-tetramethyl-[2,2'-bithiazole] 3-oxide (**2.7**)

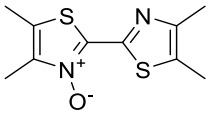

In a sealed, argon-purged microwave reaction vessel, **2.20a** (125mg, 0.40 mmol, 1.0 equiv) was dissolved in anhydrous tetrahydrofuran (8 mL, 0.05 M) allowed to stir at room temperature. *t*-BuOH (0.4 mL) and LiO*t*-Bu (0.6 mL, 1M in THF, 1.5 equiv) were then added and the mixture was immediately heated by microwave irradiation for 1 h at 60 °C. The reaction mixture was then diluted with dichloromethane (30 mL) and washed with water (3 x 20 mL) before being dried with $MgSO_4$ and concentrated. The residue was then triturated using hexanes (200 mL) to afford off-white solid **2.7** (38 mg, 79%); R_f = 0.75 (EtOAc); ^{1}H NMR ($CDCl_3$, 300 MHz) δ 2.45 (s, 6H), 2.42 (s, 3H), 2.37 (s, 3H). Data consistent with previously reported literature.[145]

[2,2'-bithiazole] 3-oxide (**2.8**)

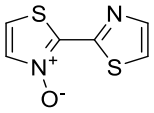

In a sealed, argon-purged microwave reaction vessel, **2.20b** (283 mg, 1.0 mmol, 1.0 equiv) was dissolved in anhydrous tetrahydrofuran (20 mL, 0.05 M) and allowed to stir at room temperature. *t*-BuOH (1.0 mL, 1 M) and LiO*t*-Bu (1.5 mL, 1 M in THF, 1.5 equiv) were then added and the mixture was immediately heated by microwave irradiation for 1 h at 60 °C. The reaction mixture was then diluted with dichloromethane (30 mL) and washed with water (3 x 20 mL) before being dried with $MgSO_4$ and concentrated. The reaction mixture was then isolated by column chromatography (0 % – 10 % gradient

MeOH in EtOAc) to yield off-white solid **2.8** (52 mg, 56%); R_f = 0.47 (EtOAc : MeOH = 1 : 9); ^{1}H-NMR ($CDCl_3$, 300 MHz) δ 8.03 (d, *J* = 2.7 Hz, 1H), 7.80 (d, *J* = 3.8 Hz, 1H), 7.56 (d, *J* = 2.8 Hz, 1H), 7.43 (d, *J* = 3.7 Hz, 1H); ^{13}C-NMR ($CDCl_3$, 75 MHz) δ 152.7, 143.4, 137.1, 120.9, 117.4; HRMS calculated for $C_6H_5ON_2S_2$ (M+H): 184.98378; Found: 184.98504 m/z.

[2,2'-bibenzo[d]thiazole] 3-oxide (**2.9**)

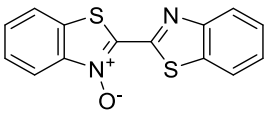

In a sealed, argon-purged microwave reaction vessel, **2.20c** (70 mg, 0.21 mmol, 1.0 equiv) was dissolved in anhydrous tetrahydrofuran (4.0 mL, 0.05 M) and allowed to stir at room temperature. *t*-BuOH (0.2 mL, 1 M) and Li*O*t-Bu (315 µL, 1 M in THF, 1.5 equiv) were then added and the mixture was immediately heated by microwave irradiation for 1 h at 60 °C. The reaction mixture was then diluted with dichloromethane (100 mL) and washed with water (2 x 100 mL) and brine (100 mL) before being dried with $MgSO_4$ and concentrated. The reaction mixture was then triturated with hexanes, filtered and redissolved in dichloromethane to yield off-white solid **2.9** (22 mg, 74%); R_f = 0.18 (EtOAc); ^{1}H-NMR ($CDCl_3$, 300 MHz) δ 8.34 – 8.30 (m, 1H), 8.19 (d, *J* = 8.3 Hz, 1H), 8.11 (d, *J* = 7.8 Hz, 1H), 7.96 – 7.93 (m, 1H), 7.72 – 7.69 (m, 2H), 7.63 (dt, *J* = 7.1, 1.2 Hz, 1H), 7.54 (dt, *J* = 8.0, 1.2 Hz, 1H); HRMS calculated for $C_{14}H_9ON_2S_2$ (M+H): 285.01563; Found: 285.01836 m/z. ^{13}C NMR was unobtainable due to poor solubility.

General procedure A: Synthesis of 5-Arylthiazoles by Direct Arylation

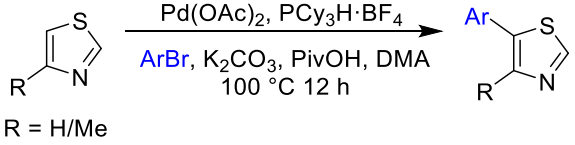

To a round bottom flask charged with $Pd(OAc)_2$ (27 mg, 2 mol %), K_2CO_3 (1.24 g, 9 mmol, 1.5 equiv), PCy_3HBF_4 (90 mg, 4 mol %), and PivOH (220 mg, 30 mol %), was added DMA (12 mL, 0.5 M) followed by thiazole (9 mmol, 1.5 equiv) and aryl halide (6 mmol, 1 equiv). The vial was sealed, purged with argon and the mixture stirred at 100 ℃ for 12 hours. The reaction mixture was then dissolved in H_2O (50 mL), and extracted with Et_2O (3x30 mL). The organic layer was then dried with $MgSO_4$ and filtered through Celite®. The filtrate was then concentrated and purified by column chromatography to yield 5-arylthiazoles.

5-phenylthiazole (**2.10a**)

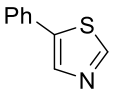

Prepared according to **General Procedure A** starting with 1-bromobenzene (352 µL, 3.3 mmol, 1.0 equiv) and purified by column chromatography (0 % – 20 % gradient EtOAc in hexanes) to afford yellow solid **2.10a** (477 mg, 90%); R_f = 0.6 (EtOAc : Hexane = 1 : 1); ^{1}H NMR ($CDCl_3$, 300 MHz) δ 8.74 (s, 1H), 8.07 (s, 1H), 7.58 (d, *J* = 8.0 Hz, 2H), 7.43 – 7.33 (m, 3H); ^{13}C NMR ($CDCl_3$, 75 MHz) δ 150.1, 139.4, 139.0, 131.1, 129.1, 128.5, 127.0; HRMS calculated for C_9H_8NS (M+H): 162.03720; Found: 162.03745 m/z.

4-methyl-5-phenylthiazole (**2.10b**)

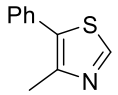

Prepared according to **General Procedure A** starting with 1-bromobenzene (352 µL, 3.3 mmol, 1.0 equiv) and 4-methylthiazole (455 µL, 5.0 mmol, 1.5 equiv), and purified by column chromatography (0 % – 20 % gradient EtOAc in hexanes) to afford yellow oil **2.10b** (568 mg, 98%); R_f = 0.57 (EtOAc : Hexane = 1 : 1); ^{1}H NMR ($CDCl_3$, 300 MHz) 8.63 (s, 1H), 7.40 – 7.31 (m, 5H), 2.51 (s, 3H); δ ^{13}C NMR ($CDCl_3$, 75 MHz) δ 150.3, 148.5, 132.0, 129.3, 128.7, 127.9, 16.1 *one peak missing due to overlap; Data consistent with previously reported literature.[145]

5-(p-tolyl)thiazole (**2.10c**)

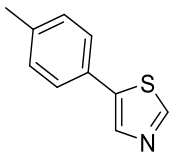

Prepared according to **General Procedure A** starting with 4-bromotoluene (855 mg, 5.0 mmol, 1.0 equiv) and purified by column chromatography (0 % – 30 % gradient EtOAc in hexanes) to afford yellow solid **2.10c** (755 mg, 86%); R_f = 0.48 (EtOAc : Hexane = 2 : 3); ^{1}H NMR ($CDCl_3$, 300 MHz) δ 8.71 (s, 1H), 8.03 (s, 1H), 7.46 (d, *J* = 7.9 Hz, 2H), 7.21 (d, *J* = 7.9 Hz, 2H), 2.37 (s, 3H); ^{13}C NMR ($CDCl_3$, 75 MHz) δ 151.6, 139.5, 138.6, 138.5, 129.8, 129.3, 126.9, 21.2; HRMS calculated for $C_{10}H_{10}NS$ (M+H): 176.05285; Found: 176.05318 m/z.

5-(naphthalen-2-yl)thiazole (**2.10d**)

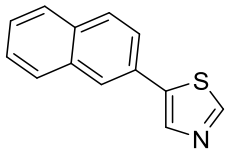

Prepared according to **General Procedure A** starting with 2-bromonaphthalene (621 mg, 3.0 mmol, 1.0 equiv) and purified by column chromatography (0 % – 30 % gradient EtOAc in hexanes) to afford yellow solid **2.10d** (483 mg, 73%); R_f = 0.42 (EtOAc : Hexane = 2 : 3); ^{1}H NMR ($CDCl_3$, 300 MHz) δ 8.79 (s, 1H), 8.20 (s, 1H), 8.02 (s, 1H), 7.89 – 7.82 (m, 3H), 7.70 (d, *J* = 8.6 Hz, 1H), 7.50 (p, *J* = 7.1 Hz, 2H); ^{13}C NMR ($CDCl_3$, 75 MHz) δ 152.2, 139.6, 139.3, 133.5, 133.1, 128.9, 128.5, 128.1, 127.8, 126.9, 126.6, 125.9, 124.8; HRMS calculated for $C_{13}H_{10}NS$ (M+H): 212.05285; Found: 212.05382 m/z.

5-(naphthalen-1-yl)thiazole (**2.10e**)

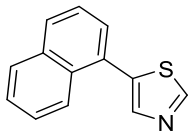

Prepared according to **General Procedure A** starting with 1-bromonaphthalene (2.07 g, 10.0 mmol, 1.0 equiv) and purified by column chromatography (0 % – 25 % gradient EtOAc in hexanes) to afford brown solid **2.10e** (1.35 g, 64%); R_f = 0.27 (EtOAc : Hexane = 1 : 4); ^{1}H NMR ($CDCl_3$, 300 MHz) δ 8.95 (s, 1H), 8.11 – 8.05 (m, 2H), 7.93 (d, *J* = 7.0 Hz, 2H), 7.59 – 7.52 (m, 4H); ^{13}C NMR ($CDCl_3$, 75 MHz) δ 153.2, 142.5, 136.3, 133.8, 132.0, 129.4, 128.9, 128.5, 128.3, 126.9, 126.3, 125.2, 125.1; HRMS calculated for $C_{13}H_{10}NS$ (M+H): 212.05285; Found: 212.05329 m/z.

5-(4-hexylphenyl)thiazole (**2.10f**)

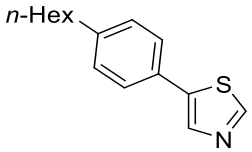

Prepared according to **General Procedure A** starting with 1-bromo-4-hexylbenzene (2.05 mL, 10.0 mmol, 1.0 equiv) and purified by column chromatography (0 % – 20 % gradient EtOAc in hexanes) to afford orange liquid **2.10f** (2.45 g, 78%); R_f = 0.6 (EtOAc : Hexane = 2 : 3); ^{1}H NMR ($CDCl_3$, 300 MHz) δ 8.70 (s, 1H), 8.03 (s, 1H), 7.47 (d, *J* = 7.9 Hz, 2H), 7.20 (d, *J* = 7.9 Hz, 2H), 2.61 (t, *J* = 7.7 Hz, 2H), 1.63 – 1.59 (m, 2H), 1.35 – 1.30 (m, 6H), 0.88 (t, *J* = 6.3 Hz, 3H); ^{13}C NMR ($CDCl_3$, 75 MHz) δ 151.5, 143.4, 139.4, 130.5, 129.0, 128.4, 126.8, 35.6, 31.6, 31.2, 28.8, 22.5, 14.0; HRMS calculated for $C_{15}H_{20}NS$ (M+H): 246.13110; Found: 246.12957 m/z.

5-(4-(hexyloxy)phenyl)thiazole (**2.10g**)

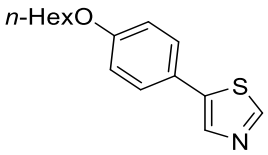

Prepared according to **General Procedure A** starting with **S1** (3.86 g, 15.0 mmol, 1.0 equiv) and purified by column chromatography (0 % – 15 % gradient EtOAc in hexanes) to afford brown oil **2.10g** (2.8 g, 72%); R_f = 0.29 (EtOAc : Hexane = 3 : 7); ^{1}H NMR ($CDCl_3$, 300 MHz) δ 8.70 (s, 1H), 7.99 (s, 1H), 7.51 (d, *J* = 8.7 Hz, 2H), 6.95 (d, *J* = 8.8 Hz, 2H), 4.00 (t, *J* = 6.6 Hz, 2H), 1.82 (p, *J* = 6.8 Hz, 2H), 1.54 – 1.44 (m, 2H), 1.39 – 1.34 (m, 4H), 0.93 (t, *J* = 6.9 Hz, 3H); ^{13}C NMR ($CDCl_3$, 75 MHz) δ 159.5, 151.1, 139.3, 138.0, 128.2,

123.5, 115.1, 68.1, 31.6, 29.1, 25.7, 22.6, 14.0; HRMS calculated for $C_{15}H_{20}ONS$ (M+H): 262.12601; Found: 262.12585 m/z.

5-(4-methoxyphenyl)thiazole (**2.10h**)

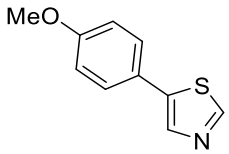

Prepared according to **General Procedure A** starting with 1-bromo-4-methoxybenzene (826 µL, 6.6 mmol, 1.0 equiv) and purified by column chromatography (0 % – 50 % gradient EtOAc in hexanes) to afford yellow solid **2.10h** (1.17 g, 93%); R_f = 0.49 (EtOAc : Hexane = 1 : 1); ^{1}H NMR ($CDCl_3$, 300 MHz) δ 8.71 (s, 1H), 7.99 (s, 1H), 7.51 (d, *J* = 8.6 Hz, 2H), 6.95 (d, *J* = 8.6 Hz, 2H), 3.85 (s, 3H); ^{13}C NMR ($CDCl_3$, 75 MHz) δ 159.9, 151.2, 139.2, 138.1, 128.3, 123.7, 114.5, 55.4; Data consistent with previously reported literature.[145]

5-(4-methoxyphenyl)-4-methylthiazole (**2.10i**)

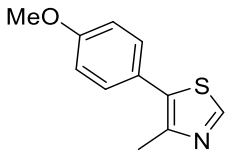

Prepared according to **General Procedure A** starting with 1-bromo-4-methoxybenzene (751 µL, 6.0 mmol, 1.0 equiv) and 4-methylthiazole (819 µL, 9.0 mmol, 1.5 equiv), and purified by column chromatography (0 % – 25 % gradient EtOAc in hexanes) to afford yellow solid **2.10i** (1.23 g, 100%); R_f = 0.27 (EtOAc : Hexane = 2 : 3); ^{1}H NMR ($CDCl_3$, 300 MHz) δ 8.65 (s, 1H), 7.37 (d, *J* = 8.8 Hz, 2H), 6.96 (d, *J* = 8.7 Hz, 2H), 3.85 (s, 3H),

2.52 (s, 3H); ^{13}C NMR ($CDCl_3$, 75 MHz) δ 159.4, 149.7, 147.9, 131.7, 130.5, 124.2, 114.2, 55.3, 16.0; Data consistent with previously reported literature.[145]

4-(thiazol-5-yl)benzonitrile (**2.10j**)

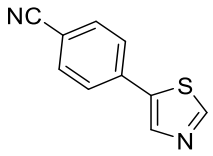

Prepared according to **General Procedure A** starting with 4-bromobenzonitrile (1.2 g, 6.6 mmol, 1.0 equiv) and purified by column chromatography (0 % – 40 % gradient EtOAc in hexanes) to afford brown solid **2.10j** (943 mg, 77%); R_f = 0.4 (EtOAc : Hexane = 1 : 1); ^{1}H NMR ($CDCl_3$, 300 MHz) δ 8.86 (s, 1H), 8.19 (s, 1H), 7.73 – 7.67 (m, 4H); ^{13}C NMR ($CDCl_3$, 75 MHz) δ 153.8, 140.7, 137.4, 135.6, 132.9, 127.3, 118.4, 111.9; HRMS calculated for $C_{10}H_7N_2S$ (M+H): 187.03245; Found: 187.03316 m/z.

4-(4-methylthiazol-5-yl)benzonitrile (**2.10k**)

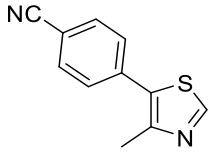

Prepared according to **General Procedure A** starting with 4-bromobenzonitrile (1.09 g, 6.0 mmol, 1.0 equiv) and 4-methylthiazole (819 µL, 9 mmol, 1.0 equiv), and purified by column chromatography (0 % – 30 % gradient EtOAc in hexanes) to afford yellow solid **2.10k** (1.17 g, 97%); R_f = 0.18 (EtOAc : Hexane = 2 : 3); ^{1}H NMR ($CDCl_3$, 300 MHz) δ 8.76 (s, 1H), 7.73 (d, *J* = 8.3 Hz, 2H), 7.57 (d, *J* = 8.3 Hz, 2H), 2.57 (s, 3H); ^{13}C NMR ($CDCl_3$, 75 MHz) δ 151.6, 150.1, 136.7, 132.5, 130.1, 129.7, 118.4, 111.5, 16.4; Data consistent with previously reported literature.[145]

5-(4-fluorophenyl)thiazole (**2.10l**)

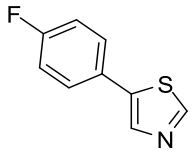

Prepared according to **General Procedure A** starting with 1-bromo-4-fluorobenzene (639 µL, 6.0 mmol, 1.0 equiv) and purified by column chromatography (0 % – 50 % gradient EtOAc in hexanes) to afford a pale yelow solid **2.10l** (828 mg, 77%); R_f = 0.51 (EtOAc : Hexane = 3 : 7); ^{1}H NMR ($CDCl_3$, 300 MHz) δ 8.76 (s, 1H), 8.03 (s, 1H), 7.56 (dd, *J* = 8.1 Hz, J_{HF} = 5.8 Hz, 2H), 7.15 – 7.10 (m, 2H); ^{13}C NMR ($CDCl_3$, 75 MHz) δ 162.8 (d, $^{1}J_{CF}$ = 248.8 Hz), 152.1, 139.0, 138.3, 128.7 (d, $^{3}J_{CF}$ = 8.2 Hz), 127.3 (d, $^{4}J_{CF}$ = 3.5 Hz), 116.2 (d, $^{2}J_{CF}$ = 22.0 Hz); ^{19}F NMR ($CDCl_3$, 470 MHz) δ -113.1; HRMS calculated for C_9H_7NFS (M+H): 180.02777; Found: 180.02871 m/z.

5-(4-(trifluoromethyl)phenyl)thiazole (**2.10m**)

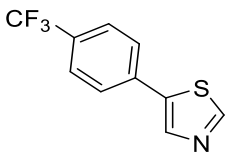

Prepared according to **General Procedure A** starting with 1-bromo-4-(trifluoromethyl)benzene (924 µL, 6.6 mmol, 1.0 equiv) and purified by column chromatography (0 % – 50 % gradient EtOAc in hexanes) to afford a brown solid **2.10m** (1.24 g, 82%); R_f = 0.50 (EtOAc : Hexane = 1 : 1); ^{1}H NMR ($CDCl_3$, 300 MHz) δ 8.84 (s, 1H), 8.18 (s, 1H), 7.71 – 7.68 (m, 4H); ^{13}C NMR ($CDCl_3$, 75 MHz) δ 153.1, 140.1, 137.8, 134.6, 130.3 (q, $^{2}J_{CF}$ = 32.8 Hz), 127.1, 126.1 (q, $^{3}J_{CF}$ = 3.8 Hz), 123.9 (q, $^{1}J_{CF}$ = 272.1

Hz); ^{19}F NMR ($CDCl_3$, 470 MHz) δ -63.0; HRMS calculated for $C_{10}H_7NF_3S$ (M+H): 230.02458; Found: 230.02609 m/z.

4-methyl-5-(4-(trifluoromethyl)phenyl)thiazole (**2.10n**)

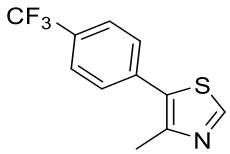

Prepared according to **General Procedure A** starting with 1-bromo-4-(trifluoromethyl)benzene (840 µL, 6.0 mmol, 1.0 equiv) and 4-methylthiazole (819 µL, 9.0 mmol, 1.5 equiv), and purified by column chromatography (0 % – 30 % gradient EtOAc in hexanes) to afford yellow solid **2.10n** (1.44 g, 99%); R_f = 0.38 (EtOAc : Hexane = 2 : 3); ^{1}H NMR ($CDCl_3$, 300 MHz) δ 8.72 (s, 1H), 7.68 (d, *J* = Hz, 2H), 7.55 (d, *J* = Hz, 2H), 2.55 (s, 3H); ^{13}C NMR ($CDCl_3$, 75 MHz) δ 151.0, 149.6, 135.7, 130.5, 129.9 (q, $^2J_{CF}$ = 32.7 Hz), 129.5, 125.7 3 (q, $^3J_{CF}$ = 3.8 Hz), 124.0 3 (d, $^1J_{CF}$ = 272.2 Hz), 16.1; ^{19}F NMR ($CDCl_3$, 470 MHz) δ -62.9; Data consistent with previously reported literature.[145]

5-(3,5-bis(trifluoromethyl)phenyl)thiazole (**2.10o**)

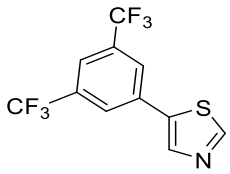

Prepared according to **General Procedure A** starting with 1-bromo-3,5-bis(trifluoromethyl)benzene (1.02 mL, 6.0 mmol, 1.0 equiv) and purified by column chromatography (0 % – 25 % gradient EtOAc in hexanes) to afford off-white solid **2.10o** (1.21 g, 68%); R_f = 0.59 (EtOAc : Hexane = 2 : 3); ^{1}H NMR ($CDCl_3$, 300 MHz) δ 8.90 (s,

1H), 8.23 (s, 1H), 8.01 (s, 2H), 7.87 (s, 1H); ^{13}C NMR ($CDCl_3$, 75 MHz) δ 153.8, 141.0, 136.3, 132.7 (q, $^{2}J_{CF}$ = 34.4 Hz), 126.8, 123.0 (q, $^{1}J_{CF}$ = 272.9 Hz), 121.9 (q, $^{3}J_{CF}$ = 3.7 Hz); ^{19}F NMR ($CDCl_3$, 470 MHz) δ -63.3; HRMS calculated for $C_{11}H_6NF_6S$ (M+H): 298.01197; Found: 298.01274 m/z.

5-(5-hexylthiophen-2-yl)thiazole (**2.10p**)

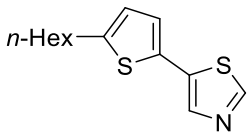

Prepared according to **General Procedure A** starting with 5-bromo-2-hexylthiophene (1.0 g, 4.0 mmol, 1.0 equiv) and purified by column chromatography (0 % – 25 % gradient EtOAc in hexanes) to afford off-white solid **2.10p** (201 mg, 20%); R_f = 0.67 (EtOAc : Hexane = 2 : 3); ^{1}H NMR ($CDCl_3$, 300 MHz) δ 8.62 (s, 1H), 7.87 (s, 1H), 6.99 (d, *J* = 3.4 Hz, 1H), 6.69 (d, *J* = 6.3 Hz, 1H), 2.78 (t, *J* = 7.6 Hz, 2H), 1.66 (quint, *J* = 7.3 Hz, 2H), 1.36 – 1.31 (m, 6H), 0.88 (t, *J* = 2.9 Hz, 1H) ; ^{13}C NMR ($CDCl_3$, 75 MHz) δ 150.9, 147.0, 138.6, 133.1, 130.1, 125.7, 124.9, 31.6, 30.1, 28.8, 22.6, 14.1 *one peak absent due to overlap; Data consistent with previously reported literature.[145]

N,N-dimethyl-4-(thiazol-5-yl)aniline (**2.10q**)

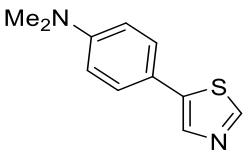

Prepared according to **General Procedure A** starting with 4-bromo-N,N-dimethylaniline (2.0 g, 10.0 mmol, 1.0 equiv) and purified by column chromatography (0 % – 15 % gradient EtOAc in hexanes) to afford off-white solid **2.10q** (1.29 g, 63%); R_f = 0.38 (EtOAc

: Hexane = 3 : 7); ^{1}H NMR ($CDCl_3$, 300 MHz) δ 8.65 (s, 1H), 7.95 (s, 1H), 7.47 (d, *J* = 8.9 Hz, 2H), 6.75 (d, *J* = 8.8 Hz, 2H), 3.01 (s, 6H); ^{13}C NMR ($CDCl_3$, 75 MHz) δ 150.5, 150.2, 140.1, 137.0, 127.9, 119.0, 112.5, 40.4; HRMS calculated for $C_{11}H_{13}N_2S$ (M+H): 205.07940; Found: 205.07958 m/z.

2-(5-phenylthiazol-2-yl)propan-2-ol (**2.11a**)

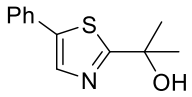

To a round-bottom flask charged with **2.10a** (2.20 g, 13.7 mmol, 1.0 equiv), purged with argon and sealed was added THF (55 mL, 0.25 M) and allowed to stir in a -78 °C bath of dry ice and acetone. *n*BuLi (10.2 mL, 1.6 M, 1.2 equiv) was added and the mixture was stirred at this temperature for 30 min. Acetone (1.53 mL, 20.6 mmol, 1.5 equiv) was then added, the vessel purged with argon, and continued to stir at this temperature for 4 h. The reaction mixture was then quenched with NH_4Cl (80 mL) and extracted with diethyl ether (3 x 100 mL). The organic layer was then dried with $MgSO_4$ and concentrated. The crude product was then purified by column chromatography (0 % – 30 % gradient EtOAc in hexanes) to yield **2.11a** (2.12 g, 71%); R_f = 0.52 (EtOAc : Hexane = 2 : 3); ^{1}H NMR ($CDCl_3$, 300 MHz) δ 7.80 (s, 1H), 7.51 (d, *J* = 7.1 Hz, 2H), 7.29 – 7.30 (m, 3H), 3.46 (br s, 1H), 1.71 (s, 6H); ^{13}C NMR ($CDCl_3$, 75 MHz) δ 178.6, 139.3, 137.5, 131.5, 129.1, 128.2, 126.7, 73.2, 30.9; HRMS calculated for $C_{12}H_{14}ONS$ (M+H): 220.07906; Found: 220.07984.

2-(4-methyl-5-phenylthiazol-2-yl)propan-2-ol (**2.11b**)

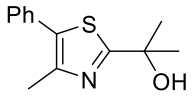

To a round-bottom flask charged with **2.10b** (175 mg, 1.0 mmol, 1.0 equiv), purged with argon and sealed was added THF (2 mL, 0.5 M) and allowed to stir in a -78 °C bath of dry ice and acetone. *n*BuLi (750 µL, 1.6 M, 1.2 equiv) was added and the mixture was stirred at this temperature for 30 min. Acetone (110 µL, 1.5 mmol, 1.5 equiv) was then added, the vessel purged with argon, and continued to stir at this temperature for 4 h. The reaction mixture was then quenched with NH_4Cl (10 mL) and extracted with diethyl ether (3 x 10 mL). The organic layer was then dried with $MgSO_4$ and concentrated. The crude product was then purified by column chromatography (0 % – 30 % gradient EtOAc in hexanes) to yield **2.11b** (233 mg, 79%); R_f = 0.55 (EtOAc : Hexane = 1 : 1); ^{1}H NMR ($CDCl_3$, 300 MHz) δ 7.41 – 7.37 (m, 4H), 7.35 – 7.33 (m, 1H), 2.45 (s, 3H), 1.68 (s, 6H); ^{13}C NMR ($CDCl_3$, 75 MHz) δ 175.9, 147.0, 132.3, 132.0, 129.2, 128.7, 127.7, 73.0, 31.1, 16.17; HRMS calculated for $C_{13}H_{16}ONS$ (M+H): 234.09471; Found: 234.09507.

2-(2-hydroxypropan-2-yl)-5-phenylthiazole 3-oxide (**2.12a**)

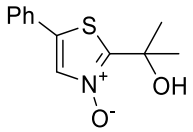

In a round-bottom flask, **2.11a** (2.12 g, 9.7 mmol, 1.0 equiv) was dissolved in 1,2-dichloroethane (30 mL, 0.3M) and allowed to stir at room temperature. *m*-CPBA (3.2 g, 77 % pure, 14.6 mmol, 1.5 equiv) was then added and the mixture was continued stirring at this temperature for 6 h. The reaction mixture was then diluted with dichloromethane

(50 mL) and then purified by column chromatography (0 % – 5 % gradient MeOH in EtOAc) to yield **2.12a** (1.84 g, 81%); R_f = 0.57 (MeOH : EtOAc = 1 : 4); ^{1}H NMR ($CDCl_3$, 300 MHz) δ 7.80 (s, 1H), 7.48 (s, 5H), 1.73 (s, 6H); ^{13}C NMR ($CDCl_3$, 75 MHz) δ 152.8, 133.9, 132.8, 130.0, 129.4, 128.7, 125.8, 71.0, 27.5; HRMS calculated for $C_{12}H_{14}O_2NS$ (M+H): 236.07398; Found: 236.07396.

2-(2-hydroxypropan-2-yl)-4-methyl-5-phenylthiazole 3-oxide (**2.12b**)

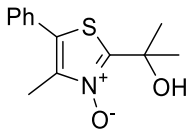

In a round-bottom flask, **2.11b** (117 mg, 0.5 mmol, 1.0 equiv) was dissolved in 1,2-dichloroethane (1.5 mL, 0.3M) and allowed to stir at room temperature. *m*-CPBA (168 mg, 77 % pure, 0.75 mmol, 1.5 equiv) was then added and the mixture was continued stirring at this temperature for 6 h. The reaction mixture was then diluted with dichloromethane (10 mL) and then purified by column chromatography (0 % – 5 % gradient MeOH in EtOAc) to yield **2.12b** (107 mg, 86%); R_f = 0.54 (MeOH : EtOAc = 1 : 4); ^{1}H NMR ($CDCl_3$, 300 MHz) δ 7.43 – 7.39 (m, 5H), 2.42 (s, 3H), 1.68 (s, 6H); ^{13}C NMR ($CDCl_3$, 75 MHz) δ 151.4, 141.6, 130.3, 129.4, 129.3, 128.7, 127.5, 70.8, 27.9, 11.8; HRMS calculated for $C_{13}H_{16}NO_2S$ (M+H): 250.08963; Found: 250.08958.

General procedure B: Activation of 5-Arylthiazoles with Benzophenone

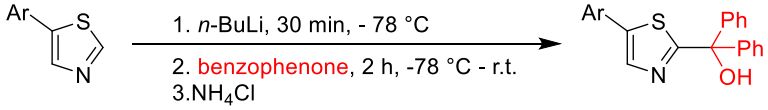

To a round-bottom flask charged with thiazole (4.0 mmol, 1.0 equiv), purged with argon and sealed was added THF (40 mL, 0.1 M) and allowed to stir in a -78 °C bath of dry ice

and acetone. *n*BuLi (4.8 mmol, 1.6 M 1.2 equiv) was added and the mixture was stirred at this temperature for 30 min. Benzophenone (6.0 mmol, 1.5 equiv) was then added, the vessel purged with argon, and continued to stir at this temperature for 4 h. The reaction mixture was then quenched with NH_4Cl (30 mL) and extracted with diethyl ether (3 x mL). The organic layer was then dried with $MgSO_4$ and concentrated. The crude product was then purified by column chromatography to yield (5-arylthiazol-2-yl) diphenylmethanols.

diphenyl(5-phenylthiazol-2-yl)methanol (**2.13a**)

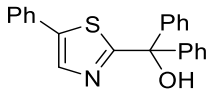

Prepared according to **General Procedure B** starting with **2.10a** (1.20 g, 7.4 mmol, 1 equiv) and purified by column chromatography (0 % – 20 % gradient EtOAc in hexanes) to afford pale yellow solid **2.13a** (2.14 g, 84%); R_f = 0.52 (EtOAc : Hexane = 1 : 4); ^{1}H NMR ($CDCl_3$, 300 MHz) δ 7.97 (s, 1H), 7.54 (d, *J* = 7.5 Hz, 2H), 7.47 (d, *J* = 6.5 Hz, 4H), 7.42 – 7.33 (m, 9H), 4.21 (br s, 1H); ^{13}C NMR ($CDCl_3$, 75 MHz) δ 176.0, 145.2, 140.6, 137.6, 131.2, 129.1, 128.4, 128.2, 128.0, 127.5, 126.7, 80.7; HRMS calculated for $C_{22}H_{18}ONS$ (M+H): 344.11036; Found: 344.11081.

(4-methyl-5-phenylthiazol-2-yl)diphenylmethanol (**2.13b**)

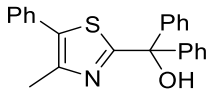

Prepared according to **General Procedure B** starting with **2.10b** (215 mg, 1.2 mmol, 1.0 equiv) and purified by column chromatography (0 % – 20 % gradient EtOAc in hexanes) to afford off-white solid **2.13b** (383 mg, 89%); R_f = 0.71 (EtOAc : Hexane = 2 : 3); ^{1}H NMR

($CDCl_3$, 300 MHz) δ 7.49 (dd, *J* = 7.9, 1.6 Hz, 4H), 7.43 – 7.36 (m, 11H), 4.57 (br s, 1H), 2.53 (s, 3H); ^{13}C NMR ($CDCl_3$, 75 MHz) δ 175.6, 147.4, 145.5, 133.7, 131.9, 129.2, 128.7, 128.1, 127.9, 127.8, 127.6, 80.4, 16.3; HRMS calculated for $C_{23}H_{20}ONS$ (M+H): 358.12601; Found: 358.12626 m/z.

diphenyl(5-(p-tolyl)thiazol-2-yl)methanol (**2.13c**)

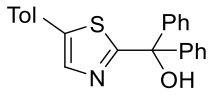

Prepared according to **General Procedure B** starting with **2.10c** (6.0 g, 34.0 mmol, 1.0 equiv) and purified by column chromatography (0 % – 10 % gradient EtOAc in hexanes) to afford pale yellow solid **2.13c** (6.98 g, 58%); R_f = 0.54 (EtOAc : Hexane = 1 : 4); ^1H NMR ($CDCl_3$, 300 MHz) δ 7.90 (s, 1H), 7.49 – 7.36 (m, 12H), 7.20 (d, *J* = 7.9 Hz, 2H), 4.45 (br s, 1H), 2.39 (s, 3H); ^{13}C NMR ($CDCl_3$, 75 MHz) δ 175.6, 145.3, 140.7, 138.4, 137.4, 129.7, 128.3, 128.2, 128.0, 127.5, 126.6, 80.7, 21.2; HRMS calculated for $C_{23}H_{20}ONS$ (M+H): 358.12601; Found: 358.12534 m/z.

diphenyl(5-(naphthalen-2-yl)thiazol-2-yl)methanol (**2.13d**)

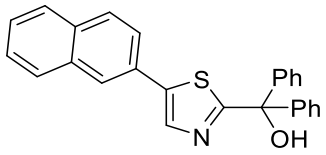

Prepared according to **General Procedure B** starting with **2.10d** (1.06 g, 5.0 mmol, 1.0 equiv) and purified by column chromatography (0 % – 30 % gradient EtOAc in hexanes) to afford orange solid **2.13d** (1.75 g, 77%); R_f = 0.62 (EtOAc : Hexane = 3 : 7); ^1H NMR ($CDCl_3$, 300 MHz) δ 8.09 (s, 1H), 7.98 (s, 1H), 7.89 – 7.83 (m, 3H), 7.67 (dd, *J* = 8.5 Hz,

1.8 Hz, 1H), 7.53 – 7.48 (m, 6H), 7.44 – 7.36 (m, 6H), 4.31 (br s, 1H); ^{13}C NMR ($CDCl_3$, 75 MHz) δ 176.2, 145.2, 140.7, 138.2, 133.5, 133.0, 128.8, 128.6, 128.2, 128.1, 128.0, 127.8, 127.5, 126.8, 126.5, 125.6, 124.4, 80.7; HRMS calculated for $C_{26}H_{20}ONS$ (M+H): 394.12601; Found: 394.12586 m/z.

(5-(naphthalen-1-yl)thiazol-2-yl)diphenylmethanol (**2.13e**)

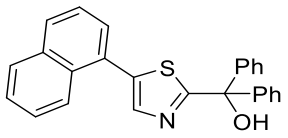

Prepared according to **General Procedure B** starting with **2.10e** (1.06 g, 5.0 mmol, 1.0 equiv) and purified by column chromatography (0 % – 20 % gradient EtOAc in hexanes) to afford pale-orange solid **2.13e** (1.60 g, 81%); R_f = 0.45 (EtOAc : Hexane = 1 : 4); ^{1}H NMR ($CDCl_3$, 300 MHz) δ 8.17 – 8.14 (m, 2H), 7.94 – 7.91 (m, 3H), 7.57 – 7.48 (m, 8H), 7.44 – 7.34 (m, 6H); ^{13}C NMR ($CDCl_3$, 75 MHz) δ 177.2, 145.3, 141.5, 137.5, 133.8, 131.7, 129.3, 128.8, 128.5, 128.4, 128.2, 128.1, 127.5, 126.9, 126.6, 126.3, 125.2, 80.8; HRMS calculated for $C_{26}H_{20}ONS$ (M+H): 394.12601; Found: 394.12590 m/z.

(5-(4-hexylphenyl)thiazol-2-yl)diphenylmethanol (**2.13f**)

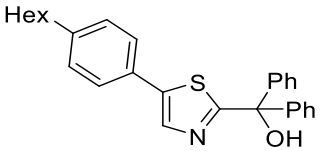

Prepared according to **General Procedure B** starting with **2.10f** (2.45 g, 10.0 mmol, 1.0 equiv) and purified by column chromatography (0 % – 10 % gradient EtOAc in hexanes) to afford brown solid **2.13f** (2.74 mg, 64%); R_f = 0.70 (EtOAc : Hexane = 3 : 7); ^{1}H NMR ($CDCl_3$, 300 MHz) δ 7.92 (s, 1H), 7.49 – 7.43 (m, 6H), 7.41 – 7.34 (m, 6H), 7.20 (d, *J* =

8.2 Hz, 2H), 4.32 (br s, 1H), 2.64 (t, *J* = 7.8 Hz, 2H), 1.64 (p, *J* = 7.5 Hz, 2H), 1.41 – 1.29 (m, 6H), 0.91 (t, *J* = 6.8 Hz, 3H); ^{13}C NMR ($CDCl_3$, 75 MHz) δ 175.5, 145.3, 143.5, 140.8, 137.4, 129.1, 128.5, 128.2, 128.0, 127.5, 126.6, 80.7, 35.7, 31.7, 31.3, 28.9 22.6, 14.1; HRMS calculated for $C_{28}H_{30}ONS$ (M+H): 428.20426; Found: 428.20425 m/z.

(5-(4-(hexyloxy)phenyl)thiazol-2-yl)diphenylmethanol (**2.13g**)

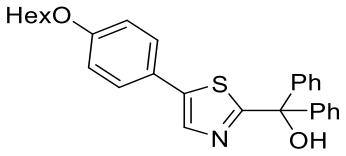

Prepared according to **General Procedure B** starting with **2.10g** (523 mg, 2.0 mmol, 1.0 equiv) and purified by column chromatography (0 % – 15 % gradient EtOAc in hexanes) to afford amber oil **2.13g** (455 mg, 51%); R_f = 0.81 (EtOAc : Hexane = 1 : 1); ^{1}H NMR ($CDCl_3$, 300 MHz) δ 7.82 (s, 1H), 7.50 – 7.36 (m, 12H), 6.92 (d, *J* = 8.6 Hz, 2H), 4.49 (br s, 1H), 4.00 (t, *J* = 6.5 Hz, 2H), 1.82 (p, *J* = 7.7 Hz, 2H), 1.52 – 1.38 (m, 6H), 0.95 (t, *J* = 6.5 Hz, 3H); ^{13}C NMR ($CDCl_3$, 75 MHz) δ 175.0, 159.4, 145.4, 140.6, 136.8, 128.2, 128.0, 127.6, 127.5, 123.6, 115.1, 80.7, 68.2, 31.6, 29.2, 25.7, 22.6, 14.1; HRMS calculated for $C_{28}H_{30}O_2NS$ (M+H): 444.19918; Found: 444.19910 m/z.

(5-(4-methoxyphenyl)thiazol-2-yl)diphenylmethanol (**2.13h**)

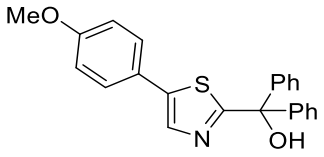

Prepared according to **General Procedure B** starting with **2.10h** (561 mg, 2.9 mmol, 1.0 equiv) and purified by column chromatography (0 % – 25 % gradient EtOAc in hexanes) to afford pale yellow solid **2.13h** (1.01 g, 93%); R_f = 0.69 (EtOAc : Hexane = 2 : 3); ^{1}H

NMR ($CDCl_3$, 300 MHz) δ 7.84 (s, 1H), 7.47 – 7.45 (m, 6H), 7.38 – 7.36 (m, 6H), 6.92 (d, *J* = 8.5 Hz, 2H), 4.39 (br s, 1H), 3.85 (s, 3H); ^{13}C NMR ($CDCl_3$, 75 MHz) δ 175.1, 159.8, 145.3, 140.5, 136.9, 128.1, 128.0, 127.5, 123.8, 114.5, 80.7, 55.4; HRMS calculated for $C_{23}H_{20}O_2NS$ (M+H): 374.12093; Found: 374.12055 m/z.

(5-(4-methoxyphenyl)-4-methylthiazol-2-yl)diphenylmethanol (**2.13i**)

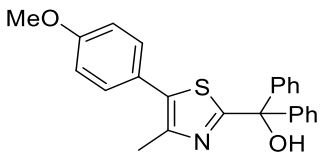

Prepared according to **General Procedure B** starting with **2.10i** (1.13 g, 5.5 mmol, 1.0 equiv) and purified by column chromatography (0 % – 20 % gradient EtOAc in hexanes) to afford yellow solid **2.13i** (1.56 g, 73%); R_f = 0.72 (EtOAc : Hexane = 2 : 3); ^1H NMR ($CDCl_3$, 300 MHz) δ 7.49 – 7.46 (m, 4H), 7.37 – 7.33 (m, 8H), 6.94 (d, *J* = 8.7 Hz, 2H), 4.51 (br s, 1H), 3.85 (s, 3H), 2.49 (s, 3H); ^{13}C NMR ($CDCl_3$, 75 MHz) δ 172.7, 159.3, 146.8, 145.6, 133.6, 130.4, 128.1, 127.9, 127.5, 124.2, 114.1, 80.3, 55.4, 16.2; HRMS calculated for $C_{24}H_{22}O_2NS$ (M+H): 388.13658; Found: 388.13618 m/z.

4-(2-(hydroxydiphenylmethyl)thiazol-5-yl)benzonitrile (**2.13j**)

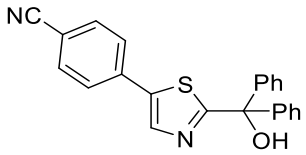

Prepared according to **General Procedure B** starting with **2.10j** (734 µL, 4.0 mmol, 1.0 equiv) and purified by column chromatography (0 % – 30 % gradient EtOAc in hexanes) to afford orange solid **2.13j** (736 mg, 50%); R_f = 0.41 (EtOAc : Hexane = 3 : 7); ^1H NMR ($CDCl_3$, 300 MHz) δ 8.07 (s, 1H), 7.70 – 7.62 (m, 4H), 7.43 – 7.37 (m, 10H), 4.00 (br s,

1H); ^{13}C NMR ($CDCl_3$, 75 MHz) δ 178.3, 144.8, 139.9, 138.3, 135.8, 132.9, 128.3, 128.2, 127.4, 126.9, 118.4, 111.7, 80.9; HRMS calculated for $C_{23}H_{17}ON_2S$ (M+H): 369.10561; Found: 369.10645 m/z.

4-(2-(hydroxydiphenylmethyl)-4-methylthiazol-5-yl)benzonitrile (**2.13k**)

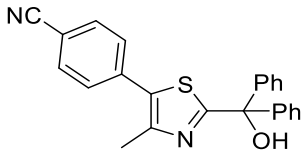

Prepared according to **General Procedure B** starting with **2.10k** (801 mg, 4.0 mmol, 1.0 equiv) and purified by column chromatography (0 % – 30 % gradient EtOAc in hexanes) to afford yellow oil **2.13k** (352 mg, 27%); R_f = 0.39 (EtOAc : Hexane = 2 : 3); ^{1}H NMR ($CDCl_3$, 300 MHz) δ 7.70 (d, *J* = 8.2 Hz, 2H), 7.54 (d, *J* = 8.2 Hz, 2H), 7.49 – 7.46 (m, 4H), 7.38 – 7.36 (m, 6H), 4.26 (br s, 1H), 2.54 (s, 3H); ^{13}C NMR ($CDCl_3$, 75 MHz) δ 175.3, 149.2, 145.0, 136.8, 132.4, 131.6, 129.5, 128.2, 128.1, 127.4, 118.5, 111.3, 80.5, 16.6; HRMS calculated for $C_{24}H_{19}ON_2S$ (M+H) 383.12126; Found: 383.12154.

(5-(4-fluorophenyl)thiazol-2-yl)diphenylmethanol (**2.13l**)

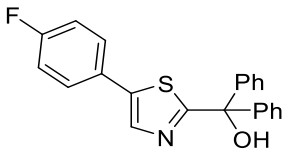

Prepared according to **General Procedure B** starting with **2.10l** (627 mg, 3.5 mmol, 1.0 equiv) and purified by column chromatography (0 % – 30 % gradient EtOAc in hexanes) to afford white solid **2.13l** (896 mg, 71%); R_f = 0.66 (EtOAc : Hexane = 1 : 4); ^{1}H NMR ($CDCl_3$, 300 MHz) δ 7.88 (s, 1H), 7.53 – 7.48 (m, 6H), 7.41 – 7.35 (m, 8H), 7.09 (t, *J* = 8.6 Hz, 2H), 4.22 (br s, 1H); ^{13}C NMR ($CDCl_3$, 75 MHz) δ 176.3, 162.7 (d, $^1J_{CF}$ = 248.7

Hz), 145.2, 143.9, 139.4, 137.9, 128.5,128.2, 128.1, 127.5, 126.6, 116.1 (d, $^{2}J_{CF}$ = 21.9 Hz), 80.7; ^{19}F NMR ($CDCl_3$, 470 MHz) δ -113.1; HRMS calculated for $C_{22}H_{17}ONFS$ (M+H): 362.10094; Found: 362.10107 m/z.

diphenyl(5-(4-(trifluoromethyl)phenyl)thiazol-2-yl)methanol (**2.13m**)

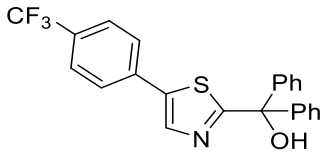

Prepared according to **General Procedure B** starting with **2.10m** (3.50 g, 15.3 mmol, 1.0 equiv) and purified by column chromatography (0 % – 20 % gradient EtOAc in hexanes) to afford orange oil **2.13m** (3.84 g, 61%); R_f = 0.70 (EtOAc : Hexane = 1 : 4); ^{1}H NMR ($CDCl_3$, 300 MHz) δ 8.00 (s, 1H), 7.63 (s, 4H), 7.47 – 7.44 (m, 4H), 7.40 – 7.34 (m, 6H), 4.17 (br s, 1H); ^{13}C NMR ($CDCl_3$, 75 MHz) δ 177.6, 144.9, 139.3, 138.7, 134.8, 130.2 (q, $^{2}J_{CF}$ = 32.9 Hz), 128.3, 128.2, 127.2, 126.8, 126.1 (q, $^{3}J_{CF}$ = 3.8 Hz), 123.9 (q, $^{1}J_{CF}$ = 272.1 Hz), 80.8; ^{19}F NMR ($CDCl_3$, 470 MHz) δ -63.0; HRMS calculated for $C_{23}H_{17}ONF_3S$ (M+H): 412.09775; Found: 412.09781 m/z.

(4-methyl-5-(4-(trifluoromethyl)phenyl)thiazol-2-yl)diphenylmethanol (**2.13n**)

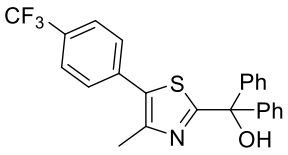

Prepared according to **General Procedure B** starting with **2.10n** (1.34 g, 5.5 mmol, 1.0 equiv) and purified by column chromatography (0 % – 20 % gradient EtOAc in hexanes) to afford orange oil **2.13n** (2.10 g, 90%); R_f = 0.77 (EtOAc : Hexane = 2 : 3); ^{1}H NMR ($CDCl_3$, 300 MHz) δ 7.67 (d, *J* = 8.1 Hz, 2H), 7.54 (d, *J* = 8.1 Hz, 2H), 7.50 – 7.46 (m,

4H), 7.38 – 7.36 (m, 6H), 4.33 (br s, 1H), 2.53 (s, 3H); ^{13}C NMR ($CDCl_3$, 75 MHz) δ 175.2, 148.8, 145.3, 135.8, 131.9, 129.8 (q, $^{2}J_{CF}$ = 32.7 Hz), 129.4, 128.2, 128.1, 127.6, 125.7 (q, $^{4}J_{CF}$ = 3.7 Hz), 124.1 (q, $^{1}J_{CF}$ = 272.1 Hz), 80.6, 16.4; ^{19}F NMR ($CDCl_3$, 470 MHz) δ -62.7; HRMS calculated for $C_{24}H_{19}ONF_3S$ (M+H): 426.11340; Found: 426.11378 m/z.

(5-(3,5-bis(trifluoromethyl)phenyl)thiazol-2-yl)diphenylmethanol (**2.13o**)

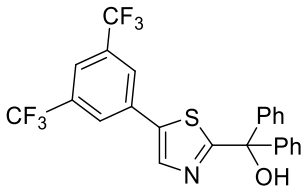

Prepared according to **General Procedure B** starting with **2.10o** (892 mg, 3.0 mmol, 1.0 equiv) and purified by column chromatography (0 % – 15 % gradient EtOAc in hexanes) to afford white solid **2.13o** (1.19 g, 83%); R_f = 0.62 (EtOAc : Hexane = 1 : 4); ^{1}H NMR ($CDCl_3$, 300 MHz) δ 7.94 (s, 2H), 7.92 (s, 1H), 7.86 (s, 1H), 7.50 (dd, *J* = 7.8, 1.6 Hz, 4H), 7.43 – 7.39 (m, 6H), 4.68 (br s, 1H); ^{13}C NMR ($CDCl_3$, 75 MHz) δ 178.8, 144.8, 140.0, 137.0, 133.6, 132.6 (q, $^{2}J_{CF}$ = 33.6 Hz), 128.3, 128.2, 127.5, 126.5, 123.0 (q, $^{1}J_{CF}$ = 272.9 Hz), 121.65 (q, $^{3}J_{CF}$ = 3.7 Hz), 80.88; ^{19}F NMR ($CDCl_3$, 470 MHz) δ -63.3; HRMS calculated for $C_{24}H_{16}ONF_6S$ (M+H): 480.08513; Found: 480.08439 m/z.

(5-(5-hexylthiophen-2-yl)thiazol-2-yl)diphenylmethanol (**2.13p**)

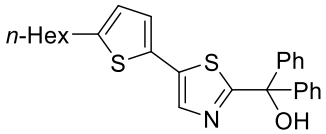

Prepared according to **General Procedure B** starting with **2.10p** (200 mg, 0.8 mmol, 1.0 equiv) and purified by column chromatography (0 % – 10 % gradient EtOAc in hexanes)

to afford yellow oil **2.13p** (234 mg, 68%); ^{1}H NMR ($CDCl_3$, 300 MHz) δ 7.76 (s, 1H), 7.47 – 7.44 (m, 4H), 7.39 – 7.34 (m, 6H), 6.95 (d, *J* = 3.5 Hz, 1H), 6.70 (d, *J* = 3.6 Hz, 1H), 4.22 (br s, 1H), 2.81 (t, *J* = 7.5 Hz, 2H), 1.69 (quint, *J* = 7.5 Hz, 2H), 1.39 – 1.29 (m, 6H), 0.92 (t, *J* = 6.7 Hz, 3H); ^{13}C NMR ($CDCl_3$, 75 MHz) δ 174.9, 146.8, 145.1, 137.5, 134.3, 130.2, 128.2, 128.0, 127.5, 125.5, 124.9, 80.6, 31.5*, 30.1, 28.7, 22.6, 14.1 *two peaks overlapping.

(5-(4-(dimethylamino)phenyl)thiazol-2-yl)diphenylmethanol (**2.13q**)

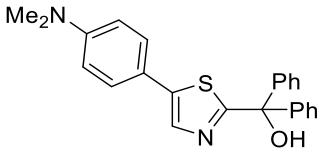

Prepared according to **General Procedure B** starting with **2.10q** (1.25 g, 6.1 mmol, 1.0 equiv) and purified by column chromatography (0 % – 20 % gradient EtOAc in hexanes) to afford orange solid **2.13q** (1.73 g, 73%); ^{1}H NMR ($CDCl_3$, 300 MHz) δ 7.81 (s, 1H), 7.48 (d, *J* = 6.4 Hz, 2H), 7.42 – 7.35 (m, 8H), 6.71 (d, *J* = 8.6 Hz, 2H), 4.37 (s, 1H), 3.00 (s, 6H); ^{13}C NMR ($CDCl_3$, 75 MHz) δ 173.9, 150.2, 145.5, 141.4, 135.8, 128.1, 127.9, 127.7, 127.5, 119.5, 112.7, 80.6, 40.6; HRMS calculated for $C_{24}H_{23}ON_2S$ (M+H): 387.15256; Found: 387.15233 m/z.

General procedure C: Oxidation of 2-Substituted Thiazoles

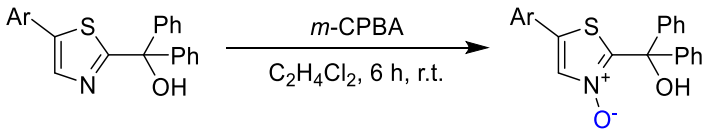

In a round-bottom flask, activated thiazole (1.0 mmol, 1.0 equiv) was dissolved in 1,2-dichloroethane (3 mL, 0.33 M) and allowed to stir at room temperature. *m*-CPBA (1.5

mmol, 1.5 equiv) was then added and the mixture was continued stirring at this temperature for 6 h. The reaction mixture was then diluted with dichloromethane (30 mL) and then purified by column chromatography to yield thiazole 3-oxides.

2-(hydroxydiphenylmethyl)-5-phenylthiazole 3-oxide (**2.14a**)

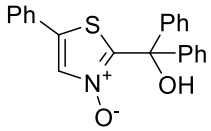

Prepared according to **General Procedure C** starting with **2.13a** (1.00 g, 2.9 mmol, 1.0 equiv) and purified by column chromatography (0 % – 50 % gradient EtOAc in hexanes) to afford white solid **2.14a** (925 mg, 89%); R_f = 0.33 (EtOAc : Hexane = 3 : 7); ^{1}H NMR ($CDCl_3$, 300 MHz) δ 8.22 (br s, 1H), 7.91 (s, 1H), 7.44 – 7.38 (m, 15H); ^{13}C NMR ($CDCl_3$, 75 MHz) δ 150.6, 143.2, 135.9, 132.7, 130.2, 129.5, 128.7, 128.6, 128.4, 127.0, 125.9, 79.1; HRMS calculated for $C_{22}H_{18}O_2NS$ (M+H): 360.10528; Found: 360.10541 m/z.

2-(hydroxydiphenylmethyl)-4-methyl-5-phenylthiazole 3-oxide (**2.14b**)

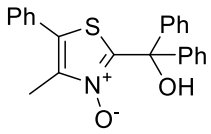

Prepared according to **General Procedure C** starting with **2.13b** (351 mg, 1.0 mmol, 1.0 equiv) and purified by column chromatography (0 % – 35 % gradient EtOAc in hexanes) to afford white solid **2.14b** (256 mg, 69%); R_f = 0.45 (EtOAc : Hexane = 2 : 3); ^{1}H NMR ($CDCl_3$, 300 MHz) δ 7.45 – 7.36 (m, 15H), 2.49 (s, 3H); ^{13}C NMR ($CDCl_3$, 75 MHz) δ 150.5, 143.4, 141.7, 130.2, 129.6, 129.4, 129.2, 128.6, 128.4, 128.3, 127.1, 79.1, 11.8; HRMS calculated for $C_{23}H_{20}O_2NS$ (M+H): 374.12093; Found: 374.12030 m/z.

2-(hydroxydiphenylmethyl)-5-(p-tolyl)thiazole 3-oxide (**2.14c**)

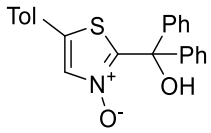

Prepared according to **General Procedure C** starting with **2.13c** (3.60 g, 10.1 mmol, 1.0 equiv) and purified by column chromatography (0 % – 50 % gradient EtOAc in hexanes) to afford white solid **2.14c** (3.48 g, 92%); R_f = 0.35 (EtOAc : Hexane = 3 : 7); ^{1}H NMR ($CDCl_3$, 300 MHz) 8.24 (br s, 1H), 7.87 (s, 1H), 7.43 – 7.33 (m, 12H), 7.23 (d, *J* = 8.1 Hz, 2H), 2.40 (s, 3H) δ ^{13}C NMR ($CDCl_3$, 75 MHz) δ 150.4, 143.2, 140.5, 136.0, 132.2, 130.1, 128.4, 128.3, 127.0, 125.9, 125.8, 79.1, 21.3; HRMS calculated for $C_{23}H_{20}O_2NS$ (M+H): 374.12093; Found: 374.12071.

2-(hydroxydiphenylmethyl)-5-(naphthalen-2-yl)thiazole 3-oxide (**2.14d**)

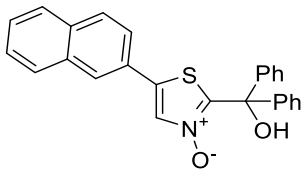

Prepared according to **General Procedure C** starting with **2.13d** (1.18 g, 3.0 mmol, 1.0 equiv) and purified by column chromatography (0 % – 30 % gradient EtOAc in hexanes) to afford white solid **2.14d** (997 mg, 81%); R_f = 0.16 (EtOAc : Hexane = 3 : 7); ^{1}H NMR ($CDCl_3$, 300 MHz) δ 8.01 (s, 1H), 7.92 – 7.84 (m, 4H), 7.59 – 7.51 (m, 3H), 7.47 – 7.39 (m, 10H); ^{13}C NMR ($CDCl_3$, 75 MHz) δ 150.9, 143.2, 136.0, 133.7, 133.1, 133.0, 129.5, 128.5, 128.4, 128.2, 127.9, 127.5, 127.4, 127.1, 126.0, 125.4, 122.9, 79.1; HRMS calculated for $C_{26}H_{20}O_2NS$ (M+H) 410.12093; Found: 410.12044 m/z.

2-(hydroxydiphenylmethyl)-5-(naphthalen-1-yl)thiazole 3-oxide (**2.14e**)

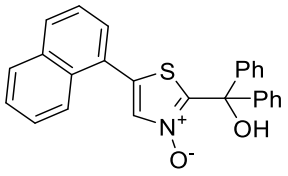

Prepared according to **General Procedure C** starting with **2.13e** (394 mg, 1.0 mmol, 1.0 equiv) and purified by column chromatography (0 % – 40 % gradient EtOAc in hexanes) to afford white solid **2.14e** (347 mg, 85%); R_f = 0.08 (EtOAc : Hexane = 1 : 4); ^{1}H NMR ($CDCl_3$, 300 MHz) δ 8.26 (br s, 1H), 8.13 (s, 1H), 7.97 – 7.94 (m, 3H), 7.63 – 7.59 (m, 2H), 7.50 – 7.39 (m, 12H); ^{13}C NMR ($CDCl_3$, 75 MHz) δ 152.1, 143.2, 136.1, 133.8, 133.7, 130.9, 130.8, 128.8, 128.6, 128.5, 128.4, 127.7, 127.0, 126.8, 125.9, 125.1, 124.2, 79.1; HRMS calculated for $C_{26}H_{20}O_2NS$ (M+H) 410.12093; Found: 410.12105 m/z.

5-(4-hexylphenyl)-2-(hydroxydiphenylmethyl)thiazole 3-oxide (**2.14f**)

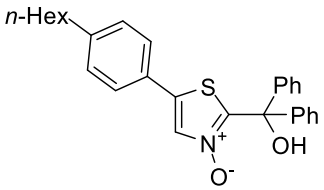

Prepared according to **General Procedure C** starting with **2.13f** (1.28 g, 3.0 mmol, 1.0 equiv) and purified by column chromatography (0 % – 30 % gradient EtOAc in hexanes) to afford white solid **2.14f** (1.07 g, 80%); R_f = 0.57 (EtOAc : Hexane = 3 : 7); ^{1}H NMR ($CDCl_3$, 300 MHz) δ 7.90 (s, 1H), 7.43 – 7.35 (m, 12H), 7.24 (d, *J* = 8.2 Hz, 2H), 2.64 (t, *J* = 7.9 Hz, 2H), 1.62 (p, *J* = 7.6 Hz, 2H), 1.32 – 1.31 (m, 6H), 0.90 (t, *J* = 6.6 Hz, 3H); ^{13}C NMR ($CDCl_3$, 75 MHz) δ 150.6, 145.6, 143.2, 136.1, 132.2, 129.5, 129.5, 128.5, 128.4,

127.0, 126.0, 125.8, 79.1, 35.7, 31.7, 21.2, 28.9, 22.6, 14.1; HRMS calculated for $C_{28}H_{30}O_2NS$ (M+H): 444.19918; Found: 444.19903 m/z.

5-(4-(hexyloxy)phenyl)-2-(hydroxydiphenylmethyl)thiazole 3-oxide (**2.14g**)

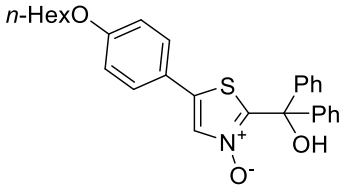

Prepared according to **General Procedure C** starting with **2.13g** (222 mg, 0.5 mmol, 1.0 equiv) and purified by column chromatography (0 % – 50 % gradient EtOAc in hexanes) to afford white solid **2.14g** (168 mg, 76%); R_f = 0.60 (EtOAc : Hexane = 1 : 1); ^{1}H NMR ($CDCl_3$, 300 MHz) δ 8.30 (s, 1H), 7.78 (s, 1H), 7.41 – 7.34 (m, 12H), 6.92 (d, *J* = 8.7 Hz, 2H), 3.99 (t, *J* = 6.5 Hz, 2H), 1.81 (p, *J* = 7.8 Hz, 2H), 1.50 – 1.36 (m, 6H), 0.93 (t, *J* = 6.6 Hz, 3H); ^{13}C NMR ($CDCl_3$, 75 MHz) δ 160.7, 149.6, 143.3, 135.9, 131.6, 128.4, 128.3, 127.3, 127.0, 120.9, 115.3, 79.1, 68.3, 31.5, 29.1, 25.7, 22.6, 14.0; HRMS calculated for $C_{28}H_{30}O_3NS$ (M+H): 460.19409; Found: 460.19382 m/z.

2-(hydroxydiphenylmethyl)-5-(4-methoxyphenyl)thiazole 3-oxide (**2.14h**)

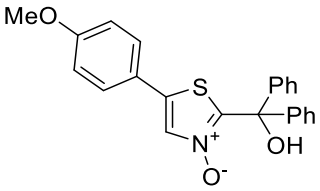

Prepared according to **General Procedure C** starting with **2.13h** (373 mg, 1.0 mmol, 1.0 equiv) and purified by column chromatography (0 % – 60 % gradient EtOAc in hexanes) to afford white solid **2.14h** (326 mg, 84%); R_f = 0.22 (EtOAc : Hexane = 2 : 3); ^{1}H NMR ($CDCl_3$, 300 MHz) δ 7.78 (s, 1H), 7.41 – 7.36 (m, 12H), 6.94 (d, *J* = 8.5 Hz, 2H), 3.86 (s,

3H); ^{13}C NMR ($CDCl_3$, 75 MHz) δ 161.1, 143.3, 135.8, 131.7, 128.4, 128.3, 127.4, 127.0, 121.2, 114.8, 79.1, 55.5; HRMS calculated for $C_{23}H_{20}O_3NS$ (M+H) 390.11584; Found: 390.11584 m/z.

2-(hydroxydiphenylmethyl)-5-(4-methoxyphenyl)-4-methylthiazole 3-oxide (**2.14i**)

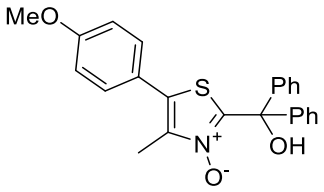

Prepared according to **General Procedure C** starting with **2.13i** (388 mg, 1.0 mmol, 1.0 equiv) and purified by column chromatography (0 % – 40 % gradient EtOAc in hexanes) to afford white solid **2.14i** (400 mg, 99%); R_f = 0.26 (EtOAc : Hexane = 2 : 3); ^{1}H NMR ($CDCl_3$, 300 MHz) δ 8.48 (br s, 1H), 7.41 – 7.32 (m, 12H), 6.97 (d, *J* = 8.7 Hz, 2H), 3.86 (s, 3H), 2.46 (s, 3H); ^{13}C NMR ($CDCl_3$, 75 MHz) δ 160.5, 149.9, 143.4, 141.0, 129.9, 129.6, 128.4, 128.2, 127.1, 122.4, 114.6, 79.1, 55.4, 11.7; HRMS calculated for $C_{24}H_{22}O_3NS$ (M+H): 404.13149; Found: 404.13134 m/z.

5-(4-cyanophenyl)-2-(hydroxydiphenylmethyl)thiazole 3-oxide (**2.14j**)

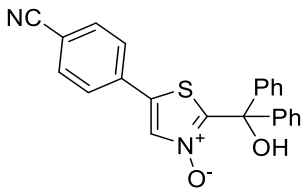

Prepared according to **General Procedure C** starting with **2.13j** (736 µL, 2.0 mmol, 1.0 equiv) and purified by column chromatography (0 % – 70 % gradient EtOAc in hexanes) to afford white solid **2.14j** (370 mg, 48%); R_f = 0.27 (EtOAc : Hexane = 1 : 1); ^{1}H NMR ($CDCl_3$, 300 MHz) δ 8.02 (br s, 1H), 8.01 (s, 1H), 7.74 (d, *J* = 8.5 Hz, 2H), 7.56 (d, *J* = 8.4

Hz, 2H), 7.41 (m, 10H); ^{13}C NMR ($CDCl_3$, 75 MHz) δ 152.5, 142.8, 134.5, 133.4, 133.2, 133.0, 128.6, 126.9, 126.4, 117.7, 113.7, 111.8, 79.1; HRMS calculated for $C_{23}H_{17}O_2N_2S$ (M+H): 385.10053; Found: 385.10067 m/z.

5-(4-cyanophenyl)-2-(hydroxydiphenylmethyl)-4-methylthiazole 3-oxide (**2.14k**)

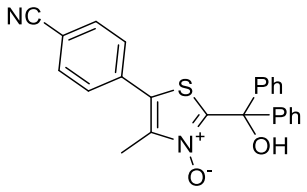

Prepared according to **General Procedure C** starting with **2.13k** (145 mg, 0.38 mmol, 1.0 equiv) and purified by column chromatography (0 % – 30 % gradient EtOAc in hexanes) to afford white solid **2.14k** (100 mg, 66%); R_f = 0.17 (EtOAc : Hexane = 1 : 4); ^{1}H NMR ($CDCl_3$, 300 MHz) δ 8.29 (br s, 1H), 7.77 (d, *J* = 7.8 Hz, 2H), 7.55 (d, *J* = 7.9 Hz, 2H), 7.39 (s, 10H), 2.51 (s, 3H); ^{13}C NMR ($CDCl_3$, 75 MHz) δ 151.5, 143.3, 143.0, 134.8, 132.9, 129.1, 128.5, 128.4, 127.5, 127.0, 117.9, 113.2, 79.1, 12.0; HRMS calculated for $C_{24}H_{19}O_2N_2S$ (M+H): 399.11618; Found: 399.11612 m/z.

5-(4-fluorophenyl)-2-(hydroxydiphenylmethyl)thiazole 3-oxide (**2.14l**)

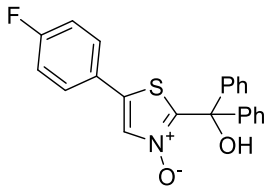

Prepared according to **General Procedure C** starting with **2.13l** (361 mg, 1.0 mmol, 1.0 equiv) and purified by column chromatography (0 % – 30 % gradient EtOAc in hexanes) to afford white solid **2.14l** (312 mg, 83%); R_f = 0.24 (EtOAc : Hexane = 2 : 3); ^{1}H NMR ($CDCl_3$, 300 MHz) δ 8.17 (br s, 1H), 7.88 (s, 1H), 7.46 – 7.38 (m, 12H), 7.13 (t, *J* = 8.5

Hz, 2H); ^{13}C NMR ($CDCl_3$, 75 MHz) δ 163.3, 162.0, 143.1, 134.7, 132.8, 131.0 (d, $^1J_{CF}$ = 229.3 Hz), 128.5, 128.4, 128.0 (d, $^3J_{CF}$ = 8.5 Hz), 127.0, 125.0 (d, $^4J_{CF}$ = 3.5 Hz), 116.7 (d, $^2J_{CF}$ = 22.3 Hz), 79.1; ^{19}F NMR ($CDCl_3$, 470 MHz) δ -109.8; HRMS calculated for $C_{22}H_{17}O_2NFS$ (M+H): 378.09585; Found: 378.09523 m/z.

2-(hydroxydiphenylmethyl)-5-(4-(trifluoromethyl)phenyl)thiazole 3-oxide (**2.14m**)

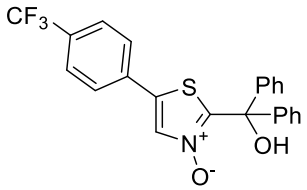

Prepared according to **General Procedure C** starting with **2.13m** (1.23 g, 3.0 mmol, 1.0 equiv) and purified by column chromatography (0 % – 60 % gradient EtOAc in hexanes) to afford white solid **2.14m** (949 mg, 74%); R_f = 0.42 (EtOAc : Hexane = 3 : 7); ^{1}H NMR ($CDCl_3$, 300 MHz) δ 8.09 (br s, 1H), 7.97 (s, 1H), 7.71 (d, *J* = 8.2 Hz, 2H), 7.57 (d, *J* = 8.3 Hz, 2H), 7.43 – 7.41 (m, 10H); ^{13}C NMR ($CDCl_3$, 75 MHz) δ 167.5, 152.1, 142.9, 134.1, 134.0, 132.1, 132.0 (q, $^2J_{CF}$ = 33.2 Hz), 128.9, 127.0, 126.5 (q, $^3J_{CF}$ = 3.7 Hz), 126.3, 123.5 (q, $^1J_{CF}$ = 272.4 Hz), 79.1; ^{19}F NMR ($CDCl_3$, 470 MHz) δ -63.2; HRMS calculated for $C_{23}H_{17}O_2NF_3S$ (M+H): 428.09266; Found: 428.09152 m/z.

2-(hydroxydiphenylmethyl)-4-methyl-5-(4-(trifluoromethyl)phenyl)thiazole 3-oxide (2.14n)

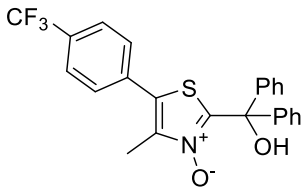

Prepared according to **General Procedure C** starting with **2.13n** (426 mg, 1.0 mmol, 1.0 equiv) and purified by column chromatography (0 % – 35 % gradient EtOAc in hexanes) to afford white solid **2.14n** (358 mg, 82%); R_f = 0.39 (EtOAc : Hexane = 2 : 3); ^{1}H NMR ($CDCl_3$, 300 MHz) δ 8.31 (br s, 1H), 7.73 (d, *J* = 8.1 Hz, 2H), 7.55 (d, *J* = 8.0 Hz, 2H), 7.41 – 7.38 (m, 10H), 2.50 (s, 3H); ^{13}C NMR ($CDCl_3$, 75 MHz) δ 167.4, 151.7, 143.1, 133.8, 132.6, 131.4 (q, $^2J_{CF}$ = 33.0 Hz), 129.0, 128.5, 128.4, 127.0, 126.2 (q, $^3J_{CF}$ = 3.7 Hz), 123.6 (q, $^1J_{CF}$ = 272.5 Hz), 79.1, 11.9; ^{19}F NMR ($CDCl_3$, 470 MHz) δ -63.1; HRMS calculated for $C_{24}H_{19}O_2NF_3S$ (M+H): 442.10831; Found: 442.10810 m/z.

5-(3,5-bis(trifluoromethyl)phenyl-2-(hydroxydiphenylmethyl)thiazole 3-oxide (2.14o)

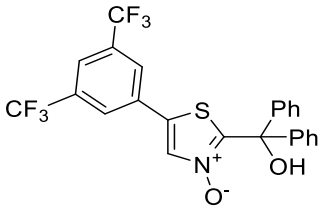

Prepared according to **General Procedure C** starting with **2.13o** (479 mg, 1.0 mmol, 1.0 equiv) and purified by column chromatography (0 % – 30 % gradient EtOAc in hexanes) to afford white solid **2.14o** (391 mg, 79%); R_f = 0.62 (EtOAc : Hexane = 2 : 3); ^{1}H NMR ($CDCl_3$, 300 MHz) δ 8.17 (s, 1H), 7.94 (s, 1H), 7.88 (s, 2H), 7.49 – 7.35 (m, 10H); ^{13}C

NMR ($CDCl_3$, 75 MHz) δ 153.0, 142.7, 133.2 (q, $^2J_{CF}$ = 34.0 Hz), 132.8, 132.5, 132.3, 131.1, 130.0, 129.5, 128.7, 128.6, 128.0, 126.9, 123.5 (q, $^3J_{CF}$ = 3.7 Hz), 122.6 (q, $^1J_{CF}$ = 273.2 Hz), 79.1; ^{19}F NMR ($CDCl_3$, 470 MHz) δ -63.3; HRMS calculated for $C_{24}H_{16}O_2NF_6S$ (M+H): 496.08005; Found: 496.08273 m/z.

General procedure D: *ipso*-Arylative Condensation of Activated Thiazole N-Oxides

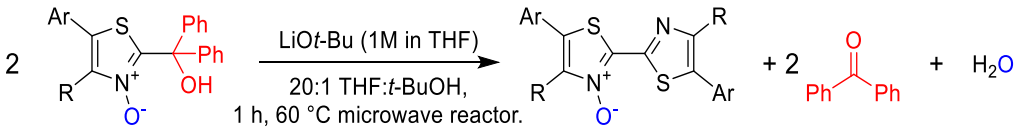

In a sealed, argon-purged microwave reaction vessel, the *N*-oxide (0.2 mmol, 1 equiv) was dissolved in anhydrous tetrahydrofuran (4 mL, 0.05 M) allowed to stir at room temperature. *t*-BuOH (0.2 mL, 1 M) and LiO*t*-Bu (0.3 mL, 1M in THF, 1.5 equiv) were then added and the mixture was immediately heated by microwave irradiation for 1 h at 60 °C. The reaction mixture was then diluted with dichloromethane (30 mL) and washed with water (3 x 20 mL) before being dried with $MgSO_4$ and concentrated. The residue was then triturated using hexanes (250 mL) to yield the pure bithiazole product.

5,5'-diphenyl-[2,2'-bithiazole] 3-oxide (**2.15a**)

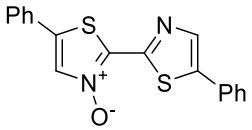

Prepared according to **General Procedure D** starting with **2.14a** (144 mg, 0.4 mmol, 1.0 equiv) to afford yellow solid **2.15a** (61 mg, 91%); R_f = 0.42 (EtOAc : Hexane = 1 : 1); ^{1}H NMR ($CDCl_3$, 300 MHz) δ 8.22 (s, 1H), 8.03 (s, 1H), 7.73 (d, *J* = 8.0 Hz, 2H), 7.62 (d, *J* = 7.8 Hz, 2H), 7.54 – 7.40 (m, 6H); ^{13}C NMR ($CDCl_3$, 75 MHz) δ 151.3, 140.7, 139.7, 139.2,

135.8, 132.0, 131.1, 130.4, 129.6, 129.3, 128.8, 128.7, 127.0, 126.1; IR (ATR) 3053, 1488, 1364, 1217, 681 cm^{-1}; HRMS calculated for $C_{18}H_{13}ON_2S_2$ (M+H): 337.04638; Found: 337.04684 m/z.

4,4'-dimethyl-5,5'-diphenyl-[2,2'-bithiazole] 3-oxide (**2.15b**)

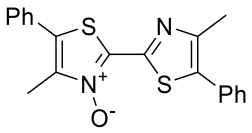

Prepared according to **General Procedure D** starting with **2.14b** (75 mg, 0.2 mmol, 1.0 equiv) to afford yellow solid **2.15b** (22 mg, 60%); R_f = 0.56 (EtOAc : Hexane = 1 : 1); ^{1}H NMR ($CDCl_3$, 300 MHz) δ 7.54 – 7.25 (m, 10H), 2.60 (s, 3H), 2.56 (s, 3H); ^{13}C NMR ($CDCl_3$, 75 MHz) δ 150.0, 148.9, 141.0, 139.3, 133.9, 132.0, 130.5, 129.6, 129.3, 129.2, 129.1, 128.8, 128.6, 128.0, 16.5, 11.9; IR (ATR) 3029, 2919, 1352, 759, 696 cm^{-1}; HRMS calculated for $C_{20}H_{17}ON_2S_2$ (M+H): 365.07768; Found: 365.07840 m/z. Data consistent with previously reported.[145]

5,5'-di-p-tolyl-[2,2'-bithiazole] 3-oxide (**2.15c**)

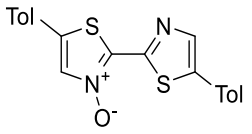

Prepared according to **General Procedure D** starting with **2.14c** (150 mg, 0.4 mmol, 1.0 equiv) to afford yellow solid **2.15c** (63 mg, 86%); R_f = 0.31 (EtOAc : Hexane = 2 : 3); ^{1}H NMR ($CDCl_3$, 300 MHz) δ 8.18 (s, 1H), 7.98 (s, 1H), 7.62 (d, *J* = 7.9 Hz, 2H), 7.51 (d, *J* = 8.0 Hz, 2H), 7.34 – 7.27 (m, 4H); ^{13}C NMR ($CDCl_3$, 75 MHz) δ 150.9, 140.9, 140.8, 138.9, 138.8, 135.9, 131.5, 130.3, 129.9, 128.3, 126.8, 126.1, 125.9, 21.4, 21.3 *one peak

missing due to overlap; IR (ATR) 3022, 2920, 2852, 1494, 1361, 793 cm^{-1}; HRMS calculated for $C_{20}H_{17}ON_2S_2$ (M+H): 365.07768; Found: 365.07768 m/z.

5,5'-di(naphthalen-2-yl)-[2,2'-bithiazole] 3-oxide (**2.15d**)

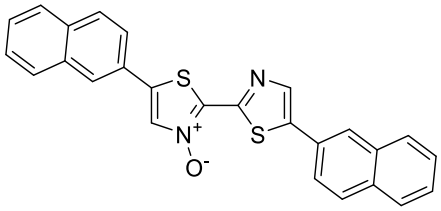

Prepared according to **General Procedure D** starting with **2.14d** (82 mg, 0.2 mmol, 1.0 equiv) to afford yellow solid **2.15d** (42 mg, 95%); R_f = 0.45 (EtOAc : Hexane = 3 : 7); IR (ATR) 3045, 2923, 1367, 1217, 805, 744, 467 cm^{-1}; HRMS calculated for $C_{26}H_{17}ON_2S_2$ (M+H): 437.07768; Found: 437.07559 m/z. ^{1}H NMR and ^{13}C NMR were unobtainable due to poor solubility.

5,5'-di(naphthalen-1-yl)-[2,2'-bithiazole] 3-oxide (**2.15e**)

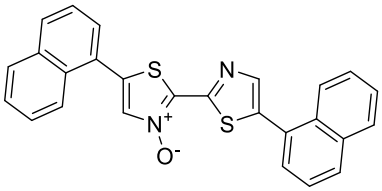

Prepared according to **General Procedure D** starting with **2.14e** (82 mg, 0.2 mmol, 1.0 equiv) to afford yellow solid **2.15e** (34 mg, 77%); R_f = 0.53 (EtOAc : Hexane = 3 : 7); ^{1}H NMR ($CDCl_3$, 300 MHz) δ 8.25 – 8.22 (m, 2H), 8.18 (s, 1H), 8.06 – 7.96 (m, 5H), 7.69 – 7.58 (m, 8H); IR (ATR) 3039, 2970, 1357, 790, 766 cm^{-1}; HRMS calculated for $C_{26}H_{17}ON_2S_2$ (M+H): 437.07768; Found: 437.07760 m/z. ^{13}C NMR was unobtainable due to poor solubility.

5,5'-bis(4-hexylphenyl)-[2,2'-bithiazole] 3-oxide (**2.15f**)

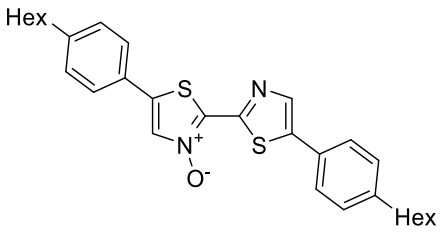

Prepared according to **General Procedure D** starting with **2.14f** (177 mg, 0.4 mmol, 1.0 equiv) to afford yellow solid **2.15f** (78 mg, 88%); R_f = 0.74 (EtOAc : Hexane = 3 : 7); ^{1}H NMR ($CDCl_3$, 300 MHz) δ 8.18 (s, 1H), 7.98 (s, 1H), 7.63 (d, *J* = 7.9 Hz, 2H), 7.52 (d, *J* = 8.0 Hz, 2H), 7.33 – 7.26 (m, 4H), 2.71 – 2.64 (m, 4H), 1.68 – 1.64 (m, 4H), 1.35 – 1.28 (m, 12H), 0.92 (t, *J* = 6.3 Hz, 6H); ^{13}C NMR ($CDCl_3$, 75 MHz) δ 150.9, 146.0, 144.0, 140.8, 138.8, 135.9, 131.5, 129.6, 129.3, 128.4, 126.9, 126.2, 125.9, 35.8, 35.7, 31.7, 31.6, 31.3, 31.2, 29.0, 28.9, 22.6, 22.5, 14.1 *two peaks missing due to overlap; IR (ATR) 3023, 2920, 2851, 1365, 819, 470 cm^{-1}; HRMS calculated for $C_{30}H_{37}ON_2S_2$ (M+H): 505.23418; Found: 505.23242 m/z.

5,5'-bis(4-(hexyloxy)phenyl)-[2,2'-bithiazole] 3-oxide (**2.15g**)

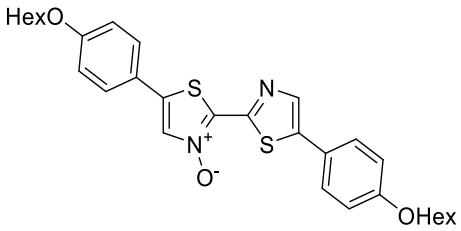

Prepared according to **General Procedure D** starting with **2.14g** (92 mg, 0.2 mmol, 1.0 equiv) to afford yellow solid **2.15g** (54 mg, 87%); R_f = 0.18 (EtOAc : Hexane = 3 : 7); ^{1}H NMR ($CDCl_3$, 300 MHz) δ 8.09 (s, 1H), 7.90 (s, 1H), 7.62 (d, *J* = 8.6 Hz, 2H), 7.51 (d, *J* = 8.6 Hz, 2H), 6.99 (t, *J* = 8.2 Hz, 4H), 4.02 (t, *J* = 5.8 Hz, 4H), 1.82 (p, *J* = 7.5 Hz, 4H),

1.51 – 1.45 (m, 4H), 1.39 – 1.37 (m, 8H), 0.94 (t, *J* = 6.8 Hz, 6H); ^{13}C NMR ($CDCl_3$, 75 MHz) δ 160.9, 159.7, 150.4, 140.6, 138.9, 138.1, 135.6, 130.8, 128.2, 127.4, 123.4, 121.1, 115.5, 115.2, 68.4, 68.2, 31.6, 31.5, 29.2, 29.1, 25.7, 25.6, 22.6, 14.0; IR (ATR) 2919, 2852, 1495, 1363, 1251, 824, 619 cm^{-1}; HRMS calculated for $C_{30}H_{37}O_3N_2S_2$ (M+H): 537.22401; Found: 537.22211 m/z.

5,5'-bis(4-methoxyphenyl)-[2,2'-bithiazole] 3-oxide (**2.15h**)

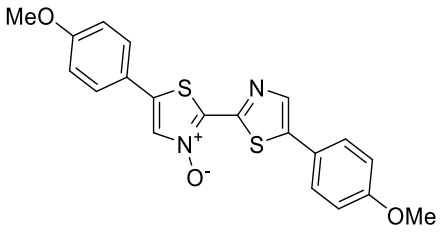

Prepared according to **General Procedure D** starting with **2.14h** (78 mg, 0.2 mmol, 1.0 equiv) to afford yellow solid **2.15h** (35 mg, 88%); R_f = 0.17 (EtOAc : Hexane = 3 : 7); ^{1}H NMR ($CDCl_3$, 300 MHz) δ 8.10 (s, 1H), 7.92 (s, 1H), 7.64 (d, *J* = 8.8 Hz, 2H), 7.53 (d, *J* = 8.8 Hz, 2H), 7.01 (t, *J* = 9.1 Hz, 4H), 3.89 (s, 3H), 3.88 (s, 3H); ^{13}C NMR ($CDCl_3$, 75 MHz) δ161.4, 160.1, 150.5*, 148.7*, 140.6, 138.2, 135.6, 130.9, 128.3, 127.5, 123.7, 121.3, 115.0, 144.7, 55.5, 55.4 *peaks poorly resolved due to poor solubility; IR (ATR) 3093, 2936, 2827, 1607, 1495, 1246, 820, 494 cm^{-1}; HRMS calculated for $C_{20}H_{17}O_3N_2S_2$ (M+H): 397.06751; Found: 397.06732 m/z.

5,5'-bis(4-methoxyphenyl)-4,4'-dimethyl-[2,2'-bithiazole] 3-oxide (**2.15i**)

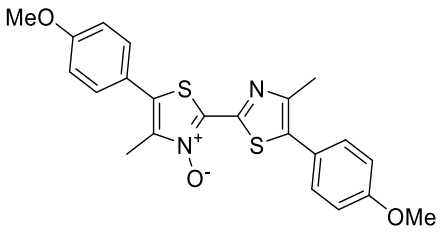

Prepared according to **General Procedure D** starting with **2.14i** (81 mg, 0.2 mmol, 1.0 equiv) to afford yellow solid **2.15i** (35 mg, 88%); R_f = 0.29 (EtOAc : Hexane = 3 : 7); ^{1}H NMR ($CDCl_3$, 300 MHz) δ 7.46 (dd, *J* = 8.2, 4.5 Hz, 4H), 7.02 (t, *J* = 9.1 Hz, 4H), 3.88 (s, 3H), 3.87 (s, 3H), 2.59 (s, 3H), 2.55 (s, 3H); ^{13}C NMR ($CDCl_3$, 75 MHz) δ 160.6, 159.5, 149.4, 148.2, 140.2, 138.8, 133.7, 130.5, 129.9, 129.0, 124.3, 122.7, 114.8, 114.3, 55.5, 55.4, 16.4, 11.8; IR (ATR) 3006, 2924, 2831, 1498, 1250, 819 cm^{-1}; HRMS calculated for $C_{22}H_{21}O_3N_2S_2$ (M+H) 425.09881; Found: 425.09859 m/z. Data consistent with previously reported.[145]

5,5'-bis(4-cyanophenyl)-[2,2'-bithiazole] 3-oxide (**2.15j**)

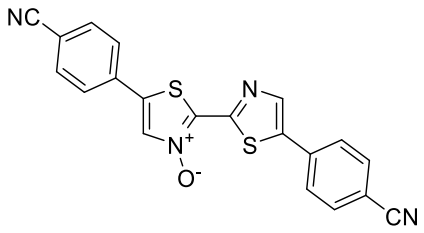

Prepared according to **General Procedure D** starting with **2.14j** (77 mg, 0.2 mmol, 1.0 equiv) to afford yellow solid **2.15j** (34 mg, 88%); R_f = 0.15 (EtOAc : Hexane = 3 : 7); IR (ATR) 3076, 2226, 1388, 832, 530 cm^{-1}; HRMS calculated for $C_{20}H_{11}ON_4S_2$ (M+H): 387.03688; Found: 387.03672 m/z. ^{1}H NMR and ^{13}C NMR were unobtainable due to poor solubility.

5,5'-bis(4-cyanophenyl)-4,4'-dimethyl-[2,2'-bithiazole] 3-oxide (**2.15k**)

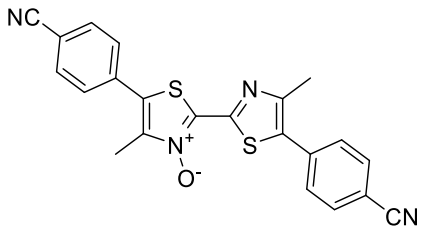

Prepared according to **General Procedure D** starting with **2.14k** (40 mg, 0.1 mmol, 1.0 equiv) to afford yellow solid **2.15k** (13 mg, 63%); R_f = 0.22 (EtOAc : Hexane = 3 : 7); ^{1}H NMR ($CDCl_3$, 300 MHz) δ 7.87 (d, *J* = 8.2 Hz, 2H), 7.79 (d, *J* = 8.1 Hz, 2H), 7.68 (d, *J* = 7.9 Hz, 4H), 2.66 (s, 3H), 2.62 (s, 3H); IR (ATR) 2970, 2227, 1351, 836, 569, 540 cm^{-1}; HRMS calculated for $C_{22}H_{15}ON_4S_2$ (M+H): 415.06818; Found: 415.06784 m/z. ^{13}C NMR was unobtainable due to poor solubility. Data consistent with previously reported.[145]

5,5'-bis(4-fluorophenyl)-[2,2'-bithiazole] 3-oxide (**2.15l**)

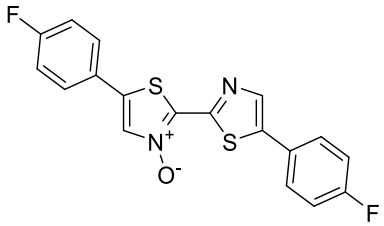

Prepared according to **General Procedure D** starting with **2.14l** (89 mg, 0.2 mmol, 1.0 equiv) to afford yellow solid **2.15l** (37 mg, 99%); R_f = 0.42 (EtOAc : Hexane = 3 : 7); ^{1}H NMR ($CDCl_3$, 300 MHz) δ 8.14 (s, 1H), 7.97 (s, 1H), 7.68 (dd, *J* = 8.6, 5.2 Hz, 2H), 7.59 (dd, *J* = 8.5, 5.0 Hz, 2H), 7.20 (dt, *J* = 17.2, 8.5 Hz, 4H); ^{13}C NMR ($CDCl_3$, 75 MHz) δ 163.9 (d, $^1J_{CF}$ = 252.4 Hz), 163.0 (d, $^1J_{CF}$ = 249.6 Hz), 151.2, 139.6, 139.2, 134.7, 131.9, 128.7 (d, $^3J_{CF}$ = 8.2 Hz), 128.1 (d, $^3J_{CF}$ = 8.6 Hz), 127.3 (d, $^4J_{CF}$ = 3.5 Hz), 125.1 (d, $^4J_{CF}$ = 4.0 Hz), 116.9 (d, $^2J_{CF}$ = 22.4 Hz), 116.4 (d, $^2J_{CF}$ = 22.0 Hz); ^{19}F NMR ($CDCl_3$, 470 MHz)

δ -109.1, -112.3; IR (ATR) 3034, 2923, 1495, 1239, 823, 487 cm^{-1}; HRMS calculated for $C_{18}H_{11}ON_2F_2S_2$ (M+H): 373.02754; Found: 373.02755 m/z.

5,5'-bis(4-(trifluoromethyl)phenyl)-[2,2'-bithiazole] 3-oxide (**2.15m**)

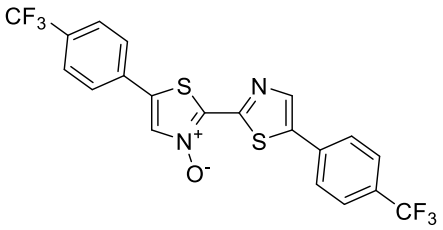

Prepared according to **General Procedure D** starting with **2.14m** (86 mg, 0.2 mmol, 1.0 equiv) to afford yellow solid **2.15m** (20 mg, 42%); R_f = 0.64 (EtOAc : Hexane = 3 : 7); ^{1}H NMR ($CDCl_3$, 300 MHz) δ 8.30 (s, 1H), 8.11 (s, 1H), 7.82 (t, *J* = 7.7 Hz, 4H), 7.74 (d, *J* = 7.5 Hz, 4H); ^{19}F NMR ($CDCl_3$, 470 MHz) δ -62.9, -63.1; IR (ATR) 3028, 1319, 1111, 1066, 833, 593 cm^{-1}; HRMS calculated for $C_{20}H_{11}ON_2F_6S$ (M+H): 473.02115; Found: 473.02030 m/z. ^{13}C NMR was unobtainable due to poor solubility.

4,4'-dimethyl-5,5'-bis(4-(trifluoromethyl)phenyl)-[2,2'-bithiazole] 3-oxide (**2.15n**)

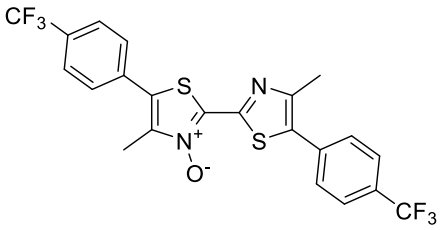

Prepared according to **General Procedure D** starting with **2.14n** (88 mg, 0.2 mmol, 1.0 equiv) to afford yellow solid **2.15n** (38 mg, 76%); R_f = 0.68 (EtOAc : Hexane = 3 : 7); ^{1}H NMR ($CDCl_3$, 300 MHz) δ 7.82 (d, *J* = 8.2 Hz, 2H), 7.75 (d, *J* = 8.3 Hz, 2H), 7.68 (d, *J* = 7.3 Hz, 4H), 2.64 (s, 3H), 2.61 (s, 3H); ^{13}C NMR ($CDCl_3$, 75 MHz) δ 150.5, 150.0, 142.1,

139.5, 135.6, 134.0, 132.4, 131.7 (q, $^{2}J_{CF}$ = 33.0 Hz), 130.0 (q, $^{2}J_{CF}$ = 32.7 Hz), 129.4, 129.0, 127.8, 126.4 (q, $^{3}J_{CF}$ = 3.7 Hz), 125.8 (q, $^{3}J_{CF}$ = 3.8 Hz), 124.0 (q, $^{1}J_{CF}$ = 272.3 Hz), 123.6 (q, $^{1}J_{CF}$ = 272.4 Hz), 16.5, 12.0; IR (ATR) 2970, 1319, 1124, 833, 601 cm^{-1}; ^{19}F NMR ($CDCl_3$, 470 MHz) δ -63.0, -63.3; HRMS calculated for $C_{22}H_{15}ON_2F_6S_2$ (M+H): 501.05245; Found: 501.05248 m/z. Data consistent with previously reported.[145]

5,5'-bis(3,5-bis(trifluoromethyl)phenyl)-[2,2'-bithiazole] 3-oxide (**2.15o**)

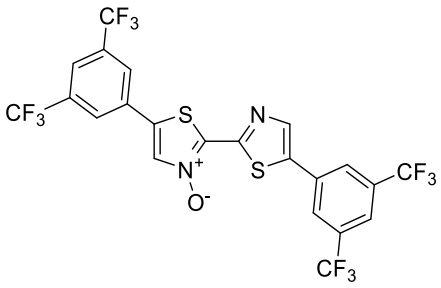

Prepared according to **General Procedure D** starting with **2.14o** (99 mg, 0.2 mmol, 1.0 equiv) to afford yellow solid **2.15o** (54 mg, 88%); R_f = 0.82 (EtOAc : Hexane = 3 : 7); ^{1}H NMR ($CDCl_3$, 300 MHz) δ 8.36 (s, 1H), 8.21 (s, 1H), 8.12 (s, 2H), 8.06 – 8.03 (m, 3H), 7.91 (s, 1H); ^{19}F NMR ($CDCl_3$, 470 MHz) δ -63.3; IR (ATR) 3062, 1362, 1283, 1134, 895, 683 cm^{-1}; HRMS calculated for $C_{22}H_9ON_2F_{12}S_2$ (M+H): 608.99592; Found: 608.99428 m/z. ^{13}C NMR was unobtainable due to poor solubility.

lithium 5-phenylthiazole-2-carboxylate (**2.16**)

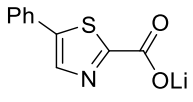

To a round-bottom flask charged with **2.10a** (645 mg, 4.0 mmol, 1.0 equiv), purged with argon and sealed was added THF (40 mL, 0.1 M) and allowed to stir in a -78 °C bath of dry ice and acetone. *n*-BuLi (3.0 mL, 1.6 M, 1.2 equiv) was added and the mixture was

stirred at this temperature for 20 min. Dry ice (265 mg, 6.0 mmol, 1.5 equiv) was then added, the vessel purged with argon, and continued to stir at this temperature for 6 h. The reaction mixture concentrated to a solid that was triturated with Et_2O (3 x 20 mL). Filtration yielded the white precipitate **2.16** (524 mg, 64%); ^{1}H NMR (CD_3OD, 300 MHz) δ 8.07 (s, 1H), 7.68 (d, *J* = 7.2 Hz, 2H), 7.47 – 7.37 (m, 3H); ^{13}C NMR (DMSO-d_6, 75 MHz) δ 161.1, 140.8, 139.3, 132.1, 129.6, 128.6, 126.8 *one peak absent due to poor solubility; HRMS calculated for $C_{10}H_8O_2NS$ (M+2H,-Li): 206.02703; Found: 206.02733.

4-(2-(4-(thiazol-5-yl)benzoyl)thiazol-5-yl)benzonitrile (**2.18**)

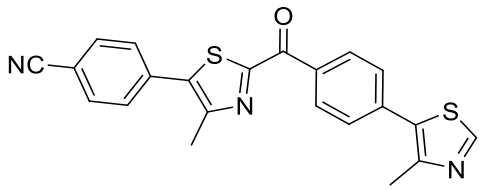

Discovered as a byproduct of the conversion of **2.10k** to **2.13k** and speculated to be caused by inadequate cooling to -78 °C. Following aqueous work-up, separation from **2.13k** by column chromatography (0 % – 30 % gradient EtOAc in hexanes) delivered byproduct **2.18**; R_f = 0.16 (EtOAc : hexanes = 2 : 3); ^{1}H NMR ($CDCl_3$, 300 MHz) δ 8.75 (s, 1H), 8.59 (d, *J* = 8.4 Hz, 2H), 7.77 (d, *J* = 8.3 Hz, 2H), 7.65 (d, *J* = 6.5 Hz, 2H), 7.62 (d, *J* = 6.8 Hz, 2H), 2.66 (s, 3H), 2.62 (s, 3H); ^{13}C NMR ($CDCl_3$, 75 MHz) δ 182.7, 165.4, 151.7, 151.3, 149.8, 138.1, 137.5, 136.0, 134.0, 132.7, 131.6, 131.0, 129.8, 129.0, 118.2, 112.5, 16.8, 16.5; HRMS calculated for $C_{22}H_{16}ON_3S_2$ (M+H): 402.07293; Found: 402.07315.

(4,5-dimethylthiazol-2-yl)diphenylmethanol (**2.19a**)

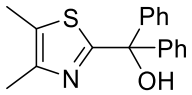

To a round-bottom flask charged with 4,5-dimethylthiazole (317 µL, 3.0 mmol, 1.0 equiv), purged with argon and sealed was added THF (30 mL, 0.1 M) and allowed to stir in a -78 °C bath of dry ice and acetone. *n*-BuLi (2.25 mL, 1.6 M, 1.2 equiv) was added and the mixture was stirred at this temperature for 30 min. Benzophenone (765 mg, 4.2 mmol, 1.4 equiv) was then added, the vessel purged with argon, and continued to stir at this temperature for 4 h. The reaction mixture was then quenched with NH_4Cl (30 mL) and extracted with ethyl acetate (3 x 30 mL). The organic layer was then dried with $MgSO_4$, concentrated and purified by column chromatography (0 % – 20 % gradient EtOAc in hexanes) to afford off-white solid **2.19a** (841 mg, 95%); R_f = 0.66 (EtOAc : Hexane = 3 : 7); ^{1}H NMR ($CDCl_3$, 300 MHz) δ 7.43 – 7.32 (m, 10H), 4.53 (s, 1H), 2.34 (s, 3H), 2.32 (s, 3H); ^{13}C NMR ($CDCl_3$, 75 MHz) δ 171.5, 147.8, 145.7, 128.0, 127.9, 127.8, 127.5, 80.2, 14.7, 11.3; HRMS calculated for $C_{18}H_{18}NOS$ (M+H): 296.11036; Found: 296.11082 m/z.

diphenyl(thiazol-2-yl)methanol (**2.19b**)

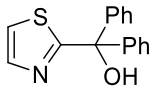

To a round-bottom flask charged with thiazole (1.42 mL, 20.0 mmol, 1.0 equiv), purged with argon and sealed was added THF (200 mL, 0.1 M) and allowed to stir in a -78 °C bath of dry ice and acetone. *n*-BuLi (15 mL, 24.0 mmol, 1.6 M, 1.2 equiv) was added and the mixture was stirred at this temperature for 45 min. Benzophenone (5.10 g, 28.0 mmol,

1.4 equiv) was then added, the vessel purged with argon, and continued to stir at this temperature for 10 h. The reaction mixture was then quenched with NH_4Cl (75 mL) and extracted with diethyl ether (3 x 50 mL). The organic layer was then dried with $MgSO_4$ and concentrated. The crude product was then purified by column chromatography (0 % – 20 % gradient EtOAc in Hexanes) to yield off-white solid **2.19b** (4.29 g, 79%); R_f = 0.27 (EtOAc : Hexanes = 1 : 4); ^{1}H-NMR ($CDCl_3$, 300 MHz) δ 7.72 (d, *J* = 3.1 Hz, 1H), 7.47 – 7.44 (m, 4H), 7.37 – 7.35 (m, 6H), 7.27 (d, *J* = 3.1 Hz, 1H), 5.06 (br s, 1H); ^{13}C-NMR ($CDCl_3$, 75 MHz) δ 177.7, 145.5, 142.7, 128.2, 128.0, 127.6, 120.0, 80.7; HRMS calculated for $C_{16}H_{14}ONS$ (M+H): 268.07906; Found: 368.07983 m/z.

benzo[d]thiazol-2-yldiphenylmethanol (**2.19c**)

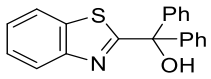

To a round-bottom flask charged with benzothiazole (330 µL, 3.0 mmol, 1.0 equiv), purged with argon and sealed was added THF (30 mL, 0.1 M) and allowed to stir in a -78 °C bath of dry ice and acetone. *n*-BuLi (2.25 mL, 1.6 M, 1.2 equiv) was added and the mixture was stirred at this temperature for 30 min. Benzophenone (765 mg, 4.2 mmol, 1.4 equiv) was then added, the vessel purged with argon, and continued to stir at this temperature for 2 h. The reaction mixture was then quenched with NH_4Cl (30 mL) and extracted with diethyl ether (3 x 30 mL). The organic layer was dried with $MgSO_4$, concentrated and purified by column chromatography (0 % – 20 % gradient EtOAc in hexanes) to afford off-white solid **2.19c** (896 mg, 94%); R_f = 0.48 (EtOAc : Hexane = 1 : 4); ^{1}H NMR ($CDCl_3$, 300 MHz) δ 8.05 (d, *J* = 8.1 Hz, 1H), 7.86 (d, *J* = 7.8 Hz, 1H), 7.54 – 7.36 (m, 12H), 4.43 (s, 1H); ^{13}C NMR ($CDCl_3$, 75 MHz) δ 177.8, 152.8, 144.9, 136.0,

128.2, 128.1, 127.7, 126.2, 125.3, 123.4, 121.6, 81.1; HRMS calculated for $C_{20}H_{16}NOS$ (M+H): 318.09471; Found: 318.09562 m/z.

2-(hydroxydiphenylmethyl)-4,5-dimethylthiazole 3-oxide (**2.20a**)

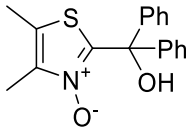

In a round-bottom flask, **2.19a** (830 mg, 2.8 mmol, 1.0 equiv) was dissolved in 1,2-dichloroethane (8.5 mL, 0.33M) and allowed to stir at room temperature. *m*-CPBA (946 mg, 77% pure, 4.2 mmol, 1.5 equiv) was then added and the mixture was continued stirring at this temperature for 16 h. The reaction mixture was then diluted with dichloromethane (30 mL) and then purified by column chromatography (0 % – 100 % gradient EtOAc in hexanes) to afford white solid **2.20a** (753 mg, 86%); R_f = 0.51 (EtOAc); ^{1}H NMR ($CDCl_3$, 300 MHz) δ 7.36 (s, 10H), 2.33 (s, 3H), 2.31 (s, 3H); ^{13}C NMR ($CDCl_3$, 75 MHz) δ 148.9, 143.5, 142.0 ,128.3, 128.2, 127.1, 124.5, 78.9, 12.7, 10.6; HRMS calculated for $C_{18}H_{18}NO_2S$ (M+H): 312.10528; Found: 312.10561 m/z.

2-(hydroxydiphenylmethyl)thiazole 3-oxide (**2.20b**)

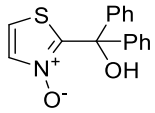

In a round-bottom flask, **2.19b** (4.2 g, 15.7 mmol, 1.0 equiv) was dissolved in 1,2-dichloroethane (50 mL, 0.3 M) and allowed to stir at room temperature. *m*-CPBA (5.3 g, 23.6 mmol, 1.5 equiv, 77% pure) was then added and the mixture was continued stirring at this temperature for 6 h. The reaction mixture was then concentrated under vacuum

and purified by column chromatography (10 % – 100 % gradient EtOAc in Hexanes) to afford white solid **2.20b** (3.87 g, 86%); R_f = 0.33 (EtOAc); ^{1}H-NMR ($CDCl_3$, 300 MHz) δ 8.38 (br s, 1H), 7.58 (d, *J* = 4.0 Hz, 1H), 7.35 – 7.33 (m, 10H), 7.20 (d, *J* = 4.0 Hz, 1H); ^{13}C-NMR ($CDCl_3$, 75 MHz) δ 151.7, 143.2, 137.7, 128.5, 128.4, 127.0, 117.8, 79.0; HRMS calculated for $C_{16}H_{14}O_2NS$ (M+H): 284.07398; Found: 284.07382 m/z.

2-(hydroxydiphenylmethyl)benzo[d]thiazole 3-oxide (**2.20c**)

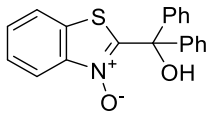

In a round-bottom flask, **2.20b** (317 mg, 1.00 mmol, 1.0 equiv) was dissolved in 1,2-dichloroethane (6 mL, 0.17 M) and allowed to stir at room temperature. *m*-CPBA (260 mg, 1.2 mmol, 1.2 equiv, 77% pure) was then added and the mixture was continued stirring at this temperature for 48 h. The reaction mixture was then concentrated under vacuum and purification was attempted by column chromatography (0 – 30 % gradient EtOAc in Hexanes) to afford white solid **2.20b** (123 mg, 37%); R_f = 0.23 (EtOAc : Hexane = 3 : 7); ^{1}H NMR ($CDCl_3$, 300 MHz) δ 8.28 (s, 1H), 8.19 (d, *J* = 8.0 Hz, 1H), 7.75 (d, *J* = 7.8 Hz, 1H), 7.62 (quint, *J* = 8.0 Hz, 2H), 7.44 – 7.37 (m, 10H); ^{13}C-NMR ($CDCl_3$, 75 MHz) δ 152.5, 143.0, 143.0, 128.5, 128.4, 127.6, 127.2, 127.1, 122.8, 117.6, 79.5; HRMS calculated for $C_{20}H_{16}NO_2S$ (M+H): 334.08963; Found: 334.09044 m/z.

(5-(2,5-dihexyl-4-(thiazol-5-yl)phenyl)thiazol-2-yl)diphenylmethanol (**2.21**)

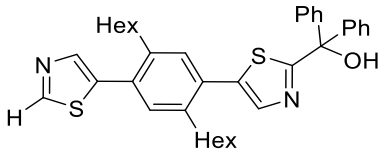

Prepared according to **General Procedure B** starting with **2.26h** (300 mg, 0.73 mmol, 1.0 equiv) and with the following deviation: *n*-BuLi (455 µL, 1.6M, 1.0 equiv) was added to the reaction mixture. The crude product was purified by column chromatography (0 % – 15 % gradient EtOAc in hexanes) to yield orange solid **2.21** (170 mg, 39%); R_f = 0.50 (EtOAc : Hexane = 1 : 4); ^{1}H NMR ($CDCl_3$, 300 MHz) δ 8.84 (s, 1H), 7.84 (s, 1H), 7.74 (s, 1H), 7.50 (dd, *J* = 7.7, 1.7 Hz, 4H), 7.39 – 7.37 (m, 6H), 7.28 – 7.24 (m, 2H), 4.44 (s, 1H), 2.71 – 2.62 (m, 4H), 1.53 – 1.48 (m, 4H), 1.26 (s, 12H), 0.88 – 0.85 (m, 6H); HRMS calculated for $C_{37}H_{43}ON_2S_2$ (M+H): 595.28113; Found: 595.27984 m/z.

5-(2,5-dihexyl-4-(thiazol-5-yl)phenyl)-2-(hydroxydiphenylmethyl)thiazole 3-oxide (**2.22a**) /

5-(2,5-dihexyl-4-(2-(hydroxydiphenylmethyl)thiazol-5-yl)phenyl)thiazole 3-oxide (**2.22b**)

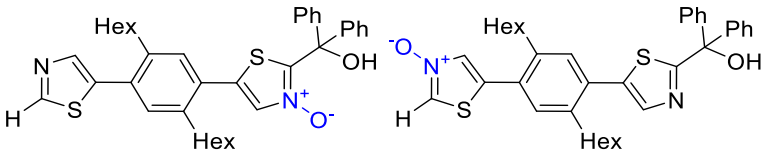

In a round bottom flask, substrate **2.21** (170 mg, 0.29 mmol, 1.0 equiv) was dissolved in 1,2-dichloroethane (1 mL, 0.3 M), and stirred. *m*-CPBA (45 mg, 0.20 mmol, 0.7 equiv, 77% pure) was added the reaction was allowed to stir at room temperature for 12 h (<1 equiv of *m*-CPBA used to ensure double *N*-oxidation did not occur). Column

chromatography (0 – 20% EtOAc in hexanes) yielded an inseparable mixture of **2.22a** and **2.22b** in a 1:1 ratio (determined by key NMR peak integration, see spectra); R_f = 0.19 (EtOAc : Hexane = 1 : 4); HRMS calculated for $C_{37}H_{43}O_2N_2S_2$ (M+H): 611.27605; Found: 611.27746 m/z.

5-(p-tolyl)thiazole 3-oxide (**2.23**)

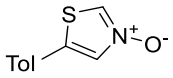

Prepared as part of competition experiment with **2.10c** (53 mg, 0.3 mmol, 1.0 equiv) and 5c (107 mg, 0.3 mmol, 1.0 equiv). Both substrates were dissolved in 1,2-dichloroethane (3 mL, 0.2 M) at room temperature at which point *m*CPBA (67 mg, 77% purity, 0.3 mmol, 1.0 equiv) was added. The mixture was continued stirring at this temperature for 6 h before then being diluted with dichloromethane (50 mL) and then purified by column chromatography (0 % – 100 % gradient EtOAc in hexanes, followed by 0 % - 10 % MeOH in EtOAc) to afford white solid **2.23** (16 mg, 28%). Note, concentration *in vacuo* was performed at 30 °C to prevent thermal degradation; ^{1}H NMR ($CDCl_3$, 300 MHz) δ 8.09 (s, 1H), 7.85 (s, 1H), 7.40 (d, *J* = 7.8 Hz, 2H), 7.27 (d, *J* = 7.3 Hz, 2H), 2.41 (s, 3H); HRMS calculated for $C_{10}H_{10}ONS$ (M+H): 192.04776; Found: 192.04797.

2-(methoxydiphenylmethyl)-5-(p-tolyl)thiazole (**2.24**)

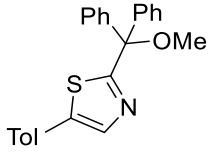

In a dry, argon-purged round-bottom flask was added **2.13c** (358 mg, 1.0 mmol, 1.0 equiv) in anhydrous THF (5 mL, 0.2M). NaH (48 mg, 60%wt, 1.2 mmol, 1.2 equiv) was added

portion-wise and stirred for 15 min at room temperature. Iodomethane (87 µL, 1.4 mmol, 1.4 equiv) was then added and the reaction mixture was allowed to continue stirring for 2 h. The crude product was purified by column chromatography (0 % – 30 % gradient EtOAc in hexanes) to afford pale yellow solid **2.24** (336 mg, 90%); R_f = 0.79 (EtOAc : Hexane = 1 : 4); ^{1}H NMR ($CDCl_3$, 300 MHz) δ 7.92 (s, 1H), 7.58 (d, *J* = 6.7 Hz, 4H), 7.45 (d, *J* = 8.1 Hz, 2H), 7.40 – 7.32 (m, 6H), 7.20 (d, *J* = 7.9 Hz, 2H), 3.28 (s, 3H), 2.38 (s, 3H); ^{13}C NMR ($CDCl_3$, 75 MHz) δ 174.3, 142.1, 139.9, 138.1, 137.8, 129.7, 128.7, 127.9, 127.8, 126.6, 86.2, 53.0, 21.2; HRMS calculated for $C_{24}H_{22}ONS$ (M+H): 372.14166; Found: 372.14150 m/z.

2-(methoxydiphenylmethyl)-5-(p-tolyl)thiazole 3-oxide (**2.25**)

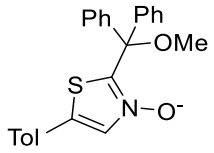

Prepared as part of competition experiment with **2.24** (112 mg, 0.3 mmol, 1.0 equiv) and **2.13c** (107 mg, 0.3 mmol, 1.0 equiv). Both substrates were dissolved in 1,2-dichloroethane (3 mL, 0.2M) at which point *m*CPBA (67 mg, 77% pure, 0.3 mmol, 1.0 equiv) was added the reaction was stirred for 6 h at room temperature. The crude mixture was purified by column chromatography (0 % – 80 % gradient EtOAc in hexanes) to afford white solid **2.25** (10 mg, 9%); R_f = 0.12 (EtOAc : Hexane = 2 : 3); ^{1}H NMR ($CDCl_3$, 300 MHz) δ 7.66 (s, 1H), 7.61 (d, *J* = 7.9 Hz, 4H), 7.39 (t, *J* = 6.8 Hz, 8H), 7.25 (d, *J* = 8.0 Hz, 2H), 3.15 (s, 3H), 2.40 (s, 3H); ^{13}C NMR ($CDCl_3$, 75 MHz) δ 149.1, 140.0, 136.6, 135.4, 133.7, 130.0, 129.0, 128.4, 127.9, 126.7, 125.7, 85.4, 52.3, 21.3; HRMS calculated for $C_{24}H_{22}O_2NS$ (M+H): 388.13658; Found: 388.13680 m/.z.

General procedure E: Double Direct Arylation of π-Spacers

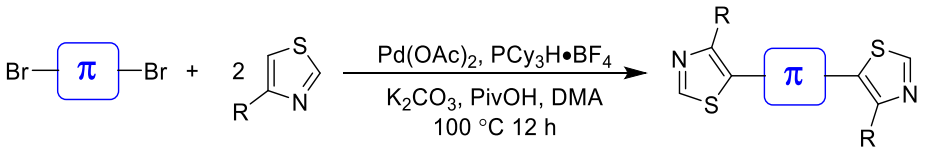

To a round bottom flask charged with $Pd(OAc)_2$ (27 mg, 4 mol %), K_2CO_3 (1.24 g, 9 mmol, 3.0 equiv), PCy_3HBF_4 (90 mg, 8 mol %), and PivOH (220 mg, 0.7 equiv), was added DMA (12 mL, 0.25 M) followed by thiazole (6.0 mmol, 2.0 equiv) and aryl dibromide (3 mmol, 1.0 equiv). The vial was sealed, purged with argon and the mixture stirred at 100 ℃ for 12 hours. The reaction mixture was then dissolved in H_2O (50 mL) and extracted with Et_2O (3x30 mL). The organic layer was then dried with $MgSO_4$ and filtered through Celite®. The filtrate was then concentrated and purified by column chromatography to yield aryldithiazoles.

5,5'-(9,9-dioctyl-9H-fluorene-2,7-diyl)dithiazole (**2.26a**)

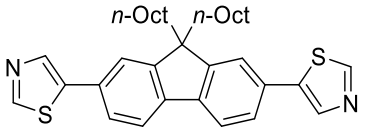

Prepared according to **General Procedure E** starting with thiazole (426 µL, 6 mmol, 2.0 equiv) and 9,9-dioctyl-2,7-dibromofluorene (1.64 g, 3.0 mmol, 1.0 equiv). The crude product was purified by column chromatography (0 % – 20 % gradient EtOAc in hexanes) to afford yellow solid **2.26a** (986 mg, 59%); R_f = 0.4 (EtOAc : Hexane = 1 : 4); ^{1}H NMR ($CDCl_3$, 300 MHz) δ 8.80 (s, 2H), 8.18 (s, 2H), 7.75 (d, *J* = 7.8 Hz, 2H), 7.60 (d, *J* = 7.8 Hz, 2H), 7.55 (s, 2H), 2.08 – 2.03 (m, 4H)), 1.09 (s, 20H), 0.81 – 0.78 (m, 6H), 0.69 (s, 4H); ^{13}C NMR ($CDCl_3$, 75 MHz) δ152.0, 151.8, 140.8, 140.0, 138.9, 130.2, 126.2, 121.2,

120.5, 55.4, 40.2, 31.7, 29.9, 29.1, 23.7, 22.6, 14.0 *one peak missing due to overlap; HRMS calculated for $C_{35}H_{45}N_2S_2$ (M+H): 557.30187; Found: 557.30084 m/z.

5,5'-(9,9-dioctyl-9H-fluorene-2,7-diyl)bis(4-methylthiazole) (**2.26b**)

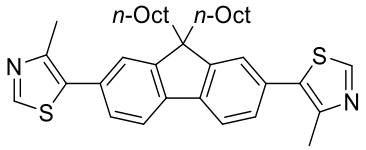

Prepared according to **General Procedure E** starting with 4-methylthiazole (546 µL, 6.0 mmol, 2.0 equiv) and 9,9-dioctyl-2,7-dibromofluorene (1.64 g, 3.0 mmol, 1.0 equiv). The crude product was purified by column chromatography (0 % – 20 % gradient EtOAc in hexanes) to afford yellow solid **2.26b** (1.40 g, 80%); R_f = 0.31 (EtOAc : Hexane = 1 : 4); ^{1}H NMR ($CDCl_3$, 300 MHz) δ 8.74 (s, 2H), 7.78 (d, *J* = 7.7 Hz, 2H), 7.47 – 7.44 (m, 4H), 2.61 (s, 6H), 2.05 – 2.00 (m, 4H), 1.22 – 1.10 (m, 20H), 0.82 (t, *J* = 6.8 Hz, 6H), 0.76 – 0.74 (m, 4H); ^{13}C NMR ($CDCl_3$, 75 MHz) δ 151.5, 150.1, 148.4, 140.2, 132.6, 130.9, 128.4, 123.7, 120.1, 55.4, 40.2, 31.7, 29.9, 29.2, 29.1, 23.8, 22.6, 16.3, 14.0; HRMS calculated for $C_{37}H_{49}N_2S_2$ (M+H): 585.33317; Found: 585.33357 m/z.

5,5'-(9,9-bis(2-ethylhexyl)-9H-fluorene-2,7-diyl)dithiazole (**2.26c**)

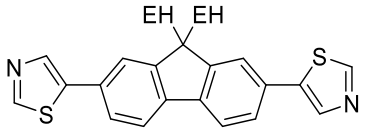

Prepared according to **General Procedure E** starting with thiazole (426 µL, 6.0 mmol, 2.0 equiv) and 9,9-di(2-ethylhexyl)-2,7-dibromofluorene (1.64 g, 3.0 mmol, 1.0 equiv). The crude product was purified by column chromatography (0 % – 20 % gradient EtOAc in hexanes) to afford yellow solid **2.26c** (786 mg, 47%); R_f = 0.28 (EtOAc : Hexane = 1 : 4);

^{1}H NMR ($CDCl_3$, 300 MHz) δ 8.76 (s, 2H), 8.11 (s, 2H), 7.71 (d, *J* = 8.3 Hz, 2H), 7.57 – 7.55 (m, 4H), 2.05 (d, *J* = 4.5 Hz, 4H), 0.86 – 0.74 (m, 18H), 0.60 (t, *J* = 5.5 Hz, 6H), 0.51 (t, *J* = 6.8 Hz, 6H); ^{13}C NMR ($CDCl_3$, 75 MHz) δ 151.9, 151.7*, 141.0, 140.1, 138.8, 129.6, 126.2, 122.6*, 120.5, 55.2, 44.3, 34.8, 33.9, 28.1, 27.2, 22.7, 14.0, 10.4(* Splitting appears due to presence of diastereomers); Data consistent with previously reported.[144]

5,5'-(9,9-bis(2-ethylhexyl)-9H-fluorene-2,7-diyl)bis(4-methylthiazole) (**2.26d**)

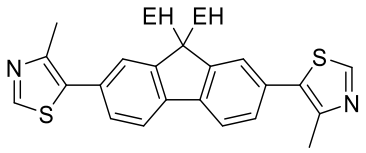

Prepared according to **General Procedure E** starting with 4-methylthiazole (437 µL, 4.8 mmol, 2.0 equiv) and 9,9-(2-ethylhexyl)-2,7-dibromofluorene (1.32 g, 2.4 mmol, 1.0 equiv). The crude product was purified by column chromatography (0 % – 20 % gradient EtOAc in hexanes) to afford yellow solid **2.26d** (1.11 g, 78%); R_f = 0.39 (EtOAc : Hexane = 1 : 4); ^{1}H NMR ($CDCl_3$, 300 MHz) δ 8.68 (s, 2H), 7.74 (d, *J* = 7.7 Hz, 2H), 7.42 – 7.40 (m, 4H), 2.55 (s, 6H), 2.02 – 1.96 (m, 4H), 0.86 – 0.74 (m, 16H), 0.63 – 0.62 (m, 6H), 0.54 – 0.49 (m, 8H); ^{13}C NMR ($CDCl_3$, 75 MHz) δ 151.2*, 150.2, 148.4, 140.5, 132.6, 130.4, 128.3*, 125.1*, 120.0, 55.3, 44.6, 34.8, 33.9*, 28.3*, 27.0*, 22.7, 16.1*, 13.9, 10.3* (* Splitting appears due to presence of diastereomers); Data consistent with previously reported.[144,145]

5,5'-(2,5-bis(decyloxy)-1,4-phenylene)dithiazole (**2.26e**)

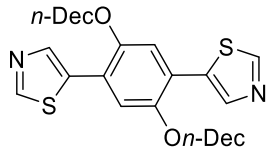

Prepared according to **General Procedure E** starting with thiazole (426 µL, 6.0 mmol, 2.0 equiv) and 1,4-dibromo-2,5-bis(decyloxy)benzene (1.64 g, 3.0 mmol, 1.0 equiv). The crude product was purified by column chromatography (0 % – 15 % gradient EtOAc in hexanes) to afford yellow solid **2.26e** (583 mg, 35%); R_f = 0.36 (EtOAc : Hexane = 1 : 4); ^{1}H NMR ($CDCl_3$, 300 MHz) δ 8.83 (s, 2H), 8.33 (s, 2H), 7.27 (s, 2H), 4.12 (t, *J* = 6.5 Hz, 4H), 1.93 (p, *J* = 7.8 Hz, 4H), 1.54 (p, *J* = 7.1 Hz, 4H), 1.35 – 1.30 (m, 24H), 0.90 (t, *J* = 6.6 Hz, 6H); ^{13}C NMR ($CDCl_3$, 75 MHz) δ 153.3, 149.1, 141.1, 133.6, 120.8, 112.5, 69.8, 31.9, 29.6, 29.4, 29.3, 26.2, 22.7, 14.1 *two peaks missing due to overlap; HRMS calculated for $C_{32}H_{49}N_2O_2S_2$ (M+H): 557.32300; Found: 557.32342 m/z.

5,5'-(2,5-bis(decyloxy)-1,4-phenylene)bis(4-methylthiazole) (**2.26f**)

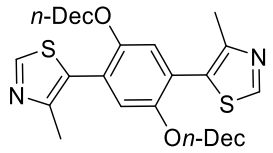

Prepared according to **General Procedure E** starting with 4-methylthiazole (546 µL, 6.0 mmol, 2.0 equiv) and 1,4-dibromo-2,5-bis(decyloxy) (1.64 g, 3.0 mmol, 1.0 equiv). The crude product was purified by column chromatography (0 % – 15 % gradient EtOAc in hexanes) to afford yellow solid **2.26f** (209 mg, 12%); R_f = 0.47 (EtOAc : Hexane = 1 : 4); ^{1}H NMR ($CDCl_3$, 300 MHz) δ 8.78 (s, 2H), 6.96 (s, 2H), 3.93 (t, *J* = 6.5 Hz, 4H), 2.52 (s, 6H), 1.73 (p, *J* = 6.9 Hz, 4H), 1.37 – 1.27 (m, 28H), 0.90 (t, *J* = 6.6 Hz, 6H); ^{13}C NMR

($CDCl_3$, 75 MHz) δ 151.3, 150.4, 150.1, 126.9, 121.8, 116.3, 69.6, 31.9, 29.5, 29.4, 29.3, 29.2, 26.0, 22.7, 16.5, 14.1 *one peak missing due to overlap; Data consistent with previously reported.[145]

5,5'-(3,4-dihexylthiophene-2,5-diyl)dithiazole (**2.26g**)

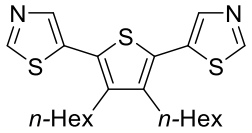

Prepared according to **General Procedure E** starting with thiazole (596 µL, 8.4 mmol, 2.1 equiv) and 2,5-dibromo-3,4-dihexylthiophene (1.25 mL, 4.0 mmol, 1.0 equiv). The crude product was purified by column chromatography (0 % – 15 % gradient EtOAc in hexanes) to afford yellow oil **2.26g** (898 mg, 54%); R_f = 0.65 (EtOAc : Hexane = 2 : 3); ^{1}H NMR ($CDCl_3$, 300 MHz) δ 8.84 (s, 1H), 7.95 (s, 1H), 2.70 – 2.64 (m, 4H), 1.57 – 1.52 (m, 4H), 1.40 – 1.29 (m, 12H), 0.93 – 0.90 (m, 3H); ^{13}C NMR ($CDCl_3$, 75 MHz) δ152.8, 141.9, 141.4, 130.7, 126.6, 31.5, 30.7, 29.5, 28.2, 22.6, 14.0; HRMS calculated for $C_{22}H_{31}N_2S_3$ (M+H): 419.16439; Found: 419.16495 m/z.

5,5'-(2,5-dihexyl-1,4-phenylene)dithiazole (**2.26h**)

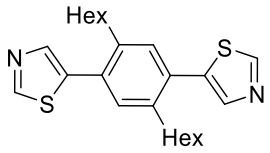

Prepared according to **General Procedure E** starting with thiazole (355 µL, 5.0 mmol, 2.0 equiv) and 1,4-dibromo-2,5-dihexylbenzene (1.0 g, 2.5 mmol, 1.0 equiv). The crude product was purified by column chromatography (0 % – 20 % gradient EtOAc in hexanes) to afford yellow solid **2.26h** (422 mg, 41%); R_f = 0.40 (EtOAc : Hexane = 1 : 4); ^{1}H NMR

($CDCl_3$, 300 MHz) δ 8.89 (s, 2H), 7.87 (s, 2H), 7.29 (s, 2H), 2.69 – 2.64 (m, 4H), 1.54 (s, 4H), 1.28 (s, 12H), 0.86 (t, *J* = 6.1 Hz, 6H); ^{13}C NMR ($CDCl_3$, 75 MHz) δ 153.0, 141.8, 139.3, 132.5, 130.4, 33.1, 31.5, 31.4, 29.2, 22.5, 14.0 *one peak missing due to overlap; HRMS calculated for $C_{24}H_{33}N_2S_2$ (M+H): 413.20797; Found: 413.20847 m/z.

General procedure F: 2,2'-Substitution of Dithiazoles

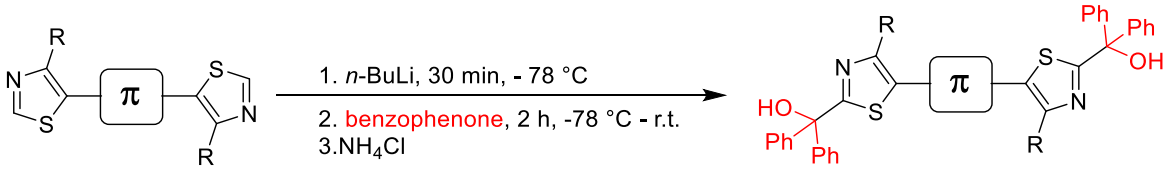

To a round-bottom flask charged with thiazole (1.4 mmol, 1.0 equiv), purged with argon and sealed, was added THF (14 mL, 0.1 M) and allowed to stir in a -78 °C bath of dry ice and acetone. *n*BuLi (3.4 mmol, 1.6 M, 2.4 equiv) was added and the mixture was stirred at this temperature for 30 min. Benzophenone (4.2 mmol, 3.0 equiv) was then added, the vessel purged with argon, and continued to stir at this temperature for 4 h. The reaction mixture was then quenched with NH_4Cl (30 mL) and extracted with diethyl ether (3 x mL). The organic layer was then dried with $MgSO_4$ and concentrated. The crude product was then purified by column chromatography to yield (arylenebis(thiazole-5,2-diyl))bis(diphenylmethanol)s.

((9,9-dioctyl-9H-fluorene-2,7-diyl)bis(thiazole-5,2-diyl))bis(diphenylmethanol) (**2.27a**)

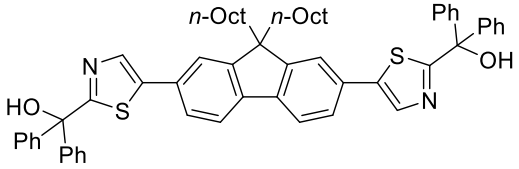

Prepared according to **General Procedure F** starting with **2.26a** (968 mg, 1.7 mmol, 1.0 equiv). The crude product was purified by column chromatography (0 % – 20 % gradient EtOAc in hexanes) to yield yellow solid **2.27a** (1.18 g, 74%); R_f = 0.30 (EtOAc : Hexane = 1 : 4); ^{1}H NMR ($CDCl_3$, 300 MHz) δ 8.01 (s, 2H), 7.69 (d, *J* = 7.9 Hz, 2H), 7.55 – 7.42 (m, 12H), 7.40 – 7.34 (m, 12H), 4.40 (br s, 2H), 2.03 – 1.98 (m, 4H), 1.21 – 1.06 (m, 20H), 0.81 (t, *J* = 0.81 Hz, 6H), 0.62 (s, 4H); ^{13}C NMR ($CDCl_3$, 75 MHz) δ 175.7, 151.8, 145.2, 141.2, 140.7, 137.8, 130.3, 128.2, 128.0, 127.5, 125.7, 120.9, 120.4, 80.7, 55.5, 40.3, 31.7, 29.9, 29.1, 23.7, 22.6, 14.0 *one peak missing due to overlap; HRMS calculated for $C_{61}H_{65}O_2N_2S_2$ (M+H): 921.44820; Found: 921.44781 m/z.

((9,9-dioctyl-9H-fluorene-2,7-diyl)bis(4-methylthiazole-5,2-diyl))bis(diphenylmethanol) (**2.27b**)

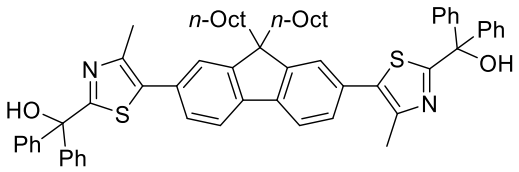

Prepared according to **General Procedure F** starting with **2.26b** (1.35 g, 2.3 mmol, 1.0 equiv). The crude product was purified by column chromatography (0 % – 40 % gradient EtOAc in hexanes) to yield yellow solid **2.27b** (707 mg, 32%); R_f = 0.39 (EtOAc : Hexane

= 1 : 4); ^{1}H NMR ($CDCl_3$, 300 MHz) δ 7.71 (d, *J* = 7.8 Hz, 2H), 7.51 (dd, *J* = 7.8 Hz, 1.6 Hz, 8H), 7.41 – 7.35 (m, 16H), 4.51 (br s, 2H), 2.56 (s, 6H), 2.01 – 1.96 (m, 4H), 1.21 – 1.06 (m, 20H), 0.82 (t, *J* = 6.9 Hz, 6H), 0.66 (s, 4H); ^{13}C NMR ($CDCl_3$, 75 MHz) δ 173.2, 151.4, 147.3, 145.5, 140.2, 134.4, 130.8, 128.2, 128.1, 127.9, 127.5, 123.5, 120.0; HRMS calculated for $C_{63}H_{69}O_2N_2S_2$ (M+H): 949.47950; Found: 949.47989 m/z.

((9,9-bis(2-ethylhexyl)-9H-fluorene-2,7-diyl)bis(thiazole-5,2-diyl))bis(diphenylmethanol) (**2.27c**)

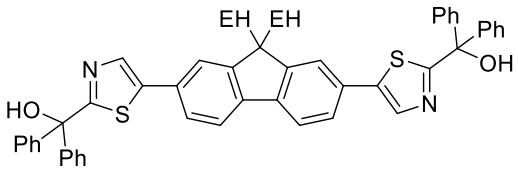

Prepared according to **General Procedure F** starting with **2.26c** (786 mg, 1.4 mmol, 1.0 equiv). The crude product was purified by column chromatography (0 % – 20 % gradient EtOAc in hexanes) to yield yellow solid **2.27c** (739 mg, 57%); R_f = 0.36 (EtOAc : Hexane = 1 : 4); ^{1}H NMR ($CDCl_3$, 300 MHz) δ 7.99 (s, 2H), 7.69 (d, *J* = 8.1 Hz, 2H), 7.51 – 7.49 (m, 10H), 7.38 (d, *J* = 6.5 Hz, 12H), 4.27 (t, *J* = 10.8 Hz, 2H), 2.03 (d, *J* = 5.3 Hz, 4H), 0.88 – 0.77 (m, 16H), 0.63 (s, 6H), 0.52 (t, *J* = 7.0 Hz, 8H); ^{13}C NMR ($CDCl_3$, 75 MHz) δ 175.7, 151.7, 145.2, 141.2, 140.9, 137.7, 129.7, 128.2, 128.0, 127.5, 125.8, 122.3, 120.4, 80.7, 55.2, 44.3, 34.8, 33.7, 28.1, 27.2, 22.7, 14.0, 10.4; HRMS calculated for $C_{61}H_{65}O_2N_2S_2$ (M+H): 921.44820; Found: 921.44414 m/z.

((9,9-bis(2-ethylhexyl)-9H-fluorene-2,7-diyl)bis(4-methylthiazole-5,2-diyl))bis(diphenylmethanol) (**2.27d**)

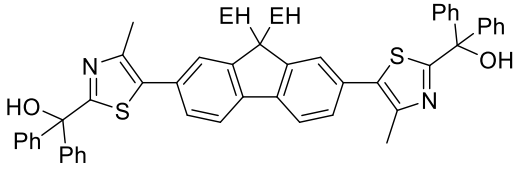

Prepared according to **General Procedure F** starting with **2.26d** (1.0 g, 1.7 mmol, 1.0 equiv). The crude product was purified by column chromatography (0 % – 15 % gradient EtOAc in hexanes) to yield yellow solid **2.27d** (1.47 g, 91%); R_f = 0.15 (EtOAc : Hexane =1: 9); ^{1}H NMR ($CDCl_3$, 300 MHz) δ 7.69 (d, *J* = 8.1 Hz, 2H), 7.47 – 7.46 (m, 8H), 7.38 – 7.33 (m, 16H), 4.46 (t, *J* = 9.4 Hz, 2H), 2.51 (s, 6H), 1.98 (d, *J* = 4.7 Hz, 4H), 0.82 – 0.71 (m, 16H), 0.60 (t, *J* = 5.9 Hz, 6H), 0.48 (t, *J* = 7.2 Hz, 8H); ^{13}C NMR ($CDCl_3$, 75 MHz) δ173.2, 151.2, 145.5, 140.4, 134.4, 134.3, 130.3, 128.2, 128.1, 127.9, 127.5, 124.8, 119.9, 80.4, 55.2, 44.6, 34.8, 33.7, 28.2, 27.1, 22.7, 16.4, 16.3, 14.0, 10.4, 10.3; HRMS calculated for $C_{63}H_{69}O_2N_2S_2$ (M+H): 949.47950; Found: 949.48241 m/z.

((2,5-bis(decyloxy)-1,4-phenylene)bis(thiazole-5,2-diyl))bis(diphenylmethanol) (**2.27e**)

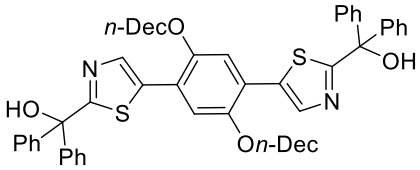

Prepared according to **General Procedure F** starting with **2.26e** (278 mg, 0.5 mmol, 1.0 equiv). The crude product was purified by column chromatography (0 % – 10 % gradient EtOAc in hexanes) to yield yellow solid **2.27e** (182 mg, 47%); R_f = 0.48 (EtOAc : Hexane

= 1 : 4); ^{1}H NMR ($CDCl_3$, 300 MHz) δ 8.20 (s, 2H), 7.47 (dd, *J* = 7.8, 1.7 Hz, 8H), 7.40 – 7.33 (m, 12H), 7.15 (s, 2H), 4.40 (br s, 2H), 4.03 (t, *J* = 6.4 Hz, 4H), 1.80 (p, *J* = 7.7 Hz, 4H), 1.46 – 1.42 (m, 4H), 1.29 (s, 24H), 0.91 (t, *J* = 6.6 Hz, 6H); ^{13}C NMR ($CDCl_3$, 75 MHz) δ 176.4, 149.1, 145.4, 140.1, 135.2, 128.1, 127.9, 127.5, 120.7, 112.1, 80.6, 69.6, 31.9, 29.6, 29.5, 29.4, 29.3, 29.2, 26.2, 22.7, 14.1; HRMS calculated for $C_{58}H_{69}O_4N_2S_2$ (M+H): 921.46933; Found: 421.46636 m/z.

((2,5-bis(decyloxy)-1,4-phenylene)bis(4-methylthiazole-5,2-diyl))bis(diphenylmethanol) (**2.27f**)

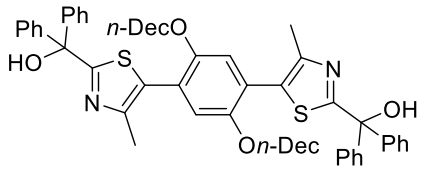

Prepared according to **General Procedure F** starting with **2.26f** (209 mg, 0.36 mmol, 1.0 equiv). The crude product was purified by column chromatography (0 % – 10 % gradient EtOAc in hexanes) to yield pale yellow solid **2.27f** (162 mg, 48%); R_f = 0.50 (EtOAc : Hexane = 1 : 4); ^{1}H NMR ($CDCl_3$, 300 MHz) δ 7.46 (dd, *J* = 7.7, 1.8 Hz, 8H), 7.36 – 7.34 (m, 12H), 6.88 (s, 2H), 4.53 (s, 2H), 3.87 (t, *J* = 6.4 Hz, 4H), 2.44 (s, 6H), 1.67 (p, *J* = 7.2 Hz, 4H), 1.26 (s, 28H), 0.90 (t, *J* = 6.6 Hz, 6H); ^{13}C NMR ($CDCl_3$, 75 MHz) δ 174.3, 150.0, 149.2, 145.6, 128.8, 128.0, 127.8, 127.5, 121.6, 116.0, 80.3, 69.5, 31.9. 29.6, 29.5, 29.3, 29.2, 26.0, 22.7, 16.7, 14.1; HRMS calculated for $C_{60}H_{72}O_4N_2S_2$ (M+H): 949.50063; Found: 949.49701 m/z.

((3,4-dihexylthiophene-2,5-diyl)bis(thiazole-5,2-diyl))bis(diphenylmethanol) (**2.27g**)

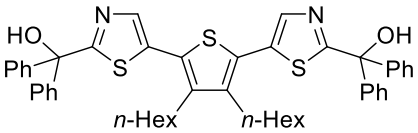

Prepared according to **General Procedure F** starting with **2.26g** (419 mg, 1.0 mmol, 1.0 equiv). The crude product was purified by column chromatography (0 % – 10 % gradient EtOAc in hexanes) to yield yellow solid **2.27g** (482 mg, 62%); ^{1}H NMR ($CDCl_3$, 300 MHz) δ 7.79 (s, 1H), 7.48 – 7.44 (m, 8H), 7.38 – 7.35 (m, 12H), 4.12 (s, 2H), 2.64 – 2.59 (m, 4H), 1.49 – 1.46 (m, 4H), 1.29 (s, 12H), 0.92 – 0.88 (m, 6H); ^{13}C NMR ($CDCl_3$, 75 MHz) δ 176.7, 145.0, 141.7, 140.2, 132.1, 128.2, 128.1, 127.4, 126.6, 80.7, 31.4, 30.6, 29.4, 28.2, 22.6, 14.0; HRMS calculated for $C_{48}H_{51}O_2N_2S_3$ (M+H): 783.31127; Found: 783.29154 m/z.

General procedure G: Oxidation of Dithiazoles

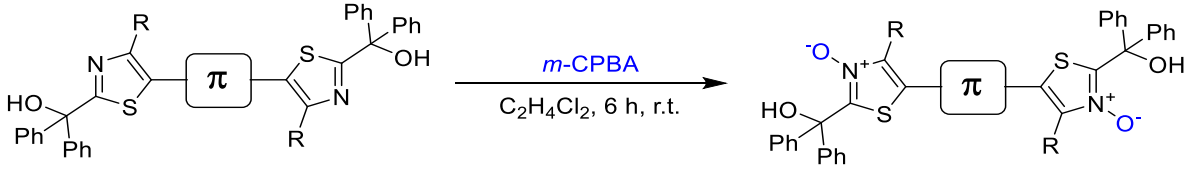

In a round-bottom flask, activated dithiazole (0.55 mmol, 1.0 equiv) was dissolved in 1,2-dichloroethane (22 mL, 0.025M) allowed to stir at room temperature. *m*-CPBA (1.2 mmol, 2.2 equiv) was then added and the mixture was continued stirring at this temperature for 6 h. The reaction mixture was then diluted with dichloromethane (30 mL) and then purified by column chromatography to yield 5,5'-(arylene)bis(2-(hydroxydiphenylmethyl)thiazole 3-oxide) monomers.

5,5'-(9,9-dioctyl-9H-fluorene-2,7-diyl)bis(2-(hydroxydiphenylmethyl)thiazole 3-oxide) (**2.28a**)

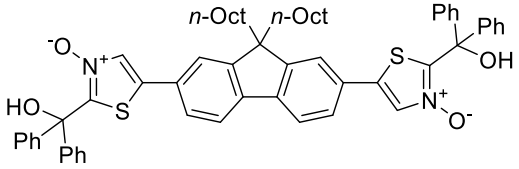

Prepared according to **General Procedure G** starting with **2.27a** (750 mg, 0.81 mmol, 1.0 equiv). The crude product was purified by column chromatography (0 % – 70 % gradient EtOAc in hexanes) to afford yellow solid **2.28a** (433 mg, 56%); R_f = 0.19 (EtOAc : Hexane = 3 : 7); ^{1}H NMR ($CDCl_3$, 300 MHz) δ 8.24 (br s, 2H), 7.94 (s, 2H), 7.71 (d, *J* = 7.9 Hz, 2H), 7.43 – 7.34 (m, 24H), 1.98 – 1.93 (m, 4H), 1.19 – 1.01 (m, 20H), 0.79 (t, *J* = 6.9 Hz, 6H), 0.52 (s, 4H); ^{13}C NMR ($CDCl_3$, 75 MHz) δ 152.4, 150.5, 143.2, 141.8, 136.0, 132.8, 128.5, 128.4, 128.2, 127.1, 125.2, 121.1, 120.0, 79.1, 55.8, 40.1, 31.7, 29.8, 29.2, 29.1, 23.7, 22.6, 14.1; HRMS calculated for $C_{61}H_{65}O_4N_2S_2$ (M+H): 953.43803; Found: 953.43615 m/z.

5,5'-(9,9-dioctyl-9H-fluorene-2,7-diyl)bis(2-(hydroxydiphenylmethyl)-4-methylthiazole 3-oxide) (**2.28b**)

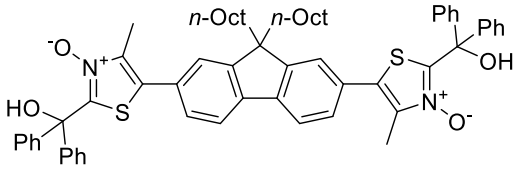

Prepared according to **General Procedure G** starting with **2.27b** (522 mg, 0.55 mmol, 1.0 equiv). The crude product was purified by column chromatography (0 % – 70 % gradient EtOAc in hexanes) to afford yellow solid **2.28b** (371 mg, 69%); R_f = 0.41 (EtOAc

: Hexane = 3 : 7); ^{1}H NMR ($CDCl_3$, 300 MHz) δ 8.47 (br s, 2H), 7.79 (d, *J* = 7.9 Hz, 2H), 7.46 – 7.37 (m, 24H), 2.52 (s, 6H), 2.03 – 1.98 (m, 4H), 1.21 – 1.05 (m, 20H), 0.82 (t, *J* = 6.9 Hz, 6H), 0.61 (s, 4H); ^{13}C NMR ($CDCl_3$, 75 MHz) δ 152.1, 150.3, 143.4, 141.7, 141.2, 130.0, 129.5, 128.4, 128.3, 127.9, 127.1, 123.0, 120.8, 79.1, 55.7, 40.1, 31.7, 29.8, 29.1, 29.0, 23.8, 22.5, 14.0, 12.0; HRMS calculated for $C_{63}H_{69}O_4N_2S_2$ (M+H): 981.46933; Found: 981.46722 m/z.

5,5'-(9,9-bis(2-ethyloctyl)-9H-fluorene-2,7-diyl)bis(2-(hydroxydiphenylmethyl)thiazole 3-oxide) (**2.28c**)

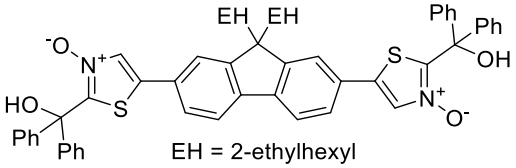

Prepared according to **General Procedure G** starting with **2.27c** (650 mg, 0.71 mmol, 1.0 equiv). The crude product was purified by column chromatography (0 % – 70 % gradient EtOAc in hexanes) to afford yellow solid **2.28c** (363 mg, 55%); R_f = 0.22 (EtOAc : Hexane = 3 : 7); ^{1}H NMR ($CDCl_3$, 300 MHz) δ 8.20 (br s, 2H), 7.96 (s, 2H), 7.75 (d, *J* = 7.5 Hz, 7.44 – 7.40 (m, 24H), 2.02 (d, *J* = 5.1 Hz, 4H), 0.85 – 0.63 (m, 22H), 0.49 (t, *J* = 7.3 Hz, 6H), 0.43 – 0.42 (m, 2H); ^{13}C NMR ($CDCl_3$, 75 MHz) δ 152.3, 150.8, 143.2, 142.0, 136.1, 132.7, 128.5, 128.4, 127.6, 127.0, 125.3, 121.4, 121.1, 79.1, 55.5, 44.2, 34.8, 33.7, 28.1, 27.1, 22.7, 14.0, 10.4; HRMS calculated for $C_{61}H_{65}O_4N_2S_2$ (M+H): 953.43803; Found: 953.43333 m/z.

5,5'-(9,9-bis(2-ethyloctyl)-9H-fluorene-2,7-diyl)bis(2-(hydroxydiphenylmethyl)-4-methylthiazole 3-oxide) (**2.28d**)

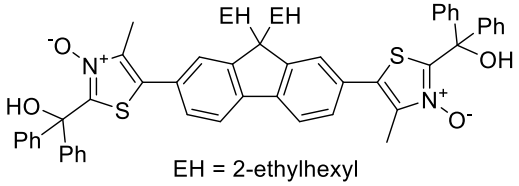

Prepared according to **General Procedure G** starting with **2.27d** (760 mg, 0.80 mmol, 1.0 equiv). The crude product was purified by column chromatography (0 % – 75 % gradient EtOAc in hexanes) to afford yellow solid **2.28d** (586 mg, 75%); R_f = 0.34 (EtOAc : Hexane = 3 : 7); ^{1}H NMR ($CDCl_3$, 300 MHz) δ 8.48 (br s, 2H), 7.82 (d, *J* = 8.2 Hz, 2H), 7.48 – 7.36 (m, 24H), 2.54 (s, 6H), 2.07 (d, *J* = 3.5 Hz, 4H), 0.85 – 0.4 (m, 16H), 0.64 (s, 6H), 0.51 (t, *J* = 7.2 Hz, 8H); ^{13}C NMR ($CDCl_3$, 75 MHz) δ 151.9*, 150.5, 143.4, 141.7, 141.2, 130.1, 129.0, 128.4, 128.3, 128.0*, 127.1, 124.3, 120.9, 79.1, 55.6, 44.4, 34.9, 33.8, 28.2, 27.1, 22.7, 14.0, 11.9, 10.4; HRMS calculated for $C_{63}H_{69}O_4N_2S_2$ (M+H): 981.46933; Found: 981.46521 m/z.

5,5'-(2,5-bis(decyloxy)-1,4-phenylene)bis(2-(hydroxydiphenylmethyl)thiazole 3-oxide) (**2.28e**)

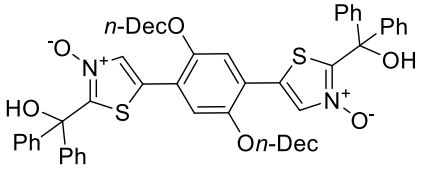

Prepared according to **General Procedure G** starting with **2.27e** (451 mg, 0.49 mmol, 1.0 equiv). The crude product was purified by column chromatography (0 % – 50 % gradient EtOAc in hexanes) to afford bright yellow solid **2.28e** (151 g, 31%); R_f = 0.28

(EtOAc : Hexane = 3 : 7); ^{1}H NMR ($CDCl_3$, 300 MHz) δ 8.28 (br s, 2H), 8.13 (s, 2H), 7.41 – 7.37 (m, 20H), 7.03 (s, 2H), 4.00 (t, *J* = 6.5 Hz, 4H), 1.73 – 1.64 (m, 8H), 1.29 (s, 24H), 0.91 (t, *J* = 6.5 Hz, 6H); ^{13}C NMR ($CDCl_3$, 75 MHz) δ 151.6, 149.6, 143.2, 134.2, 130.1, 128.4, 128.3, 127.0, 119.2, 110.5, 79.0, 70.0, 31.9, 29.6, 29.5, 29.3, 29.2, 28.9, 26.1, 22.7, 14.1; HRMS calculated for $C_{58}H_{69}O_6N_2S_2$ (M+H): 953.45916; Found: 953.45169 m/z.

5,5'-(2,5-bis(decyloxy)-1,4-phenylene)bis(2-(hydroxydiphenylmethyl)-4-methylthiazole 3-oxide) (**2.28f**)

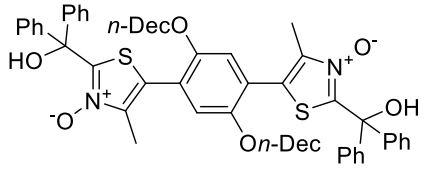

Prepared according to **General Procedure G** starting with **2.27f** (162 mg, 0.17 mmol, 1.0 equiv). The crude product was purified by column chromatography (0 % – 30 % gradient EtOAc in hexanes) to afford pale yellow solid **2.28f** (115 mg, 69%); R_f = 0.51 (EtOAc : Hexane = 3 : 7); ^{1}H NMR ($CDCl_3$, 300 MHz) δ 8.46 (s, 2H), 7.41 – 7.36 (m, 20H), 6.88 (s, 2H), 3.91 (t, *J* = 6.4 Hz, 4H), 2.40 (s, 4H), 1.69 (p, *J* = 6.6 Hz, 4H), 1.29 (s, 28H), 0.91 (t, *J* = 6.4 Hz, 6H); ^{13}C NMR ($CDCl_3$, 75 MHz) δ 151.3, 150.1, 143.4, 143.3, 128.4, 128.3, 127.1, 124.8, 120.6, 115.2, 79.1, 69.6, 31.9, 29.6, 29.5, 29.3, 29.2, 29.1, 26.0, 22.7, 14.1, 12.5; HRMS calculated for $C_{60}H_{73}O_6N_2S_2$ (M+H): 981.49046; Found: 981.48571 m/z.

3,4-dihexyl-2,5-bis(2-(hydroxydiphenylmethyl)thiazol-5-yl)thiophene 1,1-dioxide (**2.29a**)

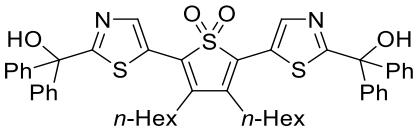

Prepared according to **General Procedure G** starting with **2.27g** (359 mg, 0.46 mmol, 1.0 equiv). The crude product was purified by column chromatography (0 % – 15 % gradient EtOAc in hexanes) to yield pale yellow solid **2.29a** (85 mg, 23%); R_f = 0.58 (EtOAc : Hexane = 1 : 4); ^{1}H NMR ($CDCl_3$, 300 MHz) δ 8.32 (s, 2H), 7.47 – 7.45 (m, 8H), 7.40 – 7.36 (m, 12H), 3.97 (s, 2H), 2.56 (t, *J* = 6.7 Hz, 4H), 1.51 – 1.29 (m, 16H), 0.93-0.89 (t, *J* = 8.7 Hz, 6H); ^{13}C NMR ($CDCl_3$, 75 MHz) δ 179.6, 144.5, 143.7, 139.4, 128.8, 128.3, 127.4, 124.4, 81.0, 31.2, 29.4, 28.6, 27.2, 22.4, 14.0 *one peak absent due to overlap; HRMS calculated for $C_{48}H_{51}O_4N_2S_3$ (M+H): 815.28334; Found: 815.29861 m/z.

5-(3,4-dihexyl-5-(2-(hydroxydiphenylmethyl)thiazol-5-yl)thiophen-2-yl)-2-(hydroxydiphenylmethyl)thiazole 3-oxide (**2.29b**)

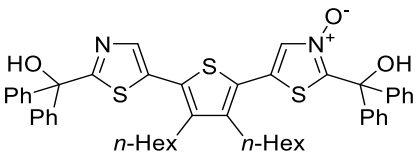

Prepared according to **General Procedure G** starting with **2.27g** (359 mg, 0.46 mmol, 1.0 equiv). The crude product was purified by column chromatography (0 % – 15 % gradient EtOAc in hexanes) to yield off-white solid **2.29b** (120 mg, 33%); R_f = 0.31 (EtOAc : Hexane = 1 : 4); ^{1}H NMR ($CDCl_3$, 300 MHz) δ 8.32 (s, 1H), 8.15 (s, 1H), 7.45 – 7.44 (m, 4H), 7.39 -7.36 (m, 16H), 2.52 (m, 4H) 1.45 – 1.28 (m, 16H), 0.90 (t, *J* = 6.7 Hz, 6H); ^{13}C

NMR ($CDCl_3$, 75 MHz) δ; HRMS calculated for $C_{48}H_{51}O_3N_2S_3$ (M+H): 799.30563; Found: 799.30799 m/z.

Chapter 3

2,2'-bithiazole (**3.1a**)

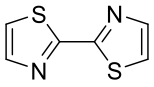

In a sealed, argon-purged pressure vessel, thiazole (710 µL, 10.0 mmol, 1.0 equiv) and $Cu(OAc)_2$ (363 mg, 2.0 mmol, 0.2 equiv) were dissolved in xylenes (33 mL, 0.3 M) and allowed to stir at 140 °C for 16 h in a sealed pressure vial. The reaction was then cooled to room temperature and depressurized in air for 10 min before being resealed and stirred at 140 °C for 16h. The reaction was then concentrated and purified by column chromatography (0 % – 10 % gradient EtOAc in Hexanes) to yield off-white solid **3.1a** (540 mg, 64%); R_f = 0.38 (EtOAc : Hexanes = 1 : 4); ^{1}H-NMR ($CDCl_3$, 300 MHz) δ 7.92 (d, *J* = 3.2 Hz, 2H), 7.46 (d, *J* = 3.2 Hz, 2H; ^{13}C-NMR ($CDCl_3$, 75 MHz) δ 161.5, 143.8, 121.0; Data consistent with previously reported literature.[216]

[2,2'-bithiazole] 3,3'-dioxide (**3.1c**)

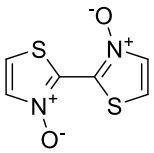

In a round bottom flask, **2.8** (41 mg, 0.22 mmol, 1.0 equiv) was dissolved in 1,2-dichloroethane (1 mL, 0.3 M) and allowed to stir at room temperature. *m*-CPBA (188 mg, 0.84 mmol, 3.0 equiv, 77% pure) was then added and the mixture stirred for 6 h. The

reaction mixture was then diluted with dichloromethane (3 mL), additional *m*-CPBA (188 mg, 0.84 mmol, 3.0 equiv, 77% pure) was added and the reaction mixture was continued to stir for 6 h. The reaction mixture was then concentrated and isolated by column chromatography (0 % – 15 % gradient MeOH in EtOAc) to yield off-white solid **3.1c** (22 mg, 50%); R_f = 0.02 (EtOAc); ^{1}H-NMR (DMSO-d_6, 300 MHz) δ 8.15 (d, *J* = 3.9 Hz, 2H), 7.98 (d, *J* = 3.9 Hz, 2H); ^{13}C-NMR (DMSO-d_6, 75 MHz) δ 136.0, 133.3, 120.8; HRMS calculated for $C_6H_5O_2N_2S_2$ (M+H): 200.97870; Found: 200.97832 m/z.

4,4'-dimethyl-2,2'-bithiazole (**3.2a**)

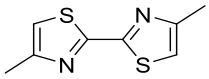

In a round bottom flask charged with 4-methylthiazole (920 µL, 10.1 mmol, 1.0 equiv) and $Cu(OAc)_2$ (405 mg, 2.0 mmol, 0.2 equiv) was added xylenes (33 mL, 0.3 M) and the mixture was stirred at reflux for 14 h. The reaction mixture was then cooled to room temperature, concentrated under vacuum, and purified by column chromatography (0 % – 20 % gradient EtOAc in Hexanes) to yield white solid **3.2a** (660 mg, 67%); R_f = 0.44 (EtOAc : Hexanes = 1 : 4); ^{1}H-NMR ($CDCl_3$, 300 MHz) δ 6.94 (s, 2H), 2.48 (s, 2H); ^{13}C-NMR ($CDCl_3$, 75 MHz) δ 160.8, 154.1, 115.4, 17.1; Data consistent with previously reported literature.[217]

4,4'-dimethyl-[2,2'-bithiazole] 3-oxide (**3.2b**)

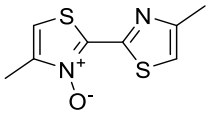

In a sealed, argon-purged microwave reaction vessel, **S2** (446 mg, 1.5 mmol, 1.0 equiv) was dissolved in anhydrous tetrahydrofuran (20 mL, 0.075 M) and allowed to stir at room temperature. *t*-BuOH (1.5 mL) and Li*O*t-Bu (2.25 mL, 1M in THF, 1.5 equiv) were then added and the mixture was immediately heated by microwave irradiation for 1 h at 60 °C. The reaction mixture was then diluted with dichloromethane (30 mL) and washed with water (3 x 20 mL) before being dried with $MgSO_4$ and concentrated. The residue was then triturated using hexanes (200 mL) to afford off-white solid **3.2b** (159 mg, 79%); R_f = 0.52 (MeOH : EtOAc = 1 : 9); ^{1}H-NMR ($CDCl_3$, 300 MHz) δ 7.10 (s, 1H), 7.09 (s, 1H), 2.54 (s, 3H), 2.45 (s, 1H); ^{13}C-NMR ($CDCl_3$, 75 MHz) δ 153.6, 152.7, 145.4, 140.1, 115.8, 111.6, 17.1, 12.6; Data consistent with previously reported literature.[145]

4,4'-dimethyl-[2,2'-bithiazole] 3,3'-dioxide (**3.2c**)

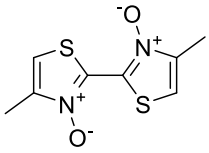

In a sealed, argon-purged microwave reaction vessel, **3.2a** (50 mg, 0.25 mmol, 1.0 equiv) was dissolved in 1,2-dichloroethane (0.5 mL, 0.5 M) and allowed to stir at room temperature. *m*-CPBA (168 mg, 0.75 mmol, 3.0 equiv, 77% pure) was then added and the mixture was continued stirring at this temperature for 6 h. The reaction mixture was then diluted with dichloromethane (2 mL) until the precipitate was fully dissolved, and a

second addition of *m*-CPBA (168 mg, 0.75 mmol, 3.0 equiv, 77% pure) was performed and the mixture was stirred for 6 h. The product was then filtered, and the filtrate was purified by column chromatography (0 % – 15 % gradient MeOH in EtOAc) to afford pale orange solid **3.2c** (42 mg, 65%); R_f = 0.36 (EtOAc : MeOH = 9 : 1); ^{1}H-NMR ($CDCl_3$, 300 MHz) δ 7.19 (s, 2H), 2.50 (s, 6H); ^{13}C-NMR ($CDCl_3$, 75 MHz) δ 144.1, 133.7, 30.8, 12.1; HRMS calculated for $C_8H_9O_2N_2S_2$ (M+H): 229.0101; Found: 229.0101 m/z.

5,5'-bis(4-hexylphenyl)-2,2'-bithiazole (**3.3a**)

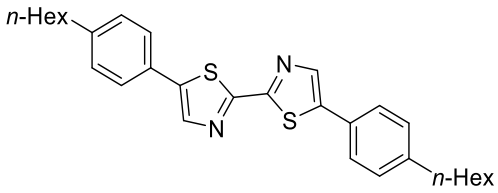

In a round bottom flask charged with **3.3c** (50 mg, 0.10 mmol, 1.0 equiv) was added tetrahydrofuran (1.5 mL, 0.07 M) and sat. NH_4Cl (1.5 mL, 0.07 M), and stirred at room temperature. Zn (63 mg, 0.10 mmol, 10.0 equiv) was then added and the reaction stirred vigorously for 2 h. The reaction mixture extracted with diethyl ether (3 x 10 mL) whereupon the organic layers were collected, dried with $MgSO_4$ and concentrated to yield, without further purification, yellow solid **3.3a** (40 mg, 80%); R_f = 0.50 (EtOAc : Hexanes = 1 : 9); ^{1}H-NMR ($CDCl_3$, 300 MHz) δ 8.03 (s, 2H), 7.56 (d, *J* = 7.3 Hz, 4H), 7.27 (d, *J* = 7.4 Hz, 4H), 2.66 (t, *J* = 6.9 Hz, 4H), 1.66 (s, 4H), 1.35 – 1.29 (m, 12H), 0.92 (s, 6H); ^{13}C-NMR ($CDCl_3$, 75 MHz) δ 159.8, 144.1, 141.6, 139.0, 129.3, 128.2, 126.7, 35.7, 31.7, 31.3, 29.0, 22.6, 14.1 *two peaks missing due to overlap; HRMS calculated for $C_{30}H_{37}N_2S_2$ (M+H): 489.23927; Found: 489.23905 m/z.

5,5'-bis(4-hexylphenyl)-[2,2'-bithiazole] 3,3'-dioxide (**3.3c**)

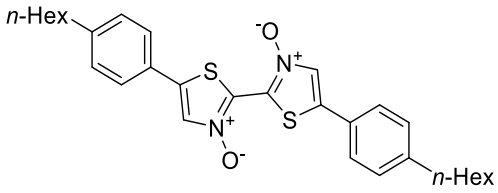

In a sealed, argon-purged microwave reaction vessel charged with **2.14f** (44 mg, 0.10 mmol, 1.0 equiv), $Cu(OAc)_2$ (9 mg, 0.05 mmol, 0.5 equiv) and K_2CO_3 (21 mg, 0.15 mmol, 1.5 equiv), was added in anhydrous tetrahydrofuran (0.5 mL, 0.1 M) and the reaction stirred at 120 °C for 2h. The reaction was then allowed to cool, diluted with H_2O (10 mL) and extracted with dichloromethane (3 x 10 mL) before being dried with $MgSO_4$ and concentrated. The residue was then triturated using Hexanes (250 mL) to yield yellow solid **3.3c** (17 mg, 66%); R_f = 0.20 (EtOAc : Hexanes = 2 : 3); ^{1}H-NMR ($CDCl_3$, 300 MHz) δ 8.06 (s, 2H), 7.56 (d, *J* = 7.8 Hz, 4H), 7.31 (d, *J* = 7.7 Hz, 4H), 2.68 (t, *J* = 7.6 Hz, 4H), 1.68 – 1.64 (m, 4H), 1.34 – 1.28 (m, 12H), 0.91 (t, *J* = 6.4 Hz, 6H); ^{13}C-NMR ($CDCl_3$, 75 MHz) δ 145.7, 136.9, 130.2, 129.6, 129.3, 126.5, 126.1, 35.8, 31.7, 31.2, 28.9, 22.6, 14.1; HRMS (APCI) calculated for $C_{30}H_{37}O_2N_2S_2$ (M+H): 521.22910; Found: 521.23110 m/z.

5,5'-bis(5-hexylthiophen-2-yl)-4,4'-dimethyl-2,2'-bithiazole (**3.5a**)

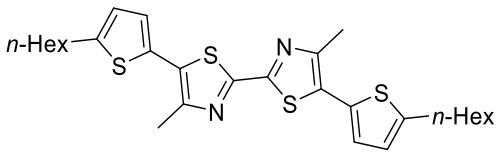

To a round bottom flask charged with $Pd(OAc)_2$ (7 mg, 4 mol %), K_2CO_3 (334 mg, 2.42 mmol, 3.0 equiv), PCy_3HBF_4 (24 mg, 8 mol %), and PivOH (49 mg, 60 mol %), was added DMA (6.5 mL, 0.12 M) followed by **3.2a** (158 mg, 0.81 mmol, 1.0 equiv) and 5-bromo-2-

hexylthiophene (323 µL, 1.61 mmol, 2.0 equiv). The vial was sealed, purged with argon and the mixture stirred at 95 °C for 16 h. The reaction mixture was then diluted in Et_2O (15 mL) and washed with H_2O (3 x 15 mL) and brine (15 mL). The organic layer was then dried with $MgSO_4$ and filtered through Celite®. The filtrate was then concentrated and purified by column chromatography (0 % – 5 % gradient EtOAc in Hexanes) to afford yellow solid **3.5a** (252 mg, 60%); R_f = 0.8 (EtOAc : Hexanes = 1 : 4); ^{1}H-NMR ($CDCl_3$, 300 MHz) δ 7.04 (d, *J* = 3.3 Hz, 2H), 6.78 (d, *J* = 3.5 Hz, 2H), 2.85 (t, *J* = 7.5 Hz, 4H), 2.64 (s, 6H), 1.72 (p, *J* = 7.0 Hz, 4H), 1.44 – 1.34 (m, 12H), 0.92 (t, *J* = 6.1 Hz, 6H); ^{13}C-NMR ($CDCl_3$, 75 MHz) δ 156.5, 148.7, 147.4, 130.4, 128.4, 126.8, 124.7, 31.4, 30.0, 28.6, 22.4, 16.7, 13.9; HRMS calculated for $C_{28}H_{37}N_2S_4$ (M+H): 529.18341; Found: 529.18330 m/z.

5,5'-bis(5-hexylthiophen-2-yl)-4,4'-dimethyl-[2,2'-bithiazole] 3-oxide (**3.5b**)

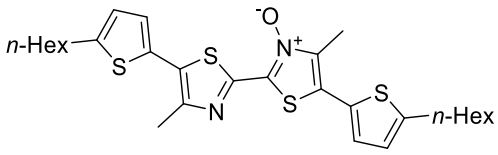

In a sealed, argon-purged microwave reaction vessel, **3.8b** (28 mg, 0.10 mmol, 1.0 equiv) was dissolved in anhydrous tetrahydrofuran (0.4 mL, 0.25 M) and allowed to stir in an ice bath. Li*O*t-Bu (150 µL, 1 M in THF, 1.5 equiv) was then added dropwise mixture was stirred for 15 min. The reaction mixture was then diluted with dichloromethane (10 mL) and sat. NH_4Cl (10 mL) and the aqueous layer was extracted with dichloromethane (10 mL). The organic layers were then combined, dried with $MgSO_4$ and concentrated to yield yellow solid **3.5b** (15 mg, 56%); *Alternatively*: in a reaction vessel charged with K_2CO_3 (245 mg, 1.77 mmol, 3.0 equiv), $Pd(OAc)_2$ (5 mg, 4 mol%), PCy_3HBF_4 (18 mg, 8 mol%),

and PivOH (36 mg, 60 mol%), was added dimethylacetamide (5 mL, 0.12 M), **3.2b** (126 mg, 0.59 mmol, 1.0 equiv) and 5-bromo-2-hexylthiophene (239 µL, 1.19 mmol, 2.0 equiv). The vessel was sealed, purged with argon, and the mixture was allowed to stir for 16 h at 95 °C. The reaction mixture was then diluted with Et_2O (50 mL) and washed with water (50 mL) and brine (50 mL). Following drying with $MgSO_4$, and concentration, the crude residue was purified by column chromatography (0 – 20% gradient EtOAc in hexanes) to yield yellow solid **3.5b** (140 mg, 44%);R_f = 0.62 (EtOAc : Hexanes = 2 : 3); ^{1}H-NMR ($CDCl_3$, 300 MHz) δ 7.16 (d, *J* = 3.6 Hz, 1H), 7.10 (d, *J* = 3.5 Hz, 1H), 6.84 (d, *J* = 3.5 Hz, 1H), 6.80 (d, *J* = 3.4 Hz, 1H), 2.88 – 2.84 (m, 4H), 2.68 (s, 3H), 2.64 (s, 3H), 1.73 (p, *J* = 6.9 Hz, 4H), 1.43 – 1.24 (m, 12H), 0.92 (t, *J* = 6.2 Hz, 6H); ^{13}C-NMR ($CDCl_3$, 75 MHz) δ 149.4, 148.5, 148.4, 147.7, 139.7, 137.8, 130.9, 129.2, 128.3, 127.4, 126.9, 125.2, 125.0, 123.8, 31.6, 31.5, 30.2, 30.1, 29.7, 28.8, 28.7, 22.6, 17.1, 14.1, 12.0; Data consistent with previously reported literature.[145]

5,5'-bis(5-hexylthiophen-2-yl)-4,4'-dimethyl-[2,2'-bithiazole] 3,3'-dioxide (**3.5c**)

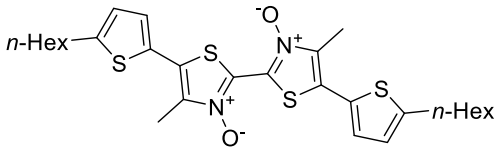

To a round bottom flask charged with $Pd(OAc)_2$ (4 mg, 4 mol %), Cs_2CO_3 (413 mg, 1.30 mmol, 3.0 equiv), tris(*O*-methoxytriphenyl)phosphine (12.4 mg, 8 mol %), and PivOH (45 mg, 0.44 mmol, 1.0 equiv), was added THF (1.5 mL, 0.3 M) followed by **3.2c** (100 mg, 0.44 mmol, 1.0 equiv) and 5-bromo-2-hexylthiophene (168 µL, 0.88 mmol, 2.0 equiv). The vial was sealed, purged with argon and the mixture stirred at 90 ℃ for 3 h. The reaction mixture was then diluted in EtOAc (15 mL) and washed with H_2O (3 x 15 mL) and brine

(15 mL). The organic layer was then dried with $MgSO_4$ and filtered through Celite®. The filtrate was then concentrated and purified by column chromatography (30 % – 70 % gradient EtOAc in Hexanes) to afford yellow solid **3.5c** (11 mg, 4%); R_f = 0.5 (EtOAc : Hexanes = 1 : 1); ^{1}H-NMR ($CDCl_3$, 300 MHz) δ 7.20 (d, *J* = 2.6 Hz, 2H), 6.85 (d, *J* = 3.2 Hz, 2H), 2.88 (t, *J* = 7.5 Hz, 4H), 2.66 (s, 6H) 1.74 (p, *J* = 7.1 Hz, 4H), 1.43 – 1.36 (m, 12H), 0.92 (t, *J* = 6.1 Hz, 6H); ^{13}C-NMR ($CDCl_3$, 75 MHz) δ 149.3, 138.8, 131.9, 129.3, 127.2, 125.3, 125.2, 31.4, 30.1, 28.6, 22.4, 13.9, 11.5; HRMS calculated for $C_{28}H_{37}N_2S_4O_2$ (M+H): 561.17324; Found: 561.17338 m/z.

5,5'-(3,4-dihexylthiophene-2,5-diyl)bis(4-methylthiazole 3-oxide) (**3.6**)

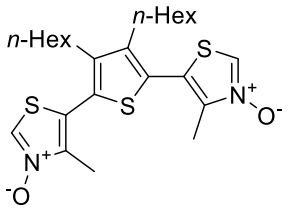

In a round-bottom flask, **S4** (560 mg, 1.25 mmol, 1.0 equiv) was dissolved in 1,2-dichloroethane (13 mL, 0.1 M) allowed to stir at room temperature. *m*-CPBA (840 mg, 3.75 mmol, 3.0 equiv, 77% pure) was then added and the mixture was continued stirring at this temperature for 6 h. The reaction mixture was then diluted with dichloromethane (30 mL) and then purified by column chromatography (0 % – 10 % gradient MeOH in EtOAc) to afford white solid **3.6** (63 mg, 10%); ^{1}H-NMR ($CDCl_3$, 300 MHz) δ 8.37 (s, 2H), 2.53 (t, *J* = 8.4 Hz, 4H), 2.37 (s, 6H), 1.45 – 1.27 (m, 16H), 0.89 (t, *J* = 6.2 Hz, 6H); ^{13}C-NMR ($CDCl_3$, 75 MHz) δ144.6, 144.5, 130.1, 126.4, 122.2, 31.3, 30.6, 29.3, 27.9, 22.4, 13.9, 12.0; Data consistent with previously reported literature.[145]

5-(5-hexylthiophen-2-yl)thiazole 3-oxide (3.7b)

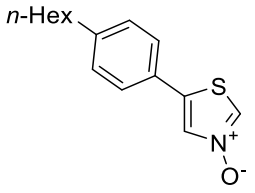

In a round-bottom flask, **2.10f** (246 mg, 1.0 mmol, 1.0 equiv) was dissolved in 1,2-dichloroethane (3 mL, 0.3 M) allowed to stir at room temperature. m-CPBA (336 mg, 1.5 mmol, 1.5 equiv, 77% pure) was then added and the mixture was continued stirring at this temperature for 6 h. The reaction mixture was then diluted with dichloromethane (30 mL) and then purified by column chromatography (0 % – 10 % gradient MeOH in EtOAc) to afford white solid **3.7b** (96 mg, 37%); Rf = 0.50 (EtOAc : Hexanes = 3 : 7); 1H-NMR (CDCl3, 300 MHz) δ 8.24 (s, 1H), 7.90 (s, 1H), 7.34 (d, J = 8.1 Hz, 2H), 7.18 (d, J = 8.1 Hz, 2H), 2.60 (t, J = 7.7 Hz, 2H), 1.61 – 1.54 (m, 2H), 1.37 – 1.29 (m, 6H), 0.90 – 0.81 (m, 3H); 13C-NMR (CDCl3, 75 MHz) δ 145.5, 137.9, 132.0, 130.2, 129.4, 126.2, 125.9, 35.7, 31.7, 31.2, 28.9, 22.6, 14.1; HRMS calculated for C15H20ONS (M+H): 262.12601; Found: 262.12577 m/z.

5-(5-hexylthiophen-2-yl)-4-methylthiazole (**3.8a**)

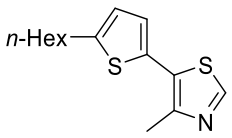

To a round bottom flask charged with $Pd(OAc)_2$ (4.5 mg, 4 mol %), Cs_2CO_3 (492 mg, 1.50 mmol, 3.0 equiv), tris(*O*-methoxytriphenyl)phosphine (14 mg, 8 mol %), and PivOH (52 mg, 0.50 mmol, 1.0 equiv), was added THF (1.8 mL, 0.3 M) followed by 4-methylthiazole (50 µL, 0.55 mmol, 1.1 equiv) and 5-bromo-2-hexylthiophene (101 µL, 0.50 mmol, 1.0

equiv). The vial was sealed, purged with argon and the mixture stirred at 90 ℃ for 3 h. The reaction mixture was then diluted in EtOAc (15 mL) and washed with H_2O (3 x 15 mL) and brine (15 mL). The organic layer was then dried with $MgSO_4$ and filtered through Celite®. The filtrate was then concentrated and purified by column chromatography (0 % – 20 % gradient EtOAc in Hexanes) to afford amber liquid **3.8a** (70 mg, 53%); R_f = 0.77 (Hexanes); ^{1}H-NMR ($CDCl_3$, 300 MHz) δ 8.55 (s, 1H), 6.93 (d, *J* = 3.3 Hz, 1H), 6.73 (d, *J* = 2.9 Hz, 1H), 2.80 (t, *J* = 7.6 Hz, 2H), 2.60 (s, 3H), 1.69 (p, *J* = 7.4 Hz, 2H), 1.41 – 1.33 (m, 6H), 0.90 (t, *J* = 6.2 Hz, 3H); ^{13}C-NMR ($CDCl_3$, 75 MHz) δ 149.2, 148.2, 147.0, 130.4, 126.7, 126.0, 124.5, 31.4, 30.0, 28.7, 22.5, 16.4, 14.0 *one peak missing due to overlap; Data consistent with previously reported literature.[145]

5-(5-hexylthiophen-2-yl)-4-methylthiazole 3-oxide (**3.8b**)

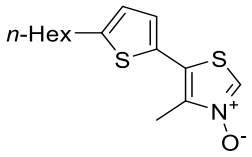

In a round-bottom flask, **3.8a** (70 mg, 0.28 mmol, 1.0 equiv) was dissolved in 1,2-dichloroethane (3 mL, 0.1 M) was allowed to stir at room temperature. *m*-CPBA (188 mg, 0.84 mmol, 3.0 equiv, 77% pure) was then added and the mixture was continued stirring at this temperature for 6 h. The reaction mixture was then diluted with dichloromethane (15 mL) and then purified by column chromatography (0 % – 10 % gradient EtOAc in Hexanes) to afford white solid **3.8b** (23 mg, 31%); R_f = 0.51 (EtOAc : Hexanes = 3 : 7); ^{1}H-NMR ($CDCl_3$, 300 MHz) δ 8.23 (s, 1H), 7.06 (d, *J* = 3.6 Hz, 1H), 6.80 (d, *J* = 3.6 Hz, 1H), 2.84 (t, *J* = 7.6 Hz, 2H), 2.53 (s, 3H), 1.70 (p, *J* = 7.5 Hz, 2H), 1.42 – 1.29 (m, 6H), 0.90 (t, *J* = 6.7 Hz, 3H); Data consistent with previously reported literature.[145]

Chapter 4

4-bromothiazole (**4.1**)

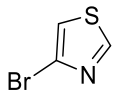

In a flame-dried round-bottom flask, 2,4-dibromothiazole (5.0 g, 20.6 mmol, 1.0 equiv) was dissolved in anhydrous THF (100 mL, 0.2 M) and allowed to stir at -78 °C. *n*-BuLi (16 mL, 1.6 M, 1.25 equiv) was then added and the mixture was continued to stir at this temperature for 30 min at which point MeOH (2.1 mL, 51.5 mmol, 2.5 equiv) was added. The reaction mixture was stirred overnight as the temperature slowly increased to room temperature. The crude mixture was filtered through a silica plug and washed with 3:7 EtOAc in hexanes and concentrated to afford clear liquid **4.1** (3.38 g, 97%); ^{1}H-NMR ($CDCl_3$, 300 MHz) δ 8.81 (d, *J* = 2.1 Hz, 1H), 7.36 (d, *J* = 2.2 Hz, 1H); Data consistent with previously reported literature.[200]

4-((2-ethylhexyl)oxy)thiazole (**4.2**)

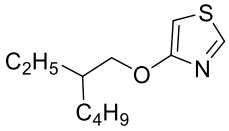

In a flame-dried, argon-purged round-bottom flask, NaH (1.60 g, 40.0 mmol, 60% wt. in mineral oil, 2.0 equiv) was dissolved in anhydrous THF (40 mL, 0.5 M) and allowed to stir at room temperature. 2-Ethylhexanol (6.25 mL, 40.0 mmol, 2.0 equiv) was then added dropwise over 15 minutes and continued stirring at this temperature for 2 h. Addition of CuI (762 mg, 4.0 mmol, 0.2 equiv) and **4.1** (3.28 g, 20.0 mmol, 1.0 equiv) was followed by reflux for 14 h with open atmosphere. The crude reaction mixture was then filtered

through Celite to remove copper solids, washed with 10% NaOH solution (100 mL), concentrated, and dried with $MgSO_4$ before being purified by column chromatography (0 % – 5 % gradient EtOAc in hexanes). This afforded yellow oil **4.2** (2.55 g, 60%); R_f = 0.81 (EtOAc : Hexanes = 1 : 9); ^{1}H-NMR ($CDCl_3$, 300 MHz) δ 8.54 (d, *J* = 1.9 Hz, 1H), 6.11 (d, *J* = 2.0 Hz, 1H), 4.01 (d, *J* = 5.7 Hz, 2H), 1.80 – 1.72 (m, 1H), 1.56 – 1.32 (m, 8H), 0.96 – 0.88 (m, 6H); ^{13}C-NMR ($CDCl_3$, 75 MHz) δ 165.7, 150.1, 88.8, 72.8, 39.4, 30.4, 29.0, 23.7, 23.0, 14.1, 11.1. HRMS calculated for $C_{11}H_{19}ONS$ (M+H): 214.12601; Found: 214.12433 m/z.

4,4'-bis((2-ethylhexyl)oxy)-2,2'-bithiazole (**4.3**)

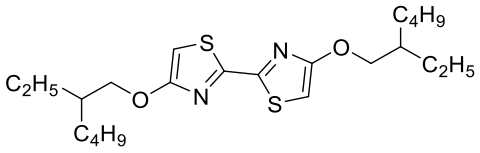

In a sealed, argon-purged pressure vessel, **4.2** (300 mg, 1.4 mmol, 1.0 equiv) and $Cu(OAc)_2$ (51 mg, 0.28 mmol, 0.2 equiv) were dissolved in xylenes (5 mL, 0.3 M) and allowed to stir at 140 °C for 16 h in a sealed pressure vial. The reaction was then cooled to room temperature and depressurized in air for 10 min before being resealed and stirred at 140 °C for 16h. The reaction was then concentrated and purified by column chromatography (0 % – 5 % gradient EtOAc in Hexanes) to yield **4.3** (45 mg, 15%); R_f = 0.85 (EtOAc : Hexanes = 9 : 1); ^{1}H-NMR ($CDCl_3$, 300 MHz) δ 6.19 (s, 2H), 4.03 (d, *J* = 5.5 Hz, 4H), 1.81 – 1.72 (m, 2H), 1.54 – 1.34 (m, 16H), 0.98 – 0.88 (m, 12H); ^{13}C-NMR ($CDCl_3$, 75 MHz) δ 164.8, 157.6, 91.6, 72.8, 39.4, 30.4, 29.1, 23.7, 23.0, 14.1, 11.1; HRMS calculated for $C_{22}H_{37}O_2N_2S_2$ (M+H): 425.22965; Found: 425.22891 m/z.

Chapter 5

4,5-dimethylthiazole 3-oxide (**5.1**)

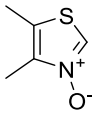

In a round-bottom flask, 4,5-dimethylthiazole (1.06 mL, 10.0 mmol, 1.0 equiv) was dissolved in 1,2-dichloroethane (30 mL, 0.33 M) and allowed to stir at room temperature. *m*-CPBA (3.36 g, 15.0 mmol, 1.5 equiv, 77% pure) was then added and the mixture was continued to stir at this temperature for 6 h. The reaction mixture was then dilu tedwith dichloromethane (30 mL), concentrated onto silica gel, and purified by column chromatography (0 % – 10 % gradient MeOH in EtOAc) to afford white solid **5.1** (1.29 g, 56%); ^{1}H-NMR ($CDCl_3$, 300 MHz) δ 8.07 (s, 1H), 2.37 (s, 3H), 2.26 (s, 3H); Data consistent with previously reported literature.[145]

General Procedure H: Addition of Arene Nucleophiles to Thiazole-*N*-Oxides.

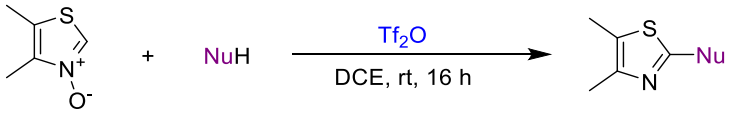

In a reaction vial, 4,5-dimethylthiazole-*N*-oxide (**5.1**) (65 mg, 0.50 mmol, 1.0 equiv) was dissolved in 1,2-dichloroethane (2 mL, 0.25 M) and allowed to stir at room temperature. Trifluoromethanesulfonic anhydride (125 µL, 0.75 mmol, 1.5 equiv) was then added and allowed to stir for 5 min before the addition of arene nucleophile (5.0 mmol, 10.0 equiv). Continued stirring at room temperature for 16 h, followed by dilution with dichloromethane (30 mL), quenching with sodium bicarbonate, and then purification by column chromatography yielded 2-aryl-4,5-dimethylthiazole products.

4,5-dimethyl-2-(5-methylthiophen-2-yl)thiazole (**5.2**)

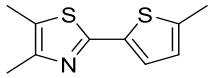

Prepared according to **General Procedure H** with 2-methylthiophene (482 µL, 5.0 mmol, 10.0 equiv) and purified by column chromatography (0 % – 5 % gradient EtOAc in hexanes) to afford beige solid **5.2** (48 mg, 46%); R_f = 0.73 (EtOAc : Hexanes = 3 : 7); ^{1}H-NMR ($CDCl_3$, 300 MHz) δ 7.18 (d, *J* = 3.5 Hz, 1H), 6.68 (d, *J* = 3.5 Hz, 1H), 2.48 (s, 3H), 2.33 (s, 3H), 2.32 (s, 3H); ^{13}C-NMR ($CDCl_3$, 75 MHz) 157.5, 148.6, 141.7, 135.4, 126.0, 125.6, 125.1, 15.5, 14.7, 11.4; HRMS calculated for $C_{10}H_{12}NS_2$ (M+H): 210.04057; Found: 210.04173 m/z.

2-(5-isopropyl-3,8-dimethylazulen-1-yl)-4,5-dimethylthiazole (**5.4**)

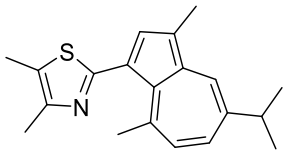

Prepared according to **General Procedure H** with guaiazulene (1.02 mL, 5.0 mmol, 10.0 equiv) and purified by column chromatography (0 % – 5 % gradient EtOAc in hexanes) to afford green solid **5.4** (84 mg, 54%); R_f = 0.62 (EtOAc : Hexanes = 1 : 4); ^{1}H-NMR ($CDCl_3$, 300 MHz) δ 8.22 (s, 1H), 7.69 (s, 1H), 7.45 (d, *J* = 10.7 Hz, 1 H), 7.07 (d, *J* = 10.7 Hz, 1H), 3.10 (quint, *J* = 6.8 Hz, 1H), 2.69 (s, 3H), 2.65 (s, 3H), 2.44 (s, 3H), 2.42 (s, 3H), 1.38 (d, *J* = 6.9 Hz, 6H); ^{13}C-NMR ($CDCl_3$, 75 MHz) δ 162.4, 146.8, 141.4, 140.2, 139.0, 135.4, 134.1, 133.3, 128.6, 126.6, 124.1, 37.9, 27.5, 24.6, 14.8, 12.8, 11.3 *two aromatic peaks absent due to overlap; HRMS calculated for $C_{20}H_{24}NS$ (M+H): 310.16240; Found: 310.16345 m/z.

4,5-dimethyl-2-(2,4,6-trimethoxyphenyl)thiazole (**5.5**)

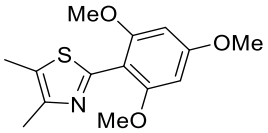

Prepared according to **General Procedure H** with 1,3,5-trimethoxybenzene (842 mg, 5.0 mmol, 10.0 equiv) and purified by column chromatography (0 % – 10 % gradient EtOAc in hexanes) to afford brown solid **5.5** (47 mg, 34%); R_f = 0.15 (EtOAc : Hexanes = 1 : 4); ^{1}H-NMR ($CDCl_3$, 300 MHz) δ 6.19 (s, 2H), 3.87 (s, 3H), 3.79 (s, 6H), 2.41 (s, 3H), 2.40 (s, 3H); ^{13}C-NMR ($CDCl_3$, 75 MHz) δ 162.1, 159.6, 156.0, 147.7, 127.3, 105.3, 90.6, 56.0, 55.4, 14.8, 11.3; HRMS calculated for $C_{14}H_{18}O_3NS$ (M+H): 280.10019; Found: 280.10132 m/z.

2-(2,3-dihydrothieno[3,4-b][1,4]dioxin-5-yl)-4,5-dimethylthiazole (**5.6**)

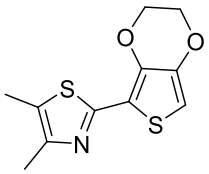

Prepared according to a modified **General Procedure H** with 3,4-ethylenedioxythiophene (53 µL, 0.5 mmol, 1.0 equiv) and **5.1** (130 mg, 1.0 mmol, 2.0 equiv), and purified by column chromatography (0 % – 10 % gradient EtOAc in hexanes) to afford brown solid **5.6** (25 mg, 20%); R_f = 0.55 (EtOAc : Hexanes = 3 : 7); ^{1}H-NMR ($CDCl_3$, 300 MHz) δ 6.37 (s, 1H), 4.39 (d, *J* = 4.0 Hz, 2H), 4.28 (d, *J* = 3.8 Hz, 2H), 2.38 (s, 3H), 2.35 (s, 3H); ^{13}C-NMR ($CDCl_3$, 75 MHz) δ 154.0, 147.4, 141.5, 139.6, 125.3, 113.0, 100.1, 65.3, 64.5, 14.6, 11.3; HRMS calculated for $C_{11}H_{12}O_2NS_2$ (M+H): 254.03040; Found: 254.03031 m/z.

Polymer Synthetic Procedures

General procedure P: *ipso*-Arylative Polycondensation

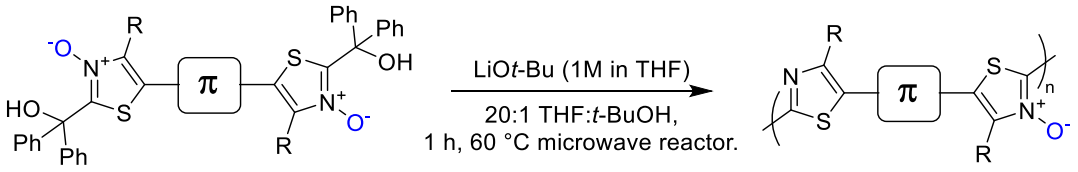

In a sealed, argon-purged microwave reaction vessel, the *N*-oxide monomer (0.1 mmol, 1 equiv) was dissolved in anhydrous tetrahydrofuran (12 mL, 0.008 M) allowed to stir at room temperature. *t*-BuOH (0.2 mL, 0.5 M) and LiO*t*-Bu (0.3 mL, 1M in THF, 3.0 equiv) were then added and the mixture was immediately heated by microwave irradiation for 1 h at 60 °C. The reaction mixture was precipitated in MeOH (150 mL) and gravity filtered to yield the polymer product.

Poly(5-(9,9-dioctyl-7-(thiazol-5-yl)-9H-fluoren-2-yl)thiazole 3-oxide) (**P1**)

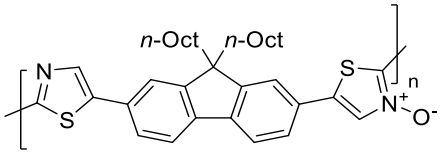

Prepared according to **General Procedure P** starting with **2.28a** (95 mg, 0.1 mmol, 1.0 equiv). Precipitation yielded yellow polymer **P1** (45 mg, 76%);^{1}H-NMR ($CDCl_3$, 300 MHz) δ 8.32 (s, 1H), 8.18 (s, 1H), 7.87 – 7.78 (m, 2H), 7.70 – 7.60 (m, 4H), 2.08 (br s, 4H), 1.70 (br s, 4H), 1.28 – 1.12 (m, 20H), 0.83 – 0.80 (m, 6H); **Mn** = 11.5 kDa; **Mw** = 23.6 kDa; **PDI** = 2.1.

Poly(4-methyl-5-(7-(4-methylthiazol-5-yl)-9,9-dioctyl-9H-fluoren-2-yl)thiazole 3-oxide) (**P2**)

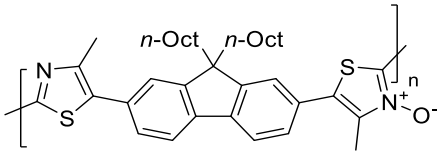

Prepared according to **General Procedure P** starting with **2.28b** (98 mg, 0.1 mmol, 1.0 equiv). Precipitation yielded yellow polymer **P2** (47 mg, 79%); ^{1}H-NMR ($CDCl_3$, 300 MHz) δ 7.94 – 7.82 (m, 2H), 7.63 – 7.56 (m, 4H), 2.73 (s, 3H), 2.69 (s, 3H), 2.07 (br s, 4H), 1.66 (br s, 4H), 1.13 (br s, 20H), 0.88 – 0.82 (m, 6H); **Mn** = 13.0 kDa; **Mw** = 26.1 kDa; **PDI** = 2.0.

Poly(5-(9,9-bis(2-ethylhexyl)-7-(thiazol-5-yl)-9H-fluoren-2-yl)thiazole 3-oxide) (**P3**)

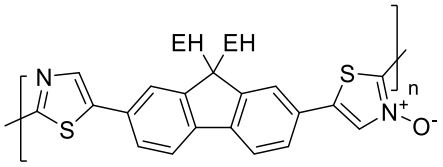

EH = 2-ethylhexyl

Prepared according to **General Procedure P** starting with **2.28c** (95 mg, 0.1 mmol, 1.0 equiv). Precipitation yielded yellow polymer **P3** (46 mg, 78%); ^{1}H-NMR ($CDCl_3$, 300 MHz) δ 8.30 (s, 1H), 8.14 (s, 1H), 7.87 – 7.77 (m, 2H), 7.65 (br s, 4H), 2.12 (br s, 4H), 1.34 – 1.21 (m, 1H), 0.89 (br s, 16H), 0.66 (br s, 6H), 0.57 (br s, 6H); **Mn** = 15.1 kDa; **Mw** = 29.8 kDa; **PDI** = 2.0.

Poly(5-(9,9-bis(2-ethylhexyl)-7-(4-methylthiazol-5-yl)-9H-fluoren-2-yl)-4-methylthiazole 3-oxide) (**P4**)

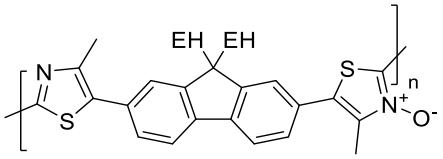

EH = 2-ethylhexyl

Prepared according to **General Procedure P** starting with **2.28d** (98 mg, 0.1 mmol, 1.0 equiv). Precipitation yielded yellow polymer **P4** (30 mg, 51%); ^{1}H-NMR ($CDCl_3$, 300 MHz) δ 7.94 – 7.84 (m, 2H), 7.61 (br s, 4H), 2.71 (s, 3H), 2.67 (s, 3H), 1.64 (br s, 4H), 1.28 – 1.24 (m, 1H), 0.92 (br s, 16H), 0.66 (s, 6H), 0.59 (s, 6H); **Mn** = 20.4 kDa; **Mw** = 45.7 kDa; **PDI** = 2.2.

Poly(5-(2,5-bis(decyloxy)-4-(thiazol-5-yl)phenyl)thiazole 3-oxide) (**P5**)

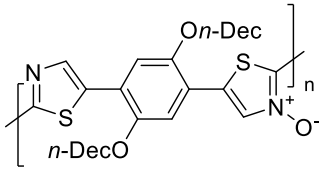

Prepared according to **General Procedure P** starting with **2.28e** (95 mg, 0.1 mmol, 1.0 equiv). Precipitation yielded yellow polymer **P5** (15 mg, 25%); Polymer highly insoluble, unable to obtain ^{1}H-NMR; **Mn** = 2.5 kDa; **Mw** = 2.6 kDa; **PDI** = 1.1.

Poly(5-(2,5-bis(decyloxy)-4-(4-methylthiazol-5-yl)phenyl)-4-methylthiazole 3-oxide) (**P6**)

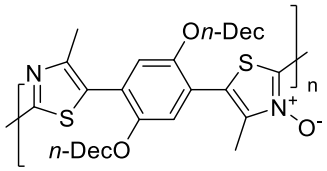

Prepared according to **General Procedure P** starting with **2.28f** (89 mg, 0.09 mmol, 1.0 equiv). Precipitation yielded yellow polymer **P6** (22 mg, 39%); ^{1}H-NMR ($CDCl_3$, 300 MHz) δ 7.06 (s, 2H), 4.01 (br s, 4H), 2.55 (s, 3H), 2.51 (s, 3H), 1.80 (br s, 4H), 1.28 (s, 28H), 0.92 – 0.86 (m, 6H); **Mn** = 5.9 kDa; **Mw** = 8.5 kDa; **PDI** = 1.4.

Poly(5,5'-(9,9-bis(2-ethylhexyl)-9H-fluorene-2,7-diyl)dithiazole) (**P7a**)

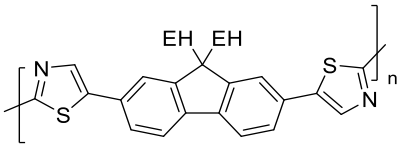

EH = 2-ethylhexyl

To a round bottom flask charged with monomer **2.26c** (145 mg, 0.26 mmol, 1.0 equiv) and $Cu(OAc)_2$ (10 mg, 0.03 mmol, 0.20 equiv) was added *p*-xylene (1.0 mL, 1.0 M). The flask was fitted with reflux condenser and $CaCl_2$-filled drying tube, and the reaction mixture was refluxed for 24 h. The reaction mixture was then concentrated *in vacuo* to remove the *p*-xylene and the residue was redissolved in minimal $CHCl_3$. Deposition into stirring methanol (20 mL) yielded a yellow precipitate which was collected by suction filtration. No further purification was required to yield polymer **P7a** (152 mg, quant.); ^{1}H-NMR ($CDCl_3$, 300 MHz) δ 8.14 (s, 2H), 7.84 – 7.78 (m 2H), 7.68 (br s, 4H), 2.09 (br s,

4H), 1.28 (s, 1H), 0.92 – 0.86 (m,16H), 0.69 (s, 3H), 0.60 (s, 3H); **Mn** = 50.0 kDa; **Mw** = 162.0 kDa; **PDI** = 3.2.

Poly(5,5'-(9,9-dioctyl-9H-fluorene-2,7-diyl)dithiazole) (**P7d**)

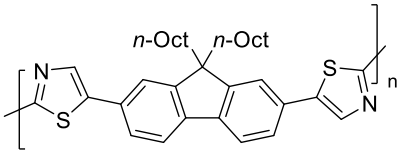

To a round bottom flask charged with monomer **2.26a** (145 mg, 0.26 mmol, 1.0 equiv) and $Cu(OAc)_2$ (10 mg, 0.03 mmol, 0.20 equiv) was added *p*-xylene (1.0 mL, 1.0 M). The flask was fitted with reflux condenser and $CaCl_2$-filled drying tube, and the reaction mixture was refluxed for 24 h. The reaction mixture was then concentrated *in vacuo* to remove the *p*-xylene and the residue was redissolved in minimal $CHCl_3$. Deposition into stirring methanol (20 mL) yielded a red-orange precipitate which was collected by suction filtration. No further purification was required to yield polymer **P7d** (152 mg, quant.); **Mn** = 13.2 kDa; **Mw** = 28.5 kDa; **PDI** = 2.2.

Poly(5,5'-(9,9-bis(2-ethylhexyl)-9H-fluorene-2,7-diyl)bis(4-methylthiazole)) (**P8a**)

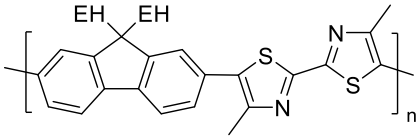

EH = 2-ethylhexyl

To a round bottom flask charged with $Pd(OAc)_2$ (2.3 mg, 4 mol %), Cs_2CO_3 (253 mg, 0.45 mmol, 3.0 equiv), tris(o-methoxyphenyl)phosphine (7 mg, 8 mol %), PivOH (26 mg, 0.25 mmol, 1.0 equiv), 9,9-Di-(2'-ethylhexyl)-2,7-dibromofluorene (125 mg, 0.25 mmol, 1.0 equiv) and **3.2a** (50 mg, 0.25 mmol, 1.0 equiv) was added anhydrous toluene (1.0 mL,

0.25 M). The vial was sealed, purged with argon and the mixture stirred at 90 ℃ for 48 h. The reaction mixture was then cooled and added dropwise to stirring methanol (20 mL) and the precipitate was collected by suction filtration. No further purification was required to yield polymer **P8a** (139 mg, quant.); ^{1}H-NMR ($CDCl_3$, 300 MHz) δ 7.84 (d, *J* = 7.7 Hz, 2H), 7.56 – 7.54 (m, 4H), 2.66 (s, 6H), 2.07 (s, 4H), 0.90 – 0.82 (m, 16H), 0.62 – 0.58 (m, 14H); **Mn** = 18.2 kDa; **Mw** = 41.9 kDa; **PDI** = 2.3.

Poly(5,5'-(9,9-bis(2-ethylhexyl)-9H-fluorene-2,7-diyl)bis(4-methylthiazole 3-oxide)) (**P8c**)

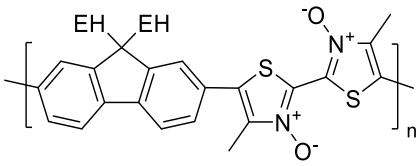

EH = 2-ethylhexyl

To a round bottom flask charged with $Pd(OAc)_2$ (1.0 mg, 4 mol %), Cs_2CO_3 (186 mg, 0.33 mmol, 3.0 equiv), tris(o-methoxyphenyl)phosphine (3 mg, 8 mol %), PivOH (11 mg, 0.11 mmol, 1.0 equiv), 9,9-Di-(2'-ethylhexyl)-2,7-dibromofluorene (55 mg, 0.11 mmol, 1.0 equiv) and **3.2c** (25 mg, 0.11 mmol, 1.0 equiv) was added anhydrous tetrahydrofuran (0.5 mL, 0.22 M). The vial was sealed, purged with argon and the mixture stirred at 90 ℃ for 48 h. The reaction mixture was then cooled and added dropwise to stirring methanol (20 mL) and the precipitate was collected by suction filtration. A Soxhlet extraction with acetone performed for 16 h yielded polymer **P8c** (25 mg, 39 %); ^{1}H-NMR ($CDCl_3$, 300 MHz) δ 7.93 (d, *J* = 7.3 Hz, 2H), 7.64 – 7.61 (m, 4H), 2.69 (s, 6H), 2.12 (s, 4H), 0.90 – 0.82 (m, 16H), 0.67 – 0.57 (m, 14H); **Mn** = 14.0 kDa; **Mw** = 32.2 kDa; **PDI** = 2.3.

Poly(5,5'-(3,4-dihexylthiophene-2,5-diyl)bis(4-methylthiazole)) (**P9a**)

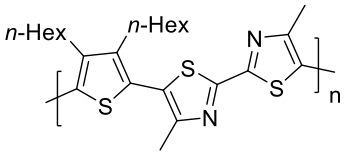

To a round bottom flask charged with $Pd(OAc)_2$ (1.4 mg, 4 mol %), Cs_2CO_3 (150 mg, 0.45 mmol, 3.0 equiv), tris(o-methoxyphenyl)phosphine (4 mg, 8 mol %), PivOH (16 mg, 0.15 mmol, 1.0 equiv) and **3.2a** (30 mg, 0.15 mmol, 1.0 equiv) was added anhydrous tetrahydrofuran (1.0 mL, 0.15 M) followed by 2,5-dibromo-3,4-dihexylthiophene (48 µL, 0.13 mmol, 1.0 equiv). The vial was sealed, purged with argon and the mixture stirred at 90 ℃ for 24 h. The reaction mixture was then cooled and added dropwise to stirring methanol (20 mL) and the precipitate was collected by suction filtration. No further purification was required to yield polymer **P9a** (63 mg, quant.); ^{1}H-NMR ($CDCl_3$, 300 MHz) δ 2.63 – 2.60 (m, 4H), 2.50 (s, 6H), 1.54 – 1.42 (m, 4H), 1.35 – 1.27 (m, 12H), 0.90 – 0.87 (m, 6H). **Mn** = 20.6 kDa; **Mw** = 45.3 kDa; **PDI** = 2.2.

Poly(5-(3,4-dihexyl-5-(4-methylthiazol-5-yl)thiophen-2-yl)-4-methylthiazole 3-oxide) (**P9b**)

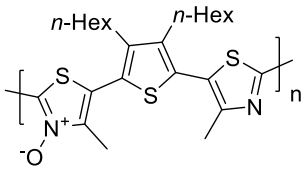

In a sealed, argon-purged microwave reaction vessel, **3.5** (87 mg, 0.20 mmol, 1.0 equiv) was dissolved in anhydrous tetrahydrofuran (7 mL, 0.03 M) and allowed to stir in an ice bath. LiO*t*-Bu (300 µL, 1 M in THF, 1.5 equiv) was then added dropwise mixture was stirred for 3 h as it warmed to room temperature. The reaction mixture was then added

dropwise to stirring methanol (20 mL) and the precipitate was collected by suction filtration as polymer **P9b** (86 mg, quant.); ^{1}H-NMR ($CDCl_3$, 300 MHz) δ 2.77 (br s, 3H), 2.60 (br s, 3H), 1.79 – 1.72 (m, 4H), 1.39 -1.22 (m, 16H), 0.90 – 0.86 (m, 6H). **Mn** = 17.0 kDa; **Mw** = 45.9 kDa; **PDI** = 2.7.

Poly(5,5'-(3,4-dihexylthiophene-2,5-diyl)bis(4-methylthiazole 3-oxide)) (**P9c**)

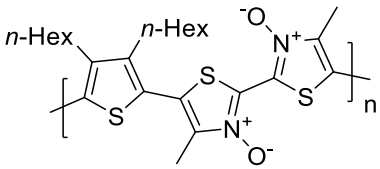

To a round bottom flask charged with $Pd(OAc)_2$ (2.5 mg, 8 mol %), Cs_2CO_3 (128 mg, 0.39 mmol, 3.0 equiv), tris(o-methoxyphenyl)phosphine (7 mg, 16 mol %), PivOH (13 mg, 0.13 mmol, 1.0 equiv) and **3.2c** (30 mg, 0.13 mmol, 1.0 equiv) was added anhydrous tetrahydrofuran (1.0 mL, 0.13 M) followed by 2,5-dibromo-3,4-dihexylthiophene (41 µL, 0.13 mmol, 1.0 equiv). The vial was sealed, purged with argon and the mixture stirred at 90 ℃ for 24 h. A second addition of $Pd(OAc)_2$ (2.5 mg, 8 mol %) and tris(o-methoxyphenyl)phosphine (7 mg, 16 mol %) was performed and the reaction was continued to stir for 42 h at 90 °C. The reaction mixture was then cooled and added dropwise to stirring methanol (20 mL) and the precipitate was collected by suction filtration. The polymer was then purified by Soxhlet extraction with acetone for 16 h to yield polymer **P9c** (45 mg, 74%); ^{1}H-NMR ($CDCl_3$, 300 MHz) δ 2.64 – 2.57 (m, 4H), 2.49 (s, 6H), 1.48 – 1.40 (m, 4H), 1.30 – 1.18 (m, 12H), 0.91 – 0.84 (m, 6H). **Mn** = 6.0 kDa; **Mw** = 12.0 kDa; **PDI** = 2.0.

General procedure Q: Direct Arylation Polymerization of Dialkoxybithiazoles

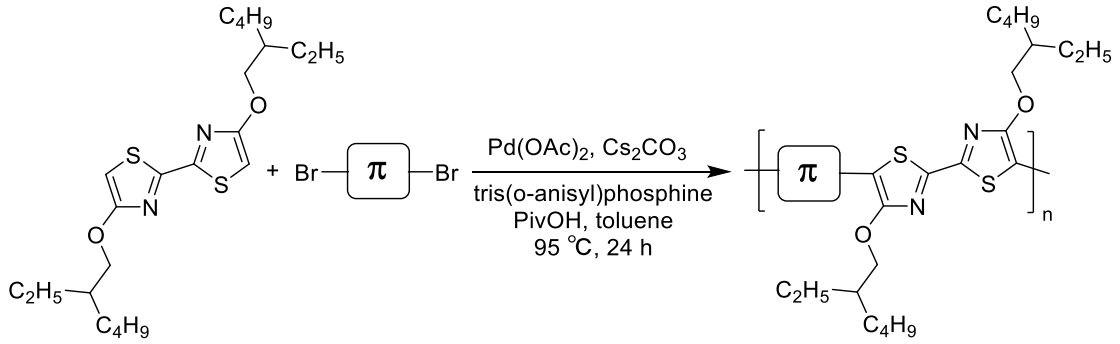

To a round bottom flask charged with $Pd(OAc)_2$ (2.5 mg, 8 mol %), Cs_2CO_3 (154 mg, 0.45 mmol, 3.0 equiv), tris(*o*-methoxyphenyl)phosphine (8 mg, 16 mol %), PivOH (15 mg, 0.15 mmol, 1.0 equiv), Dibromo-π-spacer (0.15 mmol, 1.0 equiv), and **4.3** (64 mg, 0.15 mmol, 1.0 equiv) was added anhydrous toluene (1.5 mL, 0.1 M). The vial was sealed, purged with argon and the mixture stirred at 95 ℃ for 24 h. The reaction mixture was then cooled, added dropwise to stirring methanol (20 mL), and the precipitate was collected by suction filtration. No further purification was required to yield polymer product.

Poly(5-(9,9-dioctyl-9H-fluoren-2-yl)-4,4'-bis((2-ethylhexyl)oxy)-2,2'-bithiazole) (**P10**)

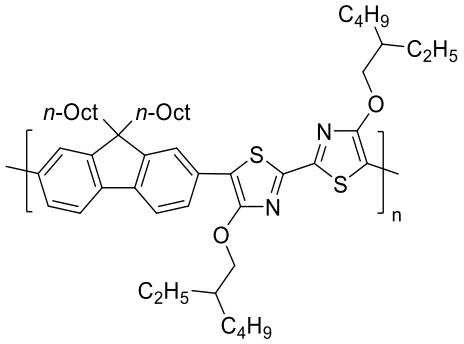

Prepared according to **General Procedure Q** starting with 9,9'-dioctyl-2,7-dibromofluorene (71 mg, 0.13 mmol, 1.0 equiv) and **4.3** (54 mg, 0.13 mmol, 1.0 equiv). Precipitation yielded black polymer **P10** (105 mg, quant.); ^{1}H-NMR ($CDCl_3$, 300 MHz) δ

7.93 (s, 2H), 7.71 (s, 4H), 4.54 (s, 4H), 2.05 (s, 4H), 1.85 (s, 2H), 1.61 (s, 8H), 1.43 (s, 12H), 1.10 – 0.96 (m, 26H), 0.83 – 0. 79 (m, 12H). **Mn** = 11.9 kDa; **Mw** = 31.5 kDa; **PDI** = 2.7.

Poly(5-(2,5-bis(decyloxy)phenyl)-4,4'-bis((2-ethylhexyl)oxy)-2,2'-bithiazole) (**P12**)

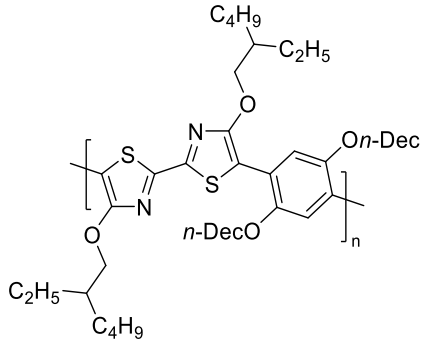

Prepared according to **General Procedure Q** starting with 1,4-dibromo-2,5-bis(decyloxy)benzene (110 mg, 0.20 mmol, 1.0 equiv) and **4.3** (85 mg, 0.20 mmol, 1.0 equiv). Precipitation yielded black polymer **P12** (162 mg, quant.); ^{1}H-NMR ($CDCl_3$, 300 MHz) δ 8.07 (s, 2H), 4.52 (s, 4H), 4.18 (s, 4H), 2.02 (s, 4H), 1.84 (s, 2H), 1.63 – 1.28 (m, 44H), 1.03 (t, *J* = 7.3 Hz, 6H), 0.96 – 0.86 (m, 12H). **Mn** = 13.6 kDa; **Mw** = 27.2 kDa; **PDI** = 2.0.

Poly(5-(3,4-dihexylthiophen-2-yl)-4,4'-bis((2-ethylhexyl)oxy)-2,2'-bithiazole) (**P13**)

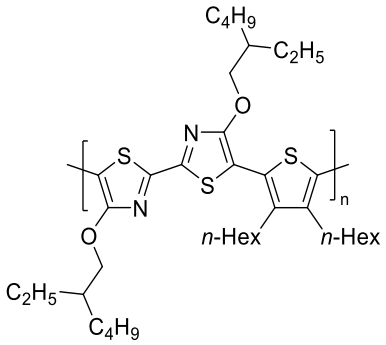

Prepared according to **General Procedure Q** starting with 2,5-dibromo-3,4-dihexylthiophene (65 µL, 0.20 mmol, 1.0 equiv) and **4.3** (85 mg, 0.20 mmol, 1.0 equiv). Precipitation yielded black polymer **P13** (116 mg, 86%); ^{1}H-NMR ($CDCl_3$, 300 MHz) δ 4.42 (d, *J* = 5.5 Hz, 4H), 2.76 (s, 4H), 1.82 (s, 2H), 1.43 – 1.36 (m, 32H), 1.00 – 0.90 (m, 18H). **Mn** = 8.7 kDa; **Mw** = 16.7 kDa; **PDI** = 1.9.

Poly(4,4'-bis((2-ethylhexyl)oxy)-5-phenyl-2,2'-bithiazole) (**P14**)

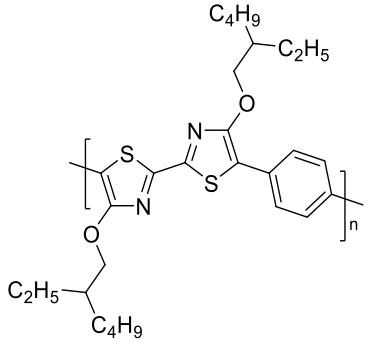

Prepared according to **General Procedure Q** starting with 1,4-dibromobenzene (35 mg, 0.15 mmol, 1.0 equiv) and **4.3** (64 mg, 0.15 mmol, 1.0 equiv). Precipitation yielded black polymer **P14** (57 mg, 76%); ^{1}H-NMR ($CDCl_3$, 300 MHz) δ 7.81 – 7.50 (m, 4H), 4.46 (s, 4H), 1.85 (s, 2H), 1.57 – 1.44 (m, 16H), 1.01 – 0.97 (m, 12H). **Mn** = 3.2 kDa; **Mw** = 5.6 kDa; **PDI** = 1.8.

Poly(4-(4,4'-bis((2-ethylhexyl)oxy)-[2,2'-bithiazol]-5-yl)benzo[c][1,2,5]thiadiazole) (**P15**)

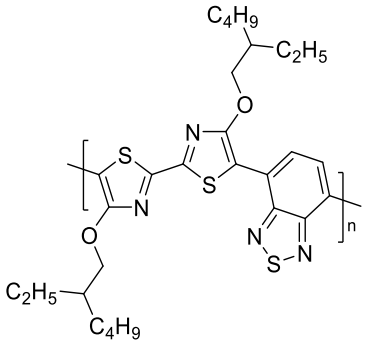

Prepared according to **General Procedure Q** starting with 4,7-dibromobenzo[c]-1,2,5-thiadiazole (44 mg, 0.15 mmol, 1.0 equiv) and **4.3** (64 mg, 0.15 mmol, 1.0 equiv). Precipitation yielded black polymer **P15** (61 mg, 73%); ^{1}H-NMR ($CDCl_3$, 300 MHz) δ 8.46 – 8.42 (m, 1H), 7.93 – 7.79 (m, 1H), 4.63 (s, 4H), 1.58 (s, 18H), 1.07 – 0.98 (m, 12). **Mn** = 2.3 kDa; **Mw** = 4.5 kDa; **PDI** = 2.0.

Poly(4,4'-bis((2-ethylhexyl)oxy)-5-(thiophen-2-yl)-2,2'-bithiazole) (**P16**)

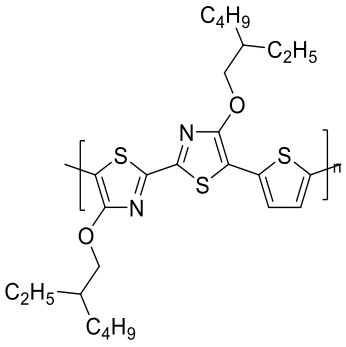

Prepared according to **General Procedure Q** starting with 2,5-dibromothiophene (17 µL, 0.15 mmol, 1.0 equiv) and **4.3** (64 mg, 0.15 mmol, 1.0 equiv). Precipitation yielded black polymer **P16** (67 mg, 88%); ^{1}H-NMR ($CDCl_3$, 300 MHz) δ 7.23 (s, 1H), 7.00 – 6.93 (s,

1H), 4.46 (s, 4H), 1.82 (s, 2H), 1.58 – 1.42 (m, 16H), 1.02 – 0.96 (m, 12H). **Mn** = 2.4 kDa; **Mw** = 5.0 kDa; **PDI** = 2.1.

Supplementary Compounds

1-bromo-4-(hexyloxy)benzene (6.1)

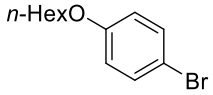

In a round-bottom flask, 4-bromophenol (3.46 g, 20.0 mmol, 1.0 equiv), K_2CO_3 (6.9 g, 50.0 mmol, 2.5 equiv) and 1-bromohexane (2.67 mL, 20.0 mmol, 1.0 equiv) were dissolved in acetonitrile (30 mL, 0.66 M). The reaction mixture was stirred for 14 h at reflux. Quenching with 1M NaOH solution (200 mL) followed by extraction with pentane (2 x 100 mL), and wash with brine (100 mL) yielded yellow oil **6.1** (4.55 g, 93%) without further purification; ^{1}H-NMR ($CDCl_3$, 300 MHz) δ 7.38 (d, *J* = 7.3 Hz, 2H), 6.80 (d, *J* = 8.9 Hz, 2H), 3.94 (t, *J* = 6.5 Hz, 2H), 1.82 – 1.77 (m, 2H), 1.48 – 1.36 (m, 6H), 0.94 (s, 3H); Data consistent with previously reported literature.[218]

(4-methylthiazol-2-yl)diphenylmethanol (6.2)

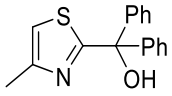

To a round-bottom flask charged with 4-methylthiazole (910 µL, 10.0 mmol, 1.0 equiv), purged with argon and sealed was added THF (100 mL, 0.1 M) and allowed to stir in a -78 °C bath of dry ice and acetone. *n*-BuLi (7.5 mL, 1.6 M, 1.2 equiv) was added and the mixture was stirred at this temperature for 30 min. Benzophenone (2.70 g, 15.0 mmol, 1.5 equiv) was then added, the vessel purged with argon, and continued to stir at this

temperature for 10 h. The reaction mixture was then quenched with NH_4Cl (30 mL) and extracted with diethyl ether (3 x 30 mL). The organic layer was then dried with $MgSO_4$ and concentrated. Column chromatography (0 – 20 % EtOAc in hexanes) yielded white solid **6.2** (2.76 g, 98%); R_f = 0.68 (EtOAc : Hexane = 3 : 7); ^{1}H NMR ($CDCl_3$, 300 MHz) δ 7.45 – 7.41 (m, 4H), 7.37 – 7.33 (m, 6H), 6.88 (s, 1H), 4.49 (s, 1H), 2.47 (s, 3H); ^{13}C NMR ($CDCl_3$, 75 MHz) δ 176.2, 152.8, 145.5, 128.1, 127.9, 127.5, 114.8, 80.5, 17.2; HRMS calculated for $C_{17}H_{16}ONS$ (M+H): 282.09471; Found: 282.09592.

2-(hydroxydiphenylmethyl)-4-methylthiazole 3-oxide (**6.3**)

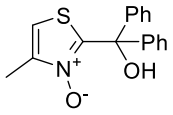

In a round-bottom flask, **6.2** (2.53 g, 9.0 mmol, 1.0 equiv) was dissolved in 1,2-dichloroethane (30 mL, 0.3 M) and allowed to stir at room temperature. *m*-CPBA (3.03 g, 77% pure, 13.5 mmol, 1.5 equiv) was then added and the mixture was continued stirring at this temperature for 12 h. The reaction mixture was then diluted with dichloromethane (30 mL) and then purified by column chromatography (0 % – 50 % gradient EtOAc in hexanes) to afford white solid **6.3** (2.29 g, 85%); R_f = 0.11 (EtOAc : Hexane = 3 : 7); ^{1}H NMR ($CDCl_3$, 300 MHz) δ 8.51 (br s, 1H), 7.36 (s, 10H), 7.01 (s, 1H), 2.39 (s, 1H); ^{13}C NMR ($CDCl_3$, 75 MHz) δ151.5, 146.2, 143.2, 128.4, 128.3, 127.0, 111.9, 79.1, 12.6; HRMS calculated for $C_8H_{14}NO_2S$ (M+H):298.08963; Found: 298.09071 m/z.

5,5'-(3,4-dihexylthiophene-2,5-diyl)bis(4-methylthiazole) (**6.4**)

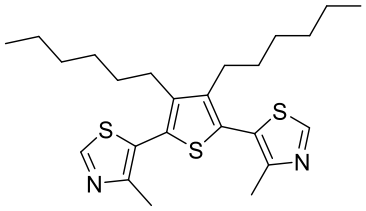

To a round bottom flask charged with $Pd(OAc)_2$ (45 mg, 4 mol %), K_2CO_3 (1.73 g, 12.5 mmol, 2.5 equiv), PCy_3HBF_4 (147 mg, 8 mol %), and PivOH (306 mg, 60 mol %), was added DMA (15 mL, 0.33 M) followed by 4-methylthiazole (1.36 mL, 15.0 mmol, 3.0 equiv) and 2,5-dibromo-3,4-dihexylthiophene (1.56 mL, 5.0 mmol, 1.0 equiv). The vial was sealed, purged with argon and the mixture stirred at 100 ℃ for 12 hours. The reaction mixture was then dissolved in H_2O (50 mL) and extracted with Et_2O (3 x 30 mL). The organic layer was then dried with $MgSO_4$ and filtered through Celite®. The filtrate was then concentrated and purified by column chromatography (0 % – 20 % gradient EtOAc in Hexanes) to afford orange liquid **6.4** (581 mg, 26%); ^{1}H-NMR ($CDCl_3$, 300 MHz) δ 8.80 (s, 2H), 2.52 - 2.45 (m, 10H), 1.45 – 1.24 (m, 16H), 0.87 (t, *J* = 6.6 Hz, 6H); ^{13}C-NMR ($CDCl_3$, 75 MHz) δ 152.3, 152.1, 143.1, 127.1, 123.4, 31.5, 30.5, 29.4, 28.1, 22.6, 16.1, 14.1; Data consistent with previously reported literature.[145]

6.3 Optical Measurements

Chapter 2

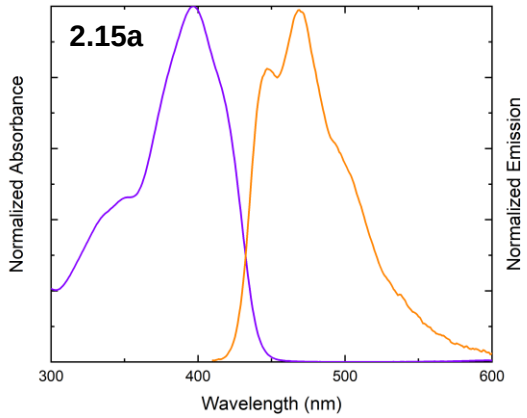

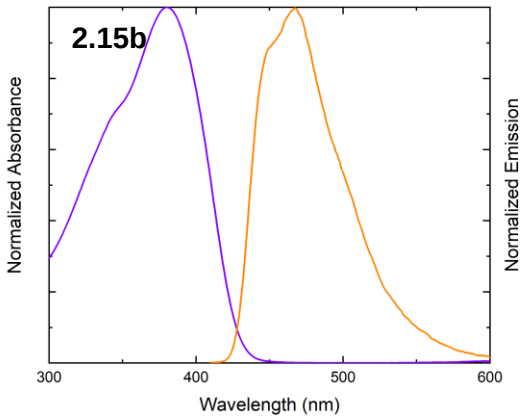

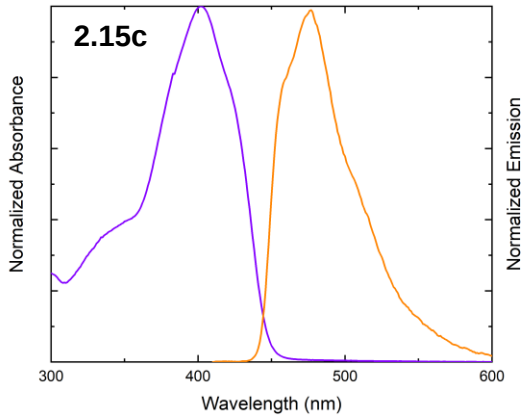

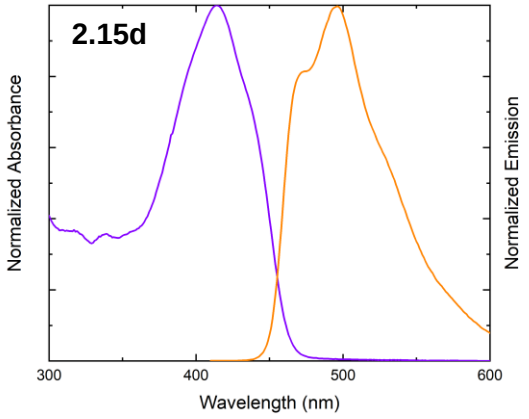

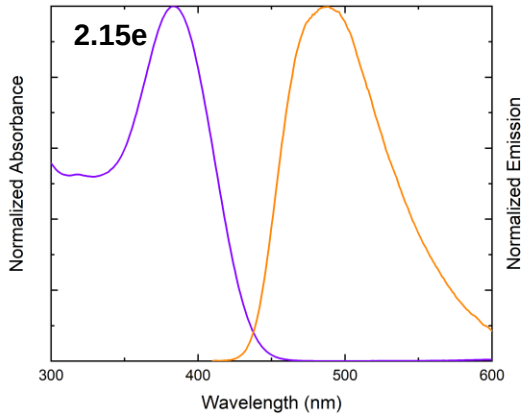

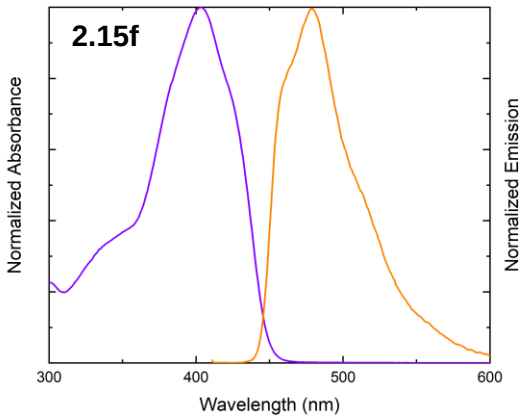

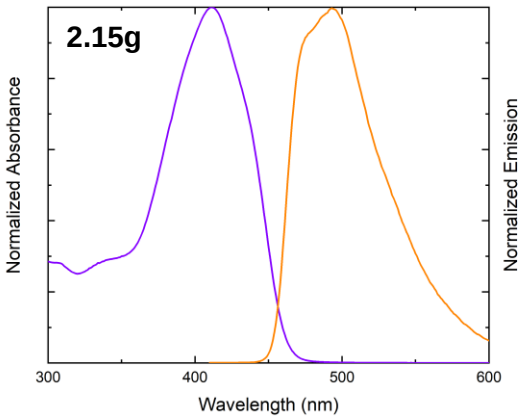
2.15g
Normalized Absorbance
Normalized Emission
300
400
500
600
Wavelength (nm)

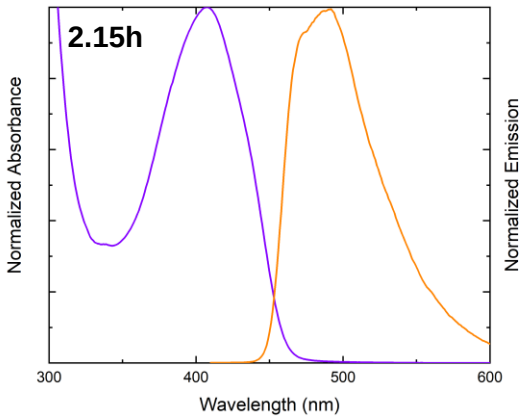
2.15h
Normalized Absorbance
Normalized Emission
300
400
500
600
Wavelength (nm)

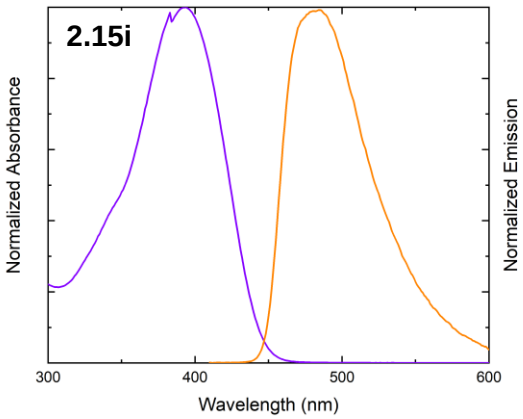
2.15i
Normalized Absorbance
Normalized Emission
300
400
500
600
Wavelength (nm)

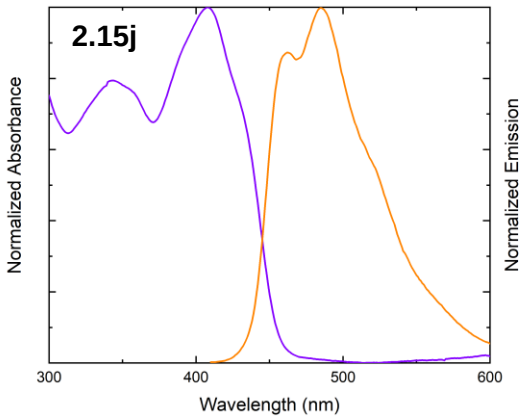
2.15j
Normalized Absorbance
Normalized Emission
300
400
500
600
Wavelength (nm)

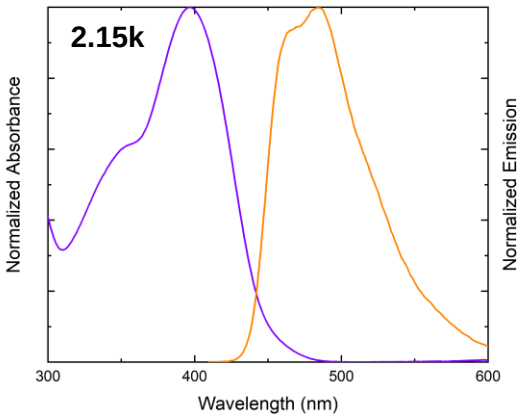
2.15k
Normalized Absorbance
Normalized Emission
300
400
500
600
Wavelength (nm)

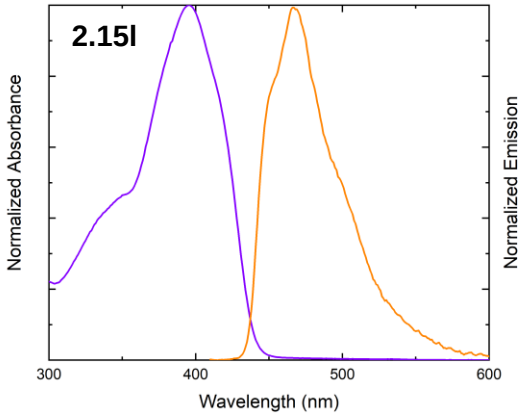
2.15l
Normalized Absorbance
Normalized Emission
300
400
500
600
Wavelength (nm)

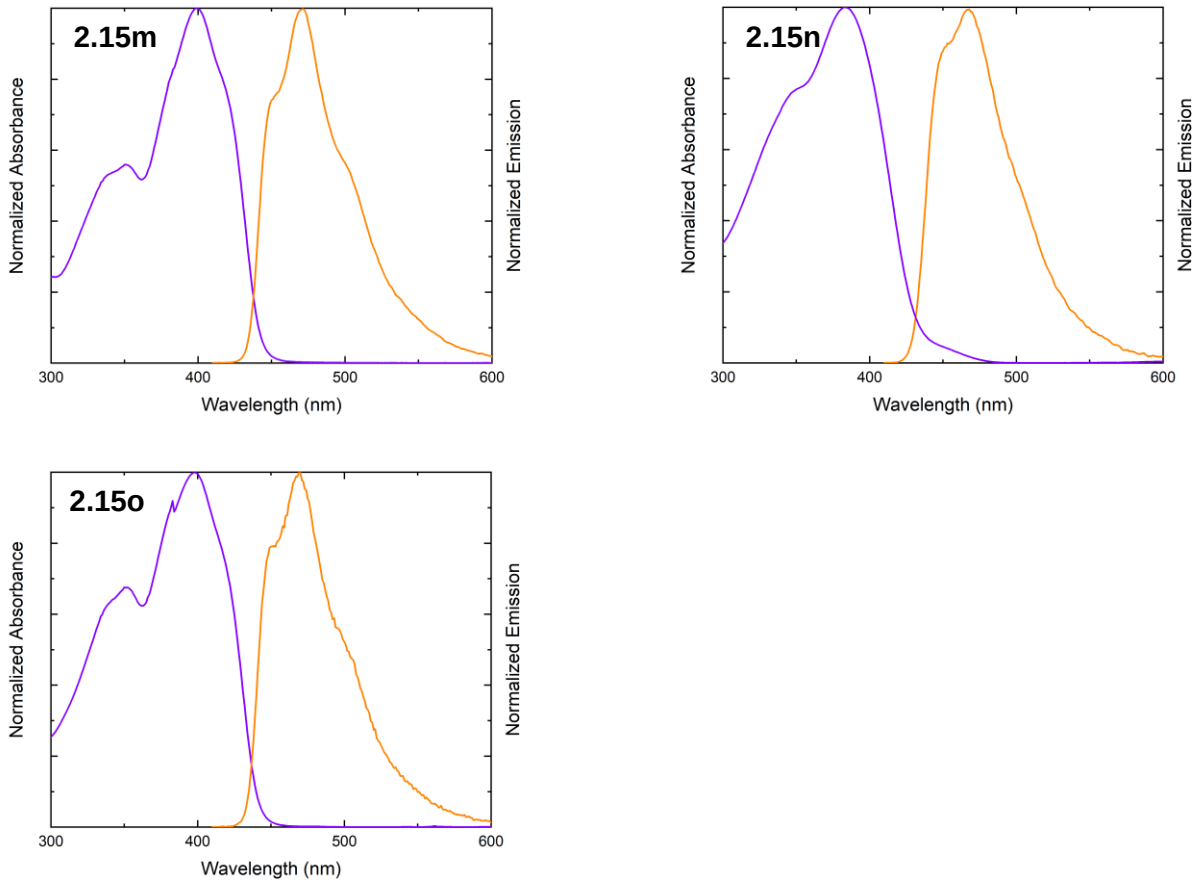

Figure 6.1 – Optical properties for 2,2'-bithiazole-*N*-oxide small molecules obtained via *ipso*-arylative coupling (**2.15**). UV-Vis absorption spectra measured in $CHCl_3$ (solid purple). Emission spectra measured in anhydrous CH_2Cl_2 (solid orange).

Chapter 3

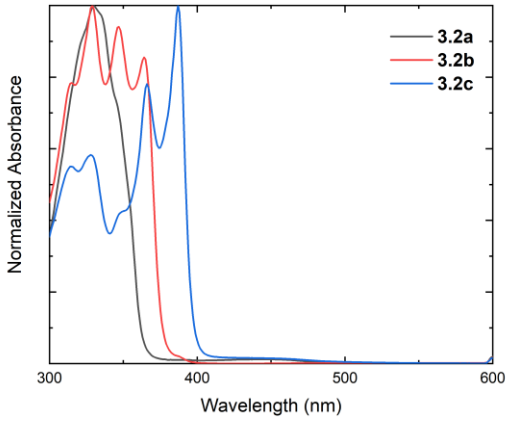

Figure 6.2 - UV-Vis absorption spectra of 4,4'-dimethyl-2,2'-bithiazoles (**3.2**) measured in $CHCl_3$.

6.4 Voltammetry Measurements

Linear-sweep voltammetry was performed by drop casting polymer solution onto Pt button working electrode. Measured in MeCN with 0.1 M nBu_4NPF_6 as the supporting electrolyte using a Pt counter electrode, and Pt reference electrode. Fc/Fc^+ used as an internal standard. Electrochemical bandgaps were determined by the difference between HOMO and LUMO levels. HOMO levels were estimated from first oxidation potential. LUMOs estimated form first reduction potential.

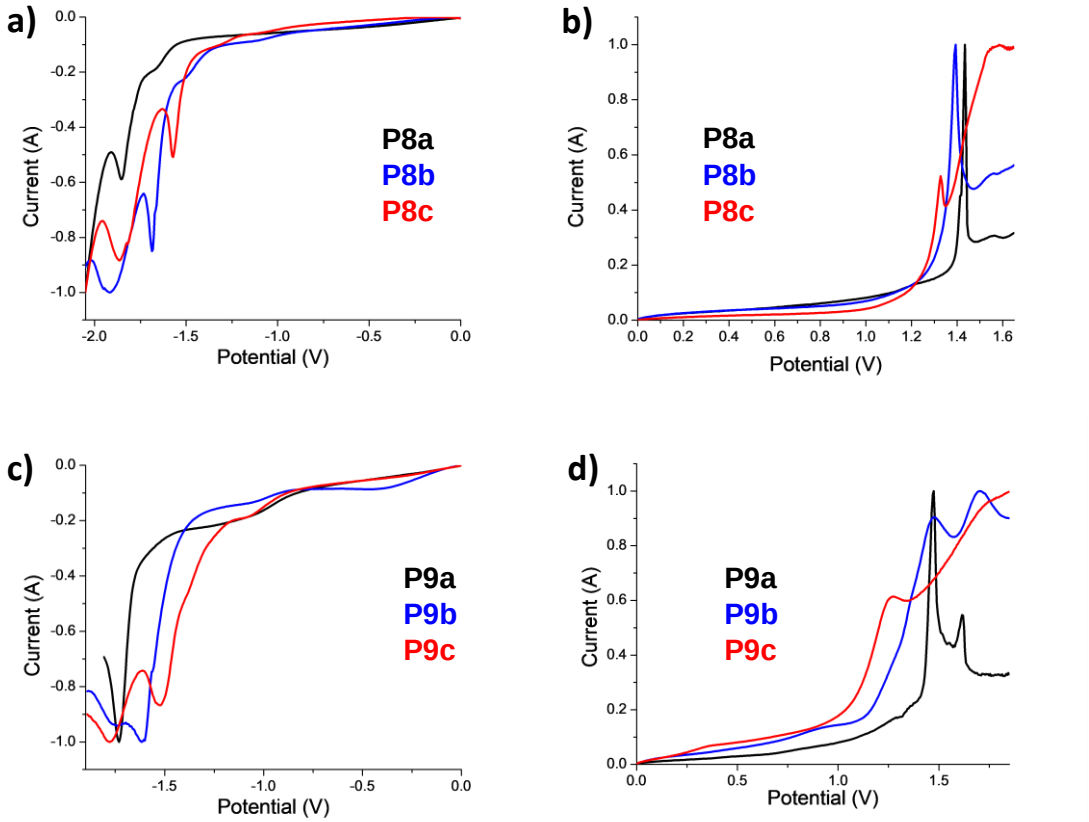

Figure 6.3 – Linear-sweep Voltammograms a) Series **P8** reduction b) Series **P8** oxidation c) Series **P9** reduction d) Series **P9** oxidation.

Table 6.1 – Summary of voltammetry results for polymer series **P8** and **P9**.

Entry	HOMO (eV)	LUMO (eV)	$Eg_{[ec]}$ (eV)
P8a	-5.75	-2.80	2.95
P8b	-5.69	-2.86	2.83
P8c	-5.65	-2.95	2.70
P9a	-5.67	-2.71	2.86
P9b	-5.57	-2.96	2.61
P9c	-5.53	-3.02	2.51

6.5 Gel Permeation Chromatography

Number-average (Mn) and weight-average (Mw) molecular weights were determined by size exclusion chromatography using a Viscotek GPCmax VE2001 at 35 °C equipped with a VE 3580 RI detector and two PAS-104 Styrene-Divinylbenzene gel columns. The flow rate was fixed at 1.0 mL/min using tetrahydrofuran (THF) as the eluent. All molecular weights are relative to a polystyrene calibration curve. All GPC samples were prepared nominally at 2 mg/mL in THF and filtered through a 0.22 µM PTFE filter into a 1 mL chromatography vial.

Chapter 2

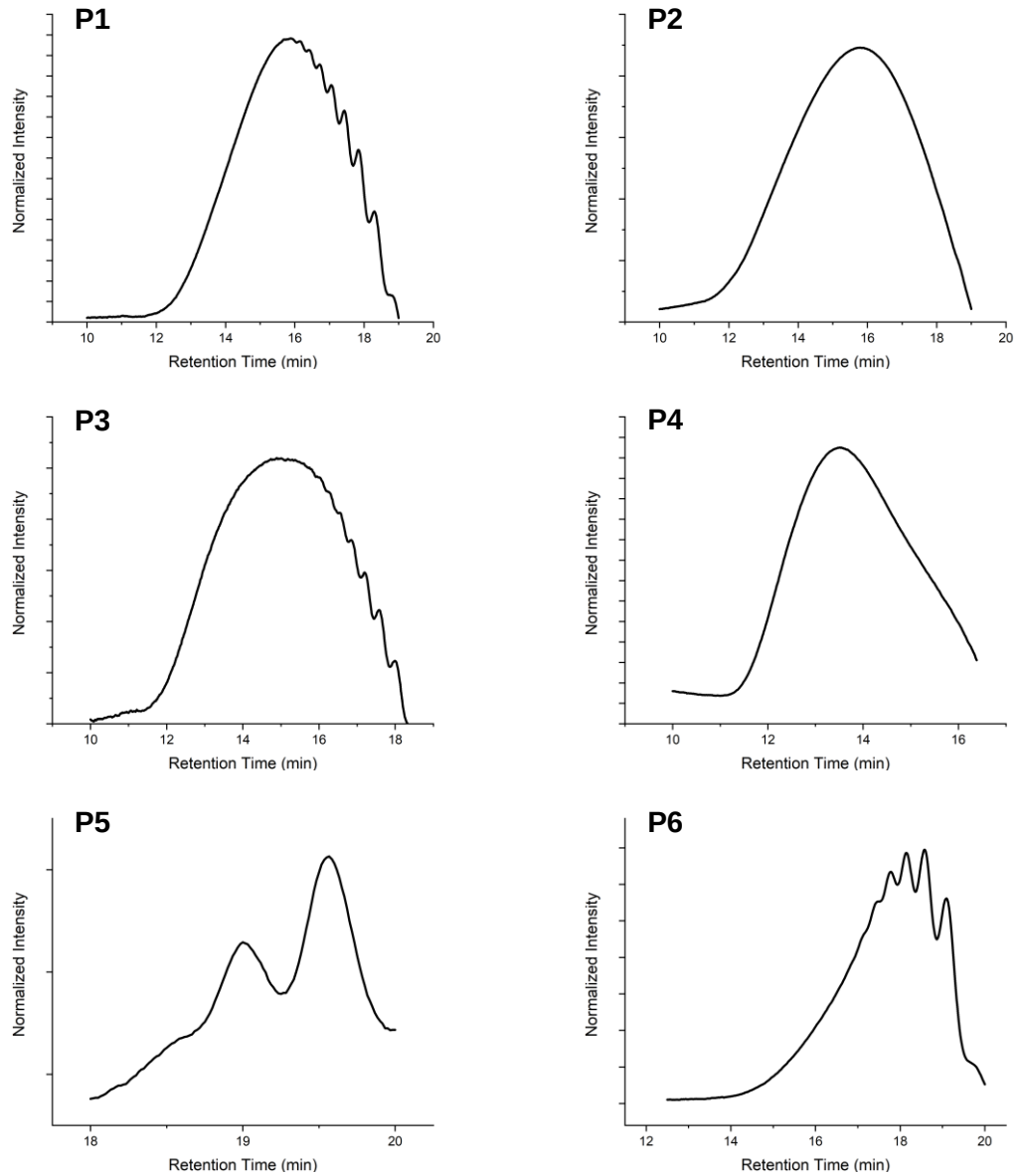

Figure 6.4 – GPC traces for **P1** – **P6** synthesized via *ipso*-arylative polycondensation.

Chapter 3

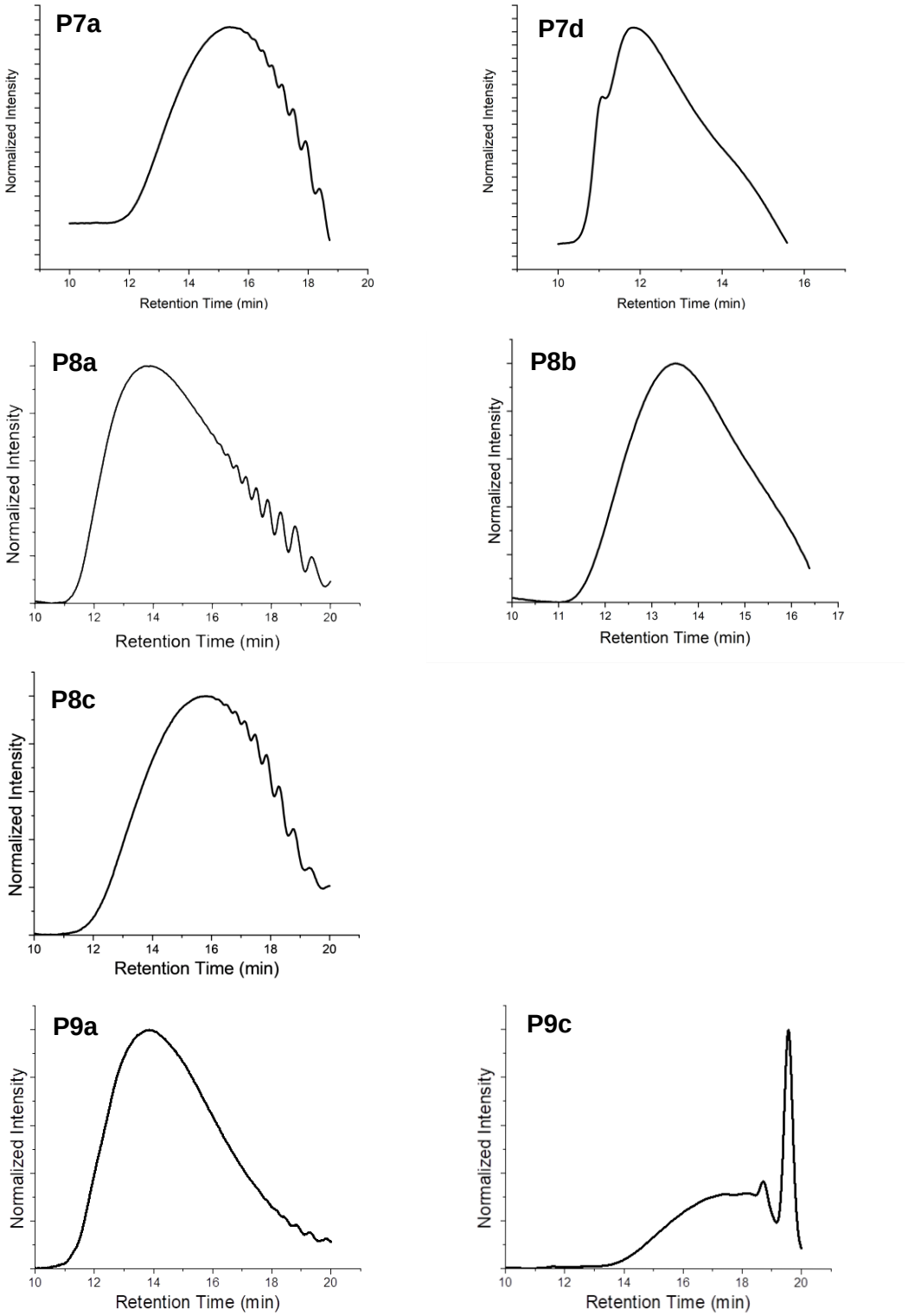

Figure 6.5 – GPC traces for **P7a/d, P8a-c** and **P9a/c**. Trace for **P9b** unavailable.

Chapter 4

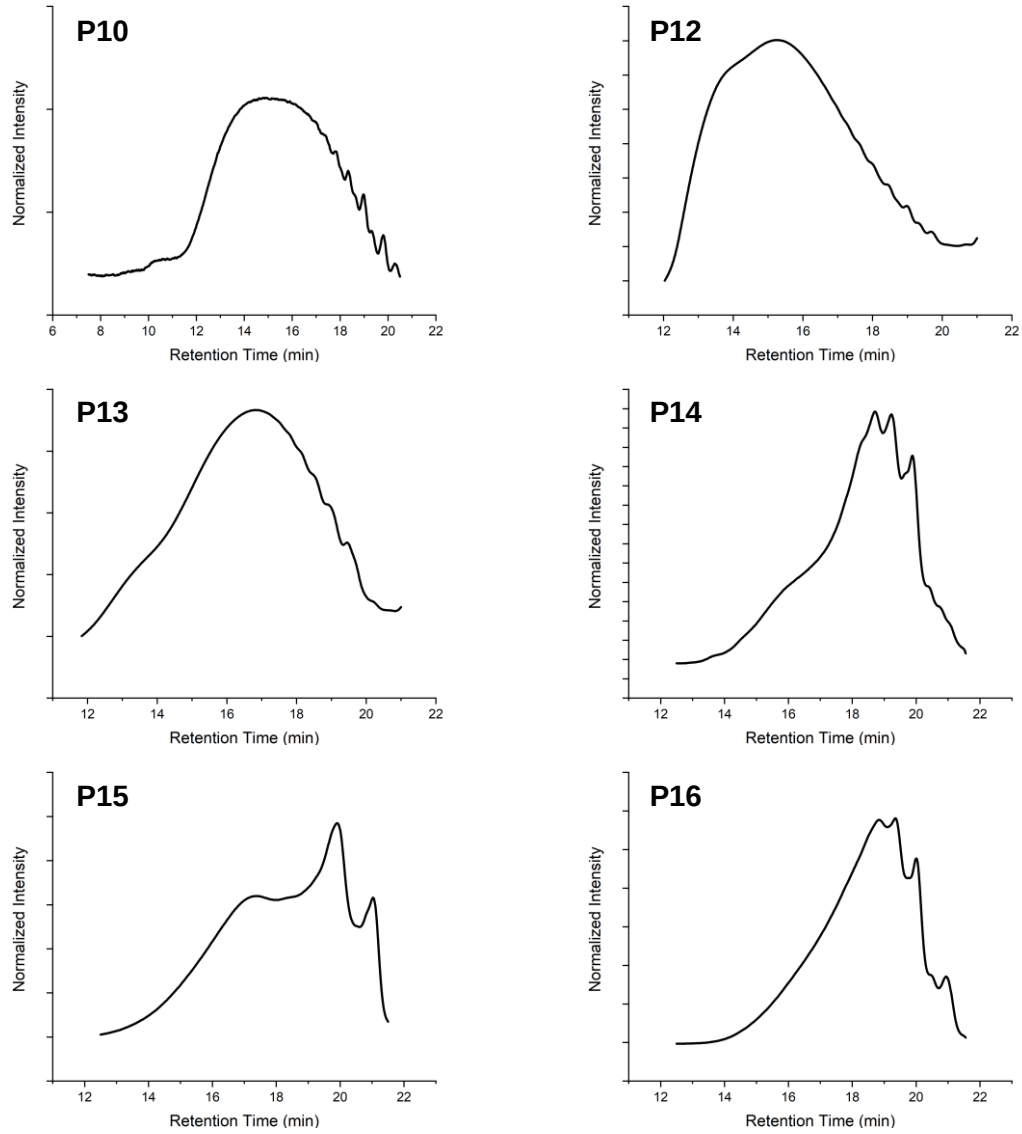

Figure 6.6 – GPC traces for **P10**, **P12** – **P16**.

6.6 X-Ray Crystal Data

Table 6.2 - X-ray data tables compiled for compound **2.15b**.

Table X1

Crystal Data and Details of the Structure Determination	
Formula	C32 H27 N O4 S
Formula Weight	364.47
Crystal System	triclinic
Space group	P-1 (No. 2)
a, b, c [Angstrom]	9.7982(2), 9.8590(2), 11.1142(3)
alpha, beta, gamma [deg]	115.5107(10), 101.2094(16), 106.8613(11)
V [Ang**3]	861.61(4)
Z	2
D(calc) [g/cm**3]	1.405
Mu(MoKa) [/mm]	0.319
F(000)	380
Crystal Size [mm]	0.00 x 0.08 x 0.32
Data Collection	
Temperature (K)	296
Radiation [Angstrom]	MoKa 0.71073
Theta Min-Max [Deg]	2.3, 28.0
Dataset	-13: 12 ; -13: 12 ; -14: 14
Tot., Uniq. Data, R(int)	17393, 4164, 0.054
Observed Data [I > 2.0 sigma(I)]	2876
Refinement	
Nref, Npar	4164, 227
R, wR2, S	0.0588, 0.1349, 1.35
w = ^2^(FO^2^)+(0.0368P)^2^+0.4399P] WHERE P=(FO^2^+2FC^2^)/3'	
Max. and Av. Shift/Error	0.00, 0.00
Min. and Max. Resd. Dens. [e/Ang^3]	-0.35, 1.23

Table X2

Final Coordinates and Equivalent Isotropic Displacement Parameters of the non-Hydrogen atoms

Atom	X	Y	Z	U(eq) Å^2
S1	0.52122(8)	0.12161(9)	0.30899(7)	0.0361(2)
S2	0.45088(9)	0.36215(9)	0.71258(8)	0.0379(3)
O1	0.3252(3)	0.2689(3)	0.3330(2)	0.0632(10)
N1	0.3489(3)	0.3160(3)	0.4653(2)	0.0363(8)
N2	0.6448(3)	0.1934(3)	0.5681(3)	0.0376(8)
C1	0.4475(3)	0.2890(3)	0.5421(3)	0.0330(9)
C2	0.3125(3)	0.4306(3)	0.6764(3)	0.0329(8)

C3	0.2704(3)	0.3981(3)	0.5396(3)	0.0348(9)
C4	0.6682(3)	0.0648(3)	0.3470(3)	0.0318(8)
C5	0.7195(3)	0.1130(3)	0.4894(3)	0.0354(9)
C6	0.5398(3)	0.2070(3)	0.4861(3)	0.0349(9)
C7	0.1567(4)	0.4309(4)	0.4597(3)	0.0461(11)
C8	0.8412(4)	0.0861(4)	0.5670(3)	0.0455(11)
C9	0.2590(3)	0.5138(3)	0.7912(3)	0.0341(9)
C10	0.2557(3)	0.4701(4)	0.8946(3)	0.0431(10)
C11	0.2108(4)	0.5500(4)	1.0048(4)	0.0510(11)
C12	0.1684(4)	0.6740(4)	1.0147(4)	0.0535(12)
C13	0.1707(4)	0.7189(4)	0.9130(4)	0.0497(11)
C14	0.2158(3)	0.6391(4)	0.8019(3)	0.0417(10)
C15	0.7222(3)	-0.0155(3)	0.2313(3)	0.0323(9)
C16	0.6207(3)	-0.1165(4)	0.0883(3)	0.0376(9)
C17	0.6724(4)	-0.1812(4)	-0.0206(3)	0.0421(10)
C18	0.8254(4)	-0.1488(4)	0.0088(3)	0.0440(11)
C19	0.9270(4)	-0.0508(4)	0.1491(3)	0.0437(11)
C20	0.8766(3)	0.0163(4)	0.2604(3)	0.0373(9)

Hydrogen Atom Positions and Isotropic Displacement Parameters				
H7A	0.1556	0.3916	0.3639	0.069
H7B	0.0566	0.3744	0.456	0.069
H7C	0.1844	0.5479	0.5076	0.069
H8A	0.8521	0.1336	0.6659	0.068
H8B	0.8133	-0.0306	0.5243	0.068
H8C	0.9367	0.1381	0.5607	0.068
H10A	0.2842	0.3861	0.8892	0.052
H11A	0.2092	0.5196	1.0732	0.061
H12A	0.1382	0.7276	1.0894	0.064
H13A	0.142	0.803	0.9192	0.06
H14A	0.217	0.67	0.7338	0.05
H16A	0.517	-0.1402	0.0666	0.045
H17A	0.6033	-0.2476	-0.1151	0.051
H18A	0.8597	-0.1927	-0.0654	0.053
H19A	1.0303	-0.0293	0.1696	0.052
H20A	0.9463	0.0827	0.3547	0.045

Table X3

Bond Distances (Å)			
S1-C4	1.732(3)	C15-C16	1.398(4)
S1-C6	1.721(3)	C15-C20	1.392(4)

S2-C1	1.702(3)	C16-C17	1.375(5)
S2-C2	1.734(3)	C17-C18	1.378(6)
O1-N1	1.284(3)	C18-C19	1.377(4)
N1-C1	1.326(4)	C19-C20	1.391(5)
N1-C3	1.400(4)	C7-H7A	0.9600
N2-C5	1.385(4)	C7-H7B	0.9600
N2-C6	1.314(4)	C7-H7C	0.9600
C1-C6	1.438(4)	C8-H8A	0.9600
C2-C3	1.358(4)	C8-H8B	0.9600
C2-C9	1.478(4)	C8-H8C	0.9600
C3-C7	1.485(5)	C10-H10A	0.9300
C4-C5	1.374(4)	C11-H11A	0.9300
C4-C15	1.480(4)	C12-H12A	0.9300
C5-C8	1.489(5)	C13-H13A	0.9300
C9-C10	1.393(5)	C14-H14A	0.9300
C9-C14	1.384(5)	C16-H16A	0.9300
C10-C11	1.376(5)	C17-H17A	0.9300
C11-C12	1.370(6)	C18-H18A	0.9300
C12-C13	1.382(6)	C19-H19A	0.9300
C13-C14	1.384(5)	C20-H20A	0.9300

Bond Angles (°)			
C4-S1-C6	88.93(14)	C10-C11-C12	120.5(4)
C1-S2-C2	90.65(15)	C11-C12-C13	119.6(4)
O1-N1-C1	123.0(3)	C12-C13-C14	120.2(4)
O1-N1-C3	122.5(3)	C9-C14-C13	120.6(3)
C1-N1-C3	114.5(2)	C4-C15-C16	120.6(3)
C5-N2-C6	110.4(3)	C4-C15-C20	121.1(3)
S2-C1-N1	112.1(2)	C16-C15-C20	118.2(3)
S2-C1-C6	124.6(2)	C15-C16-C17	120.8(3)
N1-C1-C6	123.3(3)	C16-C17-C18	120.7(3)
S2-C2-C3	111.5(2)	C17-C18-C19	119.4(3)
S2-C2-C9	119.0(2)	C18-C19-C20	120.6(4)
C3-C2-C9	129.5(3)	C15-C20-C19	120.3(3)
N1-C3-C2	111.3(3)	C3-C7-H7A	109.00
N1-C3-C7	117.5(2)	C3-C7-H7B	109.00
C2-C3-C7	131.3(3)	C3-C7-H7C	109.00
S1-C4-C5	110.2(2)	H7A-C7-H7B	109.00
S1-C4-C15	118.6(2)	H7A-C7-H7C	109.00
C5-C4-C15	131.1(3)	H7B-C7-H7C	109.00
N2-C5-C4	114.8(3)	C5-C8-H8A	109.00
N2-C5-C8	116.9(3)	C5-C8-H8B	109.00
C4-C5-C8	128.2(3)	C5-C8-H8C	109.00

S1-C6-N2	115.7(2)	H8A-C8-H8B	110.00
S1-C6-C1	122.6(2)	H8A-C8-H8C	109.00
N2-C6-C1	121.7(3)	H8B-C8-H8C	109.00
C2-C9-C10	120.0(3)	C9-C10-H10A	120.00
C2-C9-C14	121.6(3)	C11-C10-H10A	120.00
C10-C9-C14	118.4(3)	C10-C11-H11A	120.00
C9-C10-C11	120.7(4)	C12-C11-H11A	120.00
C11-C12-H12A	120.00	C16-C17-H17A	120.00
C13-C12-H12A	120.00	C18-C17-H17A	120.00
C12-C13-H13A	120.00	C17-C18-H18A	120.00
C14-C13-H13A	120.00	C19-C18-H18A	120.00
C9 -C14-H14A	120.00	C18-C19-H19A	120.00
C13-C14-H14A	120.00	C20-C19-H19A	120.00
C15-C16-H16A	120.00	C15-C20-H20A	120.00
C17-C16-H16A	120.00	C19-C20-H20A	120.00

Torsion Angles (°)			
C6-S1-C4-C5	0.4(3)	S2-C2-C9-C10	-31.2(4)
C6-S1-C4-C15	-176.7(3)	S2-C2-C9-C14	146.8(3)
C4-S1-C6-N2	-0.9(3)	C3-C2-C9-C10	149.6(4)
C4-S1-C6-C1	178.8(3)	C3-C2-C9-C14	-32.4(5)
C2-S2-C1-N1	0.2(3)	S1-C4-C5-N2	0.0(4)
C2-S2-C1-C6	-179.7(3)	S1-C4-C5-C8	178.5(3)
C1-S2-C2-C3	-0.7(3)	C15-C4-C5-N2	176.7(3)
C1-S2-C2-C9	180.0(3)	C15-C4-C5-C8	-4.8(6)
O1-N1-C1-S2	-178.8(3)	S1-C4-C15-C16	-31.7(4)
O1-N1-C1-C6	1.1(5)	S1-C4-C15-C20	143.8(3)
C3-N1-C1-S2	0.3(4)	C5-C4-C15-C16	151.9(4)
C3-N1-C1-C6	-179.8(3)	C5-C4-C15-C20	-32.6(6)
O1-N1-C3-C2	178.3(3)	C2-C9-C10-C11	177.9(3)
O1-N1-C3-C7	-0.3(5)	C14-C9-C10-C11	-0.1(5)
C1-N1-C3-C2	-0.8(4)	C2-C9-C14-C13	-177.9(3)
C1-N1-C3-C7	-179.4(3)	C10-C9-C14-C13	0.1(5)
C6-N2-C5-C4	-0.7(4)	C9-C10-C11-C12	0.0(6)
C6-N2-C5-C8	-179.3(3)	C10-C11-C12-C13	0.1(6)
C5-N2-C6-S1	1.0(4)	C11-C12-C13-C14	-0.1(6)
C5-N2-C6-C1	-178.7(3)	C12-C13-C14-C9	0.0(6)
S2-C1-C6-S1	174.95(19)	C4-C15-C16-C17	175.0(4)
S2-C1-C6-N2	-5.4(5)	C20-C15-C16-C17	-0.6(6)
N1-C1-C6-S1	-5.0(5)	C4-C15-C20-C19	-175.4(3)
N1-C1-C6-N2	174.7(3)	C16-C15-C20-C19	0.3(6)
S2-C2-C3-N1	0.9(4)	C15-C16-C17-C18	0.4(6)
S2-C2-C3-C7	179.2(3)	C16-C17-C18-C19	0.2(6)

C9-C2-C3-N1	-179.8(3)	C17-C18-C19-C20	-0.5(6)
C9-C2-C3-C7	-1.5(6)	C18-C19-C20-C15	0.3(6)

Table X4

(An)isotropic Displacement Parameters

Atom	U(1,1) or U	U(2,2)	U(3,3)	U(2,3)	U(1,3)	U(1,2)
S1	0.0368(4)	0.0471(4)	0.0340(4)	0.0221(3)	0.0148(3)	0.0269(3)
S2	0.0432(4)	0.0462(5)	0.0362(4)	0.0225(3)	0.0172(3)	0.0303(4)
O1	0.0729(17)	0.0869(19)	0.0433(14)	0.0327(13)	0.0235(13)	0.0510(15)
N1	0.0392(14)	0.0429(14)	0.0319(13)	0.0189(11)	0.0143(11)	0.0238(12)
N2	0.0363(13)	0.0408(14)	0.0419(14)	0.0214(12)	0.0146(11)	0.0242(11)
C1	0.0333(15)	0.0358(15)	0.0347(15)	0.0177(13)	0.0133(12)	0.0209(13)
C2	0.0332(14)	0.0331(15)	0.0386(15)	0.0186(13)	0.0150(12)	0.0207(12)
C3	0.0324(15)	0.0355(15)	0.0414(16)	0.0205(13)	0.0137(13)	0.0196(12)
C4	0.0319(14)	0.0343(15)	0.0353(15)	0.0190(13)	0.0129(12)	0.0197(12)
C5	0.0340(15)	0.0379(16)	0.0384(15)	0.0196(13)	0.0125(13)	0.0213(13)
C6	0.0360(15)	0.0395(16)	0.0361(15)	0.0200(13)	0.0165(13)	0.0218(13)
C7	0.0434(18)	0.0515(19)	0.0463(18)	0.0238(16)	0.0125(15)	0.0290(16)
C8	0.0469(18)	0.060(2)	0.0408(17)	0.0270(16)	0.0154(15)	0.0357(16)
C9	0.0300(14)	0.0329(15)	0.0396(16)	0.0172(13)	0.0146(12)	0.0151(12)
C10	0.0479(18)	0.0496(18)	0.0509(18)	0.0313(16)	0.0258(15)	0.0313(15)
C11	0.056(2)	0.065(2)	0.0508(19)	0.0357(18)	0.0299(17)	0.0335(18)
C12	0.053(2)	0.061(2)	0.054(2)	0.0242(18)	0.0337(17)	0.0332(18)
C13	0.055(2)	0.0495(19)	0.058(2)	0.0268(17)	0.0293(17)	0.0351(17)
C14	0.0481(18)	0.0423(17)	0.0509(18)	0.0281(15)	0.0258(15)	0.0283(15)
C15	0.0349(15)	0.0329(15)	0.0356(15)	0.0194(13)	0.0147(12)	0.0188(12)
C16	0.0344(15)	0.0410(16)	0.0380(16)	0.0196(14)	0.0128(13)	0.0185(13)
C17	0.0522(19)	0.0372(16)	0.0326(15)	0.0151(13)	0.0148(14)	0.0188(15)
C18	0.061(2)	0.0483(18)	0.0455(18)	0.0298(16)	0.0333(17)	0.0343(17)
C19	0.0425(17)	0.056(2)	0.0545(19)	0.0359(17)	0.0271(16)	0.0309(16)
C20	0.0354(15)	0.0425(17)	0.0393(16)	0.0227(14)	0.0142(13)	0.0205(13)

6.7 Computational Data

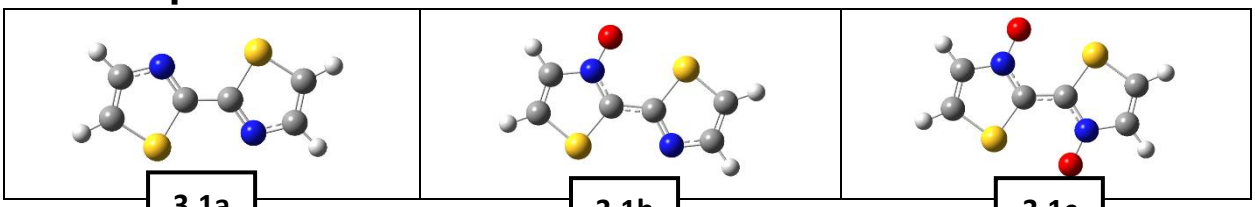

Table 6.3 – Cartesian coordinates for compounds **3.1a-c** at **N-C-C-N** 90 – 180° (10° increments) calculated at the DFT B3LYP 6-311G++(d,p) level of theory.

	3.1a 90°			**3.1a** 100°			**3.1a** 110°			**3.1a** 120°			**3.1a** 130°		
C	-0.02428	0.72508	0	-0.02428	0.72508	0	-0.02428	0.72508	0	-0.02428	0.72508	0	-0.02428	0.72508	0
C	0.44741	2.81065	-0.54114	0.49249	2.81216	-0.49191	0.53311	2.81352	-0.43893	0.56896	2.81472	-0.38262	0.59977	2.81575	-0.3234
C	-0.50496	3.07316	0.40199	-0.53845	3.07204	0.36543	-0.56862	3.07103	0.3261	-0.59526	3.07014	0.28428	-0.61815	3.06938	0.2403
S	-1.11725	1.59647	1.06305	-1.2058	1.5935	0.96634	-1.2856	1.59083	0.86227	-1.35602	1.58847	0.75165	-1.41654	1.58645	0.6353
H	0.98605	3.56038	-1.1045	1.07806	3.56346	-1.00402	1.16096	3.56624	-0.8959	1.23414	3.56869	-0.78096	1.29702	3.57079	-0.66008
H	-0.87259	4.03034	0.73747	-0.93403	4.02828	0.67041	-0.98938	4.02643	0.59825	-1.03825	4.02479	0.52153	-1.08024	4.02338	0.44084
N	0.71297	1.48691	-0.76232	0.77647	1.48903	-0.69298	0.83369	1.49095	-0.61836	0.8842	1.49264	-0.53904	0.9276	1.49409	-0.45561
C	0.02428	-0.72508	0	0.02428	-0.72508	0	0.02428	-0.72508	0	0.02428	-0.72508	0	0.02428	-0.72508	0
S	1.11725	-1.59647	1.06305	1.2058	-1.5935	0.96634	1.2856	-1.59083	0.86227	1.35602	-1.58847	0.75165	1.41654	-1.58645	0.6353
C	-0.44741	-2.81065	-0.54114	-0.49249	-2.81216	-0.49191	-0.53311	-2.81352	-0.43893	-0.56896	-2.81472	-0.38262	-0.59977	-2.81575	-0.3234
C	0.50496	-3.07316	0.40199	0.53845	-3.07204	0.36543	0.56862	-3.07103	0.3261	0.59526	-3.07014	0.28428	0.61815	-3.06938	0.2403
H	-0.98605	-3.56038	-1.1045	-1.07806	-3.56346	-1.00402	-1.16096	-3.56624	-0.8959	-1.23414	-3.56869	-0.78096	-1.29702	-3.57079	-0.66008
H	0.87259	-4.03034	0.73747	0.93403	-4.02828	0.67041	0.98938	-4.02643	0.59825	1.03825	-4.02479	0.52153	1.08024	-4.02338	0.44084
N	-0.71297	-1.48691	-0.76232	-0.77647	-1.48903	-0.69298	-0.83369	-1.49095	-0.61836	-0.8842	-1.49264	-0.53904	-0.9276	-1.49409	-0.45561
	3.1a 140°			**3.1a** 150°			**3.1a** 160°			**3.1a** 170°			**3.1a** 180°		
C	-0.02428	0.72508	0	-0.02428	0.72508	0	-0.02428	0.72508	0	-0.02428	0.72508	0.	-0.02428	0.72508	0.
C	0.6253	2.8166	-0.26171	0.64536	2.81727	-0.19803	0.6598	2.81776	-0.13285	0.66851	2.81805	-0.06665	0.67141	2.81815	0.00002
C	-0.63712	3.06874	0.19449	-0.65203	3.06824	0.14721	-0.66277	3.06788	0.0988	-0.66924	3.06766	0.04964	-0.67141	3.06759	0.00012
S	-1.4667	1.58477	0.51412	-1.50611	1.58345	0.38902	-1.53447	1.5825	0.26097	-1.55157	1.58193	0.13093	-1.55728	1.58174	-0.00005
H	1.34913	3.57254	-0.53418	1.39008	3.57391	-0.40421	1.41955	3.5749	-0.27116	1.43732	3.57549	-0.13605	1.44325	3.57569	0.00003
H	-1.11505	4.02222	0.3568	-1.1424	4.0213	0.27005	-1.16209	4.02064	0.18123	-1.17397	4.02025	0.09104	-1.17795	4.02011	0.0002
N	0.96357	1.4953	-0.36872	0.99184	1.49624	-0.27902	1.01219	1.49692	-0.1872	1.02445	1.49734	-0.09396	1.02856	1.49747	-0.00004
C	0.02428	-0.72508	0	0.02428	-0.72508	0	0.02428	-0.72508	0	0.02428	-0.72508	0.	0.02428	-0.72508	0.
S	1.4667	-1.58477	0.51412	1.50611	-1.58345	0.38902	1.53447	-1.5825	0.26097	1.55157	-1.58193	0.13093	1.55728	-1.58174	-0.00005
C	-0.6253	-2.8166	-0.26171	-0.64536	-2.81727	-0.19803	-0.6598	-2.81776	-0.13285	-0.66851	-2.81805	-0.06665	-0.67141	-2.81815	0.00002
C	0.63712	-3.06874	0.19449	0.65203	-3.06824	0.14721	0.66277	-3.06788	0.0988	0.66924	-3.06766	0.04964	0.67141	-3.06759	0.00012
H	-1.34913	-3.57254	-0.53418	-1.39008	-3.57391	-0.40421	-1.41955	-3.5749	-0.27116	-1.43732	-3.57549	-0.13605	-1.44325	-3.57569	0.00003
H	1.11505	-4.02222	0.3568	1.1424	-4.0213	0.27005	1.16209	-4.02064	0.18123	1.17397	-4.02025	0.09104	1.17795	-4.02011	0.0002
N	-0.96357	-1.4953	-0.36872	-0.99184	-1.49624	-0.27902	-1.01219	-1.49692	-0.1872	-1.02445	-1.49734	-0.09396	-1.02856	-1.49747	-0.00004
	3.1b 90°			**3.1b** 100°			**3.1b** 110°			**3.1b** 120°			**3.1b** 130°		
C	-0.78955	-0.2849	-0.00002	-0.78955	-0.2849	-0.00002	-0.78955	-0.2849	-0.00002	-0.78955	-0.2849	-0.00002	-0.78955	-0.2849	-0.00002
C	-2.76318	-1.06855	0.59258	-2.75848	-1.11773	0.53868	-2.75425	-1.16204	0.48068	-2.75052	-1.20114	0.41902	-2.74731	-1.23475	0.35417
C	-3.18487	-0.16647	-0.34558	-3.18761	-0.1378	-0.31415	-3.19007	-0.11197	-0.28034	-3.19225	-0.08917	-0.24438	-3.19412	-0.06958	-0.20657
S	-1.83846	0.66413	-1.0445	-1.84673	0.75079	-0.9495	-1.85419	0.82888	-0.84727	-1.86077	0.8978	-0.7386	-1.86643	0.95704	-0.6243
H	-3.41033	-1.7128	1.17246	-3.40104	-1.81009	1.06581	-3.39267	-1.89775	0.95106	-3.38528	-1.97513	0.82906	-3.37893	-2.04162	0.70076
H	-4.19533	0.04963	-0.65678	-4.20054	0.10412	-0.59705	-4.20522	0.15322	-0.53277	-4.20936	0.19655	-0.46445	-4.21292	0.23379	-0.39259
N	-1.41502	-1.13312	0.78502	-1.4088	-1.19826	0.71362	-1.40319	-1.25696	0.63679	-1.39825	-1.30876	0.55511	-1.394	-1.35329	0.46921
C	0.63436	-0.14898	0.00001	0.63436	-0.14898	0.00001	0.63436	-0.14898	0.00001	0.63436	-0.14898	0.00001	0.63436	-0.14898	0.00001
S	1.70339	-1.06722	-1.01547	1.71143	-1.15148	-0.92309	1.71868	-1.2274	-0.82368	1.72507	-1.29441	-0.718	1.73057	-1.352	-0.60685
C	2.68874	0.66005	0.61012	2.68391	0.71067	0.55462	2.67956	0.75628	0.4949	2.67571	0.79653	0.43141	2.67241	0.83113	0.36465
C	3.06478	-0.24051	-0.32199	3.06733	-0.26723	-0.29269	3.06963	-0.2913	-0.26117	3.07165	-0.31256	-0.22766	3.0734	-0.33082	-0.19241
H	3.29111	1.32159	1.21137	3.28152	1.4221	1.10117	3.27288	1.51266	0.9826	3.26525	1.59259	0.85654	3.2587	1.66128	0.72397
H	4.06767	-0.46902	-0.64472	4.07277	-0.52252	-0.58606	4.07737	-0.57073	-0.52295	4.08143	-0.61327	-0.45585	4.08492	-0.64984	-0.38528
N	1.3019	0.7118	0.79338	1.29562	0.77763	0.7212	1.28996	0.83694	0.64354	1.28496	0.88929	0.56098	1.28067	0.93428	0.47416
O	0.73048	1.4986	1.63083	0.71757	1.63391	1.48248	0.70593	1.75584	1.32284	0.69566	1.86345	1.15313	0.68684	1.95593	0.97465
	3.1b 140°			**3.1b** 150°			**3.1b** 160°			**3.1b** 170°			**3.1b** 180°		
C	-0.78955	-0.2849	-0.00002	-0.78955	-0.2849	-0.00002	-0.78955	-0.2849	-0.00002	-0.78955	-0.2849	-0.00002	-0.78955	-0.2849	-0.00002
C	-2.74465	-1.26261	0.28663	-2.74256	-1.2845	0.2169	-2.74105	-1.30026	0.14552	-2.74014	-1.30976	0.07304	-2.73984	-1.31294	0.00001
C	-3.19567	-0.05334	-0.16719	-3.19689	-0.04057	-0.12654	-3.19777	-0.03139	-0.08492	-3.1983	-0.02585	-0.04266	-3.19848	-0.024	-0.00008
S	-1.87111	1.00613	-0.50526	-1.8748	1.04471	-0.38237	-1.87745	1.07247	-0.25657	-1.87905	1.08922	-0.12881	-1.87959	1.09482	-0.00011
H	-3.37367	-2.09674	0.56712	-3.36953	-2.14004	0.42917	-3.36655	-2.17122	0.28795	-3.36476	-2.19002	0.14453	-3.36415	-2.19631	0.00005
H	-4.21587	0.26466	-0.31774	-4.21818	0.28892	-0.24047	-4.21985	0.30637	-0.16138	-4.22086	0.3169	-0.08106	-4.22119	0.32043	-0.00013
N	-1.39047	-1.39019	0.37974	-1.3877	-1.41918	0.28737	-1.38571	-1.44006	0.19282	-1.3845	-1.45265	0.0968	-1.3841	-1.45686	0.00006
C	0.63436	-0.14898	0.00001	0.63436	-0.14898	0.00001	0.63436	-0.14898	0.00001	0.63436	-0.14898	0.00001	0.63436	-0.14898	0.00001
S	1.73512	-1.39972	-0.49109	1.7387	-1.43722	-0.37159	1.74127	-1.4642	-0.24926	1.74282	-1.48048	-0.12503	1.74334	-1.48591	0.00012
C	2.66968	0.8598	0.2951	2.66753	0.88233	0.22331	2.66598	0.89854	0.14982	2.66505	0.90832	0.0752	2.66474	0.91158	0.00001
C	3.07484	-0.34595	-0.1557	3.07598	-0.35785	-0.11781	3.07679	-0.36641	-0.07902	3.07728	-0.37157	-0.03963	3.07745	-0.37329	0.00006
H	3.25326	1.7182	0.58589	3.249	1.76293	0.44335	3.24593	1.79512	0.29744	3.24408	1.81453	0.14927	3.24346	1.82102	-0.00002
H	4.08782	-0.68014	-0.31179	4.09009	-0.70395	-0.23591	4.09172	-0.72109	-0.15824	4.09271	-0.73143	-0.07937	4.09303	-0.73488	0.00009
N	1.27711	0.97157	0.38372	1.27432	1.00086	0.29036	1.27231	1.02195	0.1948	1.27109	1.03466	0.09775	1.27069	1.0389	-0.00003
O	0.67952	2.03257	0.78875	0.67378	2.0928	0.59685	0.66965	2.13614	0.40041	0.66716	2.16227	0.20091	0.66633	2.171	-0.00007
	3.1c 90°			**3.1c** 100°			**3.1c** 110°			**3.1c** 120°			**3.1c** 130°		
C	-0.05492	0.7044	0	-0.05492	0.7044	0	-0.05492	0.7044	0	-0.05492	0.7044	0	-0.05492	0.7044	0
C	-0.89118	2.72309	-0.67681	-0.94742	2.71871	-0.61525	-0.9981	2.71475	-0.549	-1.04283	2.71127	-0.47858	-1.08127	2.70827	-0.40451
C	0.00561	3.13393	0.2492	0.02632	3.13555	0.22653	0.04497	3.137	0.20214	0.06144	3.13829	0.17621	0.0756	3.13939	0.14894
S	0.85309	1.80978	0.99119	0.93546	1.8162	0.90103	1.00967	1.82198	0.80401	1.07518	1.82709	0.70087	1.13148	1.83148	0.59241
H	-1.55817	3.29987	-1.29695	-1.66595	3.29147	-1.17898	-1.76306	3.2839	-1.05203	-1.84877	3.27722	-0.91708	-1.92243	3.27147	-0.77515
H	0.21811	4.15037	0.54007	0.26299	4.15387	0.49094	0.30343	4.15702	0.43808	0.33912	4.1598	0.38189	0.3698	4.1622	0.32278
N	0.05492	-0.7044	0	0.05492	-0.7044	0	0.05492	-0.7044	0	0.05492	-0.7044	0	0.05492	-0.7044	0
C	-0.85309	-1.80978	0.99119	-0.93546	-1.8162	0.90103	-1.00967	-1.82198	0.80401	-1.07518	-1.82709	0.70087	-1.13148	-1.83148	0.59241
S	0.89118	-2.72309	-0.67681	0.94742	-2.71871	-0.61525	0.9981	-2.71475	-0.549	1.04283	-2.71127	-0.47858	1.08127	-2.70827	-0.40451
C	-0.00561	-3.13393	0.2492	-0.02632	-3.13555	0.22653	-0.04497	-3.137	0.20214	-0.06144	-3.13829	0.17621	-0.0756	-3.13939	0.14894
C	1.55817	-3.29987	-1.29695	1.66595	-3.29147	-1.17898	1.76306	-3.2839	-1.05203	1.84877	-3.27722	-0.91708	1.92243	-3.27147	-0.77515

H	-0.21811	-4.15037	0.54007	-0.26299	-4.15387	0.49094	-0.30343	-4.15702	0.43808	-0.33912	-4.1598	0.38189	-0.3698	-4.1622	0.32278
H	-0.92468	1.33879	-0.81782	-0.99264	1.3335	-0.74343	-1.05388	1.32872	-0.66338	-1.10793	1.32451	-0.57829	-1.15438	1.32089	-0.48879
N	0.92468	-1.33879	-0.81782	0.99264	-1.3335	-0.74343	1.05388	-1.32872	-0.66338	1.10793	-1.32451	-0.57829	1.15438	-1.32089	-0.48879
O	-1.69835	0.7147	-1.63765	-1.83443	0.70409	-1.48869	-1.95706	0.69453	-1.3284	-2.06529	0.68609	-1.158	-2.1583	0.67884	-0.97878
O	1.69835	-0.7147	-1.63765	1.83443	-0.70409	-1.48869	1.95706	-0.69453	-1.3284	2.06529	-0.68609	-1.158	2.1583	-0.67884	-0.97878
	3.1c 140°			**3.1c** 150°			**3.1c** 160°			**3.1c** 170°			**3.1c** 180°		
C	-0.05492	0.7044	0	-0.05492	0.7044	0	-0.05492	0.7044	0	-0.05492	0.7044	0	-0.05492	0.7044	0
C	-1.11313	2.70579	-0.32737	-1.13816	2.70383	-0.24773	-1.15618	2.70243	-0.16621	-1.16704	2.70158	-0.08342	-1.17067	2.7013	0
C	0.08733	3.14031	0.12053	0.09654	3.14102	0.09121	0.10318	3.14154	0.0612	0.10718	3.14185	0.03072	0.10852	3.14196	0
S	1.17813	1.83512	0.47943	1.21479	1.83798	0.3628	1.24118	1.84003	0.24341	1.25709	1.84128	0.12217	1.26241	1.84169	0
H	-1.98348	3.26671	-0.62732	-2.03145	3.26297	-0.47472	-2.06598	3.26028	-0.3185	-2.0868	3.25866	-0.15986	-2.09376	3.25812	0
H	0.39522	4.16418	0.26123	0.41519	4.16574	0.19768	0.42957	4.16686	0.13263	0.43824	4.16753	0.06657	0.44114	4.16776	0
N	0.05492	-0.7044	0	0.05492	-0.7044	0	0.05492	-0.7044	0	0.05492	-0.7044	0	0.05492	-0.7044	0
C	-1.17813	-1.83512	0.47943	-1.21479	-1.83798	0.3628	-1.24118	-1.84003	0.24341	-1.25709	-1.84128	0.12217	-1.26241	-1.84169	0
S	1.11313	-2.70579	-0.32737	1.13816	-2.70383	-0.24773	1.15618	-2.70243	-0.16621	1.16704	-2.70158	-0.08342	1.17067	-2.7013	0
C	-0.08733	-3.14031	0.12053	-0.09654	-3.14102	0.09121	-0.10318	-3.14154	0.0612	-0.10718	-3.14185	0.03072	-0.10852	-3.14196	0
C	1.98348	-3.26671	-0.62732	2.03145	-3.26297	-0.47472	2.06598	-3.26028	-0.3185	2.0868	-3.25866	-0.15986	2.09376	-3.25812	0
H	-0.39522	-4.16418	0.26123	-0.41519	-4.16574	0.19768	-0.42957	-4.16686	0.13263	-0.43824	-4.16753	0.06657	-0.44114	-4.16776	0
H	-1.19287	1.31788	-0.39557	-1.22312	1.31553	-0.29934	-1.24489	1.31383	-0.20084	-1.25802	1.3128	-0.1008	-1.26241	1.31246	0
N	1.19287	-1.31788	-0.39557	1.22312	-1.31553	-0.29934	1.24489	-1.31383	-0.20084	1.25802	-1.3128	-0.1008	1.26241	-1.31246	0
O	-2.23539	0.67282	-0.79212	-2.29596	0.6681	-0.59942	-2.33956	0.6647	-0.40217	-2.36585	0.66265	-0.20185	-2.37464	0.66197	0
O	2.23539	-0.67282	-0.79212	2.29596	-0.6681	-0.59942	2.33956	-0.6647	-0.40217	2.36585	-0.66265	-0.20185	2.37464	-0.66197	0

Table 6.4 – Total Molecular Energies (Hartrees) calculated with ccsd(t) 6-311++g(d,p) on the DFT optimized structures.

Angle (°)	**3.1a**	**3.1b**	**3.1c**
90	-1133.540487	-1208.328794	-1283.118228
100	-1133.541316	-1208.329786	-1283.119401
110	-1133.542695	-1208.331077	-1283.120752
120	-1133.544504	-1208.33269	-1283.122429
130	-1133.546524	-1208.334666	-1283.124697
140	-1133.548498	-1208.337054	-1283.127874
150	-1133.550204	-1208.339791	-1283.131978
160	-1133.55149	-1208.342535	-1283.136397
170	-1133.552278	-1208.344641	-1283.139914
180	-1133.552542	-1208.345438	-1283.141265

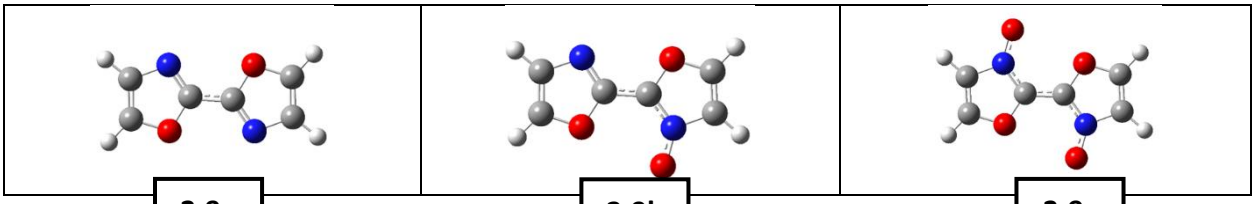

Table 6.5 – Cartesian coordinates for compounds **3.9a-c** at **N-C-C-N** 90 – 180° (10° increments) calculated at the DFT B3LYP 6-311G++(d,p) level of theory.

	3.9a 90°			**3.9a** 100°			**3.9a** 110°			**3.9a** 120°			**3.9a** 130°		
C	-0.09424	0.71694	-0.00002	-0.09424	0.71694	-0.00002	-0.09424	0.71694	-0.00002	-0.09424	0.71694	-0.00002	-0.09424	0.71694	-0.00002
C	-0.03995	2.81176	-0.32681	-0.01294	2.81531	-0.29708	0.01139	2.81851	-0.26509	0.03287	2.82133	-0.23108	0.05132	2.82375	-0.19531
C	-0.97325	2.57742	0.62914	-1.02524	2.57059	0.57192	-1.07210	2.56443	0.51035	-1.11345	2.55899	0.44490	-1.14899	2.55432	0.37605
H	0.26894	3.75126	-0.75546	0.33137	3.75947	-0.68674	0.38763	3.76686	-0.61279	0.43728	3.77339	-0.53417	0.47994	3.77900	-0.45149
H	-1.64126	3.18713	1.21208	-1.74143	3.17396	1.10185	-1.83169	3.16209	0.98323	-1.91136	3.15162	0.85712	-1.97983	3.14262	0.72449
N	0.51678	1.60809	-0.72197	0.57644	1.61594	-0.65630	0.63021	1.62300	-0.58564	0.67765	1.62924	-0.51052	0.71843	1.63460	-0.43151
C	0.09424	-0.71694	-0.00002	0.09424	-0.71694	-0.00002	0.09424	-0.71694	-0.00002	0.09424	-0.71694	-0.00002	0.09424	-0.71694	-0.00002
C	0.03995	-2.81176	-0.32681	0.01294	-2.81531	-0.29708	-0.01139	-2.81851	-0.26509	-0.03287	-2.82133	-0.23108	-0.05132	-2.82375	-0.19531
C	0.97325	-2.57742	0.62914	1.02524	-2.57059	0.57192	1.07210	-2.56443	0.51035	1.11345	-2.55899	0.44490	1.14899	-2.55432	0.37605
H	-0.26894	-3.75126	-0.75546	-0.33137	-3.75947	-0.68674	-0.38763	-3.76686	-0.61279	-0.43728	-3.77339	-0.53417	-0.47994	-3.77900	-0.45149
H	1.64126	-3.18713	1.21208	1.74143	-3.17396	1.10185	1.83169	-3.16209	0.98323	1.91136	-3.15162	0.85712	1.97983	-3.14262	0.72449
N	-0.51678	-1.60809	-0.72197	-0.57644	-1.61594	-0.65630	-0.63021	-1.62300	-0.58564	-0.67765	-1.62924	-0.51052	-0.71843	-1.63460	-0.43151
O	-1.01973	1.23043	0.85057	-1.09003	1.22119	0.77319	-1.15336	1.21286	0.68993	-1.20927	1.20551	0.60142	-1.25731	1.19920	0.50833
O	1.01973	-1.23043	0.85057	1.09003	-1.22119	0.77319	1.15336	-1.21286	0.68993	1.20927	-1.20551	0.60142	1.25731	-1.19920	0.50833
	3.9a 140°			**3.9a** 150°			**3.9a** 160°			**3.9a** 170°			**3.9a** 180°		

C	-0.09424	0.716944	-0.00001	-0.09424	0.716944	-0.00001	-0.09424	0.716944	-0.00001	-0.09424	0.716944	-0.00001	-0.09424	0.716944	-1.7E-05
C	0.066618	2.825764	-0.15806	0.078636	2.827344	-0.11960	0.087286	2.828481	-0.08023	0.092501	2.829167	-0.04026	0.094242	2.829396	0.000007
C	-1.17844	2.550449	0.304350	-1.20158	2.547406	0.230330	-1.21825	2.545216	0.154557	-1.22830	2.543895	0.077607	-1.23167	2.543453	0.000091
H	0.515301	3.783646	-0.36537	0.543085	3.787298	-0.27647	0.563081	3.789927	-0.18547	0.575137	3.791511	-0.09306	0.579162	3.792041	0.000027
H	-2.03657	3.135162	0.586351	-2.08116	3.129300	0.443746	-2.11326	3.125081	0.297765	-2.13263	3.122535	0.149516	-2.13911	3.121684	0.000176
N	0.752227	1.639042	-0.34921	0.778783	1.642532	-0.26427	0.797897	1.645045	-0.17731	0.809423	1.646560	-0.08900	0.813276	1.647067	-4.4E-05
C	0.094242	-0.71694	-0.00001	0.094242	-0.71694	-0.00001	0.094242	-0.71694	-0.00001	0.094242	-0.71694	-0.00001	0.094242	-0.71694	-1.7E-05
C	-0.06661	-2.82576	-0.15806	-0.07863	-2.82734	-0.11960	-0.08728	-2.82848	-0.08023	-0.09250	-2.82916	-0.04026	-0.09424	-2.8294	0.000007
C	1.178442	-2.55044	0.304350	1.201589	-2.54740	0.230330	1.218252	-2.54521	0.154557	1.228304	-2.54389	0.077607	1.231668	-2.54345	0.000091
H	-0.51530	-3.78364	-0.36537	-0.54308	-3.78729	-0.27647	-0.56308	-3.78992	-0.18547	-0.57513	-3.79151	-0.09306	-0.57916	-3.79204	0.000027
H	2.036573	-3.13516	0.586351	2.081166	-3.12930	0.443746	2.113266	-3.12508	0.297765	2.132630	-3.12253	0.149516	2.13911	-3.12168	0.000176
N	-0.75222	-1.63904	-0.34921	-0.77878	-1.64253	-0.26427	-0.79789	-1.64504	-0.17731	-0.80942	-1.64656	-0.08900	-0.81328	-1.64707	-4.4E-05
O	-1.29711	1.193965	0.411365	-1.32840	1.189853	0.311275	-1.35091	1.186893	0.208815	-1.36449	1.185108	0.104766	-1.36903	1.184513	-4.8E-05
O	1.297119	-1.19396	0.411365	1.328403	-1.18985	0.311275	1.350918	-1.18689	0.208815	1.364494	-1.18510	0.104766	1.369028	-1.18451	-4.8E-05
		3.9b 90°			**3.9b** 100°			**3.9b** 110°			**3.9b** 120°			**3.9b** 130°	
C	-0.87312	-0.21381	0.00001	-0.87312	-0.21381	0.00001	-0.87312	-0.21381	0.00001	-0.87312	-0.21381	0.00001	-0.87312	-0.21381	0.00001
C	-2.93486	-0.54452	0.36683	-2.93539	-0.57510	0.33347	-2.93587	-0.60265	0.29756	-2.93630	-0.62696	0.25939	-2.93667	-0.64786	0.21925
C	-2.84283	0.41207	-0.59136	-2.84197	0.46135	-0.53758	-2.84119	0.50575	-0.47971	-2.84051	0.54495	-0.41819	-2.83992	0.57863	-0.35349
H	-3.81770	-0.97414	0.81190	-3.81889	-1.04181	0.73805	-3.81996	-1.10278	0.65858	-3.82090	-1.15659	0.57410	-3.82171	-1.20284	0.48526
H	-3.54509	0.99434	-1.16133	-3.54339	1.09112	-1.05572	-3.54186	1.17833	-0.94207	-3.54051	1.25530	-0.82125	-3.53936	1.32146	-0.69418
N	-1.66444	-0.94020	0.74025	-1.66552	-1.00189	0.67292	-1.66650	-1.05748	0.60047	-1.66736	-1.10654	0.52346	-1.66810	-1.14871	0.44246
C	0.55588	-0.23889	0.00003	0.55588	-0.23889	0.00003	0.55588	-0.23889	0.00003	0.55588	-0.23889	0.00003	0.55588	-0.23889	0.00003
C	2.71676	0.06276	0.33946	2.71726	0.09104	0.30858	2.71771	0.11653	0.27535	2.71810	0.13902	0.24003	2.71844	0.15835	0.20288
C	2.54907	-0.87973	-0.60576	2.54818	-0.93022	-0.55065	2.54739	-0.97571	-0.49136	2.54668	-1.01586	-0.42833	2.54607	-1.05037	-0.36203
H	3.58475	0.50351	0.79528	3.58591	0.56978	0.72293	3.58696	0.62950	0.64508	3.58789	0.68220	0.56232	3.58868	0.72748	0.47528
H	3.23077	-1.47422	-1.18820	3.22903	-1.57325	-1.08012	3.22747	-1.66249	-0.96382	3.22608	-1.74124	-0.84018	3.22489	-1.80893	-0.71015
N	1.42596	0.47833	0.73233	1.42703	0.53936	0.66571	1.42799	0.59435	0.59403	1.42885	0.64288	0.51782	1.42958	0.68459	0.43768
O	1.18309	1.36234	1.61182	1.18545	1.49666	1.46519	1.18758	1.61769	1.30741	1.18945	1.72452	1.13968	1.19107	1.81632	0.96328
O	-1.51731	0.63655	-0.83901	-1.51608	0.70647	-0.76270	-1.51498	0.76947	-0.68058	-1.51400	0.82508	-0.59329	-1.51317	0.87287	-0.50148
O	1.22163	-1.07838	-0.82748	1.22042	-1.14734	-0.75219	1.21933	-1.20948	-0.67118	1.21837	-1.26433	-0.58506	1.21754	-1.31146	-0.49449
		3.9b 140°			**3.9b** 150°			**3.9b** 160°			**3.9b** 170°			**3.9b** 180°	
C	-0.87312	-0.21381	0.00001	-0.87312	-0.21381	0.00001	-0.87312	-0.21381	0.00001	-0.87312	-0.21381	0.00001	-0.87312	-0.21381	0.00001
C	-2.93697	-0.66518	0.17743	-2.93721	-0.67879	0.13427	-2.93738	-0.68858	0.09008	-2.93748	-0.69449	0.04521	-2.93752	-0.69647	0.00001
C	-2.83943	0.60655	-0.28609	-2.83904	0.62849	-0.21652	-2.83877	0.64428	-0.14530	-2.83860	0.65381	-0.07298	-2.83855	0.65700	-0.00011
H	-3.82238	-1.24117	0.39272	-3.82291	-1.27129	0.29719	-3.82329	-1.29298	0.19939	-3.82351	-1.30605	0.10008	-3.82359	-1.31043	0.00003
H	-3.53840	1.37628	-0.56183	-3.53764	1.41937	-0.42520	-3.53710	1.45038	-0.28534	-3.53677	1.46909	-0.14330	-3.53667	1.47535	-0.00020
N	-1.66871	-1.18366	0.35809	-1.66919	-1.21112	0.27099	-1.66953	-1.23089	0.18184	-1.66974	-1.24281	0.09130	-1.66981	-1.24680	0.00008
C	0.55588	-0.23889	0.00003	0.55588	-0.23889	0.00003	0.55588	-0.23889	0.00003	0.55588	-0.23889	0.00003	0.55588	-0.23889	0.00003
C	2.71872	0.17436	0.16418	2.71894	0.18695	0.12424	2.71910	0.19601	0.08335	2.71920	0.20147	0.04183	2.71923	0.20329	0.00000
C	2.54557	-1.07897	-0.29298	2.54517	-1.10144	-0.22170	2.54489	-1.11762	-0.14873	2.54472	-1.12738	-0.07463	2.54466	-1.13064	0.00002
H	3.58934	0.76502	0.38462	3.58986	0.79450	0.29104	3.59023	0.81573	0.19524	3.59046	0.82852	0.09796	3.59054	0.83278	-0.00005
H	3.22391	-1.86502	-0.57471	3.22313	-1.90910	-0.43489	3.22257	-1.94083	-0.29177	3.22223	-1.95997	-0.14642	3.22212	-1.96637	0.00001
N	1.43019	0.71915	0.35420	1.43067	0.74631	0.26803	1.43101	0.76586	0.17982	1.43122	0.77765	0.09024	1.43129	0.78158	0.00000
O	1.19241	1.89239	0.77955	1.19346	1.95217	0.58989	1.19422	1.99520	0.39573	1.19467	2.02114	0.19857	1.19483	2.02980	-0.00007
O	-1.51247	0.91248	-0.40585	-1.51193	0.94361	-0.30714	-1.51154	0.96601	-0.20608	-1.51130	0.97952	-0.10346	-1.51122	0.98404	-0.00007
O	1.21685	-1.35052	-0.40015	1.21631	-1.38121	-0.30277	1.21592	-1.40329	-0.20308	1.21569	-1.41661	-0.10185	1.21561	-1.42105	0.00014
		3.9c 90°			**3.9c** 100°			**3.9c** 110°			**3.9c** 120°			**3.9c** 130°	
C	0.01945	0.70642	0.00000	0.01945	0.70642	0.00000	0.01945	0.70642	0.00000	0.01945	0.70642	0.00000	0.01945	0.70642	0.00000
C	0.46862	2.83224	0.39049	0.50115	2.83135	0.35497	0.53047	2.83054	0.31675	0.55634	2.82983	0.27612	0.57858	2.82922	0.23338
C	-0.48285	2.75091	-0.55838	-0.52938	2.75219	-0.50759	-0.57130	2.75335	-0.45294	-0.60830	2.75437	-0.39484	-0.64010	2.75524	-0.33373
H	0.96569	3.65905	0.86462	1.03773	3.65707	0.78597	1.10264	3.65528	0.70134	1.15994	3.65370	0.61138	1.20917	3.65235	0.51676
H	-1.03031	3.48251	-1.12577	-1.12411	3.48509	-1.02337	-1.20863	3.48742	-0.91318	-1.28323	3.48947	-0.79604	-1.34734	3.49124	-0.67284
C	-0.01945	-0.70642	0.00000	-0.01945	-0.70642	0.00000	-0.01945	-0.70642	0.00000	-0.01945	-0.70642	0.00000	-0.01945	-0.70642	0.00000
C	-0.46862	-2.83224	0.39049	-0.50115	-2.83135	0.35497	-0.53047	-2.83054	0.31675	-0.55634	-2.82983	0.27612	-0.57858	-2.82922	0.23338
C	0.48285	-2.75091	-0.55838	0.52938	-2.75219	-0.50759	0.57130	-2.75335	-0.45294	0.60830	-2.75437	-0.39484	0.64010	-2.75524	-0.33373
H	-0.96569	-3.65905	0.86462	-1.03773	-3.65707	0.78597	-1.10264	-3.65528	0.70134	-1.15994	-3.65370	0.61138	-1.20917	-3.65235	0.51676
H	1.03031	-3.48251	-1.12577	1.12411	-3.48509	-1.02337	1.20863	-3.48742	-0.91318	1.28323	-3.48947	-0.79604	1.34734	-3.49124	-0.67284
N	0.79589	1.51212	0.75397	0.85871	1.51039	0.68539	0.91531	1.50883	0.61159	0.96527	1.50745	0.53314	1.00821	1.50627	0.45063
N	-0.79589	-1.51212	0.75397	-0.85871	-1.51039	0.68539	-0.91531	-1.50883	0.61159	-0.96527	-1.50745	0.53314	-1.00821	-1.50627	0.45063
O	1.66093	1.17985	1.62783	1.79656	1.17611	1.47976	1.91877	1.17275	1.32043	2.02664	1.16978	1.15105	2.11934	1.16722	0.97291
O	-1.66093	-1.17985	1.62783	-1.79656	-1.17611	1.47976	-1.91877	-1.17275	1.32043	-2.02664	-1.16978	1.15105	-2.11934	-1.16722	0.97291
O	0.77206	-1.44403	-0.81151	0.83967	-1.44589	-0.73770	0.90060	-1.44757	-0.65827	0.95437	-1.44905	-0.57383	1.00059	-1.45032	-0.48502
O	-0.77206	1.44403	-0.81151	-0.83967	1.44589	-0.73770	-0.90060	1.44757	-0.65827	-0.95437	1.44905	-0.57383	-1.00059	1.45032	-0.48502
		3.9c 140°			**3.9c** 150°			**3.9c** 160°			**3.9c** 170°			**3.9c** 180°	
C	0.01945	0.70642	0.00000	0.01945	0.70642	0.00000	0.01945	0.70642	0.00000	0.01945	0.70642	0.00000	0.01945	0.70642	0.00000
C	0.59701	2.82871	0.18888	0.61149	2.82831	0.14293	0.62192	2.82802	0.09589	0.62820	2.82785	0.04813	0.63030	2.82779	0.00000
C	-0.66645	2.75597	-0.27008	-0.68716	2.75654	-0.20438	-0.70206	2.75695	-0.13713	-0.71105	2.75720	-0.06882	-0.71406	2.75728	0.00000
H	1.24998	3.65122	0.41821	1.28204	3.65034	0.31647	1.30512	3.64970	0.21233	1.31904	3.64932	0.10657	1.32369	3.64919	0.00000
H	-1.40047	3.49270	-0.54452	-1.44222	3.49385	-0.41206	-1.47227	3.49468	-0.27646	-1.49039	3.49518	-0.13876	-1.49644	3.49534	0.00000
C	-0.01945	-0.70642	0.00000	-0.01945	-0.70642	0.00000	-0.01945	-0.70642	0.00000	-0.01945	-0.70642	0.00000	-0.01945	-0.70642	0.00000
C	-0.59701	-2.82871	0.18888	-0.61149	-2.82831	0.14293	-0.62192	-2.82802	0.09589	-0.62820	-2.82785	0.04813	-0.63030	-2.82779	0.00000
C	0.66645	-2.75597	-0.27008	0.68716	-2.75654	-0.20438	0.70206	-2.75695	-0.13713	0.71105	-2.75720	-0.06882	0.71406	-2.75728	0.00000
H	-1.24998	-3.65122	0.41821	-1.28204	-3.65034	0.31647	-1.30512	-3.64970	0.21233	-1.31904	-3.64932	0.10657	-1.32369	-3.64919	0.00000
H	1.40047	-3.49270	-0.54452	1.44222	-3.49385	-0.41206	1.47227	-3.49468	-0.27646	1.49039	-3.49518	-0.13876	1.49644	-3.49534	0.00000
N	1.04379	1.50529	0.36469	1.07175	1.50452	0.27597	1.09188	1.50397	0.18516	1.10402	1.50363	0.09293	1.10807	1.50352	0.00000
N	-1.04379	-1.50529	0.36469	-1.07175	-1.50452	0.27597	-1.09188	-1.50397	0.18516	-1.10402	-1.50363	0.09293	-1.10807	-1.50352	0.00000
O	2.19616	1.16511	0.78736	2.25653	1.16345	0.59583	2.29998	1.16225	0.39975	2.32619	1.16153	0.20064	2.33494	1.16129	0.00000
O	-2.19616	-1.16511	0.78736	-2.25653	-1.16345	0.59583	-2.29998	-1.16225	0.39975	-2.32619	-1.16153	0.20064	-2.33494	-1.16129	0.00000
O	1.03889	-1.45138	-0.39252	1.06898	-1.45221	-0.29703	1.09064	-1.45280	-0.19929	1.10371	-1.45316	-0.10002	1.10807	-1.45328	0.00000
O	-1.03889	1.45138	-0.39252	-1.06898	1.45221	-0.29703	-1.09064	1.45280	-0.19929	-1.10371	1.45316	-0.10002	-1.10807	1.45328	0.00000

Table 6.6 – Total Molecular Energies (Hartrees) calculated with ccsd(t) 6-311++g(d,p) on the DFT optimized structures of 2,2'-bioxazole **3.9c**, **3.9b** and **3.9c**.

Angle (°)	**3.9a**	**3.9b**	**3.9c**
90	-488.2228535	-563.0043741	-637.7869715
100	-488.2230806	-563.0048065	-637.7877221
110	-488.2237822	-563.0055669	-637.7886273
120	-488.2248653	-563.006558	-637.7895533
130	-488.2261751	-563.0076576	-637.7903795
140	-488.2275251	-563.008748	-637.7910558
150	-488.2287406	-563.0097271	-637.7915741
160	-488.2296907	-563.0105091	-637.7919404
170	-488.2302934	-563.0110216	-637.7921662
180	-488.2305007	-563.0112026	-637.7922458

Table 6.7 – Second order perturbative stabilization energies from Natural Bonding Orbital (pop=nbo) calculations

	Donor	**Acceptor**	**Energy (kcal/mol)**
3.1b	O15 (LP1)	BD*(1) S4 - C3	0.64
	O15 (LP2)	BD*(1) S4 - C3	2.70
3.1c	O15 (LP1)	BD*(1) S8 - C10	0.64
	O15 (LP2)	BD*(1) S8 - C10	3.11
	O16 (LP1)	BD*(1) S4 - C3	0.65
	O16 (LP2)	BD*(1) S4 - C3	3.09
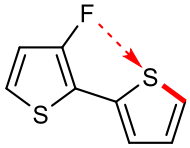	F16 (LP2)	BD*(1) S4 - C3	0.57
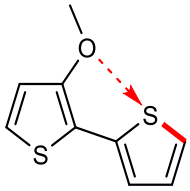	O16 (LP1)	BD*(1) S4 - C3	1.14
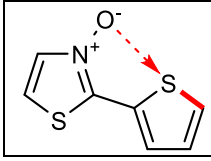	O14 (LP1)	BD*(1) S4 - C3	0.66
	O14 (LP2)	BD*(1) S4 - C3	2.87

Table 6.8 – QTAIM Calculation Summary

Compound	ρ / a.u.	$\nabla^2\rho$ / a.u.
3.1b	0.0199	+0.0622
3.1c	0.0210	+0.0642
	0.0210	+0.0642
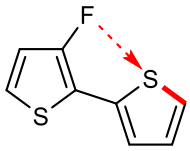	0.0105	+0.0401
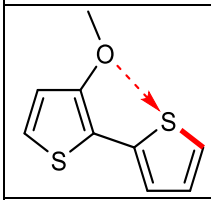	0.0209	+0.0650
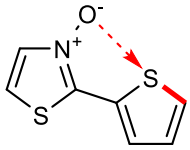	0.0133	+0.0471

Table 6.9 – QTAIM Calculation Structures

Compound	**Charge Densities (ρ)**	**Laplacians ($\nabla^2\rho$)**
3.1b	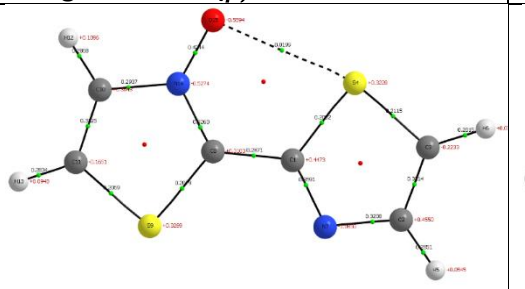	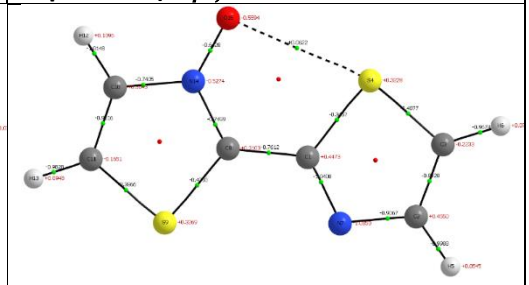
3.1c	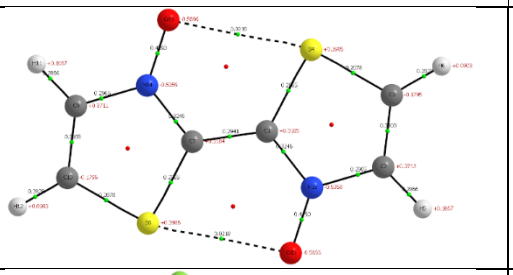	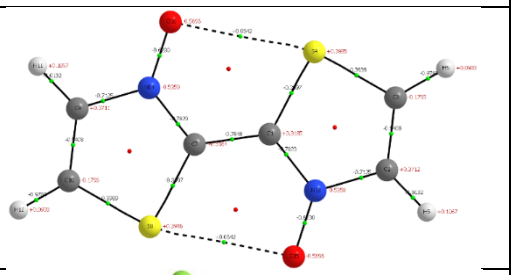
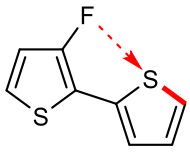	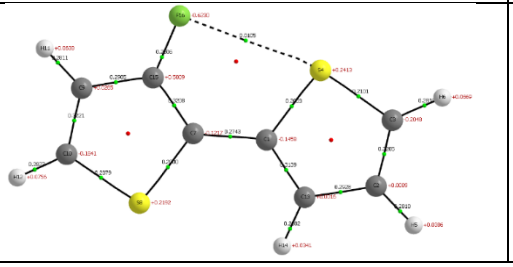	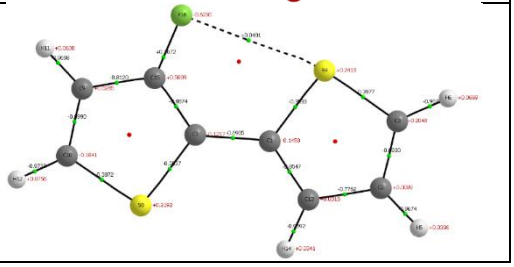

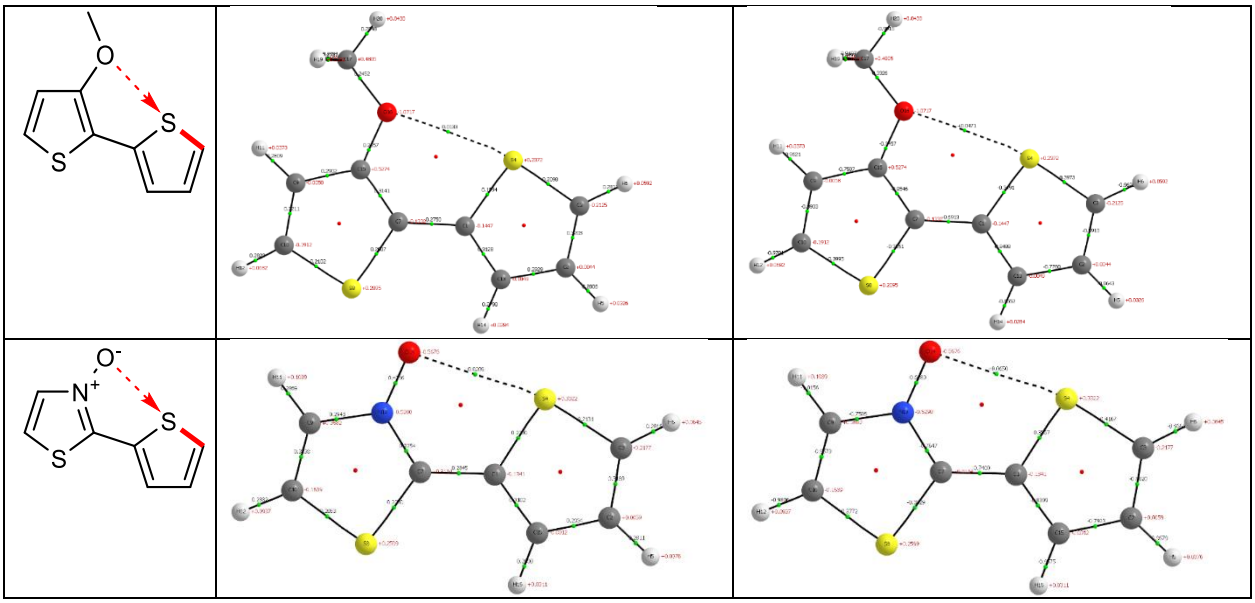

Table 6.10 – Cartesian coordinates for Distortion-Interaction Analysis of 4-Methoxythiazole in the CMD transition state; optimized at the DFT B3LYP 6-311G++(d,p) level of theory.

	Pd Ground (A)				Pd Dist. (B)				4-MeOTz – Pd TS (C)				4-MeOTz – Pd Complex (D)		
Pd	-0.59399	-0.15629	0.004507	Pd	-0.27836	-0.4952	-0.19379	Pd	0.265116	-0.45597	-0.19863	Pd	-0.41101	0.340154	-0.13693
C	3.284976	-1.49847	1.200403	C	3.676867	-0.98884	1.330942	C	2.937616	2.666173	-1.34855	C	-1.39018	-3.69141	-1.20986
C	1.995157	-0.96147	1.203367	C	2.304723	-0.78411	1.195973	C	2.180686	1.496898	-1.29597	C	-1.12535	-2.31987	-1.25329
C	1.329502	-0.69438	0.000377	C	1.715967	-0.6426	-0.06554	C	1.443807	1.163979	-0.15393	C	-0.71559	-1.63244	-0.10391
C	1.989307	-0.96578	-1.20487	C	2.548761	-0.6812	-1.18634	C	1.513578	2.022921	0.945425	C	-0.55663	-2.3556	1.084746
C	3.27914	-1.5028	-1.20626	C	3.921552	-0.8835	-1.05248	C	2.272176	3.191413	0.894878	C	-0.82576	-3.72576	1.127213
C	3.932756	-1.76792	-0.00403	C	4.491081	-1.0452	0.205771	C	2.981984	3.522135	-0.25425	C	-1.2474	-4.39988	-0.01815
H	1.505936	-0.77098	2.153128	H	1.691998	-0.7569	2.090255	H	2.15452	0.854011	-2.16885	H	-1.23324	-1.79381	-2.19612
H	3.769335	-1.71754	-2.1505	H	4.546245	-0.91937	-1.93799	H	2.303014	3.847395	1.757664	H	-0.69542	-4.26775	2.058827
H	4.933581	-2.18524	-0.0057	H	5.556992	-1.20751	0.309133	H	3.567169	4.432678	-0.29503	H	-1.45158	-5.46444	0.015192
H	3.779773	-1.70982	2.143012	H	4.108824	-1.10782	2.31851	H	3.490907	2.909233	-2.24901	H	-1.7031	-4.20504	-2.11367
H	1.495561	-0.77859	-2.15294	H	2.129069	-0.57776	-2.17994	H	0.954865	1.799822	1.84661	H	-0.20409	-1.85572	1.980128
P	0.067793	1.991594	-0.00279	P	-0.23572	1.794075	0.060107	P	1.969962	-1.85075	0.476013	P	-2.71787	0.774059	0.212141
C	1.05533	2.560736	1.437667	C	-1.07795	2.432401	1.555925	C	2.449215	-3.14271	-0.7304	C	-3.53718	1.619905	-1.20787
H	1.991801	2.003249	1.475897	H	-0.48825	2.175671	2.437061	H	2.965001	-2.67571	-1.5706	H	-3.51383	0.966608	-2.08213
H	1.2684	3.63038	1.362224	H	-1.20098	3.51702	1.51391	H	3.107831	-3.88787	-0.27844	H	-4.57577	1.87404	-0.97809
H	0.500525	2.368565	2.357586	H	-2.05576	1.959333	1.641852	H	1.549588	-3.63179	-1.10289	H	-2.98509	2.530675	-1.44574
C	-1.4002	3.097753	-0.0028	C	-1.18854	2.529976	-1.31899	C	1.375356	-2.8071	1.919332	C	-3.03733	1.933723	1.609993
H	-2.00797	2.890351	0.879139	H	-2.17708	2.072619	-1.34418	H	0.438489	-3.29546	1.653246	H	-2.46317	2.847026	1.448414
H	-1.10035	4.149206	-0.00491	H	-1.28451	3.612205	-1.20541	H	2.107112	-3.55577	2.231342	H	-4.09996	2.178334	1.692801
H	-2.01019	2.88748	-0.88253	H	-0.68131	2.308689	-2.25868	H	1.185097	-2.12126	2.745581	H	-2.70064	1.477496	2.542891
C	1.050168	2.553759	-1.44951	C	1.3316	2.7354	0.028314	C	3.578147	-1.1953	1.04849	C	-3.85146	-0.62839	0.570883
H	0.491646	2.358107	-2.36644	H	1.902823	2.467702	-0.8605	H	3.414322	-0.44008	1.817091	H	-3.51534	-1.1444	1.471632
H	1.2644	3.623539	-1.37951	H	1.130555	3.808943	0.022625	H	4.194428	-2.00055	1.45434	H	-4.8774	-0.27764	0.710648
H	1.986039	1.995353	-1.48893	H	1.938087	2.48117	0.897499	H	4.101576	-0.71475	0.222028	H	-3.81625	-1.34519	-0.25062
O	-2.80629	-0.14864	0.012119	O	-2.49022	-0.29402	-0.12481	O	-0.93722	-2.31074	-0.42609	O	-0.17935	2.625705	-0.14653
C	-2.79997	-1.42055	0.012243	C	-3.21987	-1.2964	0.063462	C	-2.01143	-2.30345	-1.0731	C	0.867775	3.272066	-0.1562
O	-1.69742	-2.04981	0.014482	O	-2.79424	-2.49499	0.151678	O	-2.54459	-1.26153	-1.57876	O	2.06221	2.727637	-0.19537
C	-4.09787	-2.18538	-0.01747	C	-4.71322	-1.10937	0.191222	C	-2.75748	-3.60027	-1.28059	C	0.8908	4.774976	-0.12371
H	-4.91152	-1.57471	0.373357	H	-4.98244	-0.05871	0.11459	H	-2.22564	-4.43287	-0.82653	H	-0.12349	5.166747	-0.09973
H	-4.32679	-2.44686	-1.05494	H	-5.21184	-1.67732	-0.59557	H	-3.75226	-3.51305	-0.84124	H	1.444424	5.111502	0.755921
H	-4.00362	-3.11231	0.548998	H	-5.05194	-1.51713	1.144979	H	-2.89297	-3.7766	-2.34886	H	1.418254	5.150731	-1.00337
	4-MeOTz Ground (A)				4-MeOTz Dist. (B)			C	-2.23552	1.081925	0.739258	C	2.550937	-0.48055	0.534232
C	-1.09031	C	-1.09031	C	0.481276	-0.27805	-0.05664	C	-1.49633	0.821349	-0.42133	C	1.59628	-0.12511	-0.40458
C	0.498673	C	0.498673	C	-0.57672	-1.19489	-0.09304	S	-1.58923	2.293074	-1.3459	S	2.296016	-0.5363	-1.95719
C	-0.57048	C	-0.57048	S	-2.0142	-0.21612	-0.02177	C	-2.54701	3.045149	-0.15097	C	3.755308	-1.08075	-1.19812
S	-2.0354	S	-2.0354	C	-1.09613	1.220374	0.044831	N	-2.81187	2.299764	0.895208	N	3.747184	-0.99136	0.103367
H	-1.56374	H	-1.56374	N	0.203698	1.047578	0.016157	H	-2.90213	4.061528	-0.25028	H	4.598166	-1.45039	-1.76708
H	-0.56504	H	-0.56504	H	-1.5554	2.197581	0.10092	H	-1.98874	-0.26203	-1.10625	H	1.974307	1.726272	-0.23098
N	0.199536	N	0.199536	H	-0.50369	-2.09803	0.938607	O	-2.39515	0.131677	1.676925	O	2.325842	-0.32041	1.866063
O	1.776281	O	1.776281	O	1.756578	-0.70366	-0.06797	C	-3.21121	0.435266	2.810875	C	3.393383	-0.661	2.753921
C	2.80605	C	2.80605	C	2.793784	0.275074	0.033286	H	-3.14235	-0.43735	3.456389	H	3.011656	-0.46036	3.754641
H	3.741449	H	3.741449	H	3.723692	-0.28053	-0.064	H	-2.84161	1.318678	3.332879	H	3.66493	-1.71484	2.658665
H	2.739938	H	2.739938	H	2.712675	1.014208	-0.76459	H	-4.248	0.604406	2.513868	H	4.279161	-0.05052	2.560656
H	2.743212	H	2.743212	H	2.758185	0.785889	0.997424								

6.8 NMR Spectral Data of All Compounds

Table 6.11 – Index of NMR spectral data.

2.1

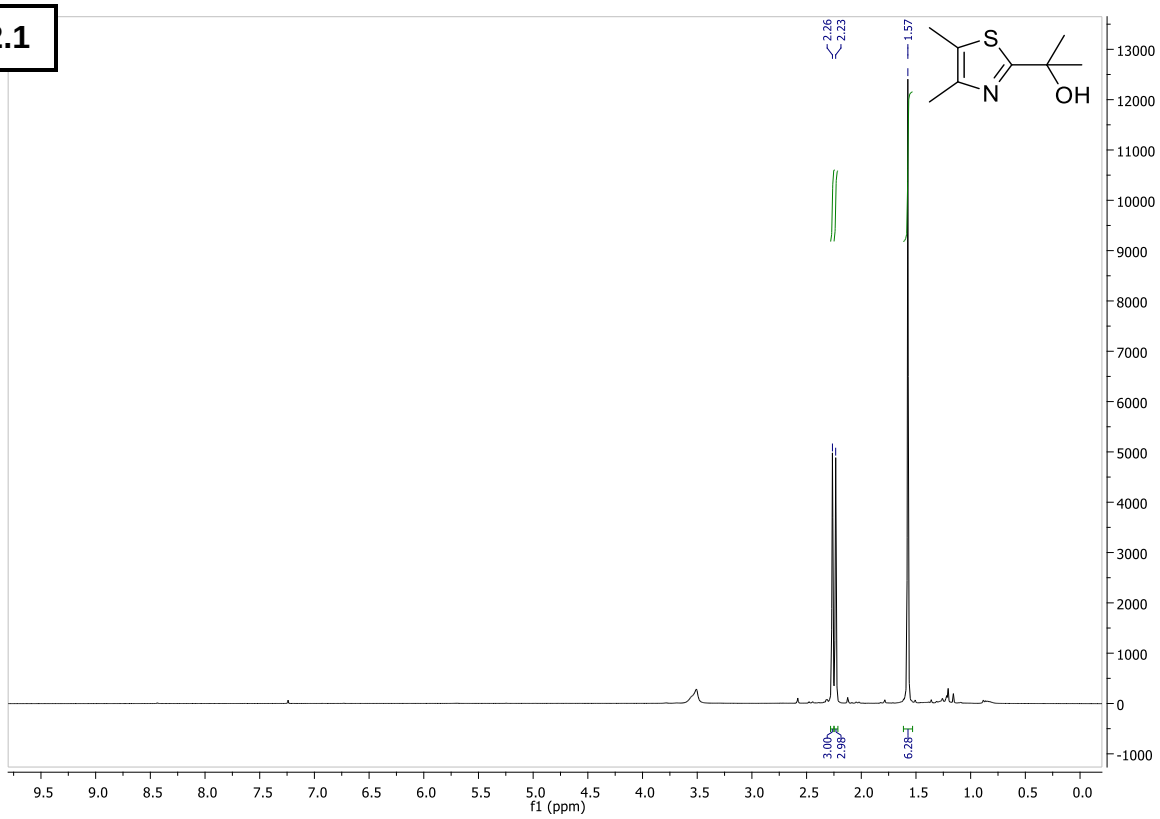
2.26
2.23
1.57
S
N
OH
3.00
2.98
6.28
f1 (ppm)

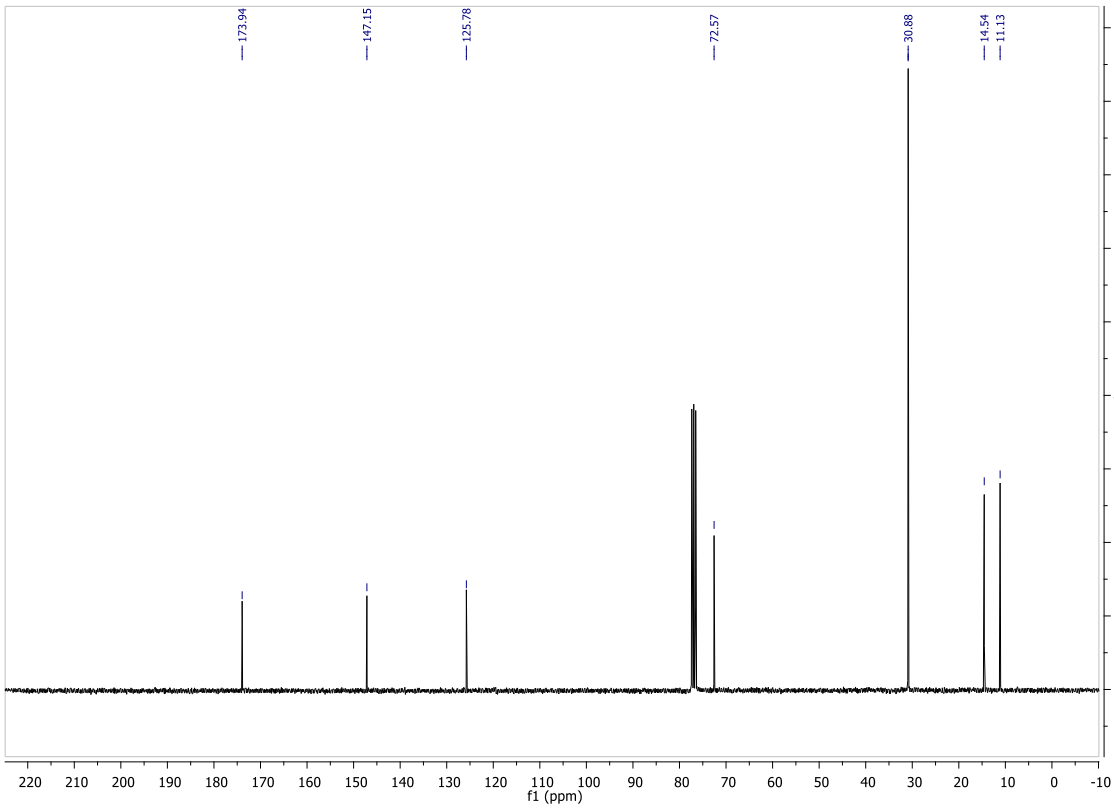
173.94
147.15
125.78
72.57
30.88
14.54
11.13
f1 (ppm)

2.2

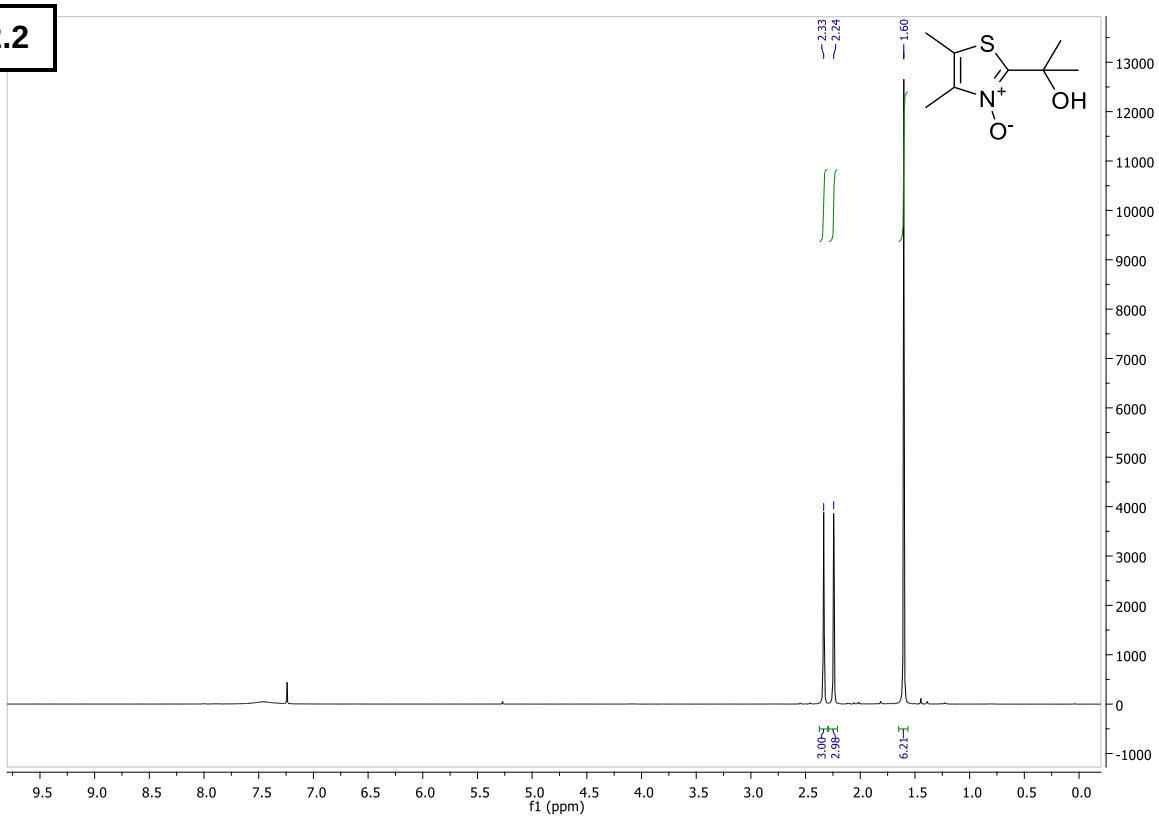
2.33
2.24
1.60
S
N+
O-
OH
3.00
2.98
6.21
f1 (ppm)

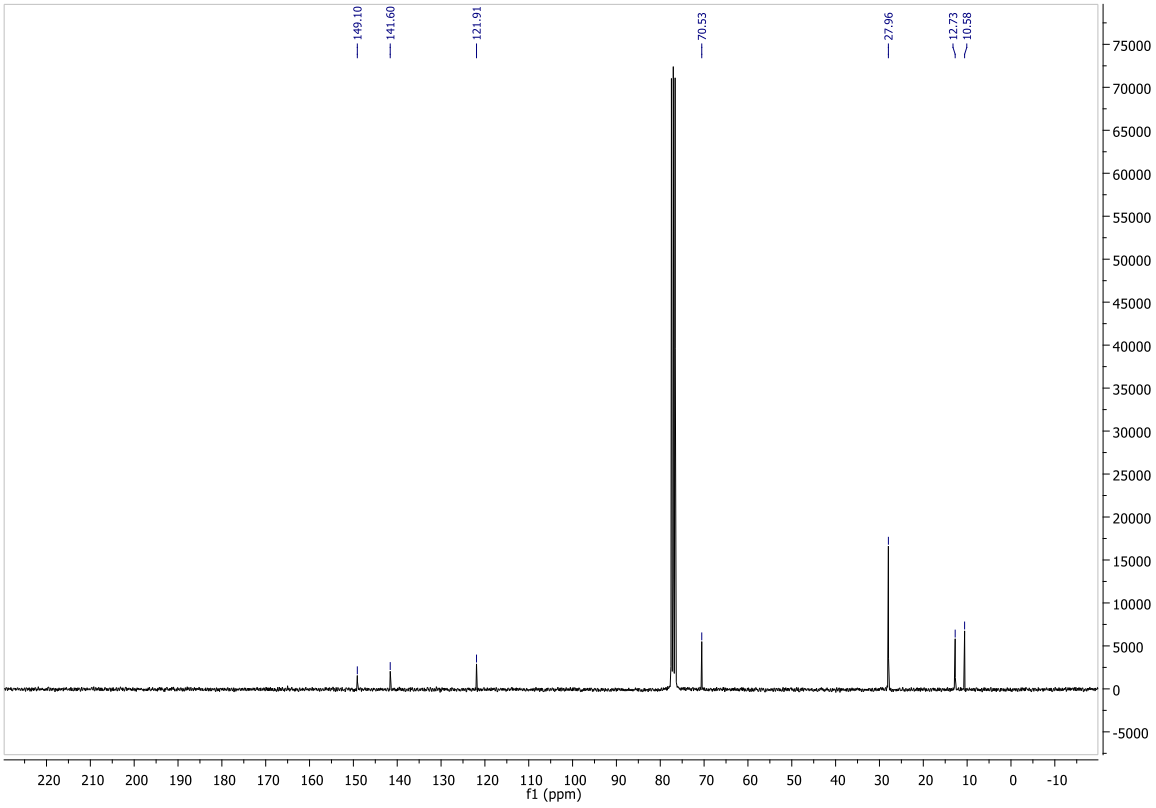
149.10
141.60
121.91
70.53
27.96
12.73
10.58
f1 (ppm)

2.3

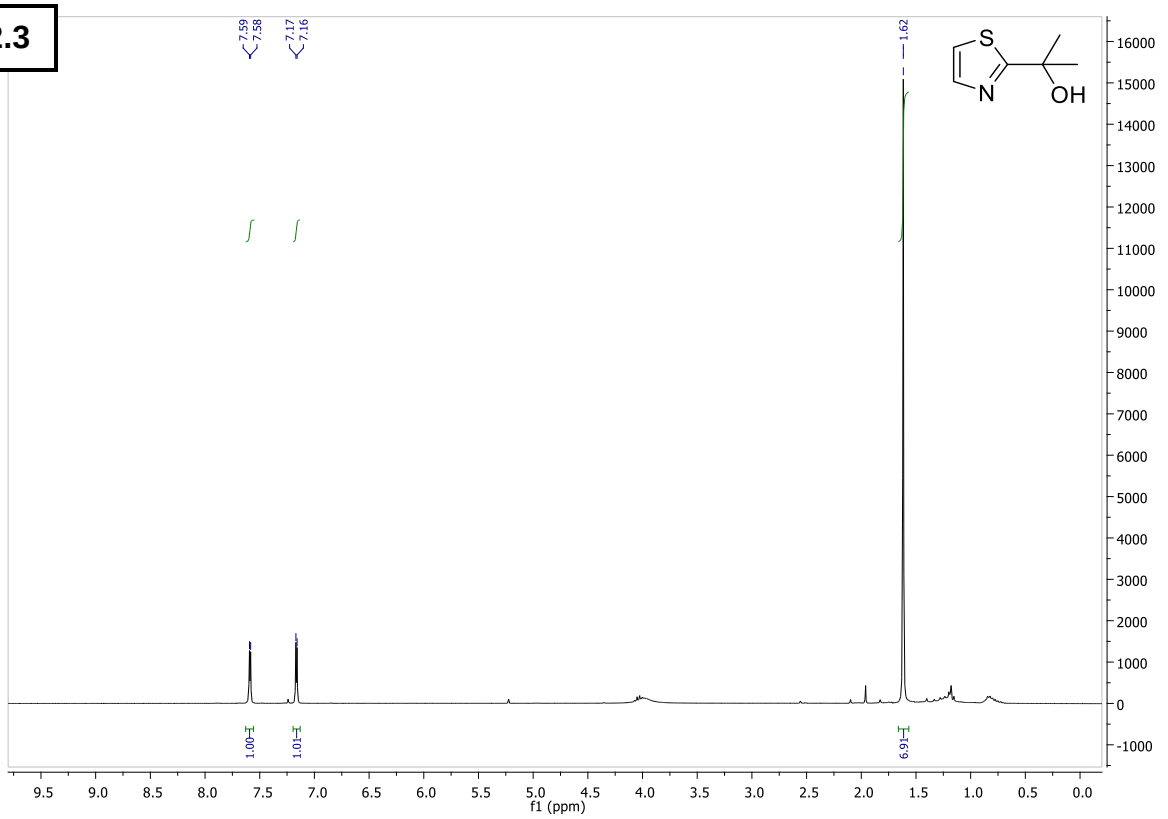
7.59
7.58
7.17
7.16
1.62
S
N
OH
1.00
1.01
6.91
f1 (ppm)

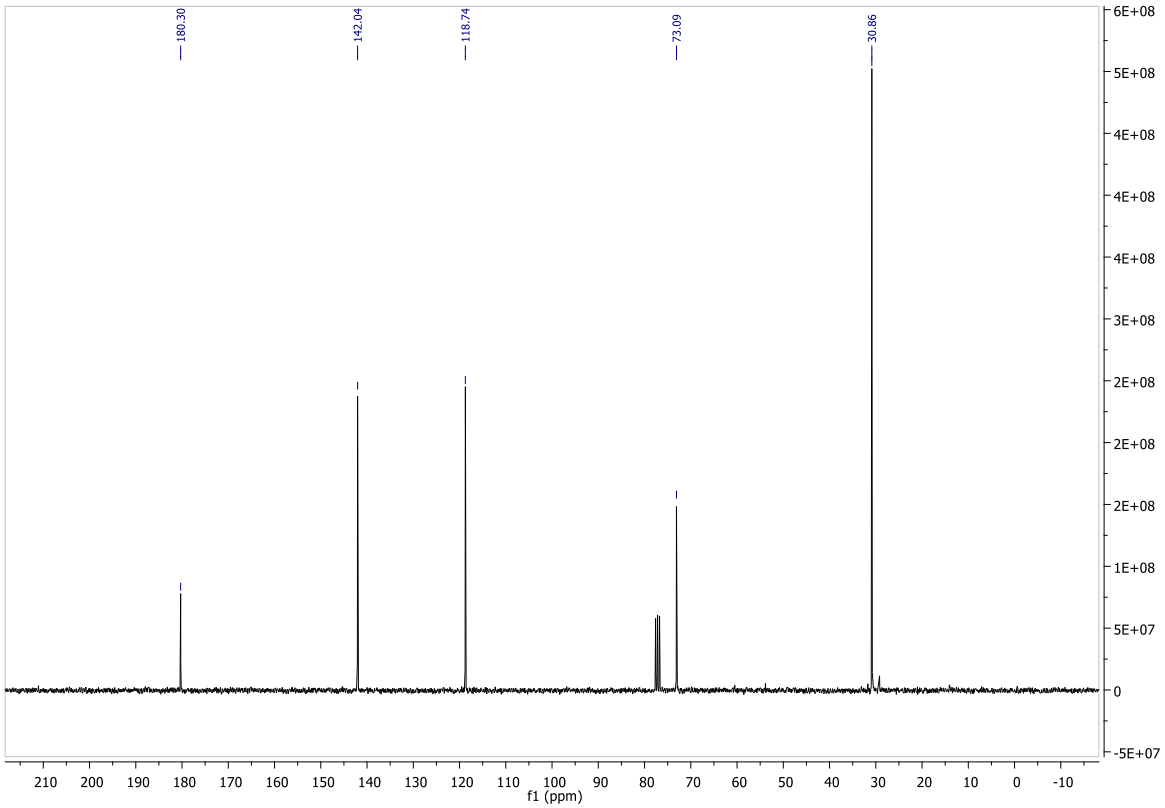
180.30
142.04
118.74
73.09
30.86
f1 (ppm)

2.4

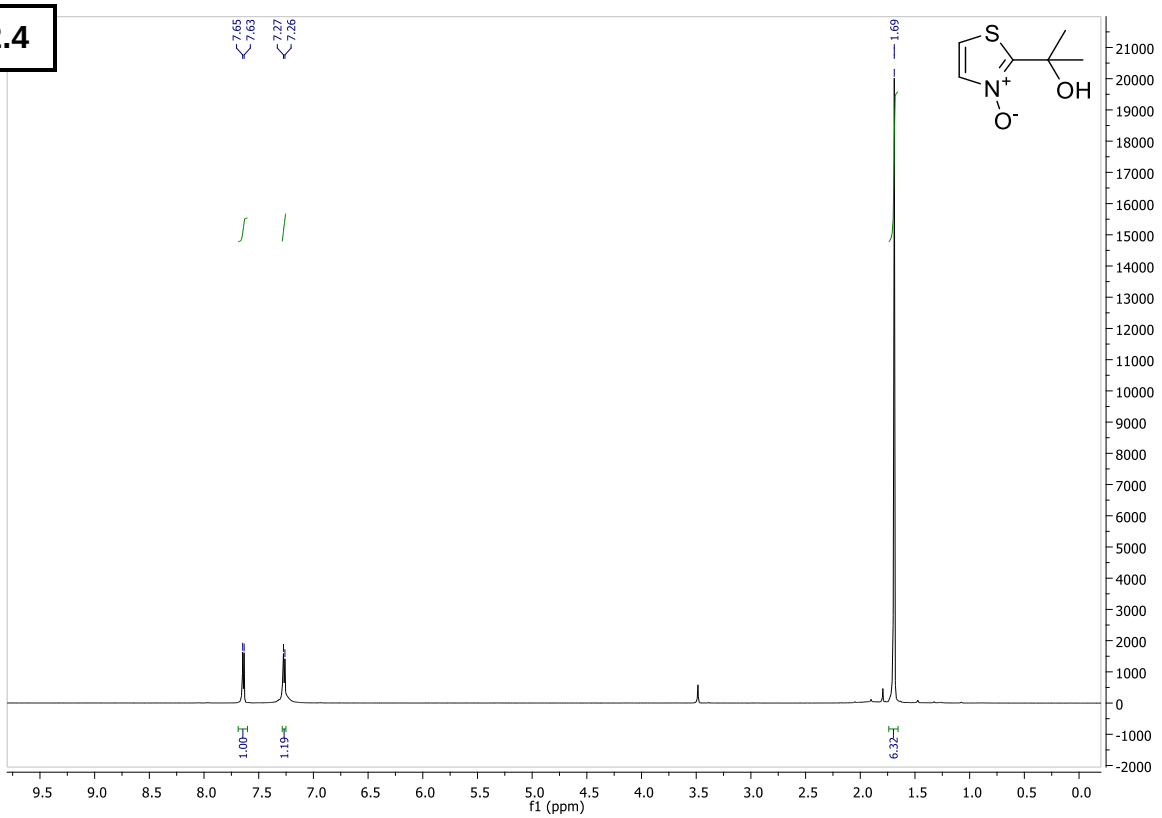
7.65
7.63
7.27
7.26
1.69
1.00
1.19
6.32
f1 (ppm)

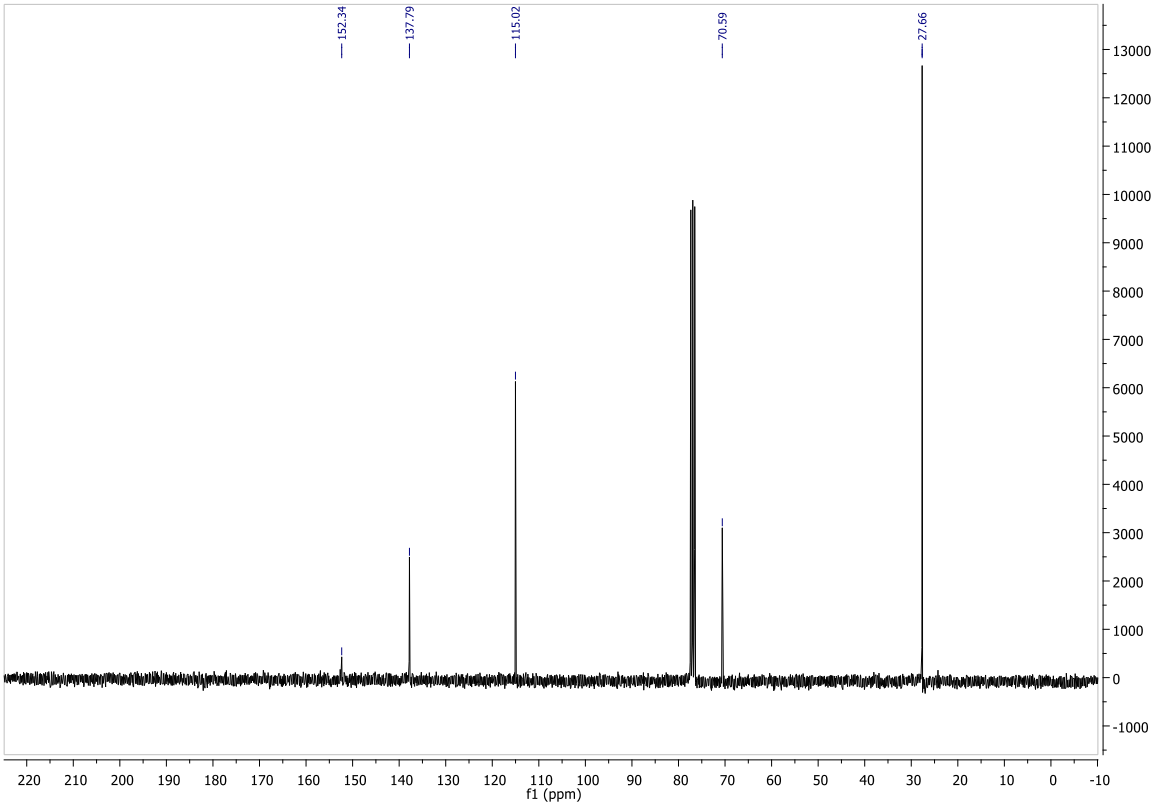
152.34
137.79
115.02
70.59
27.66
f1 (ppm)

2.5

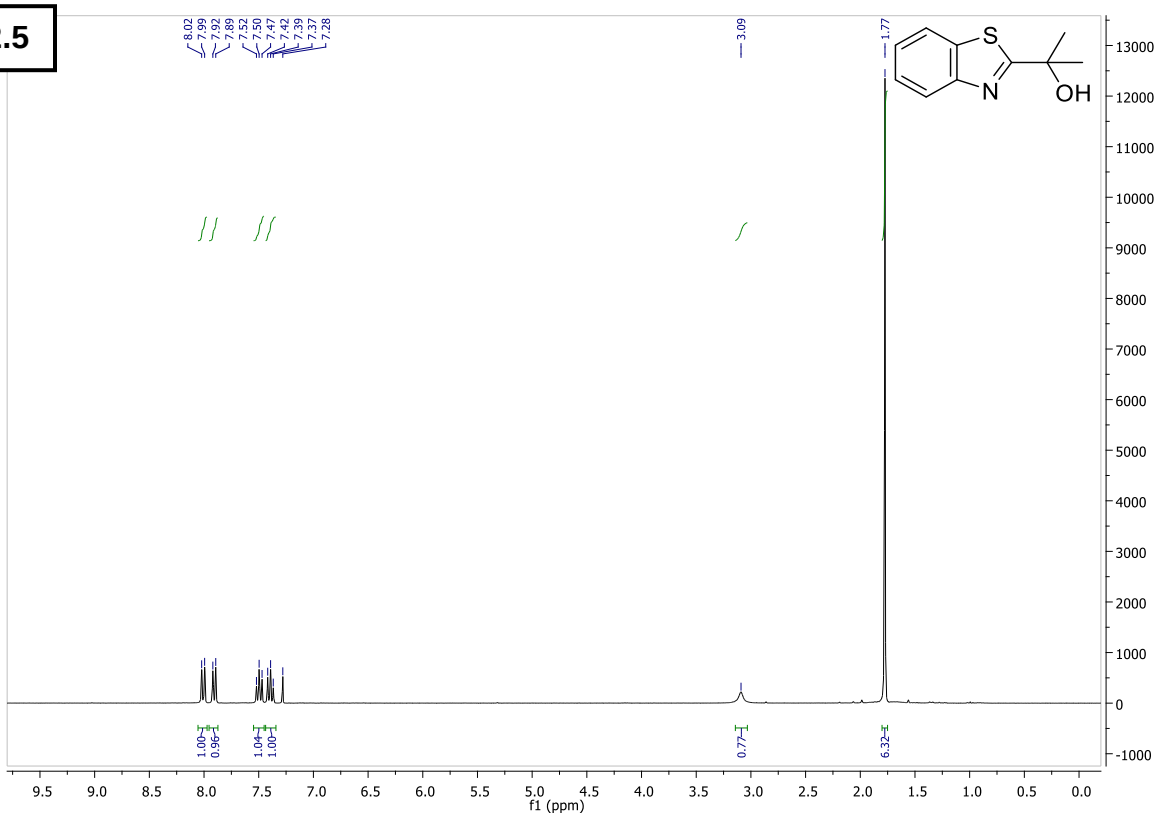
8.02
7.99
7.92
7.89
7.52
7.50
7.47
7.42
7.39
7.37
7.28
3.09
1.77
S
N
OH
1.00
0.96
1.04
1.00
0.77
6.32
f1 (ppm)

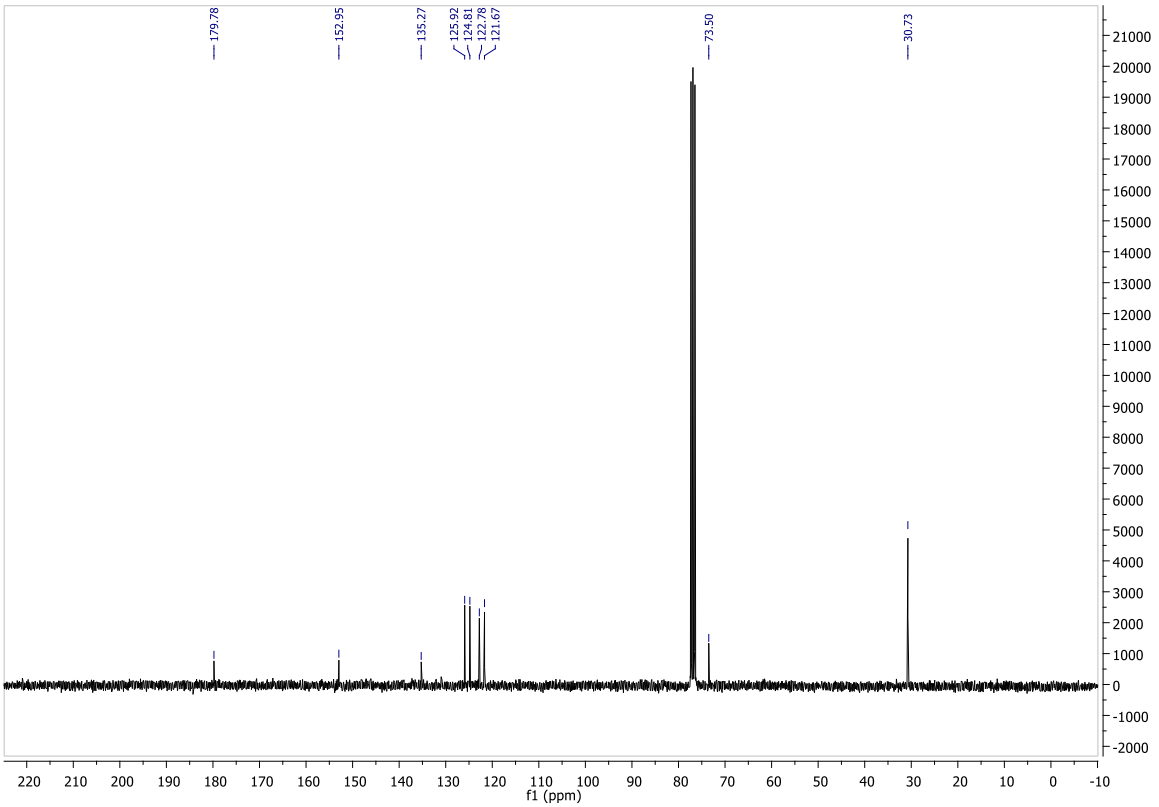
179.78
152.95
135.27
125.92
124.81
122.78
121.67
73.50
30.73
f1 (ppm)

2.6

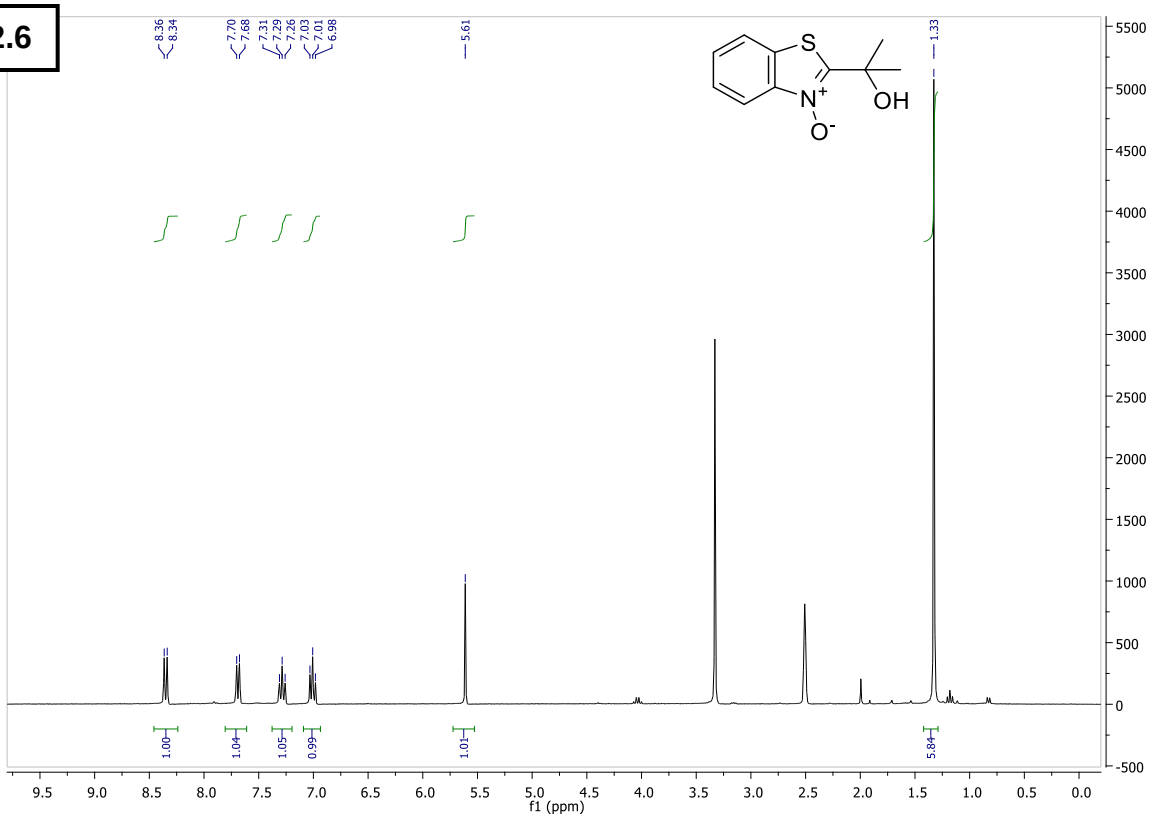
8.36
8.34
7.70
7.68
7.31
7.29
7.26
7.03
7.01
6.98
5.61
1.33
S
N+
O-
OH
1.00
1.04
1.05
0.99
1.01
5.84
f1 (ppm)

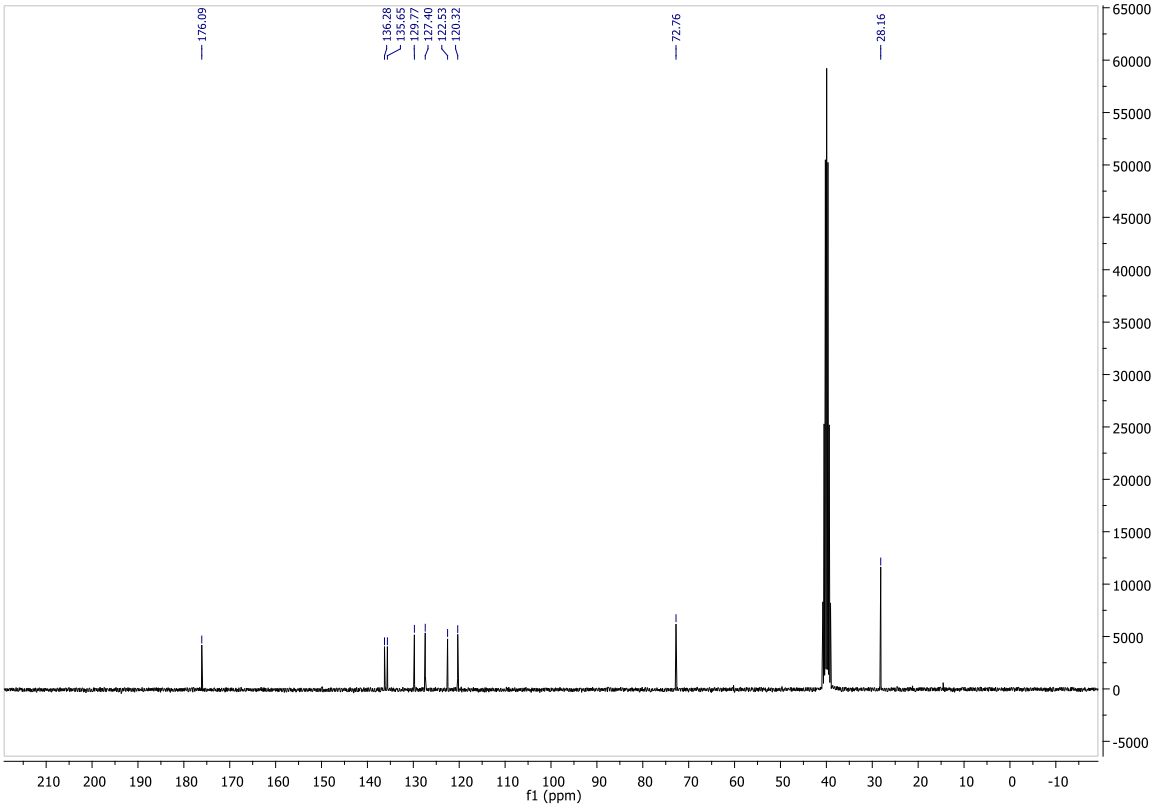
176.09
136.28
135.65
129.77
127.40
122.53
120.32
72.76
28.16
f1 (ppm)

2.7

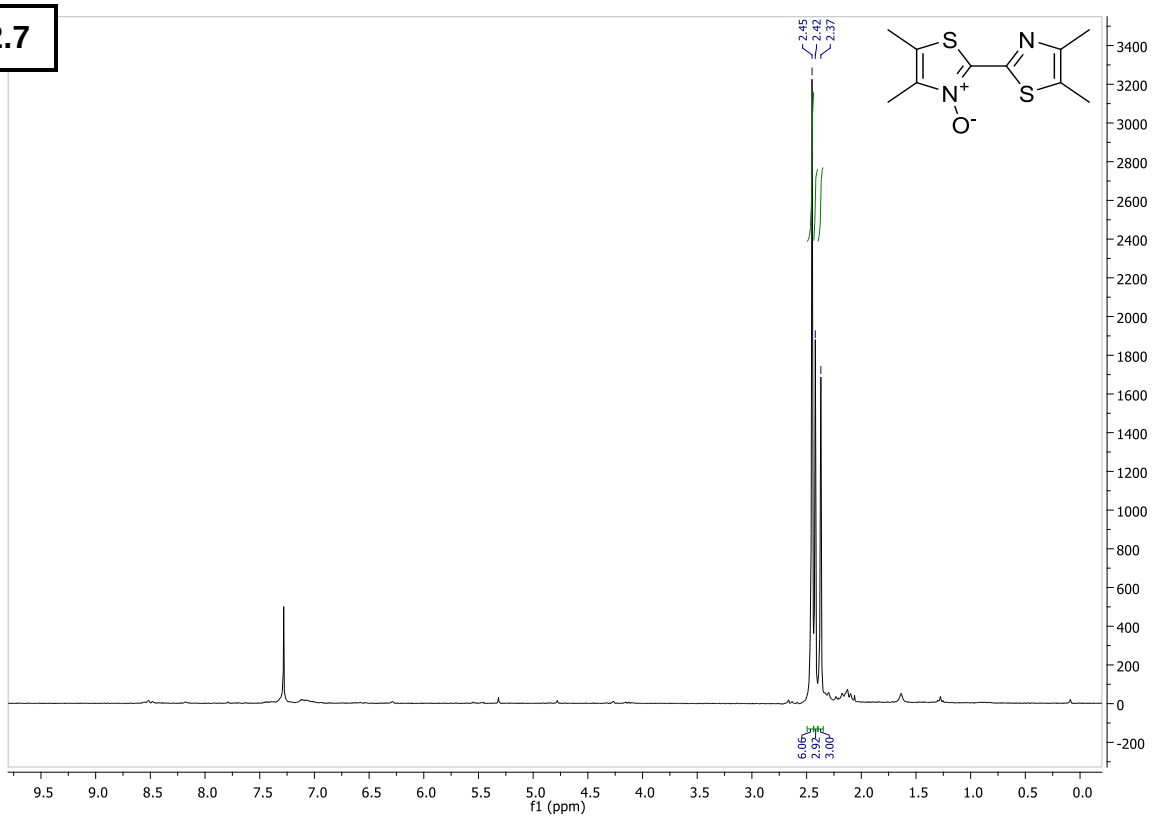

2.8

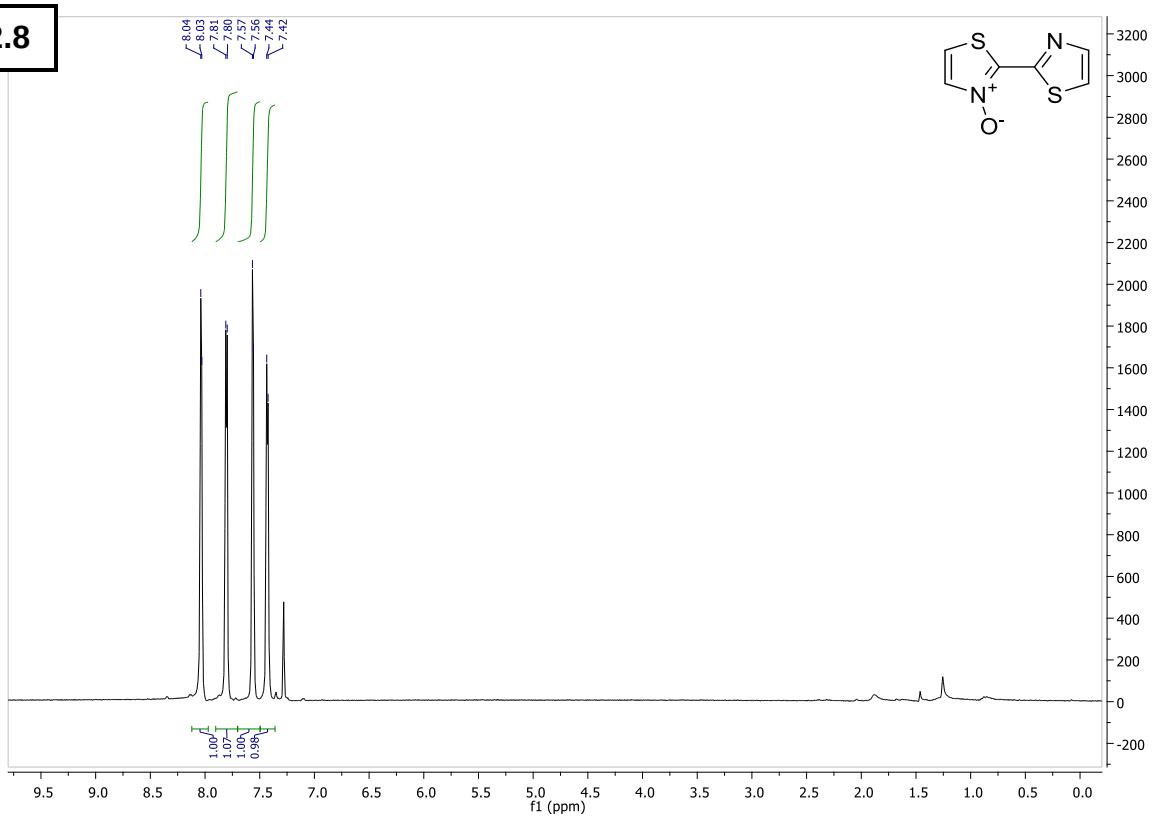
8.04
8.03
7.81
7.80
7.57
7.56
7.44
7.42
1.00
1.07
1.06
0.98
f1 (ppm)

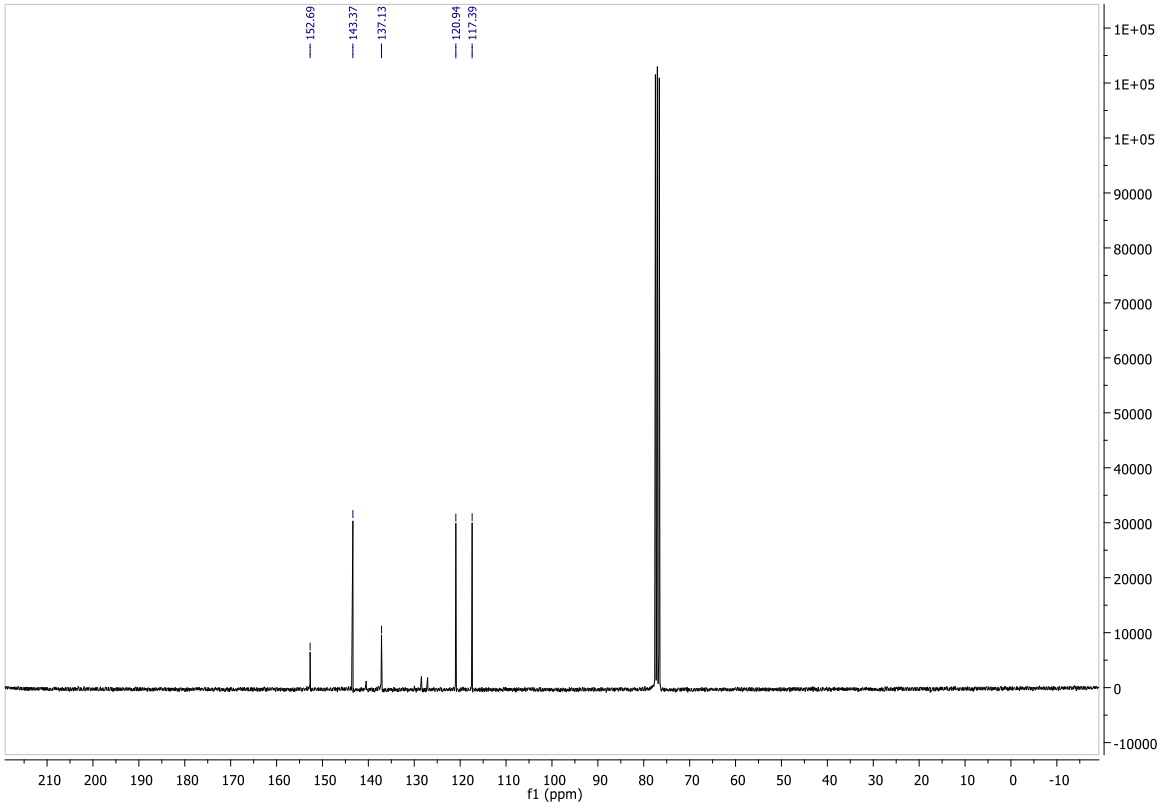
152.69
143.37
137.13
120.94
117.39
f1 (ppm)

2.9

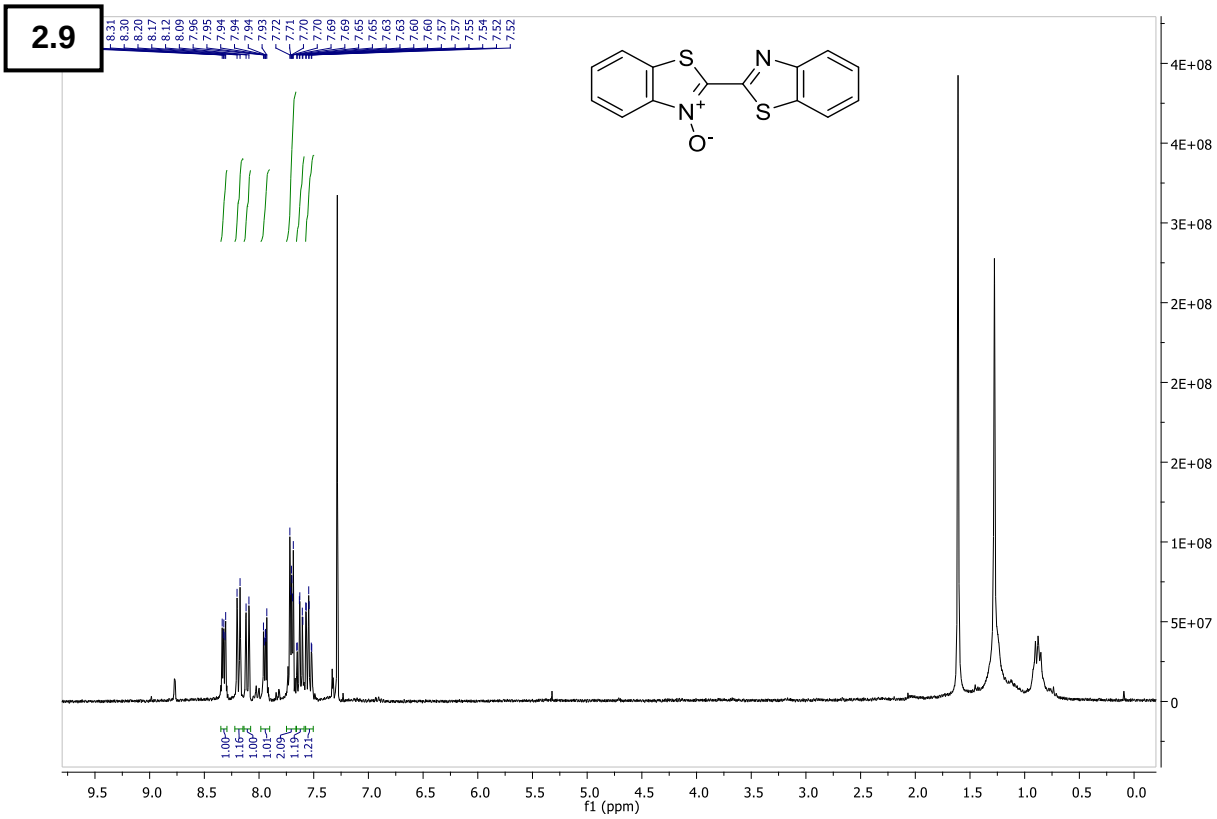
8.31
8.30
8.20
8.17
8.12
8.09
7.96
7.95
7.94
7.94
7.94
7.93
7.72
7.71
7.70
7.70
7.69
7.69
7.65
7.65
7.63
7.63
7.60
7.60
7.57
7.57
7.55
7.54
7.52
7.52
S
N
N+
O-
S
4E+08
4E+08
3E+08
2E+08
2E+08
2E+08
1E+08
5E+07
0
1.00
1.16
1.00
1.01
2.09
1.19
1.21
9.5
9.0
8.5
8.0
7.5
7.0
6.5
6.0
5.5
5.0
4.5
4.0
3.5
3.0
2.5
2.0
1.5
1.0
0.5
0.0
f1 (ppm)

2.10a

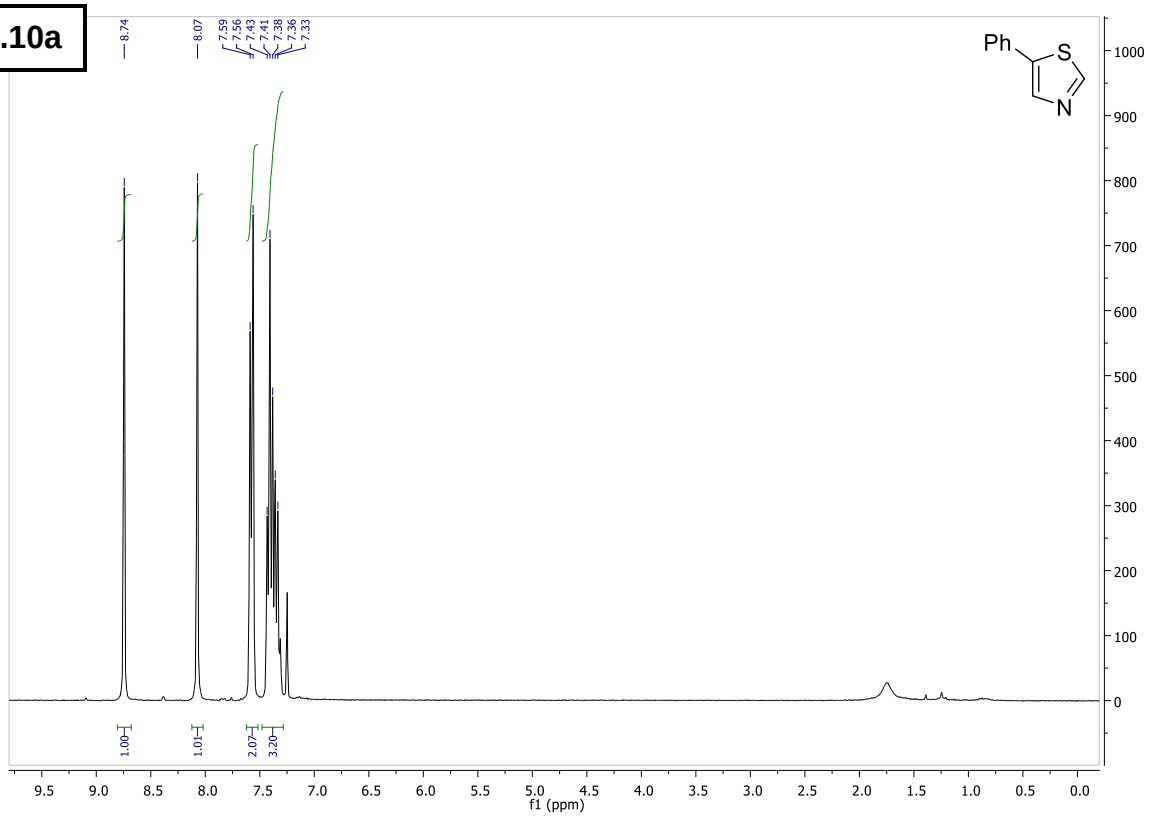
8.74
8.07
7.59
7.56
7.43
7.41
7.38
7.36
7.33
Ph
S
N
1.00
1.01
2.07
3.20
f1 (ppm)

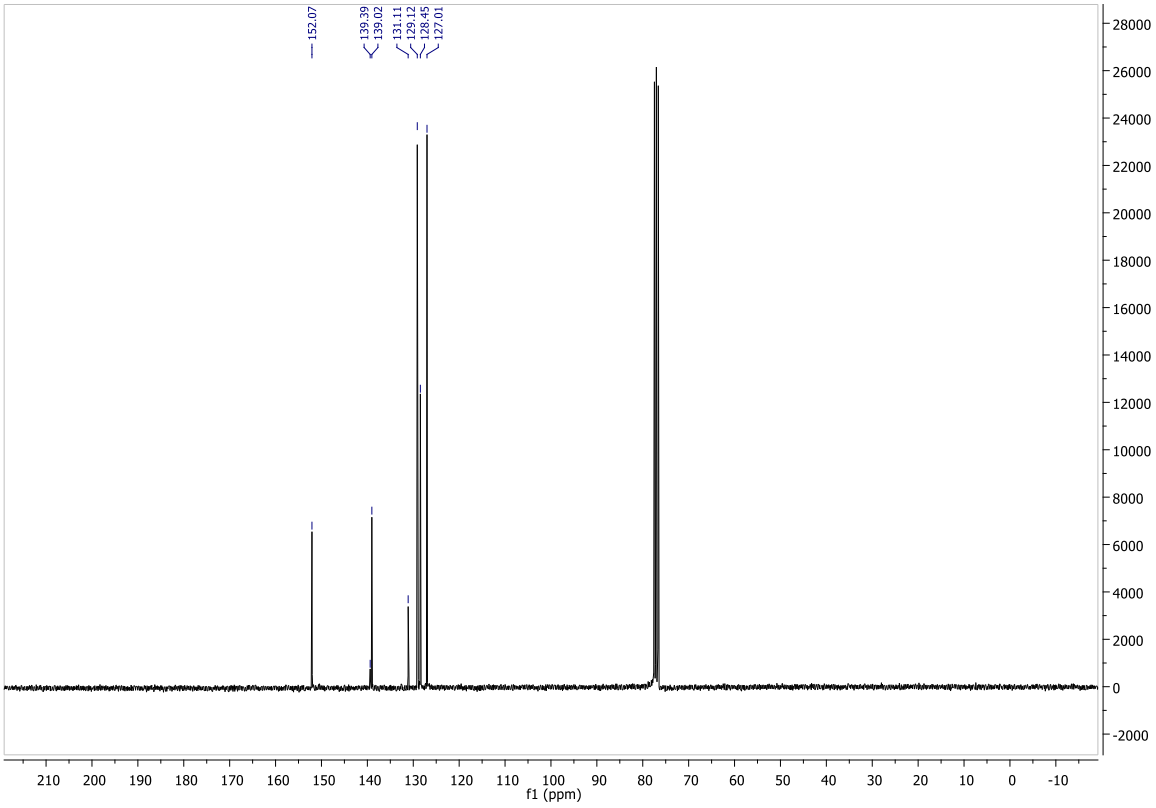
152.07
139.39
139.02
131.11
129.12
128.45
127.01
f1 (ppm)

2.10b

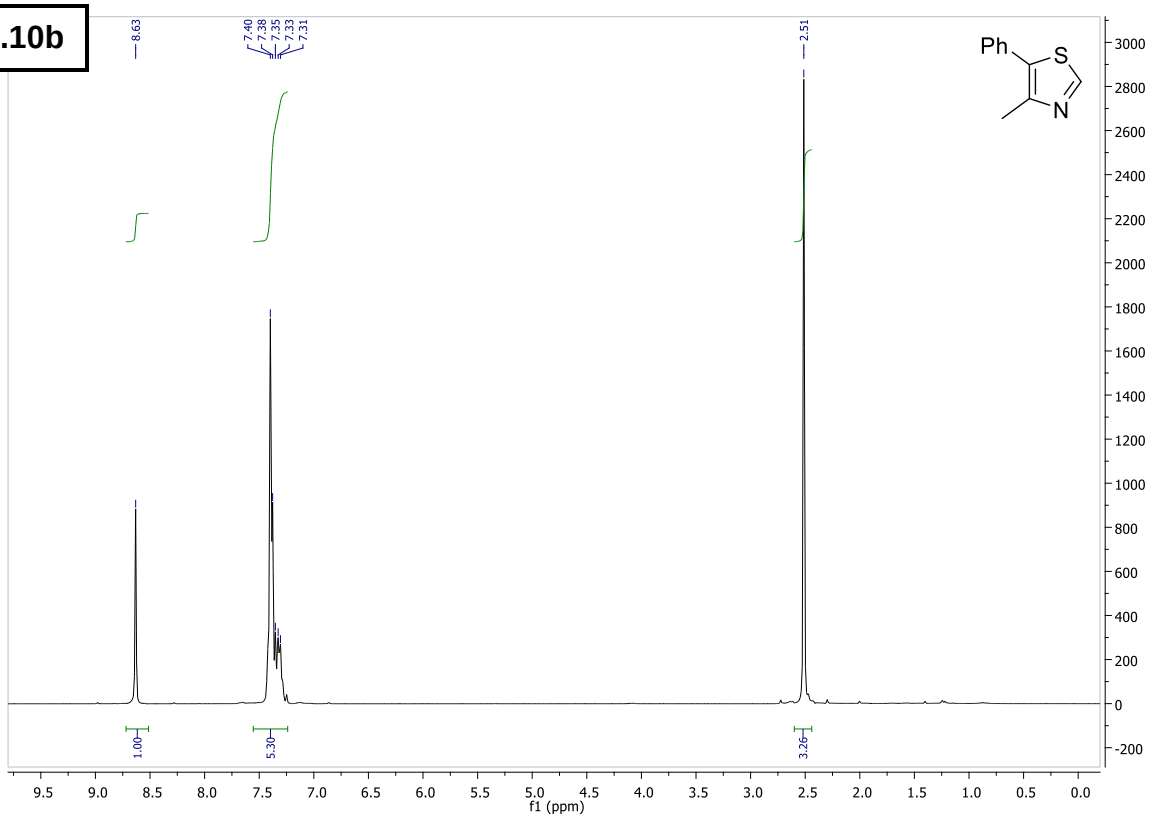
8.63
7.40
7.38
7.35
7.33
7.31
2.51
Ph
S
N
1.00
5.30
3.26
f1 (ppm)

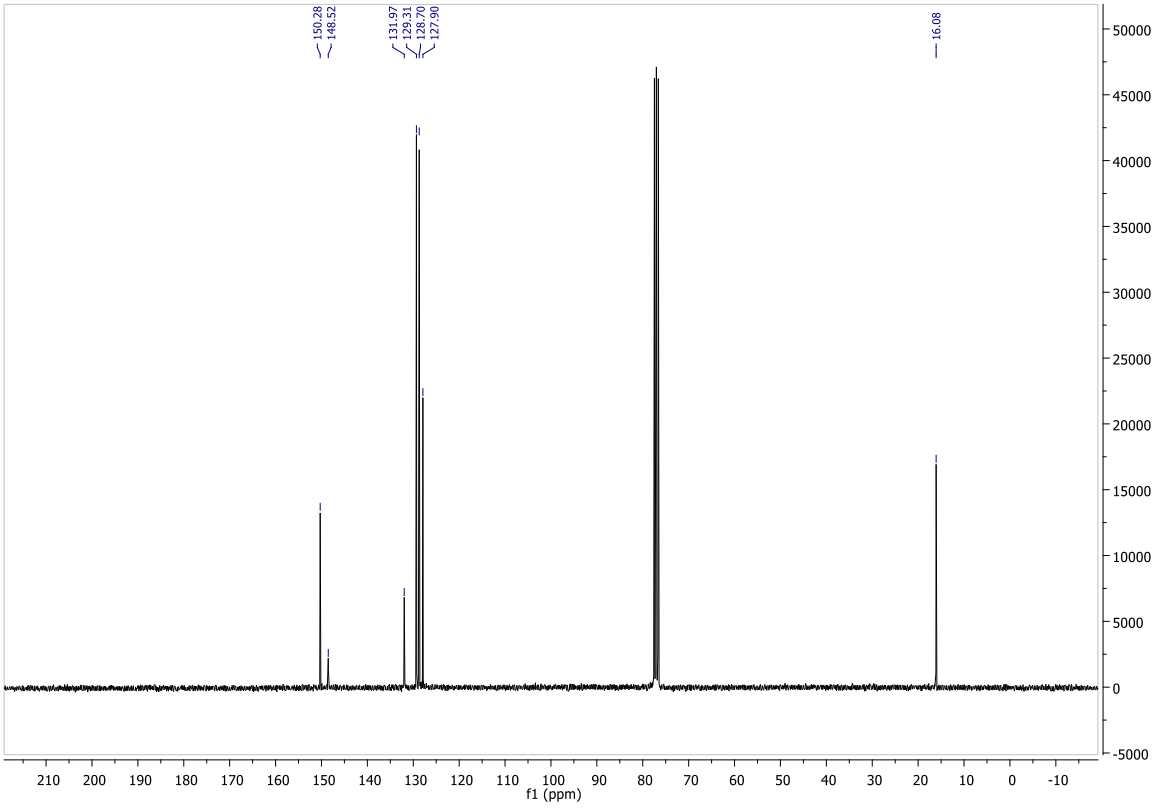
150.28
148.52
131.97
129.31
128.70
127.90
16.08
f1 (ppm)

2.10c

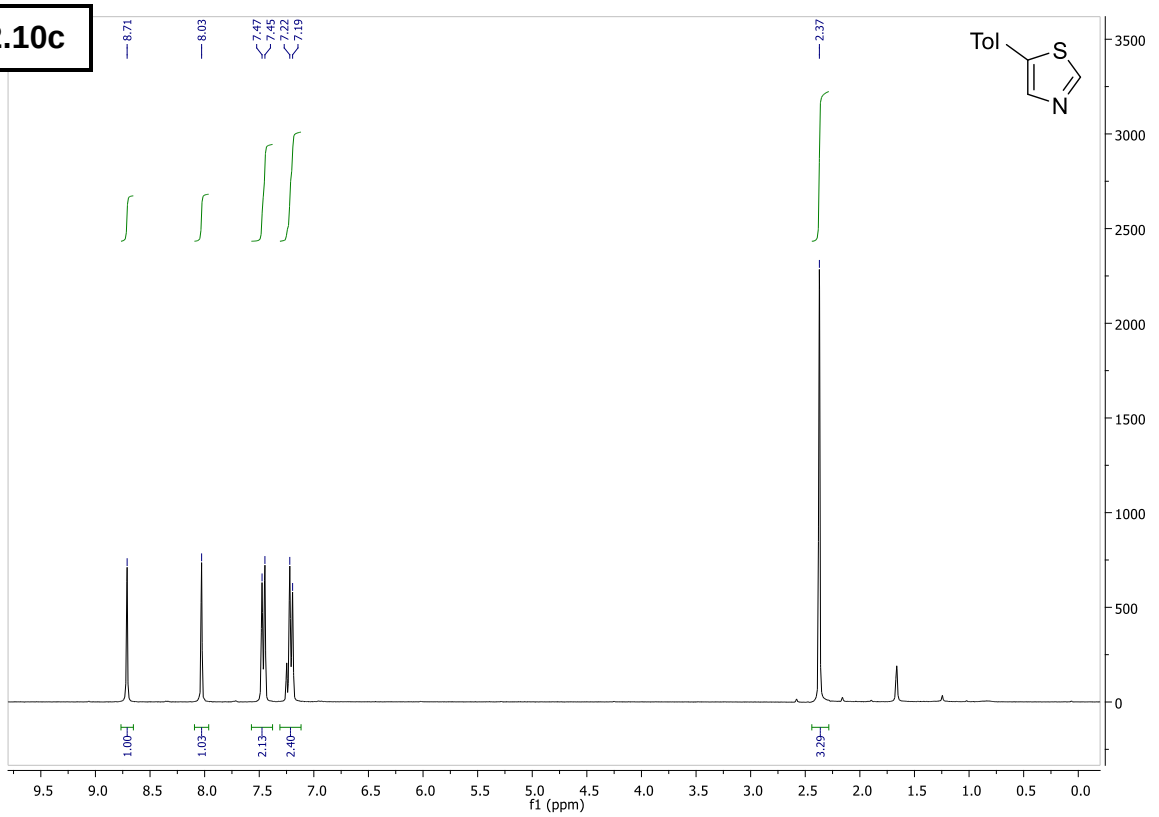
8.71
8.03
7.47
7.45
7.22
7.19
2.37
Tol
S
N
1.00
1.03
2.13
2.40
3.29
f1 (ppm)

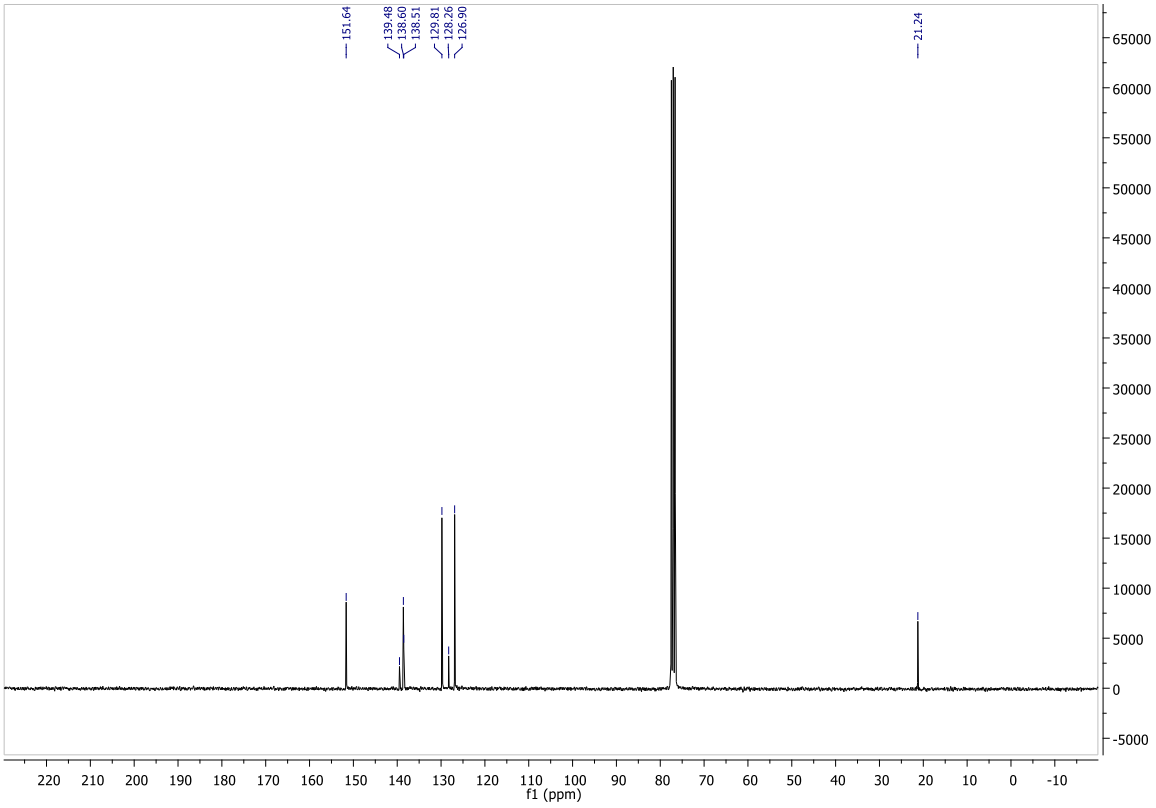
151.64
139.48
138.60
138.51
129.81
128.26
126.90
21.24
f1 (ppm)

2.10d

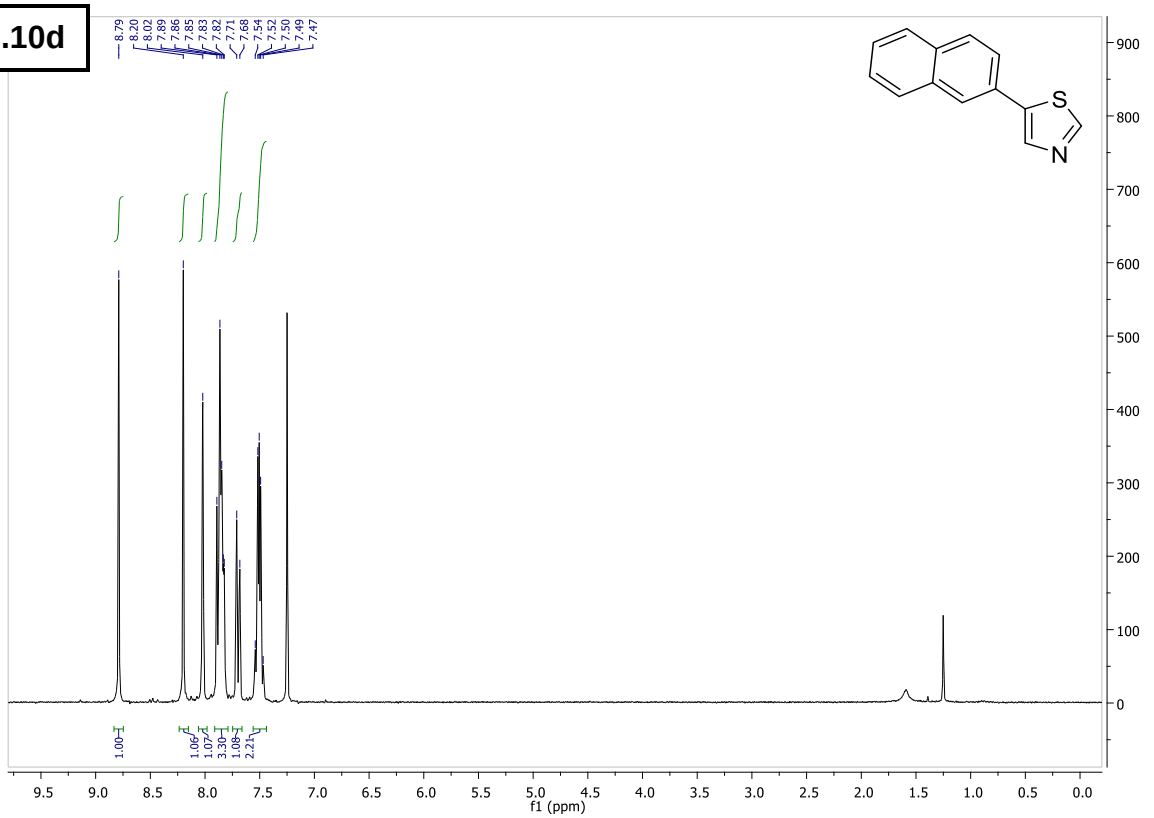
8.79
8.20
8.02
7.89
7.86
7.85
7.83
7.82
7.71
7.68
7.54
7.52
7.50
7.49
7.47
S
N
1.00
1.06
1.07
3.30
1.08
2.21
f1 (ppm)

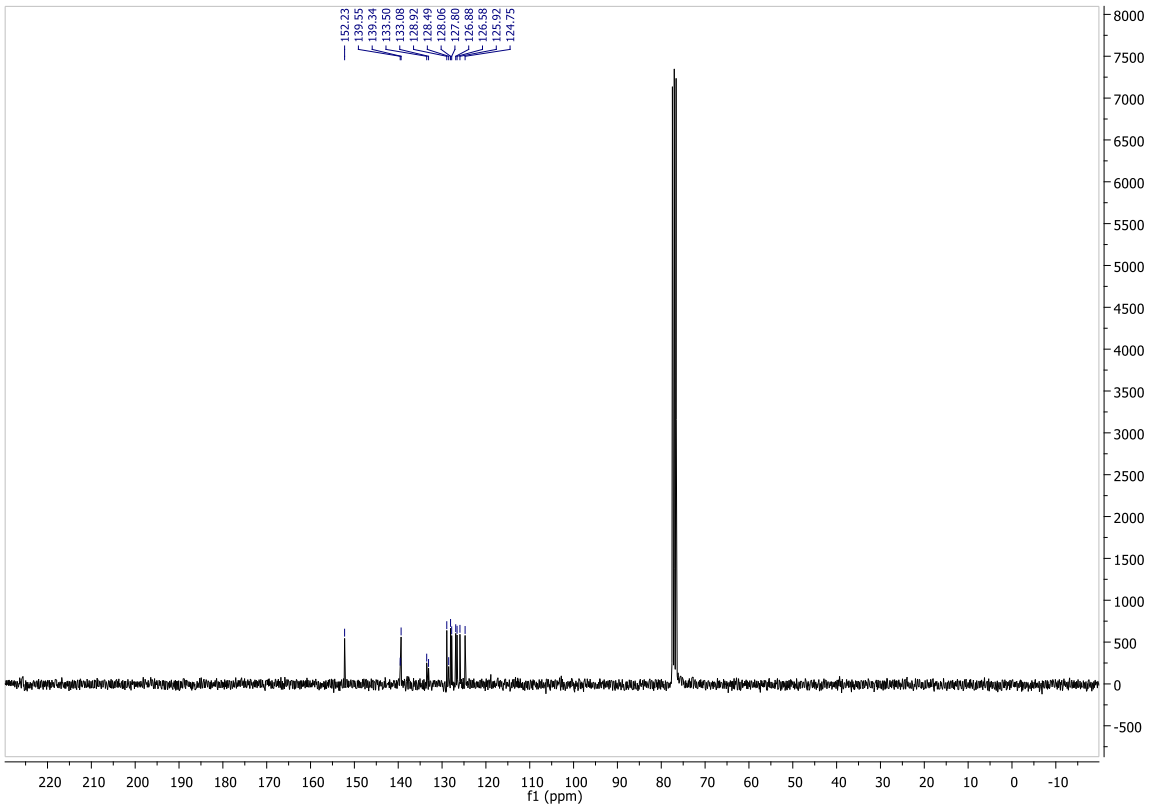
152.23
139.55
139.34
133.50
133.08
128.92
128.49
128.06
127.80
126.88
126.58
125.92
124.75
f1 (ppm)

2.10e

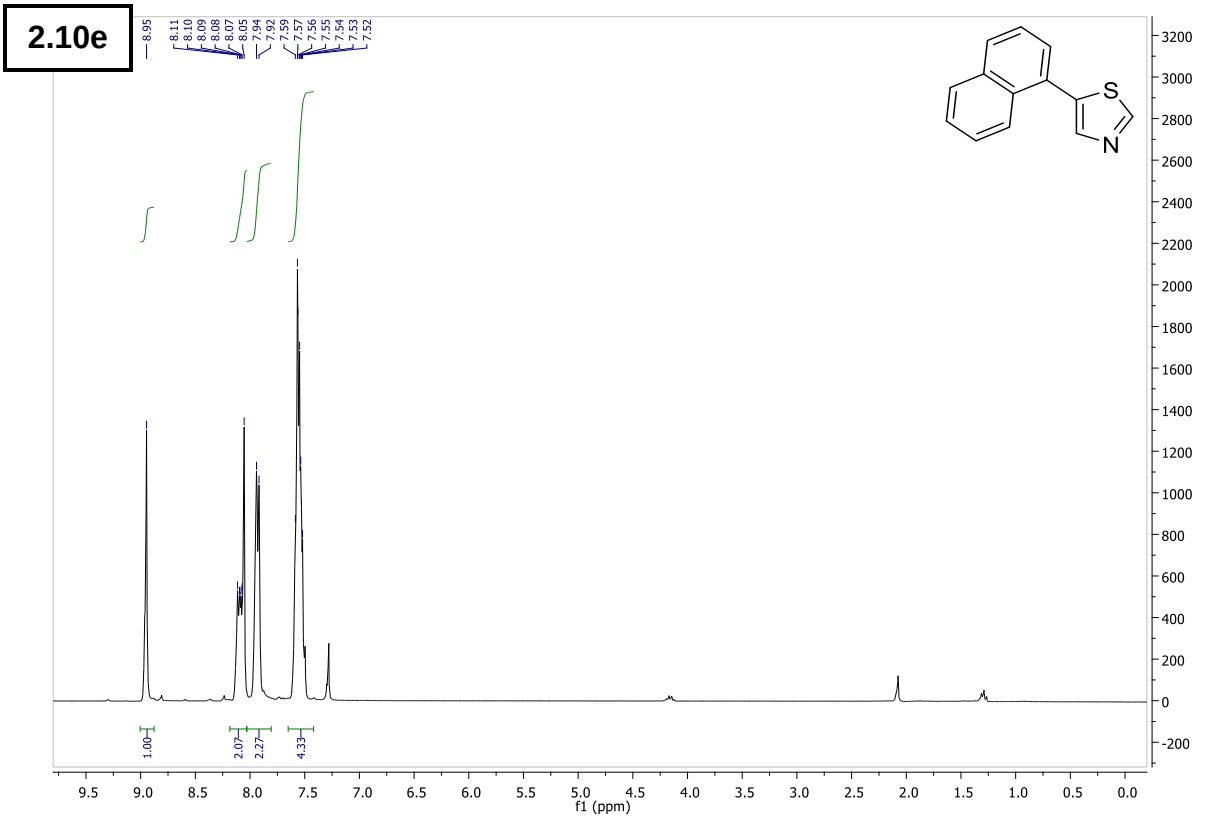
8.95
8.11
8.10
8.09
8.08
8.07
8.05
7.94
7.92
7.59
7.57
7.56
7.55
7.54
7.53
7.52
S
N
1.00
2.07
2.27
4.33
f1 (ppm)

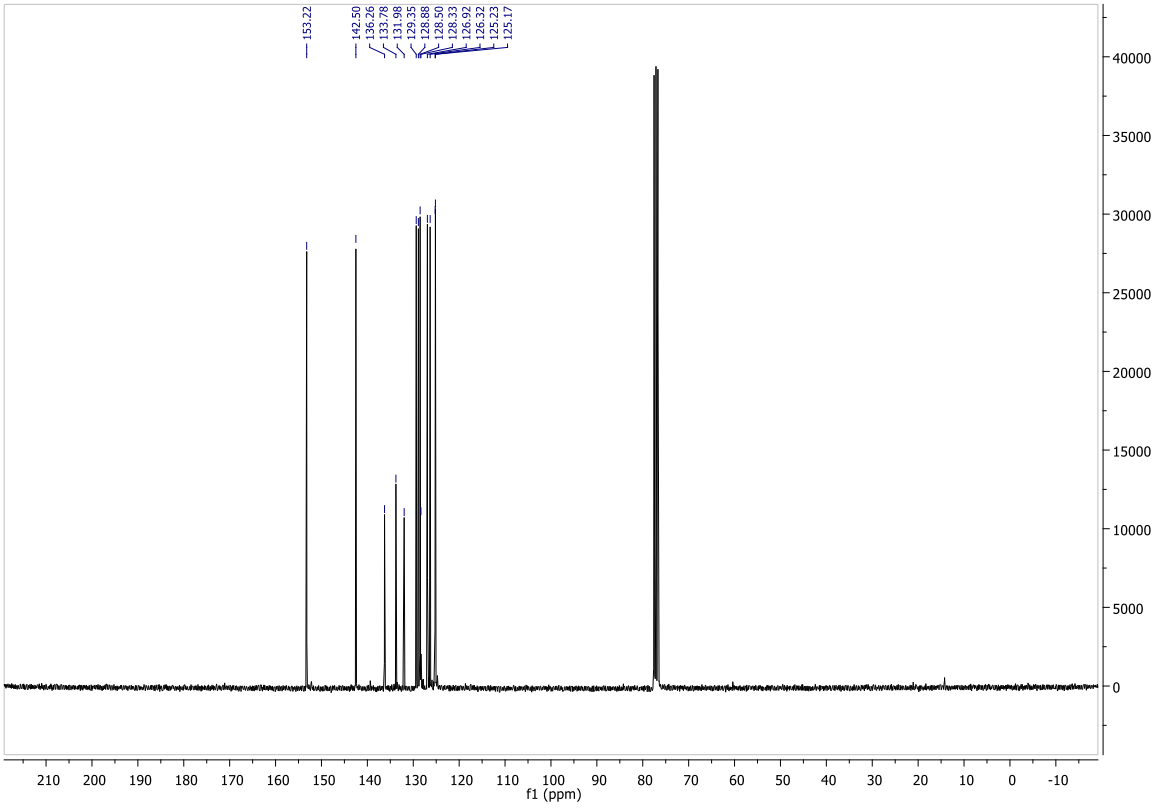
153.22
142.50
136.26
133.78
131.98
129.35
128.88
128.50
128.33
126.92
126.32
125.23
125.17
f1 (ppm)

2.10f

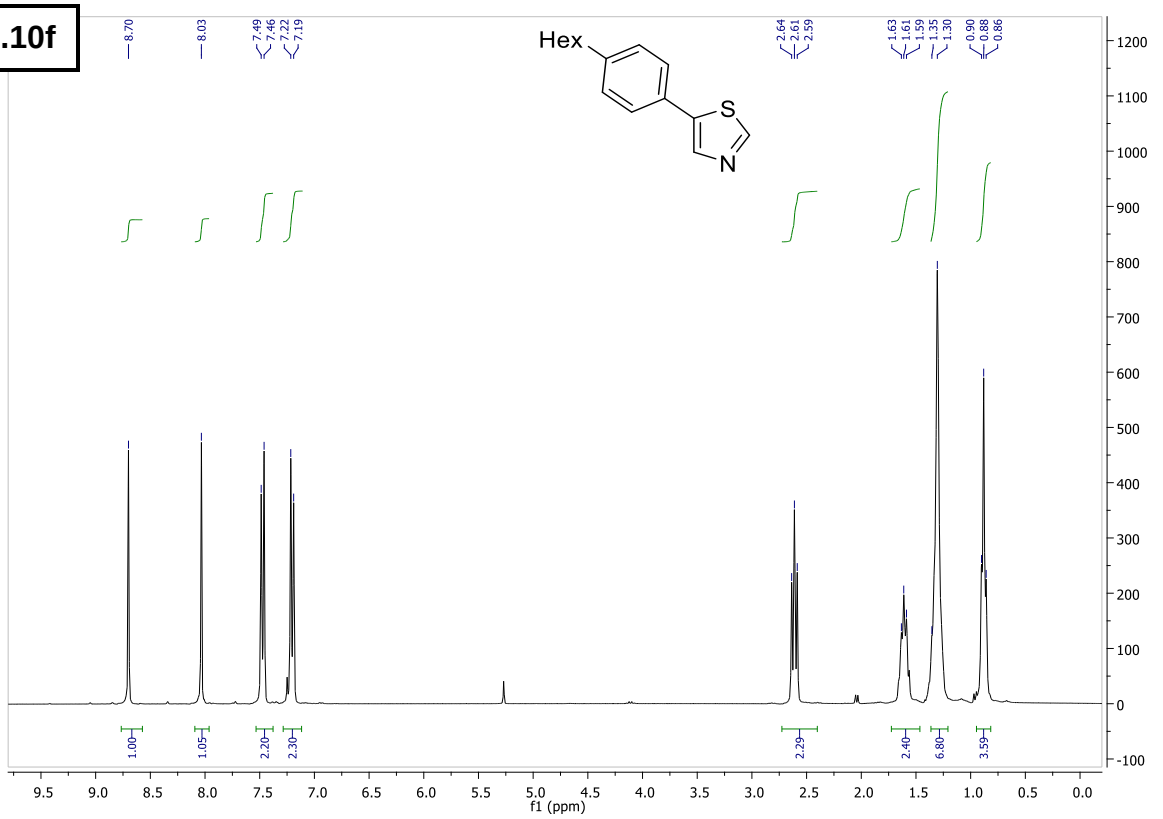
Hex
S
N
8.70
8.03
7.49
7.46
7.22
7.19
2.64
2.61
2.59
1.63
1.61
1.59
1.35
1.30
0.90
0.88
0.86
1.00
1.05
2.20
2.30
2.29
2.40
6.80
3.59
f1 (ppm)

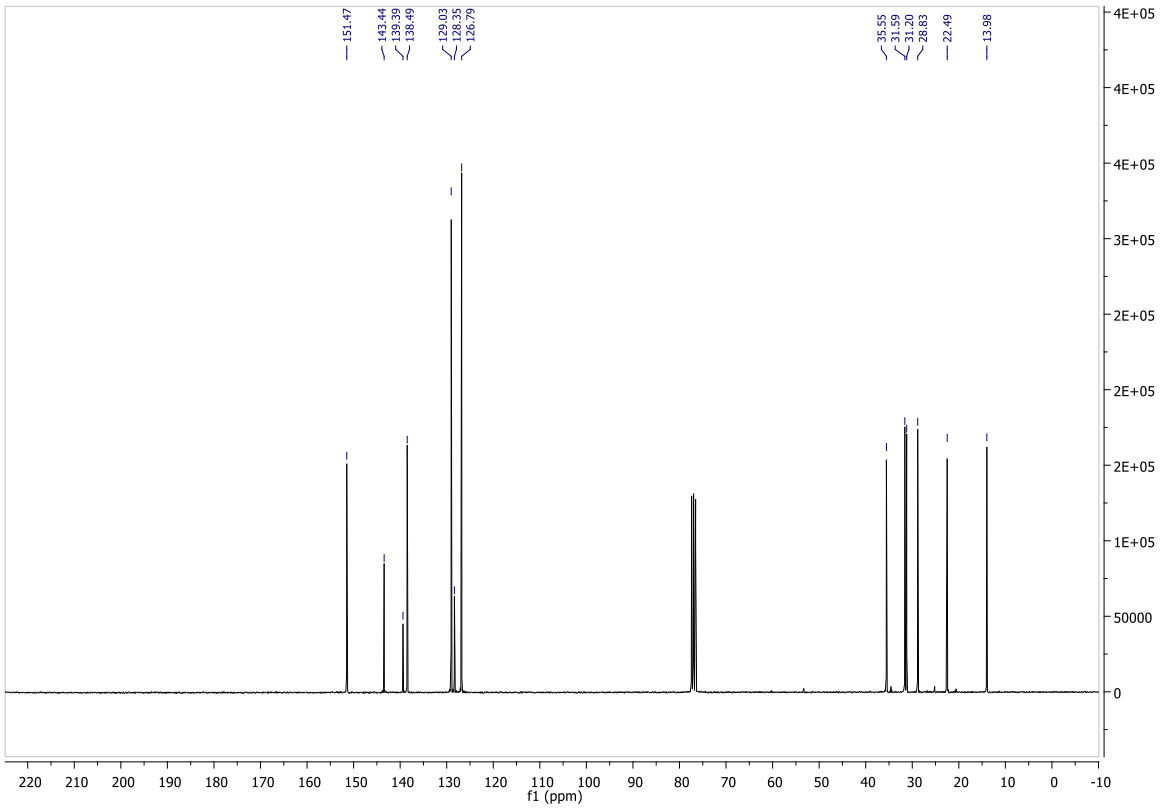
151.47
143.44
139.39
138.49
129.03
128.35
126.79
35.55
31.59
31.20
28.83
22.49
13.98
f1 (ppm)

2.10g

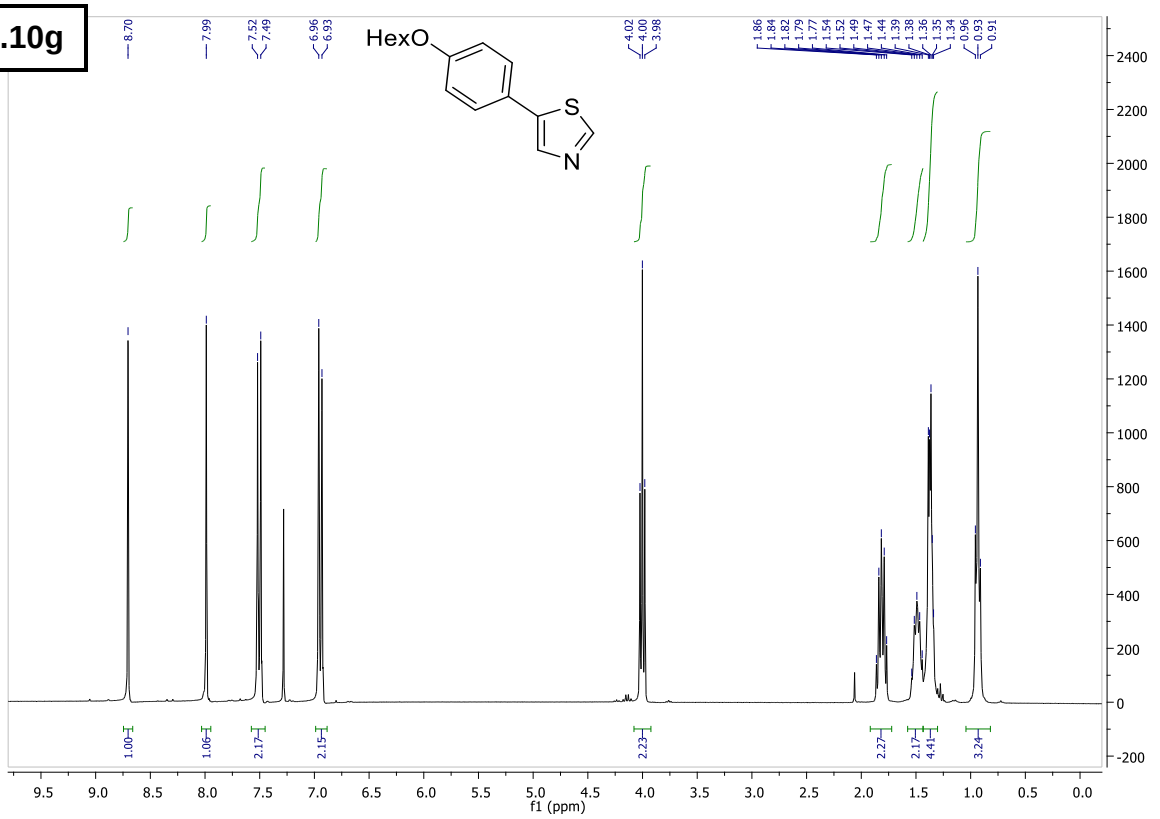
HexO
S
N
8.70
7.99
7.52
7.49
6.96
6.93
4.02
4.00
3.98
1.86
1.84
1.82
1.79
1.77
1.54
1.52
1.49
1.47
1.44
1.39
1.38
1.36
1.35
1.34
0.96
0.93
0.91
1.00
1.06
2.17
2.15
2.23
2.27
2.17
4.41
3.24
f1 (ppm)

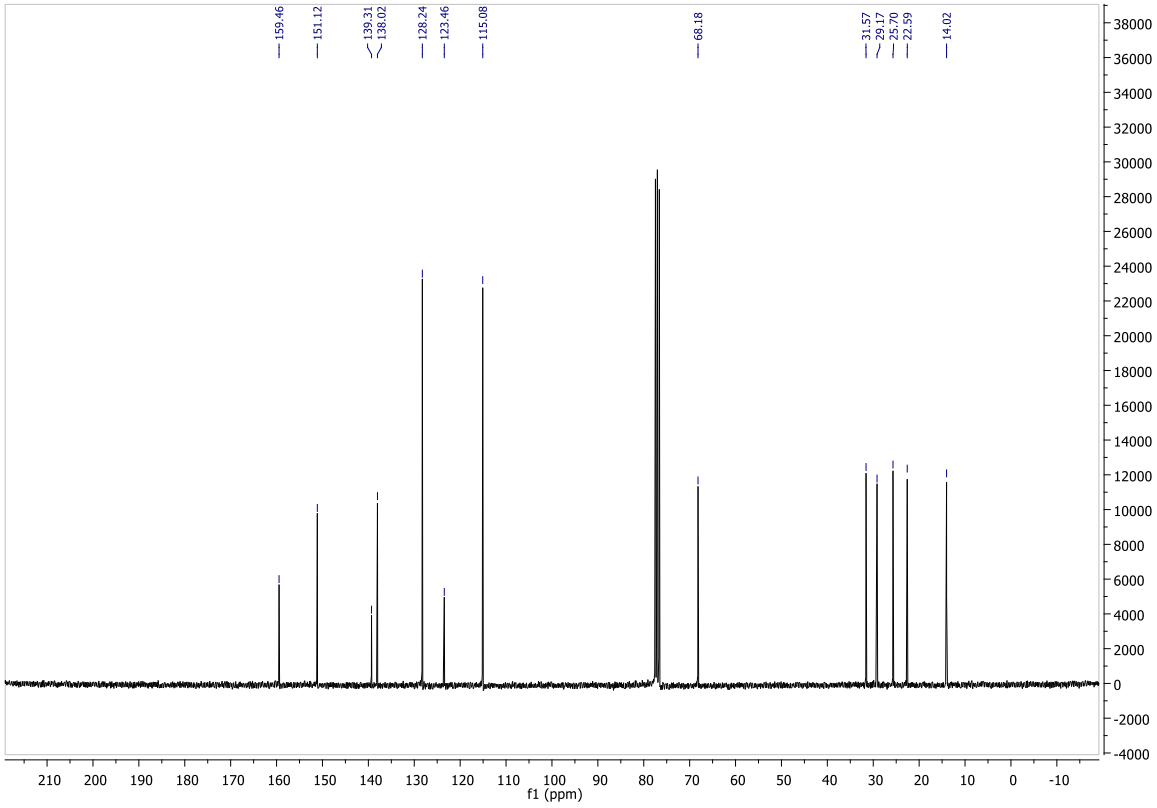
159.46
151.12
139.31
138.02
128.24
123.46
115.08
68.18
31.57
29.17
25.70
22.59
14.02
f1 (ppm)

2.10h

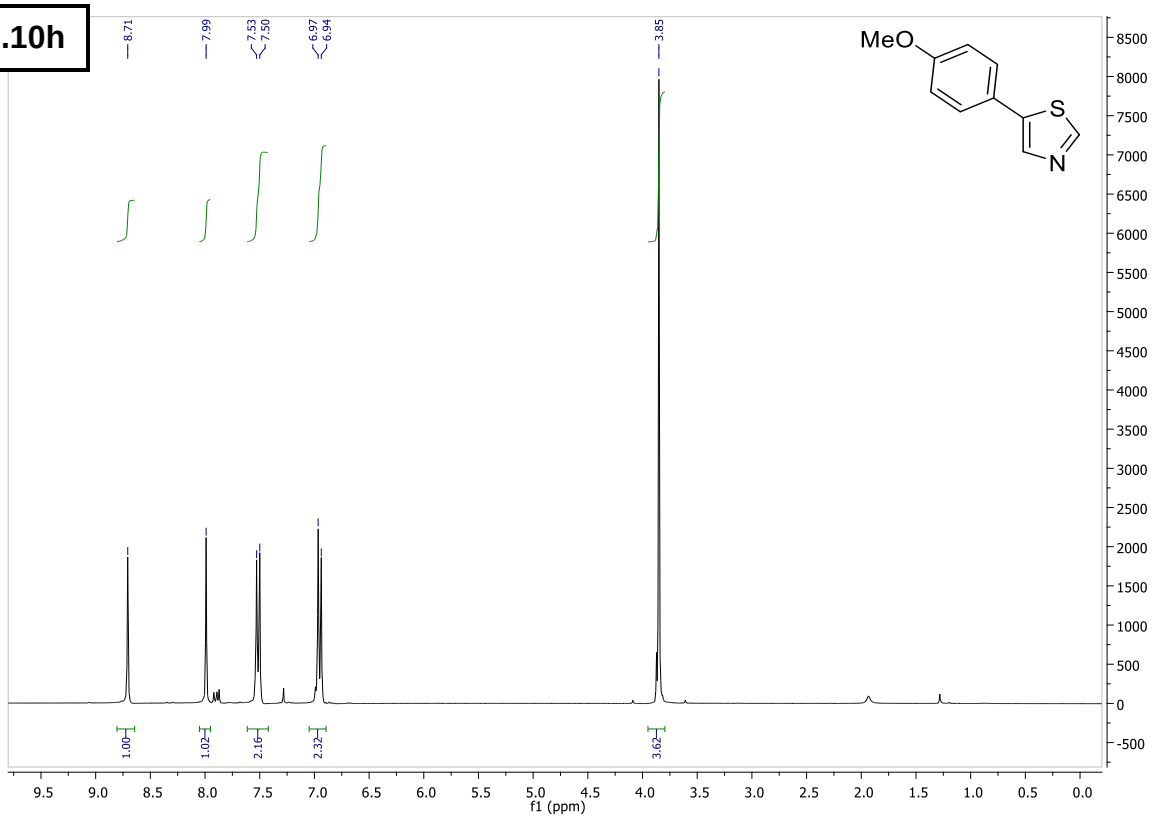
8.71
7.99
7.53
7.50
6.97
6.94
3.85
MeO
S
N
1.00
1.02
2.16
2.32
3.62
f1 (ppm)

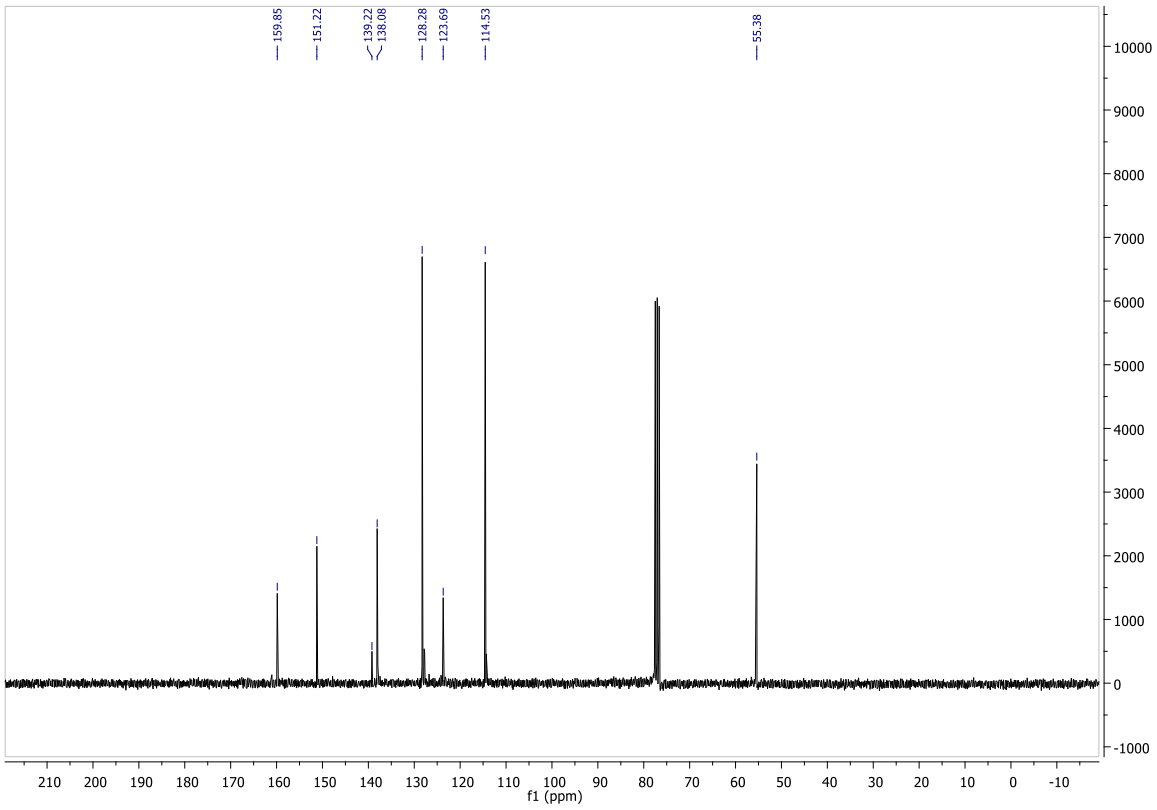
159.85
151.22
139.22
138.08
128.28
123.69
114.53
55.38
f1 (ppm)

2.10i

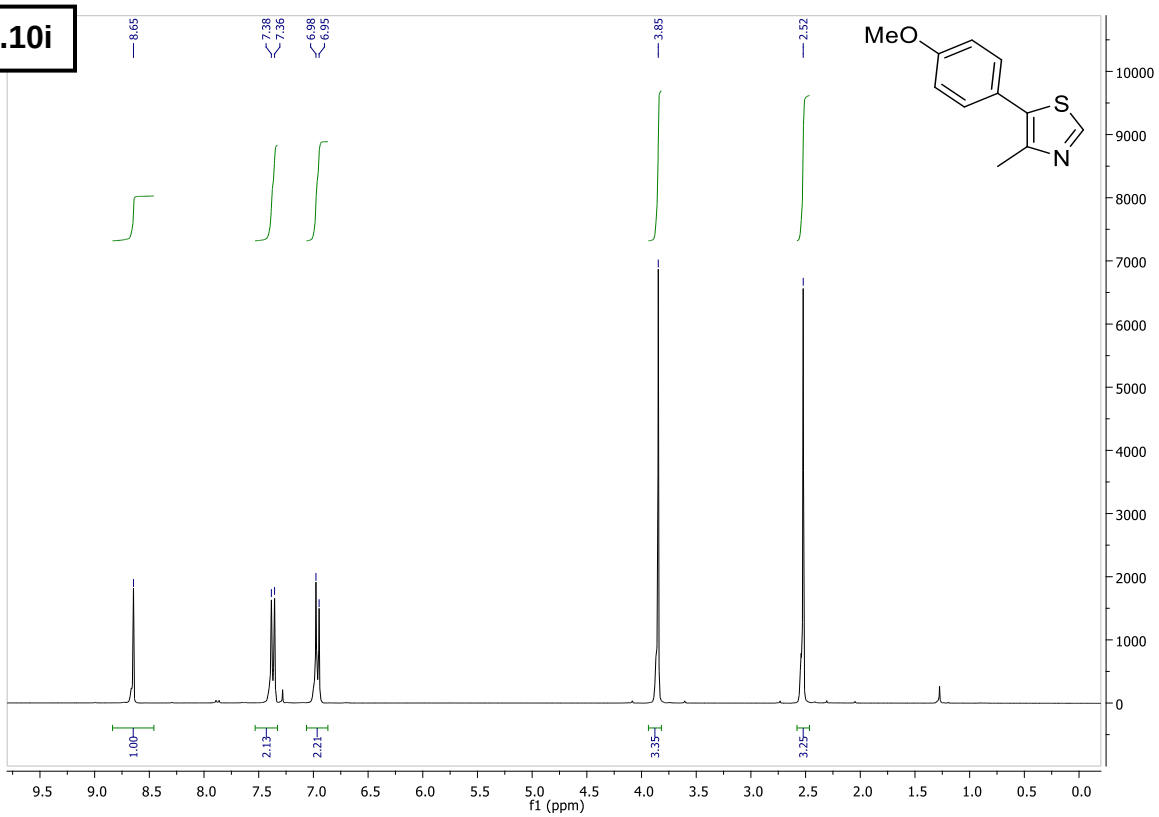
8.65
7.38
7.36
6.98
6.95
3.85
2.52
MeO
S
N
1.00
2.13
2.21
3.35
3.25
f1 (ppm)

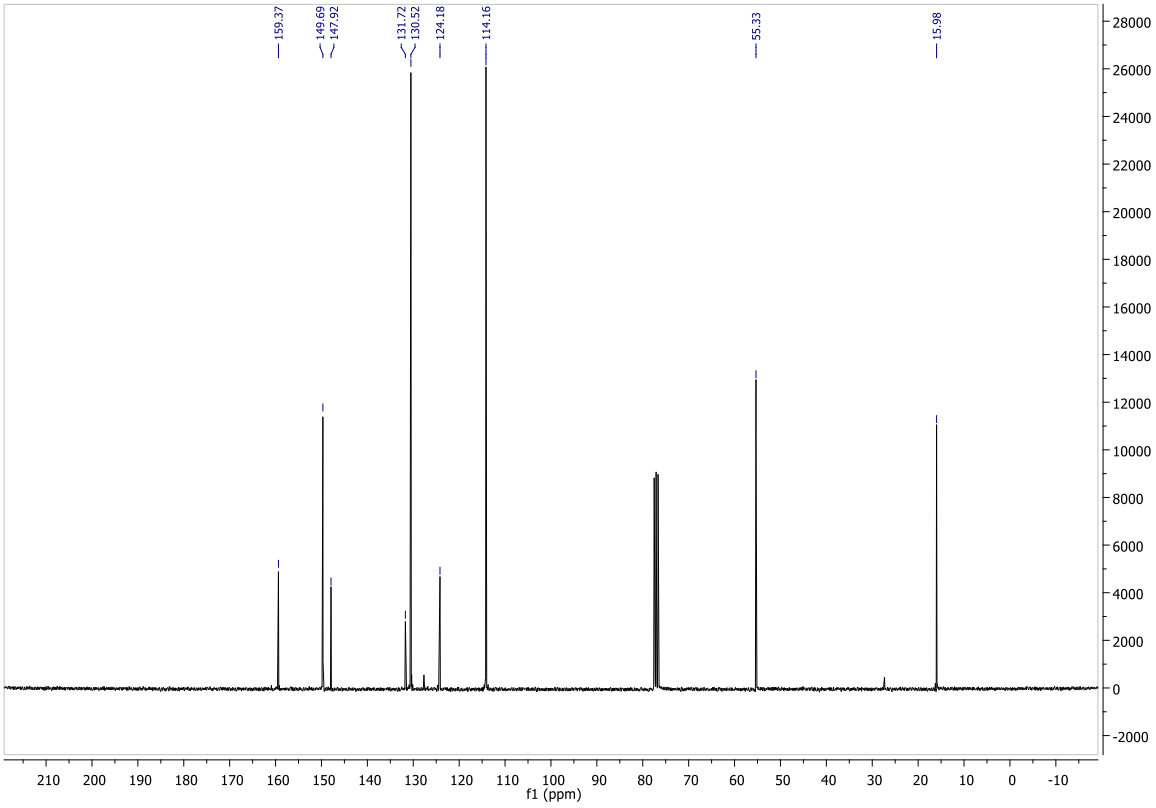
159.37
149.69
147.92
131.72
130.52
124.18
114.16
55.33
15.98
f1 (ppm)

2.10j

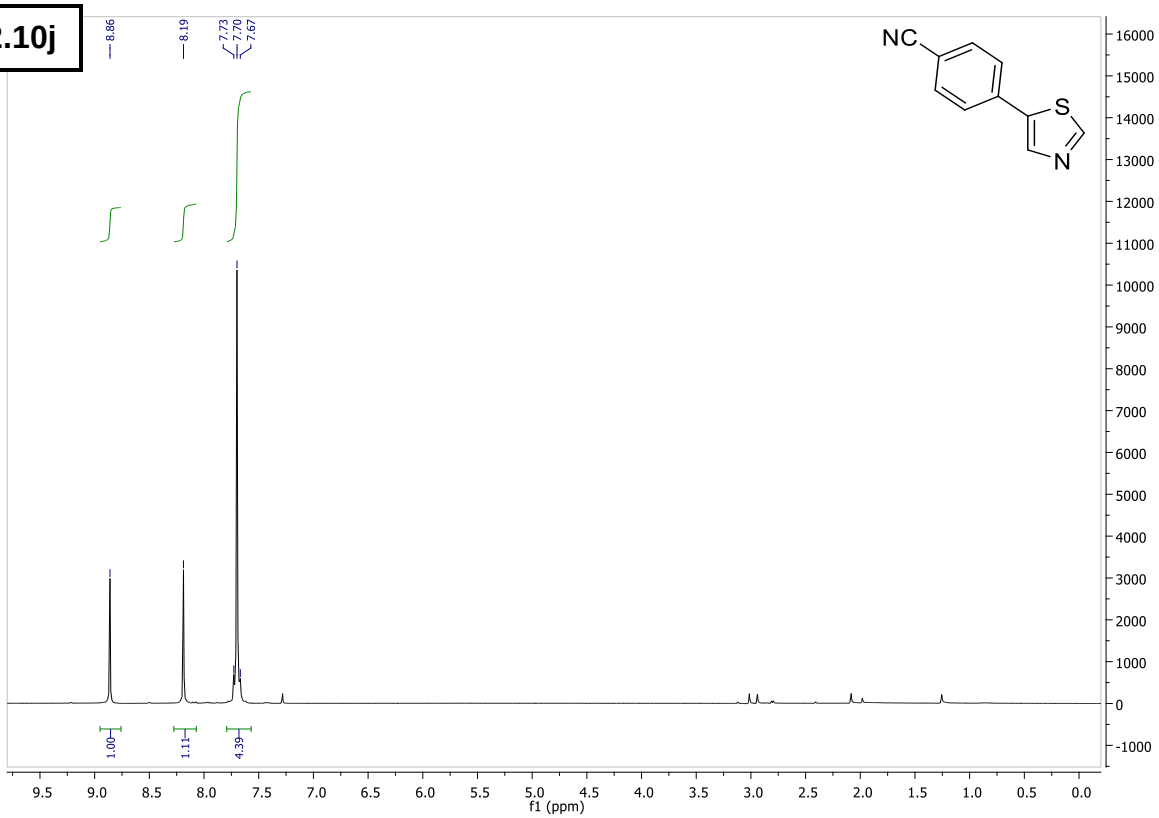
8.86
8.19
7.73
7.70
7.67
NC
S
N
1.00
1.11
4.39
f1 (ppm)

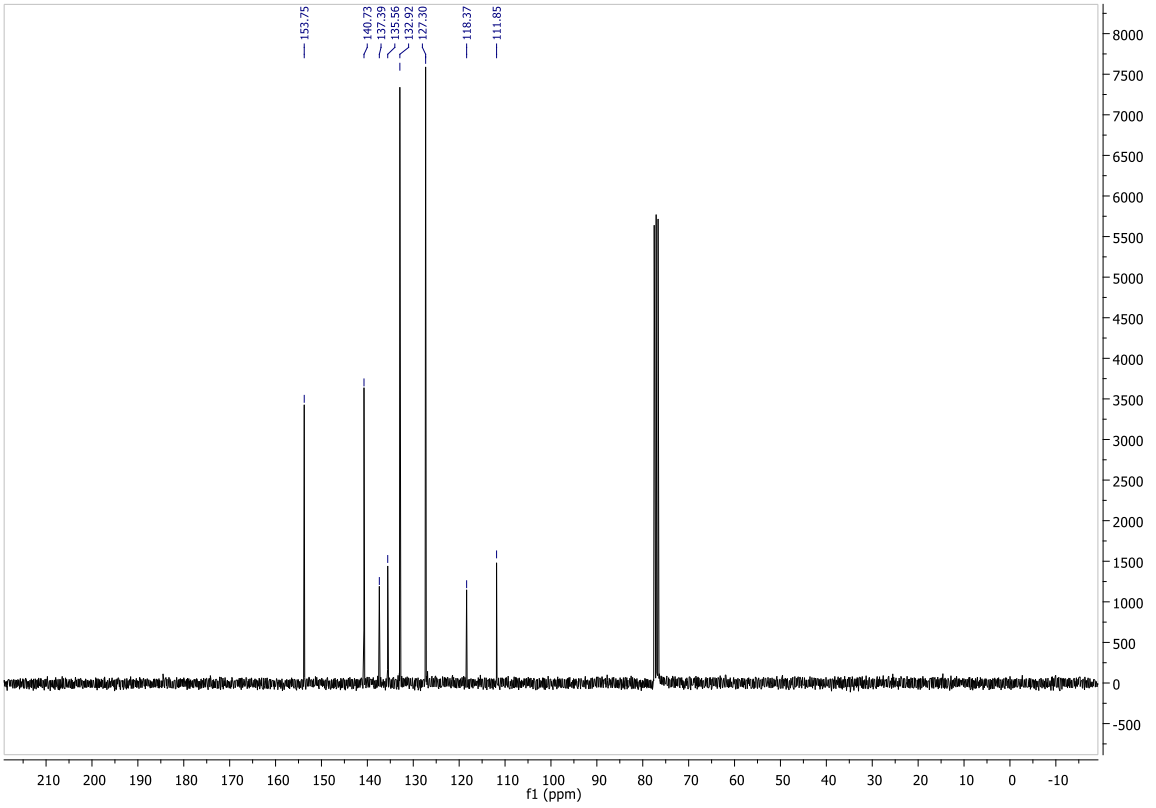
153.75
140.73
137.39
135.56
132.92
127.30
118.37
111.85
f1 (ppm)

2.10k

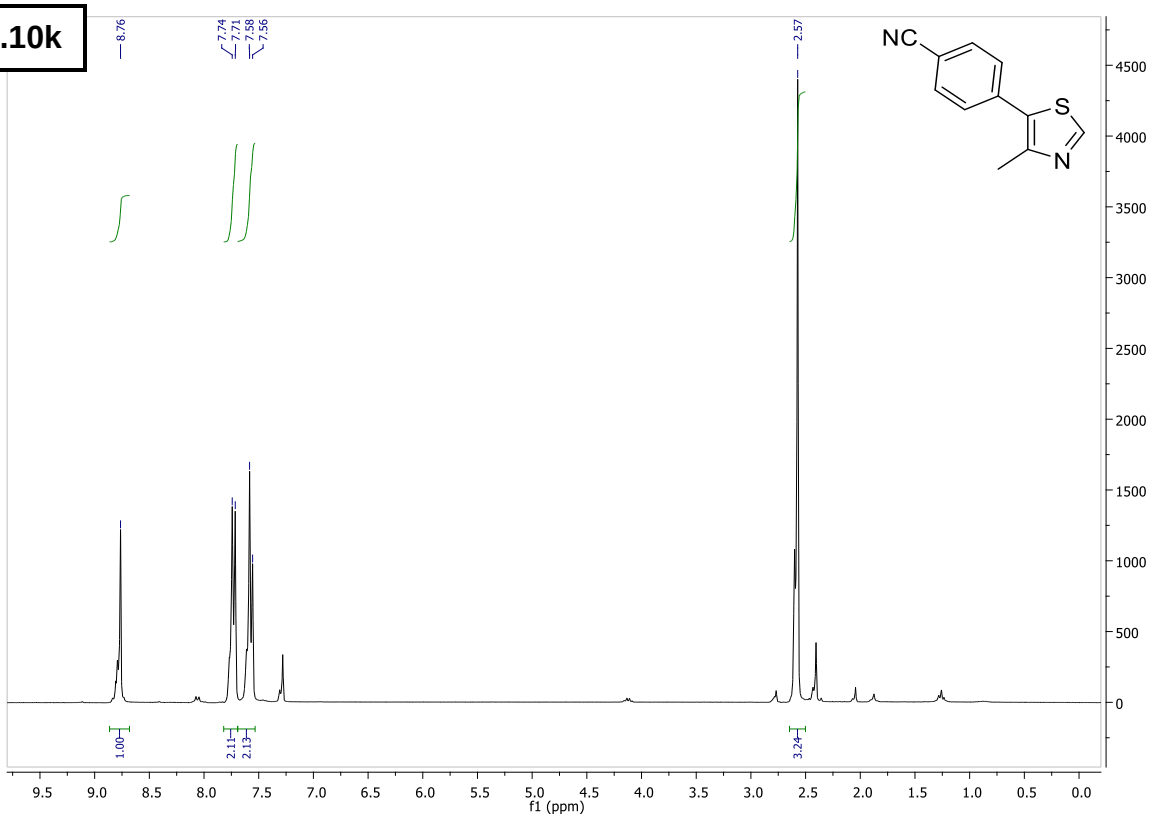
8.76
7.74
7.71
7.58
7.56
2.57
NC
S
N
1.00
2.11
2.13
3.24
f1 (ppm)

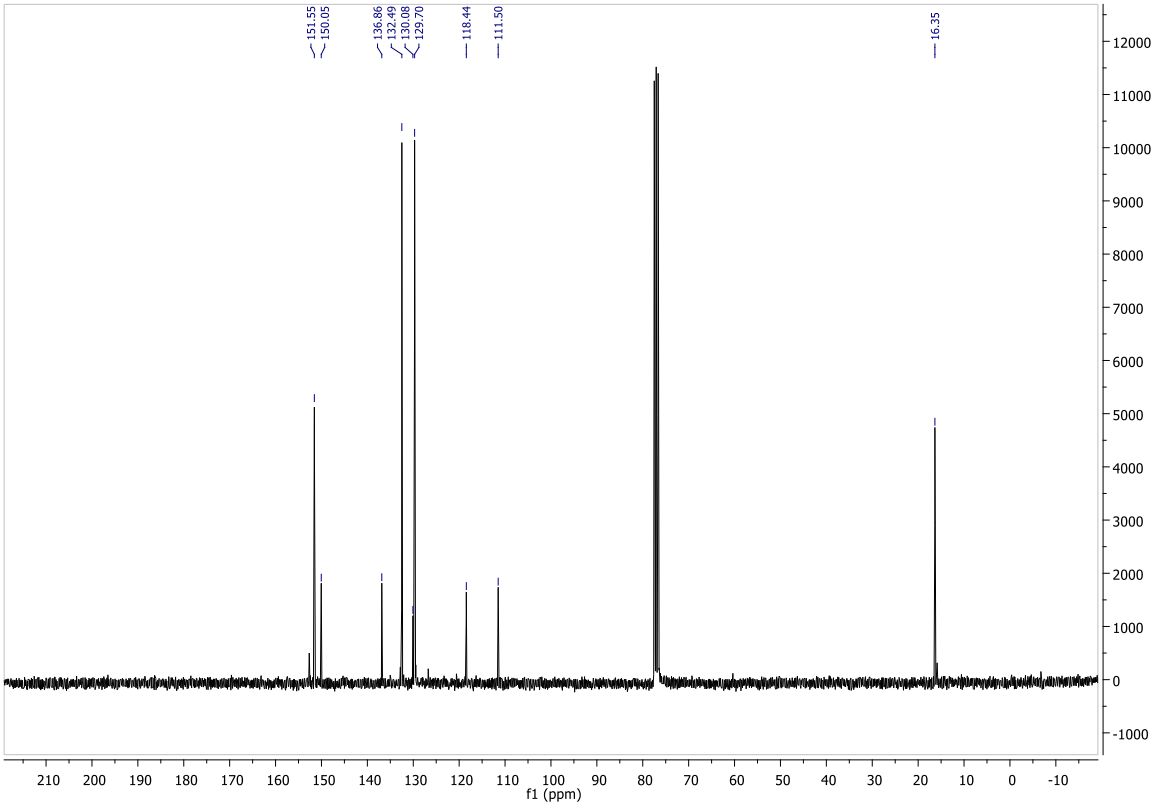
151.55
150.05
136.86
132.49
130.08
129.70
118.44
111.50
16.35
f1 (ppm)

2.10l

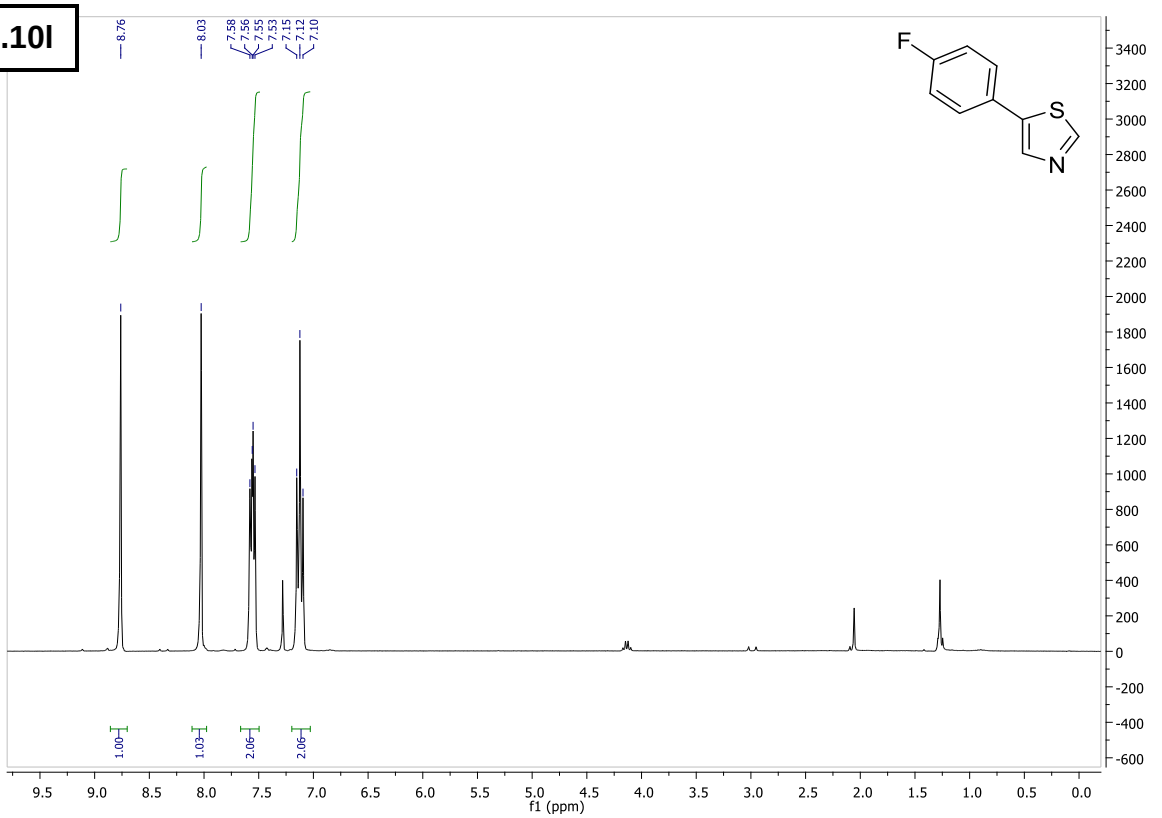
8.76
8.03
7.58
7.56
7.55
7.53
7.15
7.12
7.10
F
S
N
1.00
1.03
2.06
2.06
f1 (ppm)

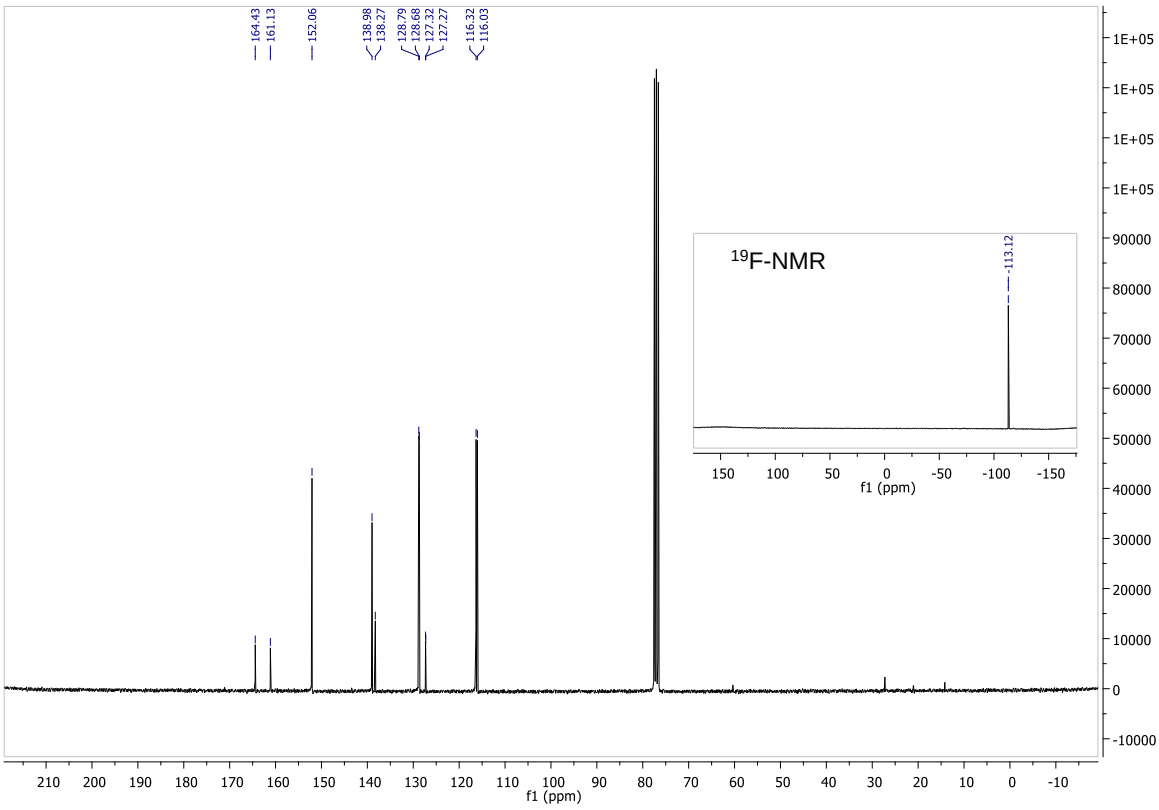
164.43
161.13
152.06
138.98
138.27
128.79
128.68
127.32
127.27
116.32
116.03
^{19}F-NMR
-113.12
f1 (ppm)
f1 (ppm)

2.10m

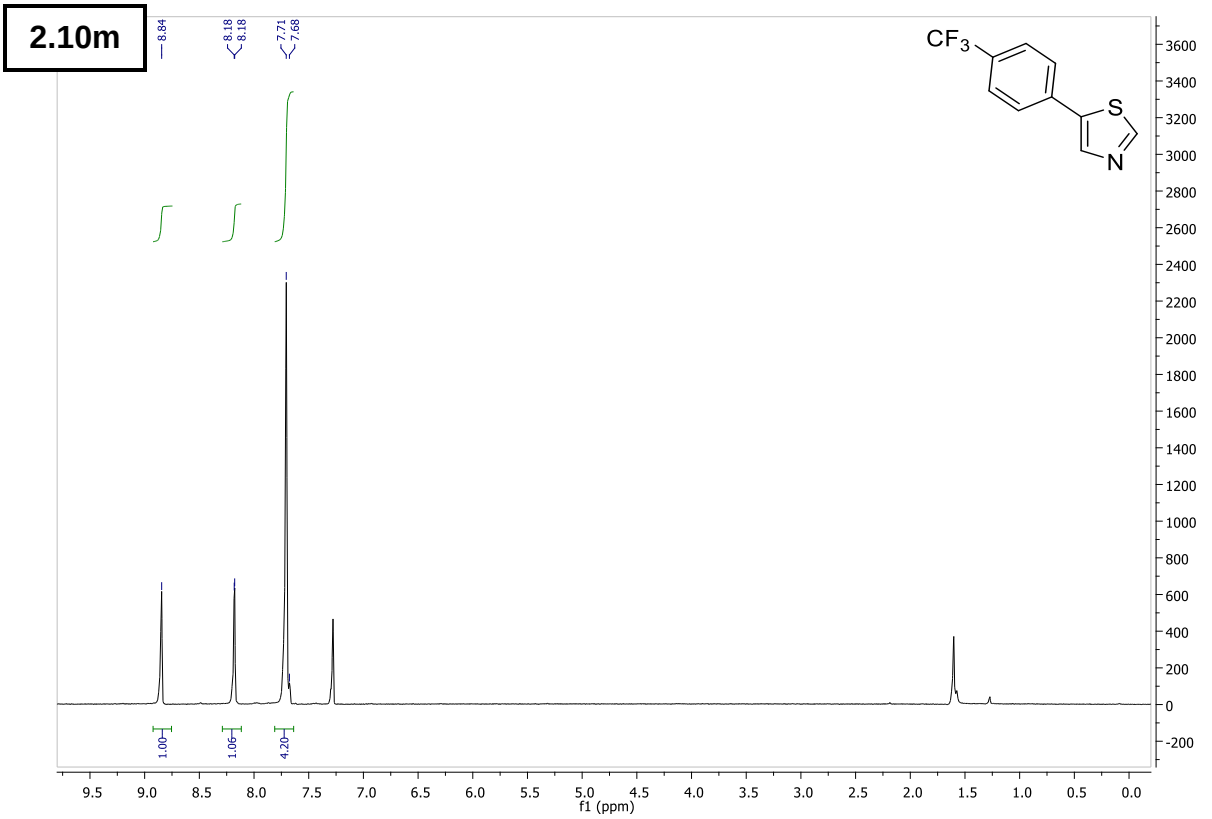
8.84
8.18
8.18
7.71
7.68
CF3
S
N
1.00
1.06
4.20
f1 (ppm)

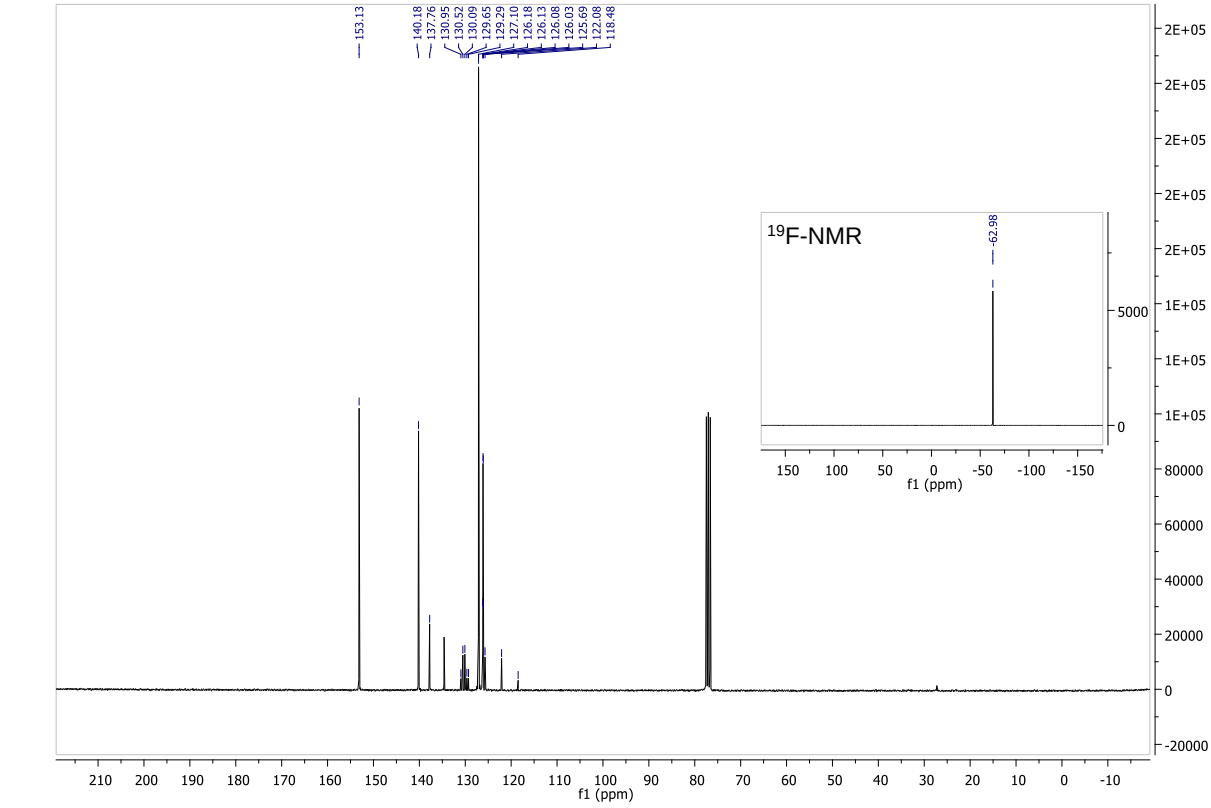
153.13
140.18
137.76
130.95
130.52
130.09
129.65
129.29
127.10
126.18
126.13
126.08
126.03
125.69
122.08
118.48
19F-NMR
-62.98
f1 (ppm)

2.10n

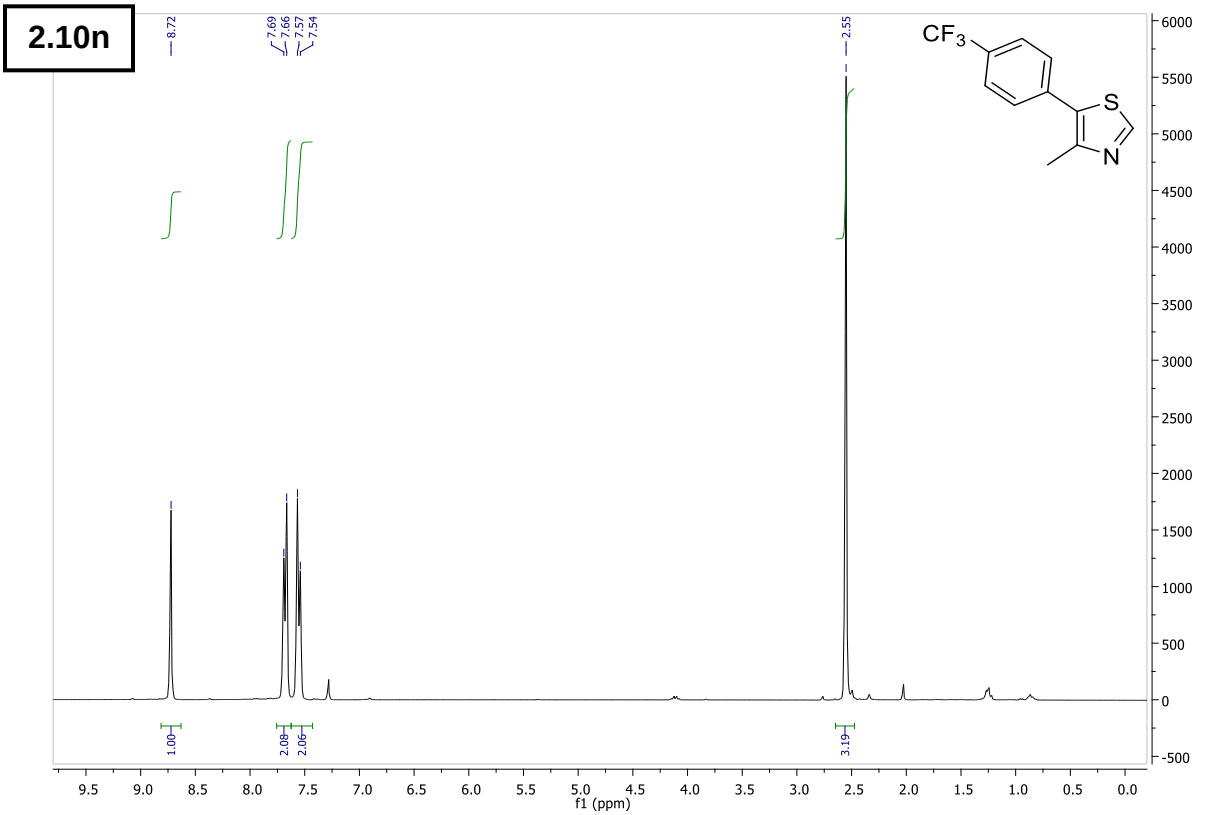
8.72
7.69
7.66
7.57
7.54
2.55
CF3
S
N
1.00
2.08
2.06
3.19
f1 (ppm)

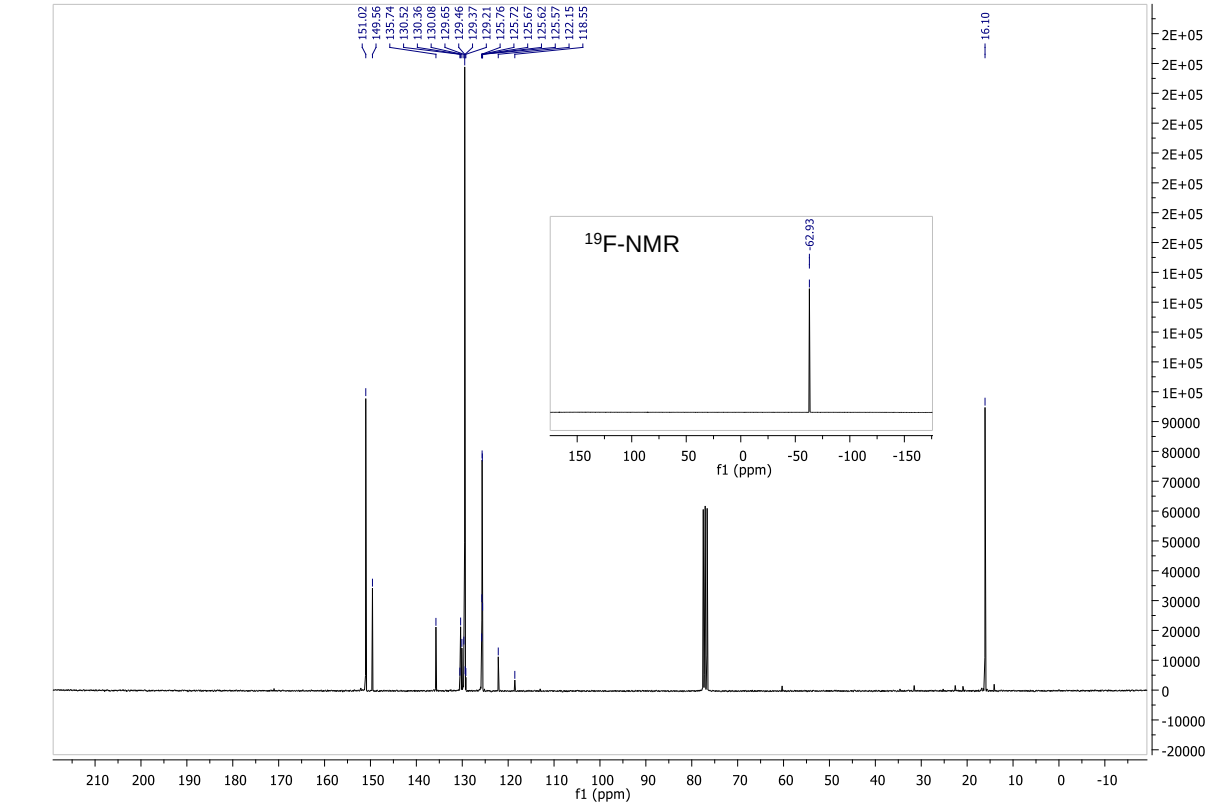
151.02
149.56
135.74
130.52
130.36
130.08
129.65
129.46
129.37
129.21
125.76
125.72
125.67
125.62
123.57
122.15
118.55
16.10
19F-NMR
-62.93
f1 (ppm)

2.10o

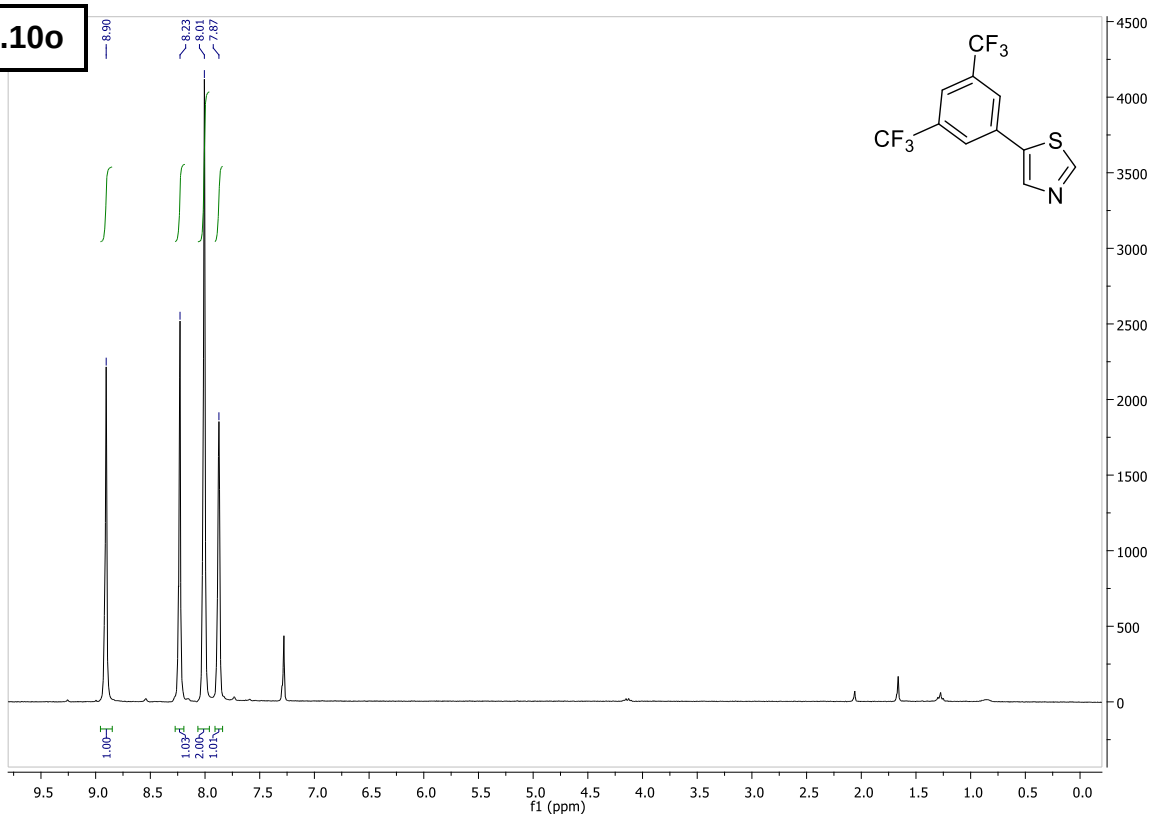
8.90
8.23
8.01
7.87
CF3
CF3
S
N
1.00
1.03
2.00
1.01
f1 (ppm)

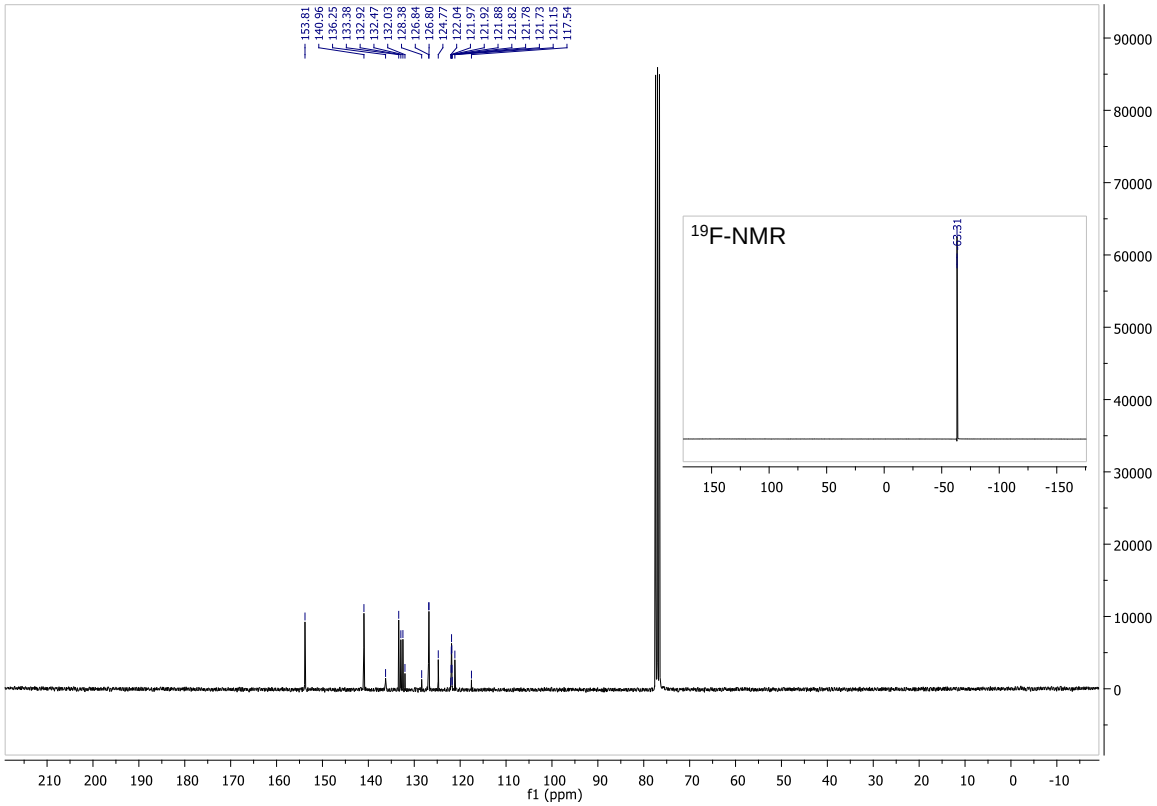
153.81
140.96
136.25
133.38
132.92
132.47
132.03
128.38
126.84
126.80
124.77
122.04
121.97
121.92
121.88
121.82
121.78
121.73
121.15
117.54
19F-NMR
-63.31
f1 (ppm)

2.10p

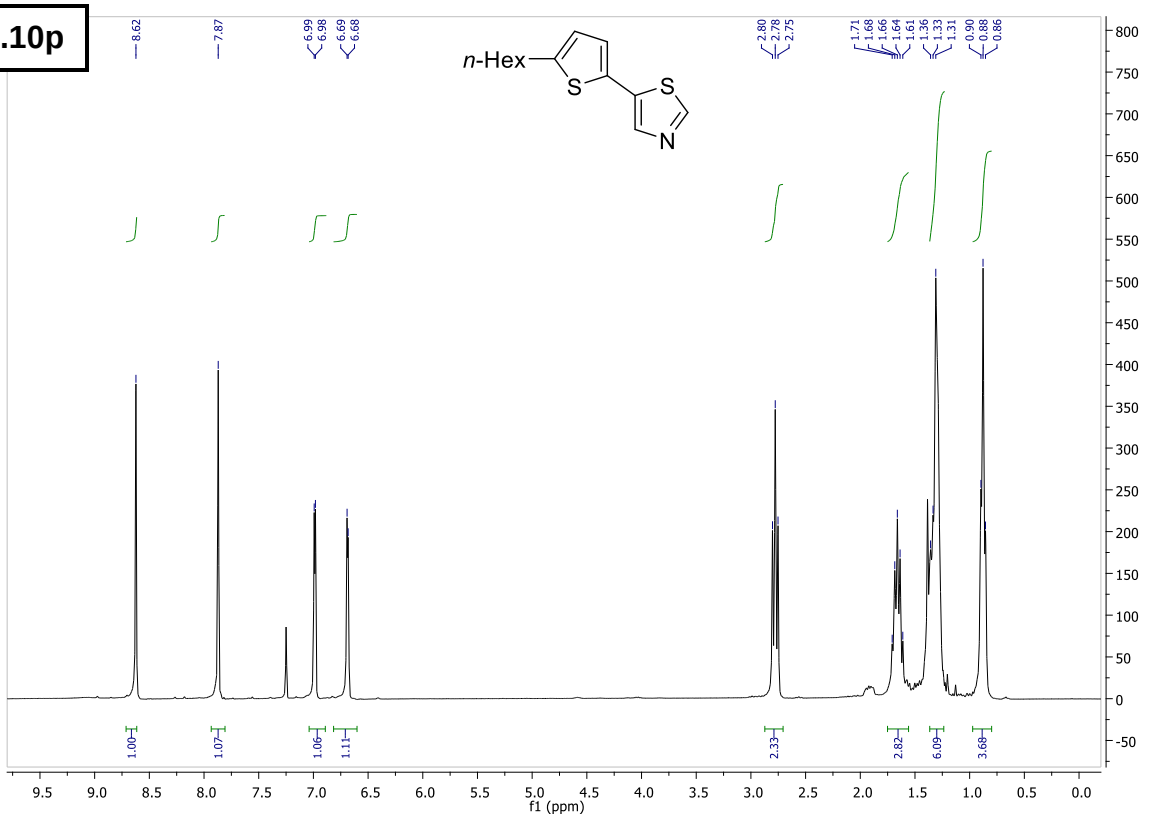
8.62
7.87
6.99
6.98
6.69
6.68
2.80
2.78
2.75
1.71
1.68
1.66
1.64
1.61
1.36
1.33
1.31
0.90
0.88
0.86
n-Hex
S
S
N
1.00
1.07
1.06
1.11
2.33
2.82
6.09
3.68
f1 (ppm)

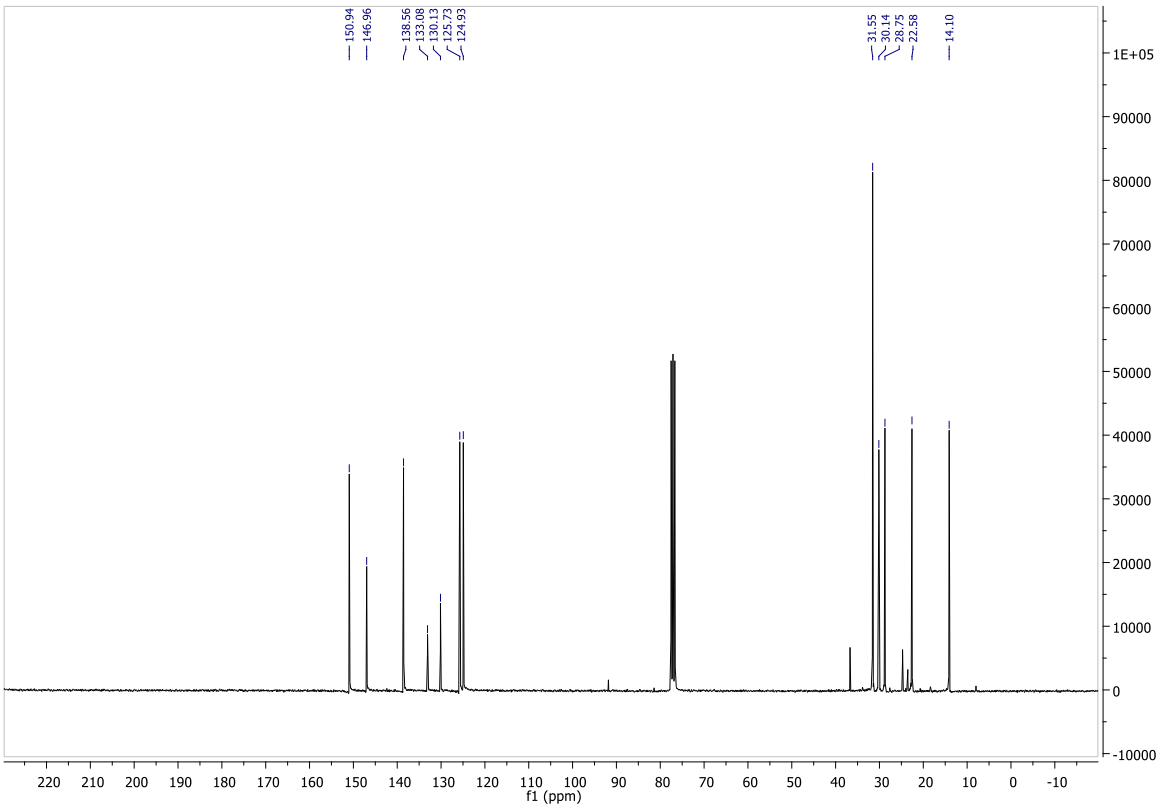
150.94
146.96
138.56
133.08
130.13
125.73
124.93
31.55
30.14
28.75
22.58
14.10
f1 (ppm)

2.10q

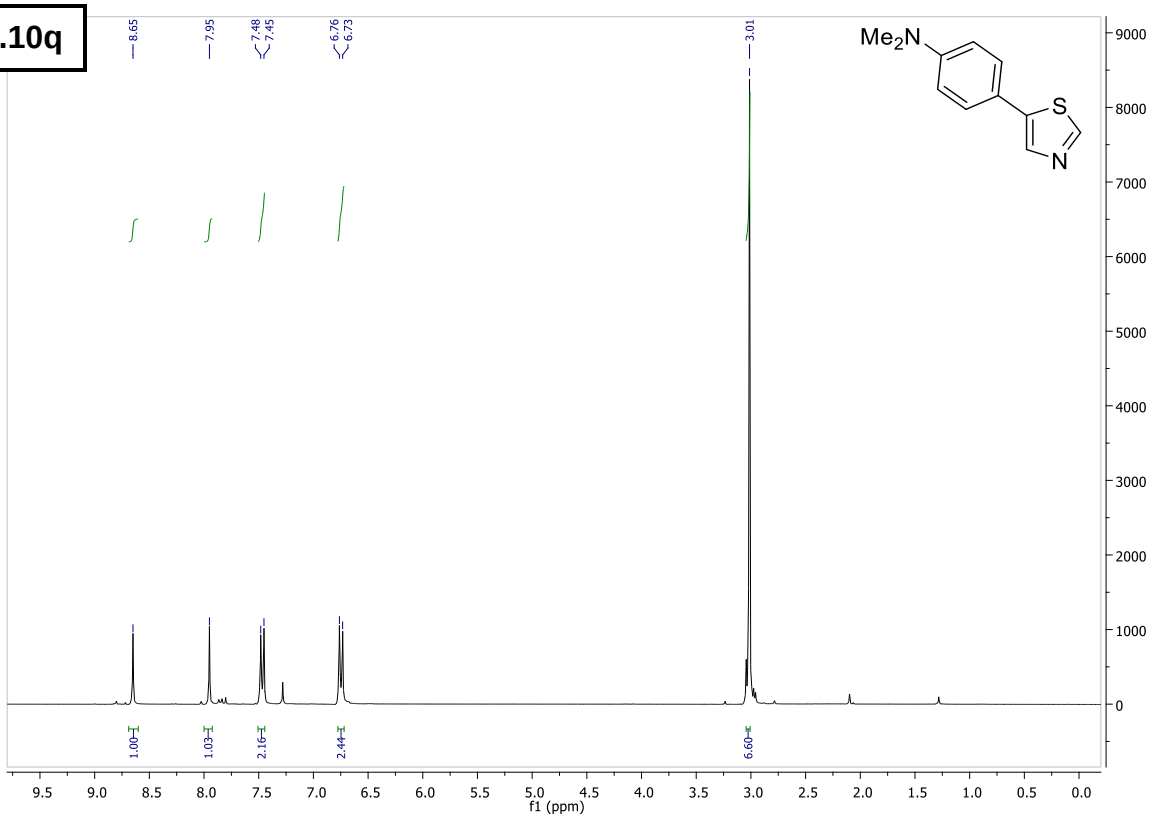
8.65
7.95
7.48
7.45
6.76
6.73
3.01
Me2N
S
N
1.00
1.03
2.16
2.44
6.60
f1 (ppm)

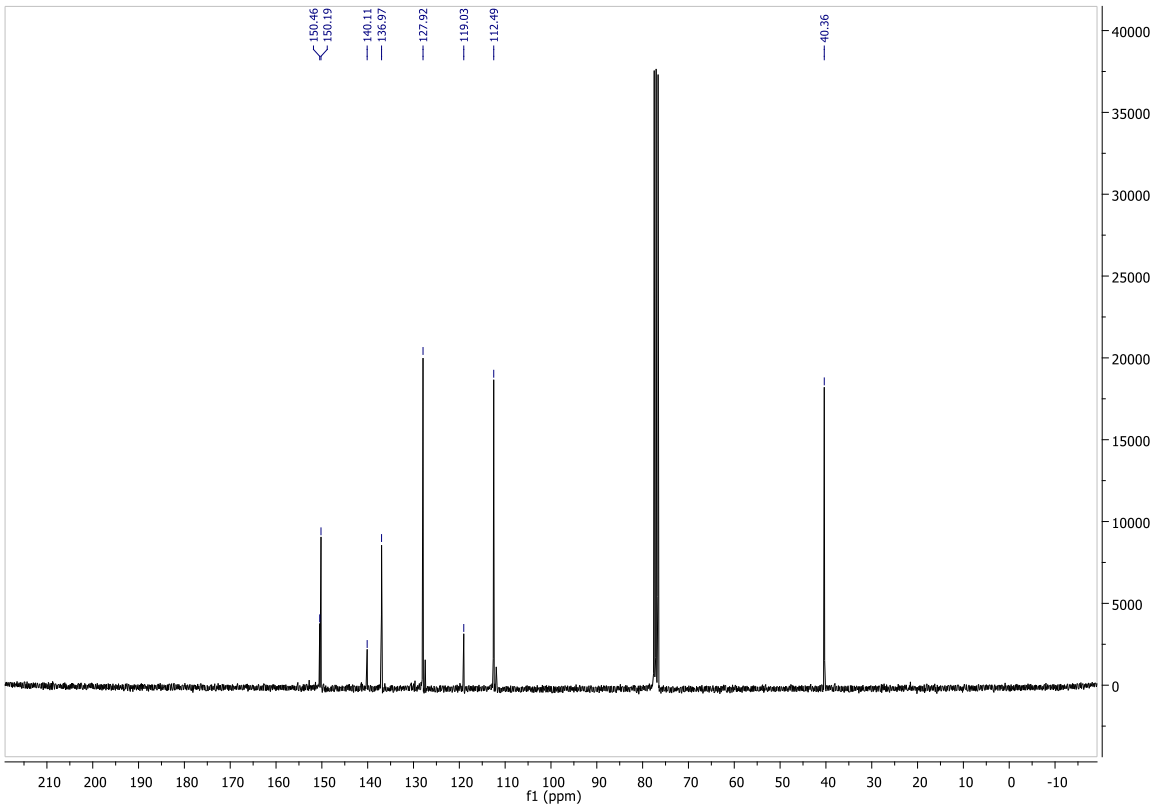
150.46
150.19
140.11
136.97
127.92
119.03
112.49
40.36
f1 (ppm)

2.11a

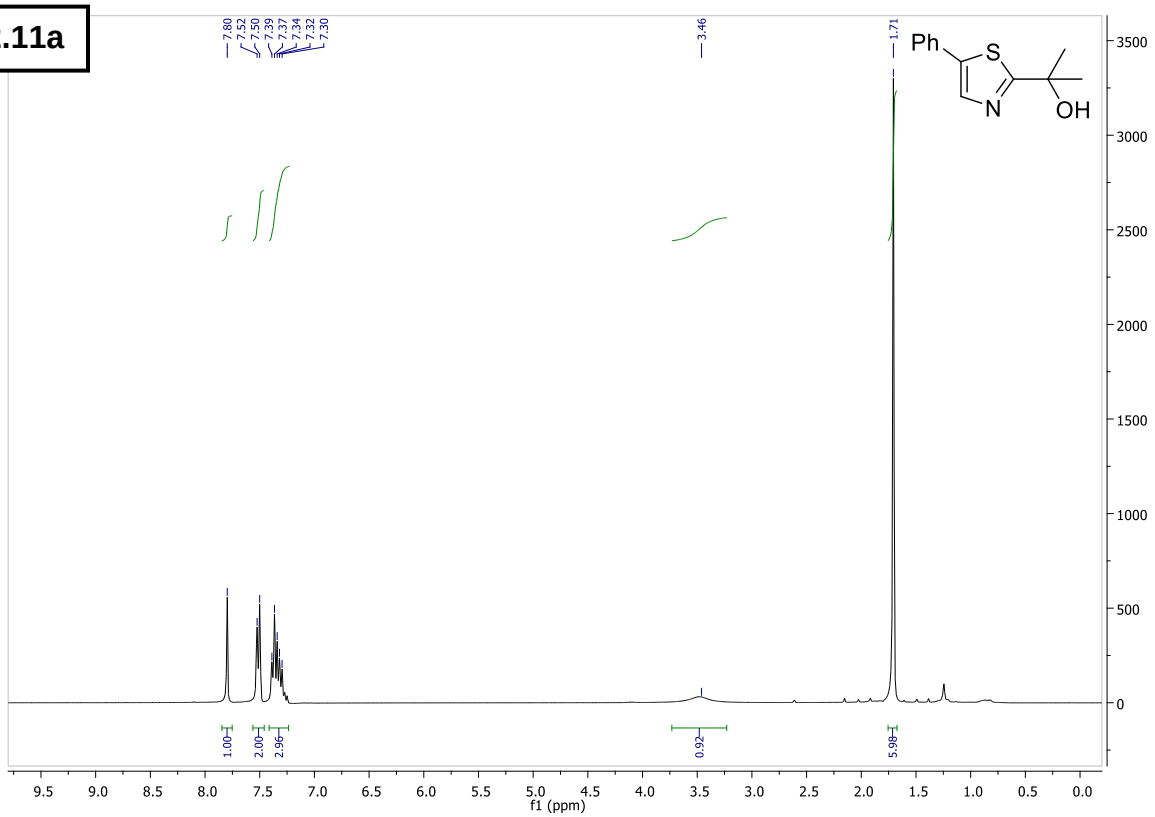
7.80
7.52
7.50
7.39
7.37
7.34
7.32
7.30
3.46
1.71
Ph
S
N
OH
1.00
2.00
2.96
0.92
5.98
f1 (ppm)

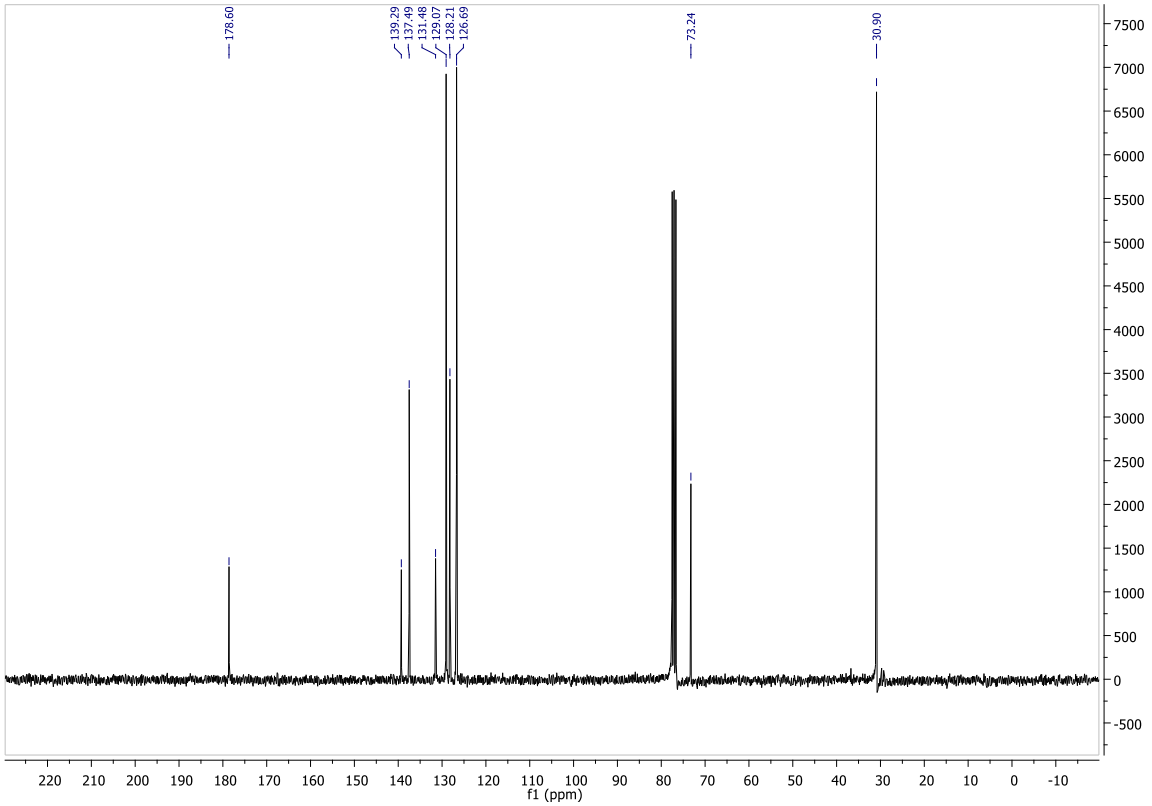
178.60
139.29
137.49
131.48
129.07
128.21
126.69
73.24
30.90
f1 (ppm)

2.11b

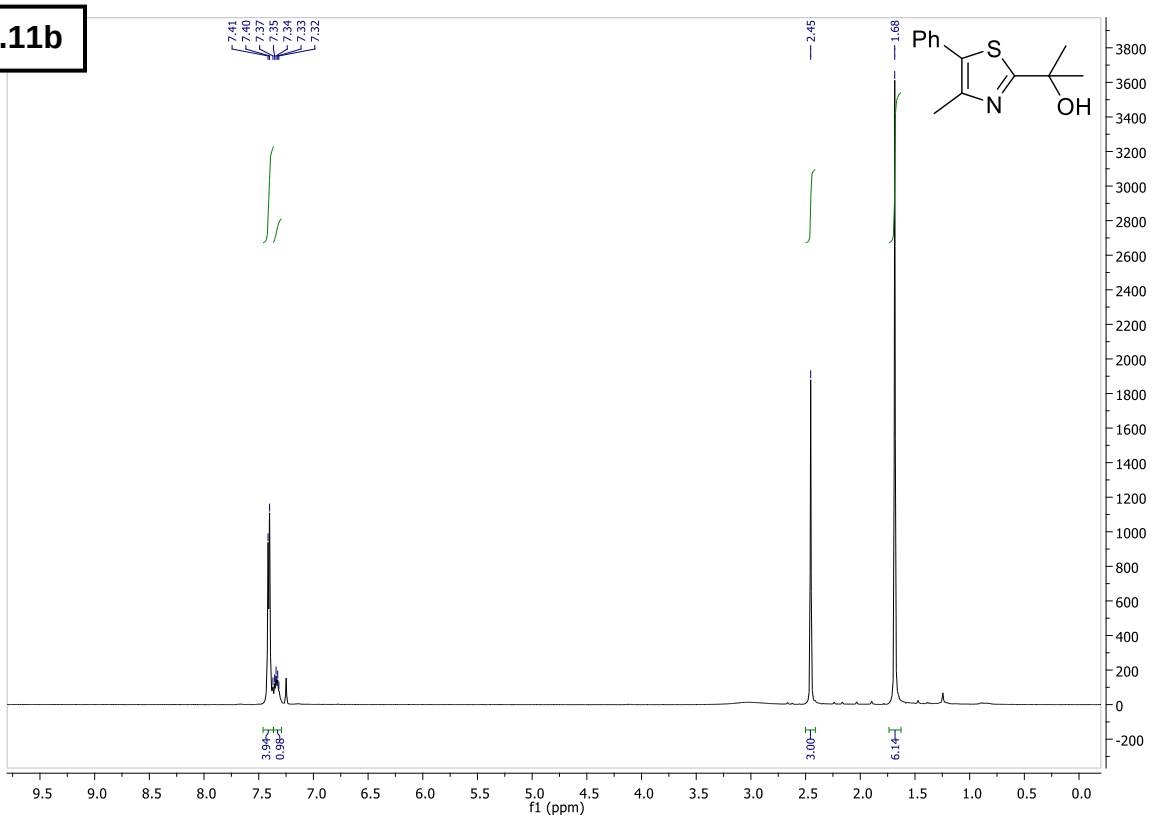
7.41
7.40
7.37
7.35
7.34
7.33
7.32
2.45
1.68
Ph
S
N
OH
3.94
0.98
3.00
6.14
f1 (ppm)

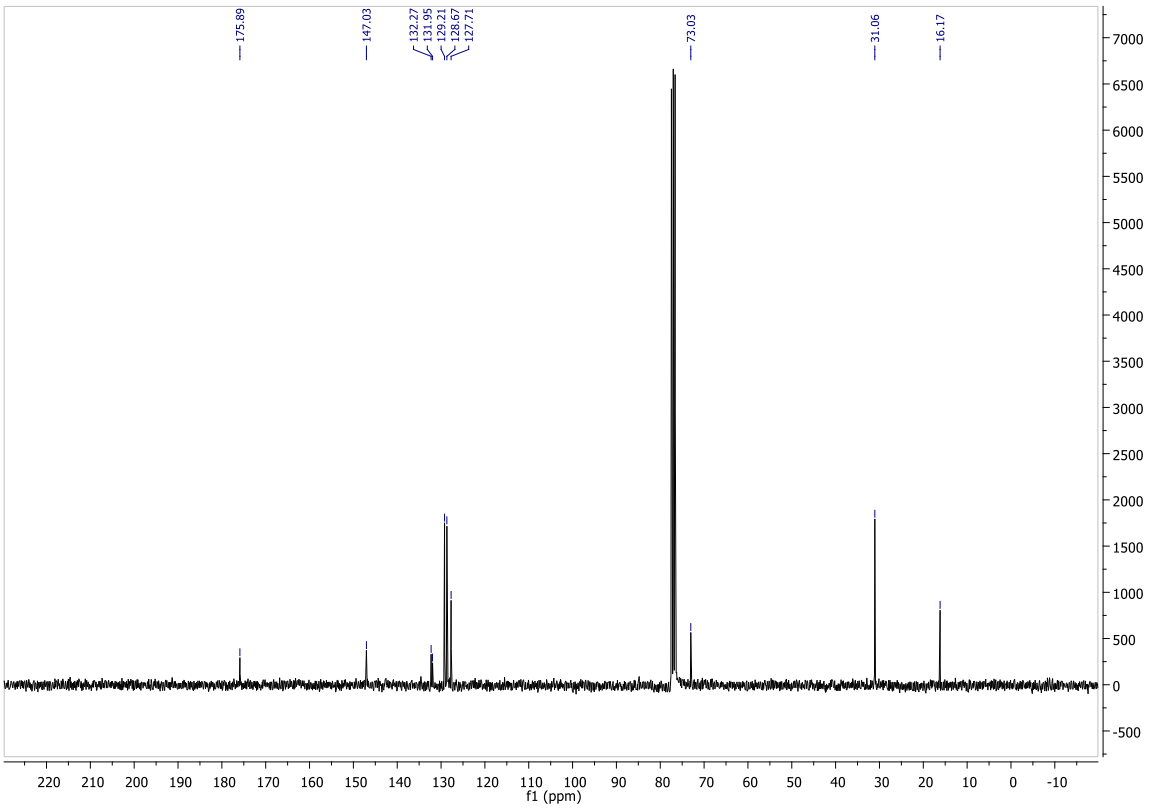
175.89
147.03
132.27
131.95
129.21
128.67
127.71
73.03
31.06
16.17
f1 (ppm)

2.12a

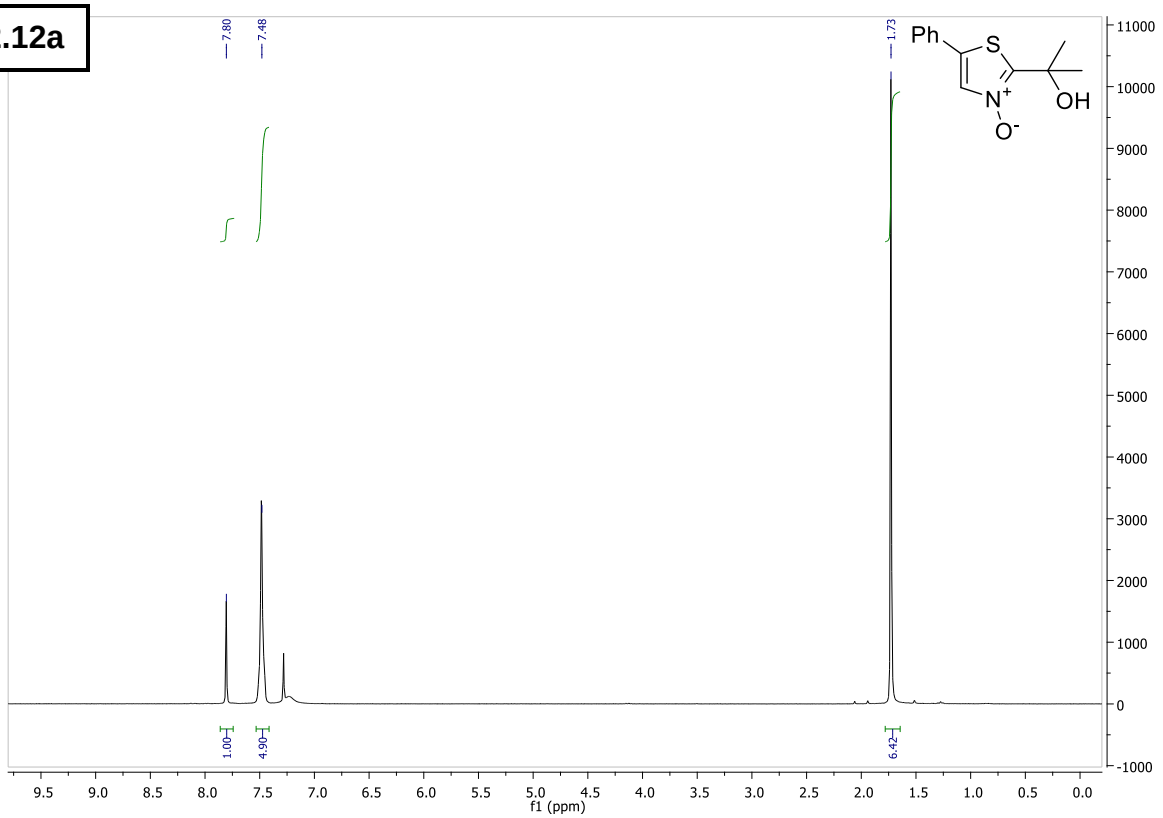
7.80
7.48
1.73
Ph
S
N+
O-
OH
1.00
4.90
6.42
f1 (ppm)

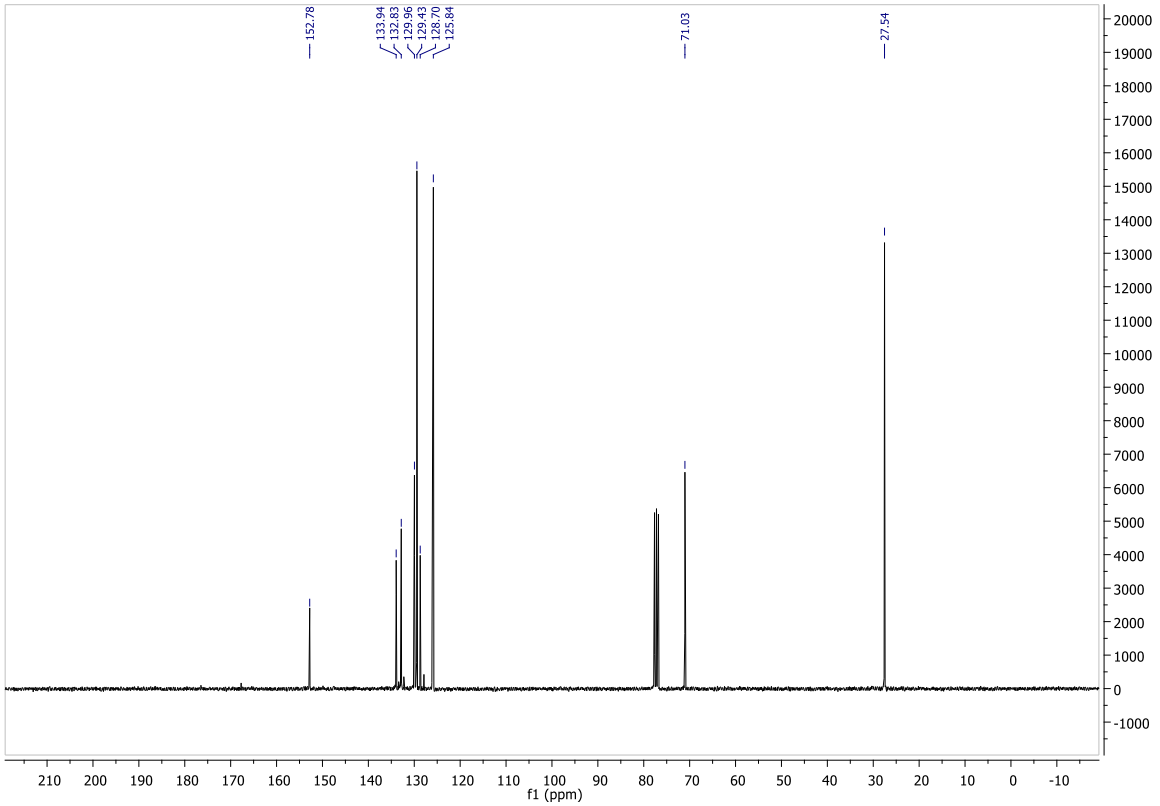
152.78
133.94
132.83
129.96
129.43
128.70
125.84
71.03
27.54
f1 (ppm)

2.12b

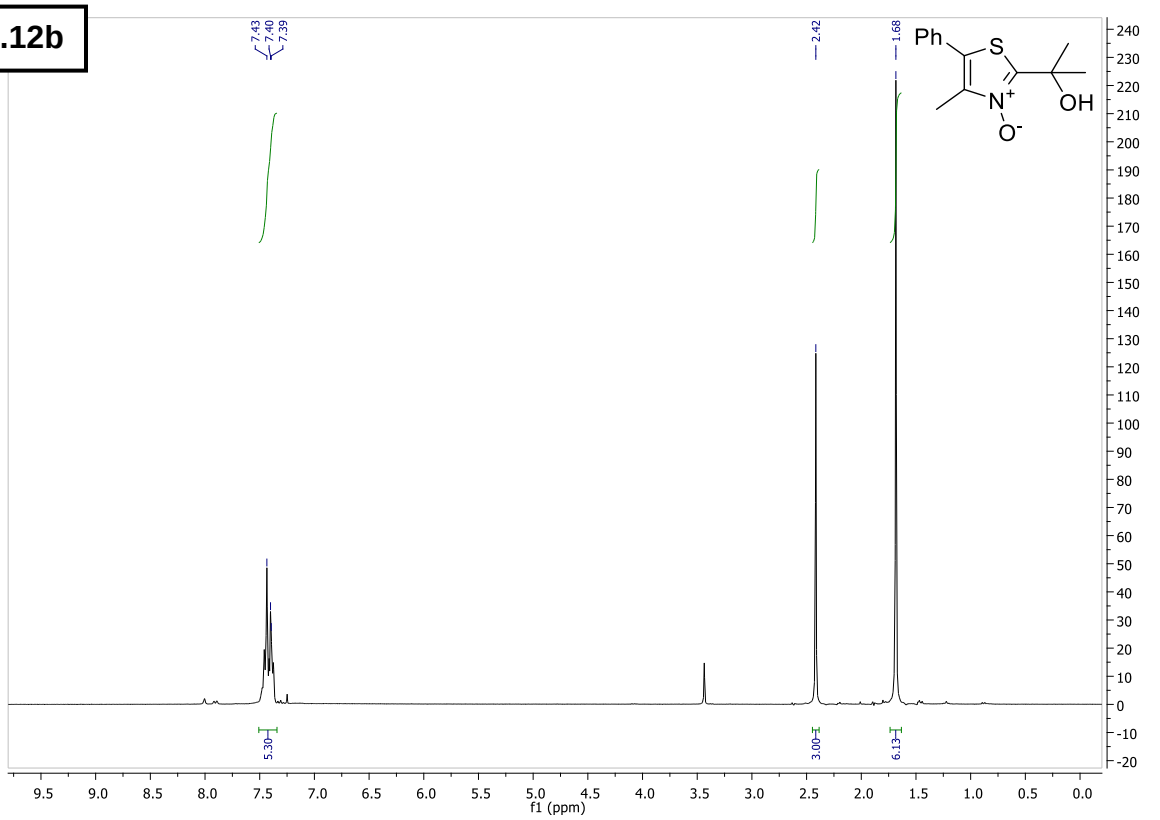
7.43
7.40
7.39
2.42
1.68
Ph
S
N+
O-
OH
5.30
3.00
6.13
f1 (ppm)

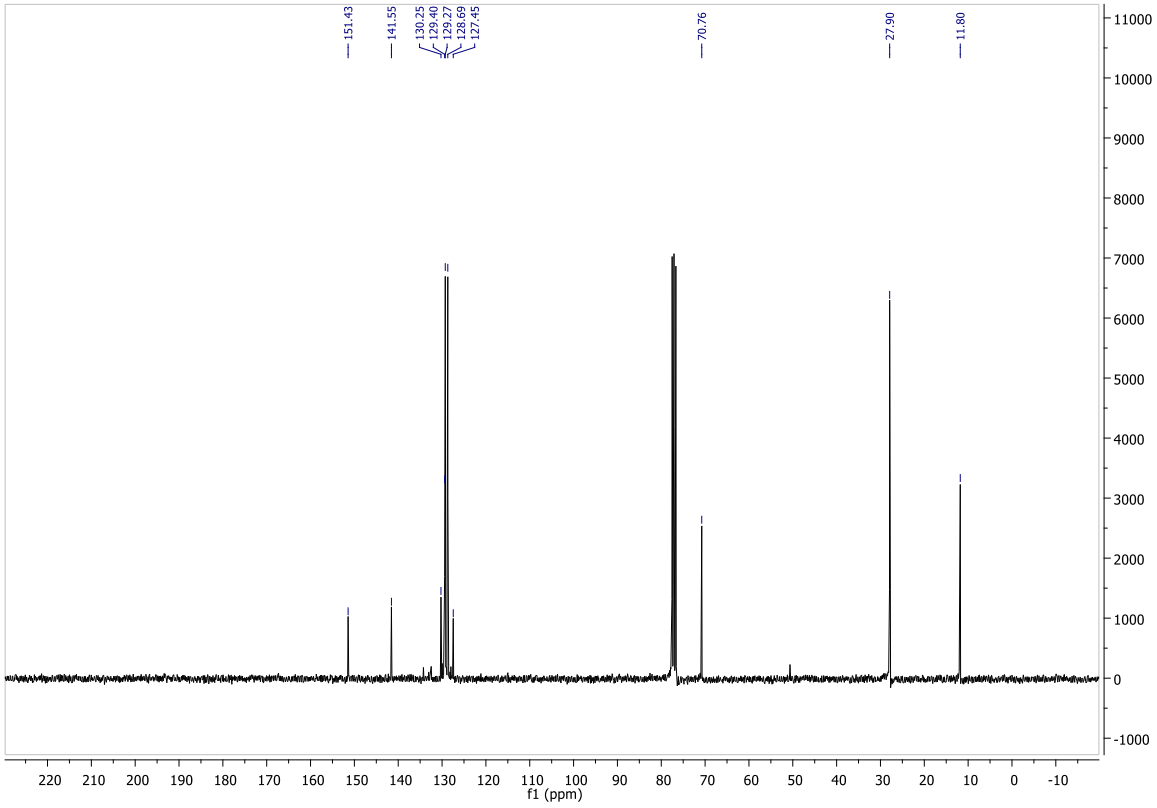
151.43
141.55
130.25
129.40
129.27
128.69
127.45
70.76
27.90
11.80
f1 (ppm)

2.13a

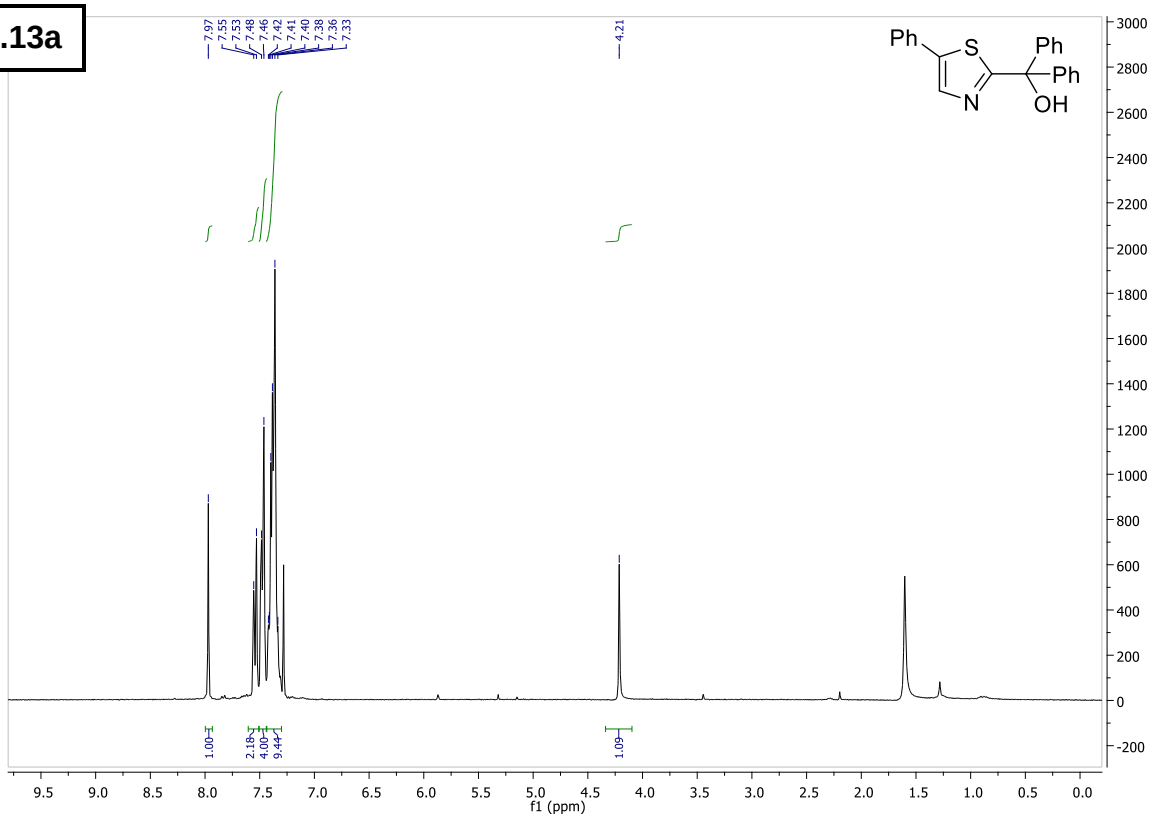
7.97
7.55
7.53
7.48
7.46
7.42
7.41
7.40
7.38
7.36
7.33
4.21
Ph
S
Ph
Ph
N
OH
1.00
2.18
4.00
9.44
1.09
f1 (ppm)

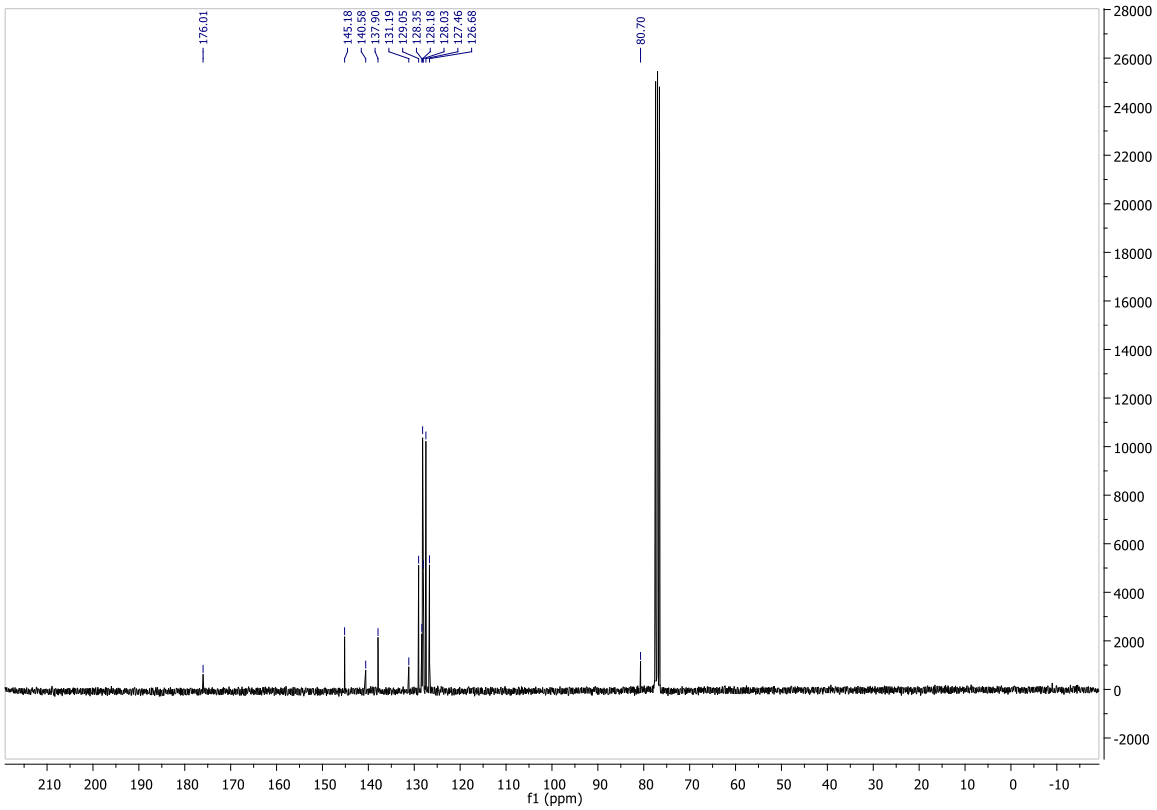
176.01
145.18
140.58
137.90
131.19
129.05
128.35
128.18
128.03
127.46
126.68
80.70
f1 (ppm)

2.13b

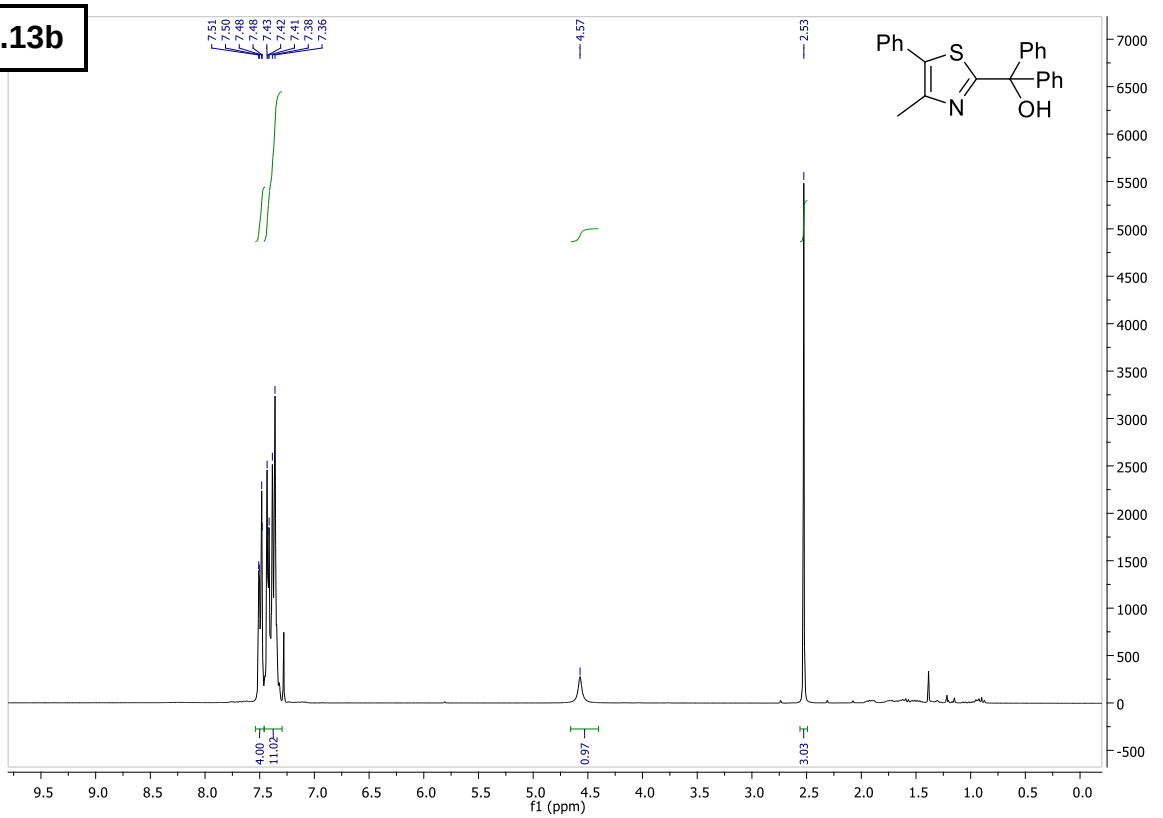
7.51
7.50
7.48
7.48
7.43
7.42
7.41
7.38
7.36
4.57
2.53
Ph
S
Ph
Ph
N
OH
4.00
11.02
0.97
3.03
f1 (ppm)

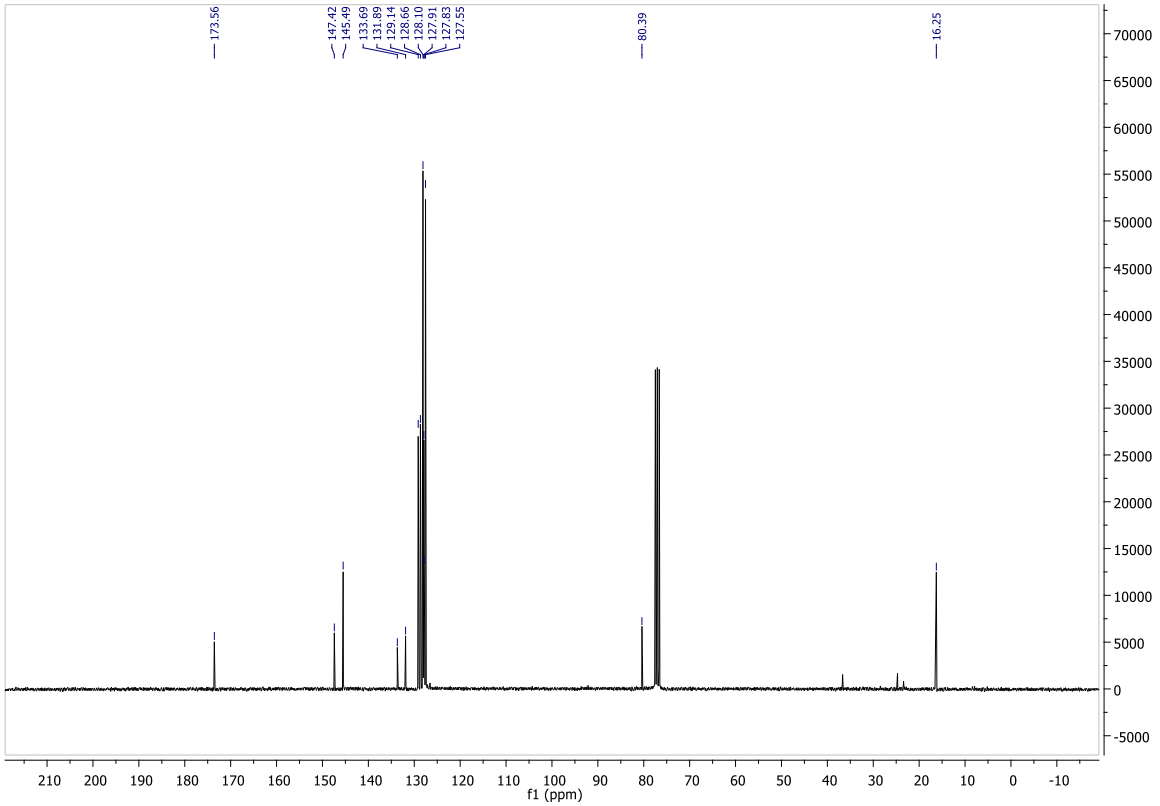
173.56
147.42
145.49
133.69
131.89
129.14
128.66
128.10
127.91
127.83
127.55
80.39
16.25
f1 (ppm)

2.13c

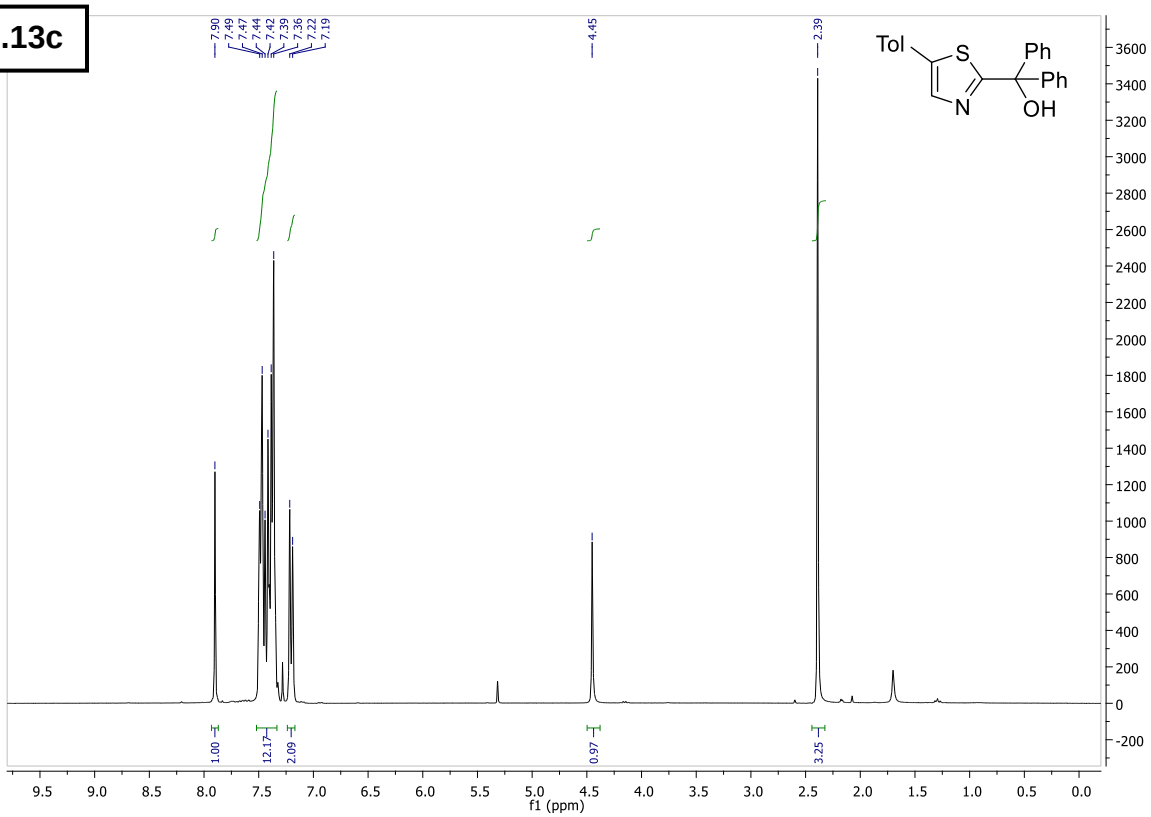
7.90
7.49
7.47
7.44
7.42
7.36
7.35
7.22
7.19
4.45
2.39
Tol
S
N
Ph
Ph
OH
1.00
12.17
2.09
0.97
3.25
f1 (ppm)

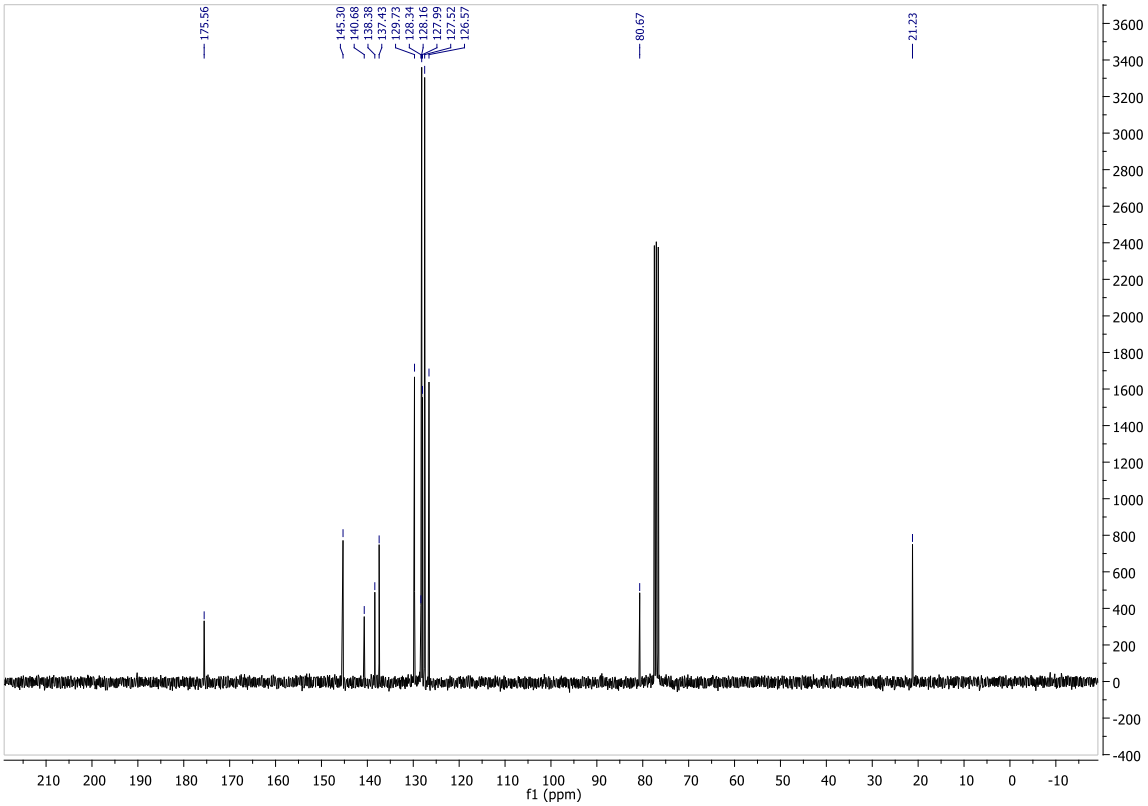
175.56
145.30
140.68
138.38
137.43
129.73
128.34
128.16
127.99
127.52
126.57
80.67
21.23
f1 (ppm)

2.13d

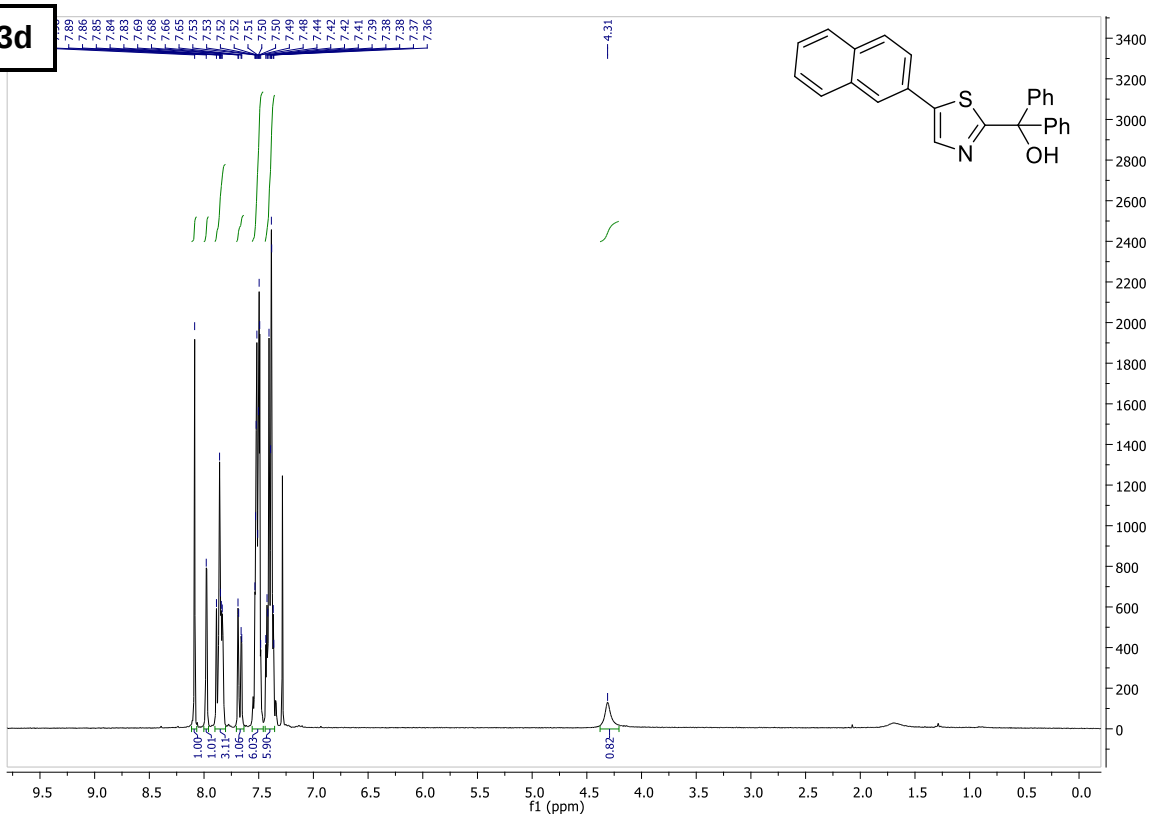
7.89
7.86
7.85
7.84
7.83
7.69
7.68
7.66
7.65
7.53
7.53
7.52
7.52
7.51
7.50
7.50
7.49
7.48
7.44
7.42
7.42
7.41
7.39
7.38
7.38
7.37
7.36
4.31
S
Ph
Ph
N
OH
1.00
1.01
3.11
1.06
6.03
5.90
0.82
f1 (ppm)

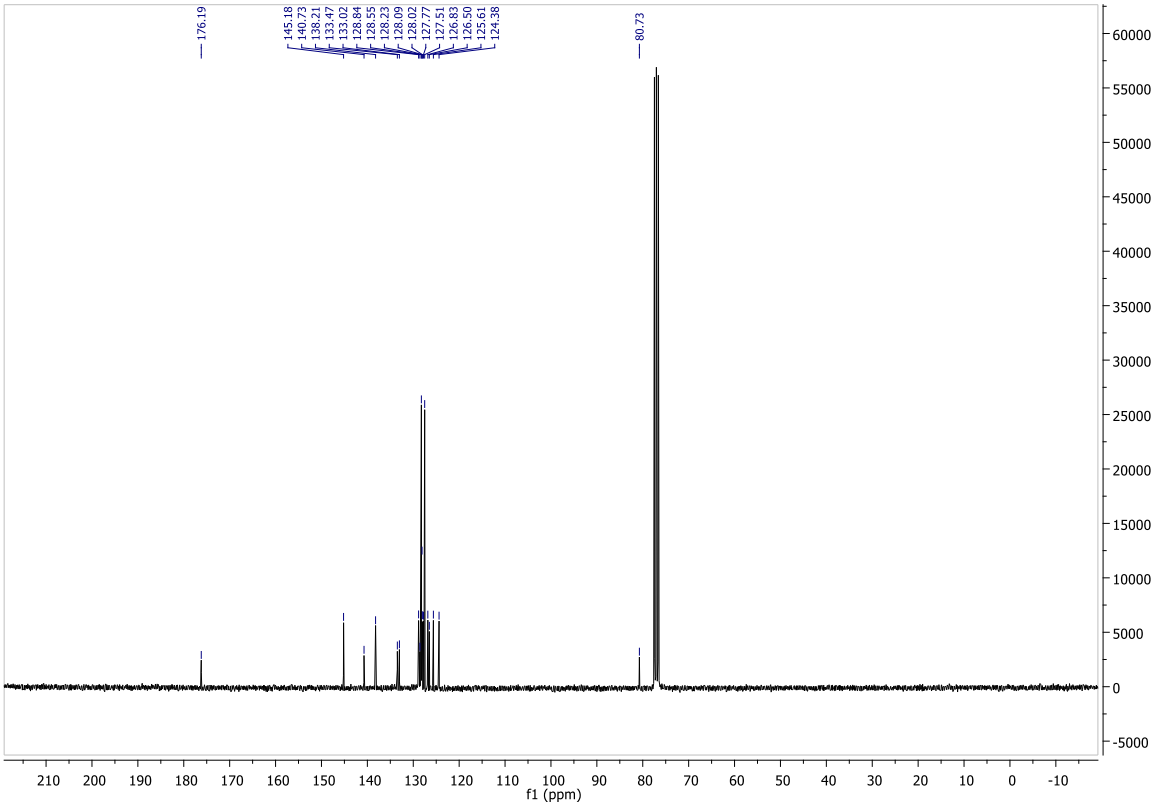
176.19
145.18
140.73
138.21
133.47
133.02
128.84
128.55
128.23
128.09
128.02
127.77
127.51
126.83
126.50
125.61
124.38
80.73
f1 (ppm)

2.13e

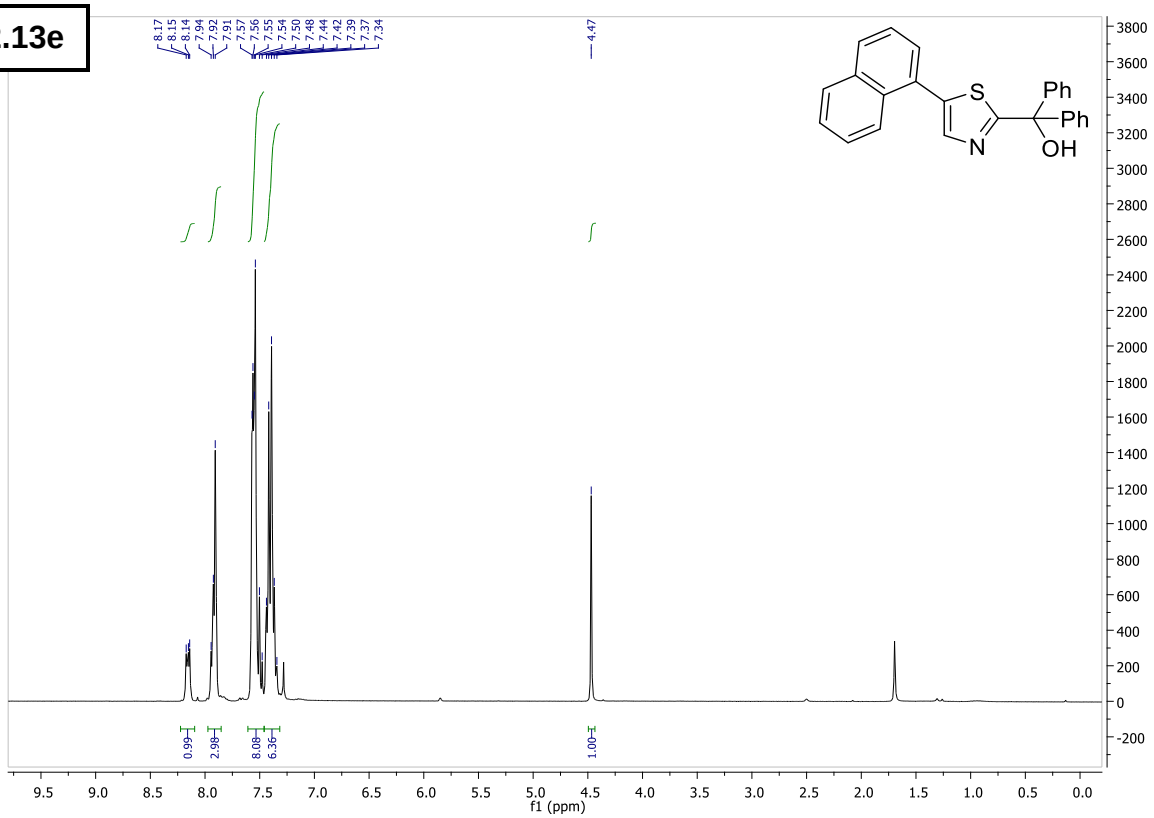
8.17
8.15
8.14
7.94
7.92
7.91
7.57
7.56
7.55
7.54
7.50
7.48
7.44
7.42
7.39
7.37
7.34
4.47
S
Ph
Ph
N
OH
0.99
2.98
8.08
6.36
1.00
f1 (ppm)

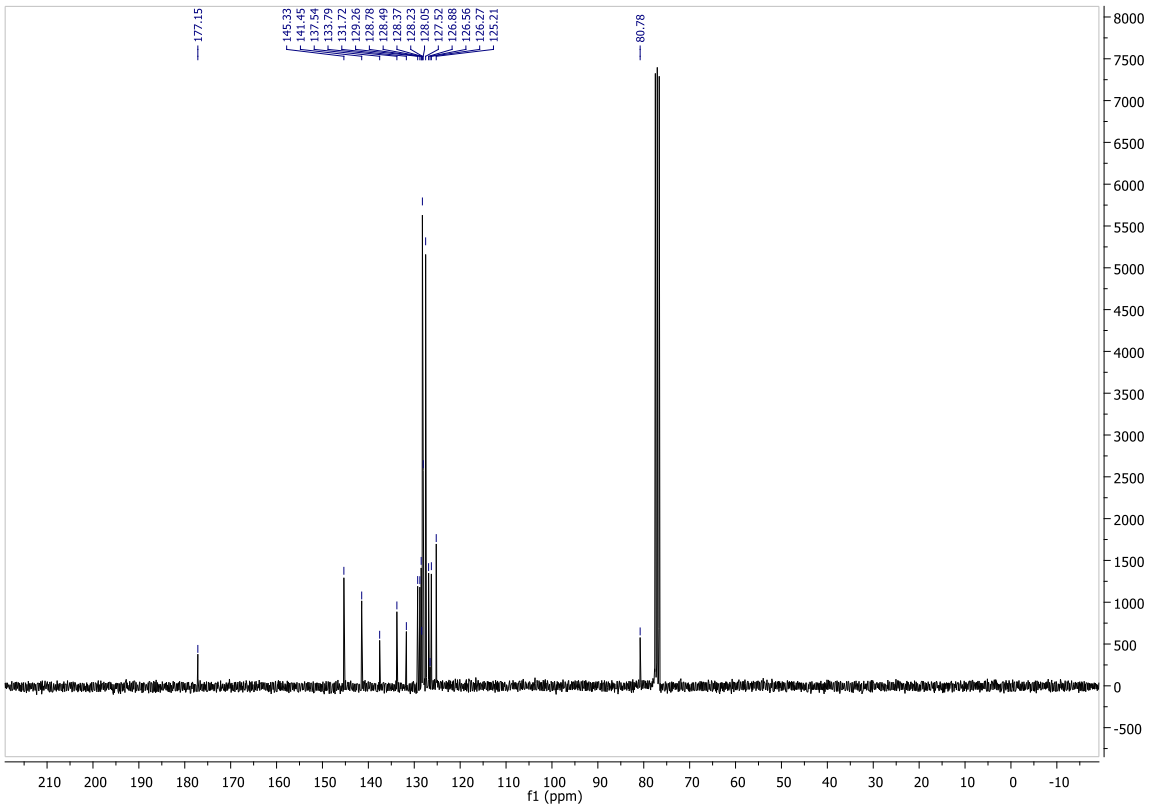
177.15
145.33
141.45
137.54
133.79
131.72
129.26
128.78
128.49
128.37
128.23
128.05
127.52
126.88
126.56
126.27
125.21
80.78
f1 (ppm)

2.13f

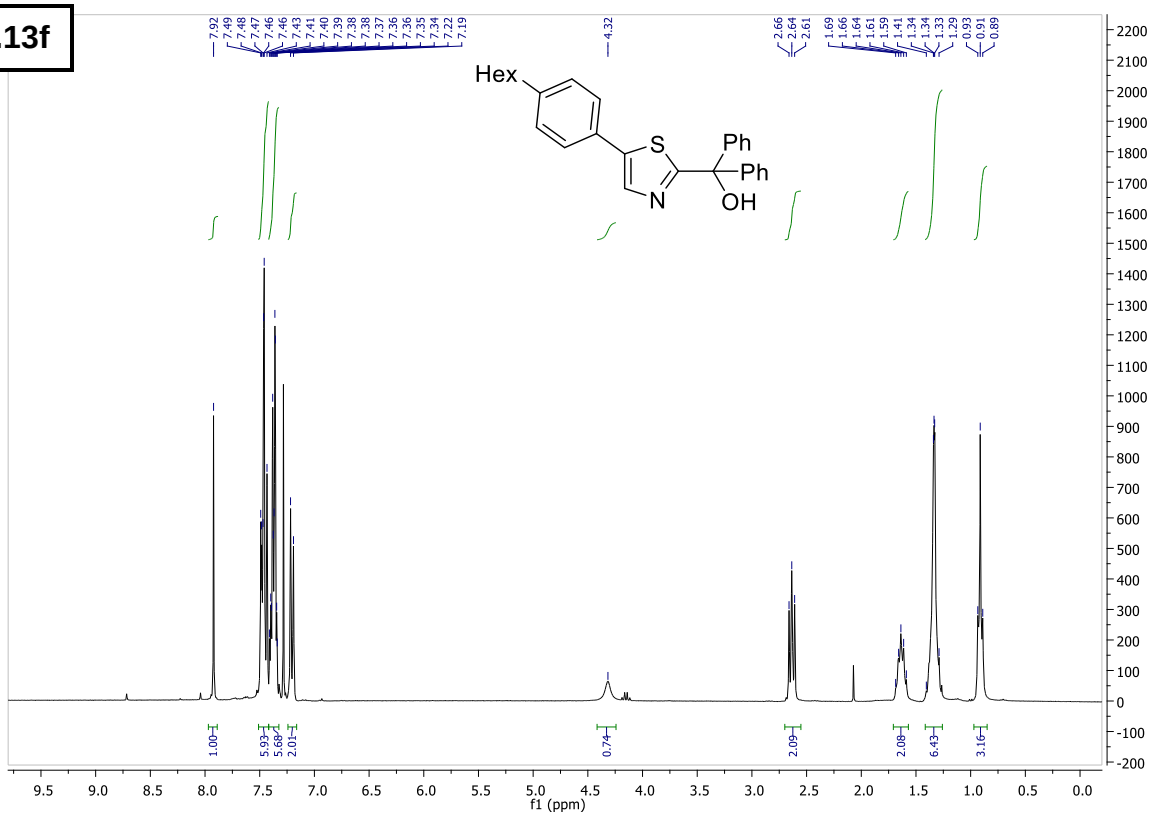
7.92
7.49
7.48
7.47
7.46
7.46
7.43
7.41
7.40
7.39
7.38
7.38
7.37
7.36
7.36
7.35
7.34
7.22
7.19
4.32
2.66
2.64
2.61
1.69
1.66
1.64
1.61
1.59
1.41
1.34
1.33
1.29
0.93
0.91
0.89
Hex
S
N
Ph
Ph
OH
1.00
5.93
5.68
2.01
0.74
2.09
2.08
6.43
3.16
f1 (ppm)

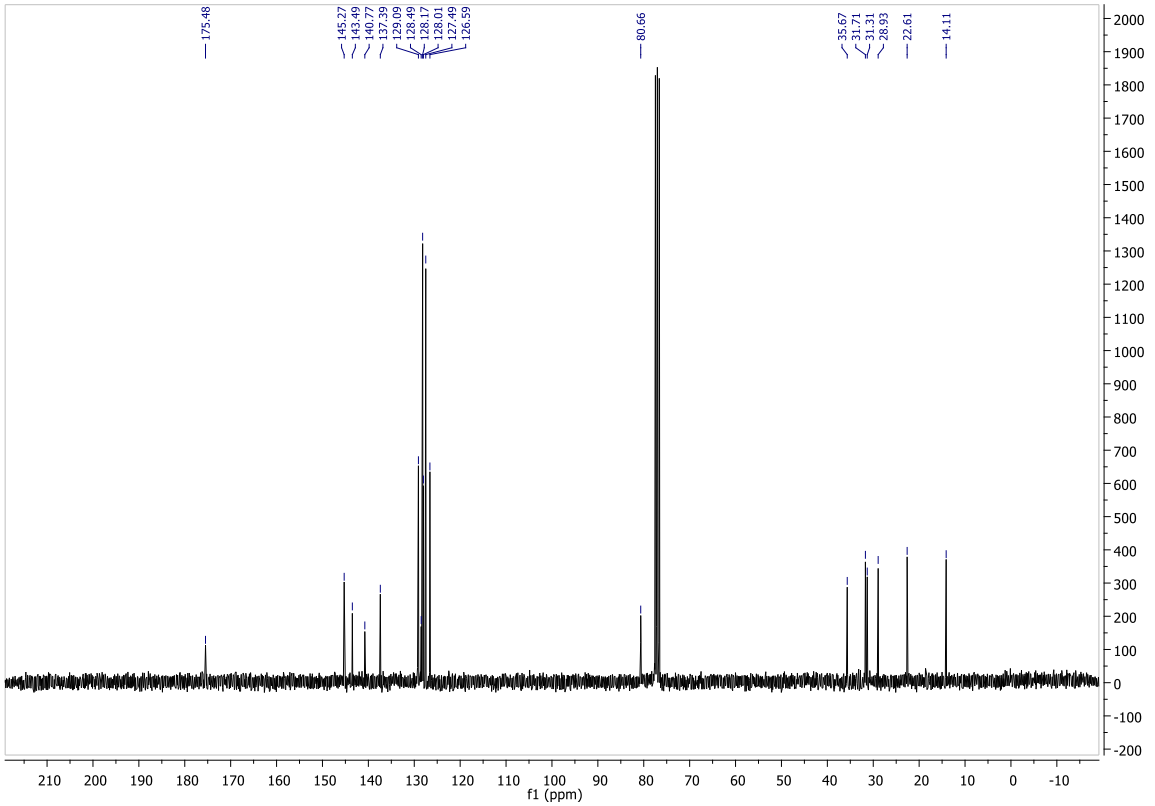
175.48
145.27
143.49
140.77
137.39
129.09
128.49
128.17
128.01
127.49
126.59
80.66
35.67
31.71
31.31
28.93
22.61
14.11
f1 (ppm)

2.13g

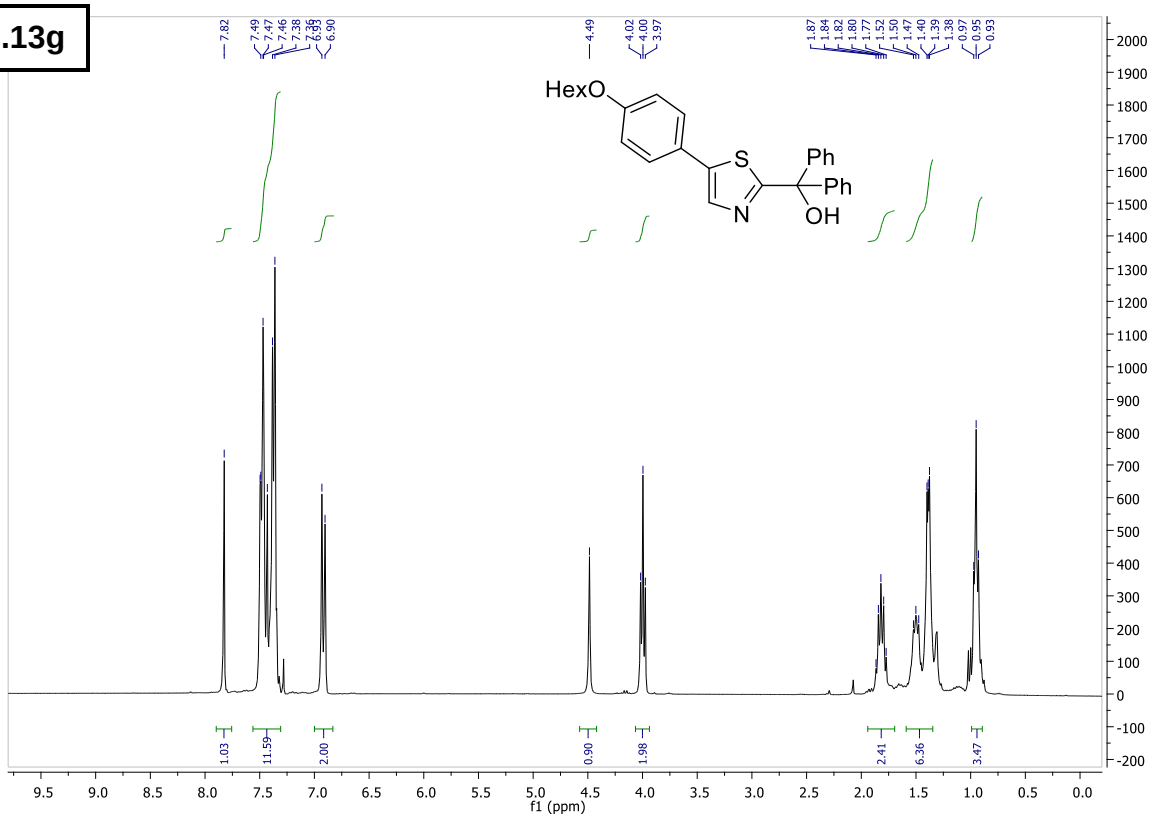
7.82
7.49
7.47
7.46
7.38
7.36
6.93
6.90
4.49
4.02
4.00
3.97
1.87
1.84
1.82
1.80
1.77
1.52
1.50
1.47
1.40
1.39
1.38
0.97
0.95
0.93
HexO
S
N
Ph
Ph
OH
1.03
11.59
2.00
0.90
1.98
2.41
6.36
3.47
f1 (ppm)

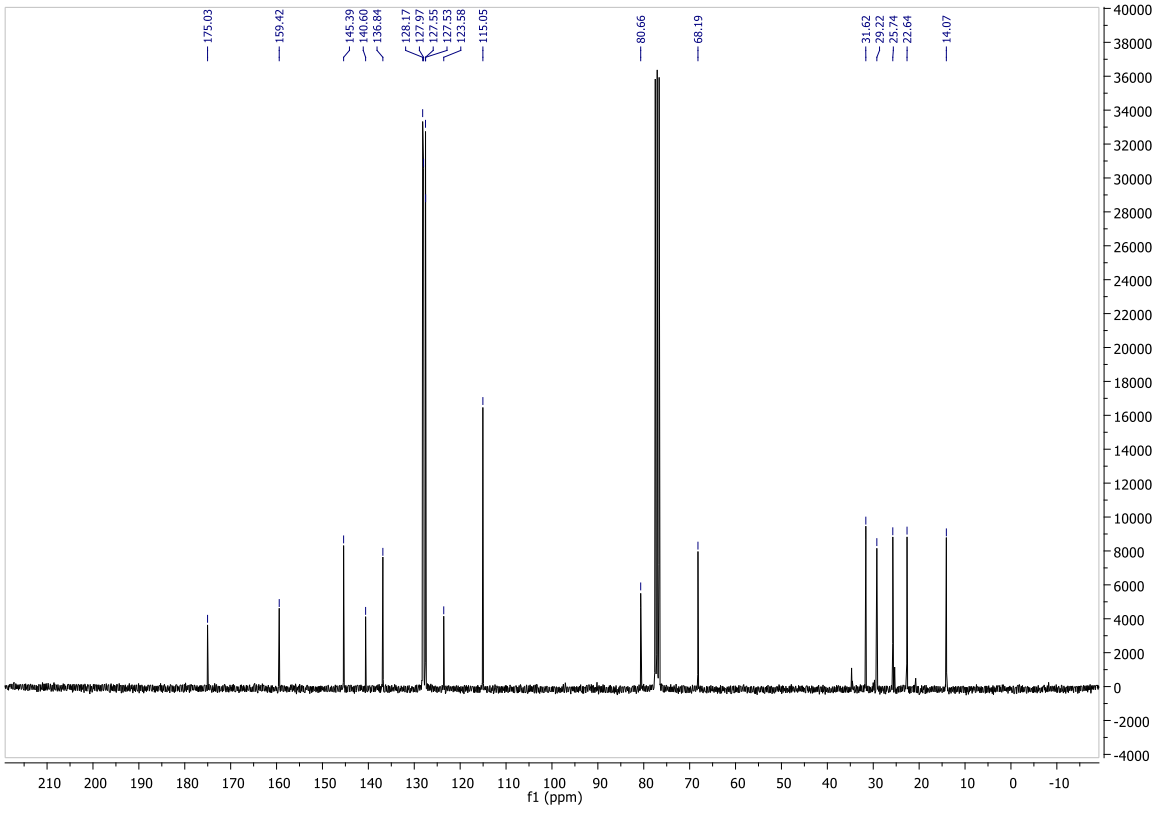
175.03
159.42
145.39
140.60
136.84
128.17
127.97
127.55
127.53
123.58
115.05
80.66
68.19
31.62
29.22
25.74
22.64
14.07
f1 (ppm)

2.13h

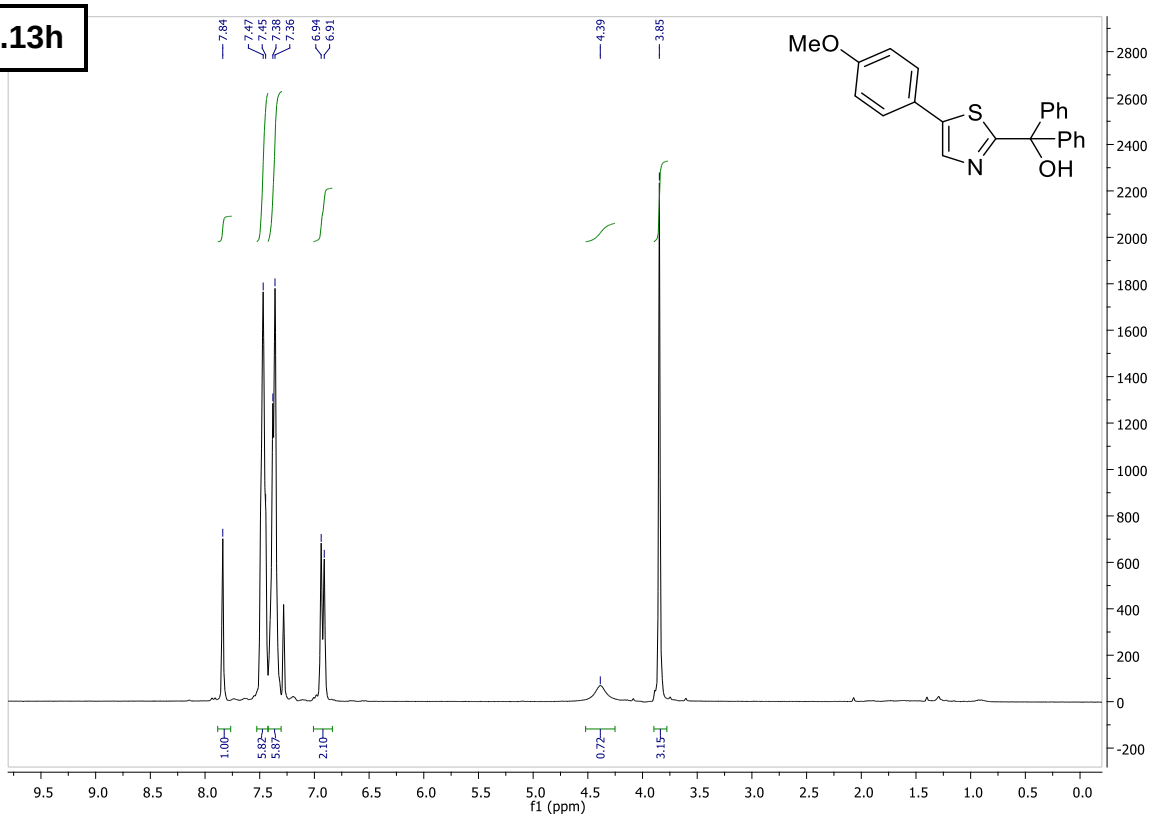
7.84
7.47
7.45
7.38
7.36
6.94
6.91
4.39
3.85
MeO
S
N
Ph
Ph
OH
1.00
5.82
5.87
2.10
0.72
3.15
f1 (ppm)

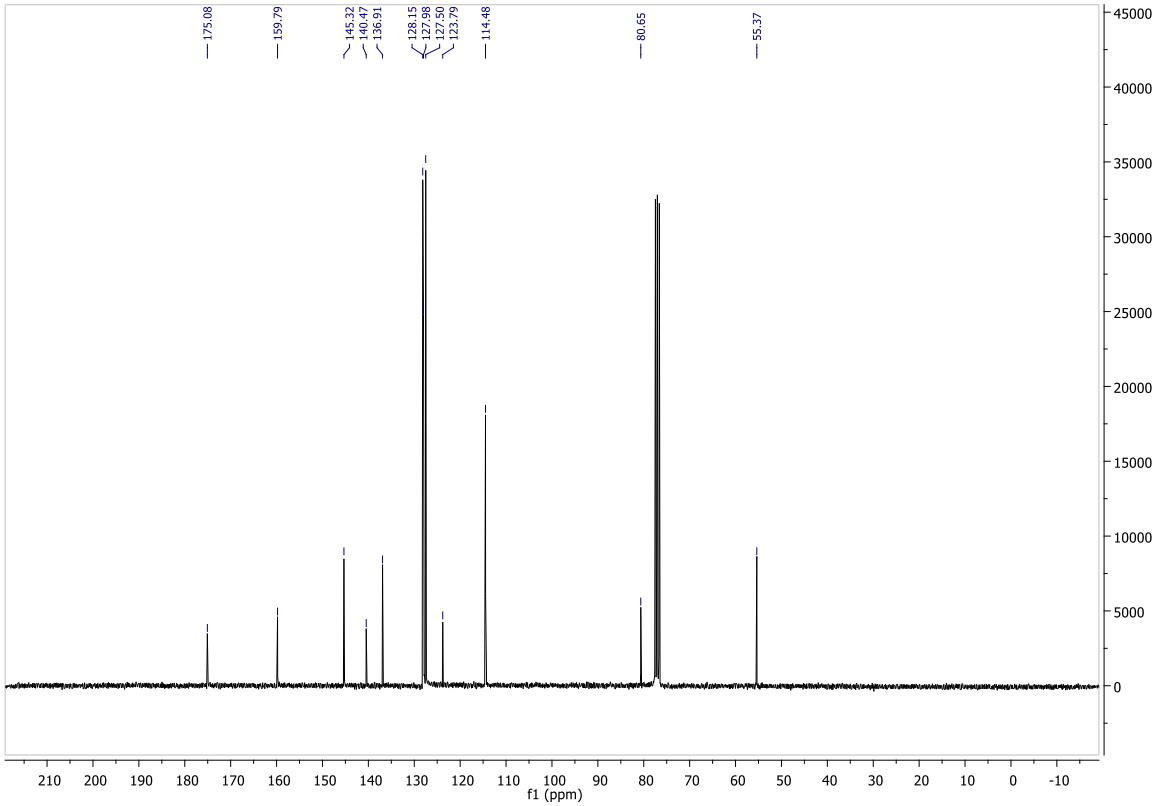
175.08
159.79
145.32
140.47
136.91
128.15
127.98
127.50
123.79
114.48
80.65
55.37
f1 (ppm)

2.13i

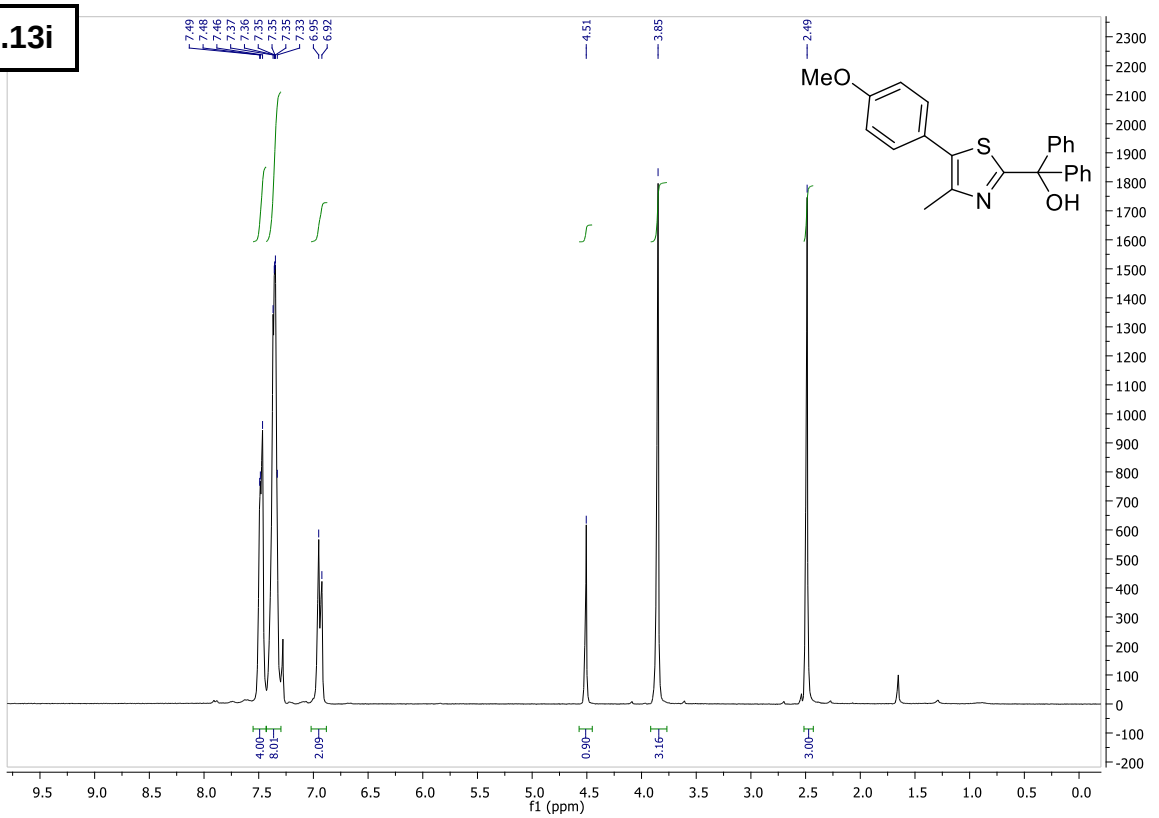
7.49
7.48
7.46
7.37
7.36
7.35
7.35
7.35
7.33
6.95
6.92
4.51
3.85
2.49
MeO
S
N
Ph
Ph
OH
4.00
8.01
2.09
0.90
3.16
3.00
f1 (ppm)

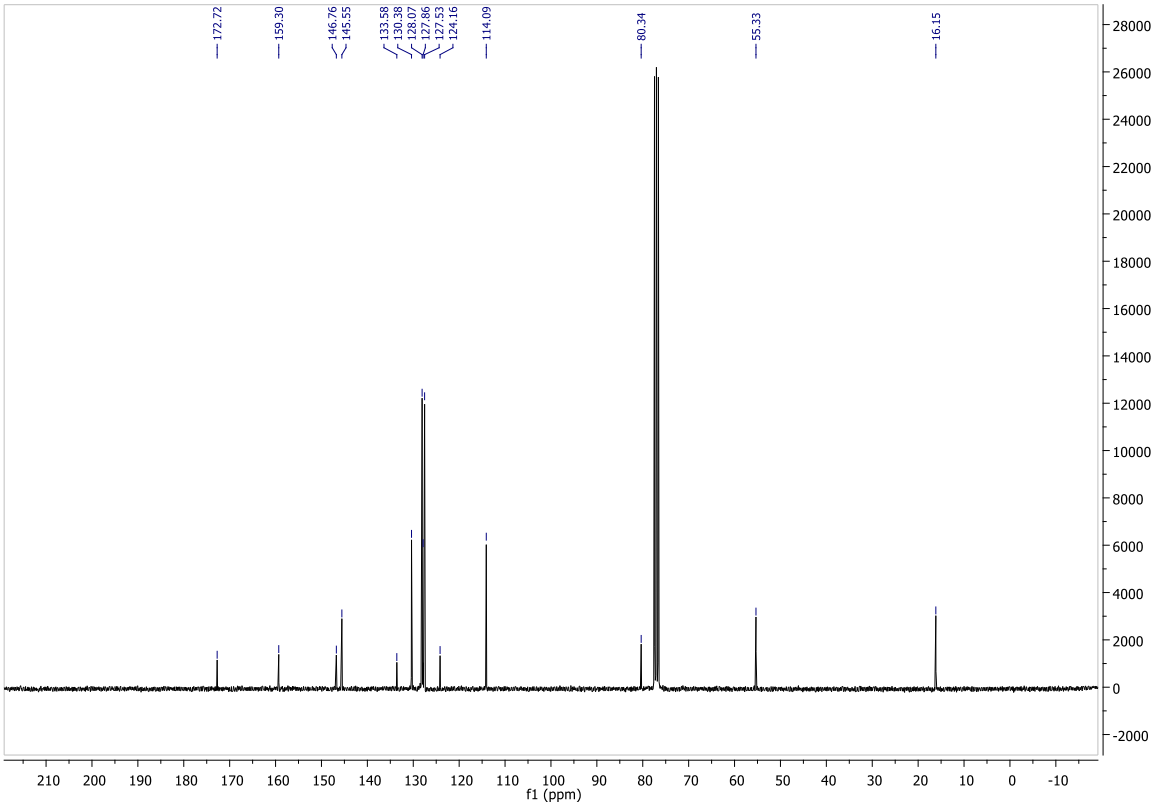
172.72
159.30
146.76
145.55
133.58
130.38
128.07
127.86
127.53
124.16
114.09
80.34
55.33
16.15
f1 (ppm)

2.13j

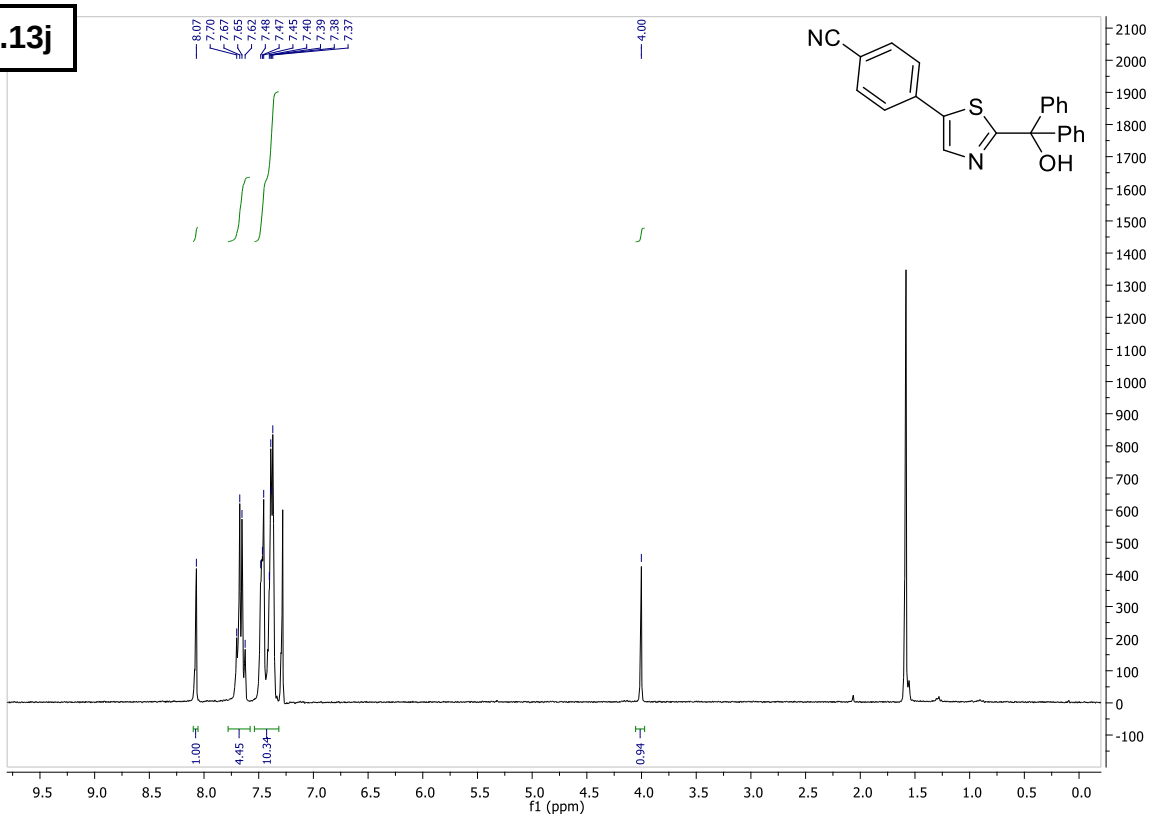
8.07
7.70
7.67
7.65
7.62
7.48
7.47
7.45
7.40
7.39
7.38
7.37
4.00
NC
S
N
Ph
Ph
OH
1.00
4.45
10.34
0.94
f1 (ppm)

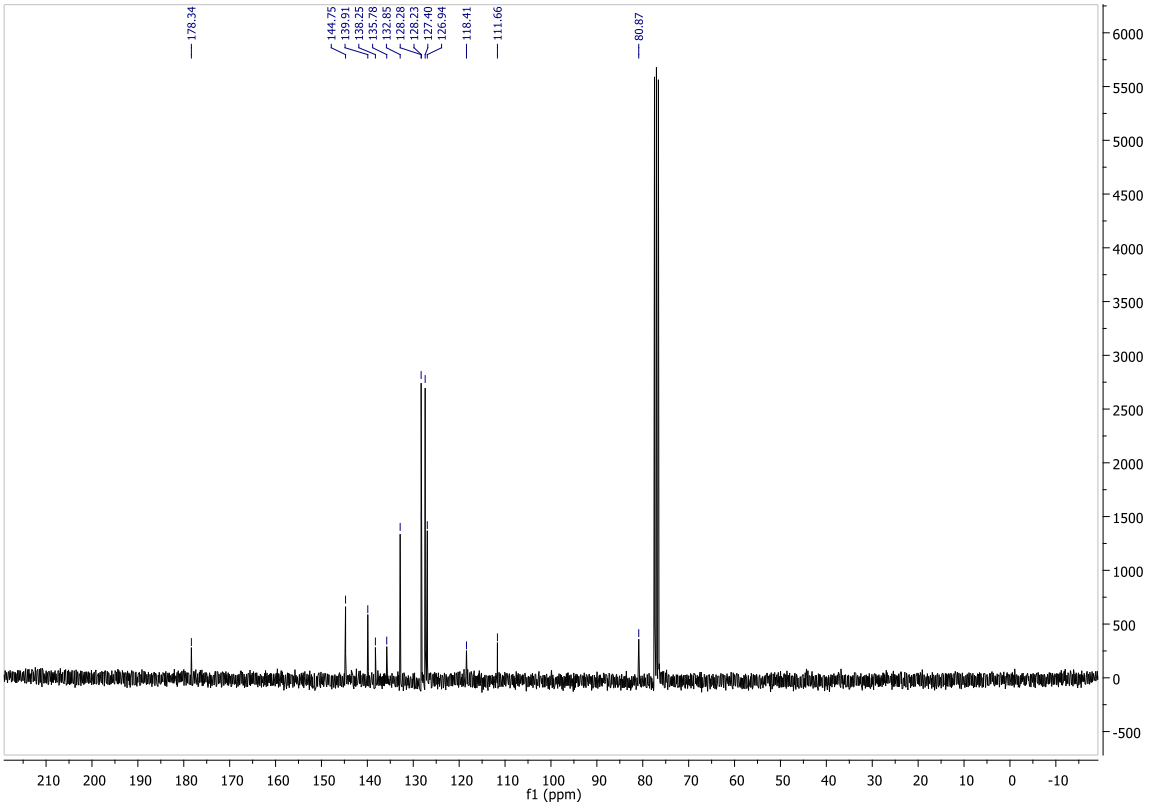
178.34
144.75
139.91
138.25
135.78
132.85
128.28
128.23
127.40
126.94
118.41
111.66
80.87
f1 (ppm)

2.13k

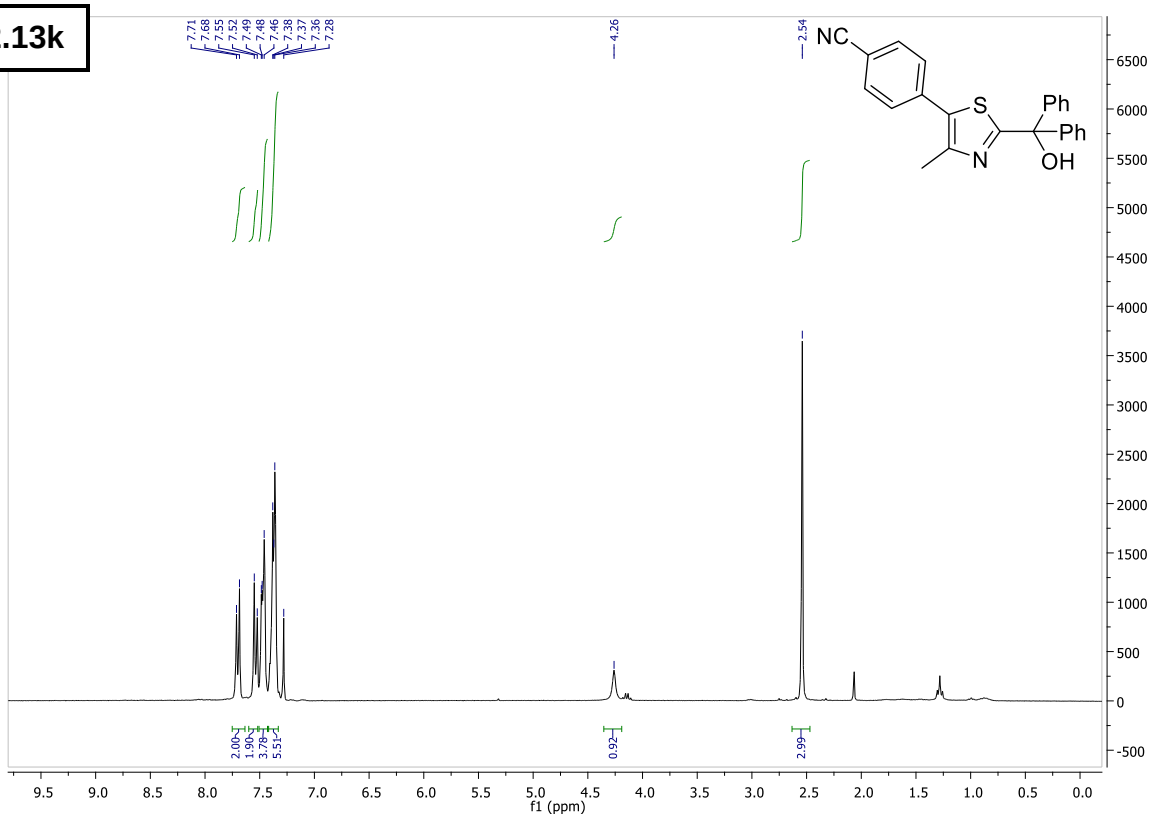
7.71
7.68
7.55
7.52
7.49
7.48
7.46
7.38
7.37
7.36
7.28
4.26
2.54
NC
S
N
Ph
Ph
OH
2.00
1.90
3.78
5.51
0.92
2.99
f1 (ppm)

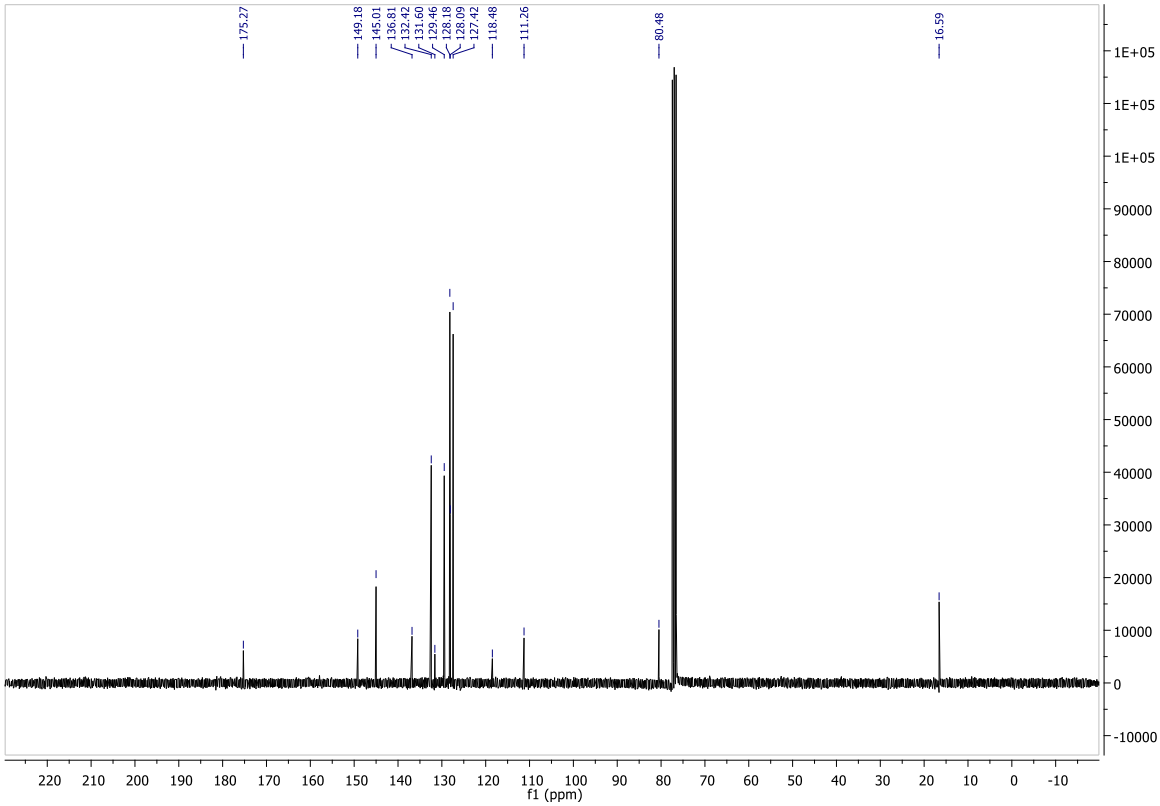
175.27
149.18
145.01
136.81
132.42
131.60
129.46
128.18
128.09
127.42
118.48
111.26
80.48
16.59
f1 (ppm)

2.13l

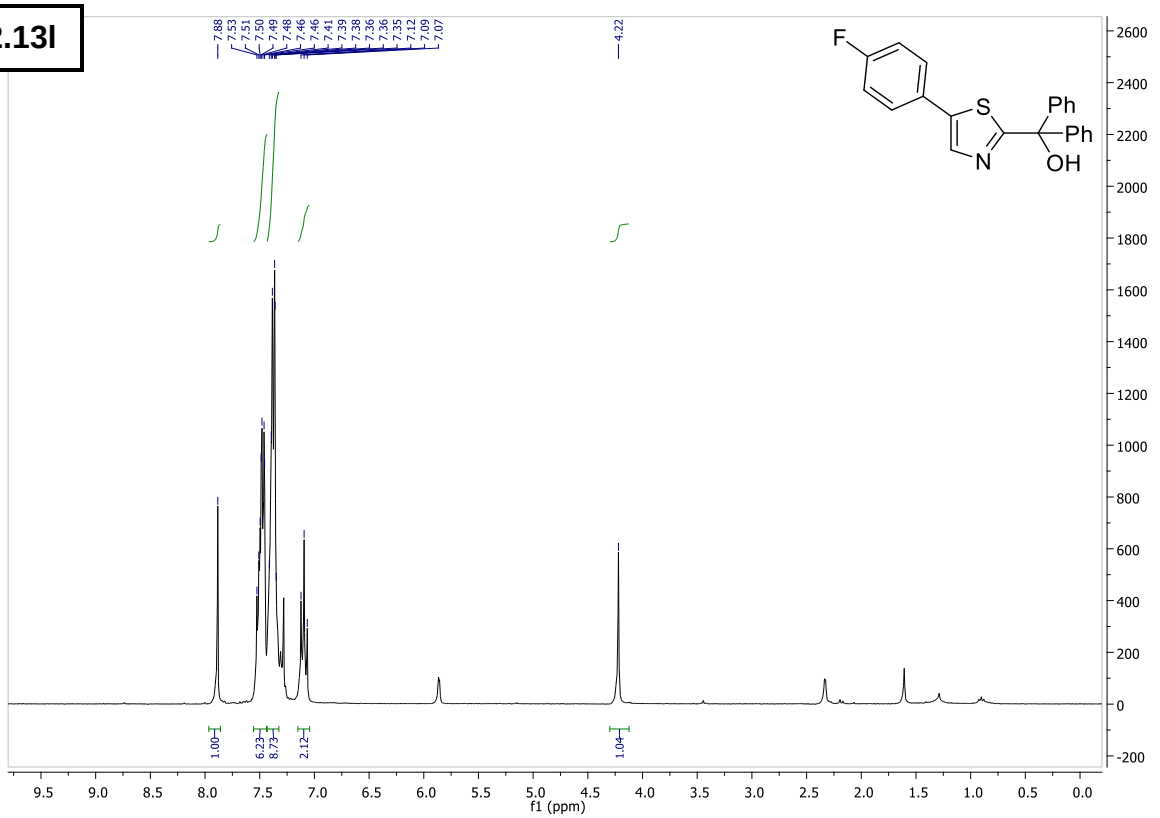
7.88
7.53
7.51
7.50
7.49
7.48
7.46
7.46
7.41
7.39
7.38
7.36
7.35
7.12
7.09
7.07
4.22
F
S
N
Ph
Ph
OH
1.00
6.23
8.73
2.12
1.04
f1 (ppm)

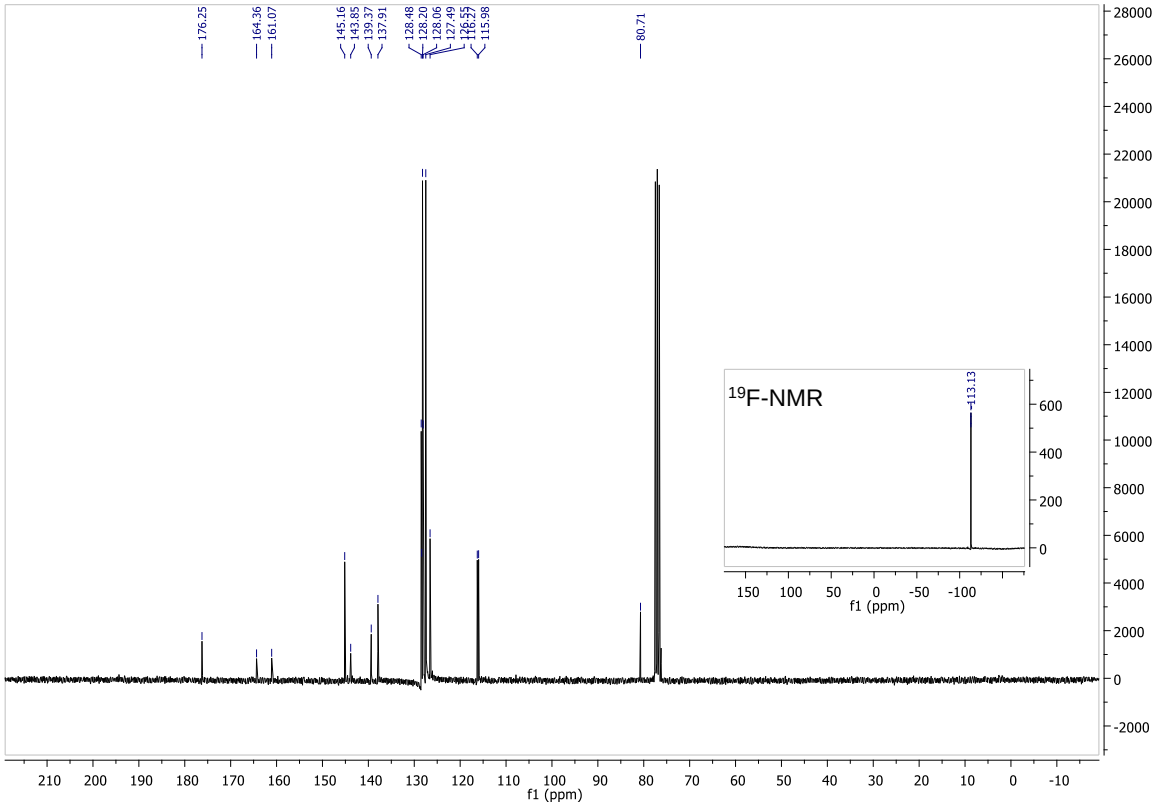
176.25
164.36
161.07
145.16
143.85
139.37
137.91
128.48
128.20
128.06
127.49
116.55
116.27
115.98
80.71
^{19}F-NMR
-113.13
f1 (ppm)
f1 (ppm)

2.13m

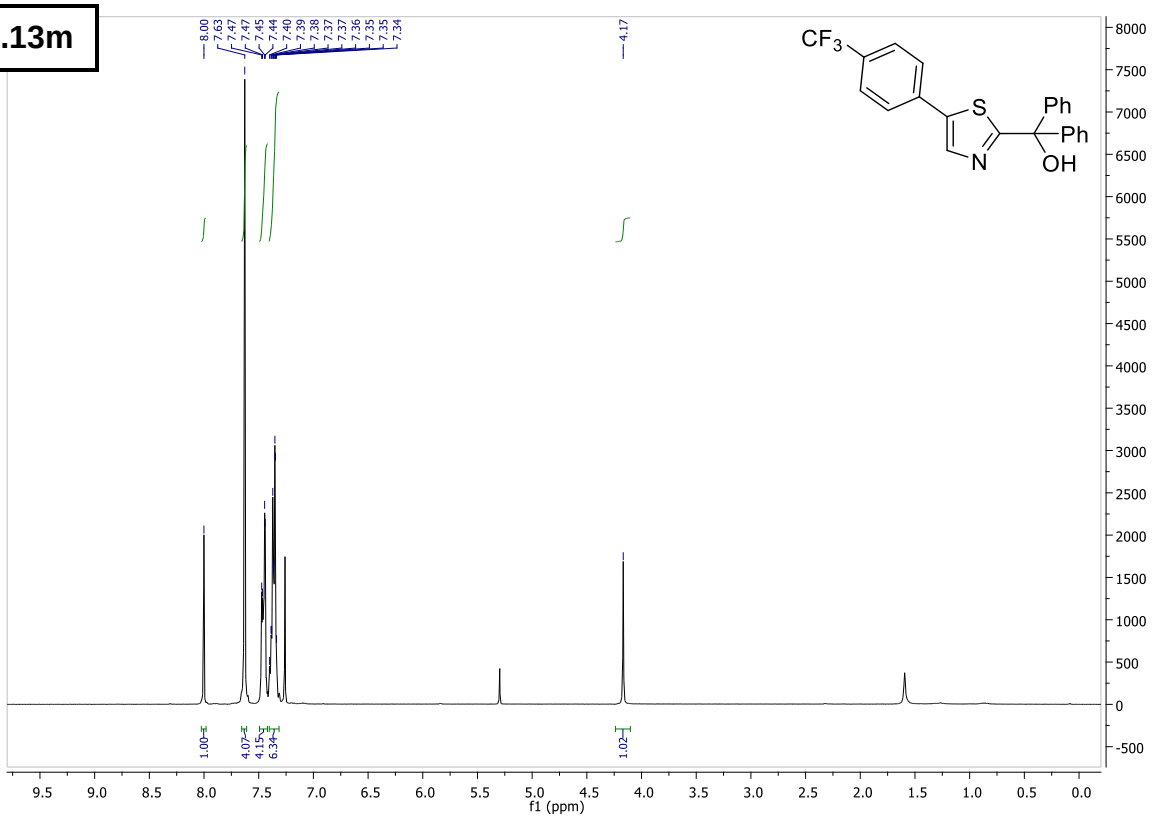
8.00
7.63
7.47
7.47
7.45
7.44
7.40
7.39
7.38
7.37
7.37
7.36
7.35
7.35
7.34
4.17
CF3
S
N
Ph
Ph
OH
1.00
4.07
4.15
6.34
1.02
f1 (ppm)

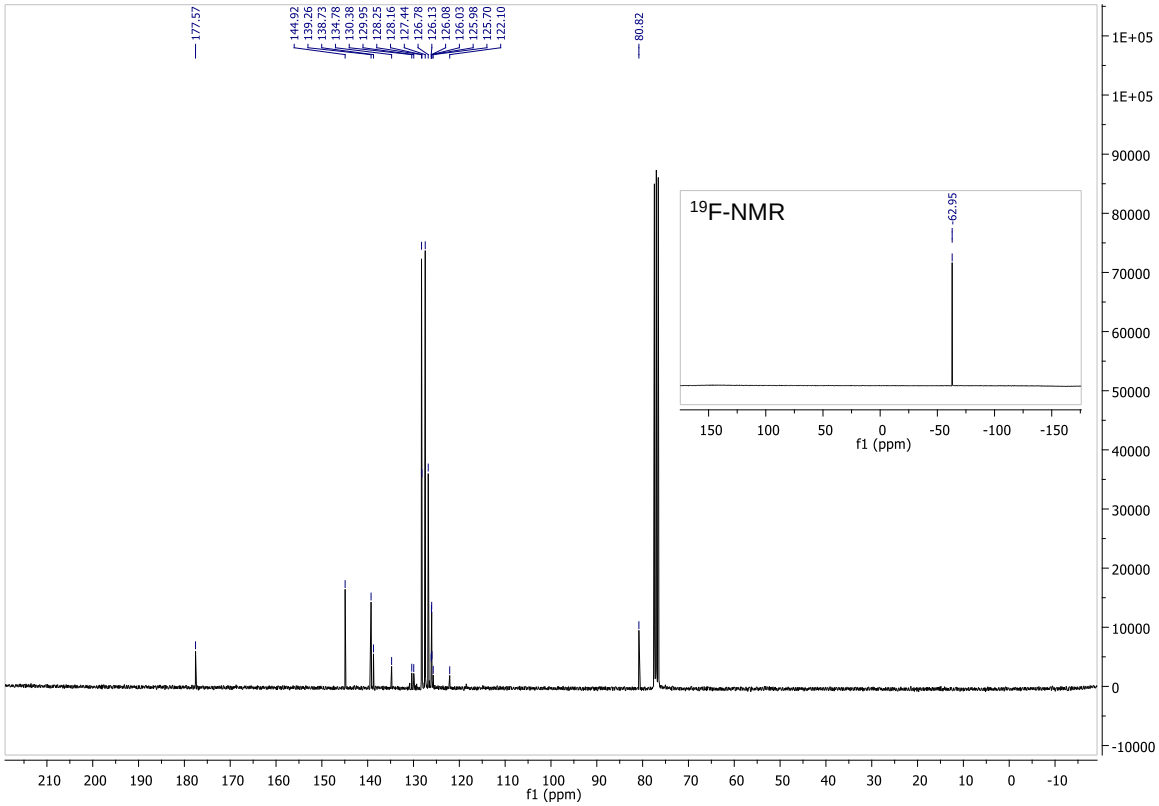
177.57
144.92
139.26
138.73
134.78
130.38
129.95
128.25
128.16
127.44
126.78
126.13
126.08
126.03
125.98
125.70
122.10
80.82
19F-NMR
-62.95
f1 (ppm)
f1 (ppm)

2.13n

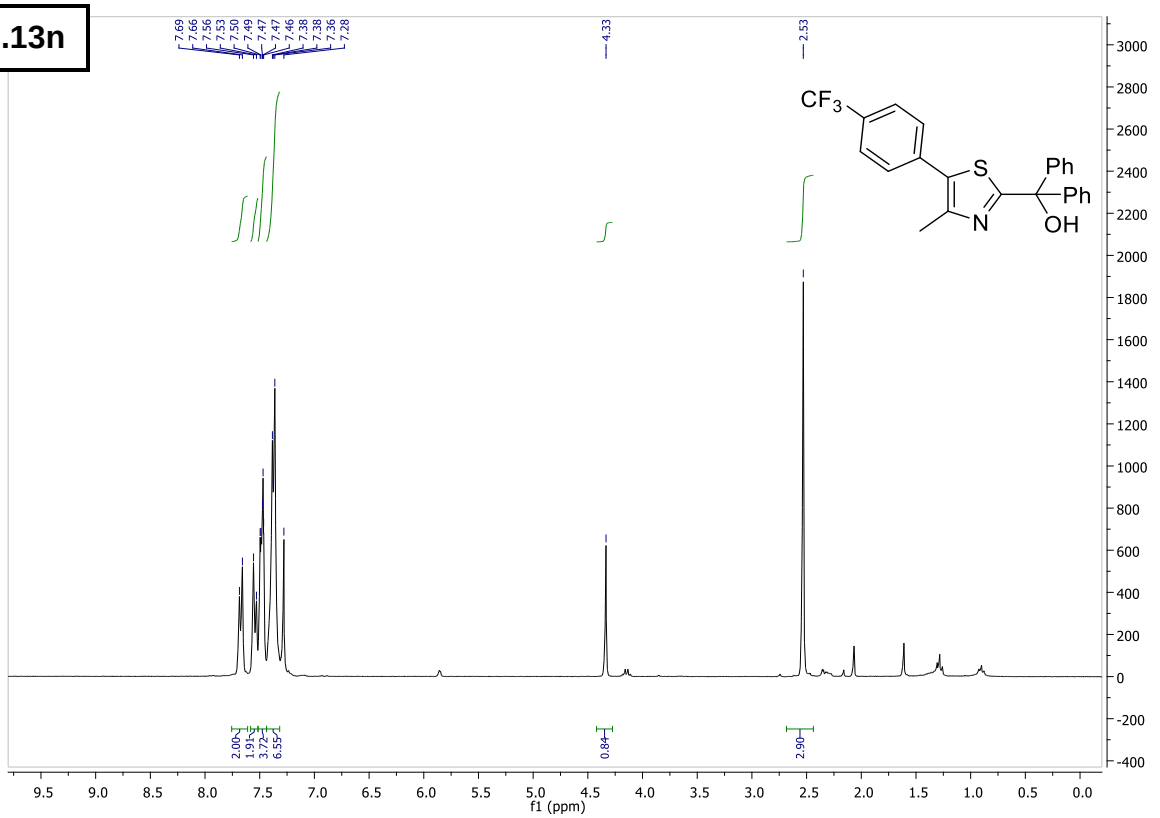
7.69
7.66
7.56
7.53
7.50
7.49
7.47
7.47
7.46
7.38
7.38
7.36
7.28
4.33
2.53
CF3
S
N
Ph
Ph
OH
2.00
1.91
3.72
6.55
0.84
2.90
f1 (ppm)

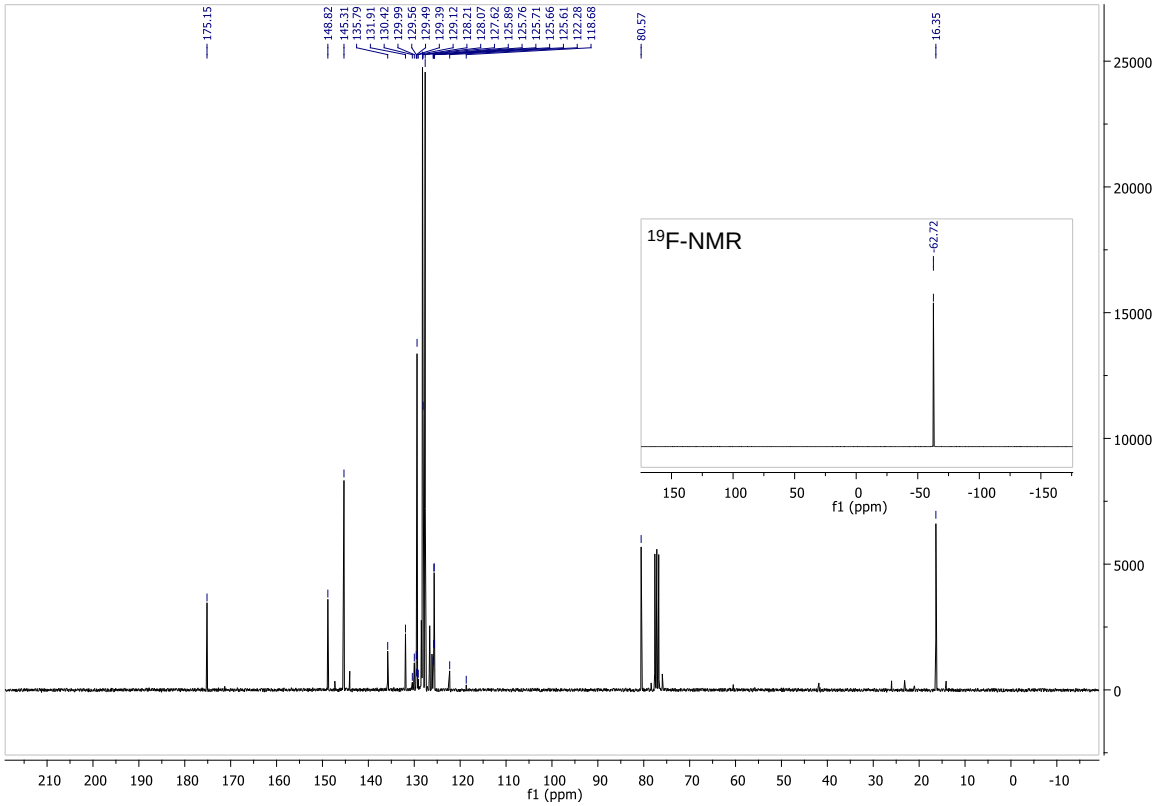
175.15
148.82
145.31
135.79
131.91
130.42
129.99
129.56
129.49
129.39
129.12
128.21
128.07
127.62
125.89
125.76
125.71
125.66
125.61
122.28
118.68
80.57
16.35
19F-NMR
-62.72
f1 (ppm)
f1 (ppm)

2.13o

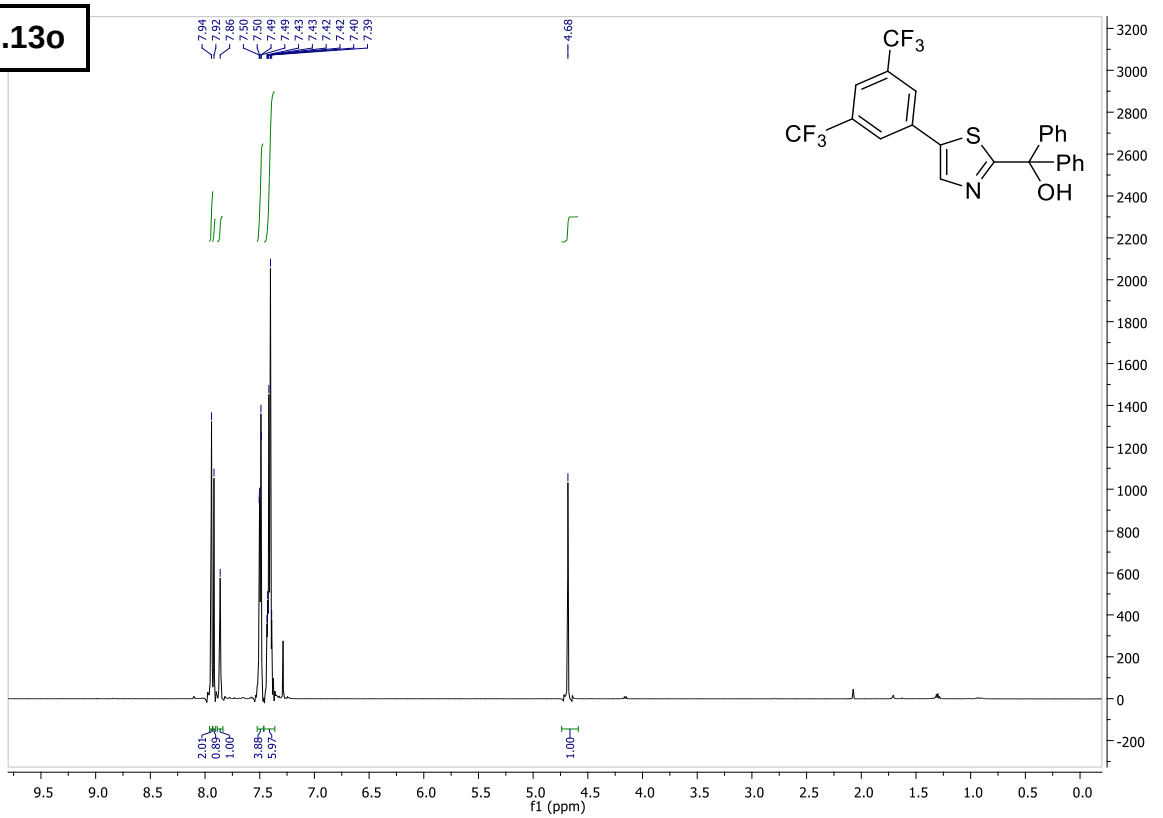
7.94
7.92
7.86
7.50
7.49
7.49
7.43
7.42
7.42
7.40
7.39
4.68
CF3
CF3
S
N
Ph
Ph
OH
2.01
0.89
1.00
3.89
5.97
1.00
f1 (ppm)

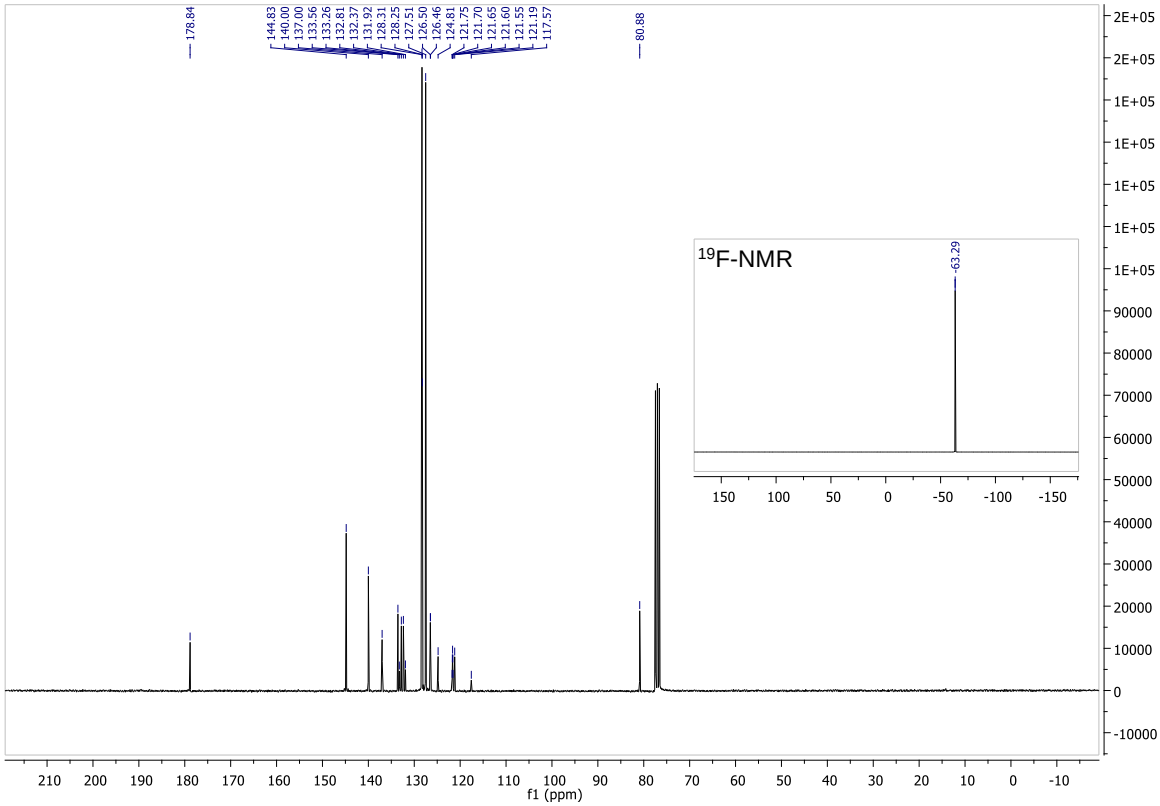
178.84
144.83
140.00
137.00
133.56
133.26
132.81
132.37
131.92
128.31
128.25
127.51
126.50
126.46
124.81
121.75
121.70
121.65
121.60
121.55
121.19
117.57
80.88
19F-NMR
-63.29
f1 (ppm)

2.13p

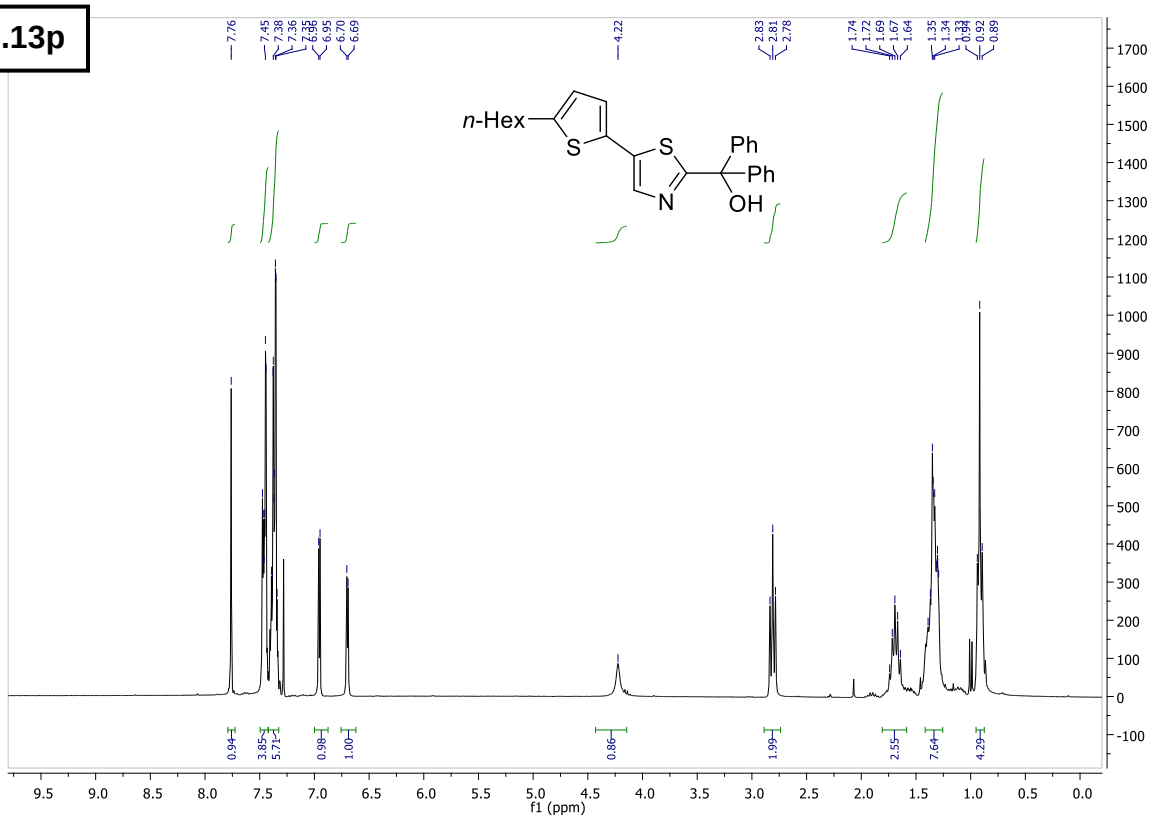
7.76
7.45
7.38
7.36
7.35
6.95
6.70
6.69
4.22
2.83
2.81
2.78
1.74
1.72
1.69
1.67
1.64
1.35
1.34
0.94
0.92
0.89
n-Hex
S
S
N
Ph
Ph
OH
0.94
3.85
5.71
0.98
1.00
0.86
1.99
2.55
7.64
4.29
f1 (ppm)

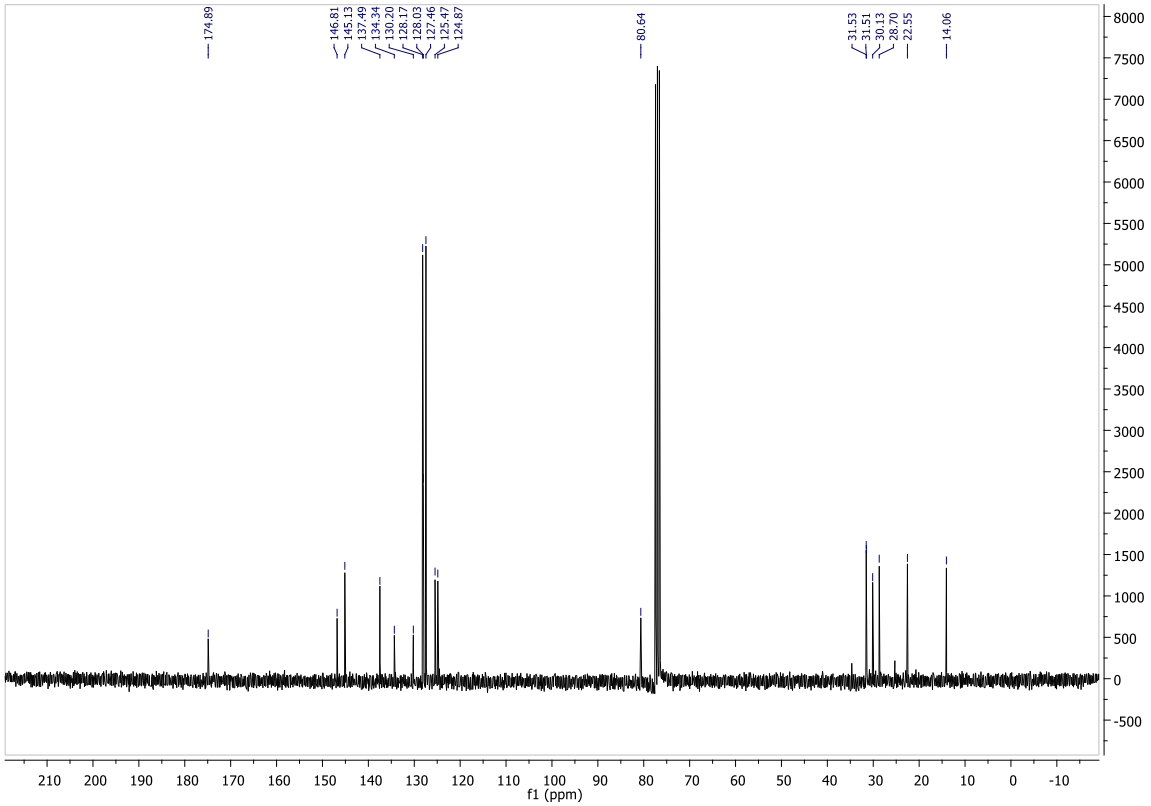
174.89
146.81
145.13
137.49
134.34
130.20
128.17
128.03
127.46
125.47
124.87
80.64
31.53
31.51
30.13
28.70
22.55
14.06
f1 (ppm)

2.13q

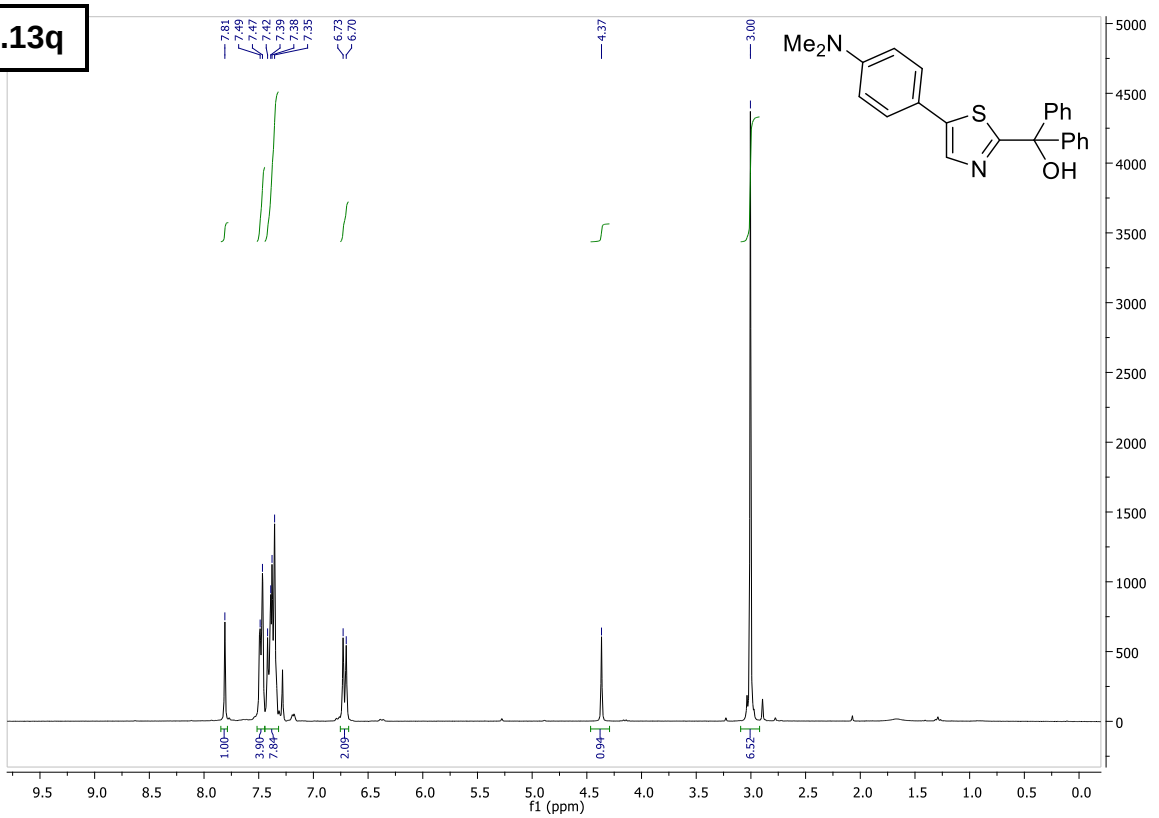
7.81
7.49
7.47
7.42
7.39
7.38
7.35
6.73
6.70
4.37
3.00
Me2N
S
Ph
Ph
N
OH
1.00
3.90
7.84
2.09
0.94
6.52
f1 (ppm)

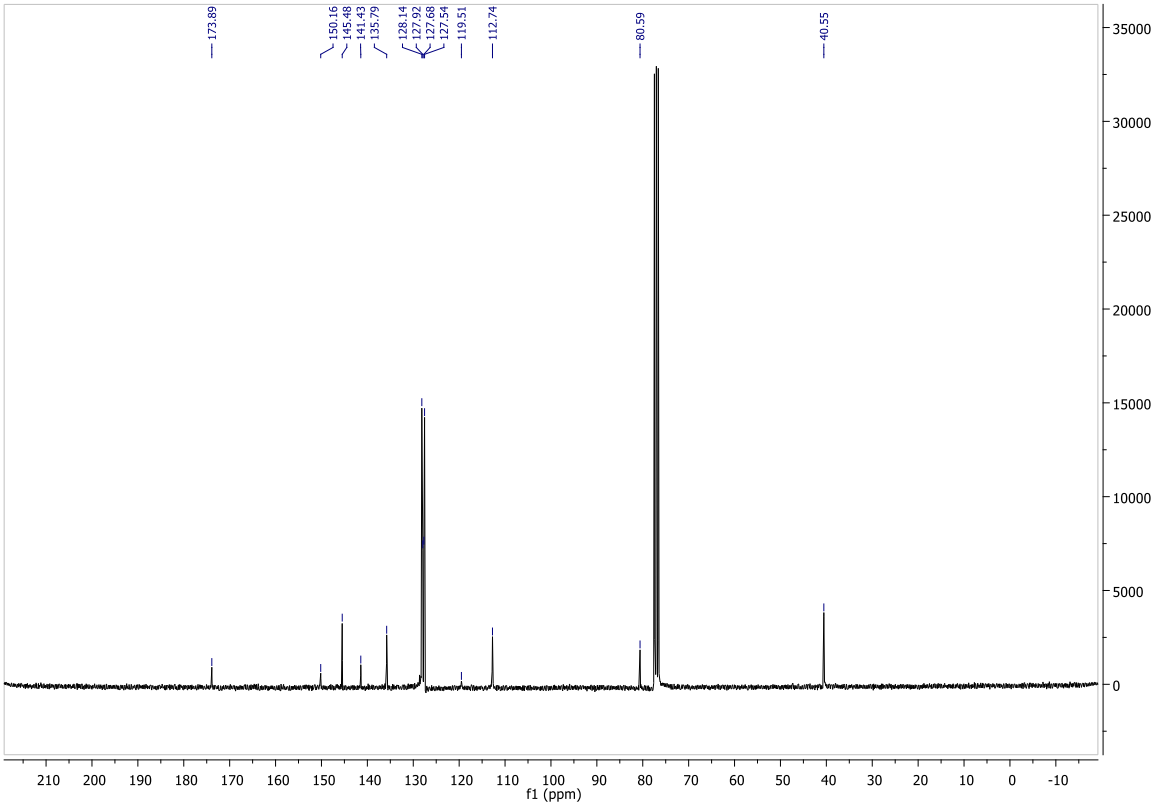
173.89
150.16
145.48
141.43
135.79
128.14
127.92
127.68
127.54
119.51
112.74
80.59
40.55
f1 (ppm)

2.14a

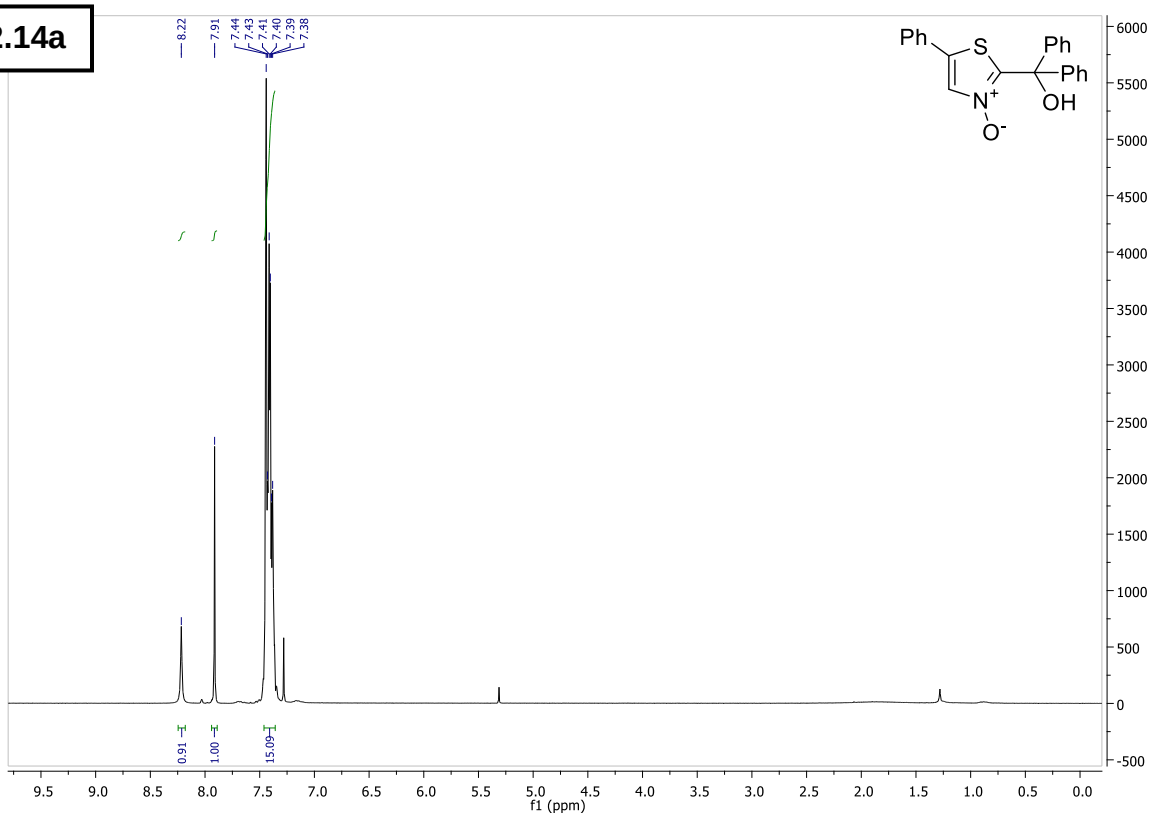
8.22
7.91
7.44
7.43
7.41
7.40
7.39
7.38
Ph
S
Ph
Ph
OH
N+
O-
0.91
1.00
15.09
f1 (ppm)

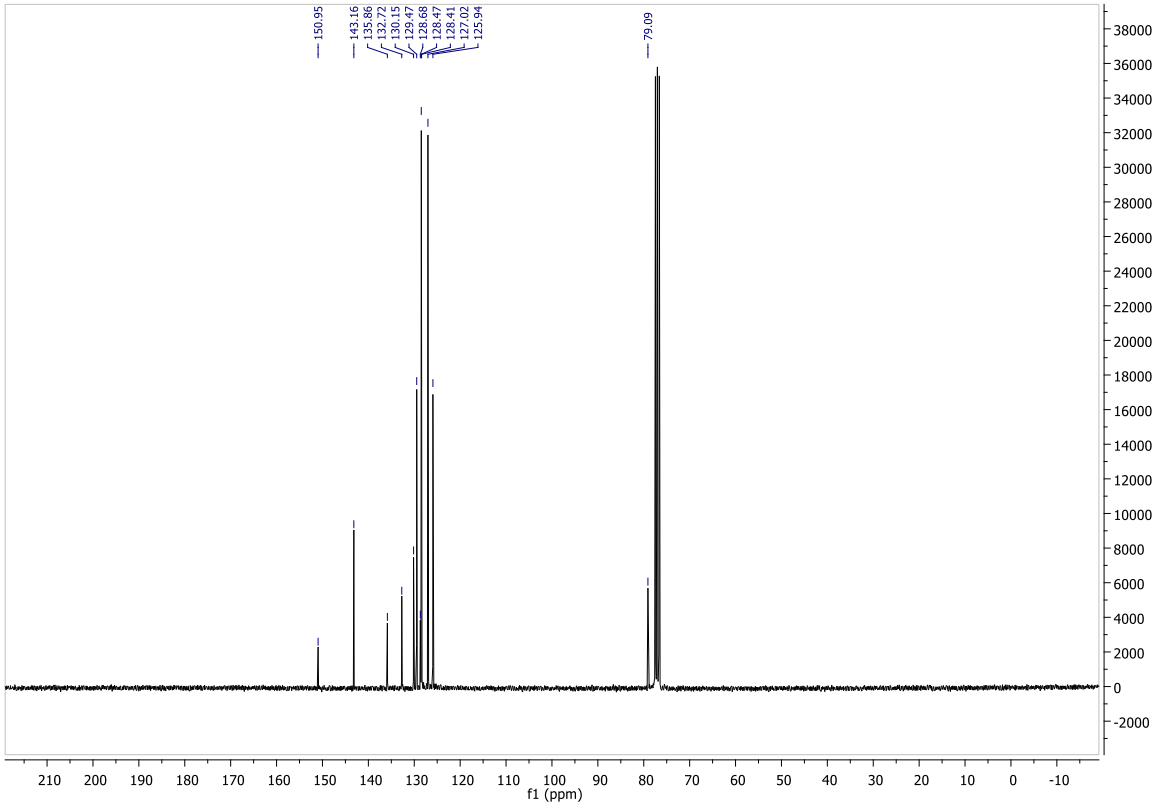
150.95
143.16
135.86
132.72
130.15
129.47
128.68
128.47
128.41
127.02
125.94
79.09
f1 (ppm)

2.14b

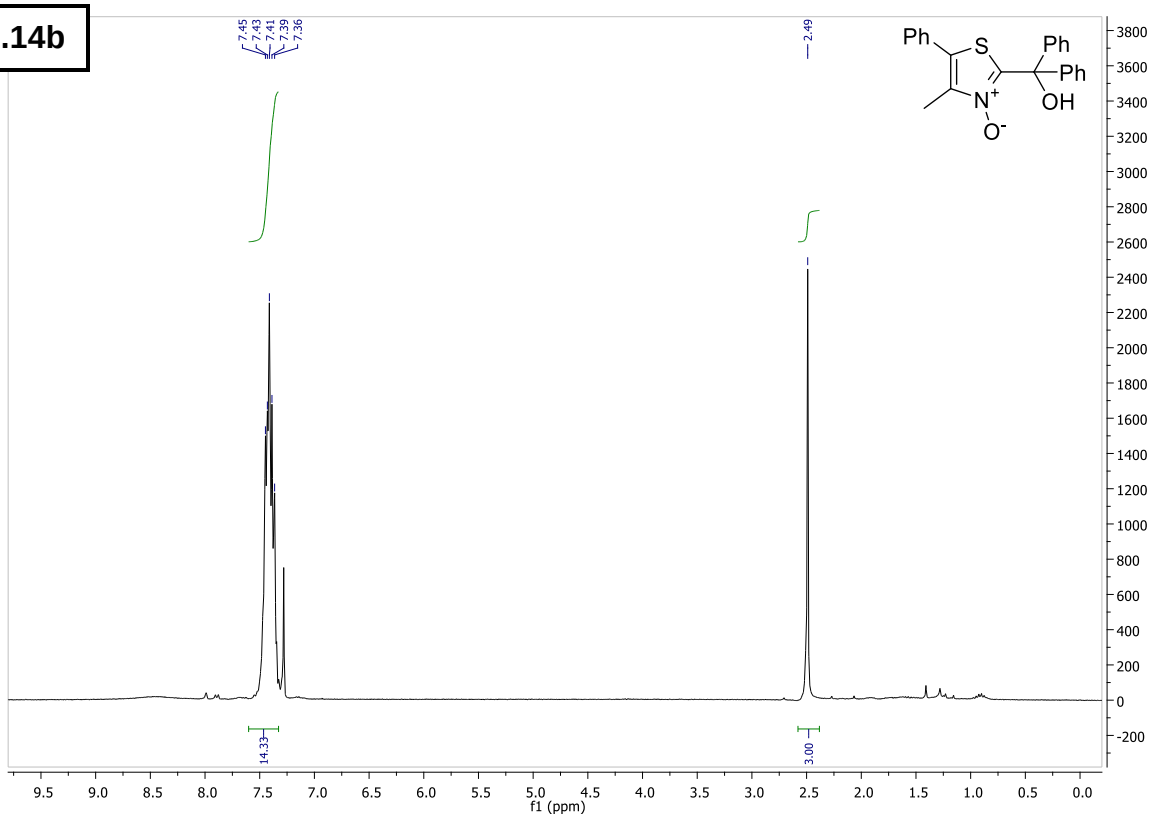
7.45
7.43
7.41
7.39
7.36
2.49
Ph
S
Ph
Ph
N+
O-
OH
14.33
3.00
f1 (ppm)

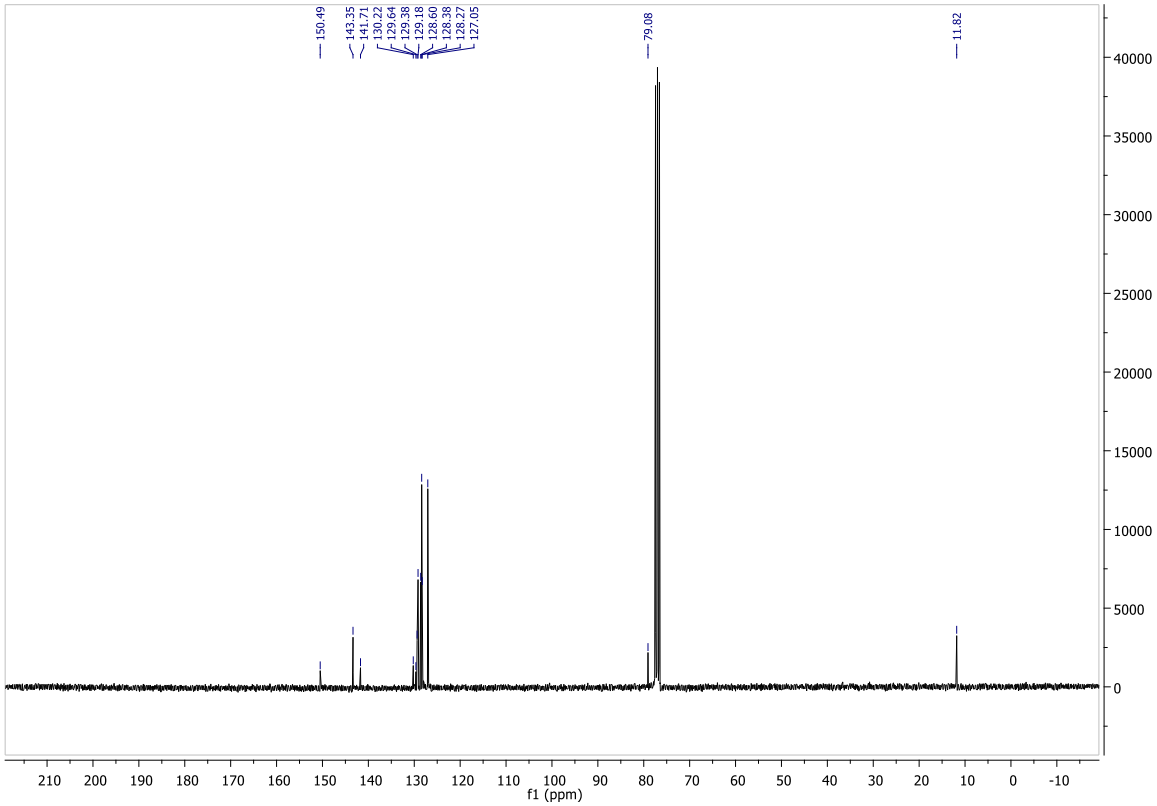
150.49
143.35
141.71
130.22
129.64
129.38
129.18
128.60
128.38
128.27
127.05
79.08
11.82
f1 (ppm)

2.14c

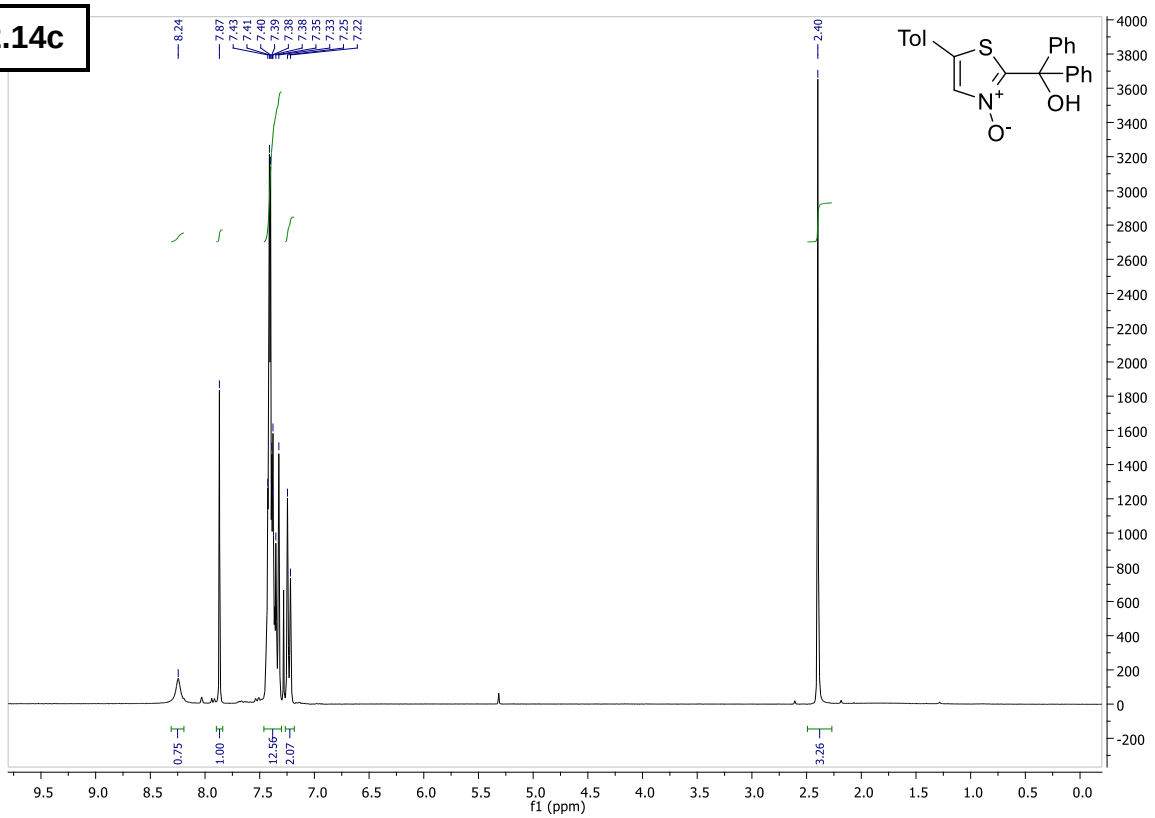
8.24
7.87
7.43
7.41
7.40
7.39
7.38
7.38
7.35
7.33
7.25
7.22
2.40
Tol
S
Ph
Ph
OH
N+
O-
0.75
1.00
12.56
2.07
3.26
f1 (ppm)

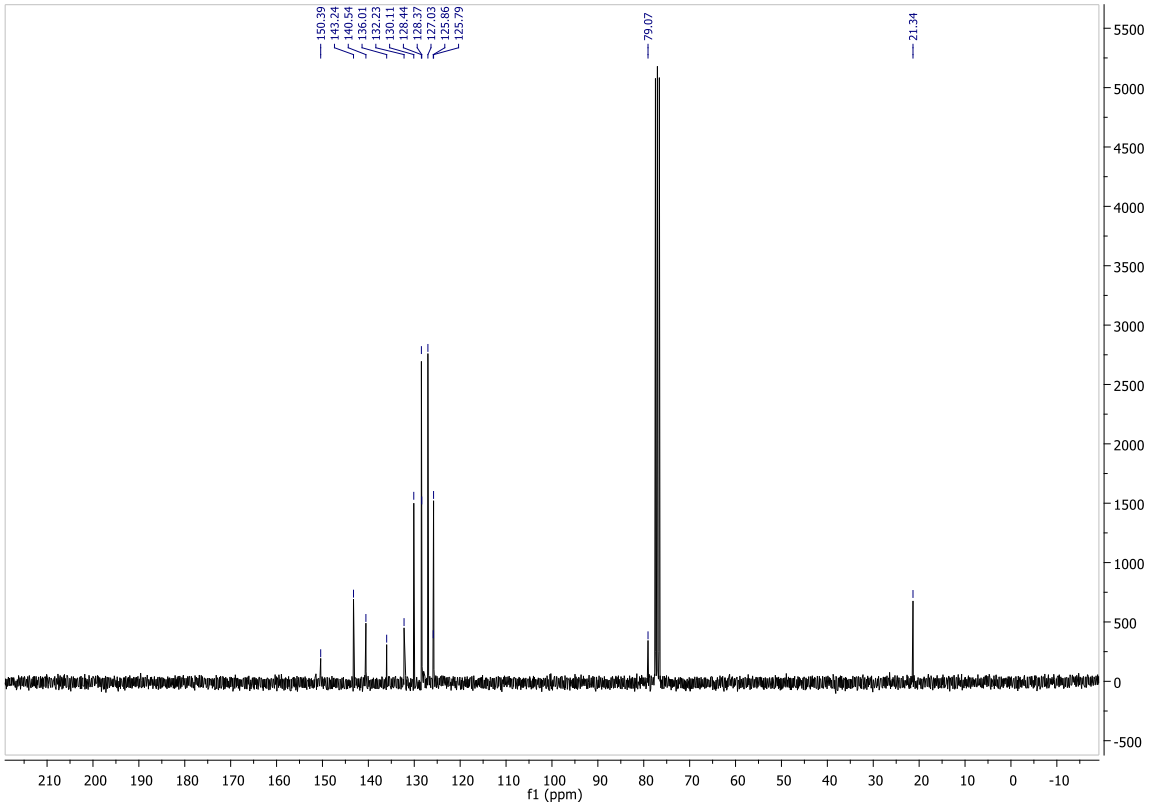
150.39
143.24
140.54
136.01
132.23
130.11
128.44
128.37
127.03
125.86
125.79
79.07
21.34
f1 (ppm)

2.14d

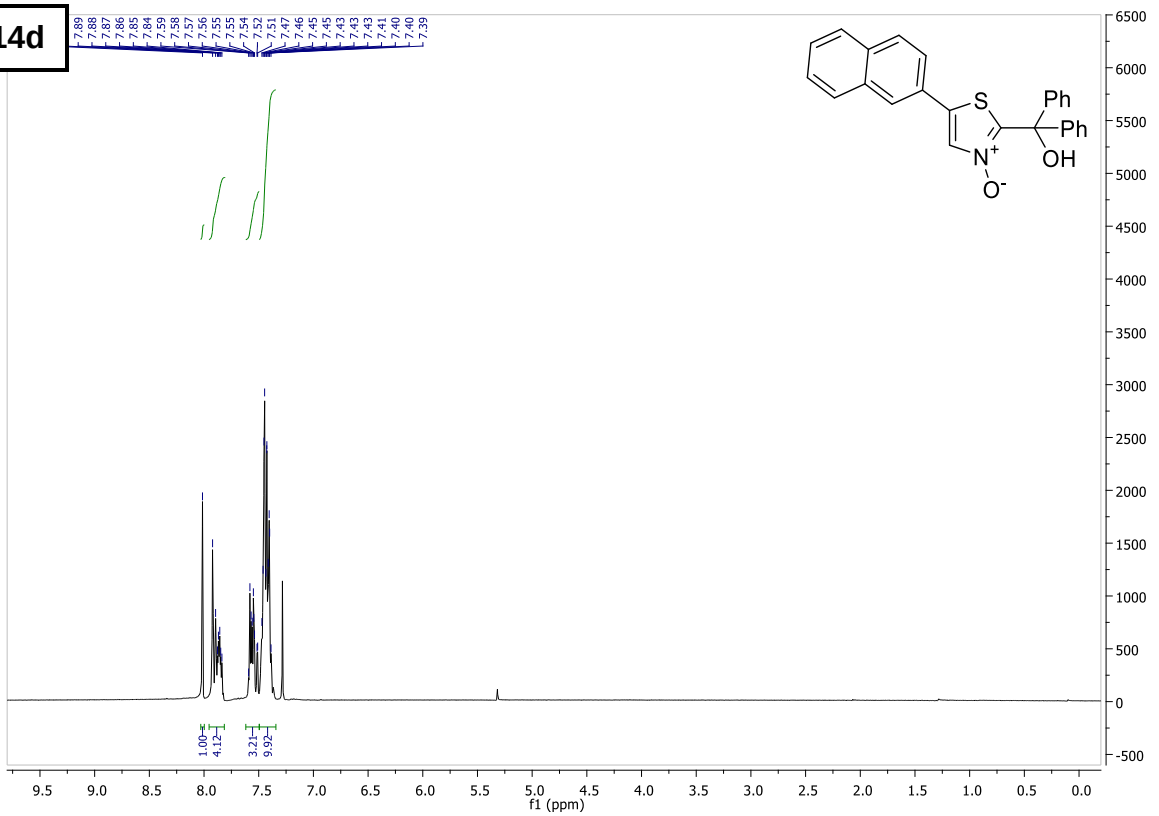
7.89
7.88
7.87
7.86
7.85
7.84
7.59
7.58
7.57
7.56
7.55
7.55
7.54
7.52
7.51
7.47
7.46
7.45
7.45
7.43
7.43
7.41
7.40
7.40
7.39
S
Ph
Ph
OH
N+
O-
1.00
4.12
3.21
9.92
f1 (ppm)

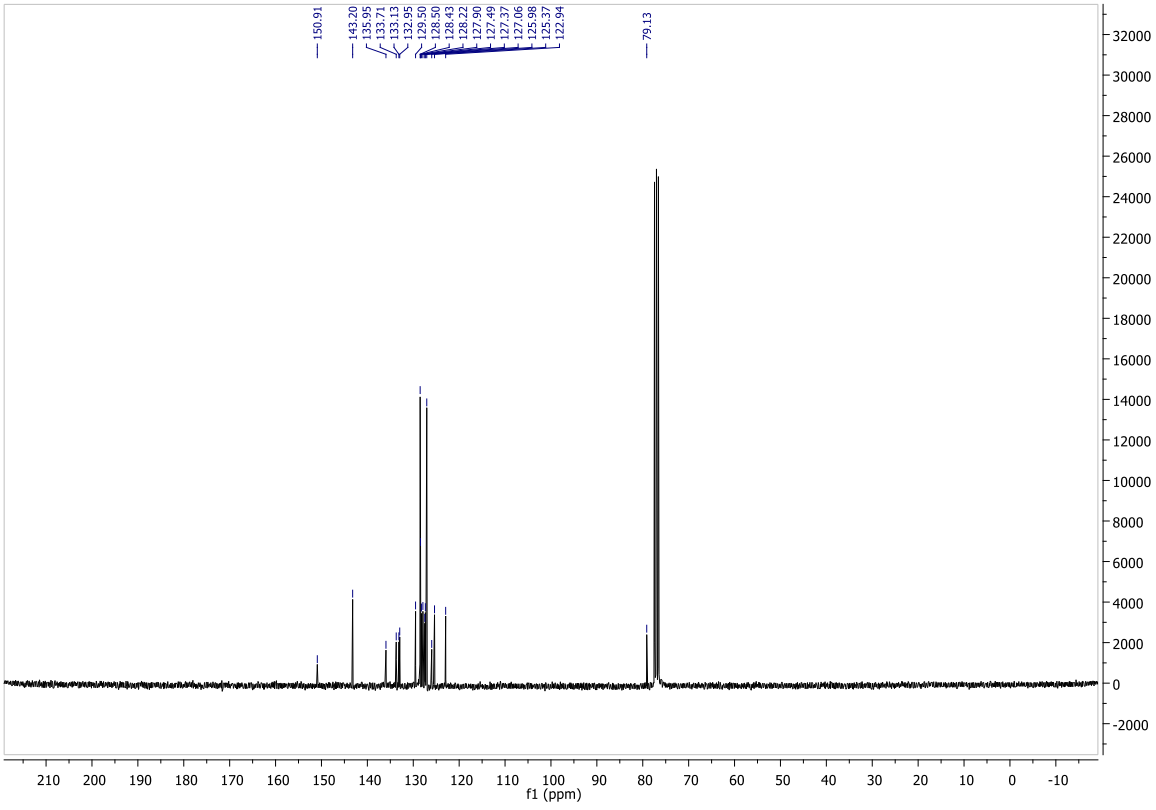
150.91
143.20
133.95
133.71
133.13
132.95
129.50
128.45
128.22
127.90
127.49
127.37
127.06
125.98
125.37
122.94
79.13
f1 (ppm)

2.14e

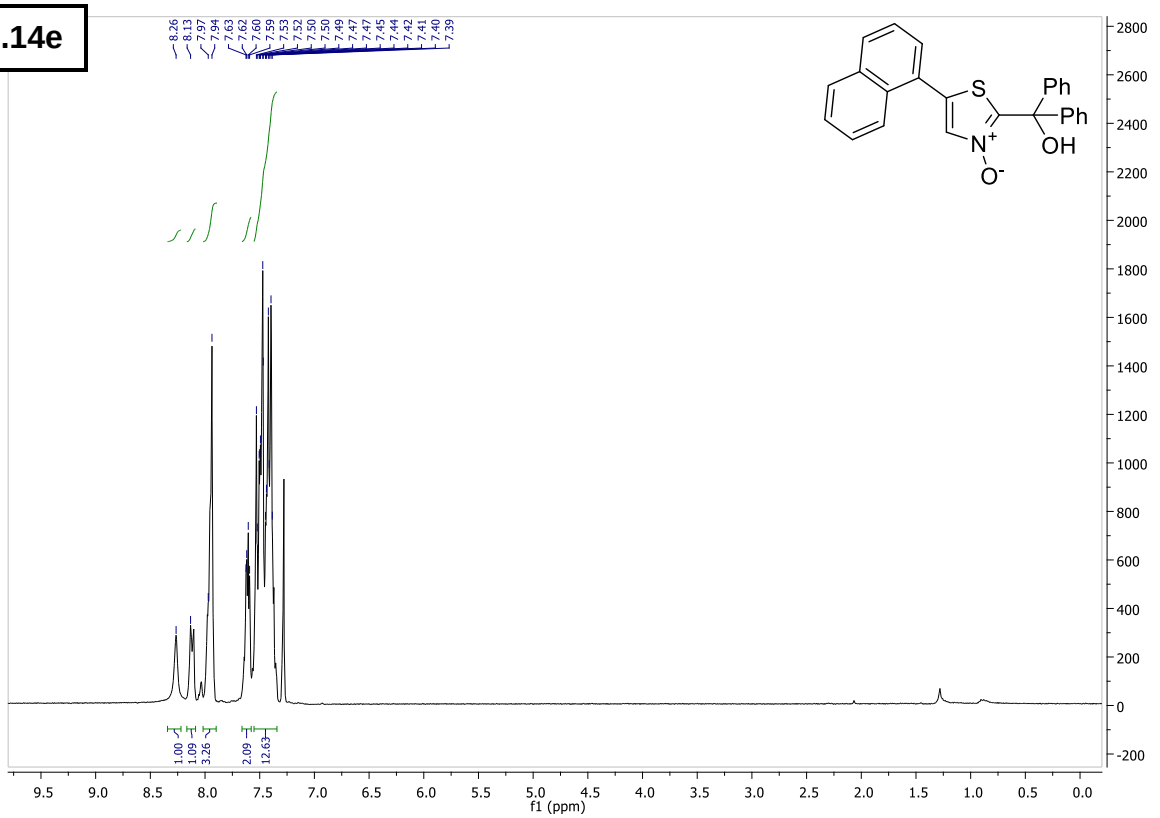
8.26
8.13
7.97
7.94
7.63
7.62
7.60
7.59
7.53
7.52
7.50
7.50
7.49
7.47
7.47
7.45
7.44
7.42
7.41
7.40
7.39
S
Ph
Ph
OH
N+
O-
1.00
1.09
3.26
2.09
12.63
f1 (ppm)

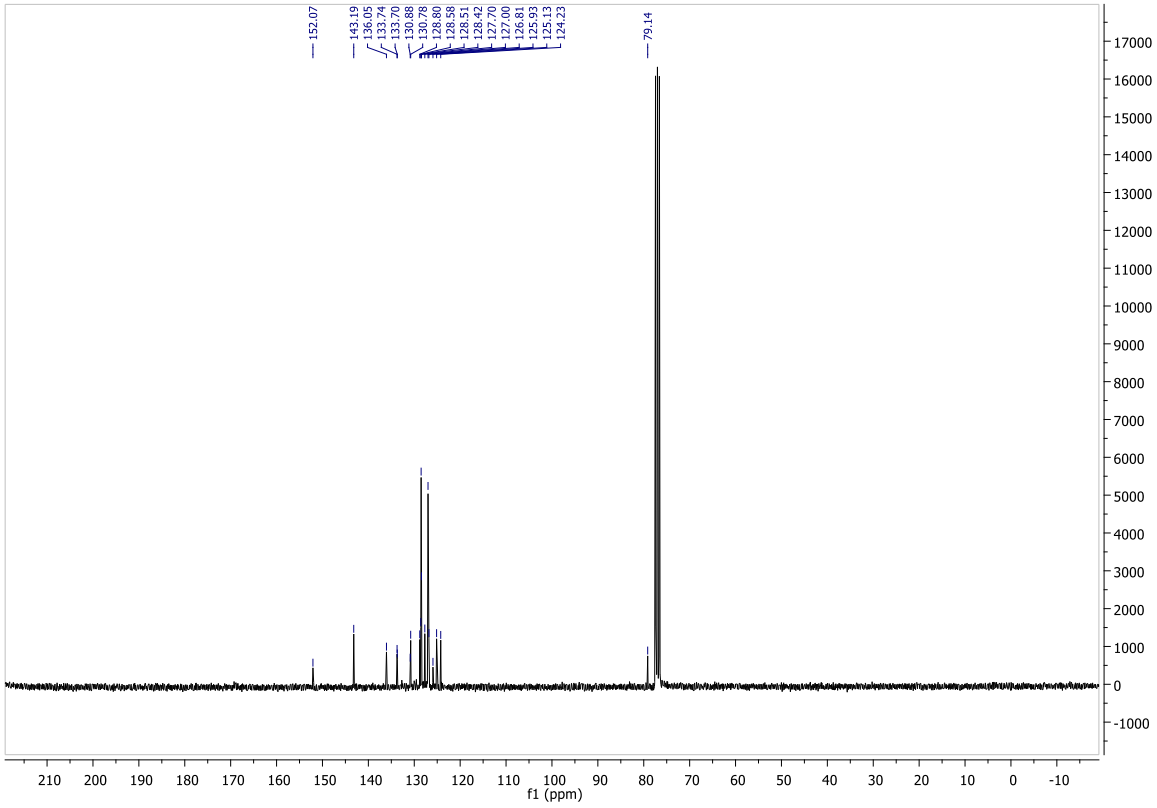
152.07
143.19
136.05
133.74
133.70
130.88
130.78
130.80
128.58
128.51
128.42
127.70
127.00
126.81
125.93
125.13
124.23
79.14
f1 (ppm)

2.14f

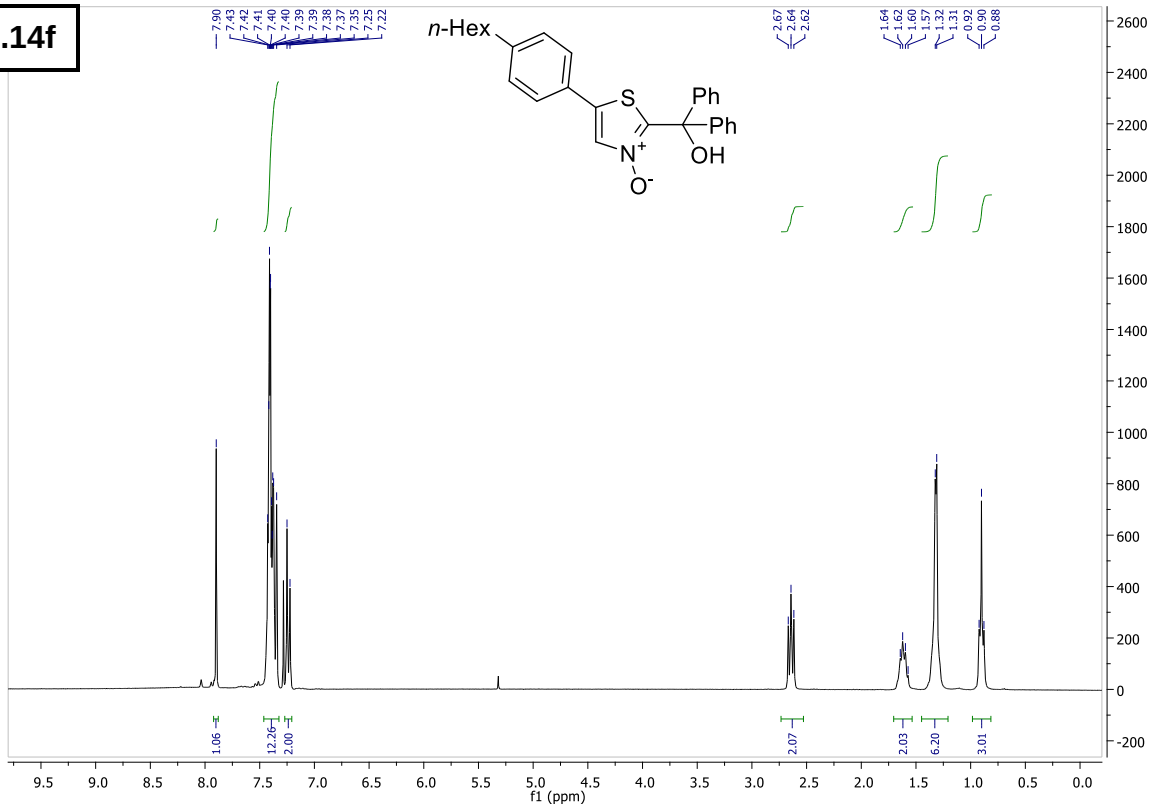
7.90
7.43
7.42
7.42
7.41
7.40
7.40
7.39
7.38
7.38
7.37
7.35
7.25
7.22
n-Hex
S
Ph
Ph
OH
N+
O-
2.67
2.64
2.62
1.64
1.62
1.60
1.57
1.32
1.31
0.92
0.90
0.88
1.06
12.26
2.00
2.07
2.03
6.20
3.01
f1 (ppm)

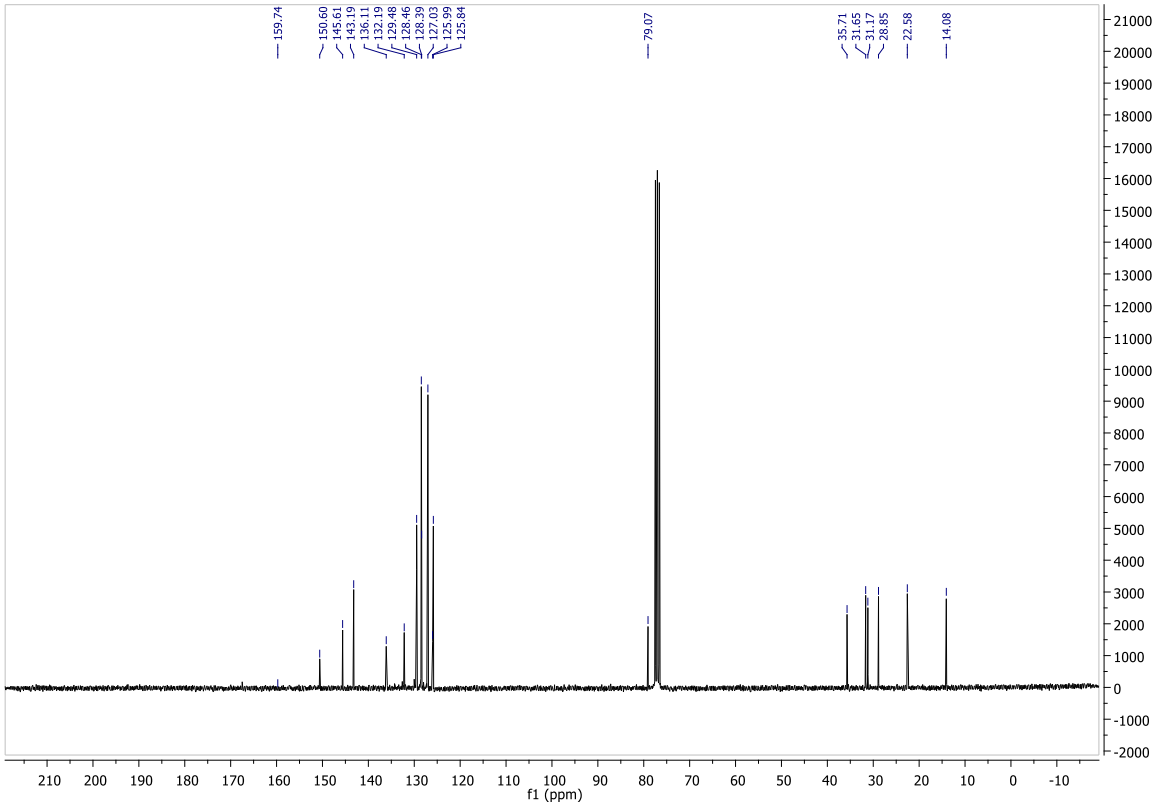
159.74
150.60
145.61
143.19
136.11
132.19
129.48
128.46
128.39
127.03
125.99
125.84
79.07
35.71
31.65
31.17
28.85
22.58
14.08
f1 (ppm)

2.14g

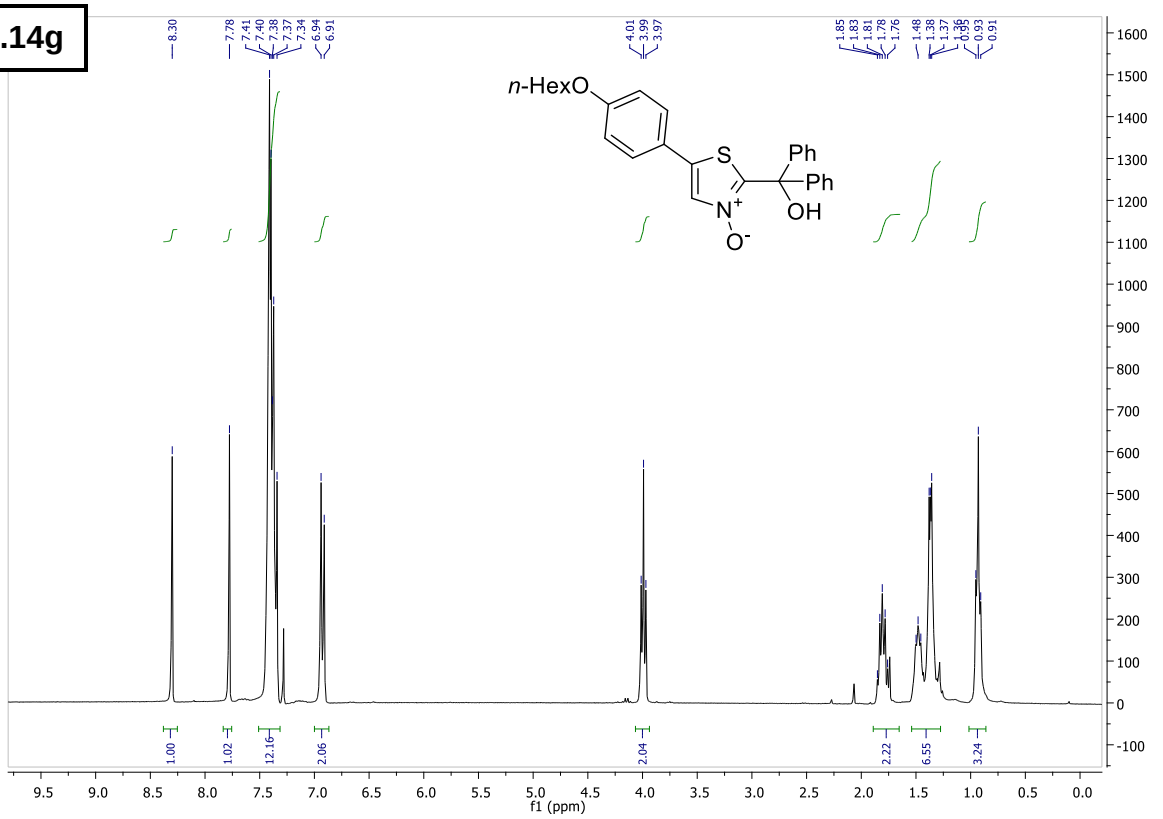
8.30
7.78
7.41
7.40
7.38
7.37
7.34
6.94
6.91
4.01
3.99
3.97
1.85
1.83
1.81
1.78
1.76
1.48
1.38
1.37
0.95
0.93
0.91
n-HexO
S
Ph
Ph
OH
N+
O-
1.00
1.02
12.16
2.06
2.04
2.22
6.55
3.24
f1 (ppm)

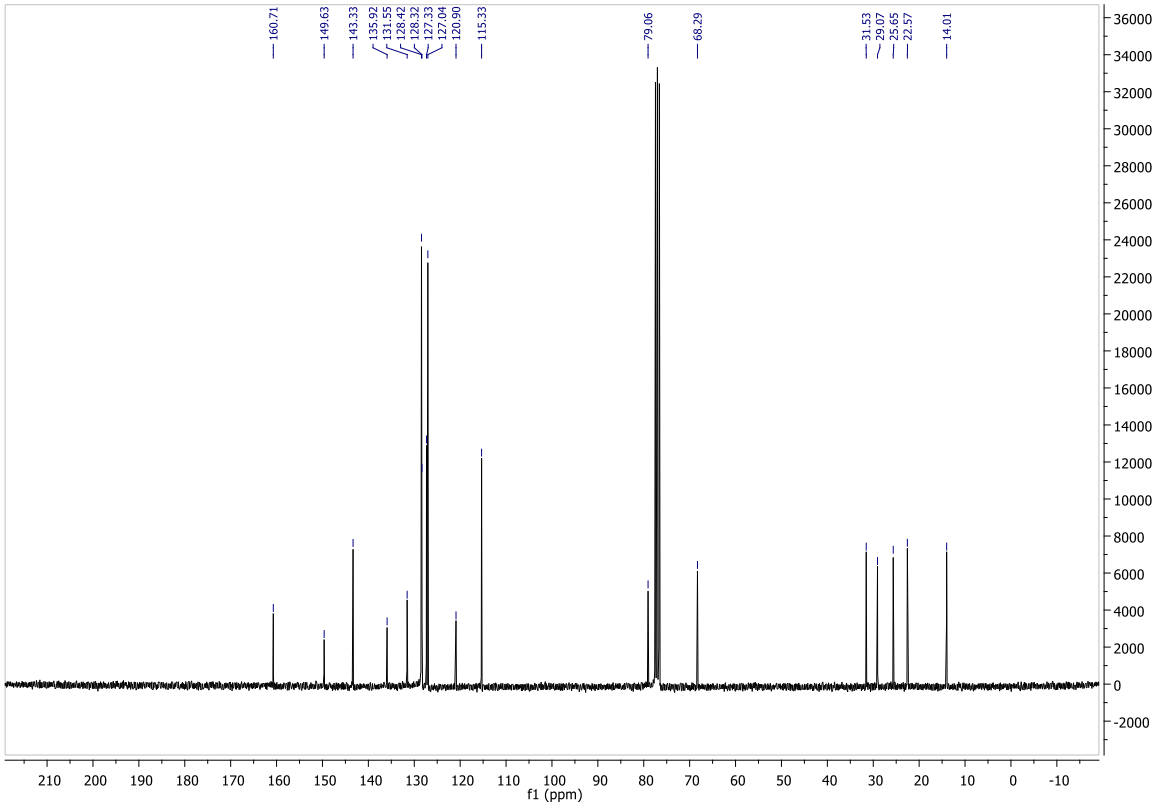
160.71
149.63
143.33
135.92
131.55
128.42
128.32
127.33
127.04
120.90
115.33
79.06
68.29
31.53
29.07
25.65
22.57
14.01
f1 (ppm)

2.14h

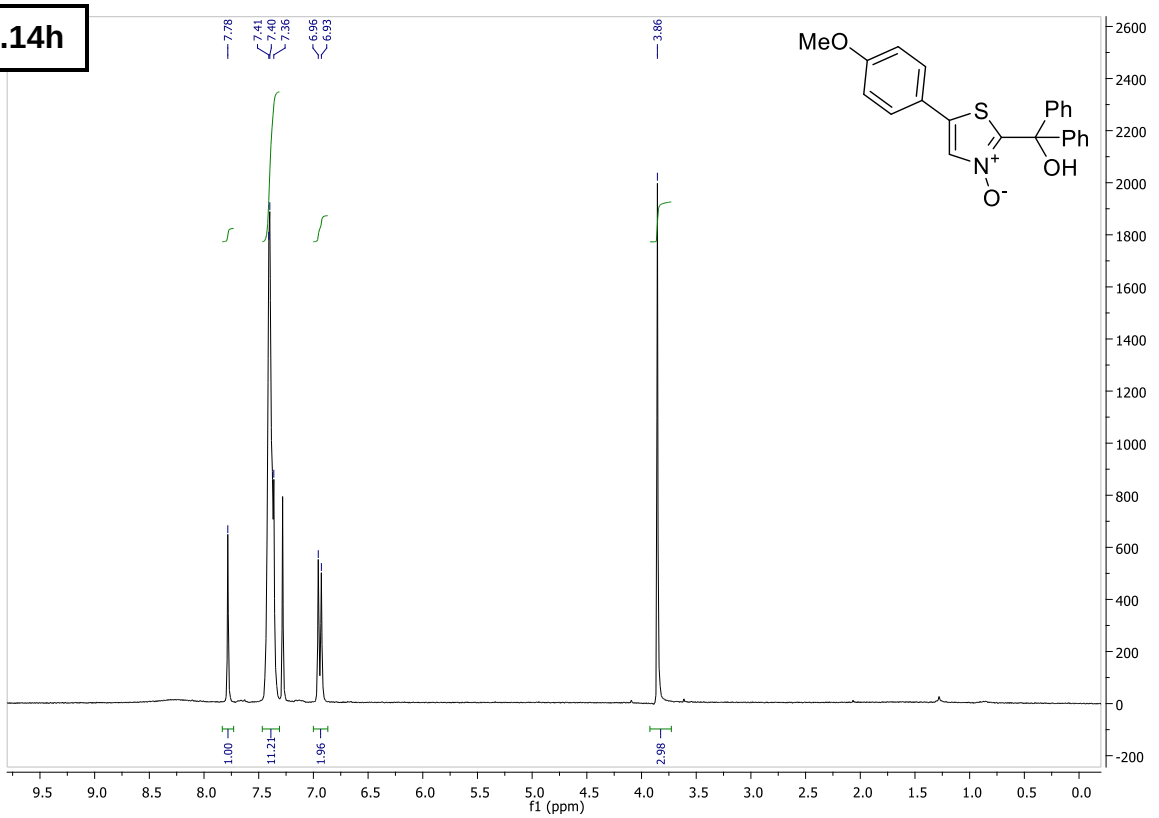
7.78
7.41
7.40
7.36
6.96
6.93
3.86
MeO
S
Ph
Ph
OH
N+
O-
1.00
11.21
1.96
2.98
f1 (ppm)

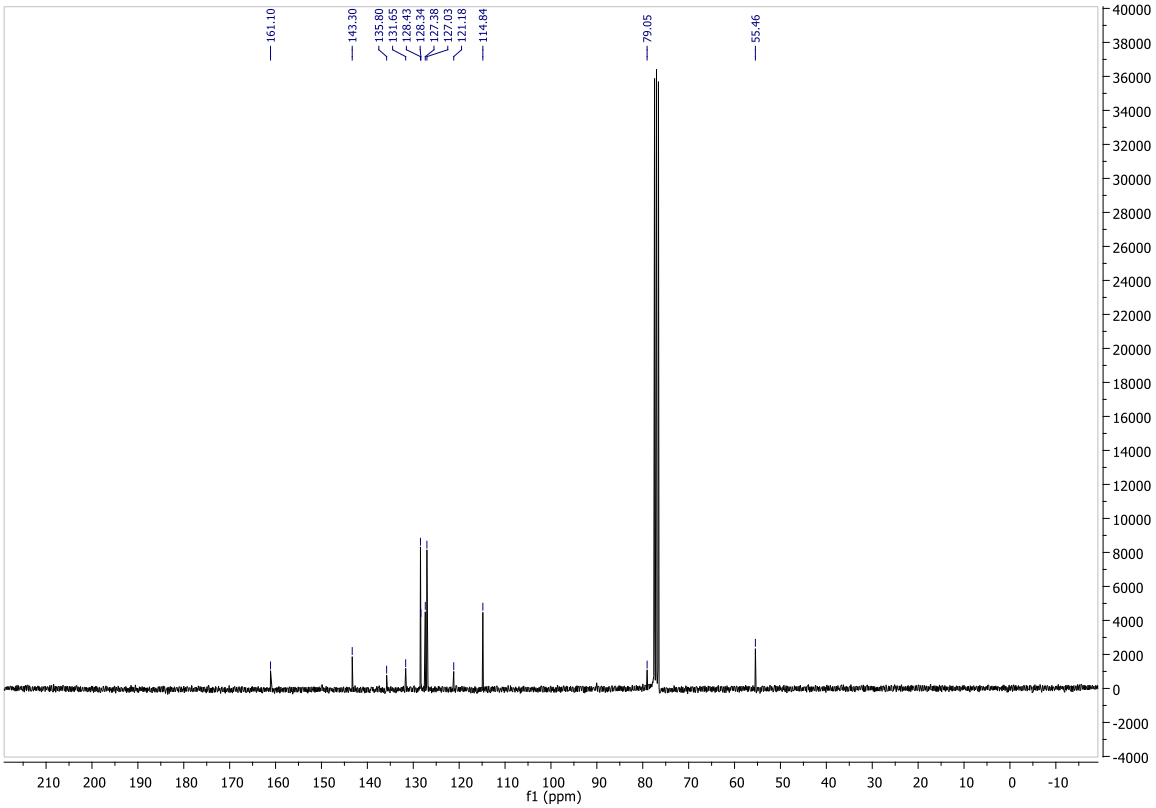
161.10
143.30
135.80
131.65
128.43
128.34
127.38
127.03
121.18
114.84
79.05
55.46
f1 (ppm)

2.14i

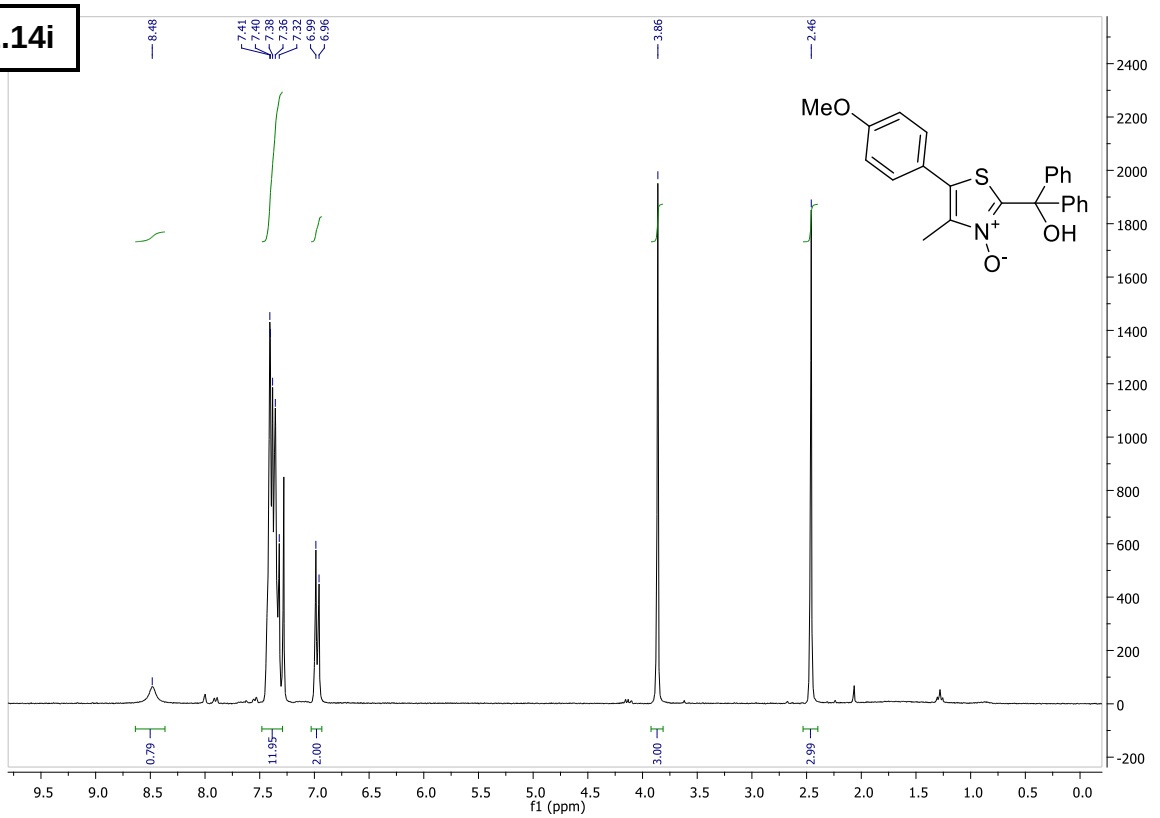
8.48
7.41
7.40
7.38
7.36
7.32
6.99
6.96
3.86
2.46
MeO
S
Ph
Ph
OH
N+
O-
0.79
11.95
2.00
3.00
2.99
f1 (ppm)

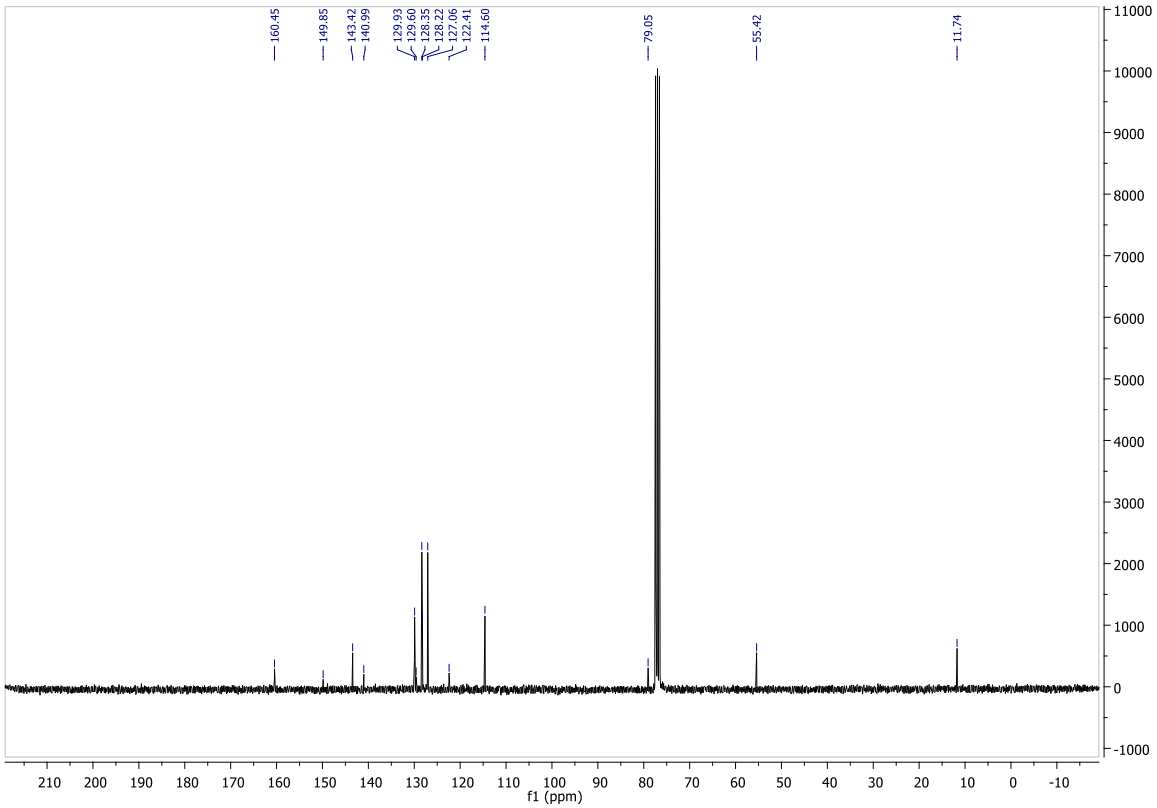
160.45
149.85
143.42
140.99
129.93
129.60
128.35
128.22
127.06
122.41
114.60
79.05
55.42
11.74
f1 (ppm)

2.14j

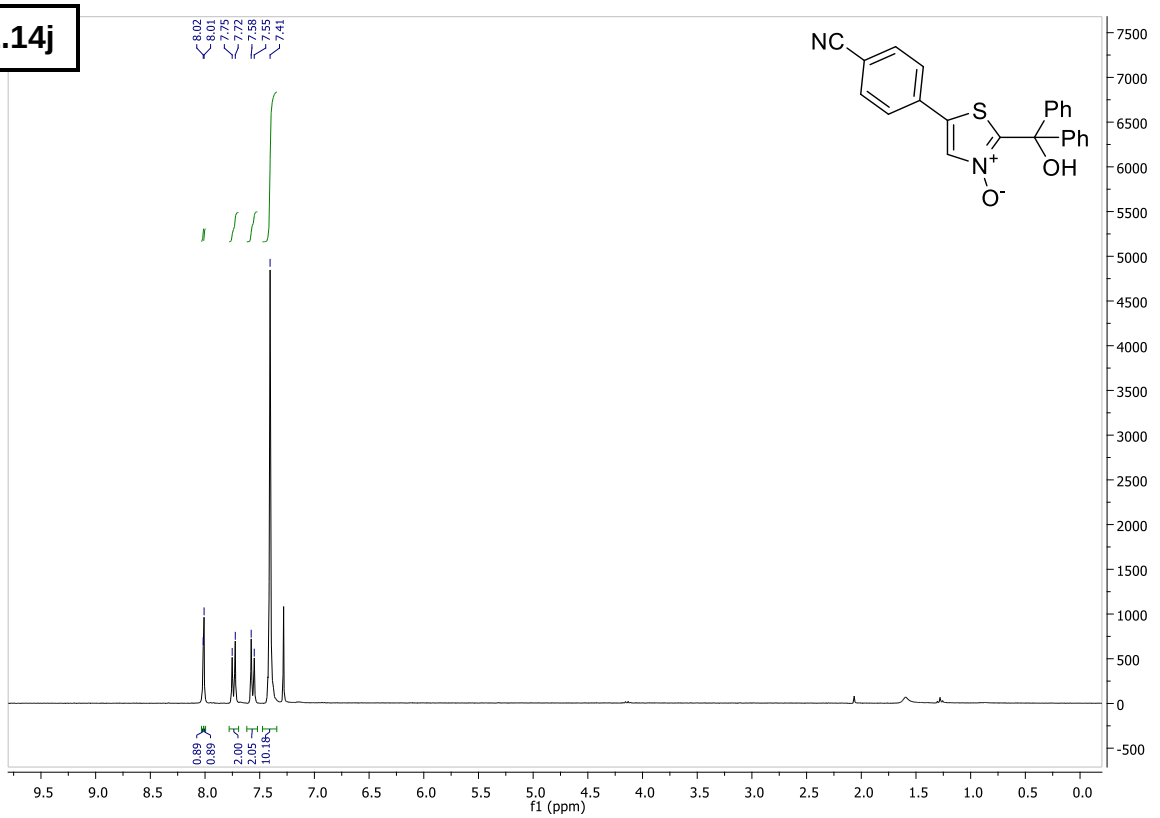
8.02
8.01
7.75
7.72
7.58
7.55
7.41
NC
S
Ph
Ph
OH
N+
O-
0.89
0.89
2.00
2.05
10.18
f1 (ppm)

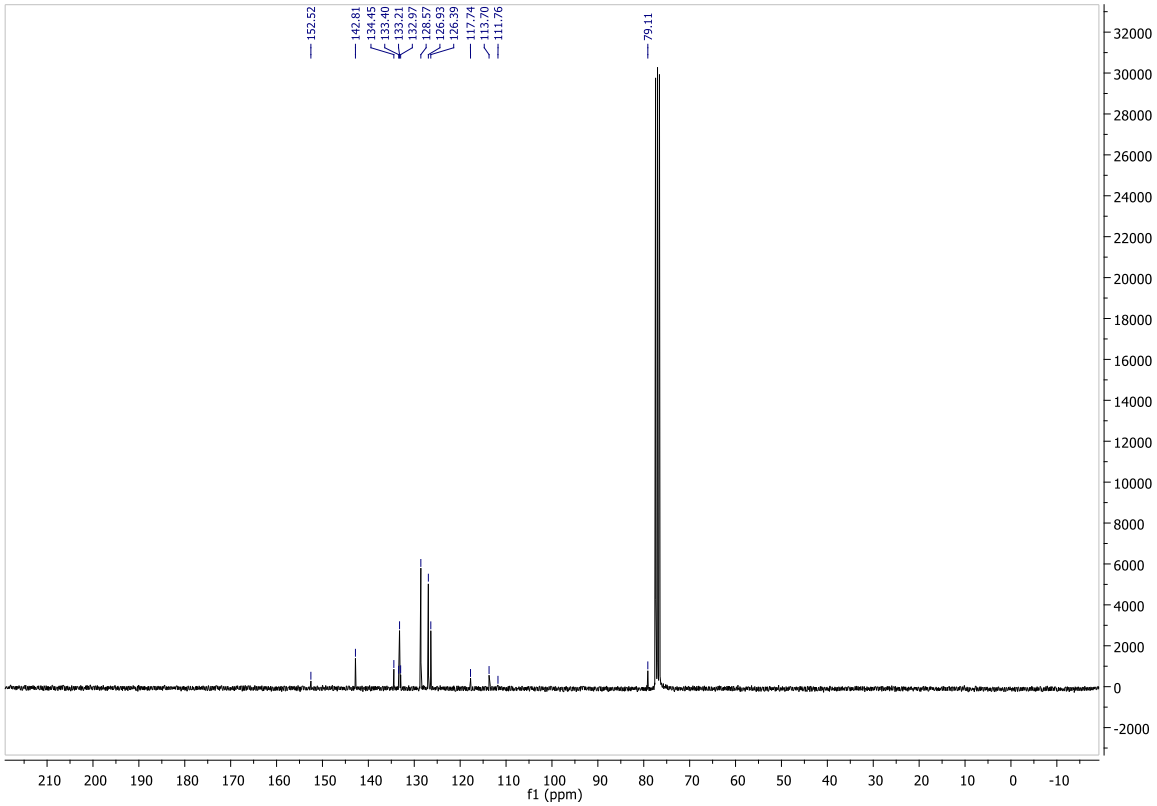
152.52
142.81
134.45
133.40
133.21
132.97
128.57
126.93
126.39
117.74
113.70
111.76
79.11
f1 (ppm)

2.14k

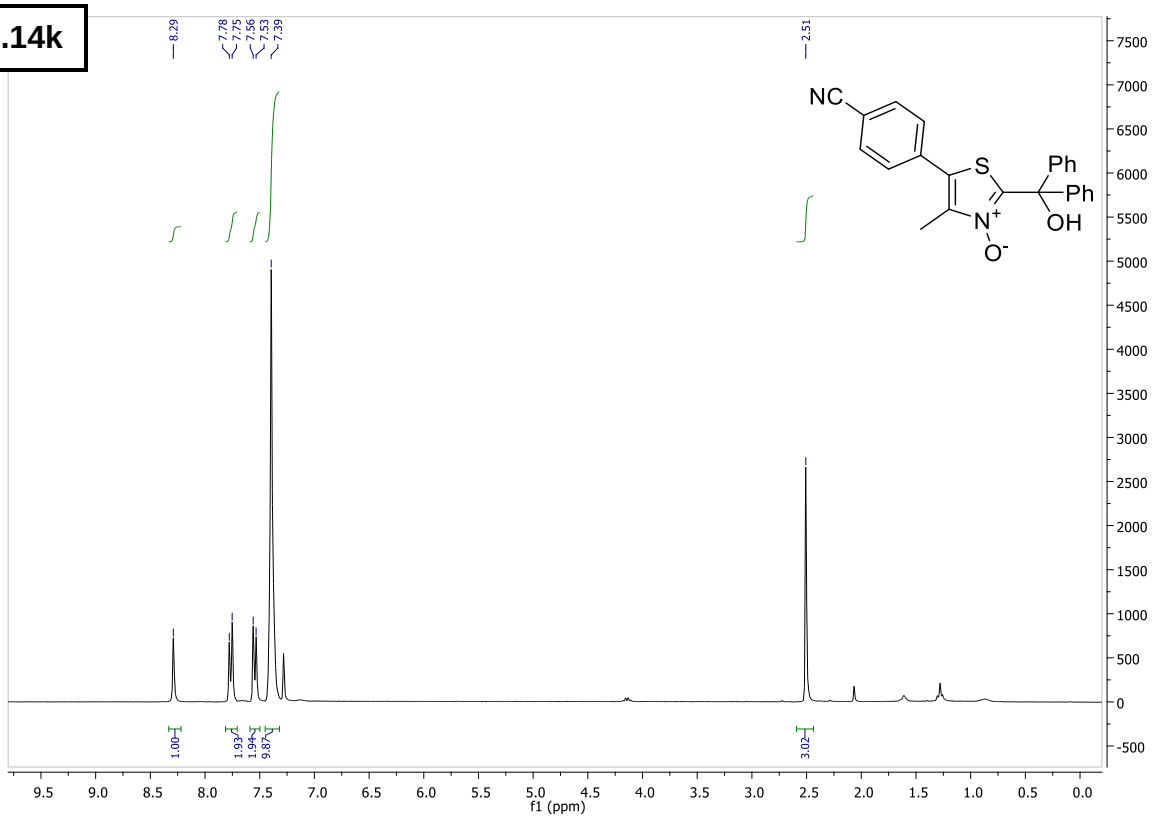
8.29
7.78
7.75
7.56
7.53
7.39
2.51
NC
S
Ph
Ph
OH
N+
O-
1.00
1.93
1.94
9.87
3.02
f1 (ppm)

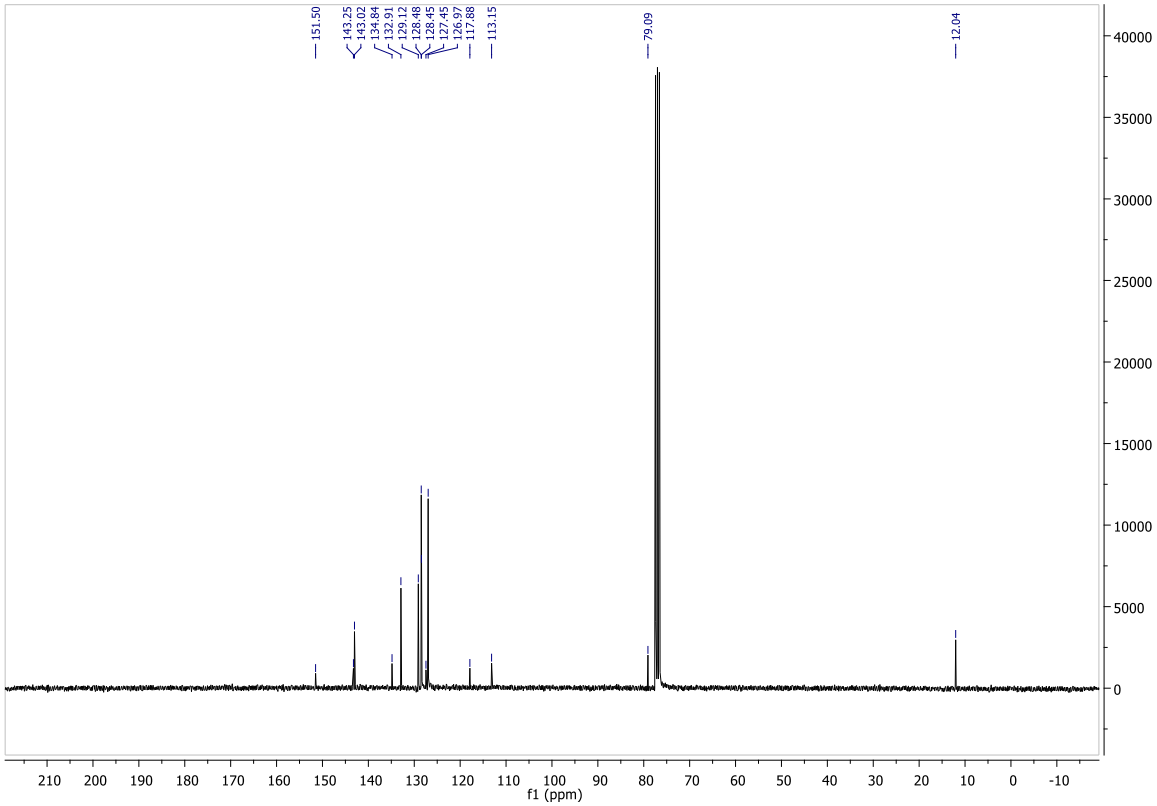
151.50
143.25
143.02
134.84
132.91
129.12
128.48
128.45
127.45
126.97
117.88
113.15
79.09
12.04
f1 (ppm)

2.14l

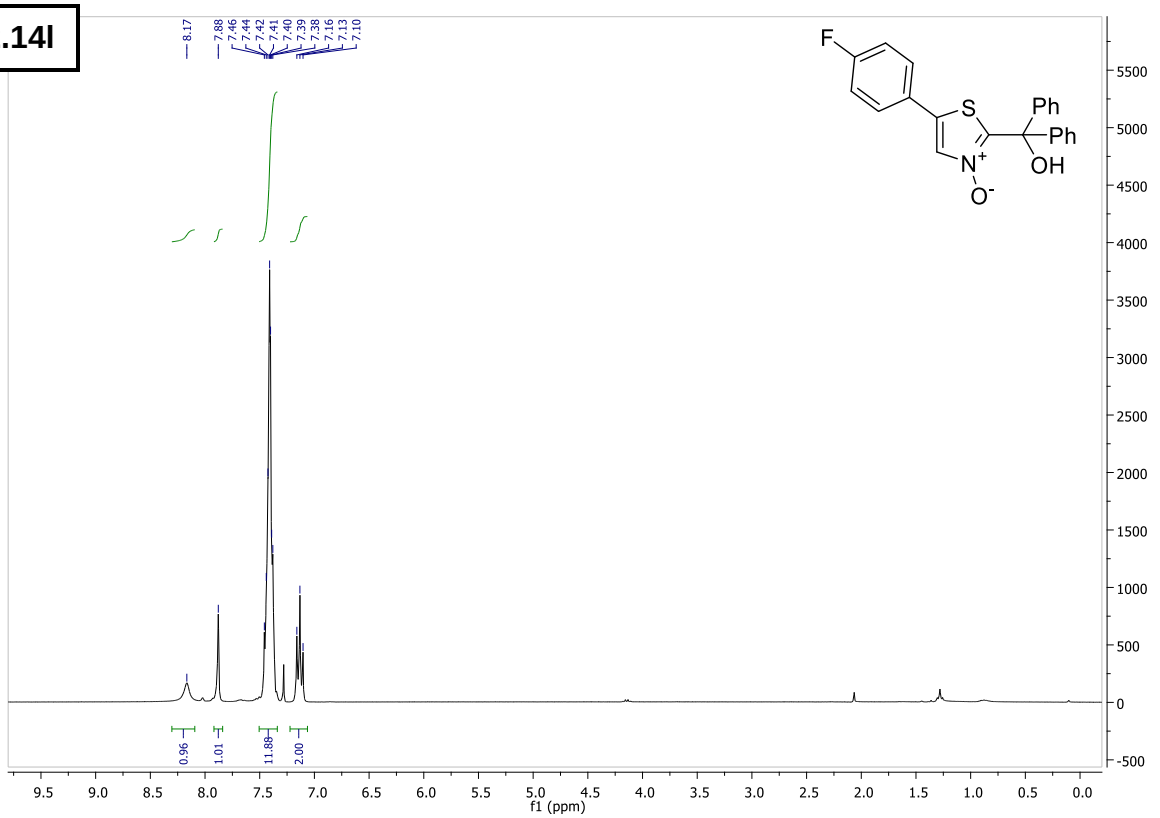
8.17
7.88
7.46
7.44
7.42
7.41
7.40
7.39
7.38
7.16
7.13
7.10
F
S
Ph
Ph
OH
N+
O-
0.96
1.01
11.88
2.00
f1 (ppm)

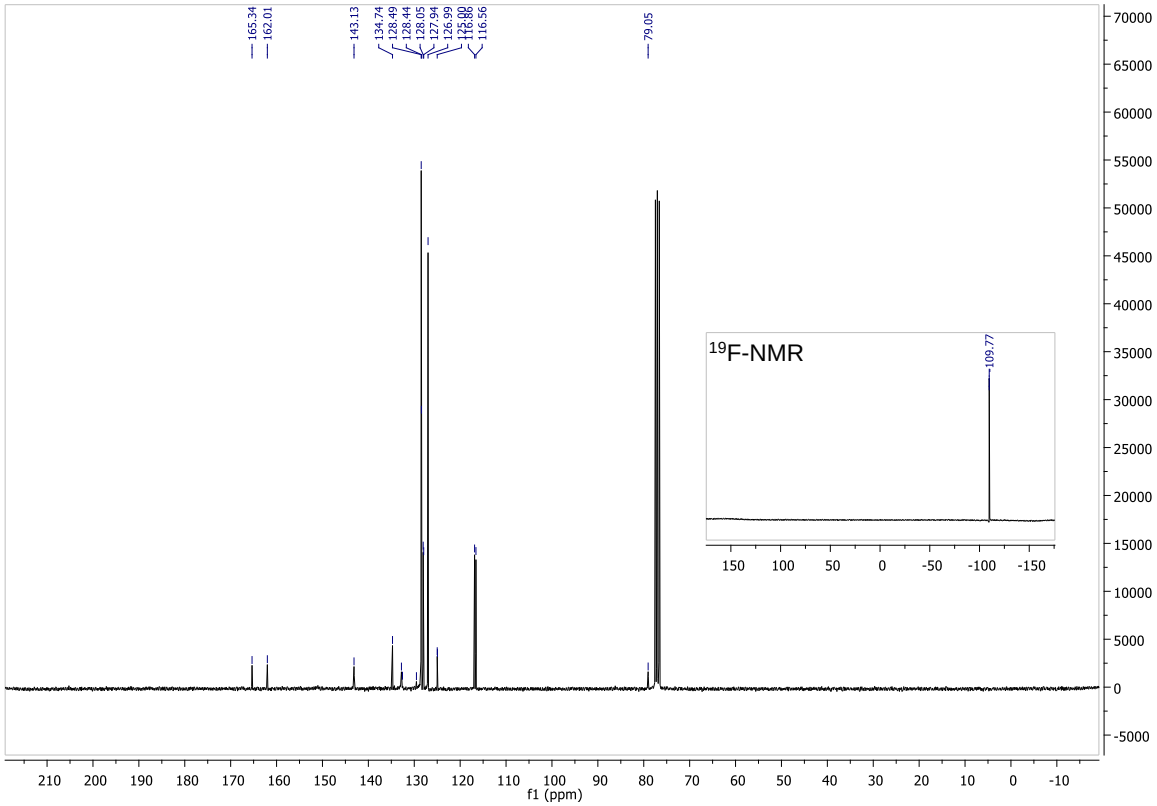
165.34
162.01
143.13
134.74
128.49
128.44
128.05
127.94
126.99
125.00
116.86
116.56
79.05
19F-NMR
-109.77
f1 (ppm)

2.14m

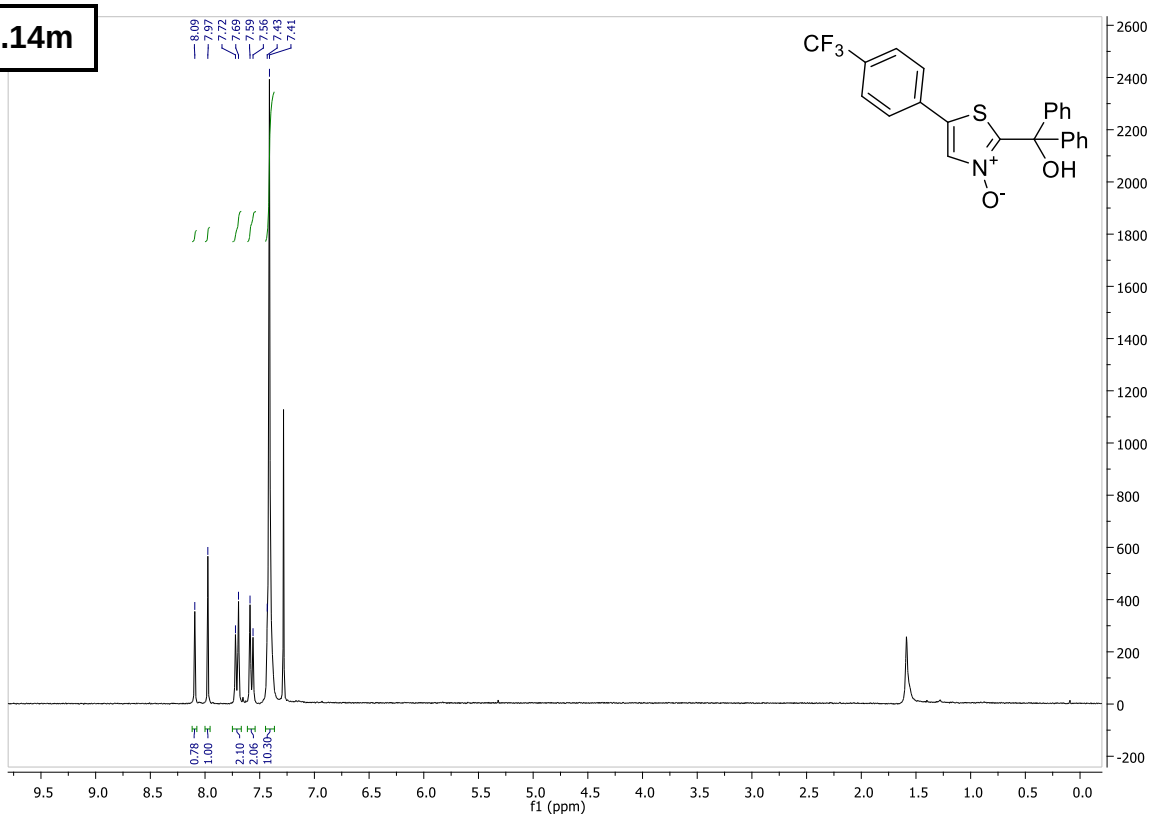
8.09
7.97
7.72
7.69
7.59
7.56
7.43
7.41
CF3
S
Ph
Ph
OH
N+
O-
0.78
1.00
2.10
2.06
10.30
f1 (ppm)

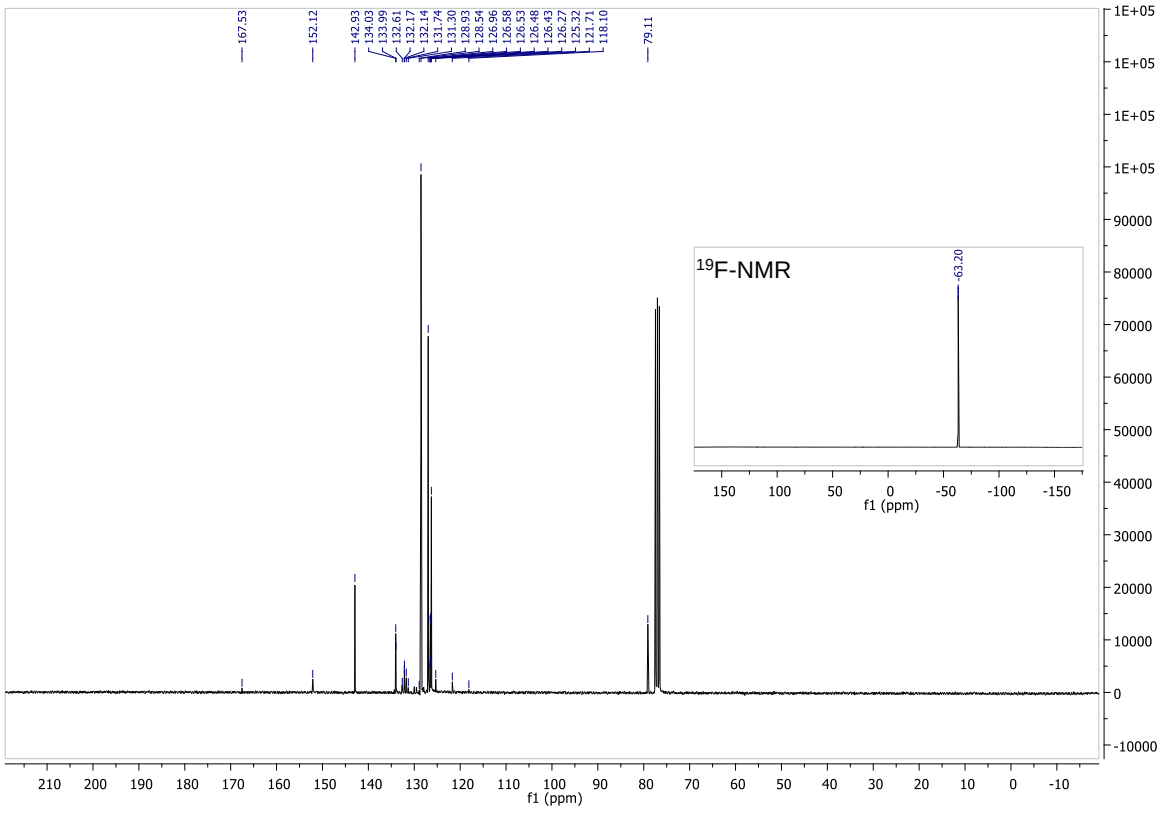
167.53
152.12
142.93
134.03
133.99
132.61
132.17
132.14
131.74
131.30
128.93
128.54
126.96
126.58
126.53
126.48
126.43
126.27
125.32
121.71
118.10
79.11
19F-NMR
-63.20
f1 (ppm)
f1 (ppm)

2.14n

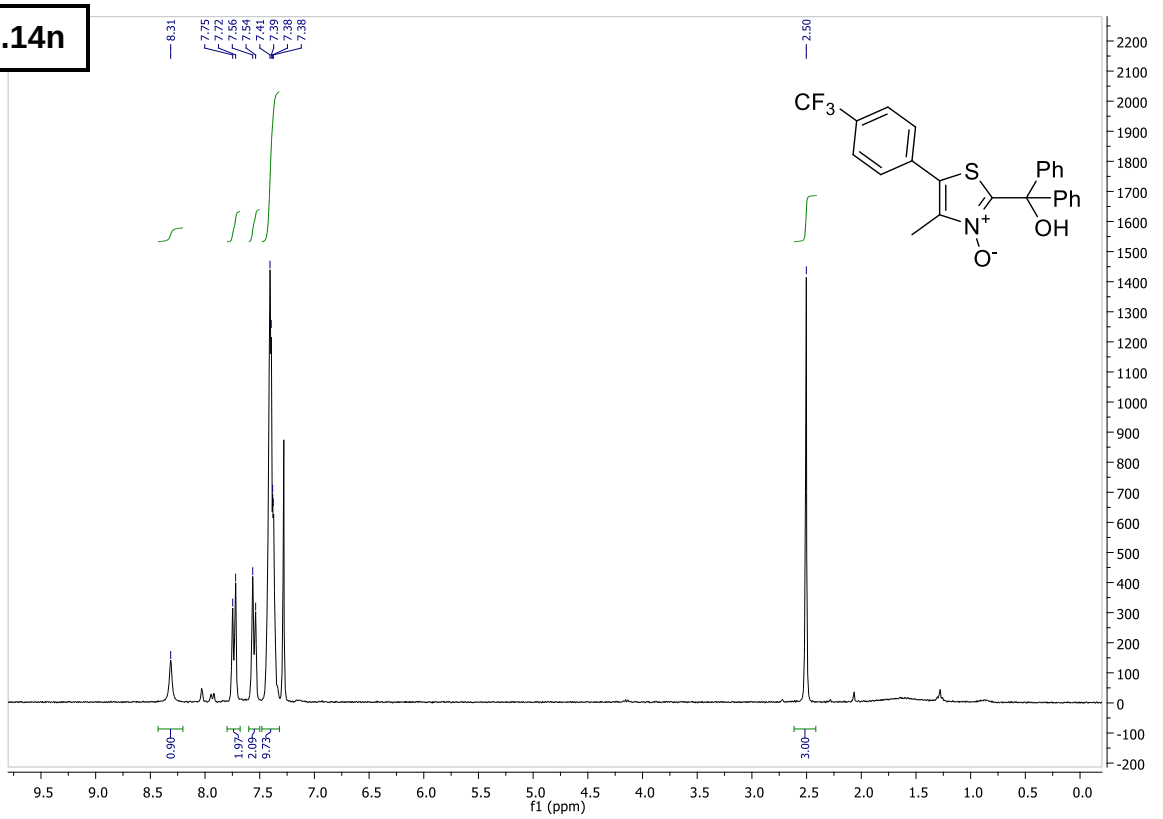
8.31
7.75
7.72
7.56
7.54
7.41
7.39
7.38
7.38
2.50
CF3
S
Ph
Ph
OH
N+
O-
0.90
1.97
2.09
9.73
3.00
f1 (ppm)

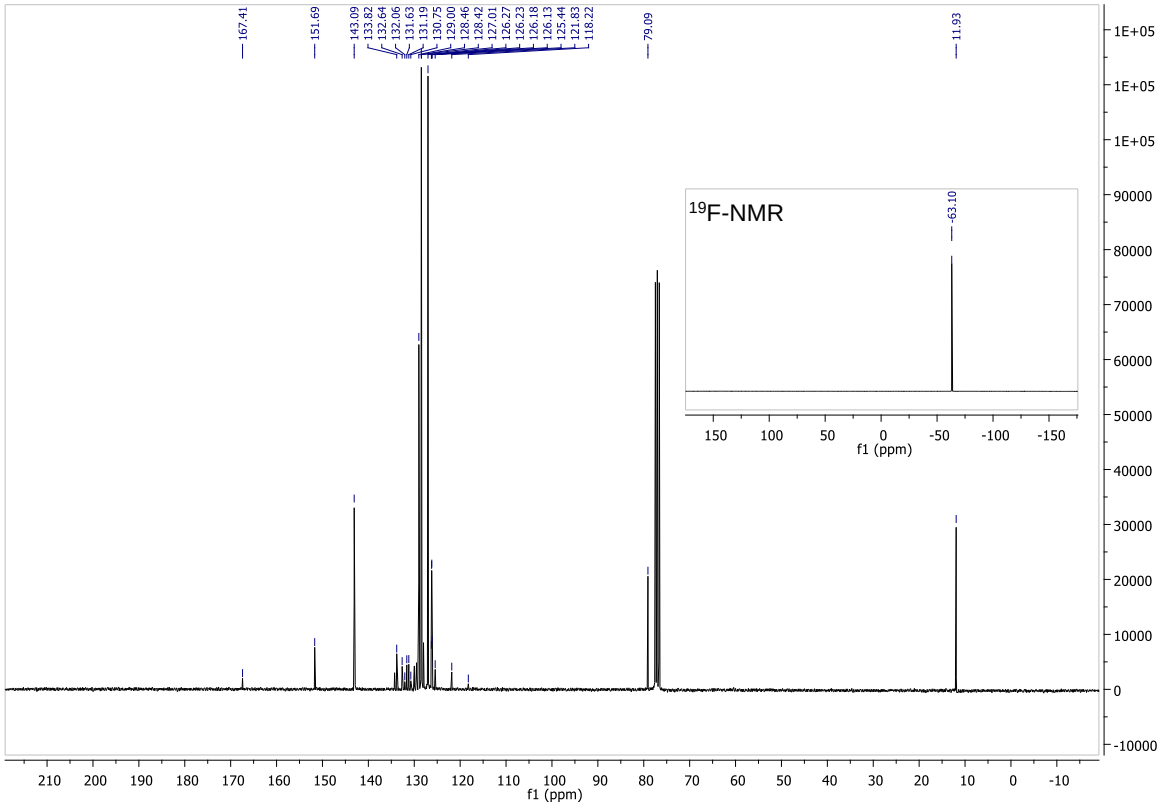
167.41
151.69
143.09
133.82
132.64
132.06
131.63
131.19
130.75
129.00
128.46
128.42
127.01
126.27
126.23
126.18
126.13
125.44
121.83
118.22
79.09
11.93
19F-NMR
-63.10
f1 (ppm)
f1 (ppm)

2.14o

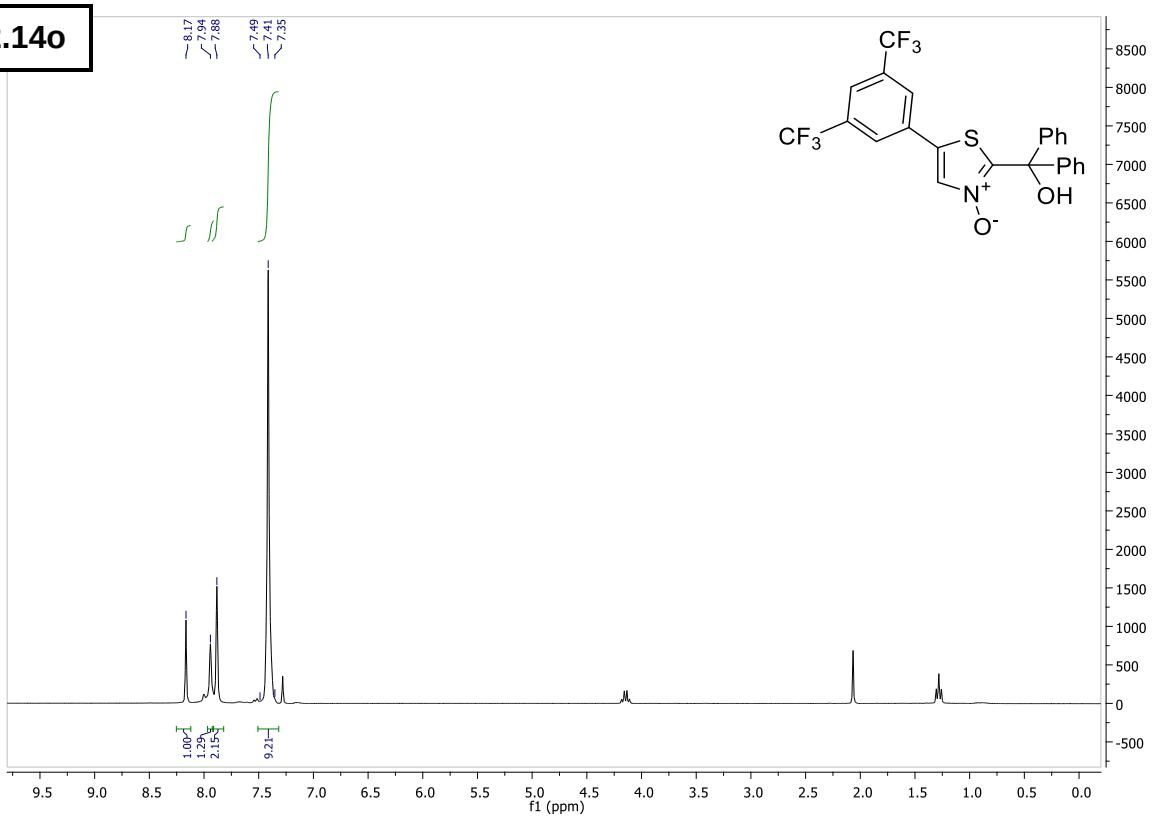
8.17
7.94
7.88
7.49
7.41
7.35
CF3
CF3
S
Ph
Ph
OH
N+
O-
1.00
1.29
2.15
9.21
f1 (ppm)

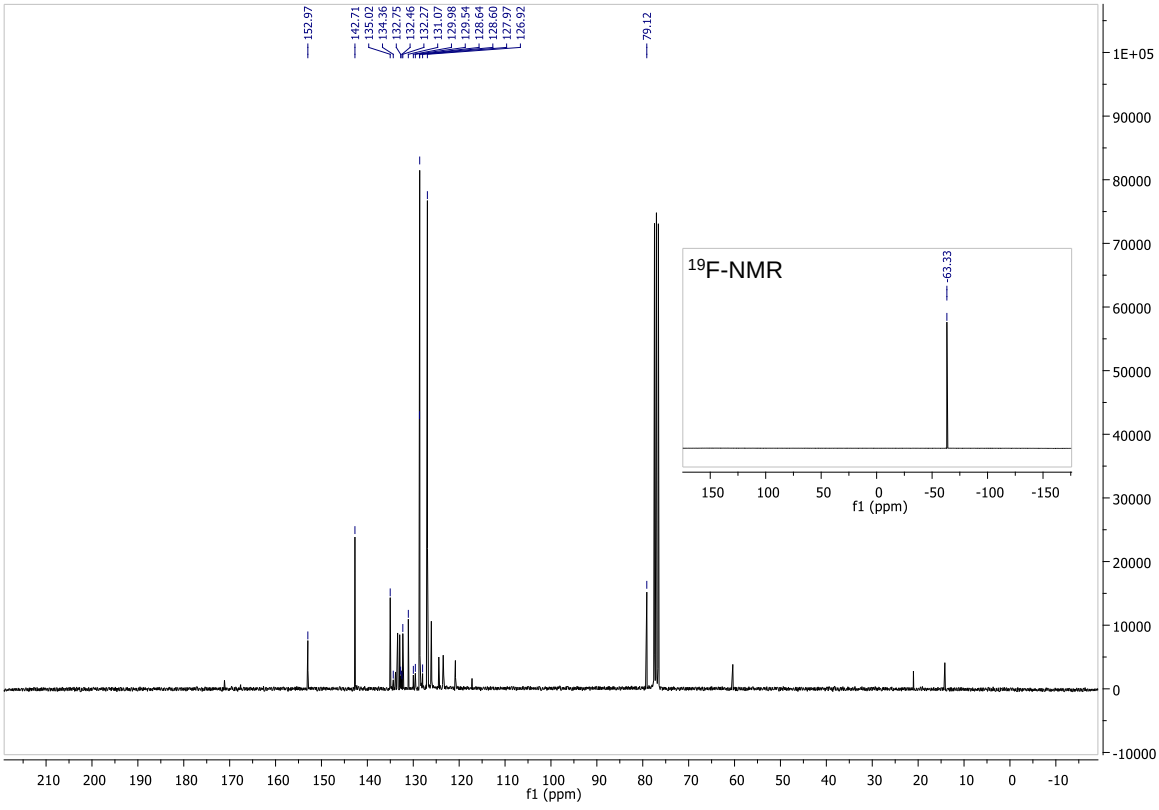
152.97
142.71
135.02
134.36
132.75
132.46
132.27
131.07
129.98
129.54
128.64
128.60
127.97
126.92
79.12
19F-NMR
-63.33
f1 (ppm)
f1 (ppm)

2.15a

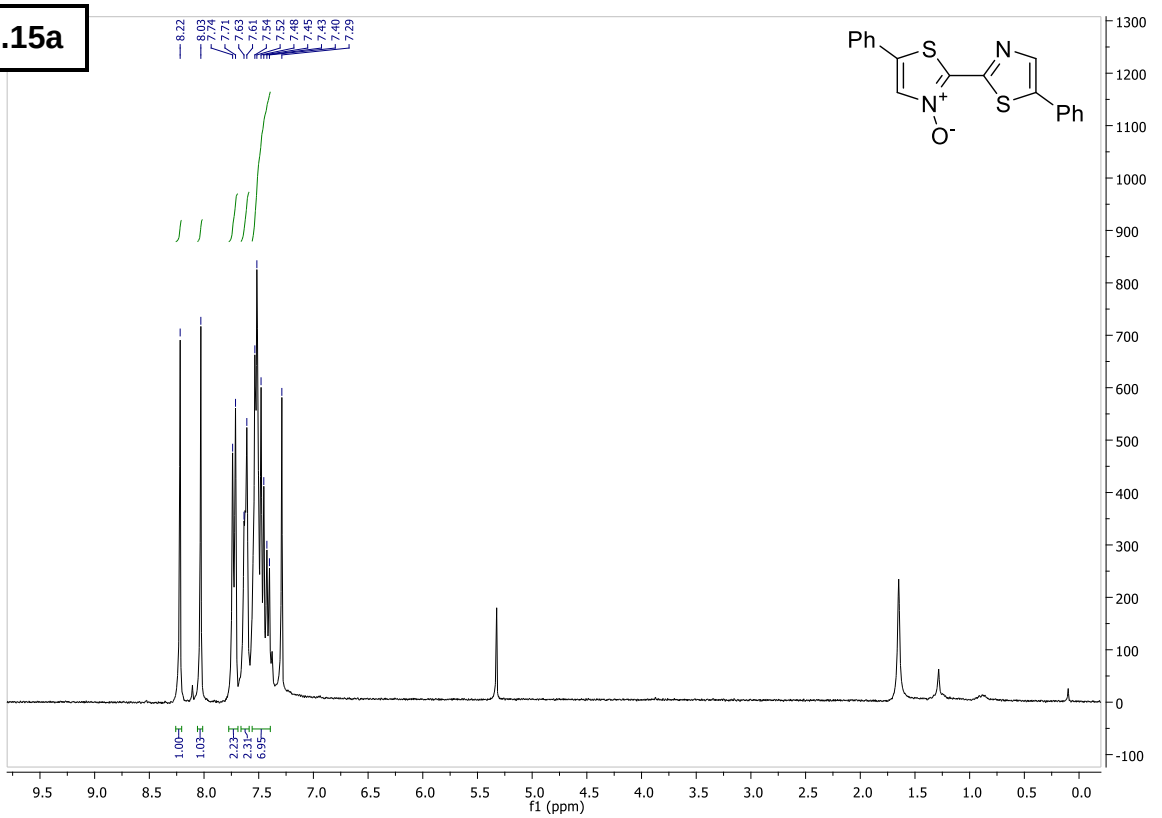
8.22
8.03
7.74
7.71
7.63
7.61
7.54
7.52
7.48
7.45
7.43
7.40
7.29
Ph
S
N
N+
O-
S
Ph
1.00
1.03
2.23
2.31
6.95
f1 (ppm)

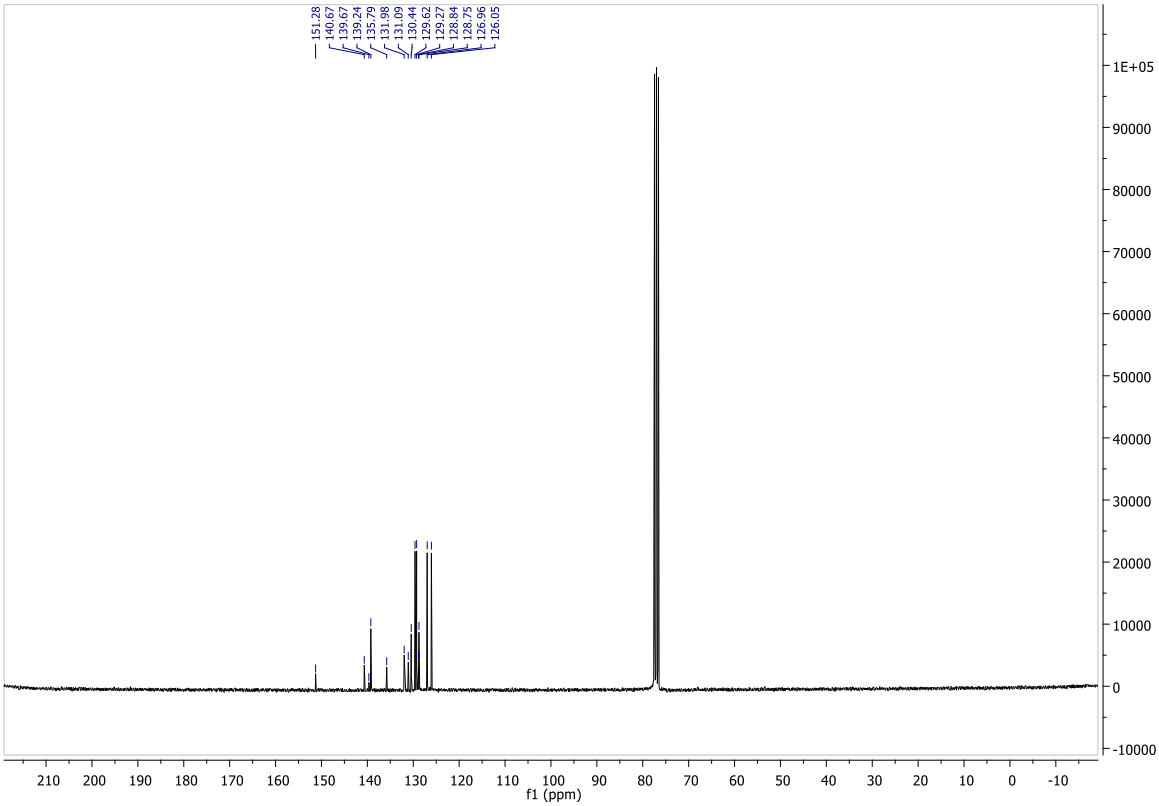
151.28
140.67
139.67
139.24
135.79
131.98
131.09
130.44
129.62
129.27
128.84
128.75
126.96
126.05
f1 (ppm)

2.15b

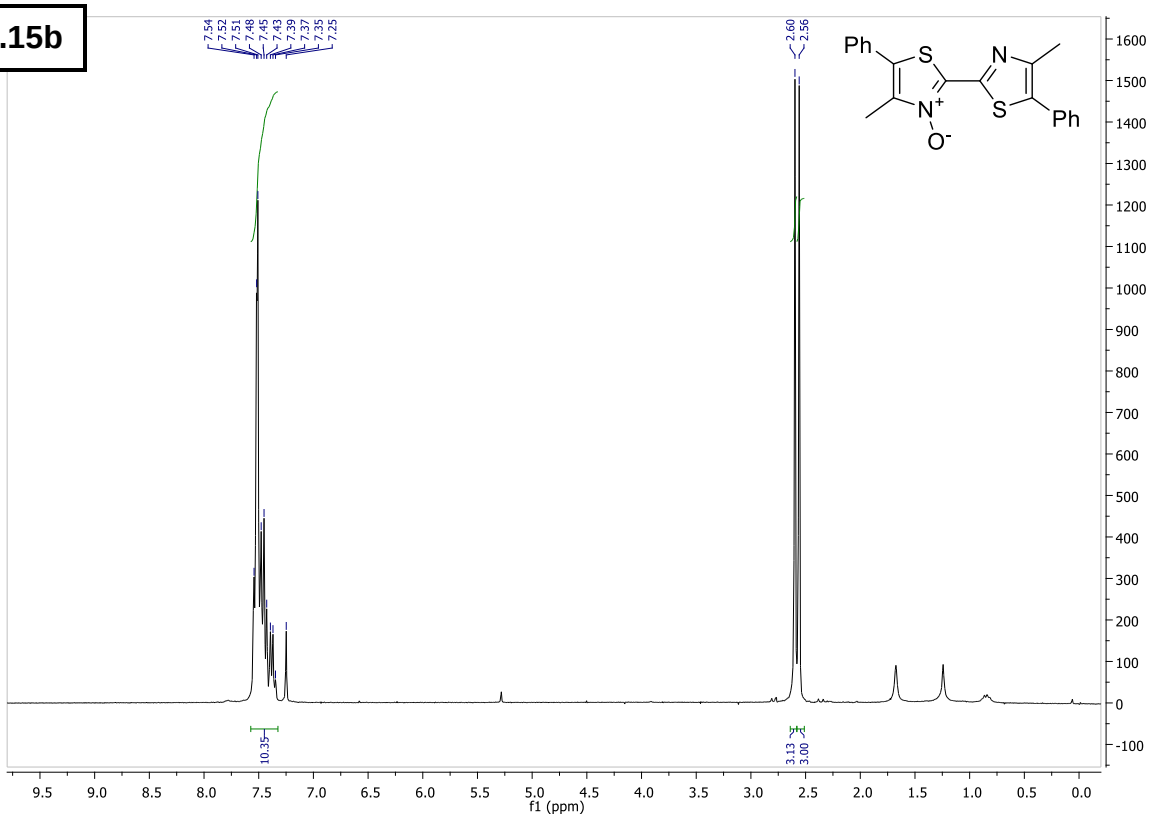
7.54
7.52
7.51
7.48
7.45
7.43
7.39
7.37
7.35
7.25
2.60
2.56
Ph
S
N
N+
O-
S
Ph
10.35
3.13
3.00
f1 (ppm)

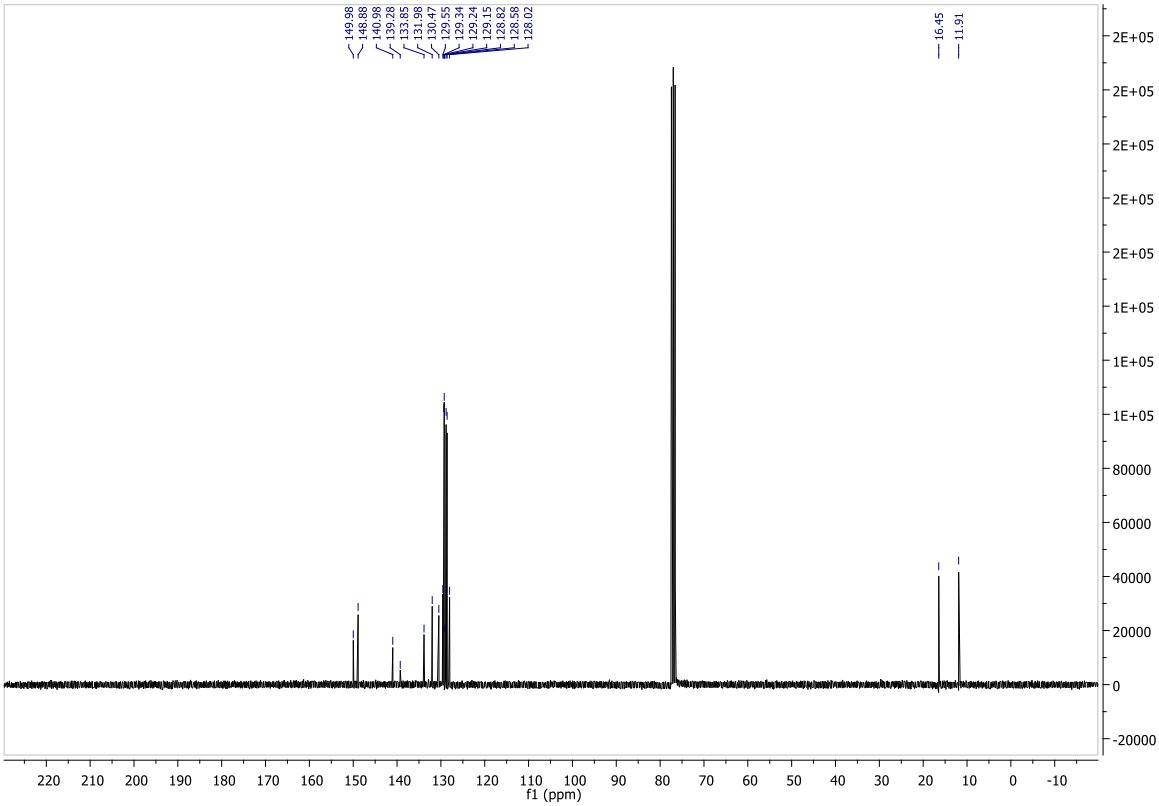
149.98
148.88
140.98
139.28
133.85
131.98
130.47
129.55
129.34
129.24
129.15
128.82
128.58
128.02
16.45
11.91
f1 (ppm)

2.15c

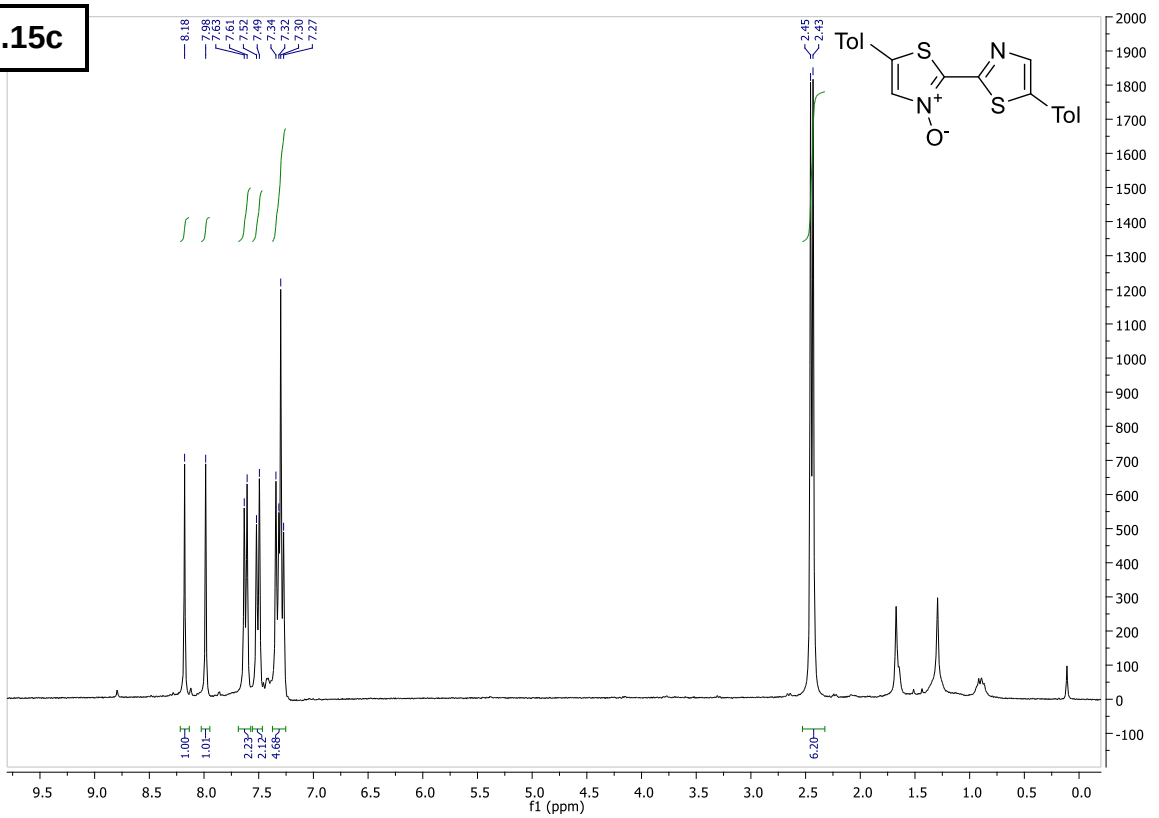
8.18
7.98
7.63
7.61
7.52
7.49
7.34
7.32
7.30
7.27
2.45
2.43
Tol
S
N
N+
O-
S
Tol
1.00
1.01
2.23
2.12
4.68
6.20
f1 (ppm)

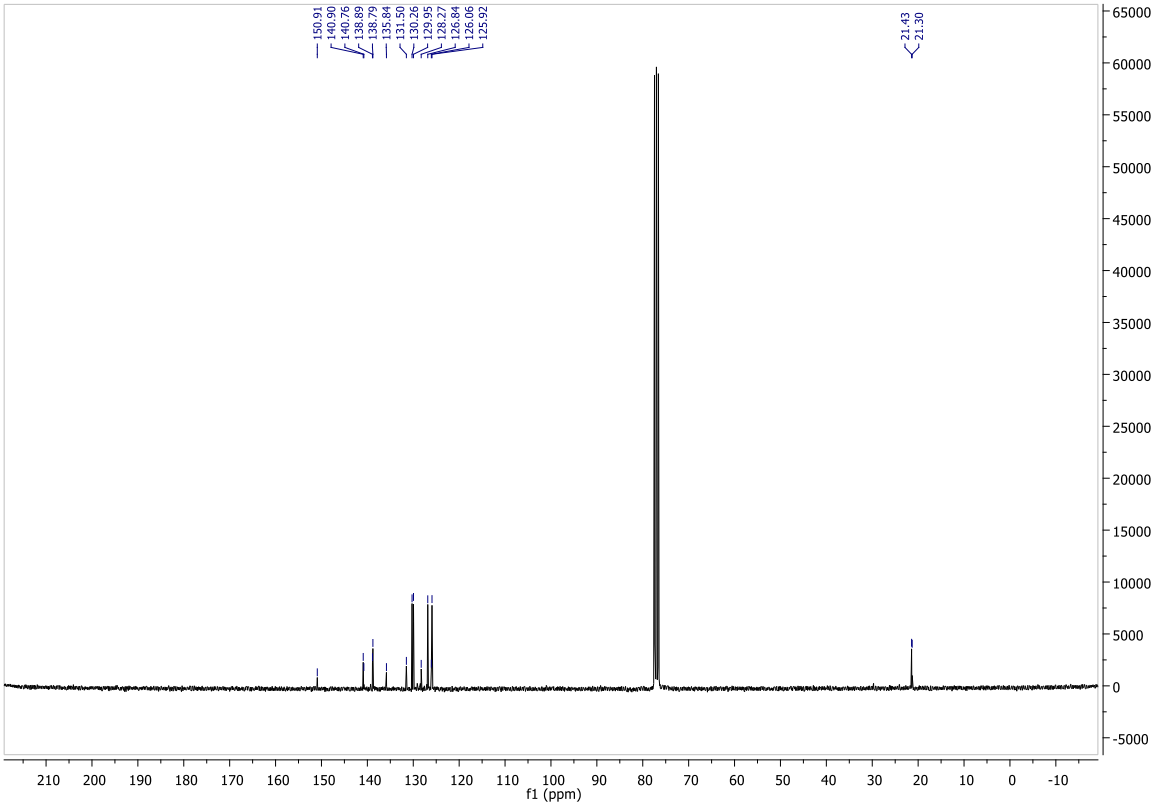
150.91
140.90
140.76
138.89
138.79
135.84
131.50
130.26
129.95
128.27
126.84
126.06
125.92
21.43
21.30
f1 (ppm)

2.15e

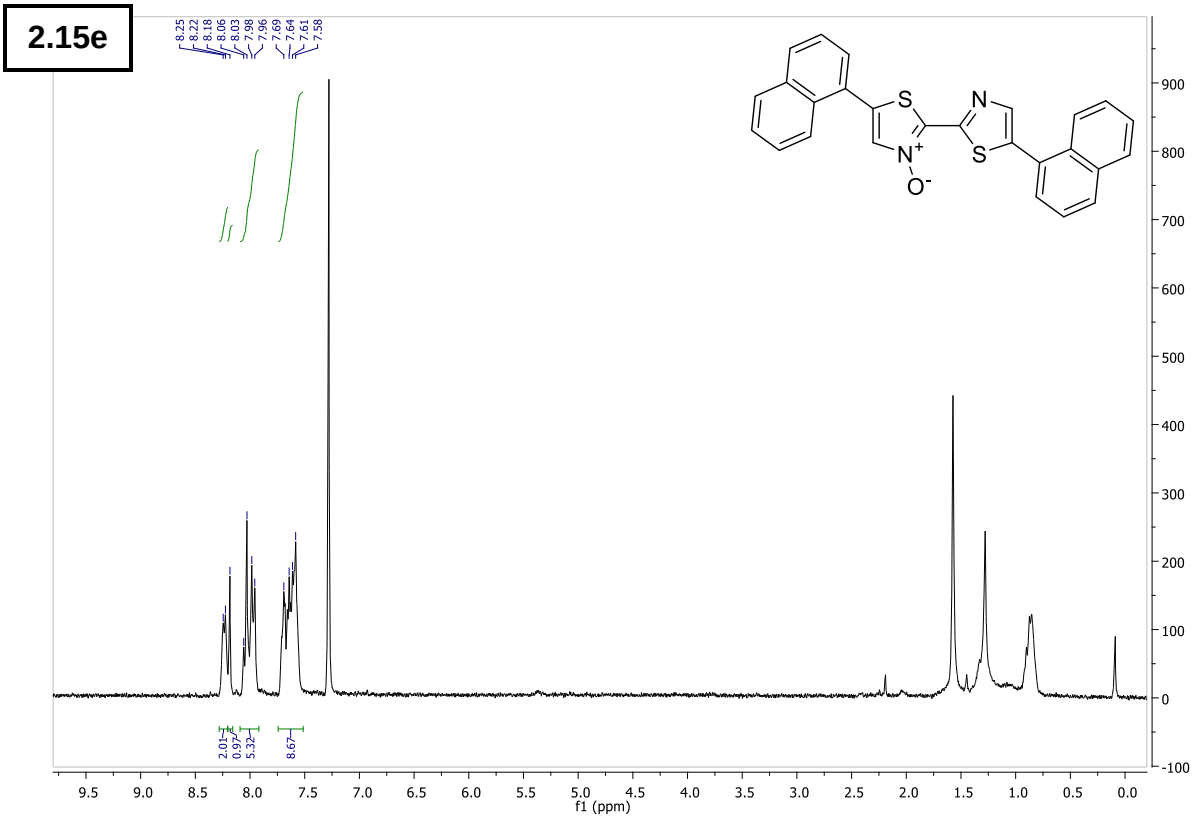
8.25
8.22
8.18
8.06
8.03
7.98
7.96
7.69
7.64
7.61
7.58
S
N
N+
O-
S
2.01
0.97
5.32
8.67
f1 (ppm)

2.15f

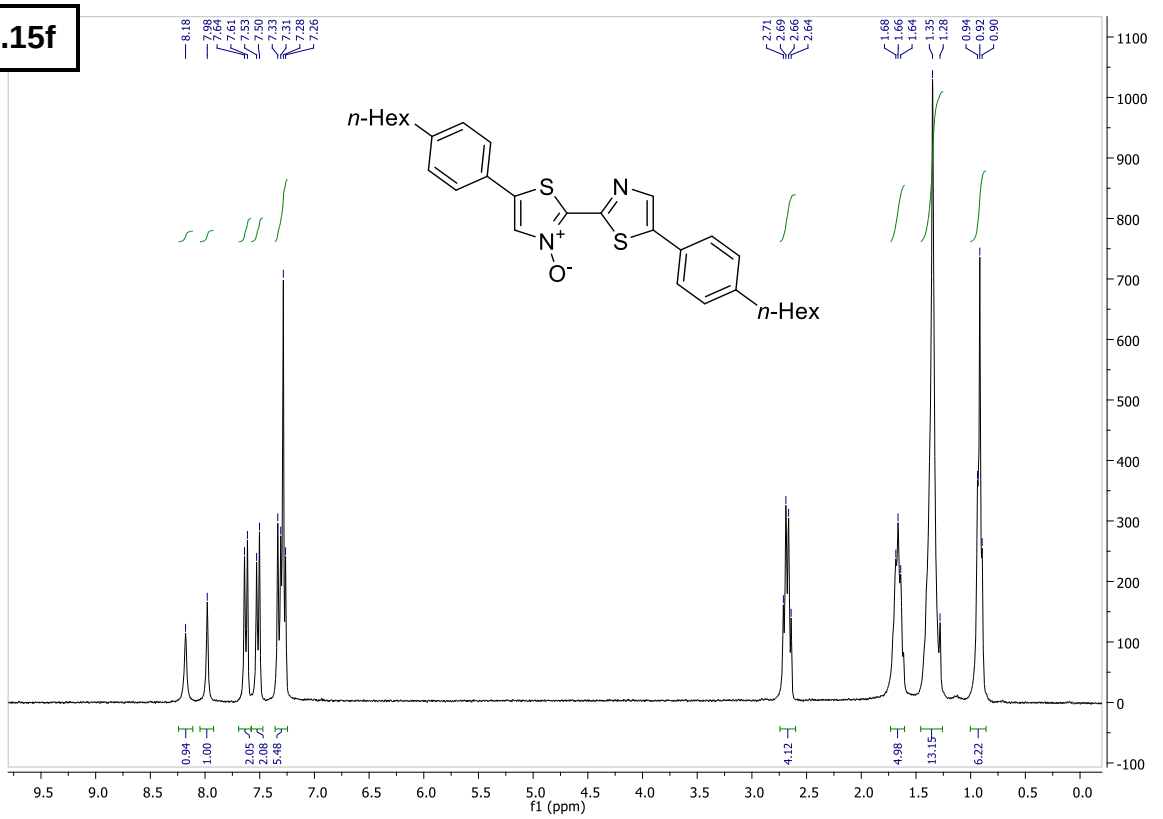
8.18
7.98
7.64
7.61
7.53
7.50
7.33
7.31
7.28
7.26
2.71
2.69
2.66
2.64
1.68
1.66
1.64
1.35
1.28
0.94
0.92
0.90
n-Hex
S
N
N+
O-
S
n-Hex
0.94
1.00
2.05
2.08
5.48
4.12
4.98
13.15
6.22
f1 (ppm)

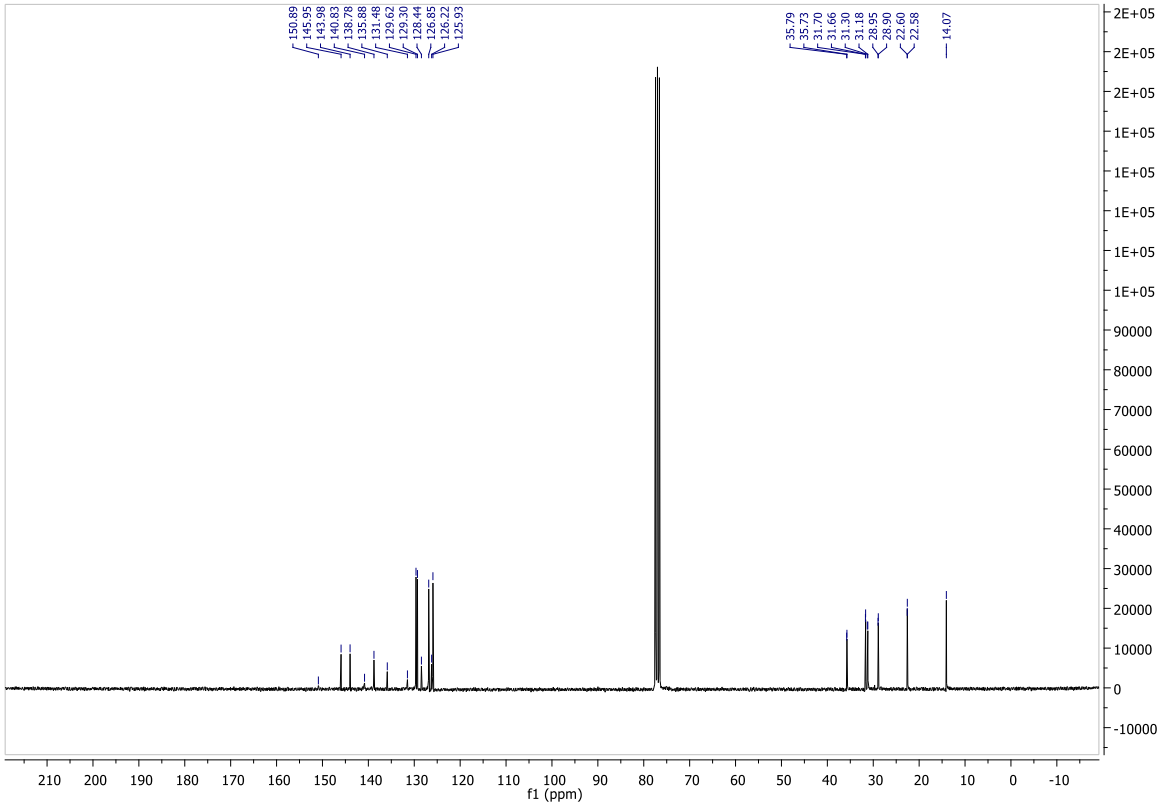
150.89
145.95
143.98
140.83
138.78
135.88
131.48
129.62
129.30
128.44
126.85
126.22
125.93
35.79
35.73
31.70
31.66
31.30
31.18
28.95
28.90
22.60
22.58
14.07
f1 (ppm)

2.15g

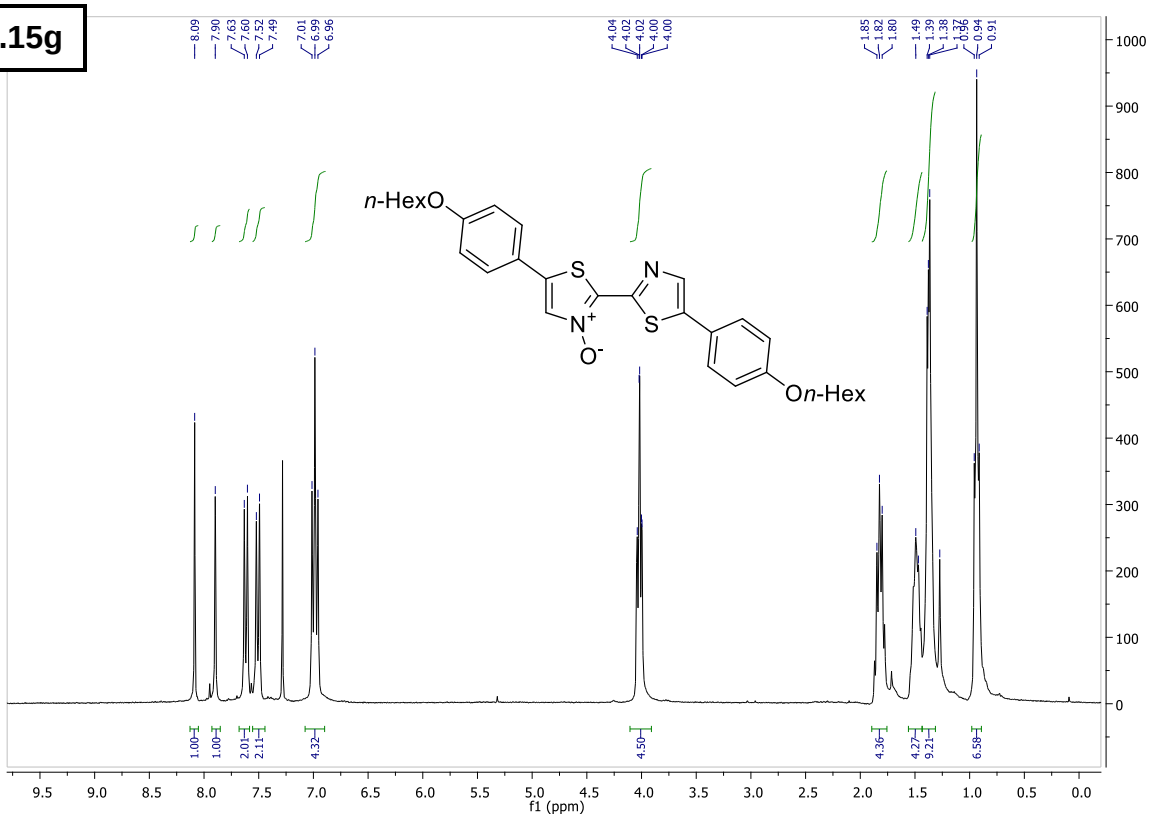
8.09
7.90
7.63
7.60
7.52
7.49
7.01
6.99
6.96
4.04
4.02
4.02
4.00
4.00
1.85
1.82
1.80
1.49
1.39
1.38
1.37
0.96
0.94
0.91
n-HexO
S
N
N+
O-
S
On-Hex
1.00
1.00
2.01
2.11
4.32
4.50
4.36
4.27
9.22
6.58
f1 (ppm)

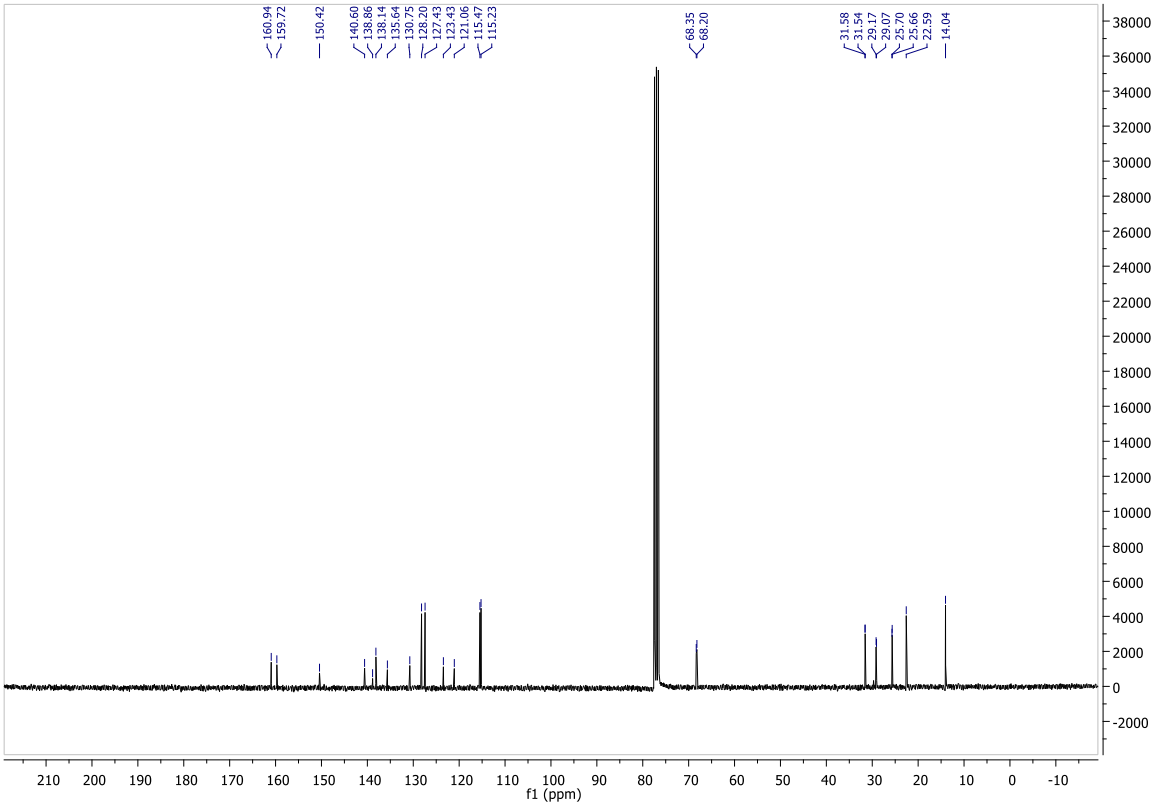
160.94
159.72
150.42
140.60
138.86
138.14
135.64
130.75
128.20
127.43
123.43
121.06
115.47
115.23
68.35
68.20
31.58
31.54
29.17
29.07
25.70
25.66
22.59
14.04
f1 (ppm)

2.15h

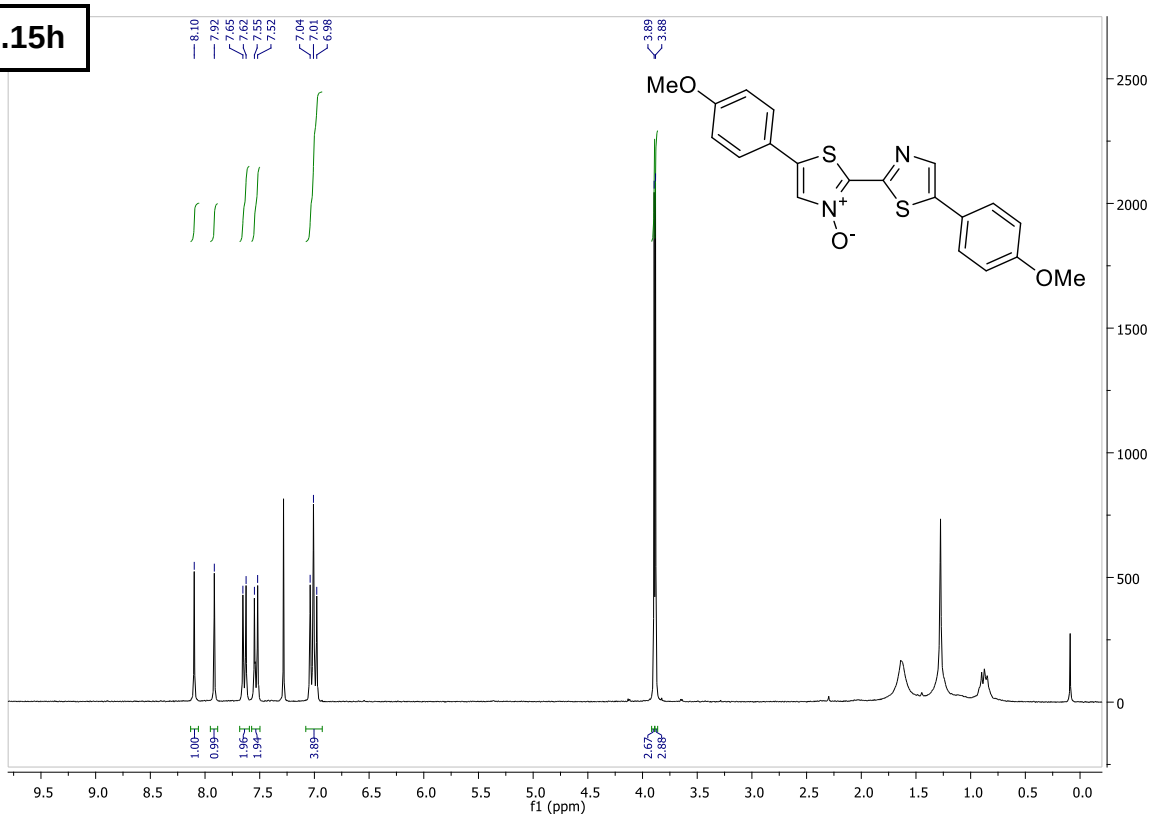
8.10
7.92
7.65
7.62
7.55
7.52
7.04
7.01
6.98
3.89
3.88
MeO
S
N
N+
O-
S
OMe
1.00
0.99
1.96
1.94
3.89
2.67
2.88
f1 (ppm)

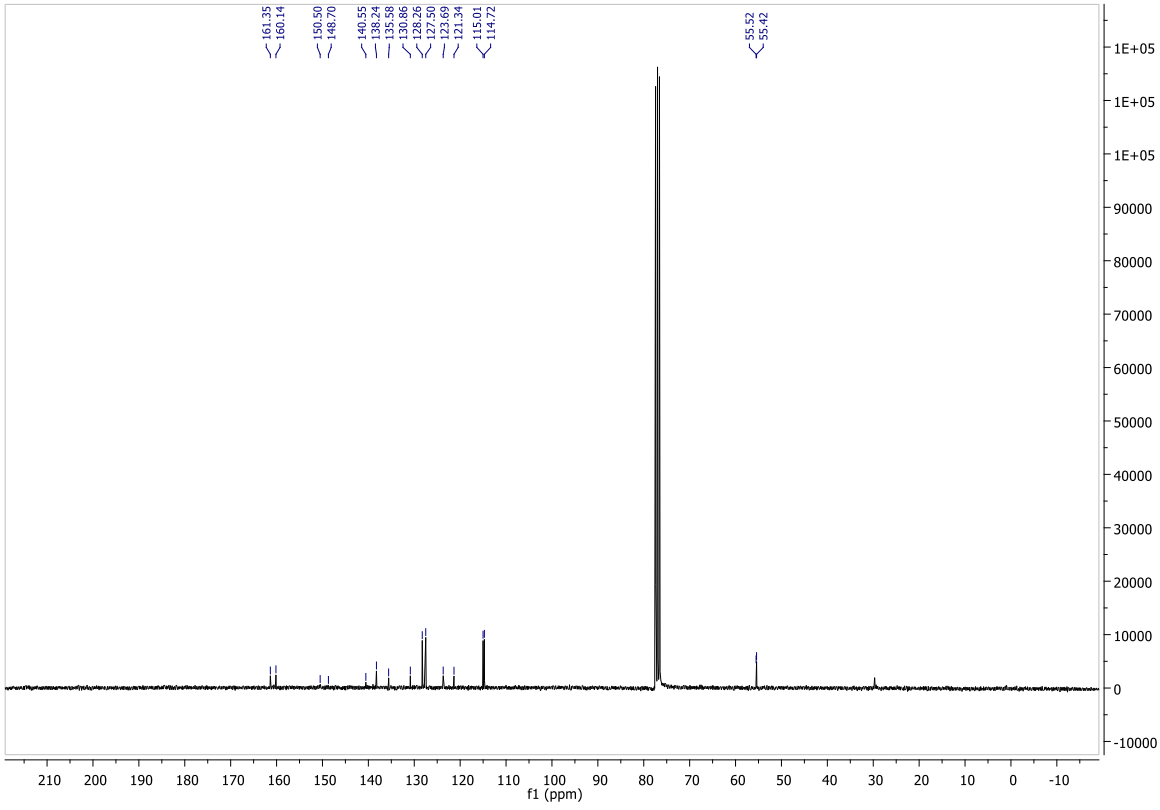
161.35
160.14
150.50
148.70
140.55
138.24
135.58
130.86
128.26
127.50
123.69
121.34
115.01
114.72
55.52
55.42
f1 (ppm)

2.15i

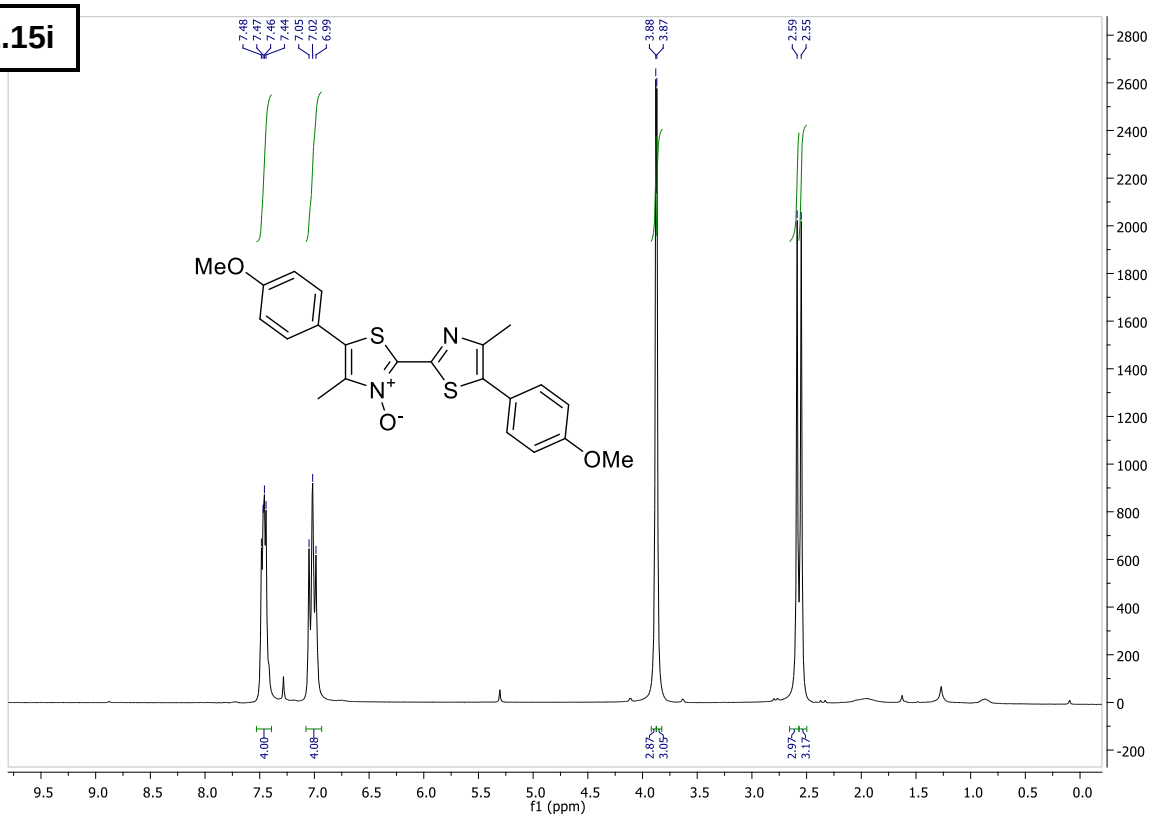
7.48
7.47
7.46
7.44
7.05
7.02
6.99
3.88
3.87
2.59
2.55
MeO
OMe
S
N
N+
O-
4.00
4.08
2.87
3.05
2.97
3.17
f1 (ppm)

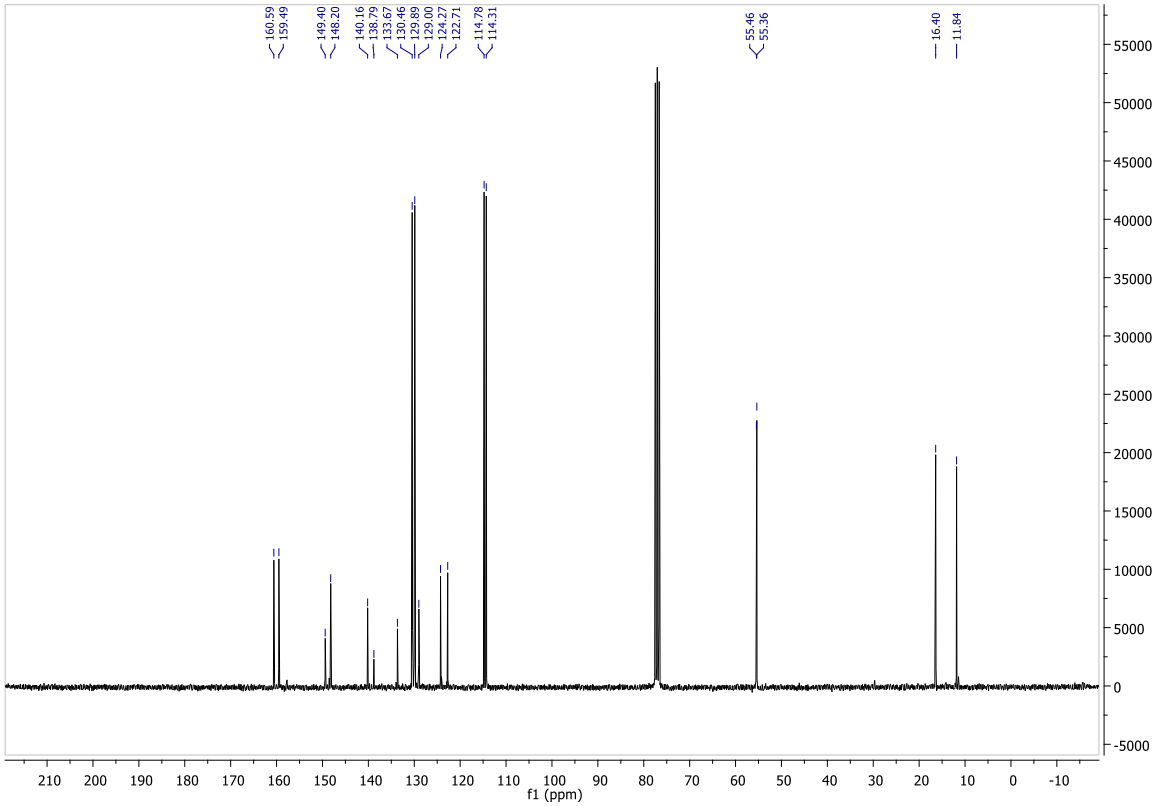
160.59
159.49
149.40
148.20
140.16
138.79
133.67
130.46
129.89
129.00
124.27
122.71
114.78
114.31
55.46
55.36
16.40
11.84
f1 (ppm)

2.15k

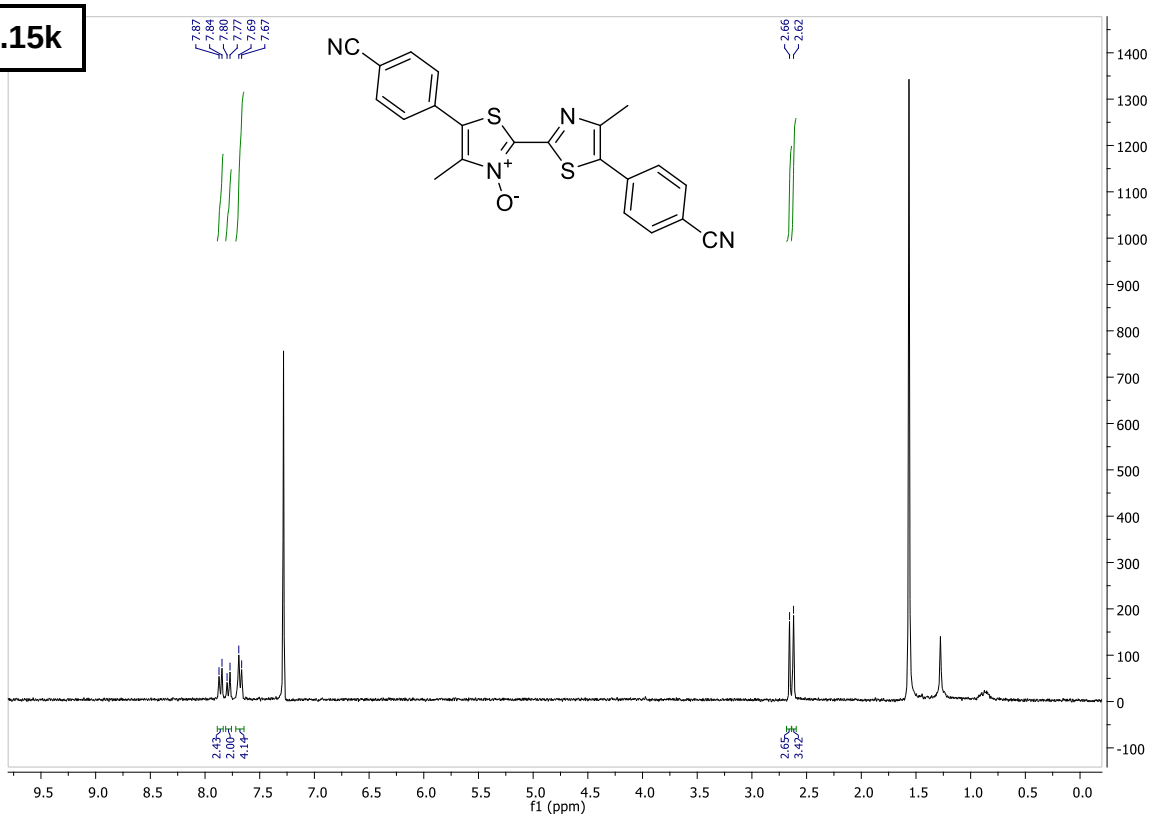
7.87
7.84
7.80
7.77
7.69
7.67
2.66
2.62
NC
S
N
N+
O-
S
CN
2.43
2.00
4.14
2.65
3.42
f1 (ppm)

2.15l

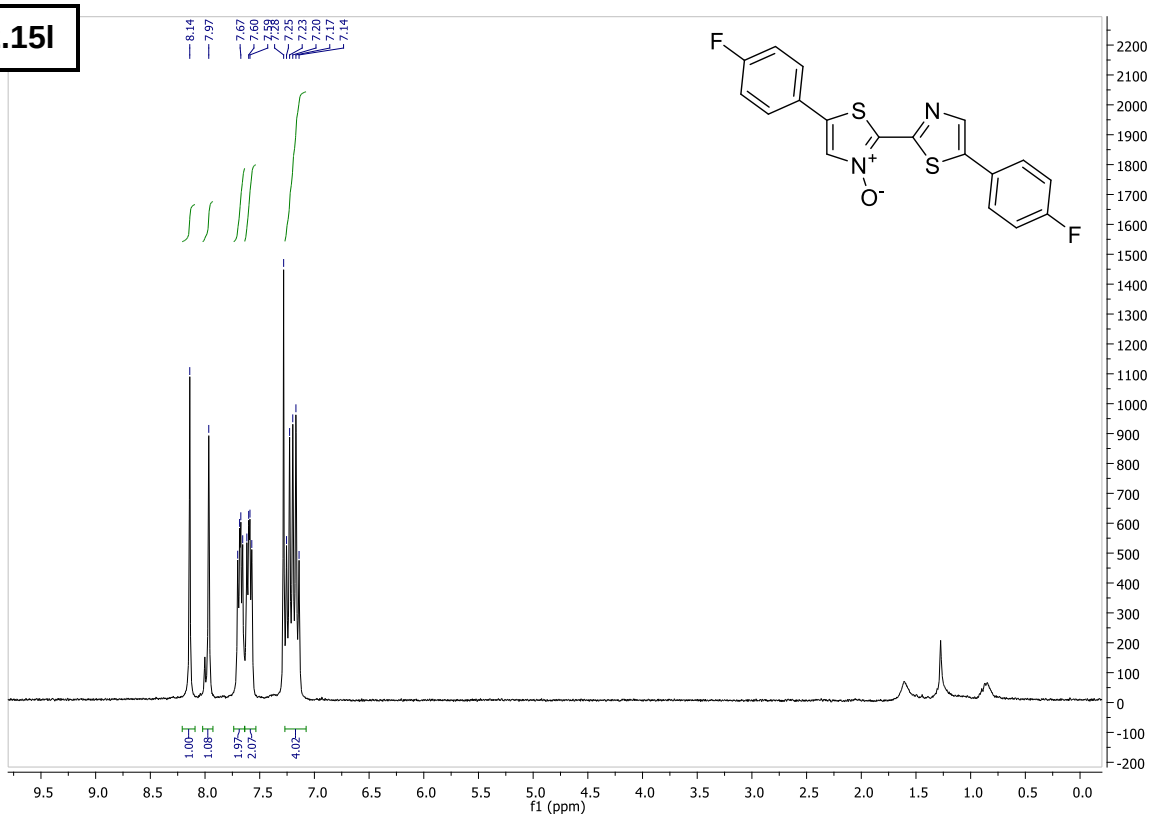
8.14
7.97
7.67
7.60
7.59
7.28
7.25
7.23
7.20
7.17
7.14
F
S
N
N+
O-
S
F
1.00
1.08
1.97
2.07
4.02
f1 (ppm)

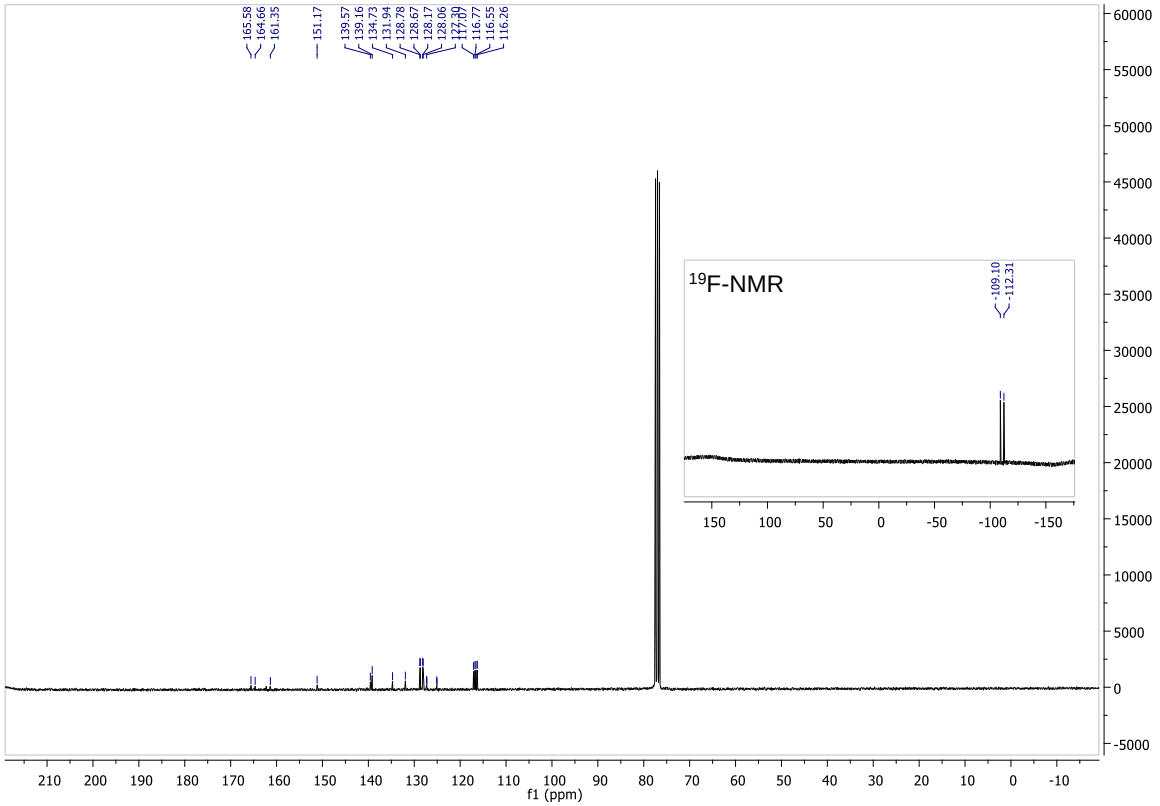
165.58
164.66
161.35
151.17
139.57
139.16
134.73
131.94
128.78
128.67
128.17
128.06
116.77
116.55
116.26
19F-NMR
-109.10
-112.31
f1 (ppm)

2.15m

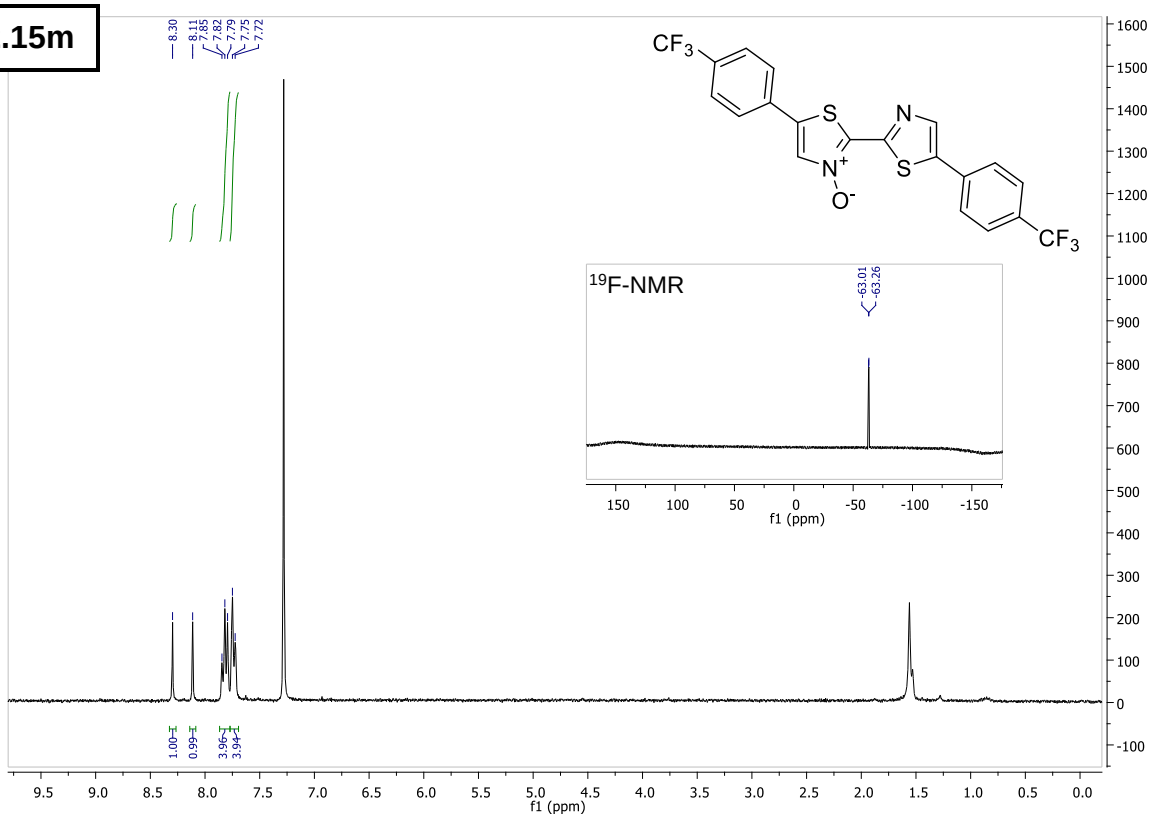
8.30
8.11
7.85
7.82
7.79
7.75
7.72
CF3
S
N
N+
O-
S
CF3
19F-NMR
-63.01
-63.26
150 100 50 0 -50 -100 -150
f1 (ppm)
1.00
0.99
3.96
3.94
9.5 9.0 8.5 8.0 7.5 7.0 6.5 6.0 5.5 5.0 4.5 4.0 3.5 3.0 2.5 2.0 1.5 1.0 0.5 0.0
f1 (ppm)
1600 1500 1400 1300 1200 1100 1000 900 800 700 600 500 400 300 200 100 0 -100

2.15n

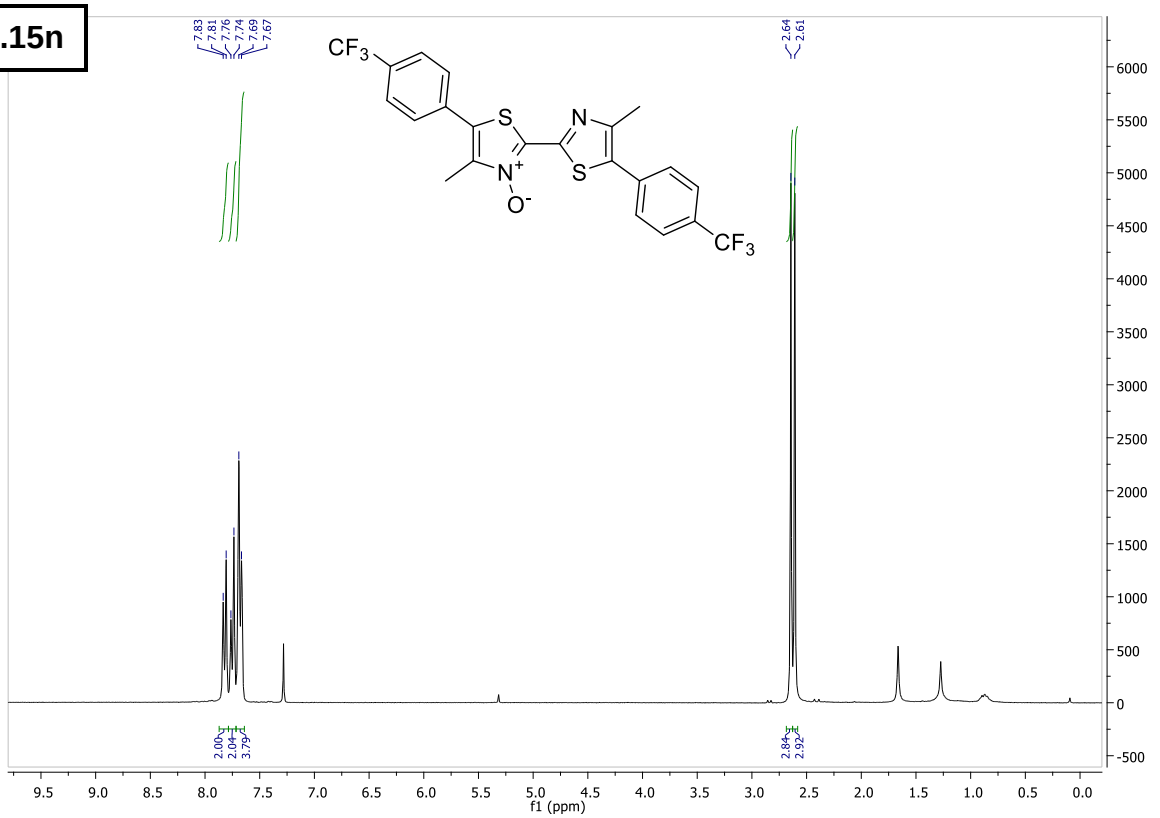
7.83
7.81
7.76
7.74
7.69
7.67
2.64
2.61
CF3
S
N
N+
O-
S
CF3
2.00
2.04
3.79
2.84
2.92
f1 (ppm)

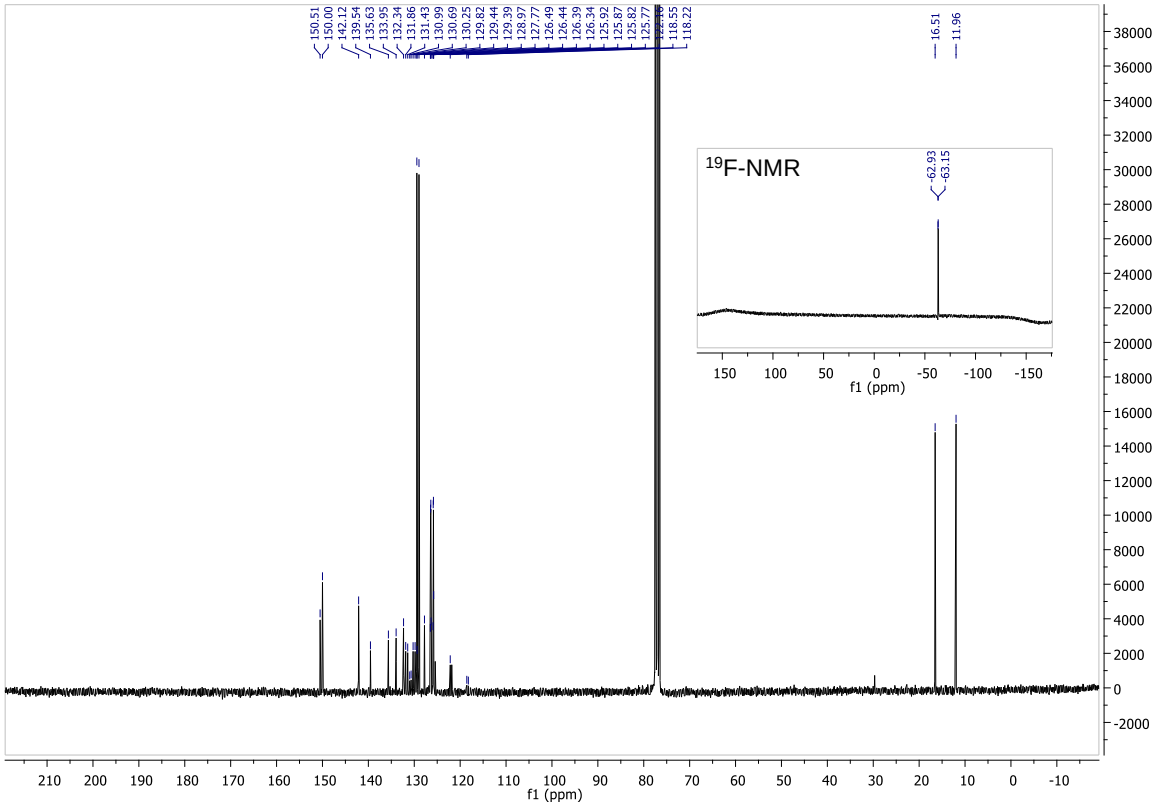
150.51
150.00
142.12
139.54
135.63
133.95
132.34
131.86
131.43
130.99
130.69
130.25
129.82
129.44
129.39
128.97
127.77
126.49
126.44
126.39
126.34
125.92
125.87
125.82
125.77
118.55
118.22
16.51
11.96
19F-NMR
-62.93
-63.15
f1 (ppm)
f1 (ppm)

2.15o

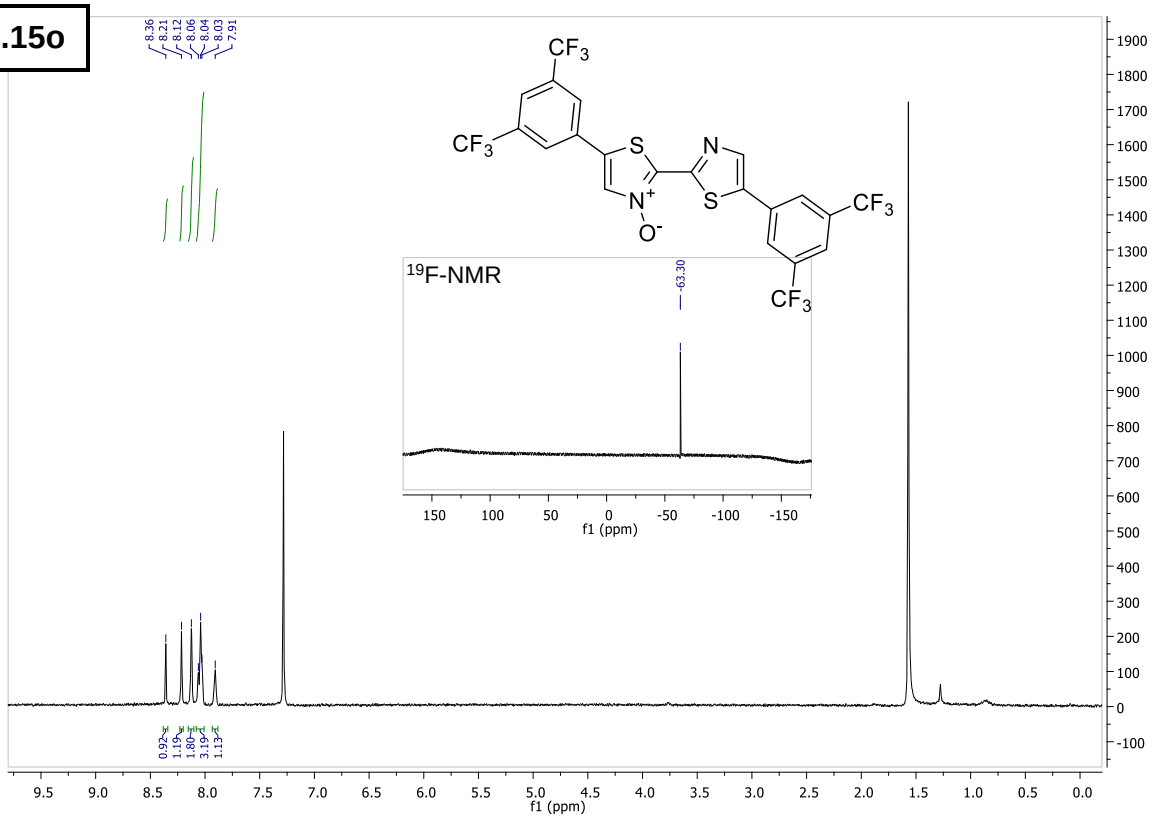
8.36
8.21
8.12
8.06
8.04
8.03
7.91
CF3
CF3
S
N
N+
O-
S
CF3
CF3
19F-NMR
-63.30
150
100
50
0
-50
-100
-150
f1 (ppm)
0.92
1.15
1.80
3.19
1.13
9.5
9.0
8.5
8.0
7.5
7.0
6.5
6.0
5.5
5.0
4.5
4.0
3.5
3.0
2.5
2.0
1.5
1.0
0.5
0.0
f1 (ppm)
1900
1800
1700
1600
1500
1400
1300
1200
1100
1000
900
800
700
600
500
400
300
200
100
0
-100

2.16

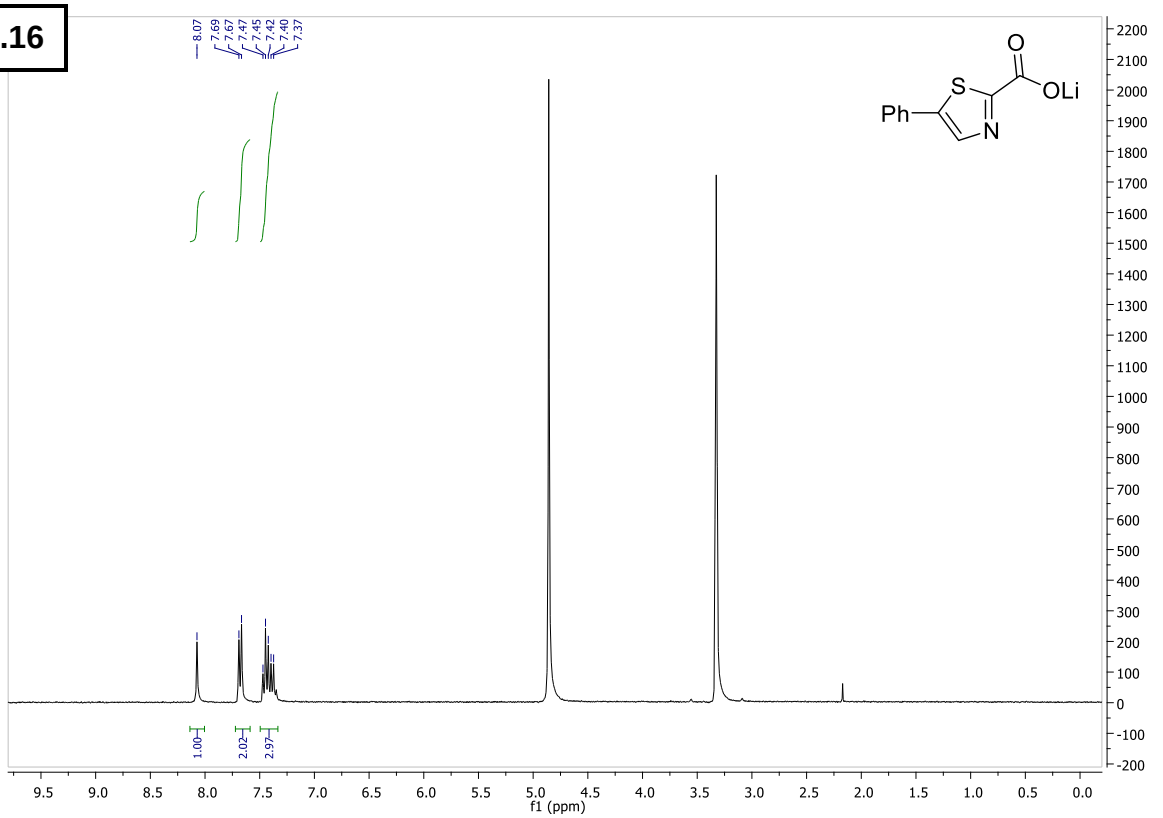
8.07
7.69
7.67
7.47
7.45
7.42
7.40
7.37
O
S
OLi
Ph
N
1.00
2.02
2.97
f1 (ppm)

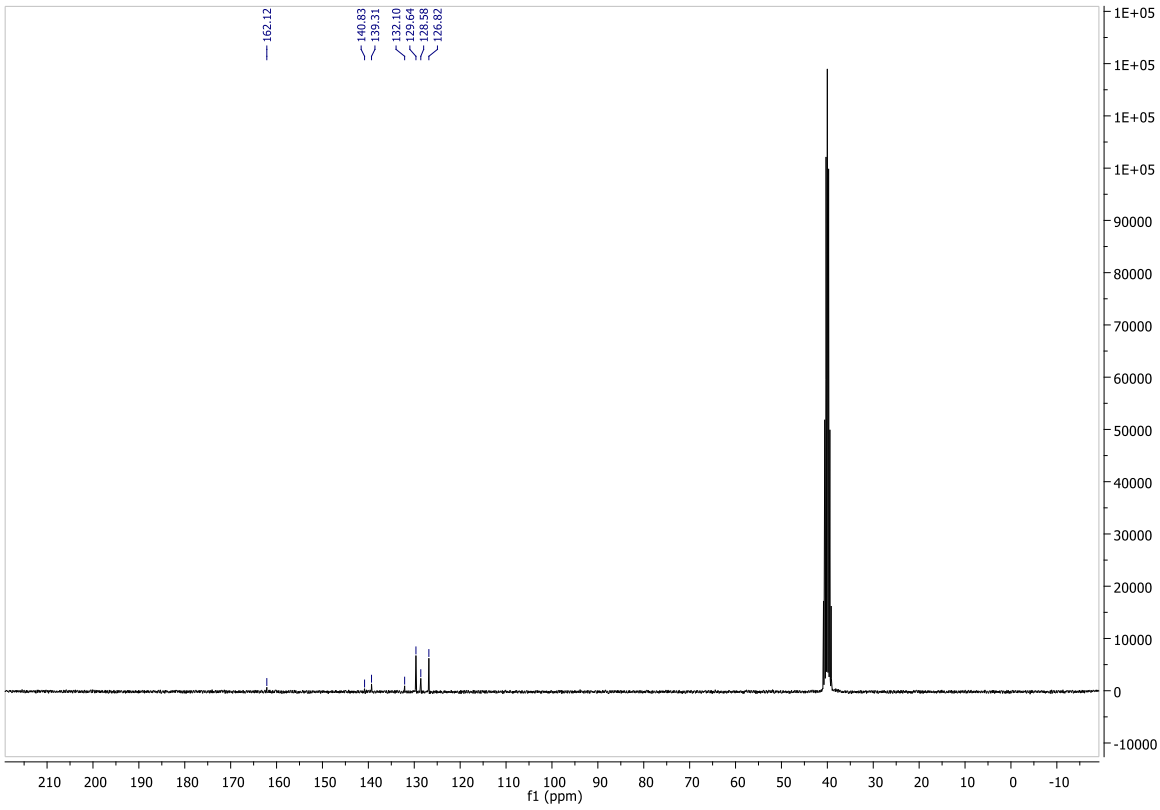
162.12
140.83
139.31
132.10
129.64
128.58
126.82
f1 (ppm)

2.18

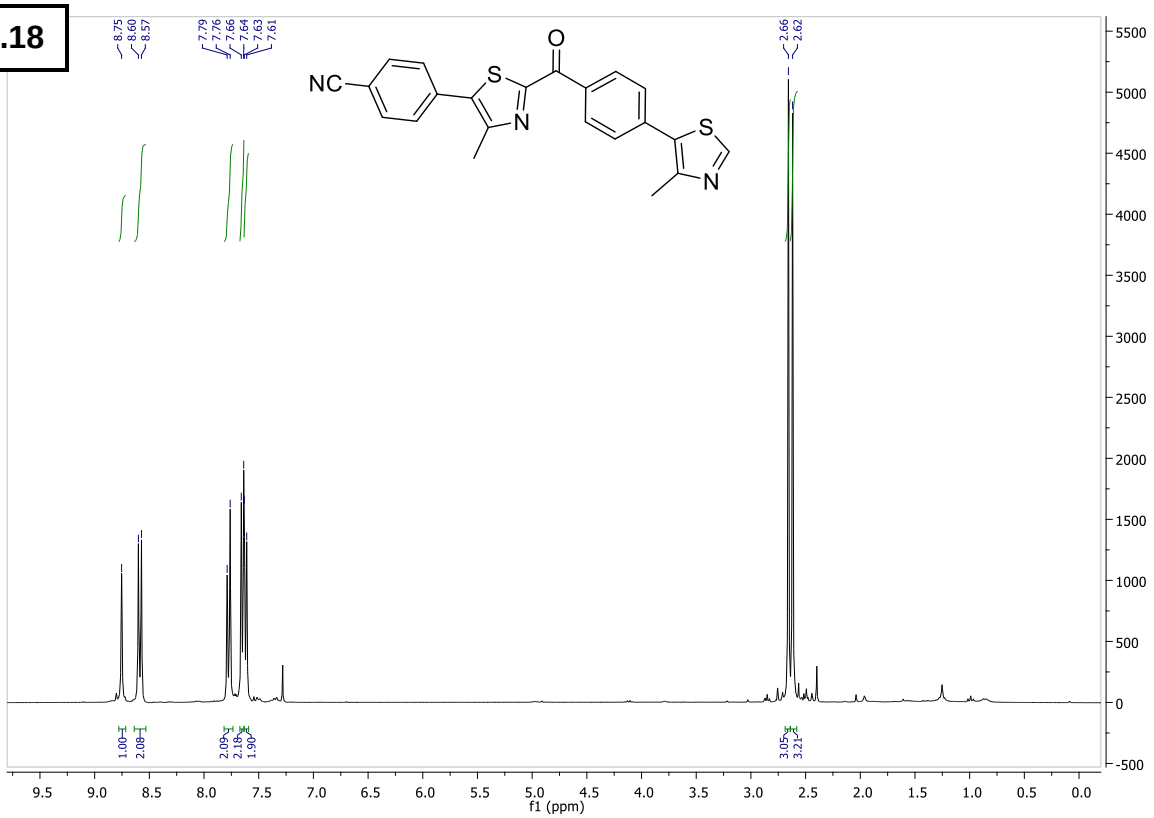
8.75
8.60
8.57
7.79
7.76
7.66
7.64
7.63
7.61
2.66
2.62
NC
O
S
N
S
N
1.00
2.08
2.09
2.18
1.90
3.05
3.21
f1 (ppm)

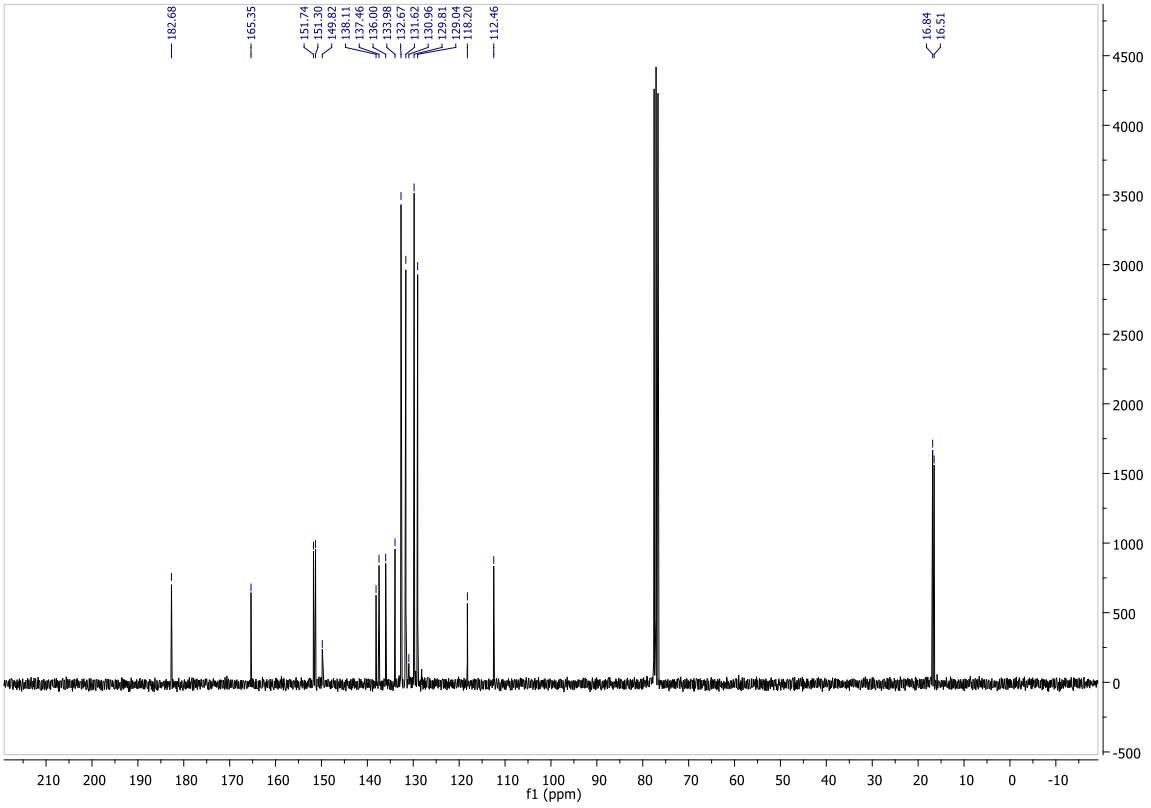
182.68
165.35
151.74
151.30
149.82
138.11
137.46
136.00
133.98
132.67
131.62
130.96
129.81
129.04
118.20
112.46
16.84
16.51
f1 (ppm)

2.19a

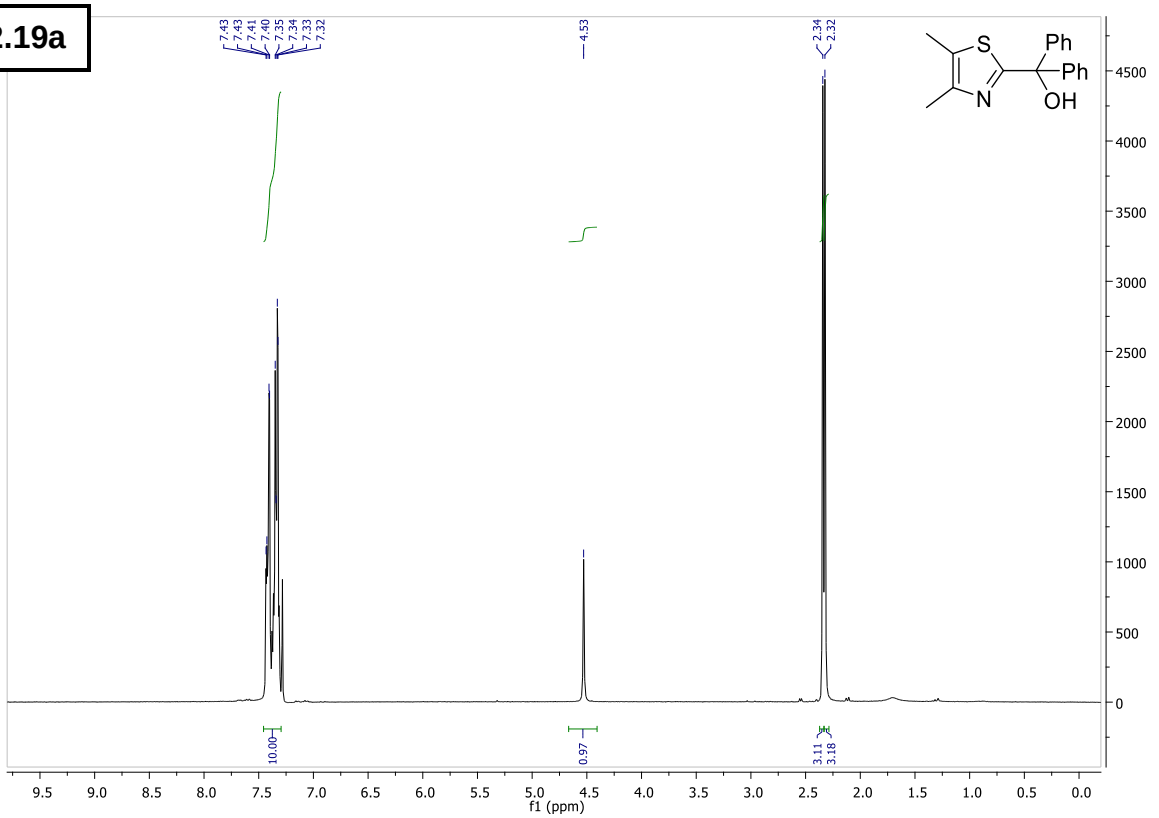
7.43
7.43
7.41
7.40
7.35
7.34
7.33
7.32
4.53
2.34
2.32
S
N
Ph
Ph
OH
10.00
0.97
3.11
3.18
f1 (ppm)

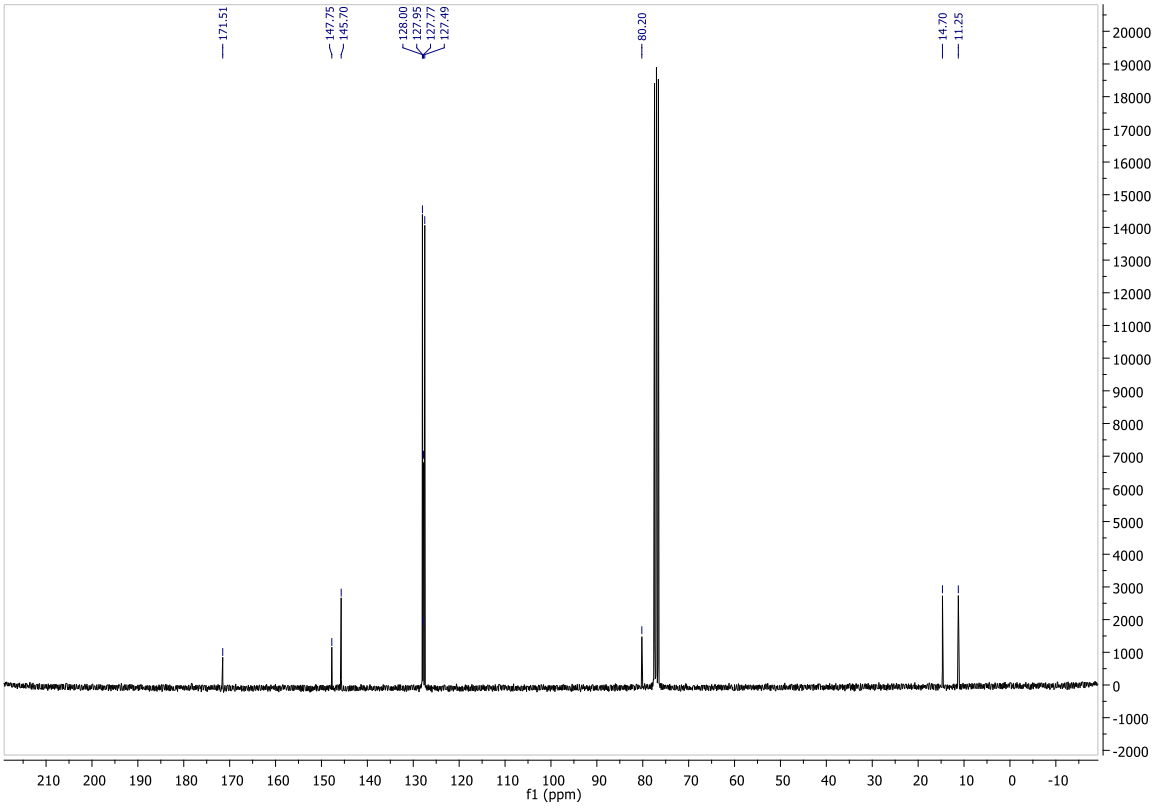
171.51
147.75
145.70
128.00
127.95
127.77
127.49
80.20
14.70
11.25
f1 (ppm)

2.19b

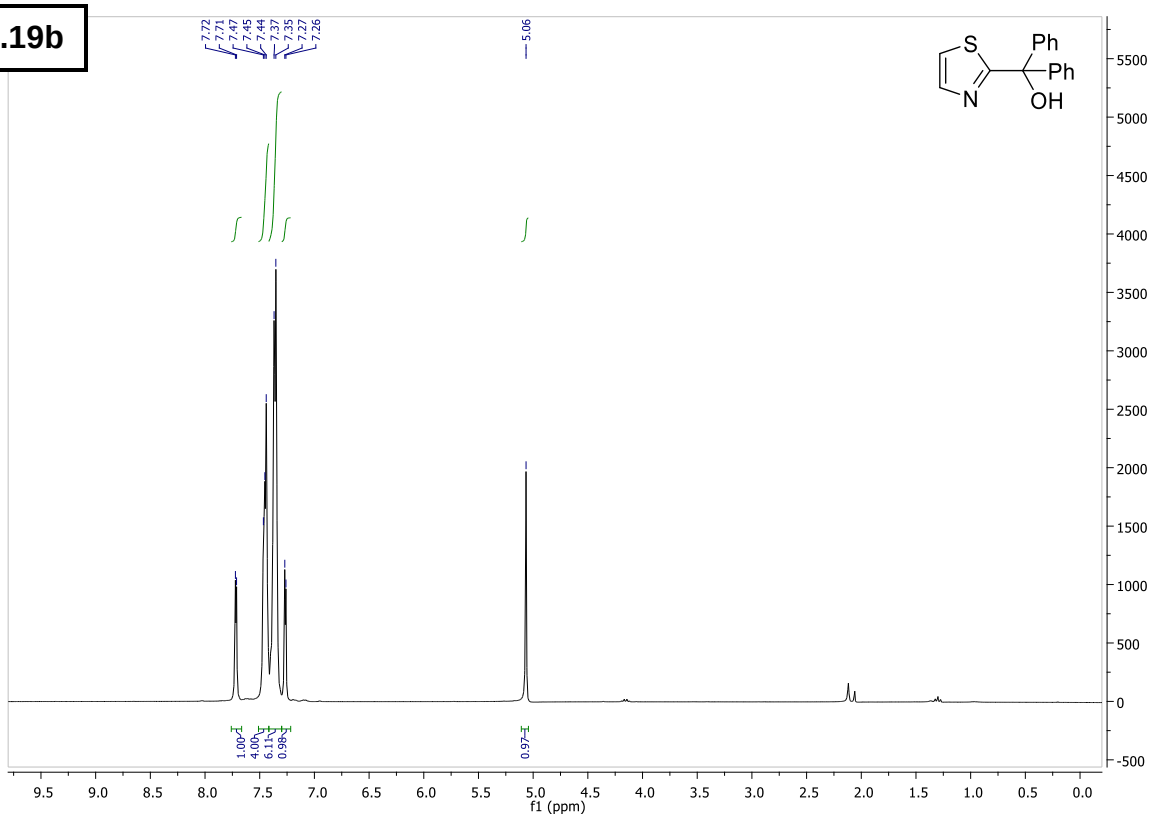
7.72
7.71
7.47
7.45
7.44
7.37
7.35
7.27
7.26
5.06
S
N
Ph
Ph
OH
1.00
4.00
6.11
0.98
0.97
f1 (ppm)

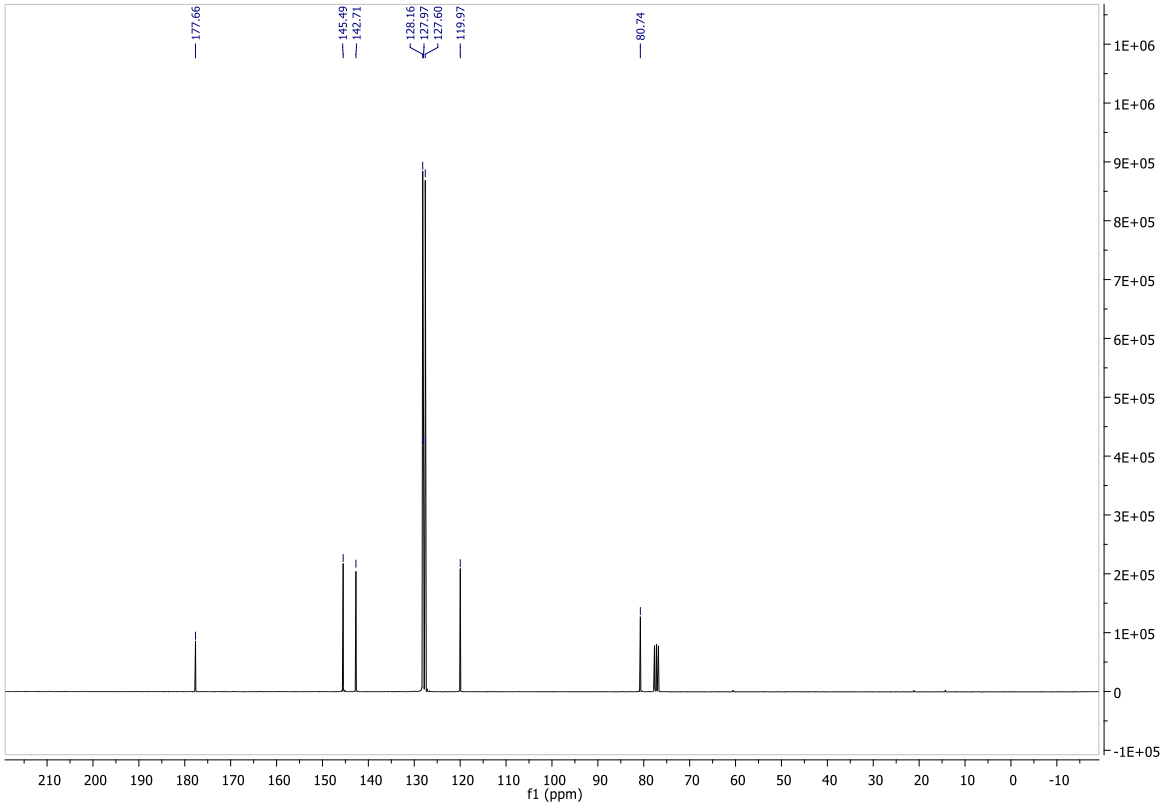
177.66
145.49
142.71
128.16
127.97
127.60
119.97
80.74
f1 (ppm)

2.19c

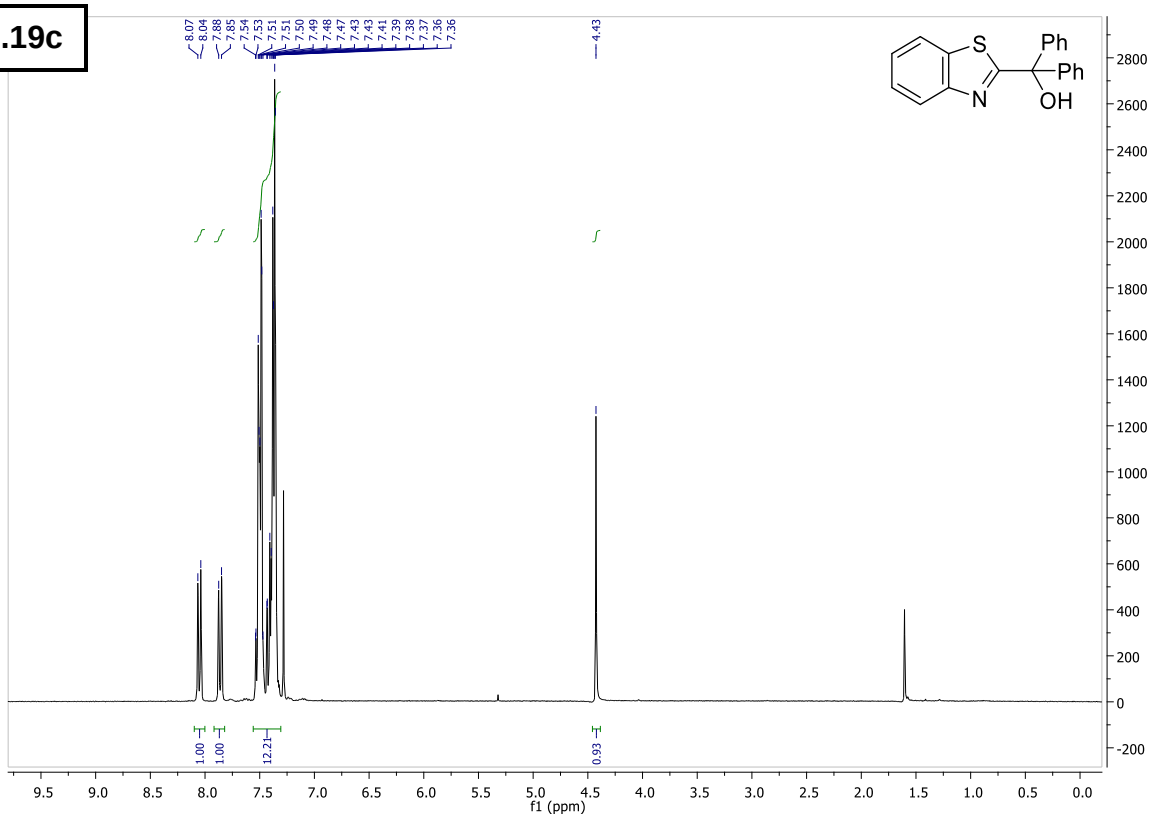
8.07
8.04
7.88
7.85
7.54
7.53
7.51
7.51
7.50
7.49
7.48
7.47
7.43
7.43
7.41
7.39
7.38
7.37
7.36
7.36
4.43
S
N
Ph
Ph
OH
1.00
1.00
12.21
0.93
f1 (ppm)

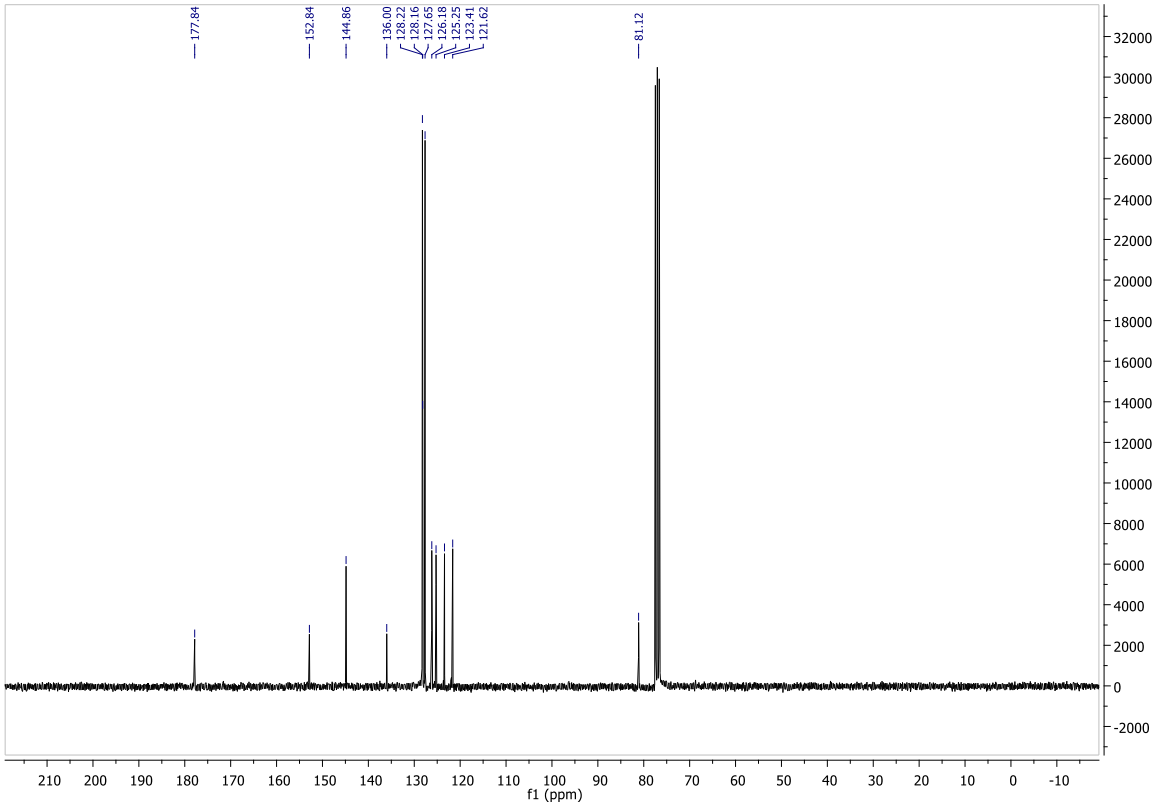
177.84
152.84
144.86
136.00
128.22
128.16
127.65
126.18
125.25
123.41
121.62
81.12
f1 (ppm)

2.20a

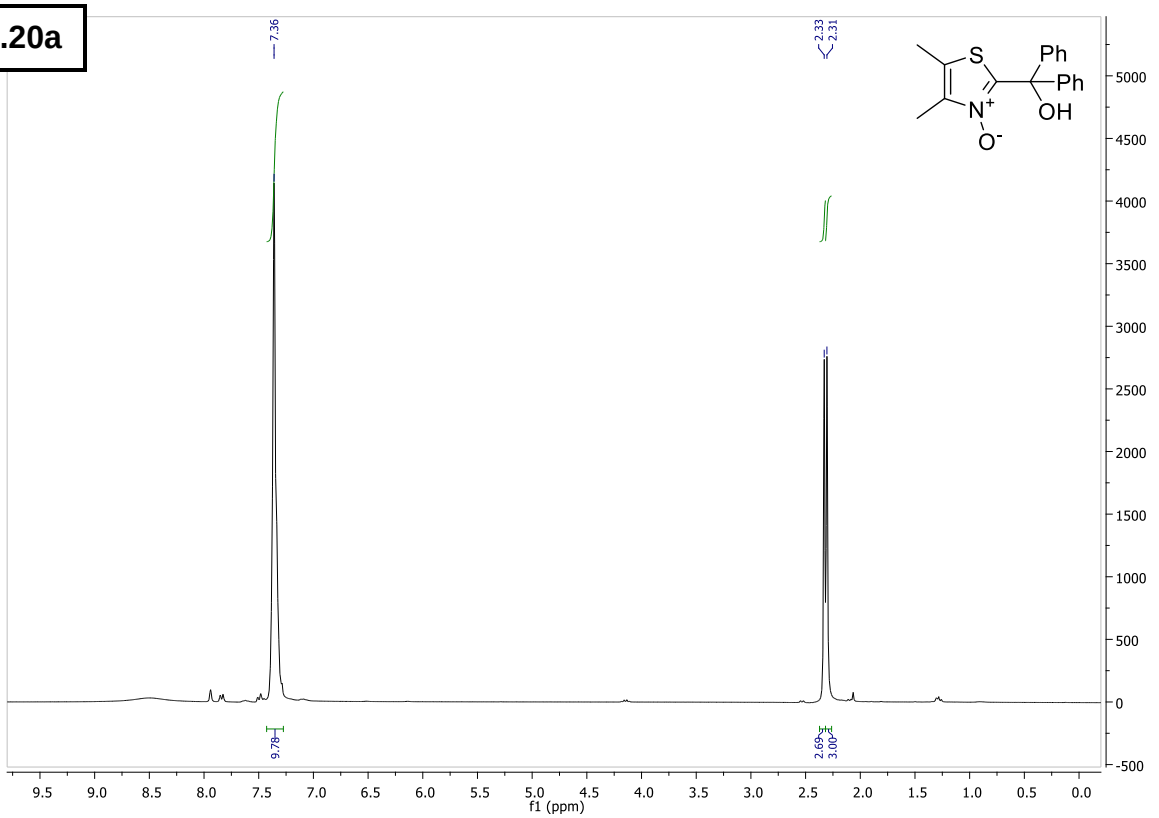
7.36
2.33
2.31
S
Ph
Ph
N+
OH
O-
9.78
2.69
3.00
f1 (ppm)

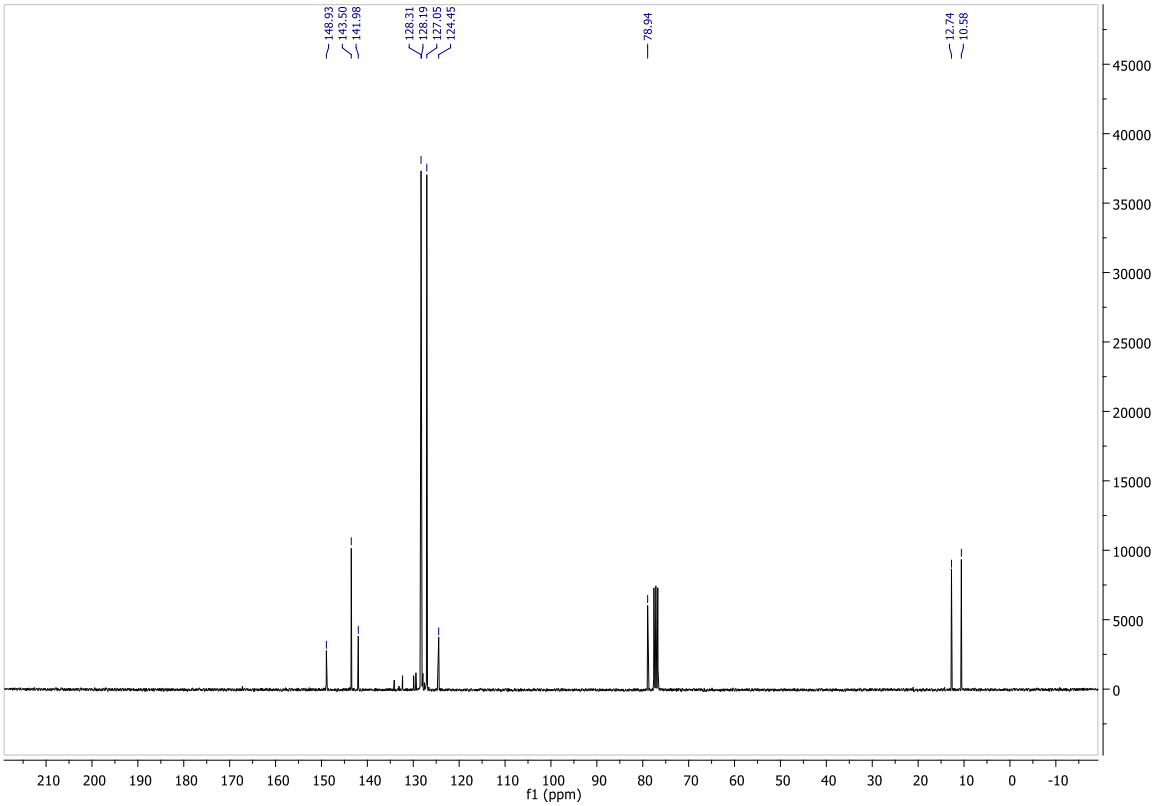
148.93
143.50
141.98
128.31
128.19
127.05
124.45
78.94
12.74
10.58
f1 (ppm)

2.20b

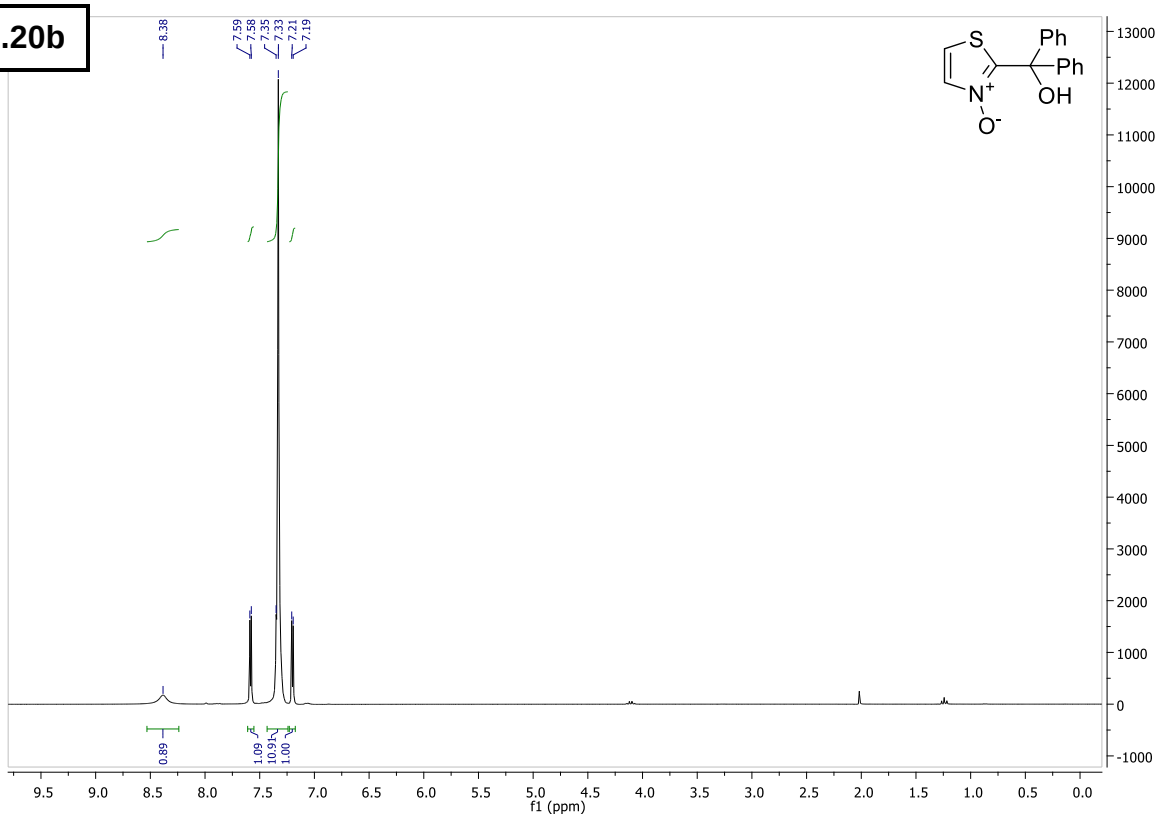
8.38
7.59
7.58
7.35
7.33
7.21
7.19
S
Ph
Ph
N+
OH
O-
0.89
1.09
10.91
1.00
f1 (ppm)

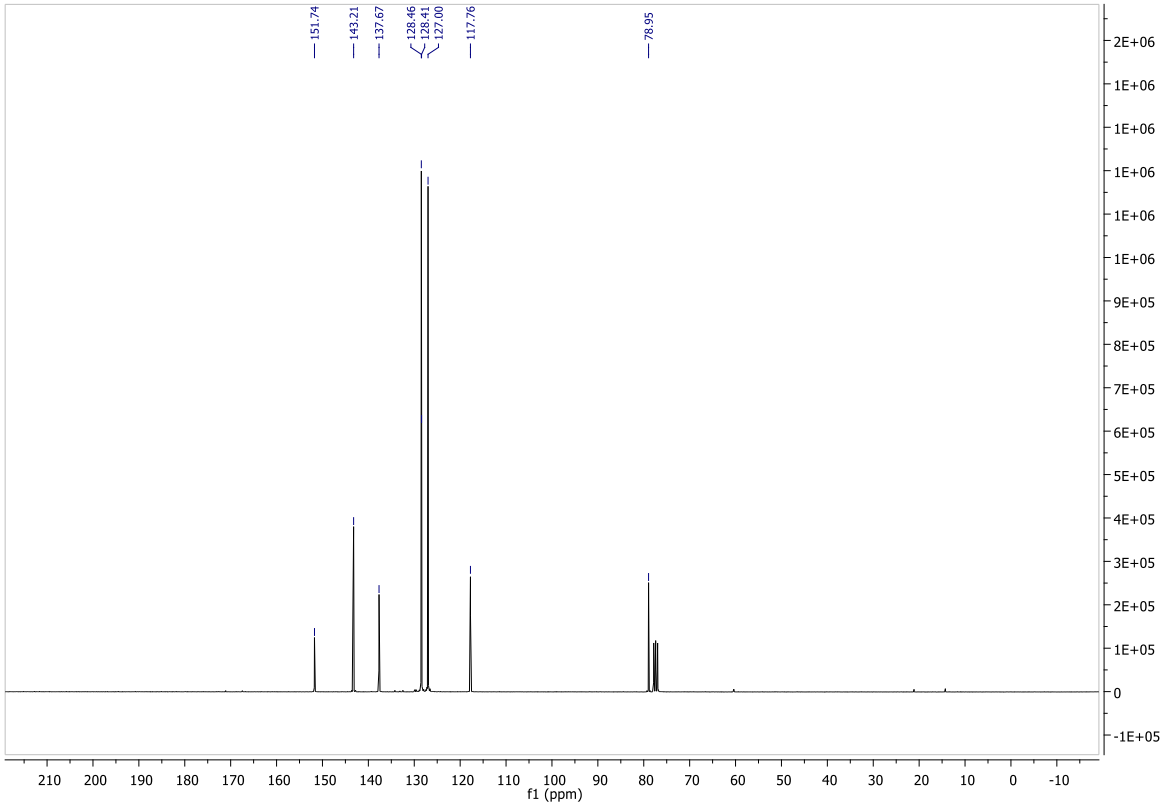
151.74
143.21
137.67
128.46
128.41
127.00
117.76
78.95
f1 (ppm)

2.20c

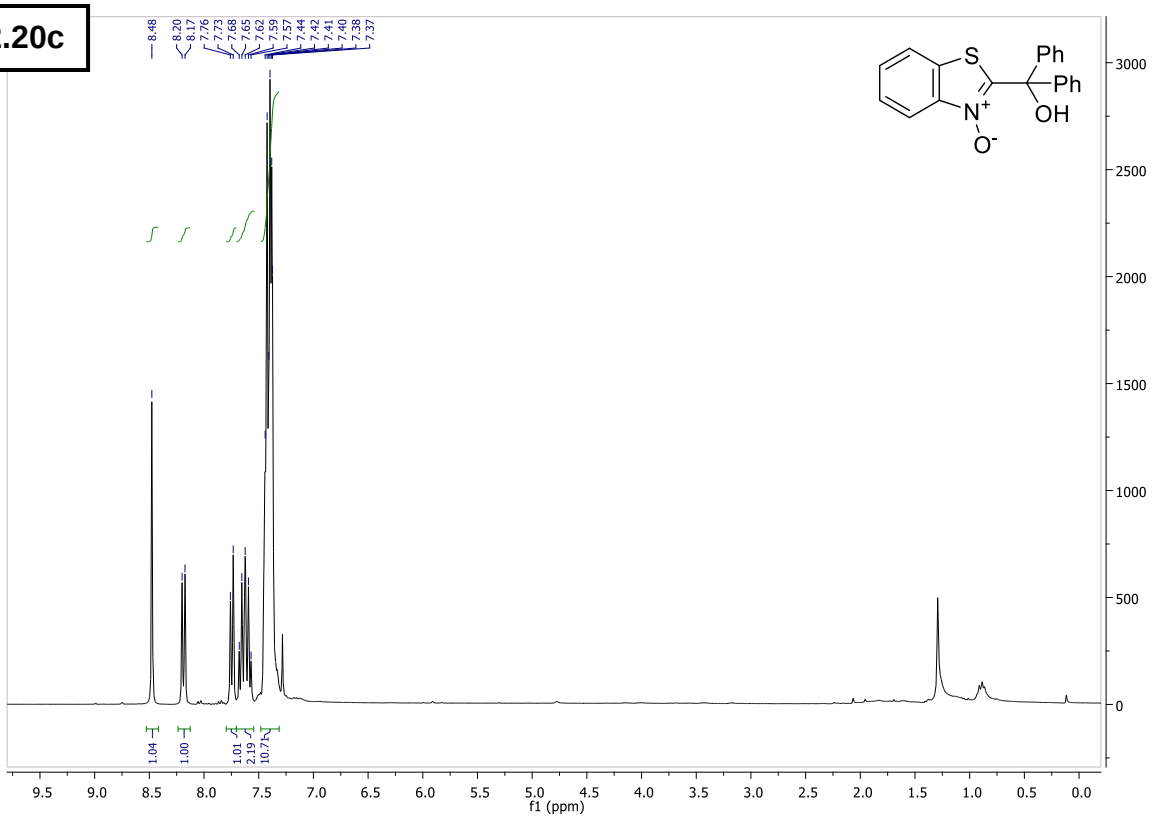
8.48
8.20
8.17
7.76
7.73
7.68
7.65
7.62
7.59
7.57
7.44
7.42
7.41
7.40
7.38
7.37
S
Ph
Ph
N+
O-
OH
1.04
1.00
1.01
2.19
10.71
f1 (ppm)

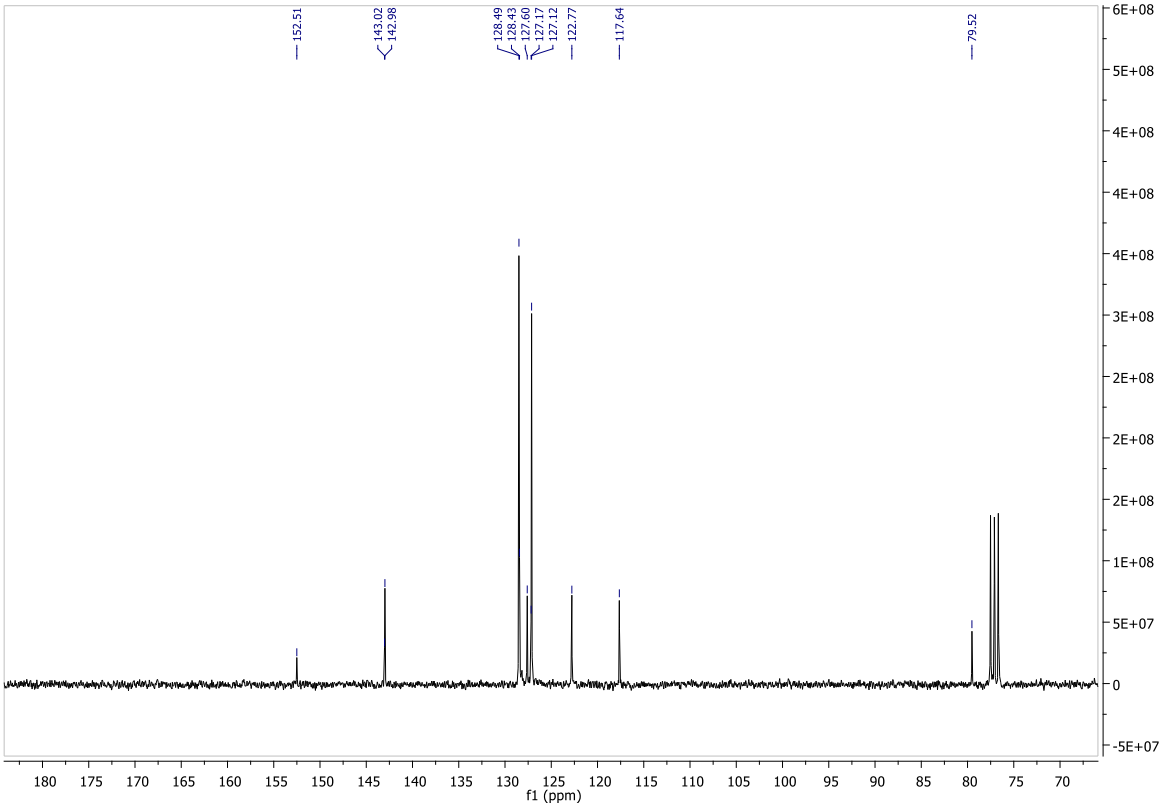
152.51
143.02
142.98
128.49
128.43
127.60
127.17
127.12
122.77
117.64
79.52
f1 (ppm)

2.21

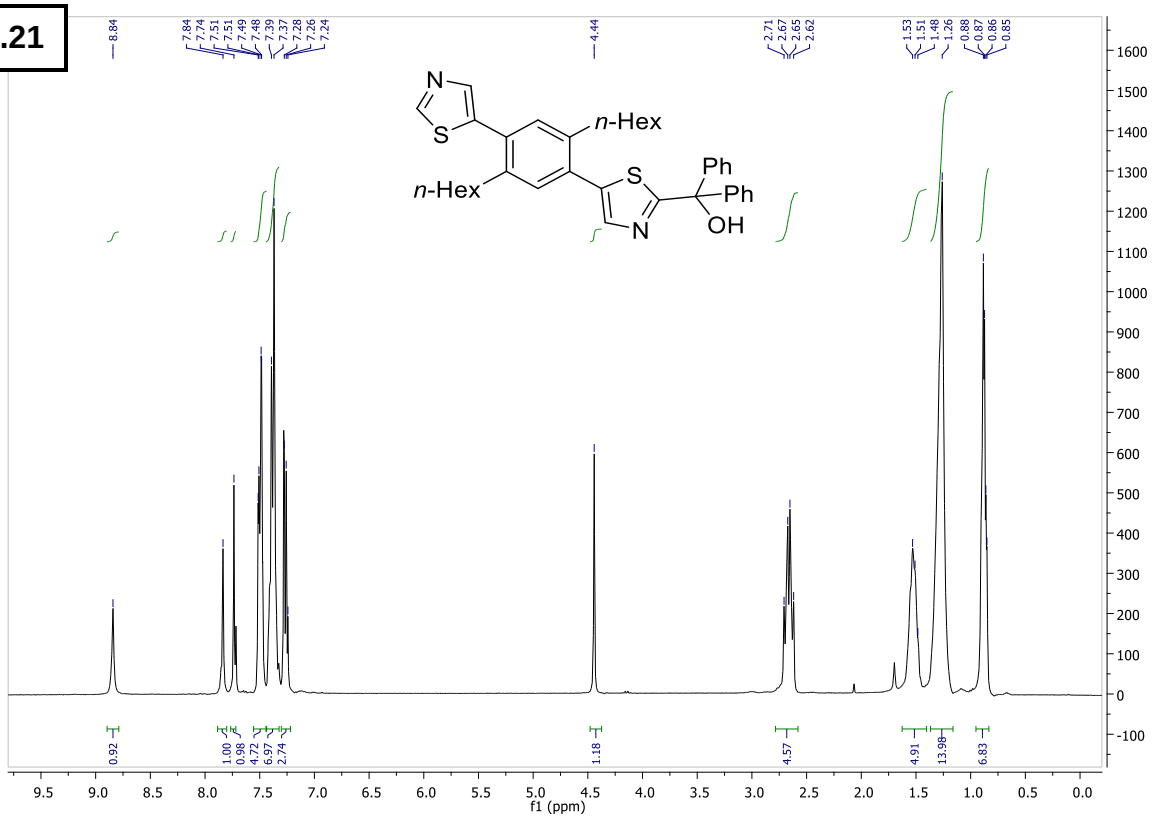
8.84
7.84
7.74
7.51
7.51
7.49
7.48
7.39
7.37
7.28
7.26
7.24
4.44
2.71
2.67
2.65
2.62
1.53
1.51
1.48
1.26
0.88
0.87
0.86
0.85
N
S
n-Hex
n-Hex
S
Ph
Ph
OH
N
0.92
1.00
0.98
4.72
6.97
2.74
1.18
4.57
4.91
13.98
6.83
f1 (ppm)

2.22

a/b

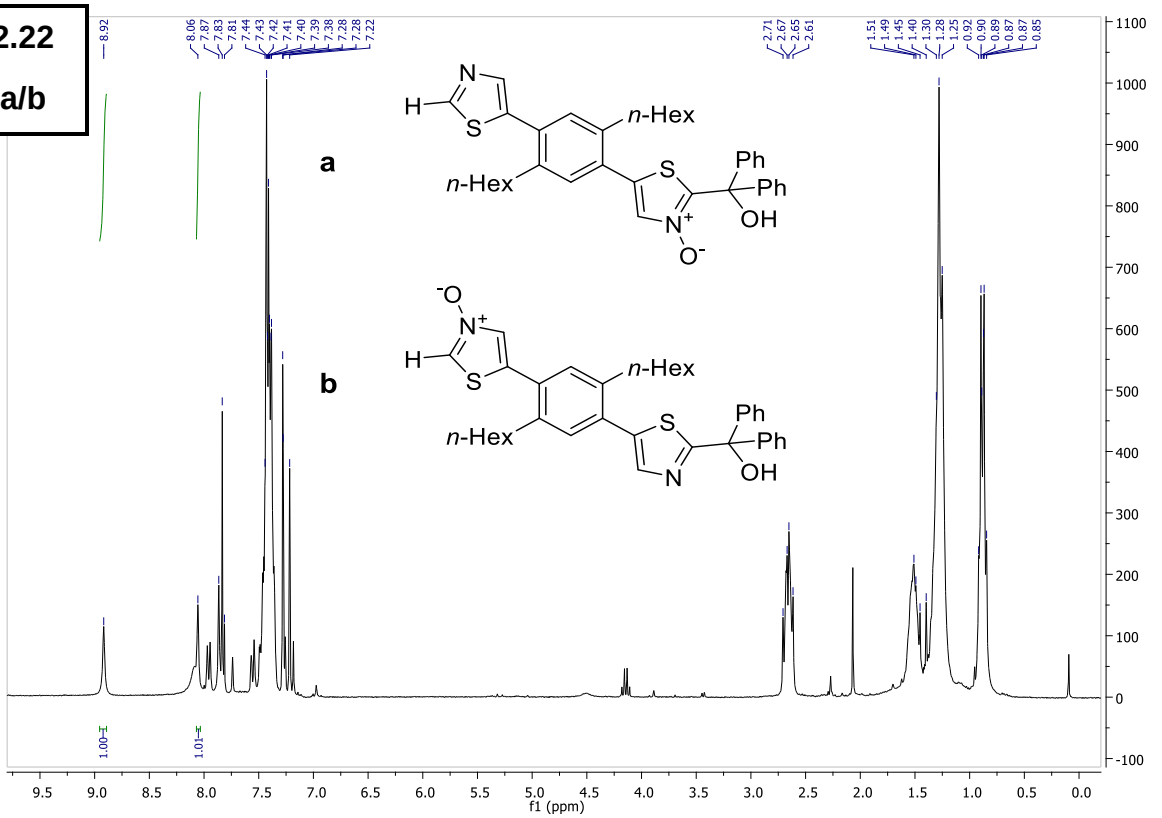

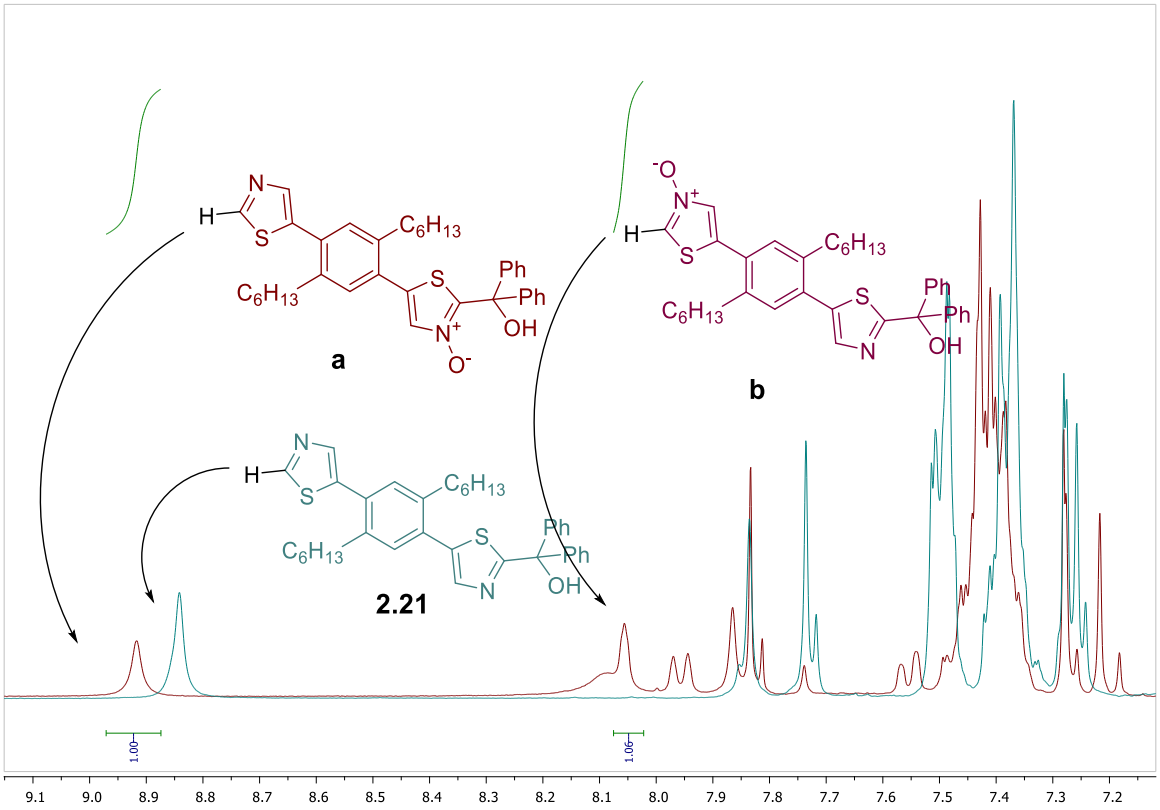

2.23

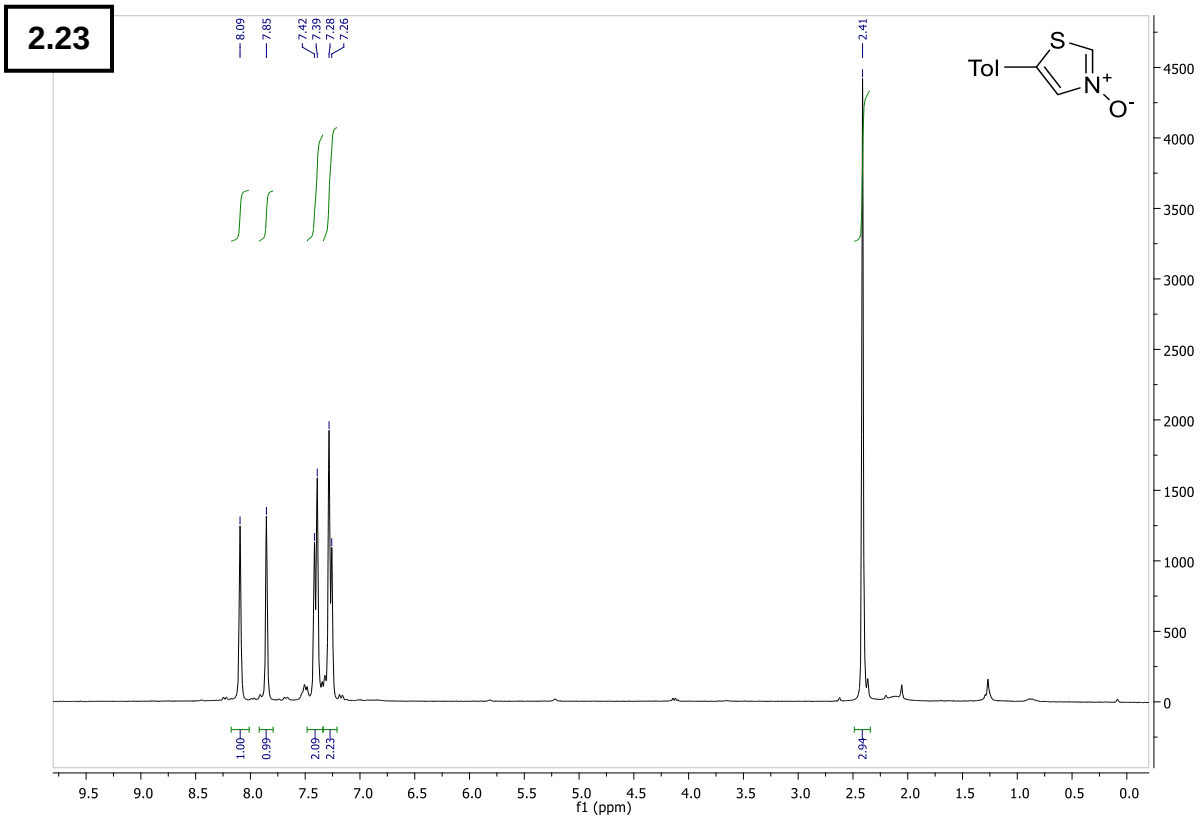

2.24

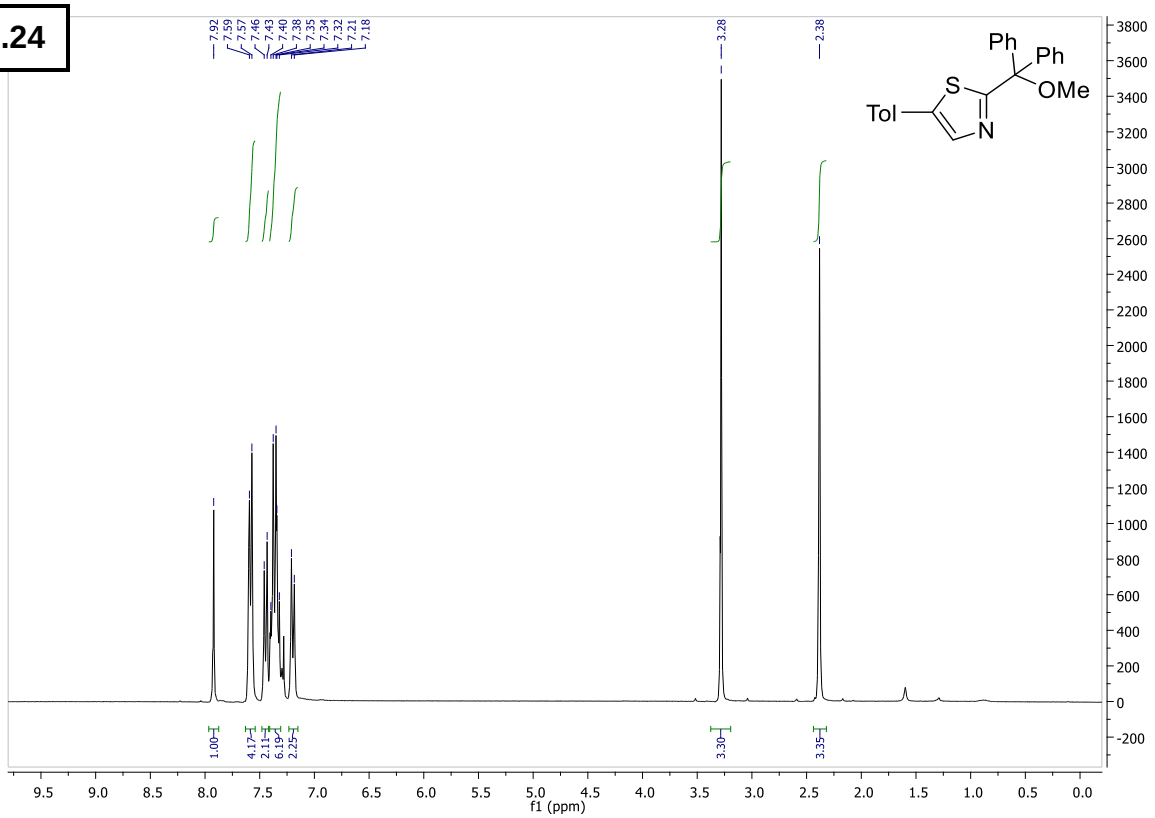
7.92
7.59
7.57
7.46
7.43
7.40
7.38
7.35
7.34
7.32
7.21
7.18
3.28
2.38
Ph
Ph
OMe
S
N
Tol
1.00
4.17
2.11
6.19
2.25
3.30
3.35
f1 (ppm)

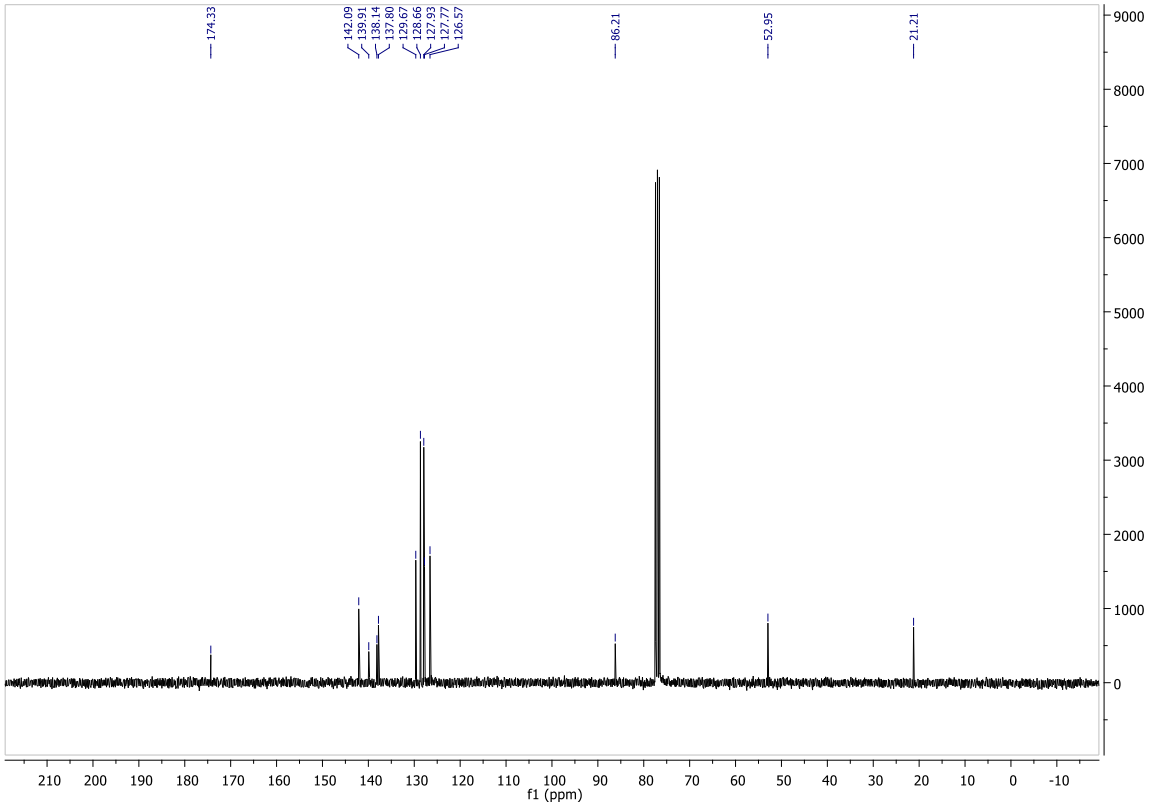
174.33
142.09
139.91
138.14
137.80
129.67
128.66
127.93
127.77
126.57
86.21
52.95
21.21
f1 (ppm)

2.25

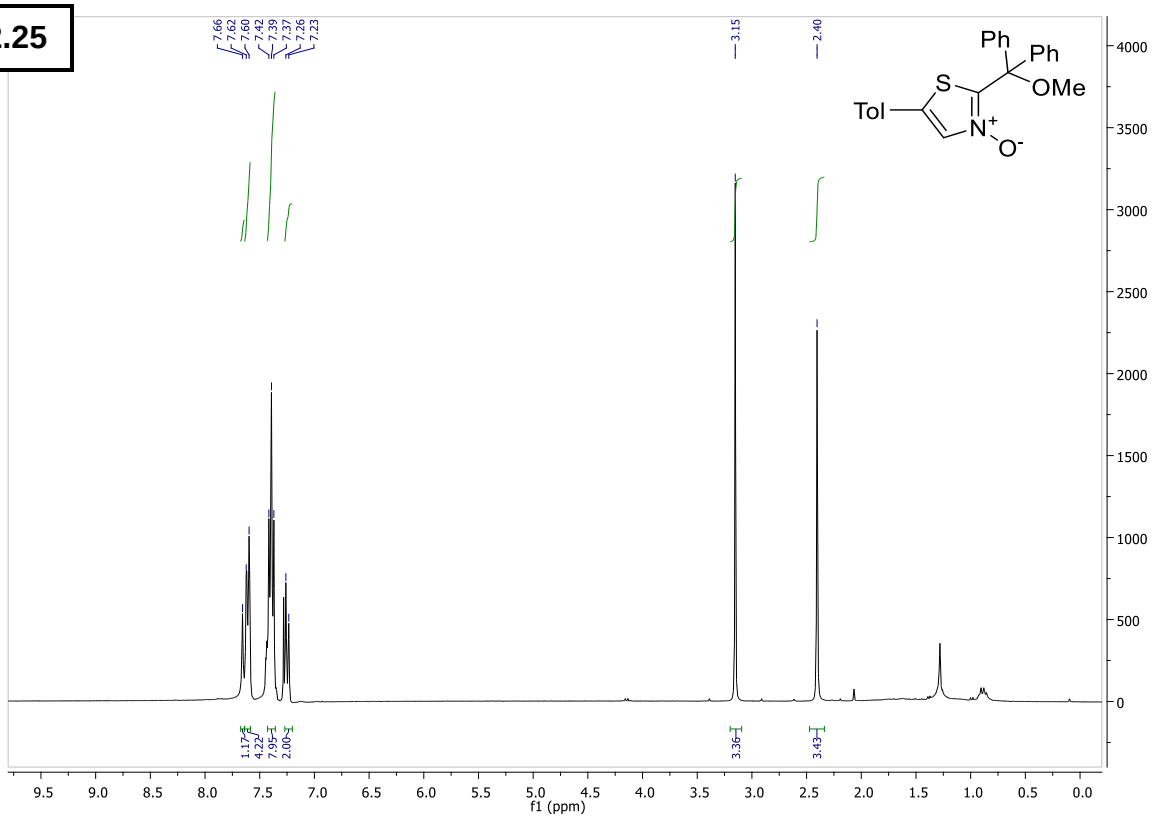
7.66
7.62
7.60
7.42
7.39
7.37
7.26
7.23
3.15
2.40
Ph
Ph
OMe
S
Tol
N+
O-
1.17
4.22
7.95
2.00
3.36
3.43
f1 (ppm)

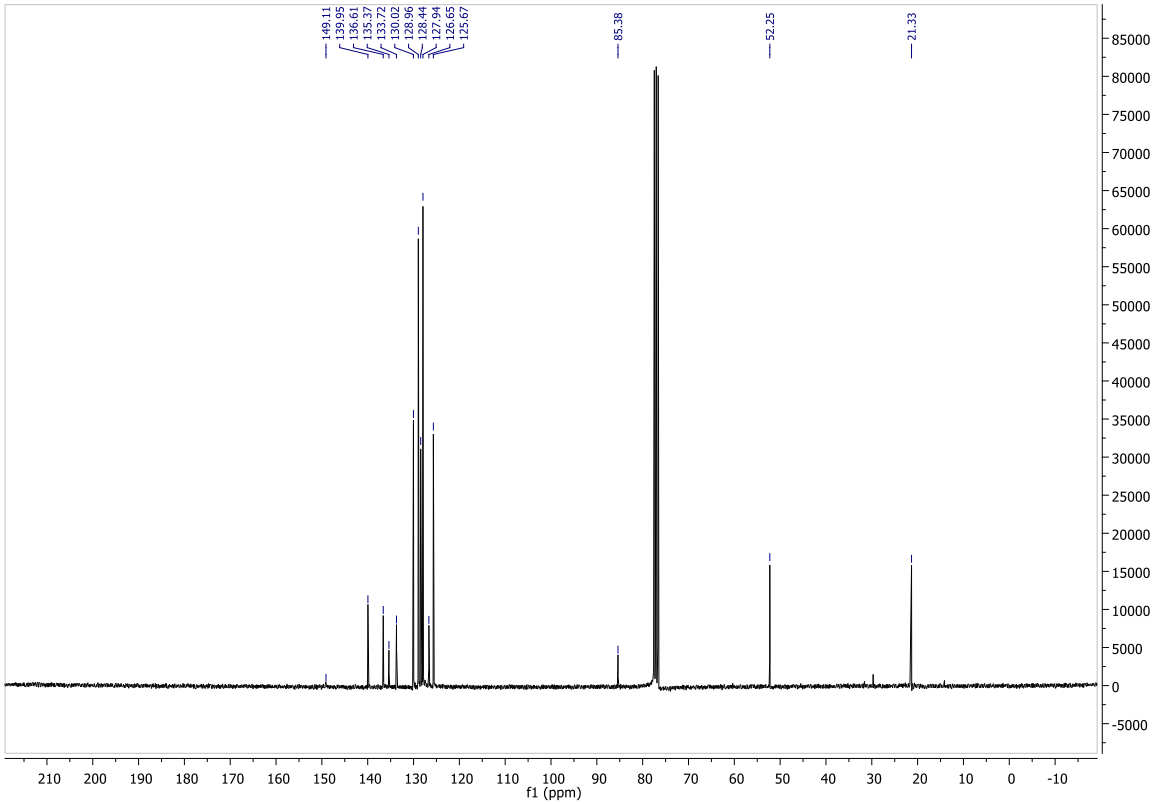
149.11
139.95
136.61
135.37
133.72
130.02
128.96
128.44
127.94
126.65
125.67
85.38
52.25
21.33
f1 (ppm)

2.26a

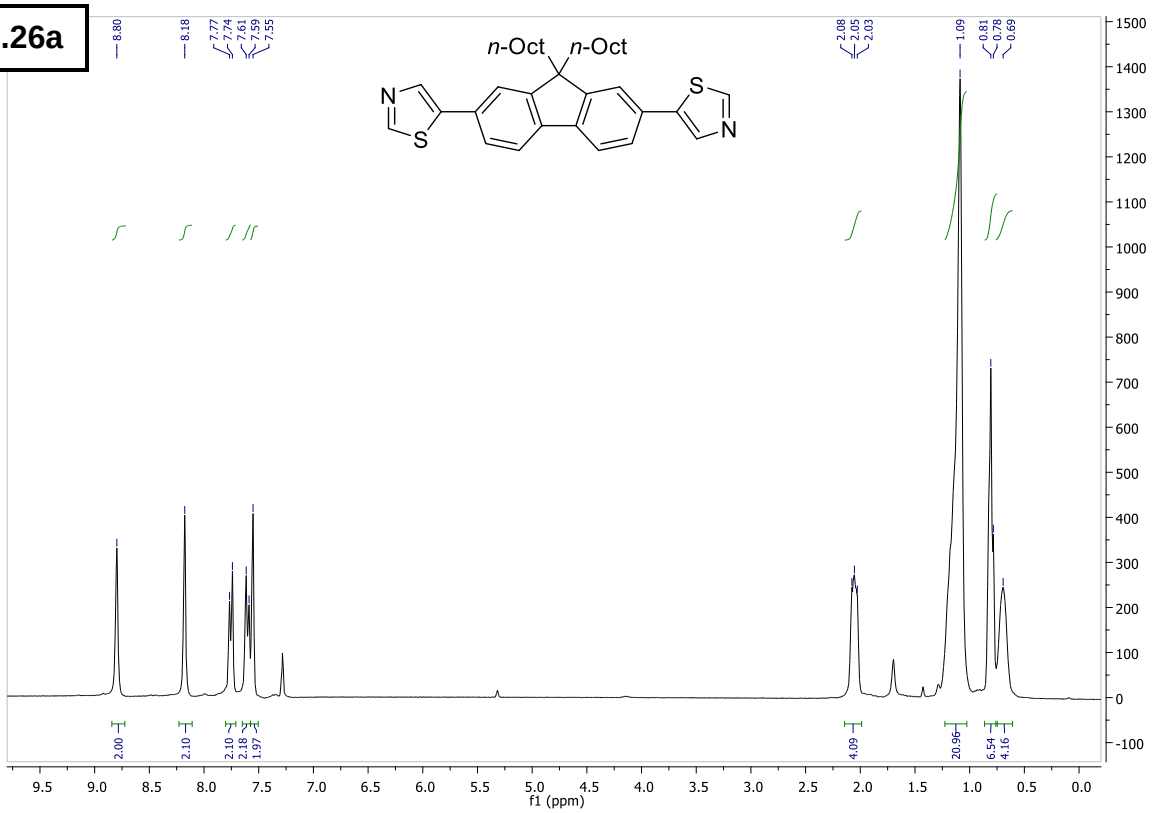
n-Oct
n-Oct
N
S
S
N
8.80
8.18
7.77
7.74
7.61
7.59
7.55
2.08
2.05
2.03
1.09
0.81
0.78
0.69
2.00
2.10
2.10
2.18
1.97
4.09
20.96
6.54
4.16
f1 (ppm)

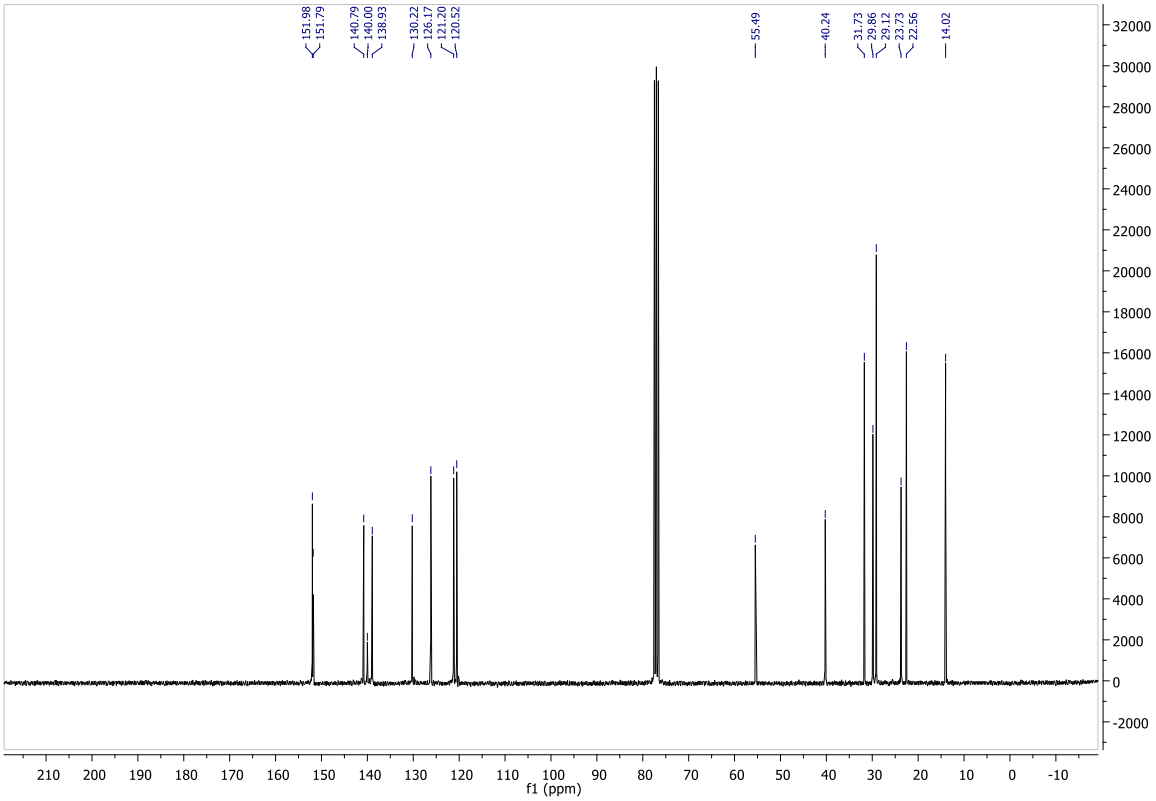
151.98
151.79
140.79
140.00
138.93
130.22
126.17
121.20
120.52
55.49
40.24
31.73
29.86
29.12
23.73
22.56
14.02
f1 (ppm)

2.26b

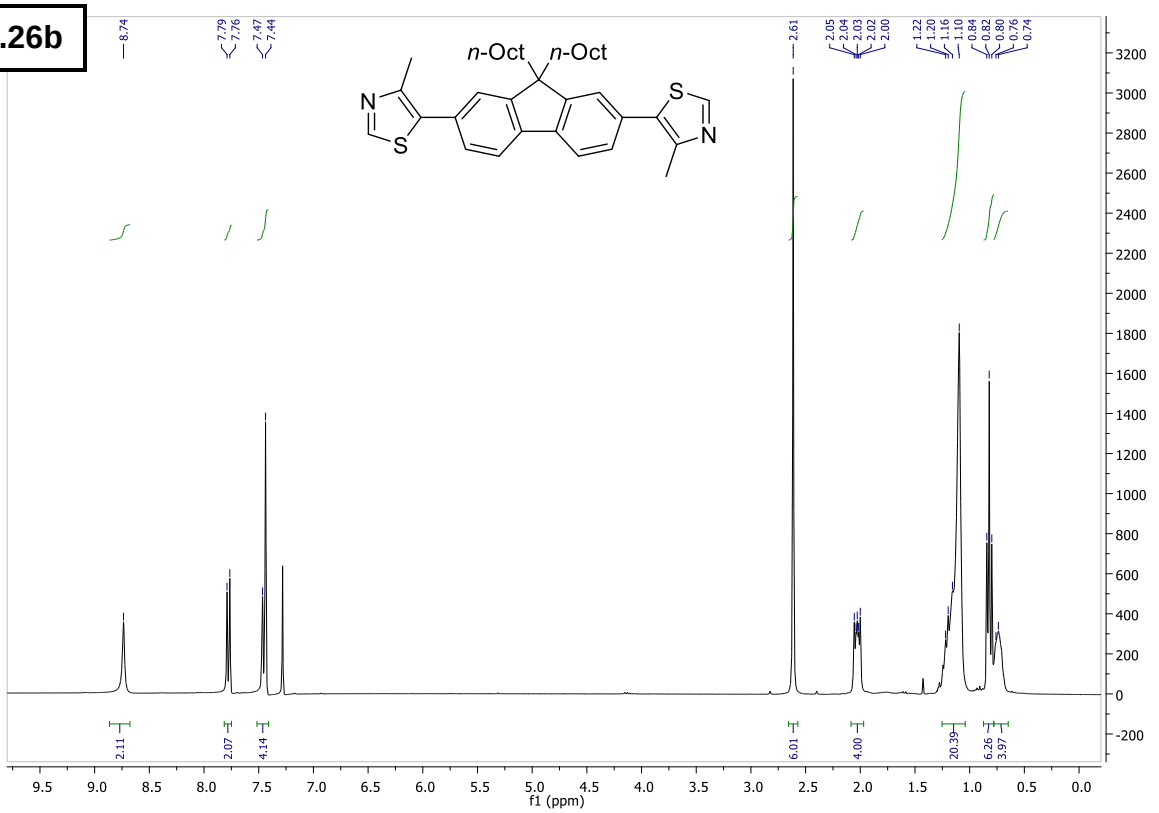
8.74
7.79
7.76
7.47
7.44
2.61
2.05
2.04
2.03
2.02
2.00
1.22
1.20
1.16
1.10
0.84
0.82
0.80
0.76
0.74
n-Oct
n-Oct
N
S
S
N
2.11
2.07
4.14
6.01
4.00
20.39
6.26
3.97
f1 (ppm)

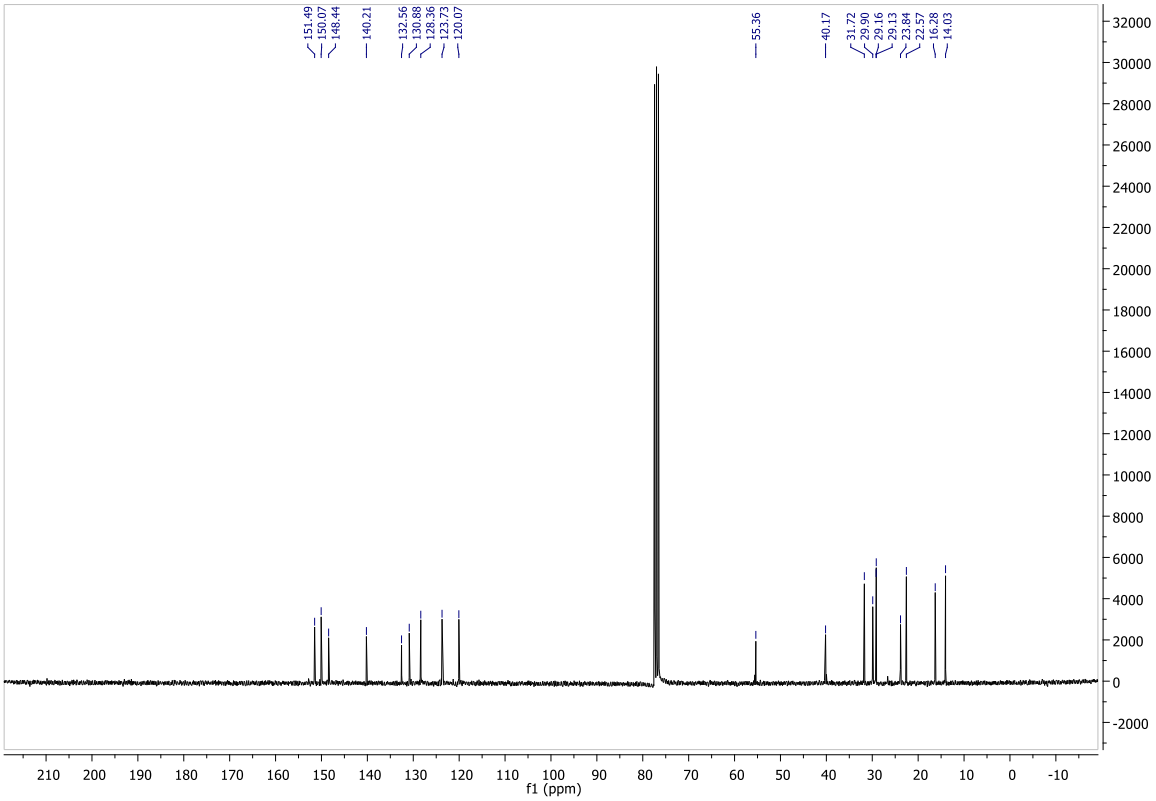
151.49
150.07
148.44
140.21
132.56
130.88
128.36
123.73
120.07
55.36
40.17
31.72
29.90
29.16
29.13
23.84
22.57
16.28
14.03
f1 (ppm)

2.26c

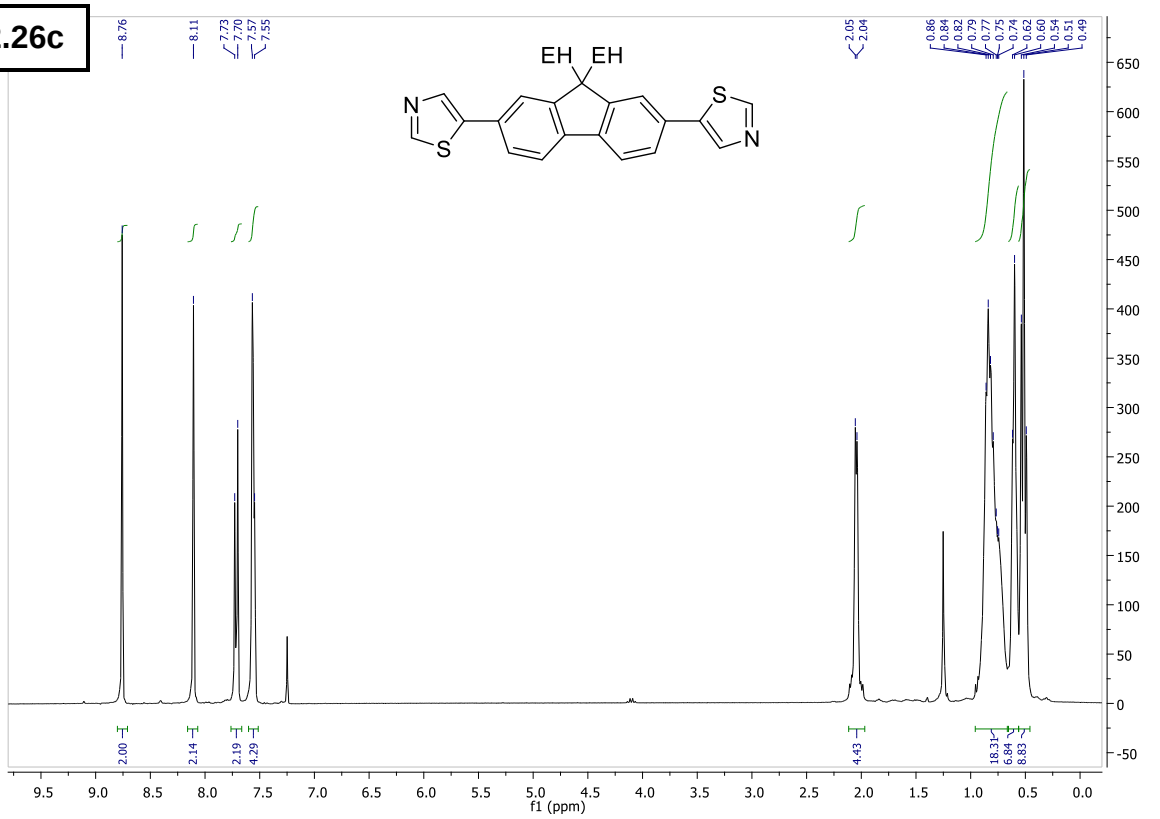
8.76
8.11
7.73
7.70
7.57
7.55
2.05
2.04
0.86
0.84
0.82
0.79
0.77
0.75
0.74
0.62
0.60
0.54
0.51
0.49
EH EH
N
S
S
N
2.00
2.14
2.19
4.29
4.43
18.31
6.84
8.83
f1 (ppm)

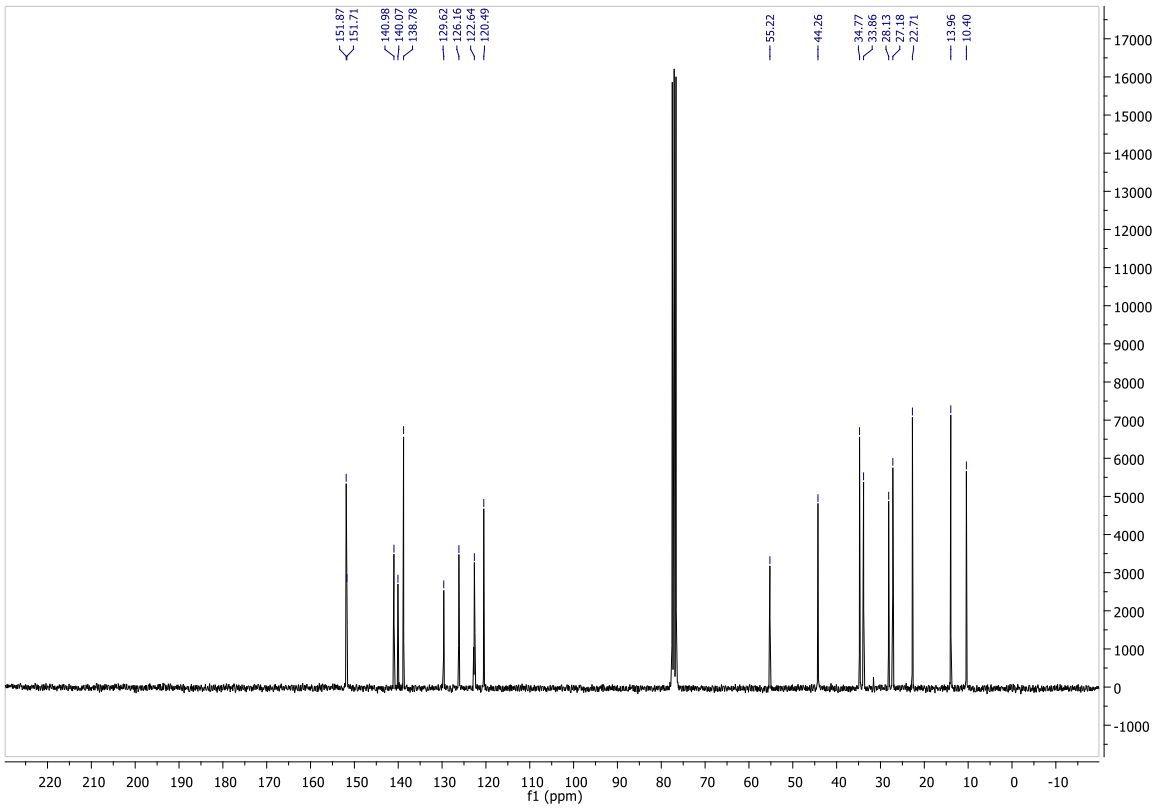
151.87
151.71
140.98
140.07
138.78
129.62
126.16
122.64
120.49
55.22
44.26
34.77
33.86
28.13
27.18
22.71
13.96
10.40
f1 (ppm)

2.26d

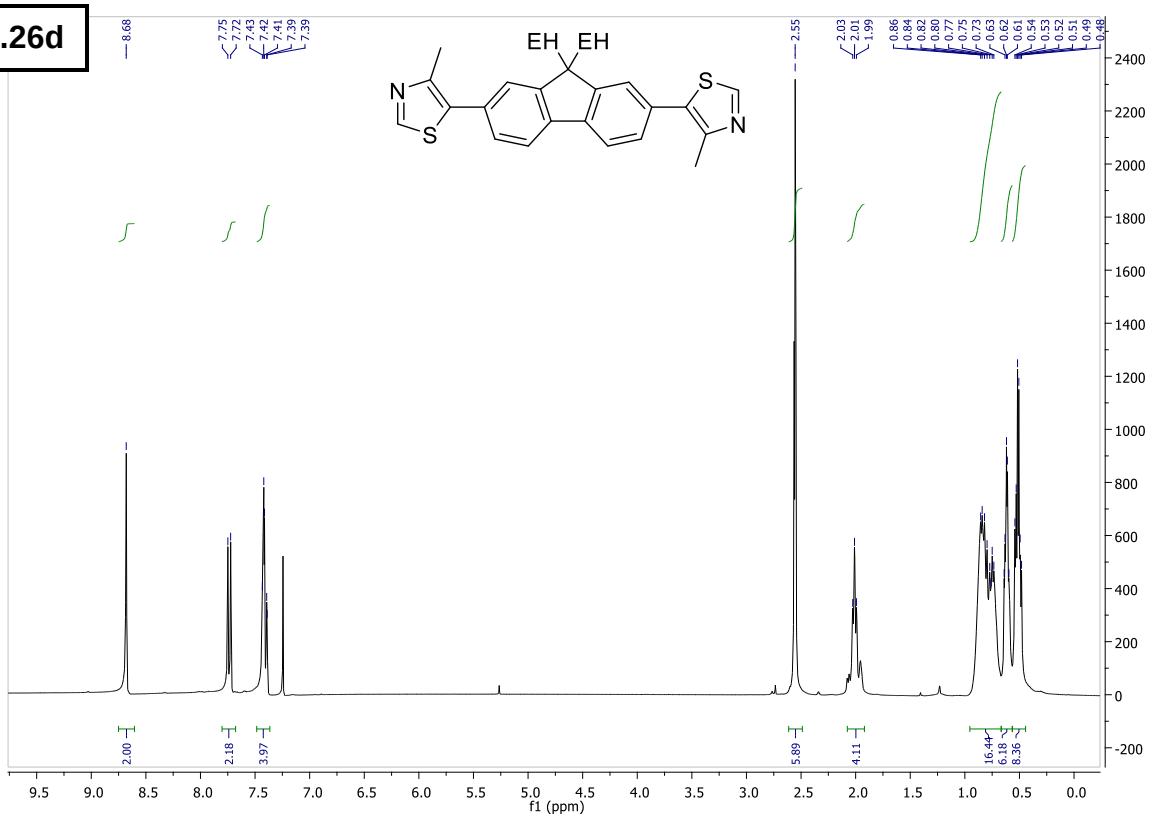
8.68
7.75
7.72
7.43
7.42
7.41
7.39
7.39
EH EH
N
S
S
N
2.55
2.03
2.01
1.99
0.86
0.84
0.82
0.80
0.77
0.75
0.73
0.63
0.62
0.61
0.54
0.53
0.52
0.51
0.49
0.48
2.00
2.18
3.97
5.89
4.11
16.44
6.18
8.36
f1 (ppm)

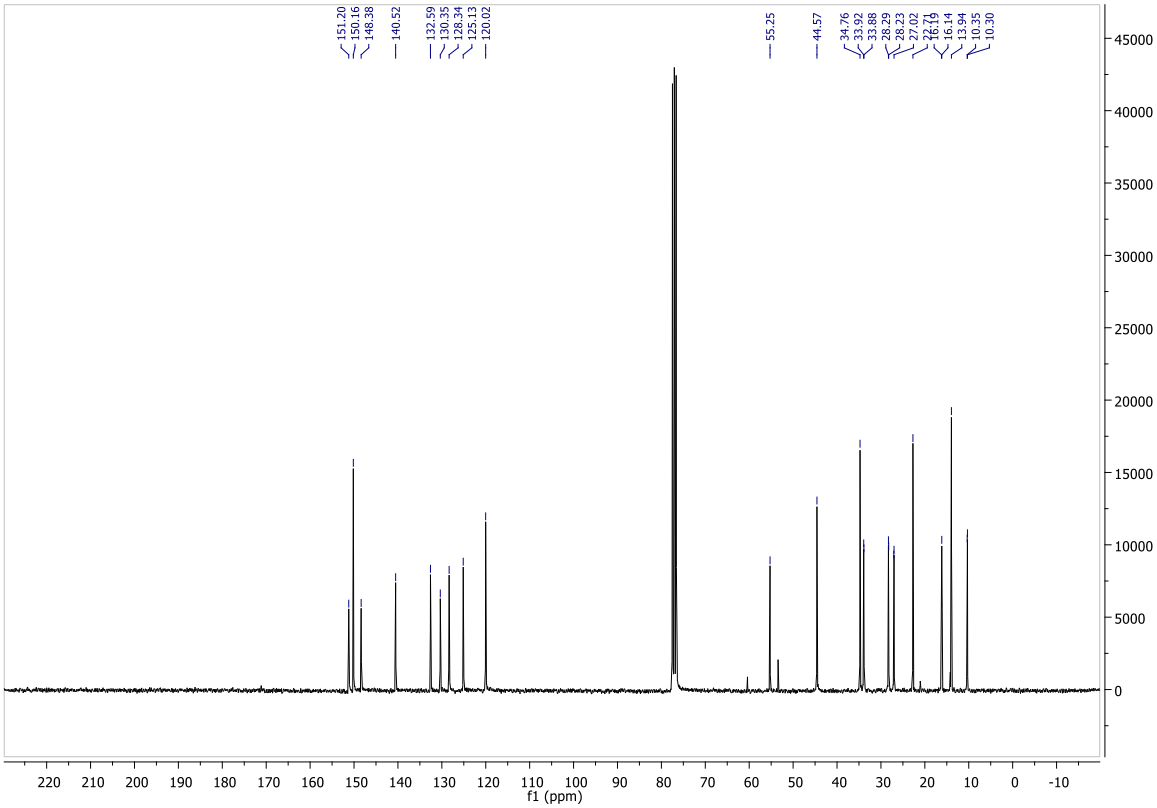
151.20
150.16
148.38
140.52
132.59
130.35
128.34
125.13
120.02
55.25
44.57
34.76
33.92
33.88
28.29
28.23
27.02
16.14
13.94
10.35
10.30
f1 (ppm)

2.26e

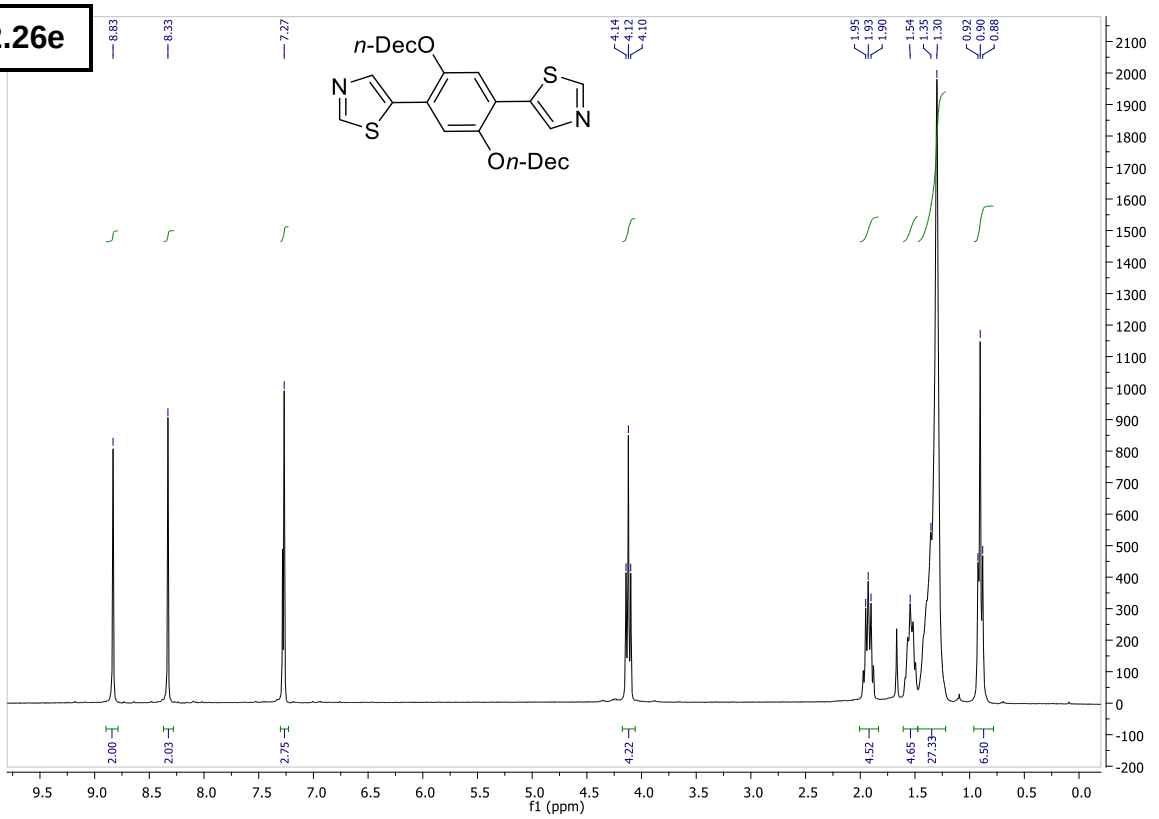
8.83
8.33
7.27
4.14
4.12
4.10
1.95
1.93
1.90
1.54
1.35
1.30
0.92
0.90
0.88
n-DecO
On-Dec
N
S
S
N
2.00
2.03
2.75
4.22
4.52
4.65
27.33
6.50
f1 (ppm)

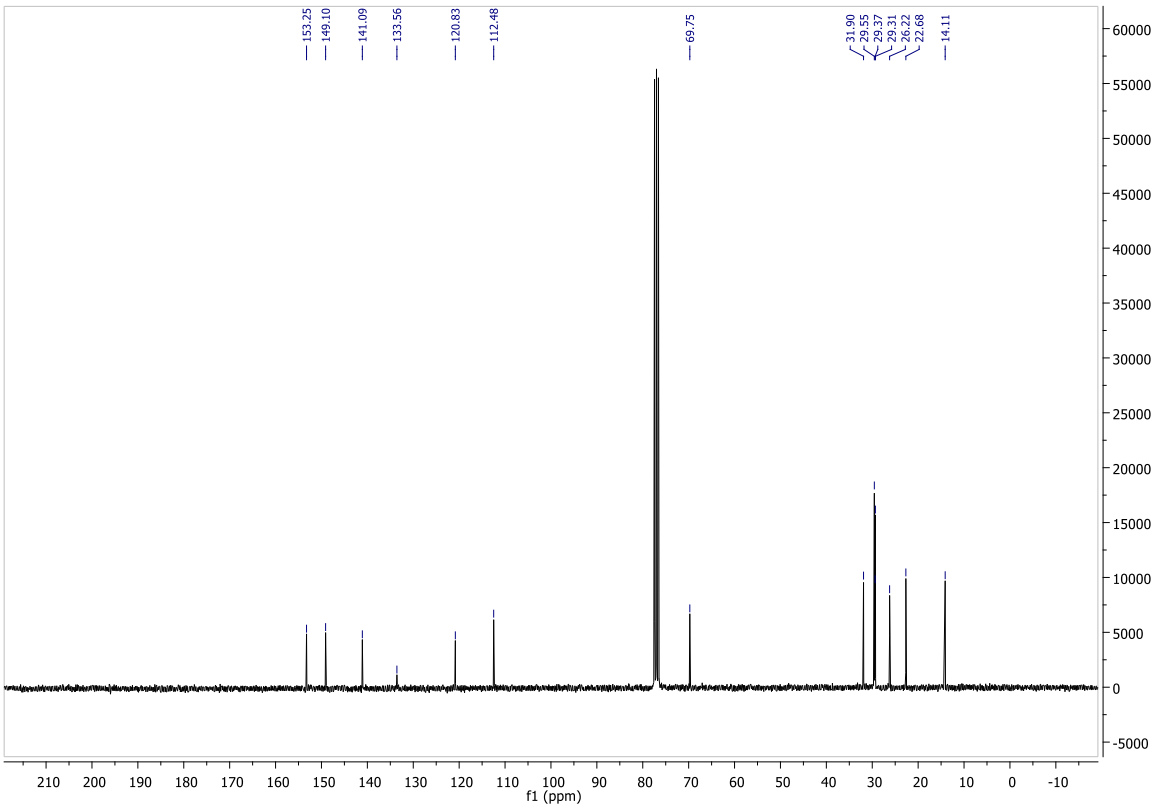
153.25
149.10
141.09
133.56
120.83
112.48
69.75
31.90
29.55
29.37
29.31
26.22
22.68
14.11
f1 (ppm)

2.26f

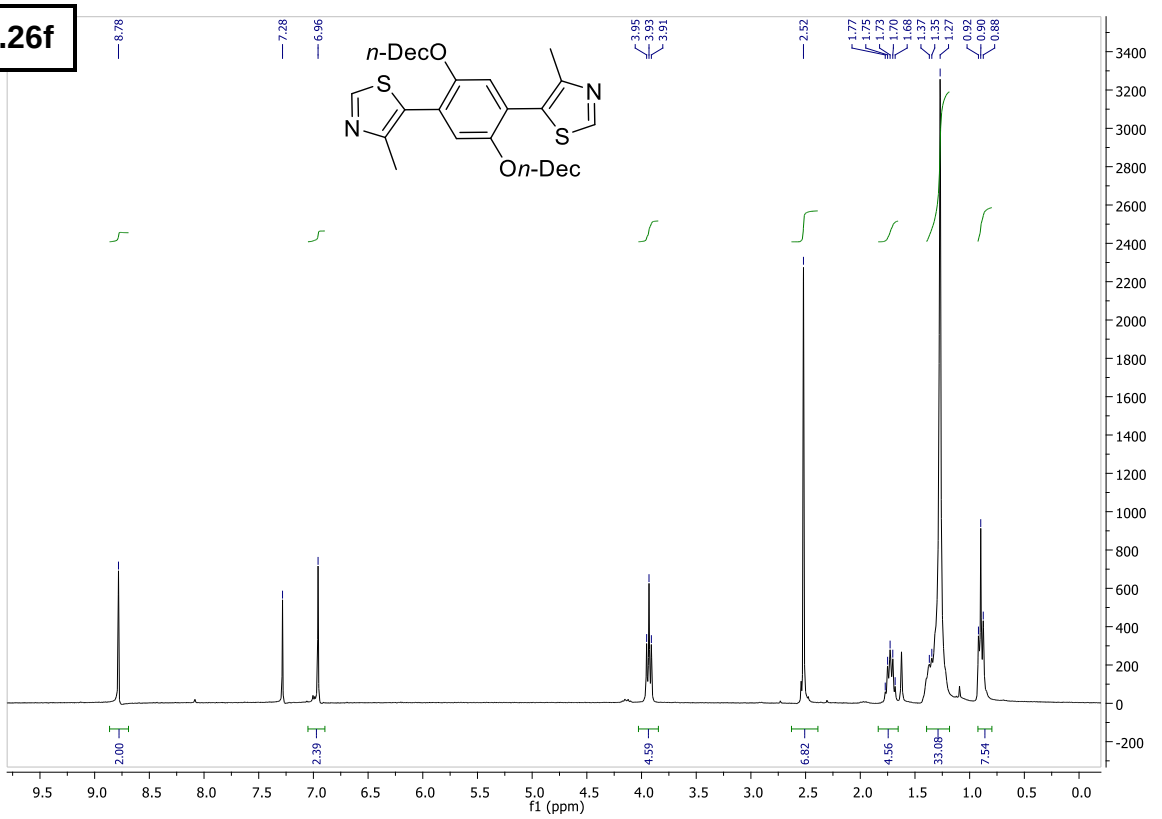
8.78
7.28
6.96
3.95
3.93
3.91
2.52
1.77
1.75
1.73
1.70
1.68
1.37
1.35
1.27
0.92
0.90
0.88
n-DecO
On-Dec
S
N
N
S
2.00
2.39
4.59
6.82
4.56
33.08
7.54
f1 (ppm)

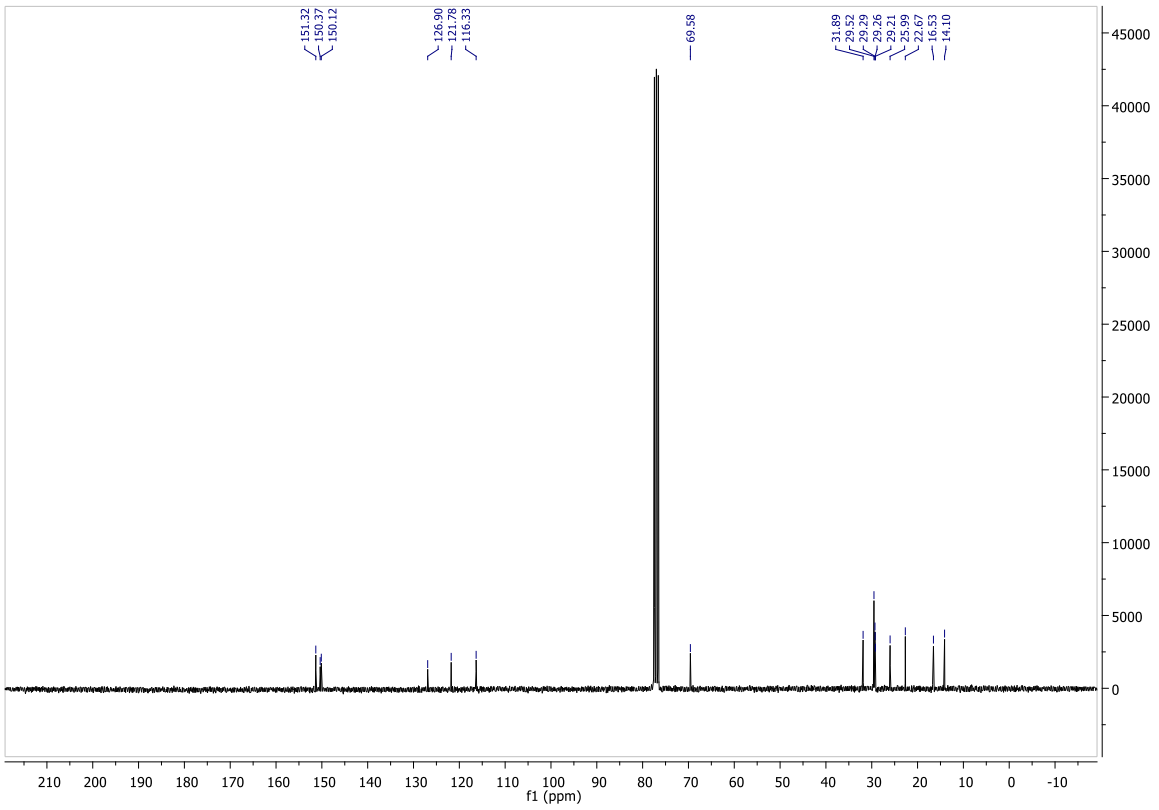
151.32
150.37
150.12
126.90
121.78
116.33
69.58
31.89
29.52
29.29
29.26
29.21
25.99
22.67
16.53
14.10
f1 (ppm)

2.26g

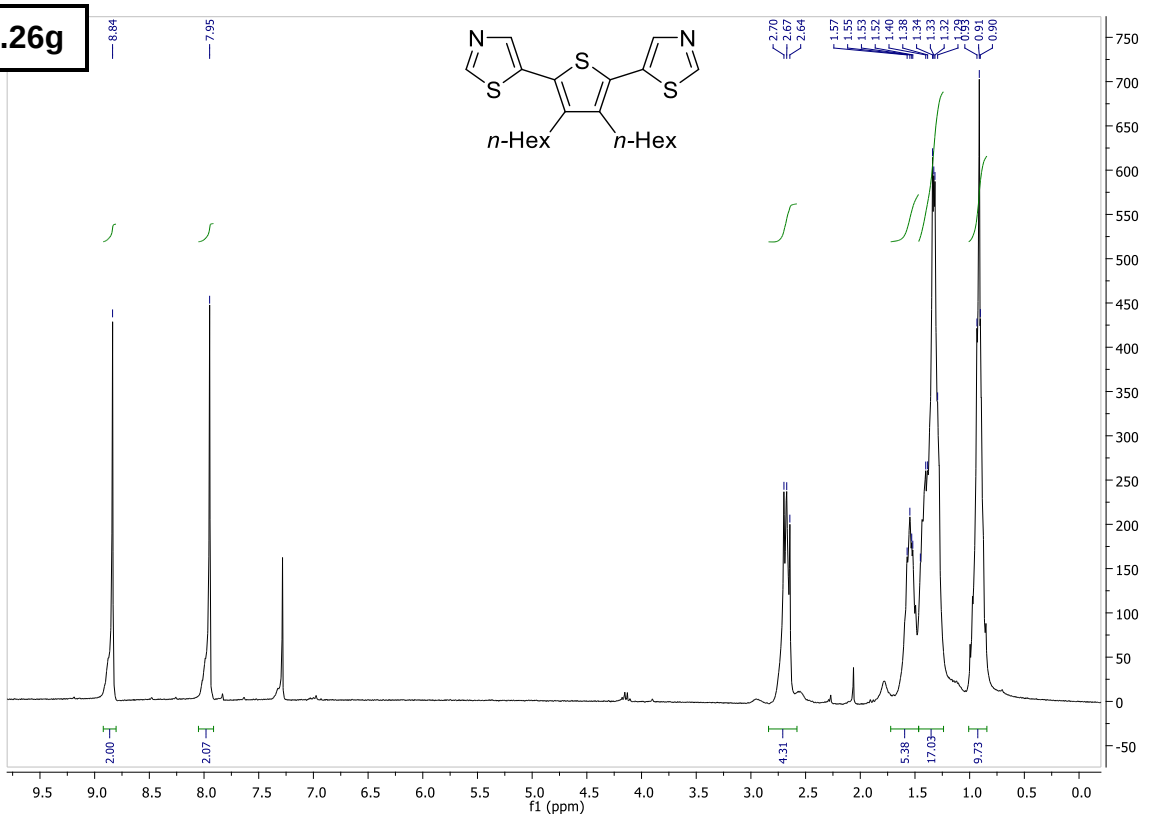
8.84
7.95
2.70
2.67
2.64
1.57
1.55
1.53
1.52
1.40
1.38
1.34
1.33
1.32
0.93
0.91
0.90
N
S
S
N
S
n-Hex
n-Hex
2.00
2.07
4.31
5.38
17.03
9.73
f1 (ppm)

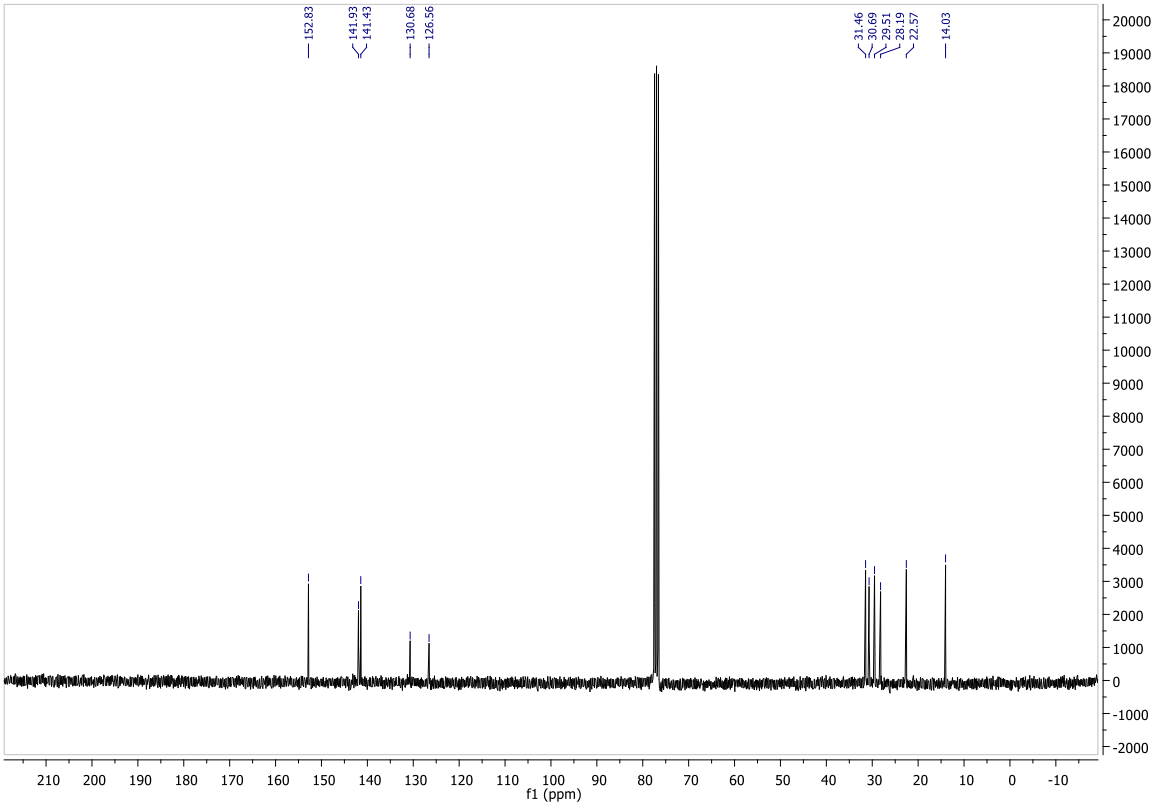
152.83
141.93
141.43
130.68
126.56
31.46
30.69
29.51
28.19
22.57
14.03
f1 (ppm)

2.26h

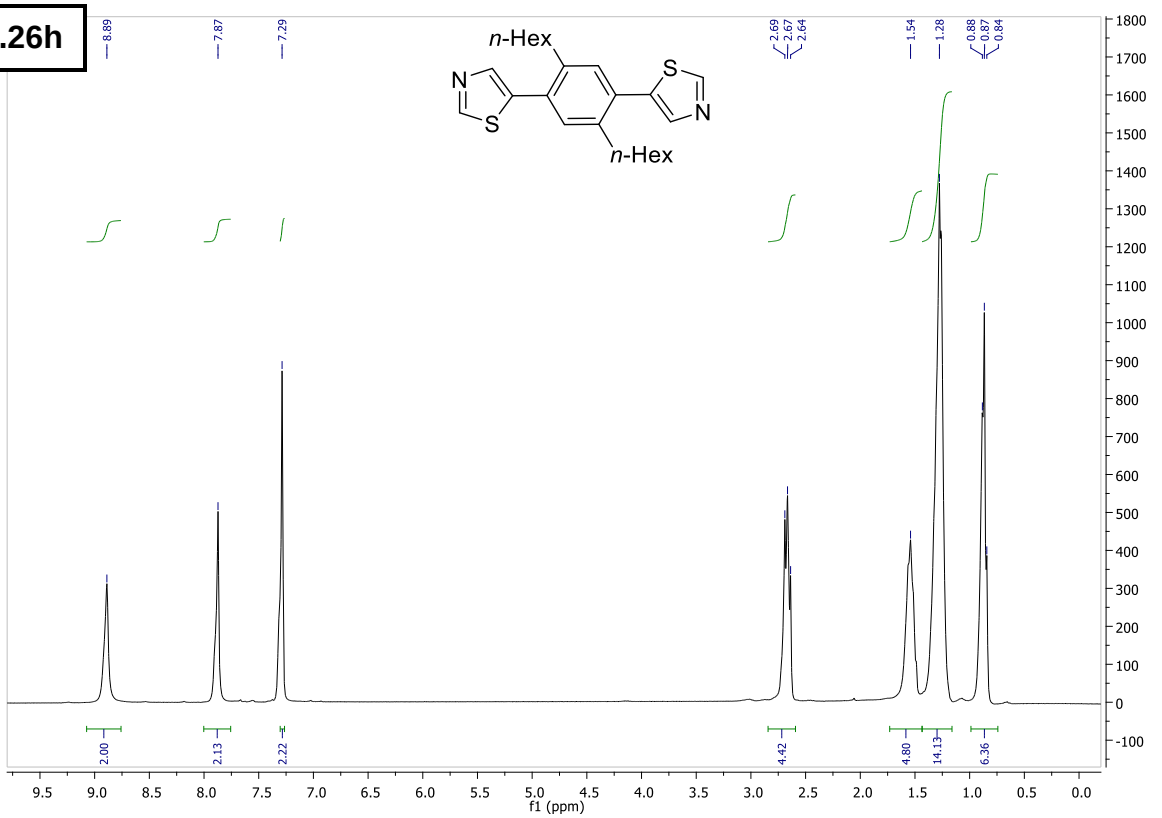
8.89
7.87
7.29
2.69
2.67
2.64
1.54
1.28
0.88
0.87
0.84
n-Hex
n-Hex
N
S
S
N
2.00
2.13
2.22
4.42
4.80
14.13
6.36
f1 (ppm)

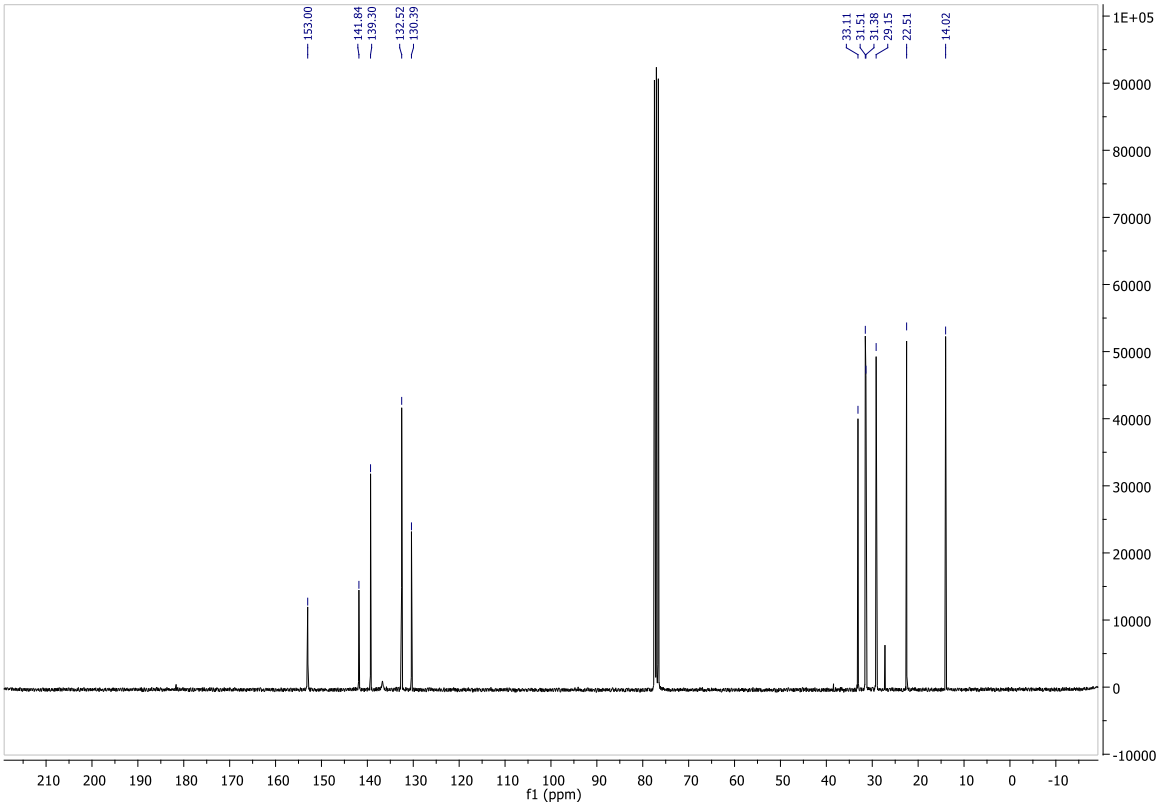
153.00
141.84
139.30
132.52
130.39
33.11
31.51
31.38
29.15
22.51
14.02
f1 (ppm)

2.27a

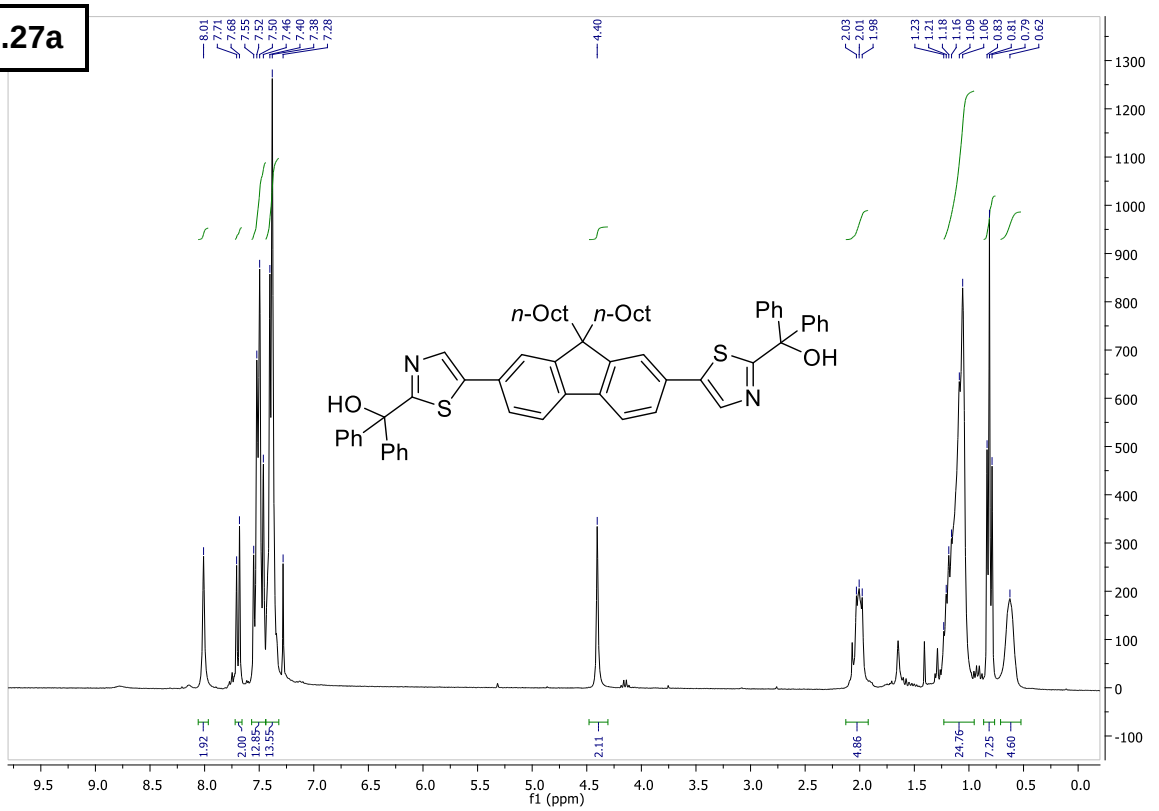
8.01
7.71
7.68
7.55
7.52
7.50
7.46
7.40
7.38
7.28
4.40
2.03
2.01
1.98
1.23
1.21
1.18
1.16
1.09
1.06
0.83
0.81
0.79
0.62
n-Oct
n-Oct
Ph
Ph
OH
S
N
HO
Ph
Ph
1.92
2.00
12.85
13.55
2.11
4.86
24.76
7.25
4.60
f1 (ppm)

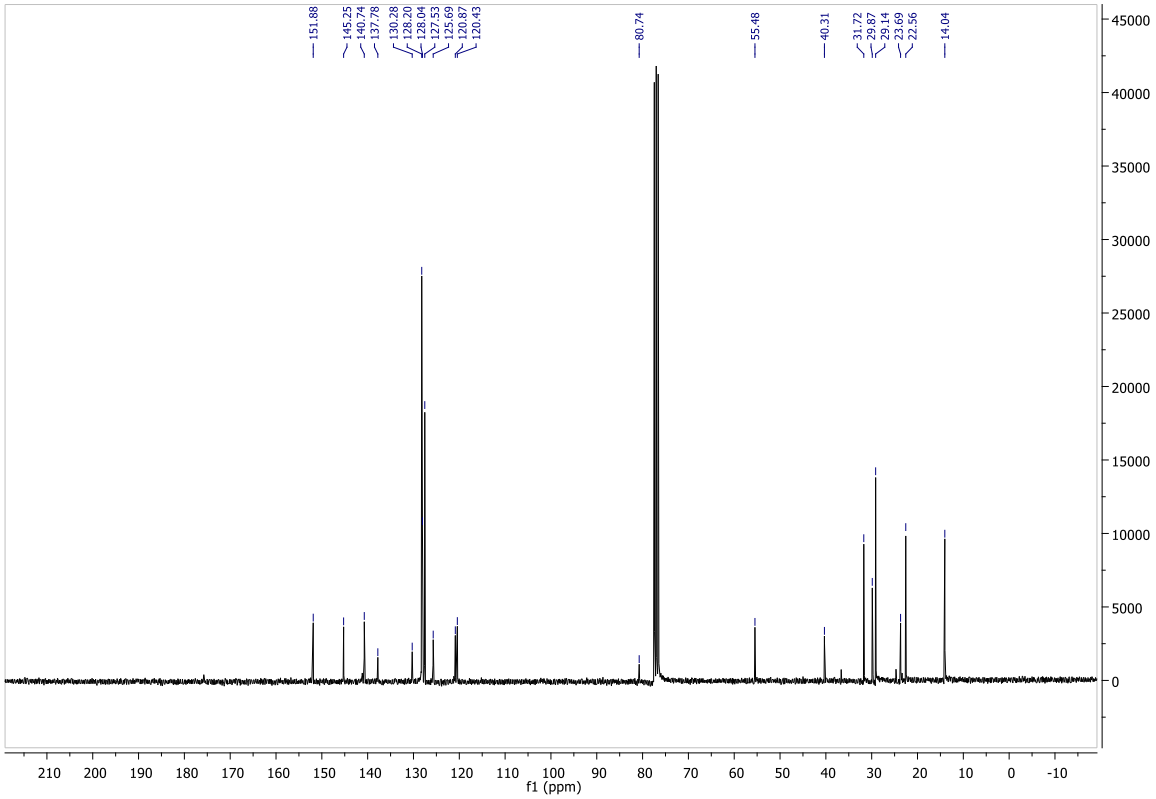
151.88
145.25
140.74
137.78
130.28
128.20
128.04
127.53
125.69
120.87
120.43
80.74
55.48
40.31
31.72
29.87
29.14
23.69
22.56
14.04
f1 (ppm)

2.27b

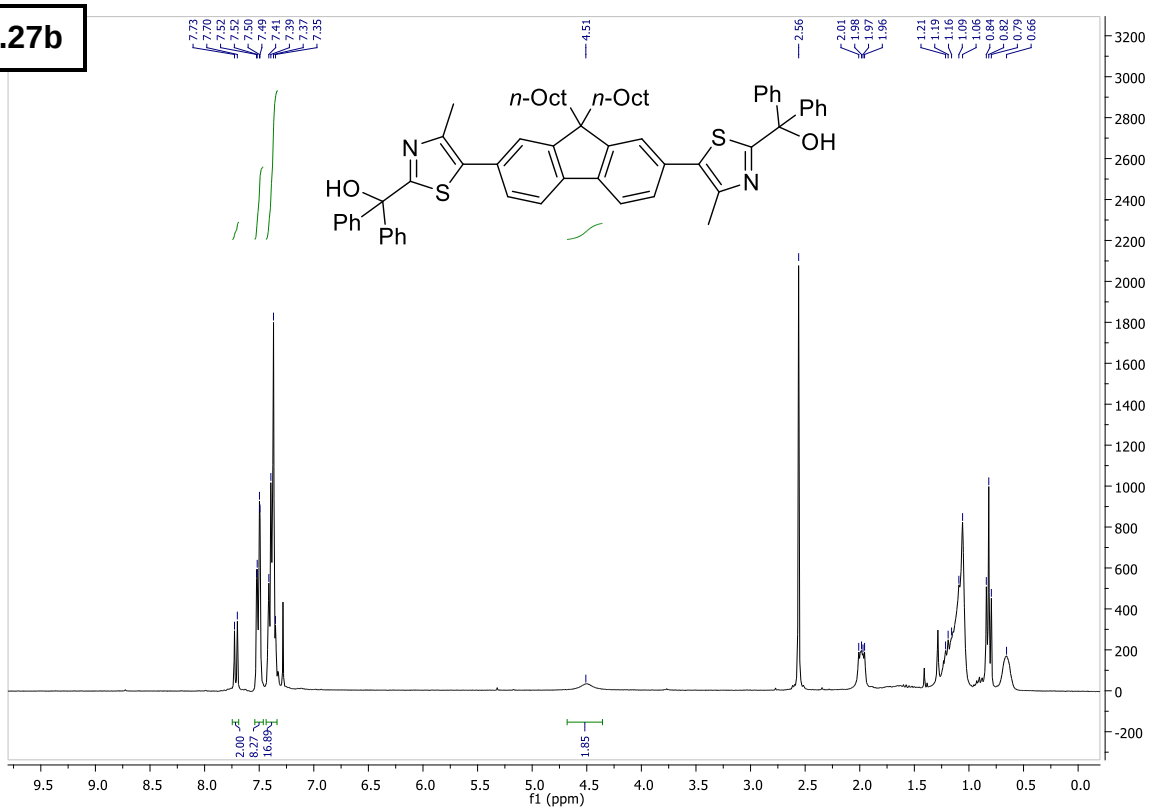
7.73
7.70
7.52
7.52
7.50
7.49
7.41
7.39
7.37
7.35
4.51
2.56
2.01
1.98
1.97
1.96
1.21
1.19
1.16
1.09
1.06
0.84
0.82
0.79
0.66
n-Oct
n-Oct
Ph
Ph
OH
S
N
HO
Ph
Ph
2.00
8.27
16.89
1.85
f1 (ppm)

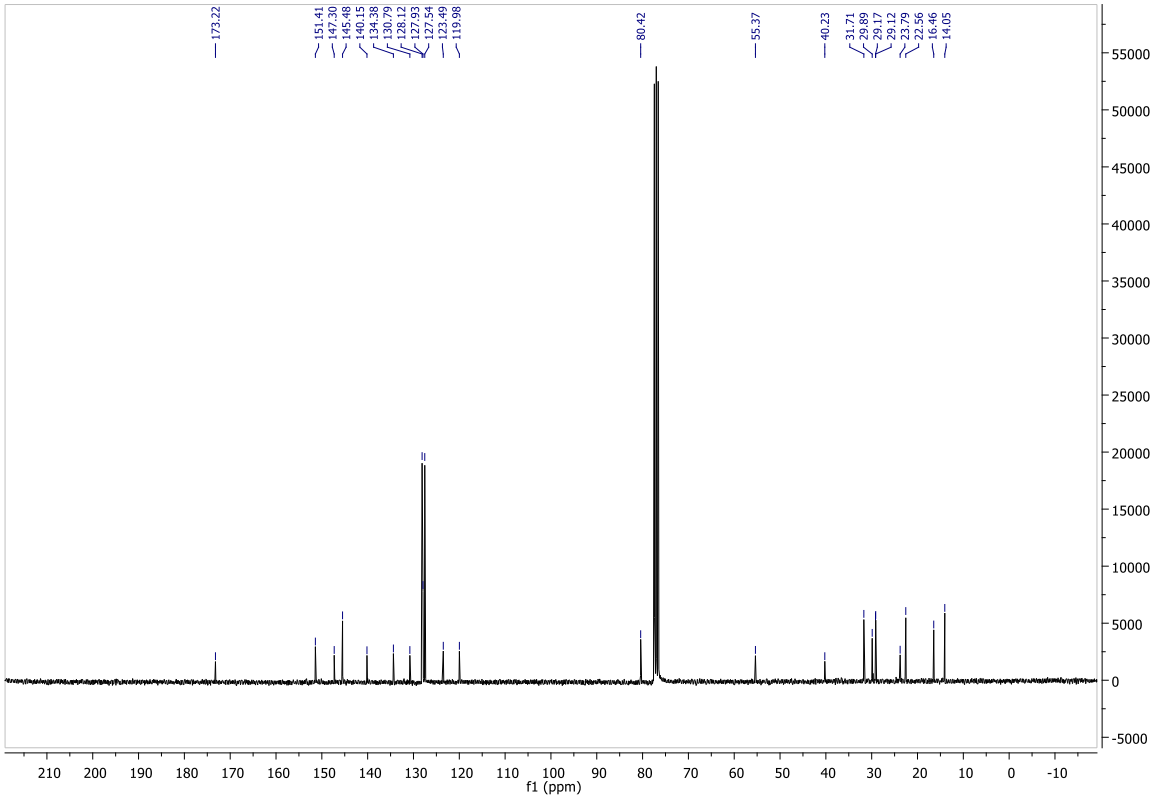
173.22
151.41
147.30
145.48
140.15
134.38
130.79
128.12
127.93
127.54
123.49
119.98
80.42
55.37
40.23
31.71
29.89
29.17
29.12
23.79
22.56
16.46
14.05
f1 (ppm)

2.27c

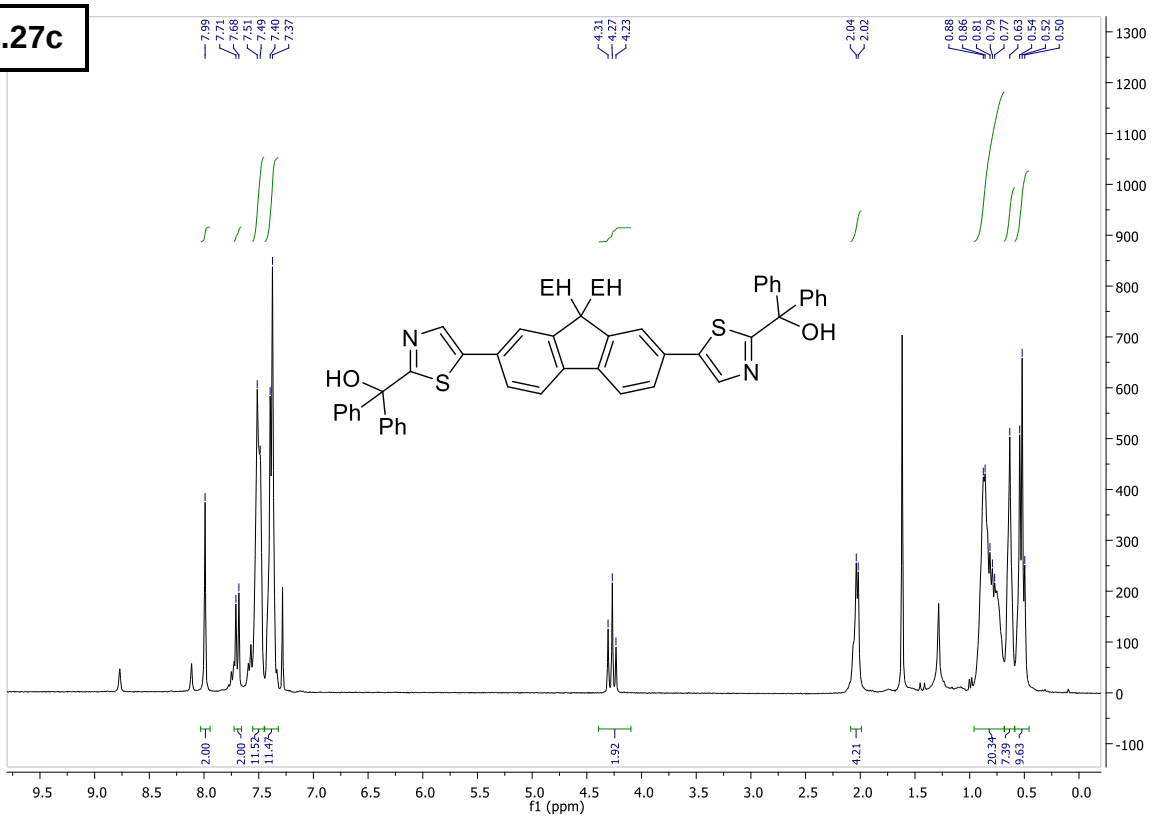
7.99
7.71
7.68
7.51
7.49
7.40
7.37
4.31
4.27
4.23
2.04
2.02
0.88
0.86
0.81
0.79
0.77
0.63
0.54
0.52
0.50
EH EH
Ph Ph
OH
HO
Ph Ph
N
S
S
N
2.00
2.00
11.52
11.47
1.92
4.21
20.34
7.39
9.63
f1 (ppm)

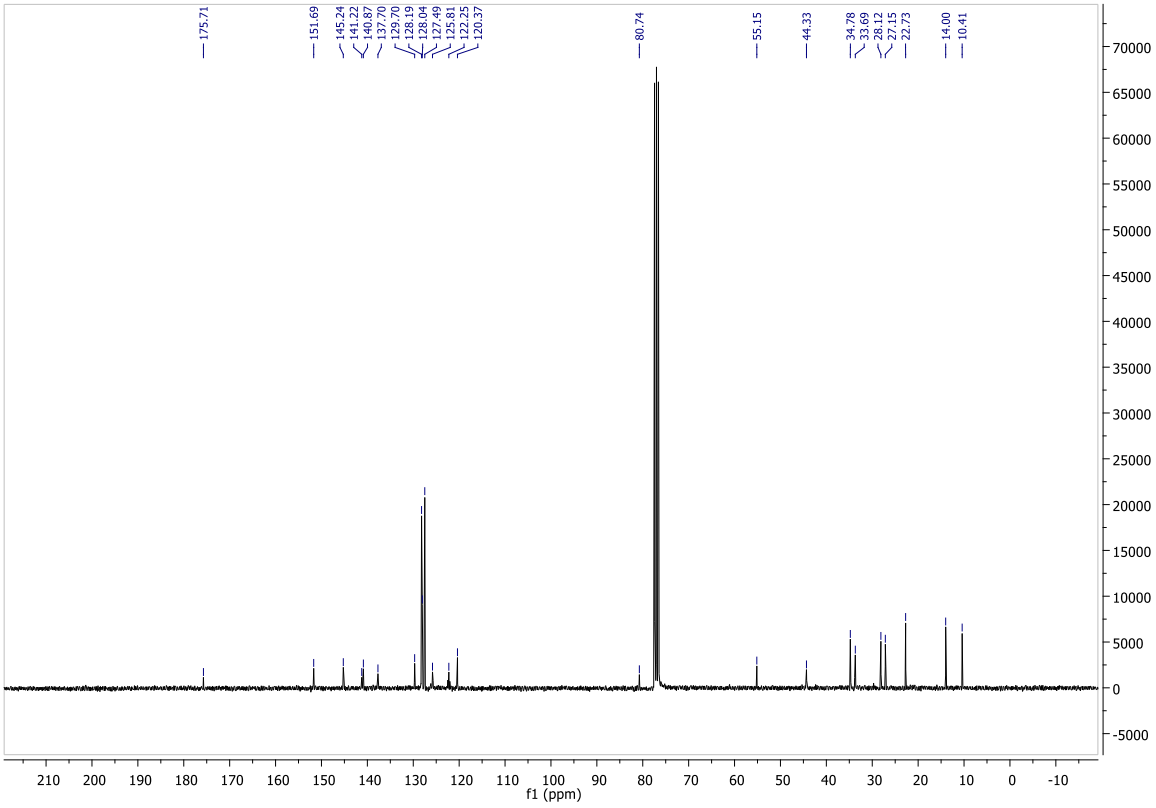
175.71
151.69
145.24
141.22
140.87
137.70
129.70
128.19
128.04
127.49
123.81
122.25
120.37
80.74
55.15
44.33
34.78
33.69
28.12
27.15
22.73
14.00
10.41
f1 (ppm)

2.27d

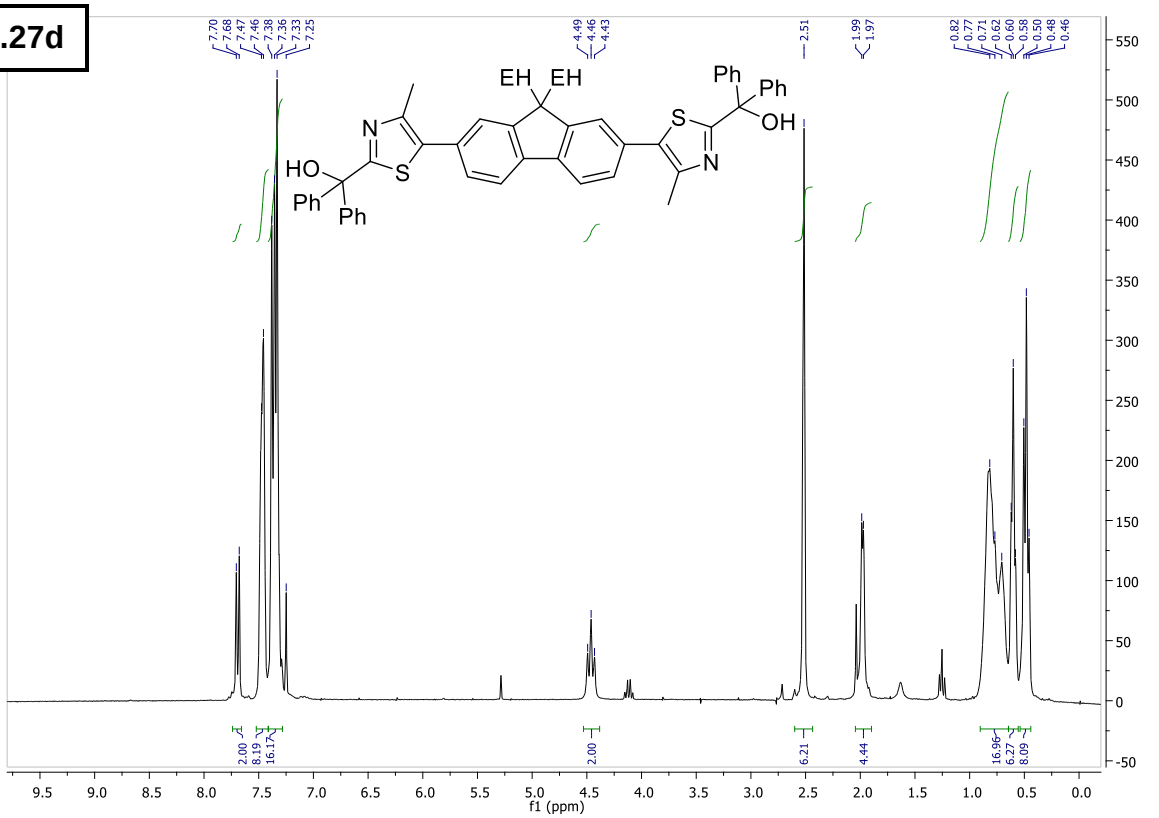
7.70
7.68
7.47
7.46
7.38
7.36
7.33
7.25
4.49
4.46
4.43
2.51
1.99
1.97
0.82
0.77
0.71
0.62
0.60
0.58
0.50
0.48
0.46
EH EH
Ph Ph
OH
N
S
HO
Ph Ph
2.00
8.19
16.17
2.00
6.21
4.44
16.96
6.27
8.09
f1 (ppm)

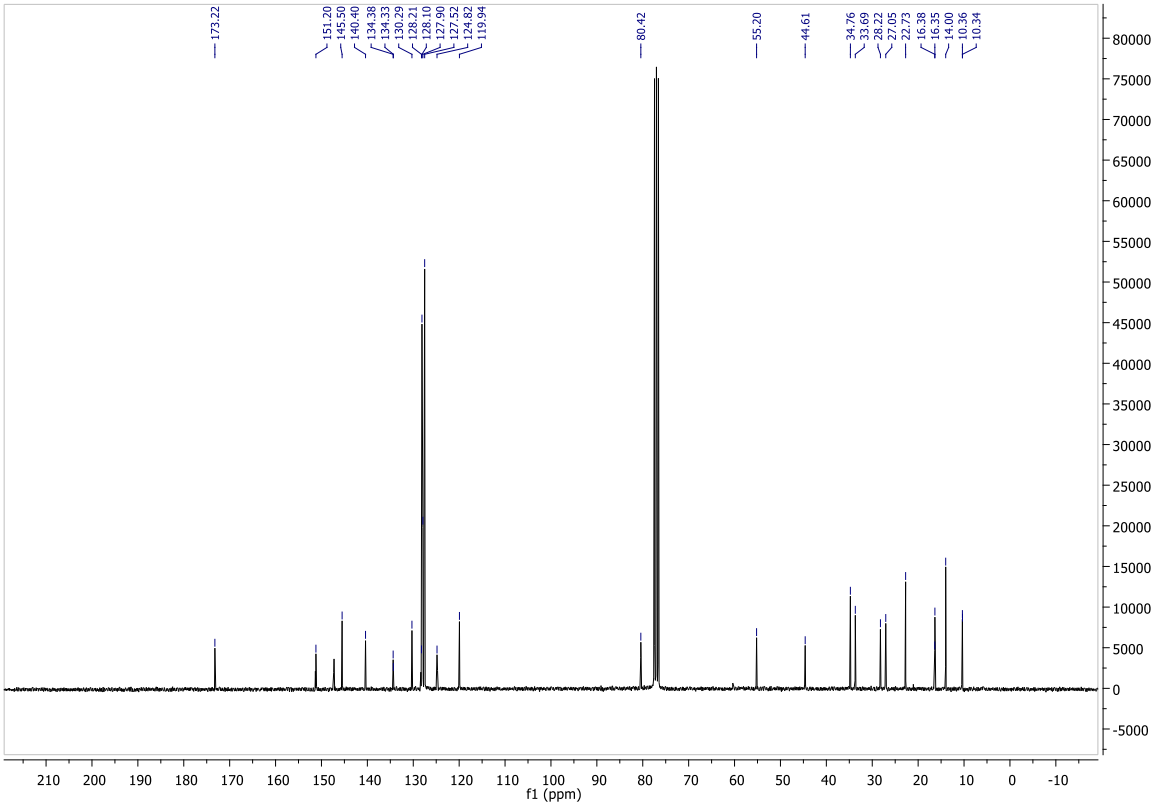
173.22
151.20
145.50
140.40
134.38
134.33
130.29
128.21
128.10
127.90
127.52
124.82
119.94
80.42
55.20
44.61
34.76
33.69
28.22
27.05
22.73
16.38
16.35
14.00
10.36
10.34
f1 (ppm)

2.27e

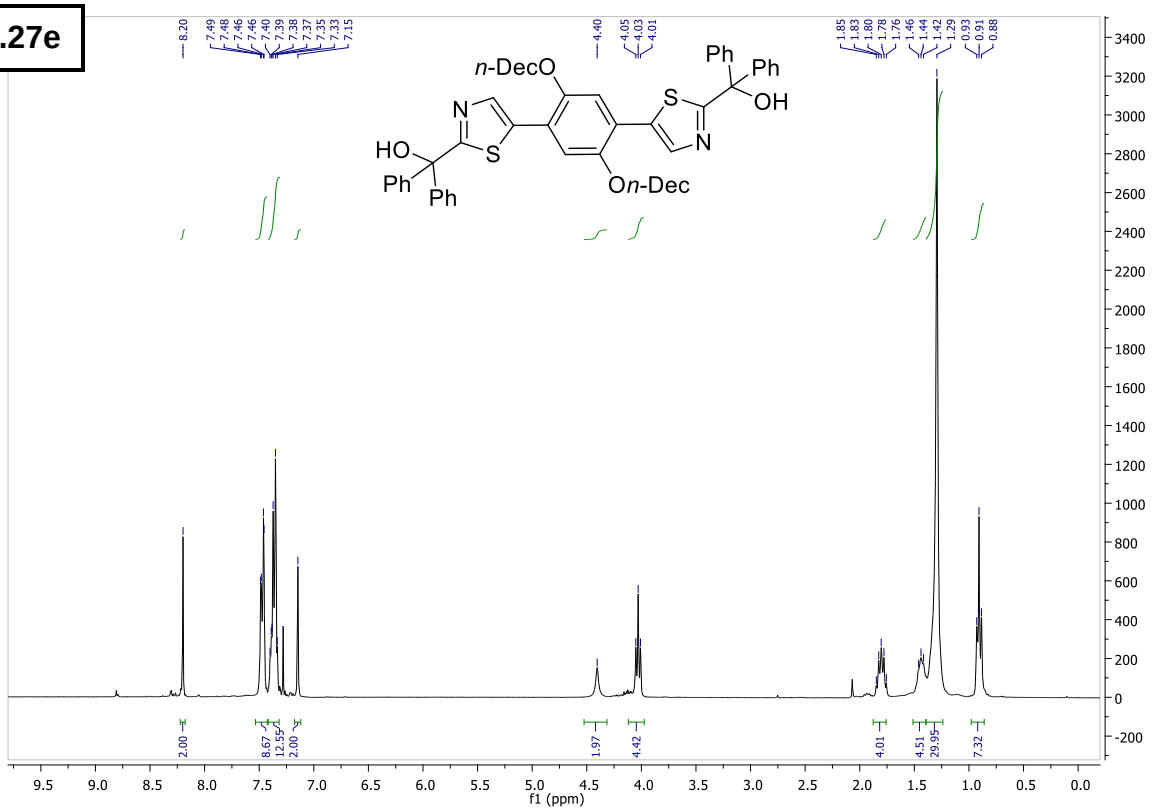
8.20
7.49
7.48
7.46
7.46
7.40
7.39
7.38
7.37
7.35
7.33
7.15
4.40
4.05
4.03
4.01
1.85
1.83
1.80
1.78
1.76
1.46
1.44
1.42
1.29
0.93
0.91
0.88
n-DecO
Ph
Ph
OH
S
N
N
S
HO
Ph
Ph
On-Dec
2.00
8.67
12.55
2.00
1.97
4.42
4.01
4.51
29.99
7.32
f1 (ppm)

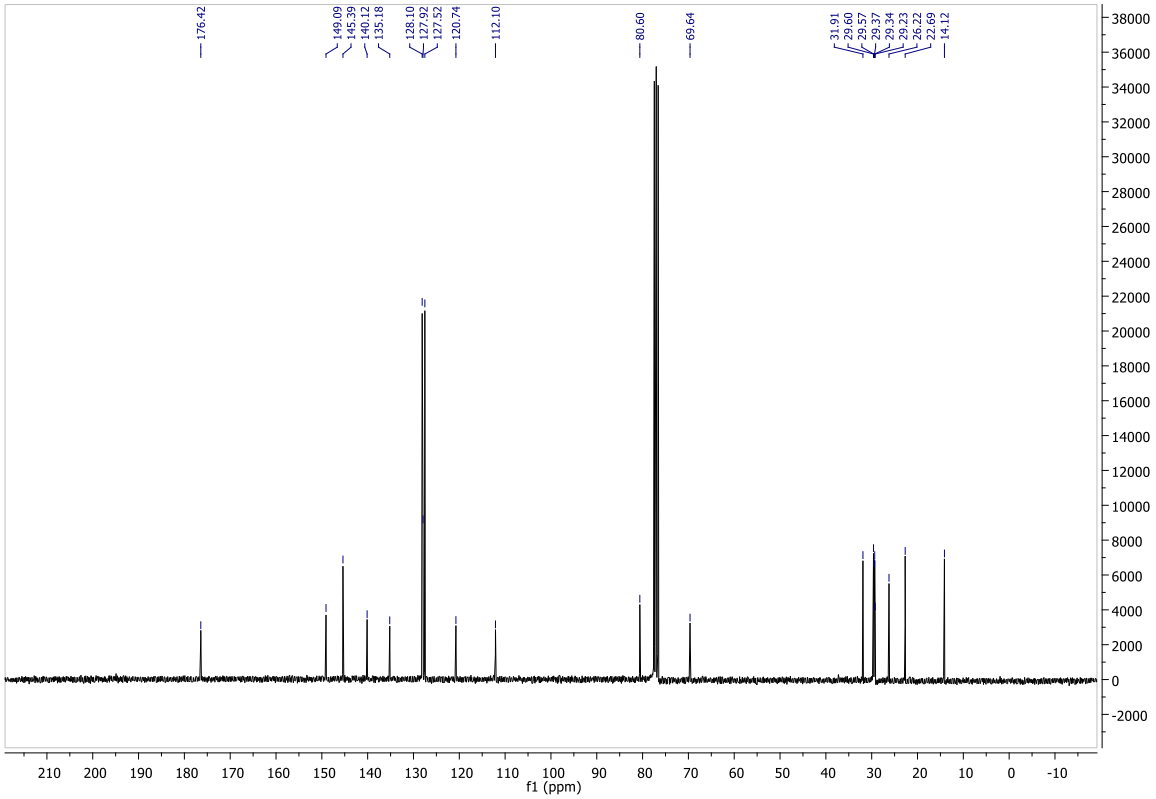
176.42
149.09
145.39
140.12
135.18
128.10
127.92
127.52
120.74
112.10
80.60
69.64
31.91
29.60
29.57
29.37
29.34
29.23
26.22
22.69
14.12
f1 (ppm)

2.27f

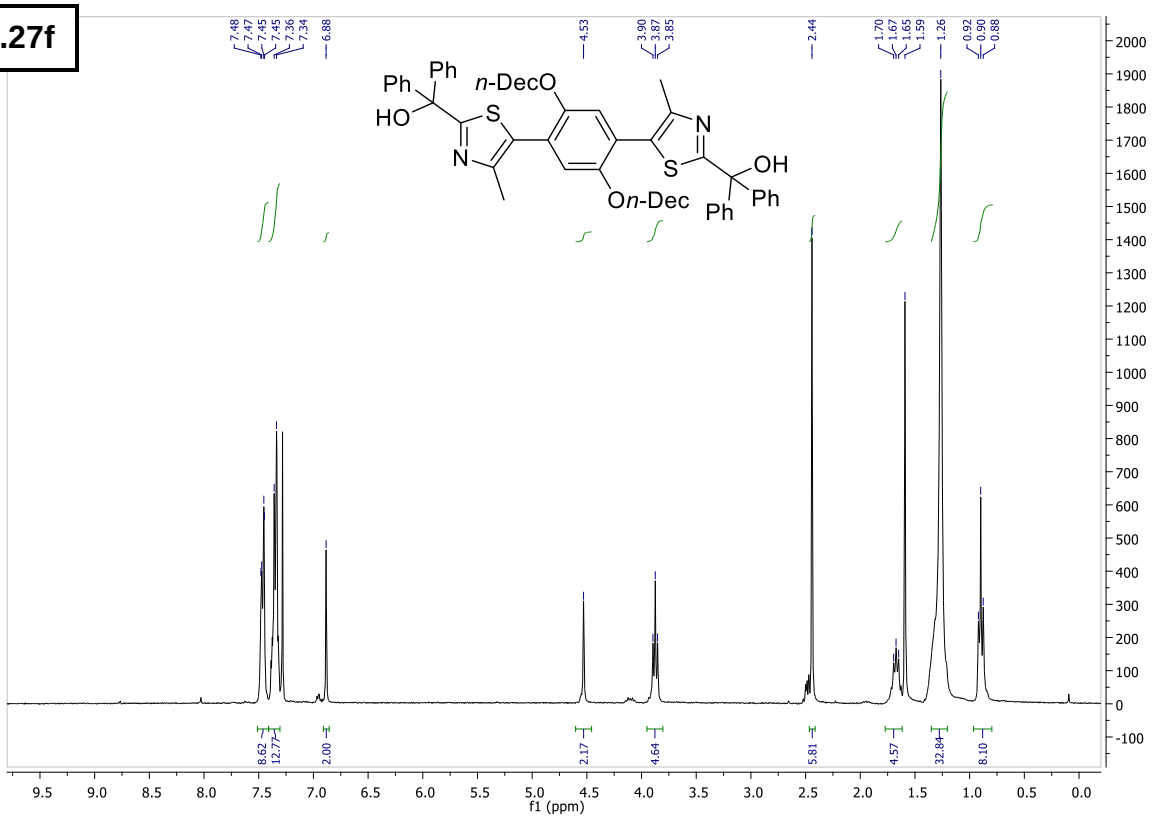
7.48
7.47
7.45
7.45
7.36
7.34
6.88
4.53
3.90
3.87
3.85
2.44
1.70
1.67
1.65
1.59
1.26
0.92
0.90
0.88
Ph
Ph
HO
n-DecO
S
N
N
S
OH
Ph
On-Dec
Ph
8.62
12.77
2.00
2.17
4.64
5.81
4.57
32.84
8.10
f1 (ppm)

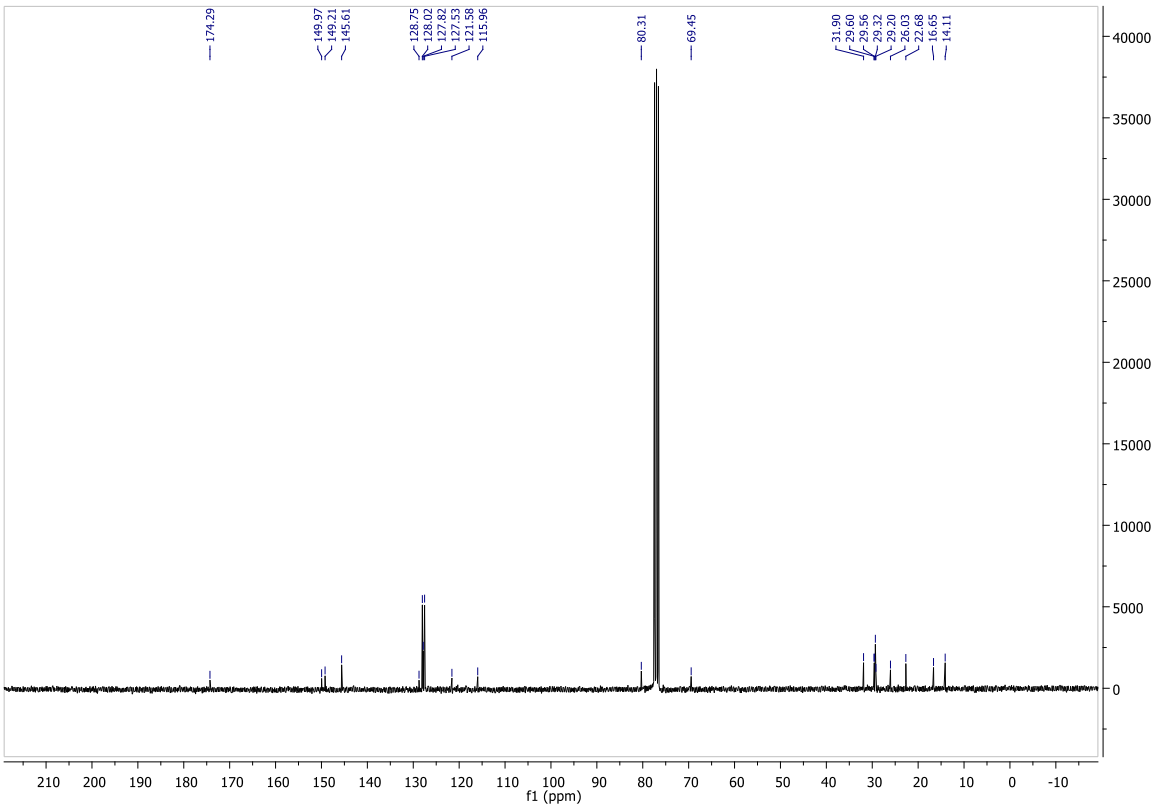
174.29
149.97
149.21
145.61
128.75
128.02
127.82
127.53
121.58
115.96
80.31
69.45
31.90
29.60
29.56
29.32
29.20
26.03
22.68
16.65
14.11
f1 (ppm)

2.27g

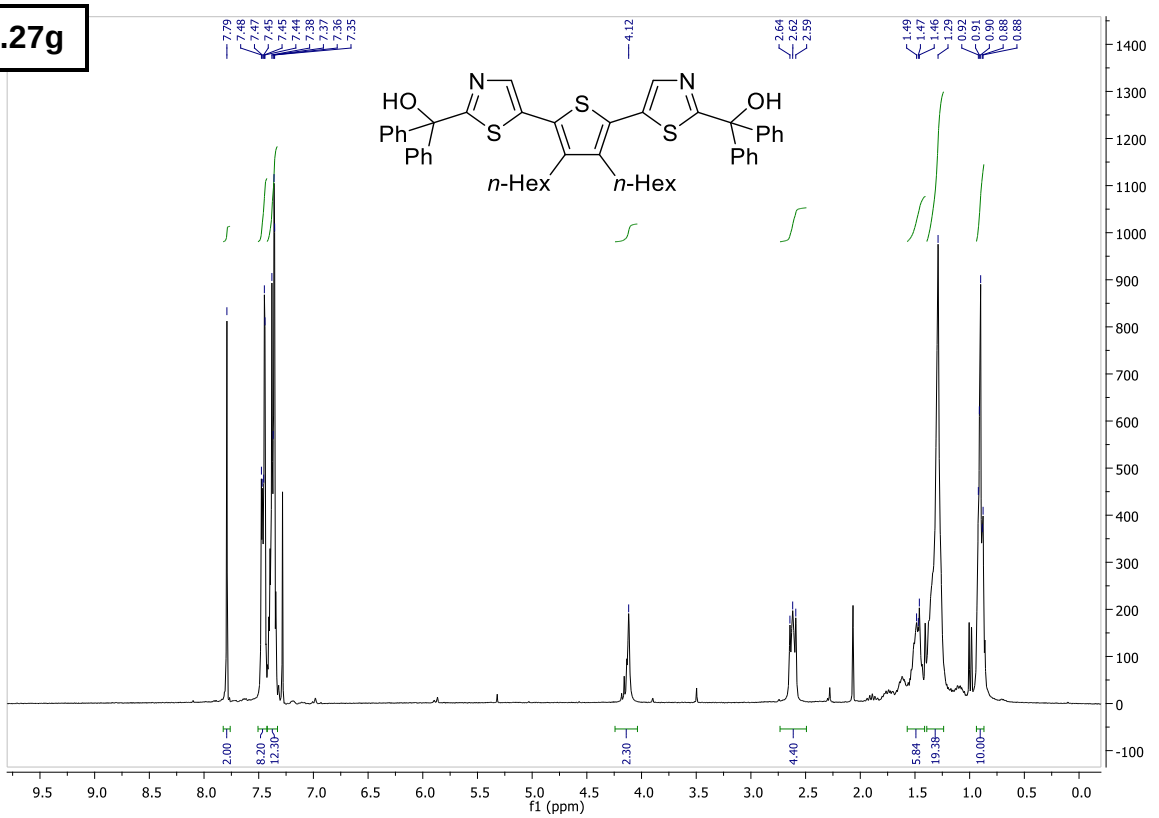
7.79
7.48
7.47
7.45
7.45
7.44
7.38
7.37
7.36
7.35
4.12
2.64
2.62
2.59
1.49
1.47
1.46
1.29
0.92
0.91
0.90
0.88
0.88
HO
Ph
Ph
N
S
S
N
OH
Ph
Ph
n-Hex
n-Hex
2.00
8.20
12.30
2.30
4.40
5.84
19.38
10.00
f1 (ppm)

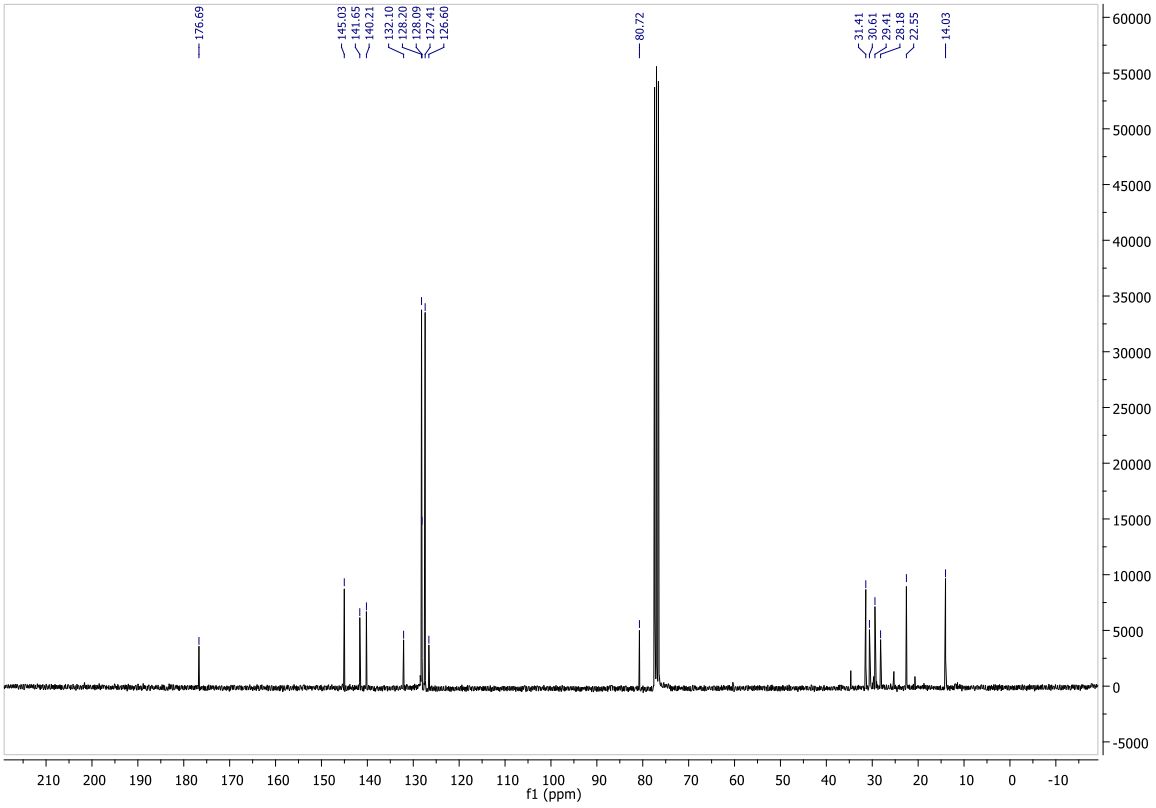
176.69
145.03
141.65
140.21
132.10
128.20
128.09
127.41
126.60
80.72
31.41
30.61
29.41
28.18
22.55
14.03
f1 (ppm)

2.28a

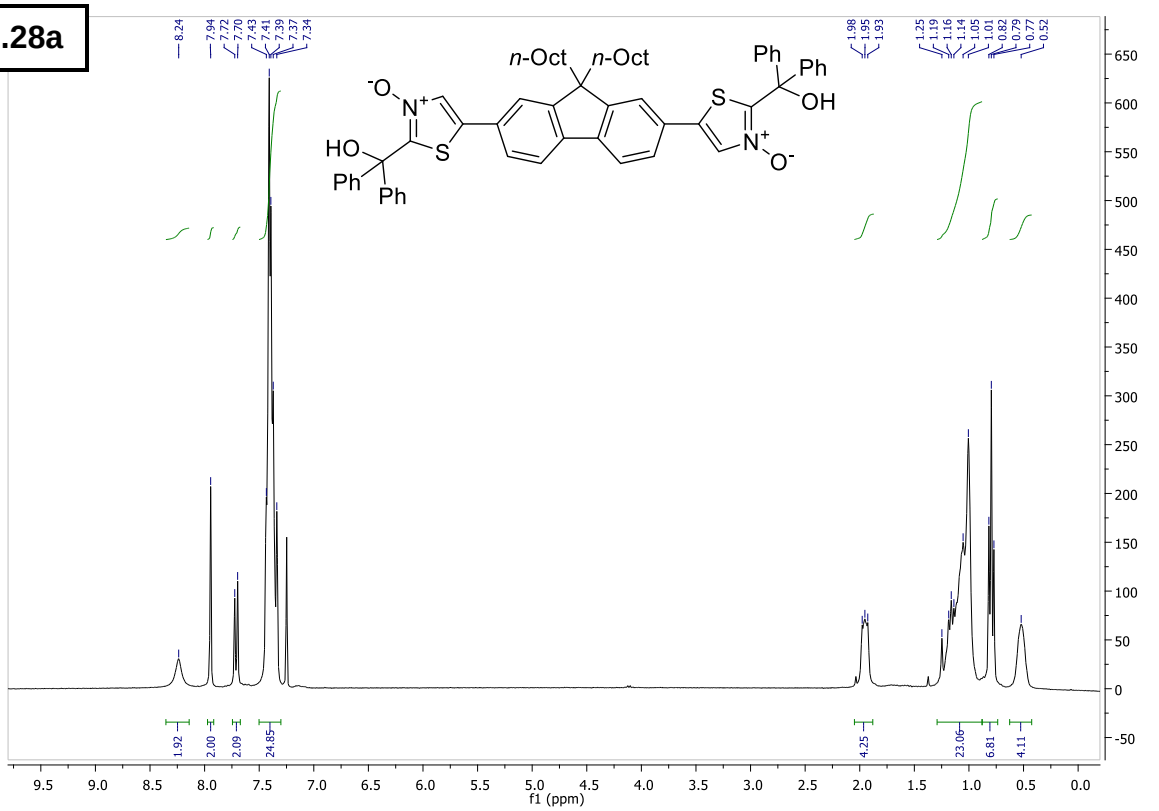
8.24
7.94
7.72
7.70
7.43
7.41
7.39
7.37
7.34
1.98
1.95
1.93
1.25
1.19
1.16
1.14
1.05
1.01
0.82
0.79
0.77
0.52
n-Oct
n-Oct
Ph
Ph
OH
S
N+
O-
HO
Ph
Ph
1.92
2.00
2.09
24.85
4.25
23.06
6.81
4.11
f1 (ppm)

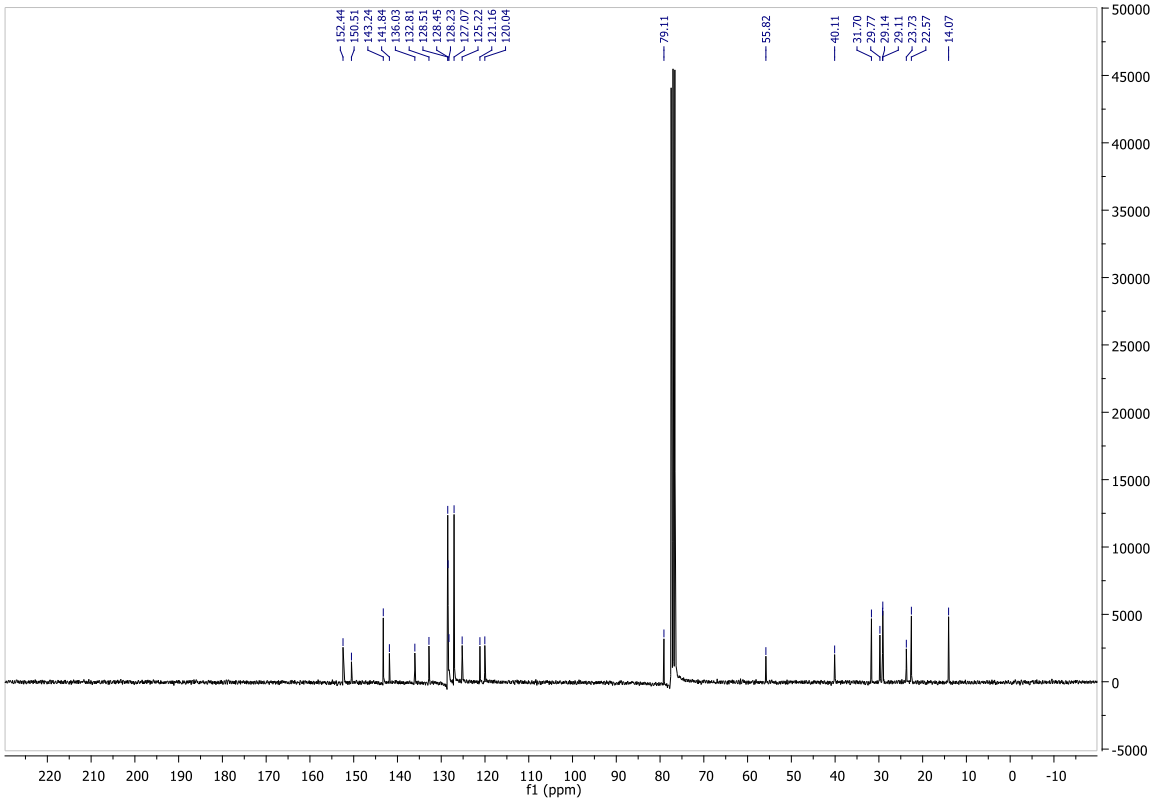
152.44
150.51
143.24
141.84
136.03
132.81
128.51
128.45
128.23
127.07
125.22
121.16
120.04
79.11
55.82
40.11
31.70
29.77
29.14
29.11
23.73
22.57
14.07
f1 (ppm)

2.28b

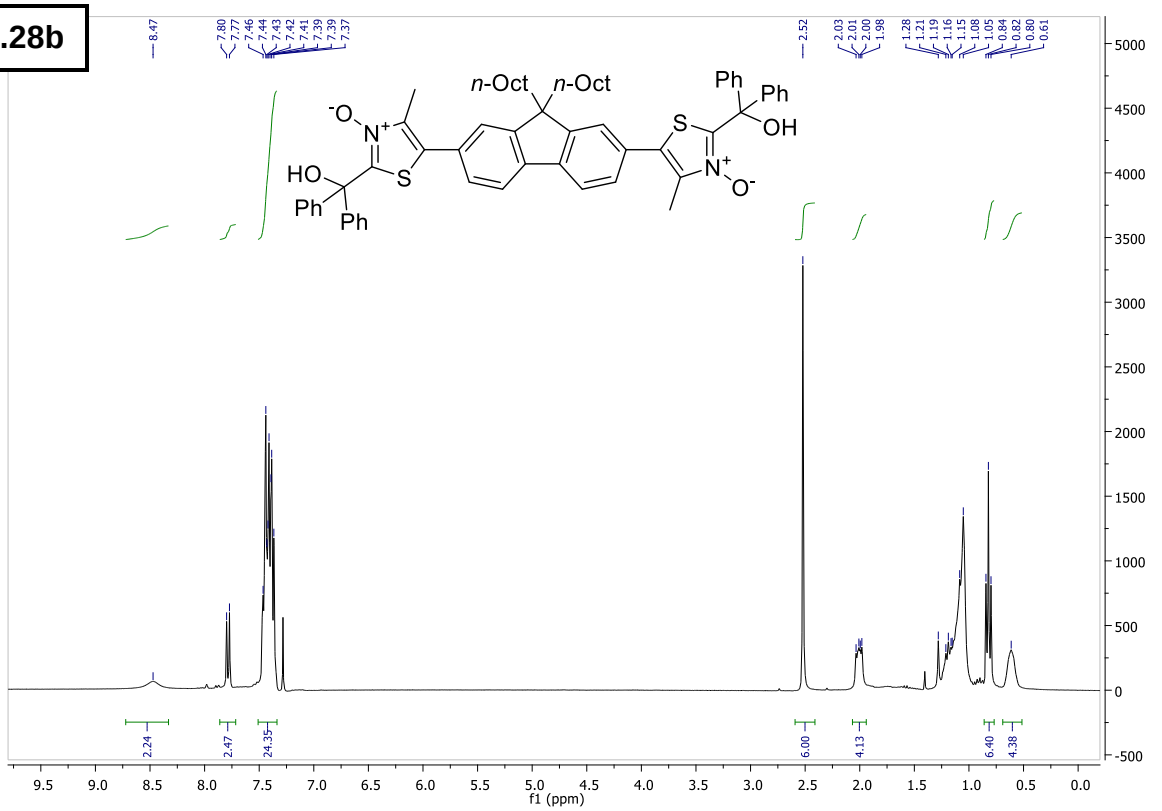
8.47
7.80
7.77
7.46
7.44
7.43
7.42
7.41
7.39
7.39
7.37
2.52
2.03
2.01
2.00
1.98
1.28
1.21
1.19
1.16
1.15
1.08
1.05
0.84
0.82
0.80
0.61
n-Oct
n-Oct
Ph
Ph
OH
HO
Ph
Ph
2.24
2.47
24.35
6.00
4.13
6.40
4.38
f1 (ppm)

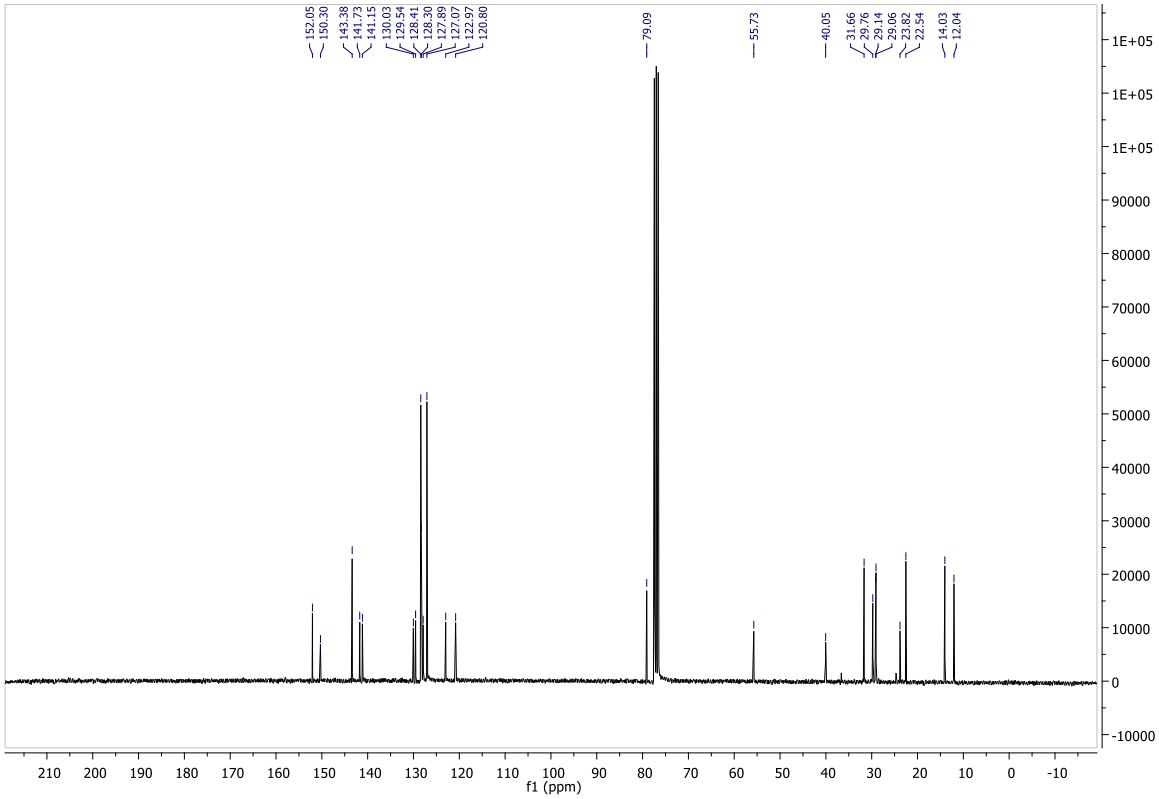
152.05
150.30
143.38
141.73
141.15
130.03
129.54
128.41
128.30
127.89
127.07
122.97
120.80
79.09
55.73
40.05
31.66
29.76
29.14
29.06
23.82
22.54
14.03
12.04
f1 (ppm)

2.28c

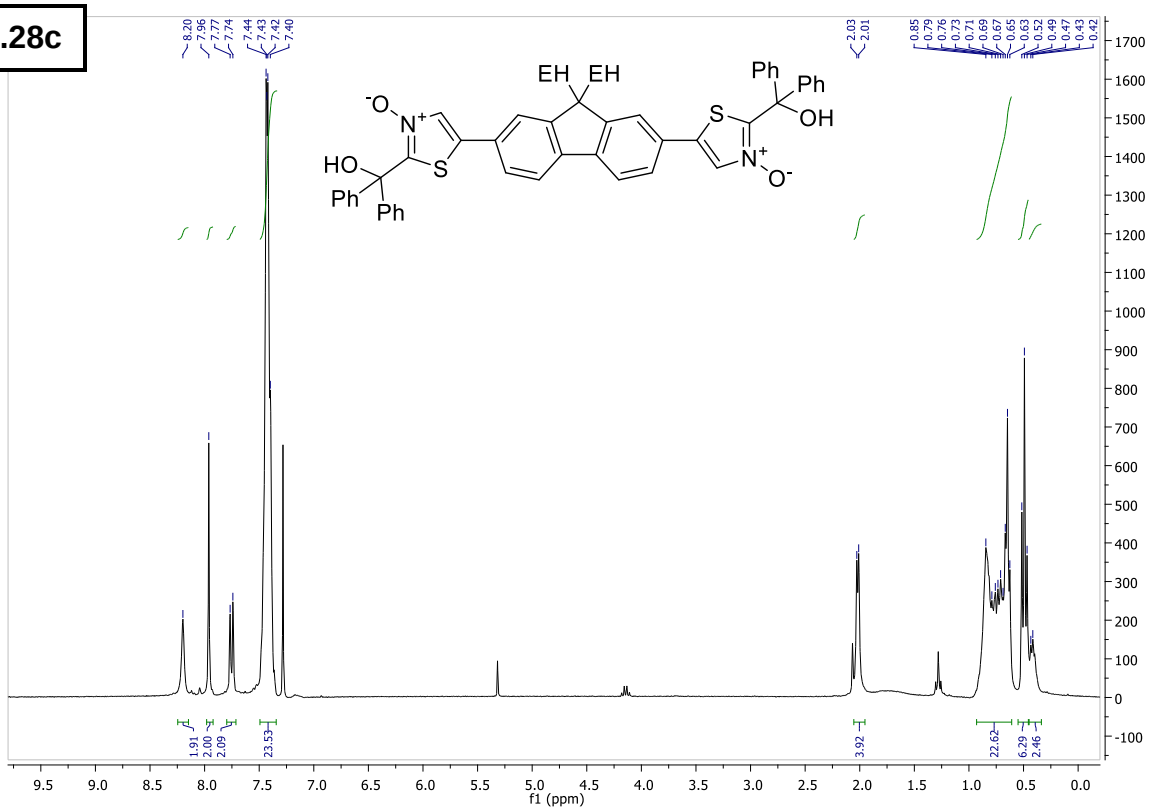
8.20
7.96
7.77
7.74
7.44
7.43
7.42
7.40
2.03
2.01
0.85
0.79
0.76
0.73
0.71
0.69
0.67
0.65
0.63
0.52
0.49
0.47
0.43
0.42
EH EH
Ph Ph
OH
HO
Ph Ph
1.91
2.00
2.09
23.53
3.92
22.62
6.29
2.46
f1 (ppm)

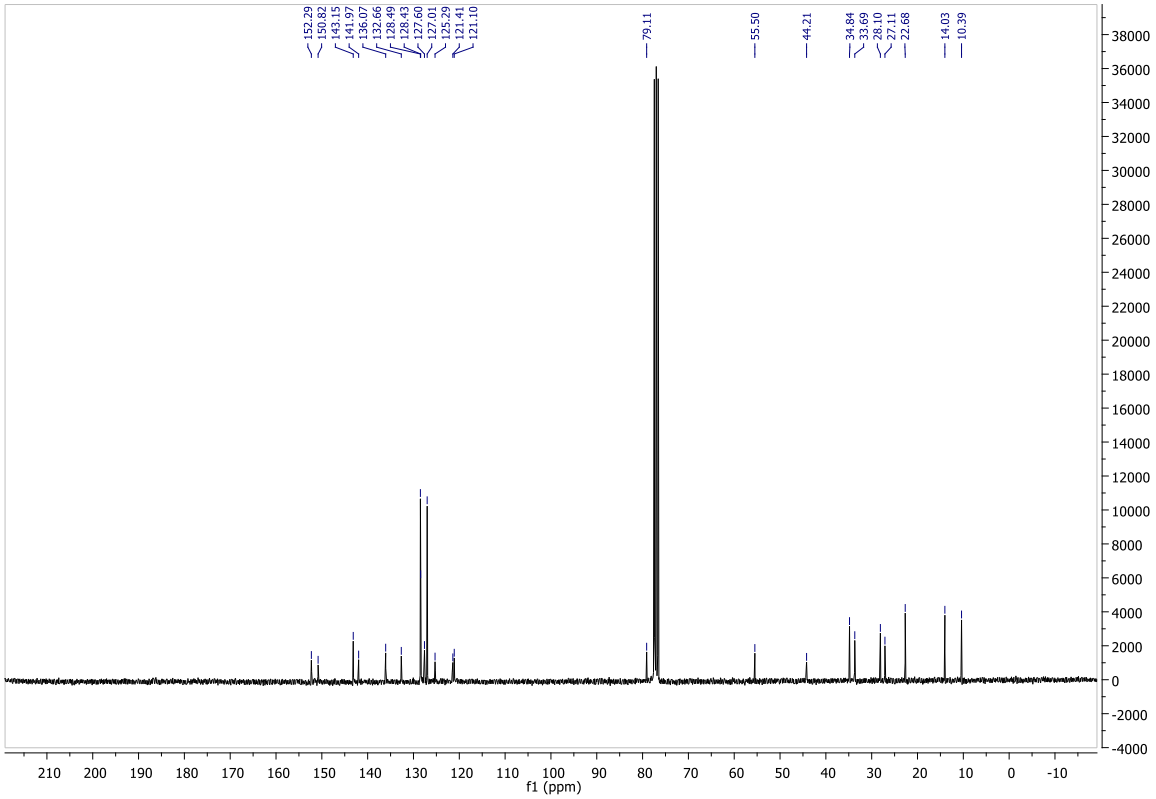
152.29
150.82
143.15
141.97
136.07
132.66
128.49
128.43
127.60
127.01
125.29
121.41
121.10
79.11
55.50
44.21
34.84
33.69
28.10
27.11
22.68
14.03
10.39
f1 (ppm)

2.28d

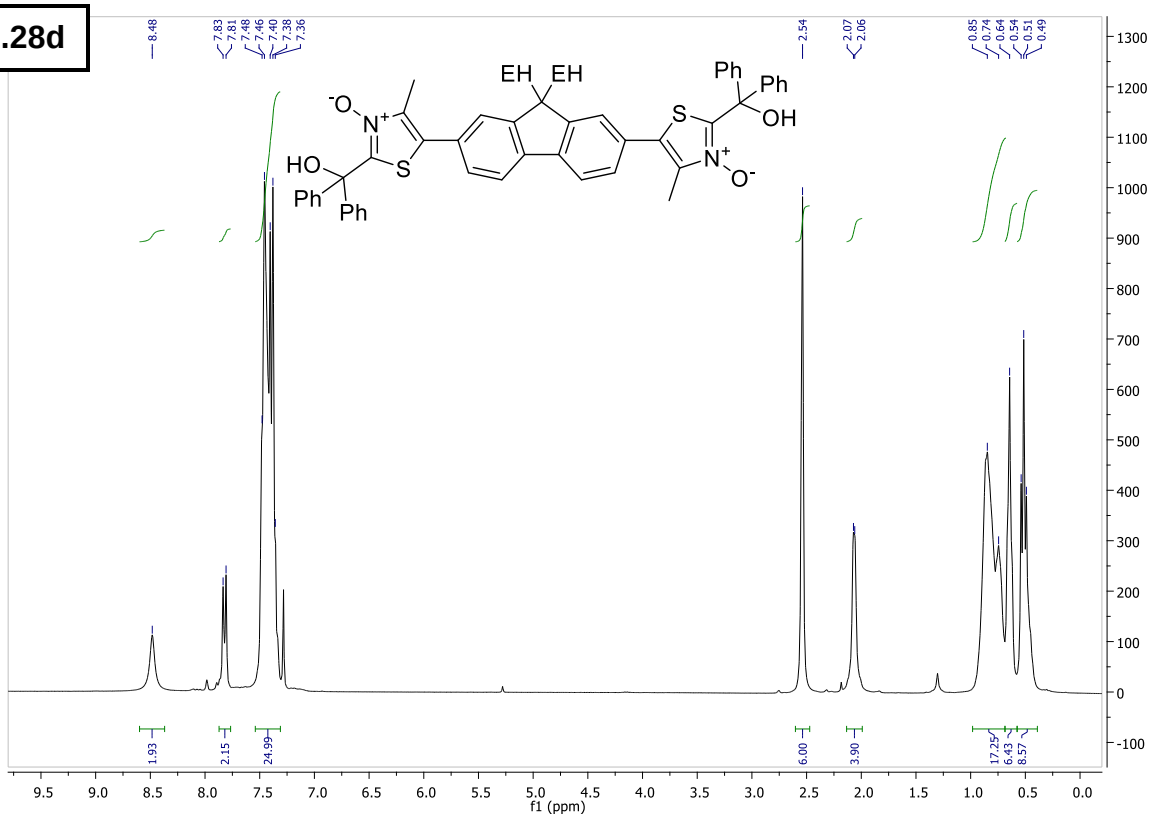
8.48
7.83
7.81
7.48
7.46
7.40
7.38
7.36
2.54
2.07
2.06
0.85
0.74
0.64
0.54
0.51
0.49
EH EH
Ph
Ph
OH
HO
Ph
Ph
1.93
2.15
24.99
6.00
3.90
17.25
6.43
8.57
f1 (ppm)

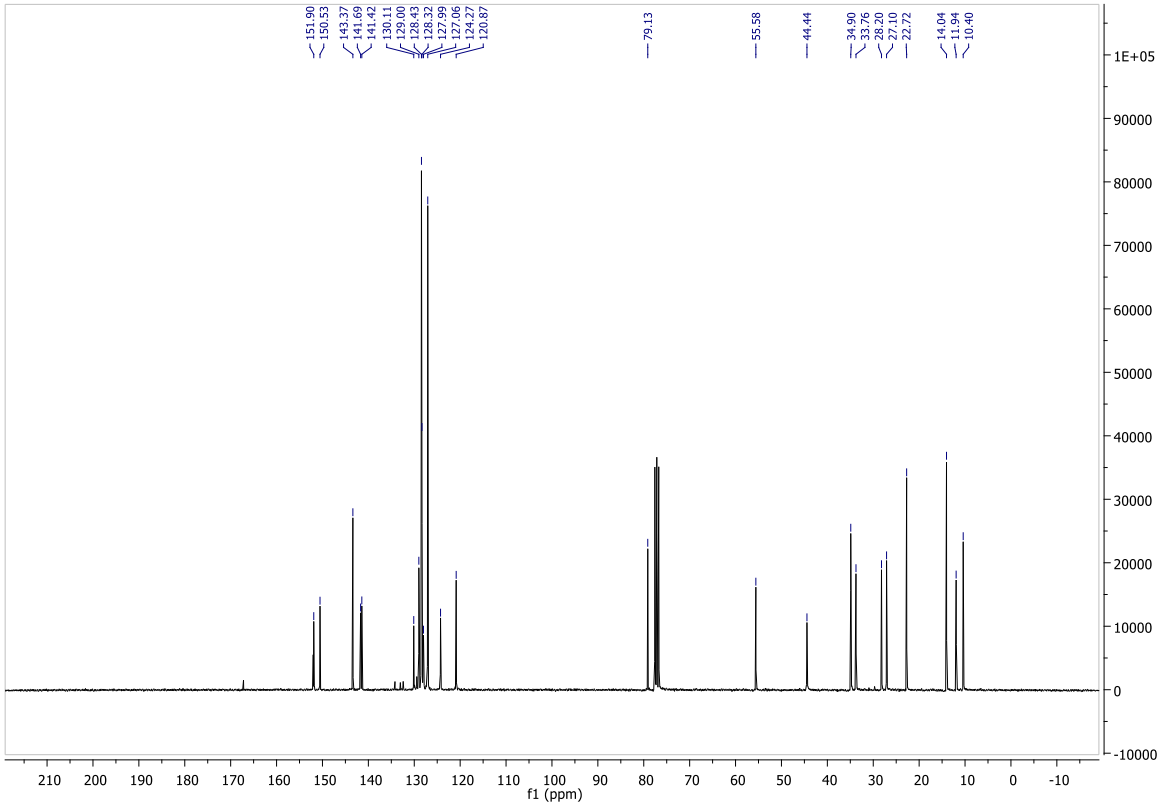
151.90
150.53
143.37
141.69
141.42
130.11
129.00
128.43
128.32
127.99
127.06
124.27
120.87
79.13
55.58
44.44
34.90
33.76
28.20
27.10
22.72
14.04
11.94
10.40
f1 (ppm)

2.28e

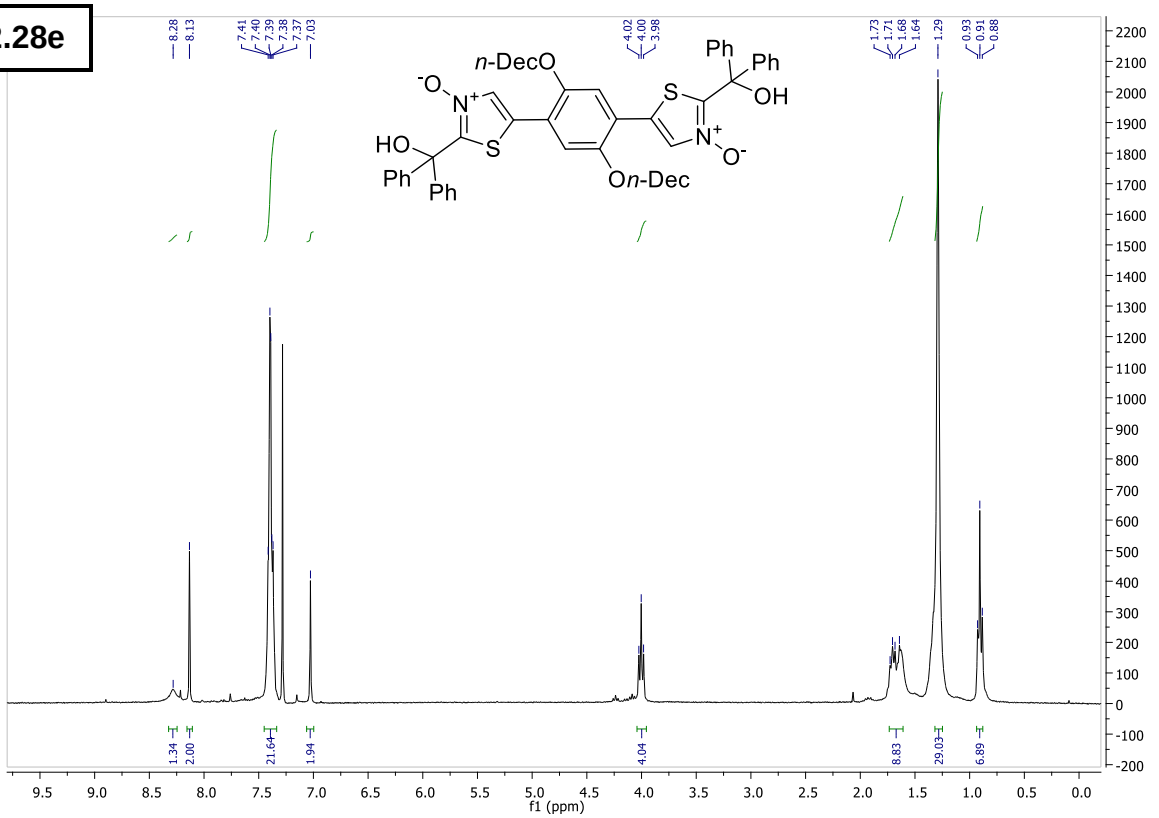
8.28
8.13
7.41
7.40
7.39
7.38
7.37
7.03
4.02
4.00
3.98
1.73
1.71
1.68
1.64
1.29
0.93
0.91
0.88
n-DecO
Ph
Ph
OH
HO
Ph
Ph
On-Dec
1.34
2.00
21.64
1.94
4.04
8.83
29.03
6.89
f1 (ppm)

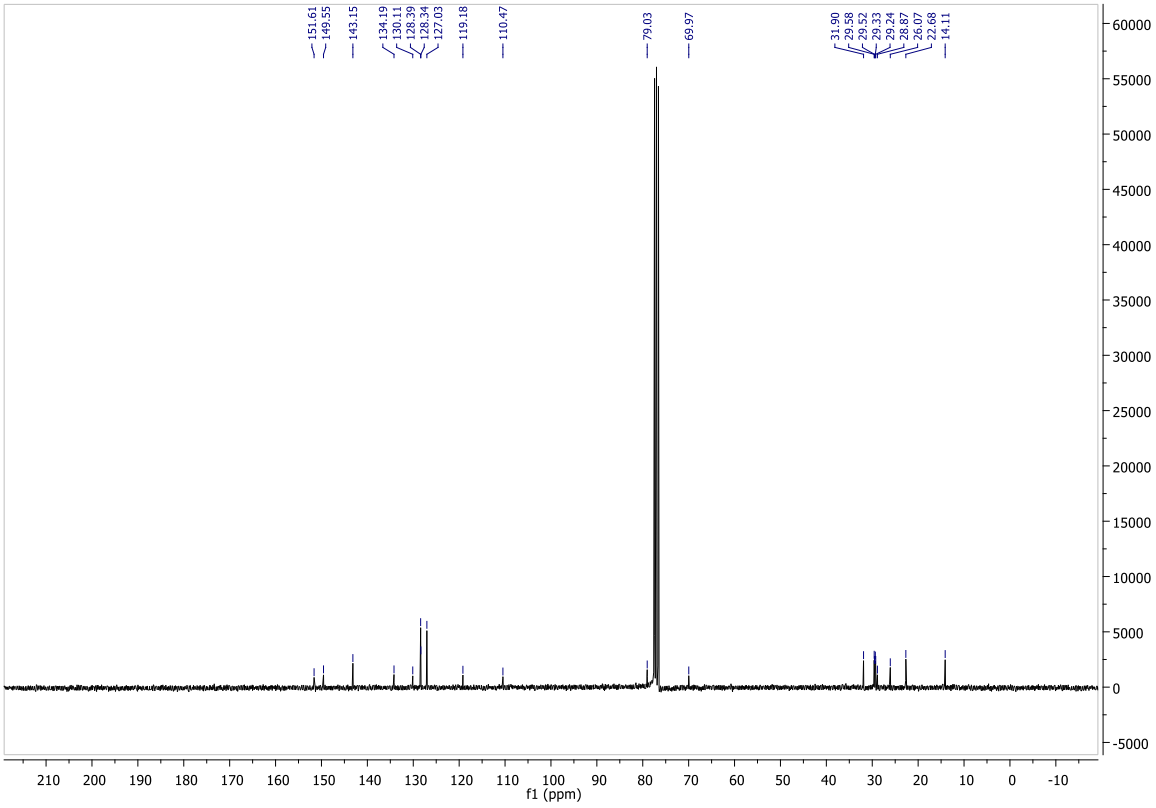
151.61
149.55
143.15
134.19
130.11
128.39
128.34
127.03
119.18
110.47
79.03
69.97
31.90
29.58
29.52
29.33
29.24
28.87
26.07
22.68
14.11
f1 (ppm)

2.28f

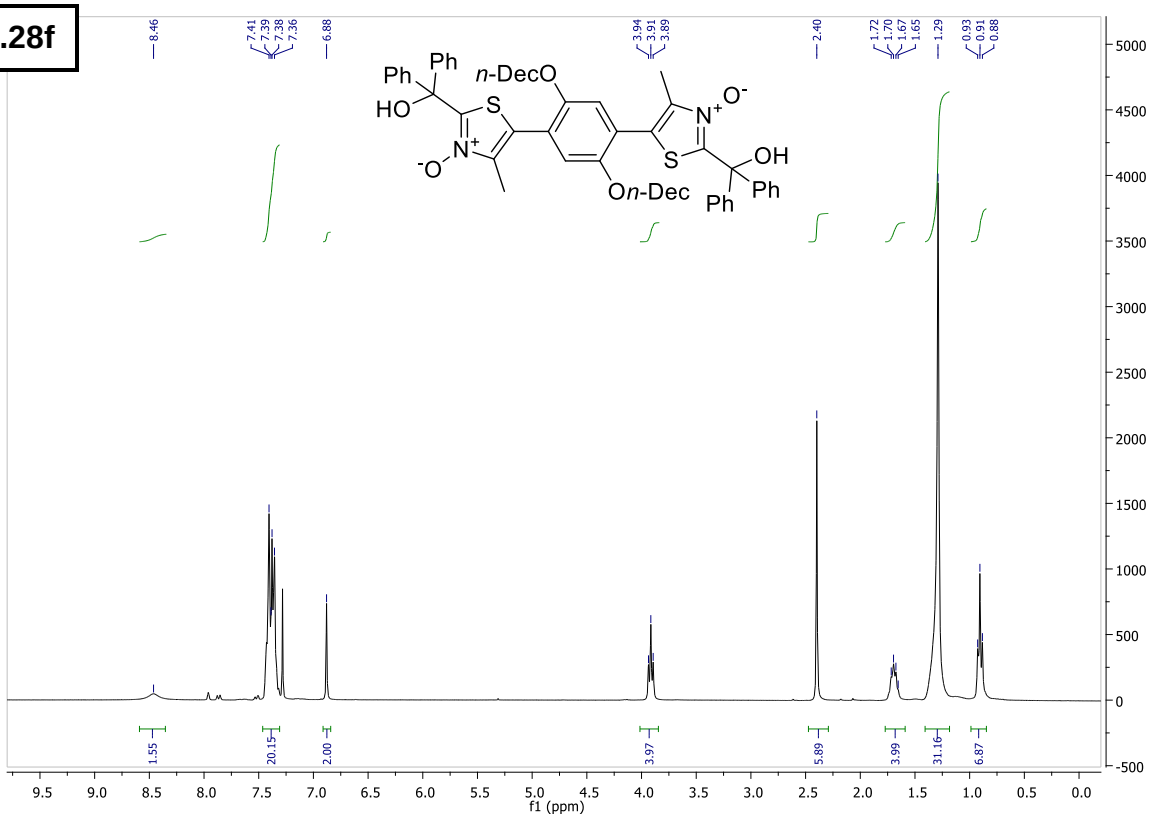
8.46
7.41
7.39
7.38
7.36
6.88
3.94
3.91
3.89
2.40
1.72
1.70
1.67
1.65
1.29
0.93
0.91
0.88
Ph
Ph
HO
n-DecO
S
N+
O-
O-
N+
S
OH
Ph
Ph
On-Dec
1.55
20.15
2.00
3.97
5.89
3.99
31.16
6.87
f1 (ppm)

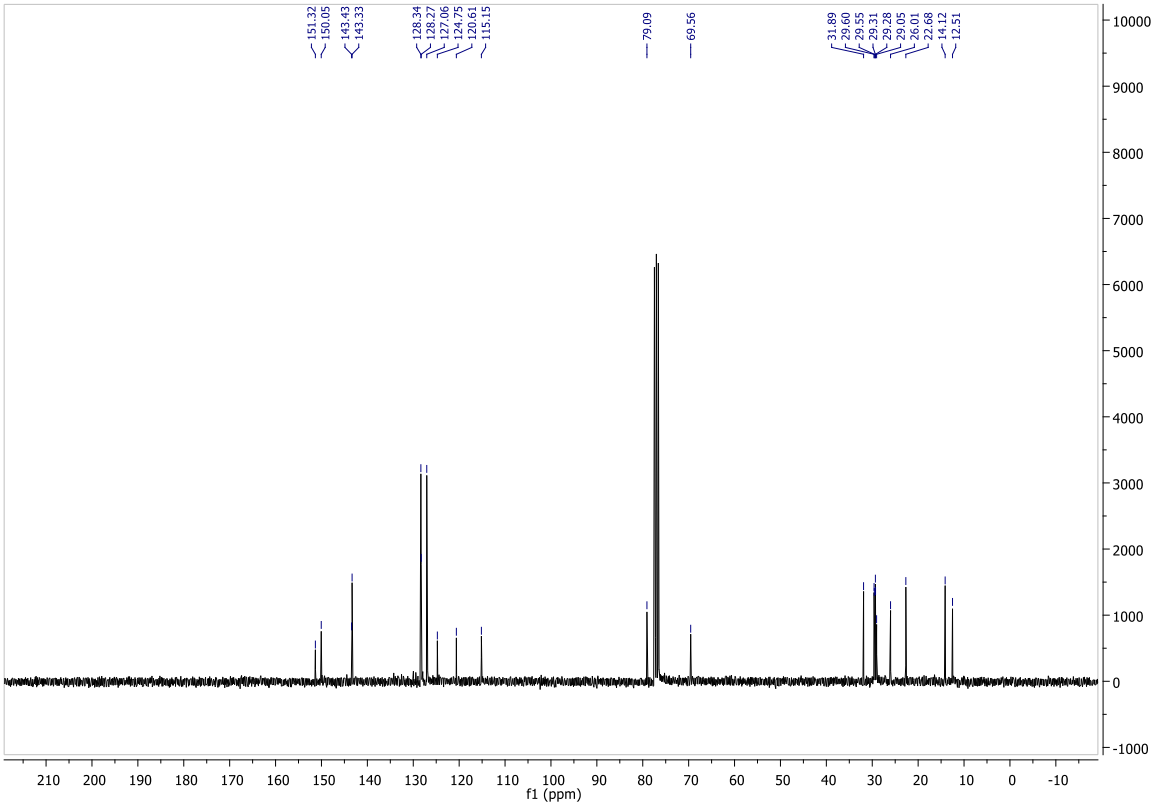
151.32
150.05
143.43
143.33
128.34
128.27
127.06
124.75
120.61
115.15
79.09
69.56
31.89
29.60
29.55
29.31
29.28
29.05
26.01
22.68
14.12
12.51
f1 (ppm)

2.29a

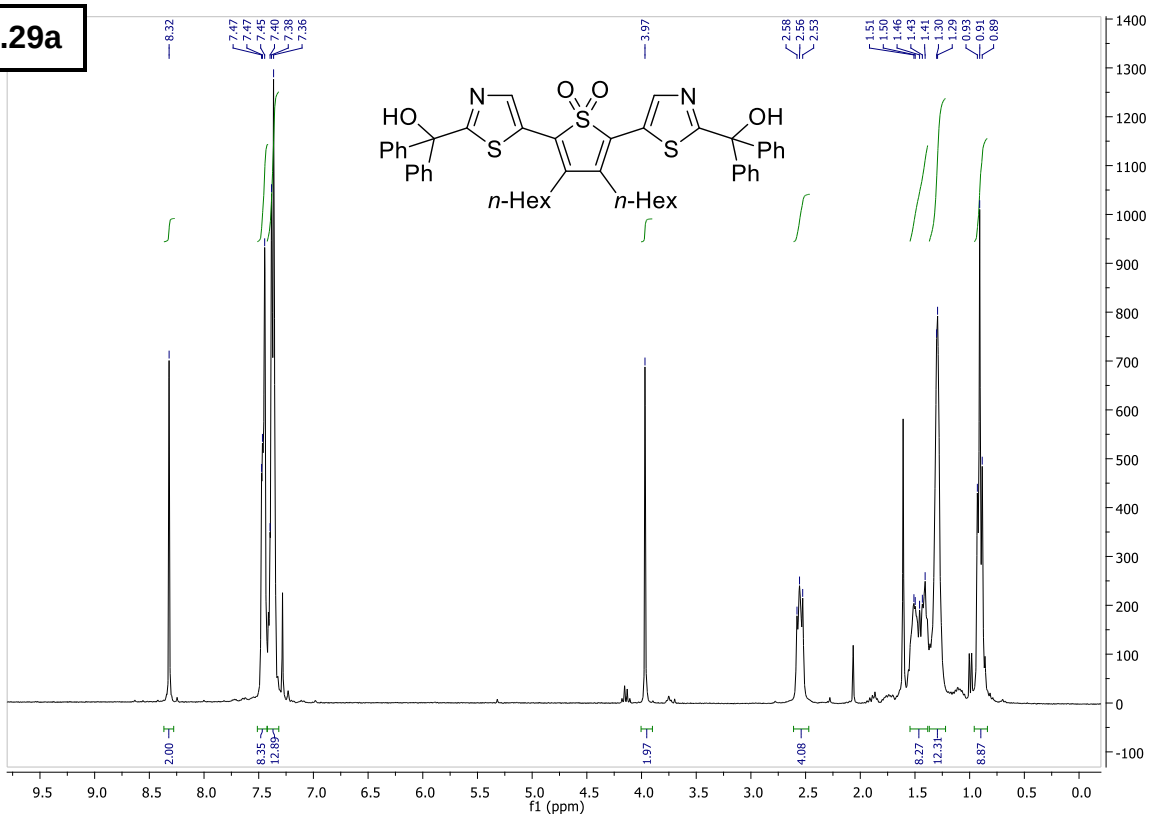
8.32
7.47
7.47
7.45
7.40
7.38
7.36
3.97
2.58
2.56
2.53
1.51
1.50
1.46
1.43
1.41
1.30
1.29
0.93
0.91
0.89
HO
Ph
Ph
N
S
O
O
S
N
S
OH
Ph
Ph
n-Hex
n-Hex
2.00
8.35
12.89
1.97
4.08
8.27
12.31
8.87
f1 (ppm)

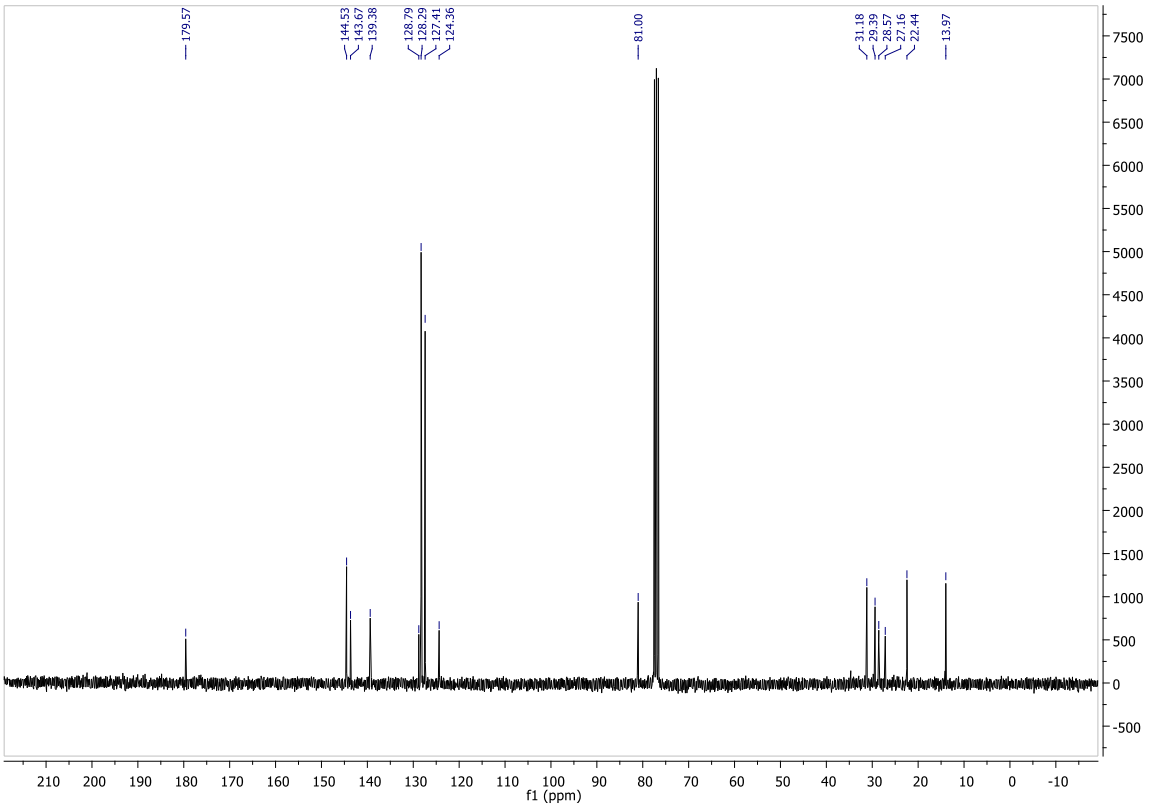
179.57
144.53
143.67
139.38
128.79
128.29
127.41
124.36
81.00
31.18
29.39
28.57
27.16
22.44
13.97
f1 (ppm)

2.29b

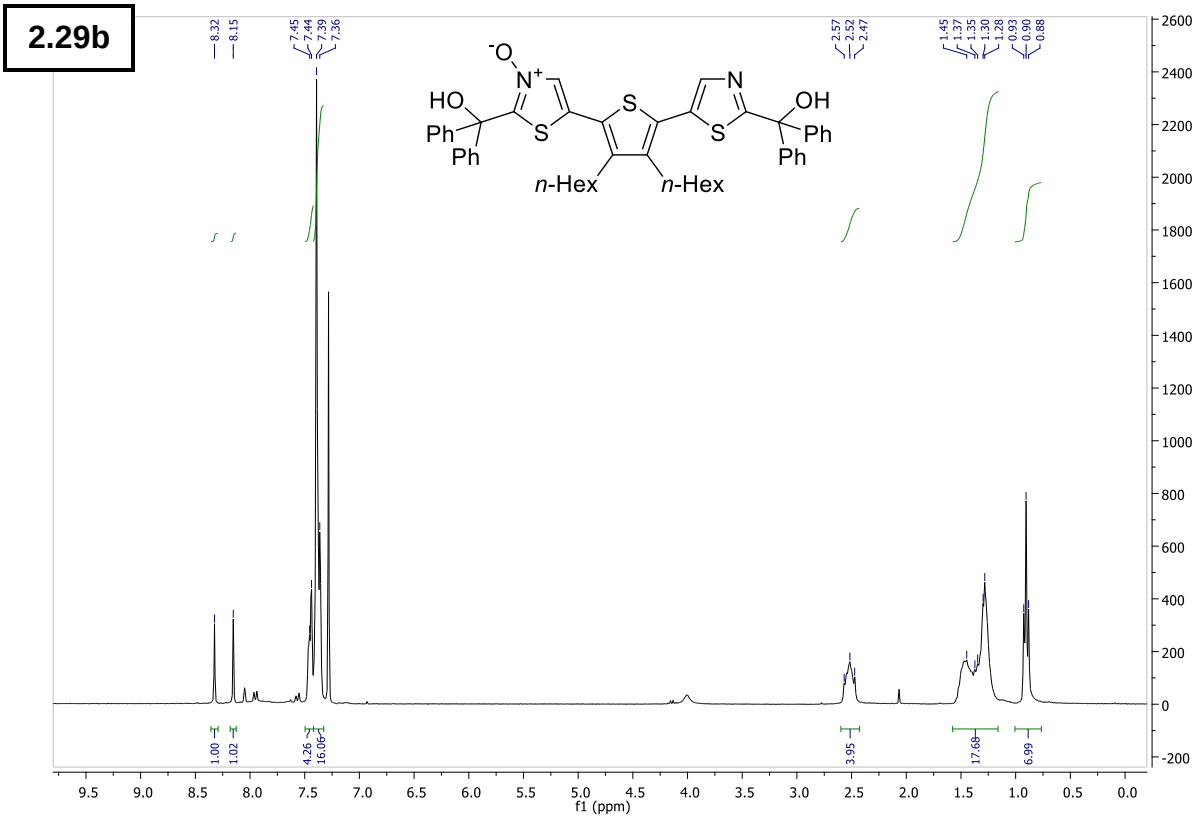
8.32
8.15
7.45
7.44
7.39
7.36
2.57
2.52
2.47
1.45
1.37
1.35
1.30
1.28
0.93
0.90
0.88
HO
Ph
Ph
OH
Ph
Ph
n-Hex
n-Hex
1.00
1.02
4.26
16.06
3.95
17.68
6.99
f1 (ppm)

3.1a

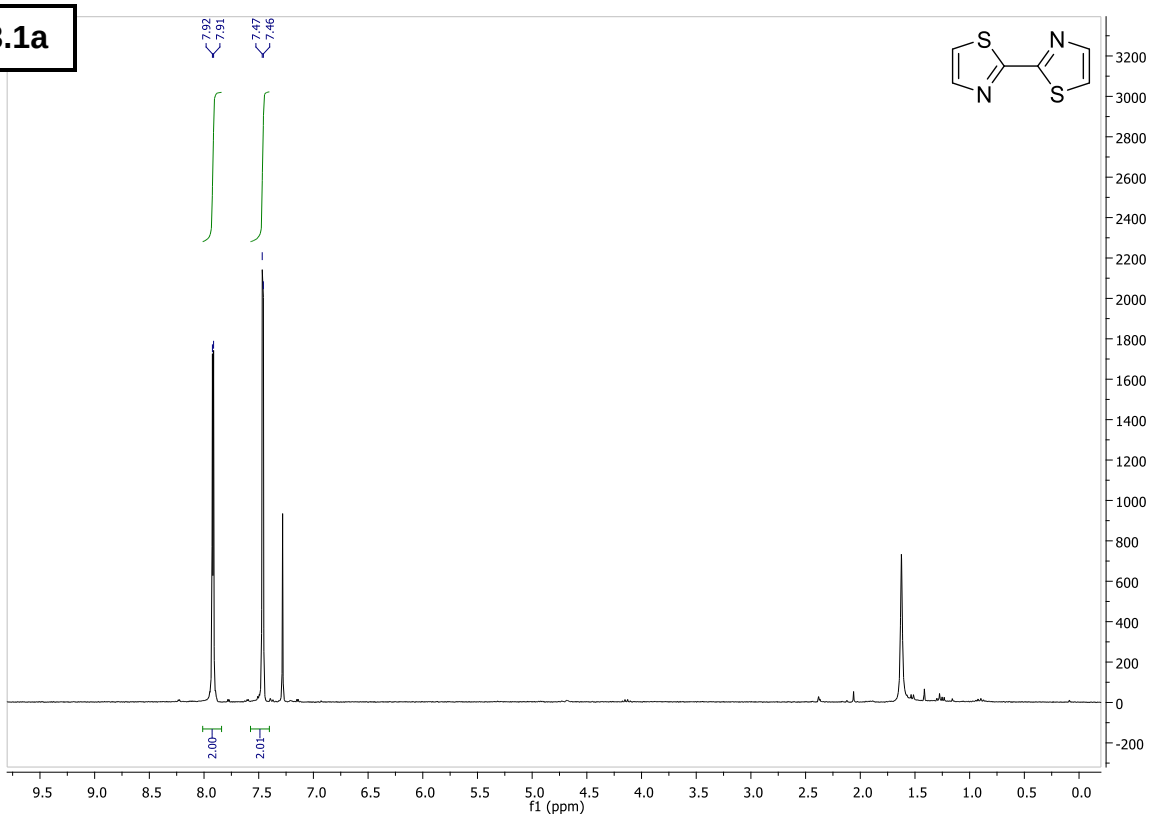

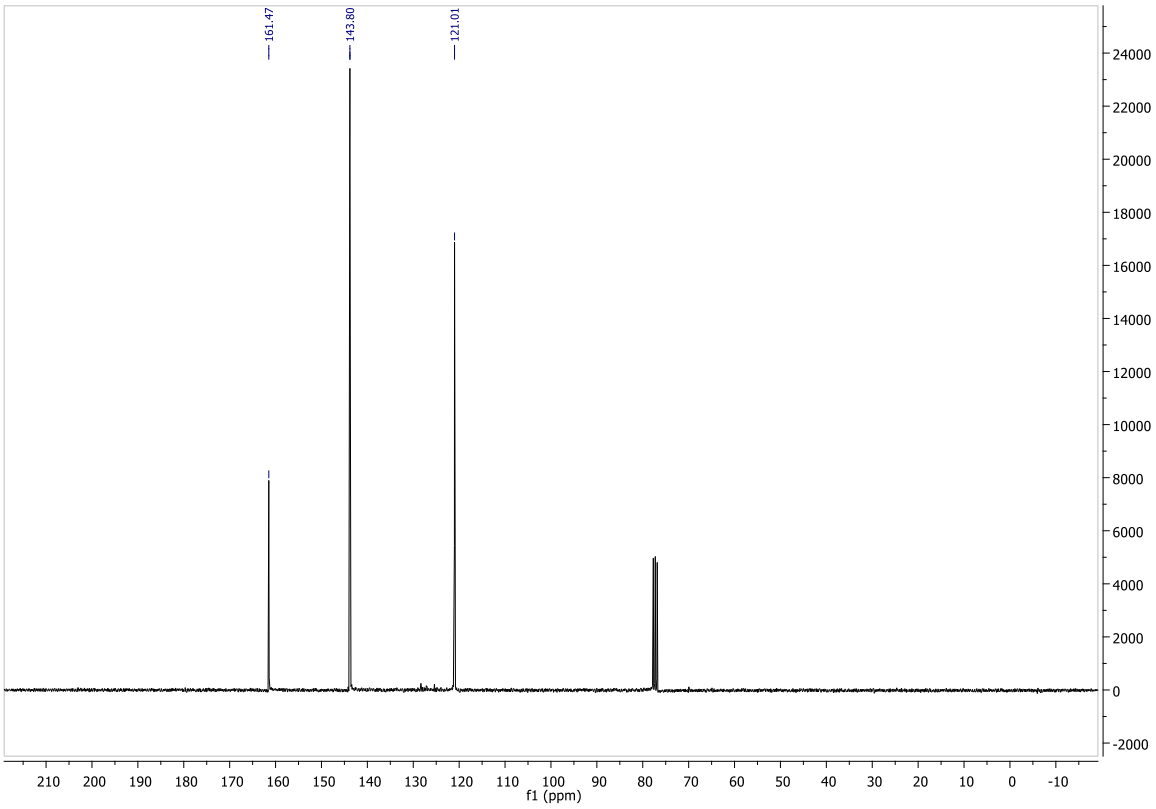

3.1c

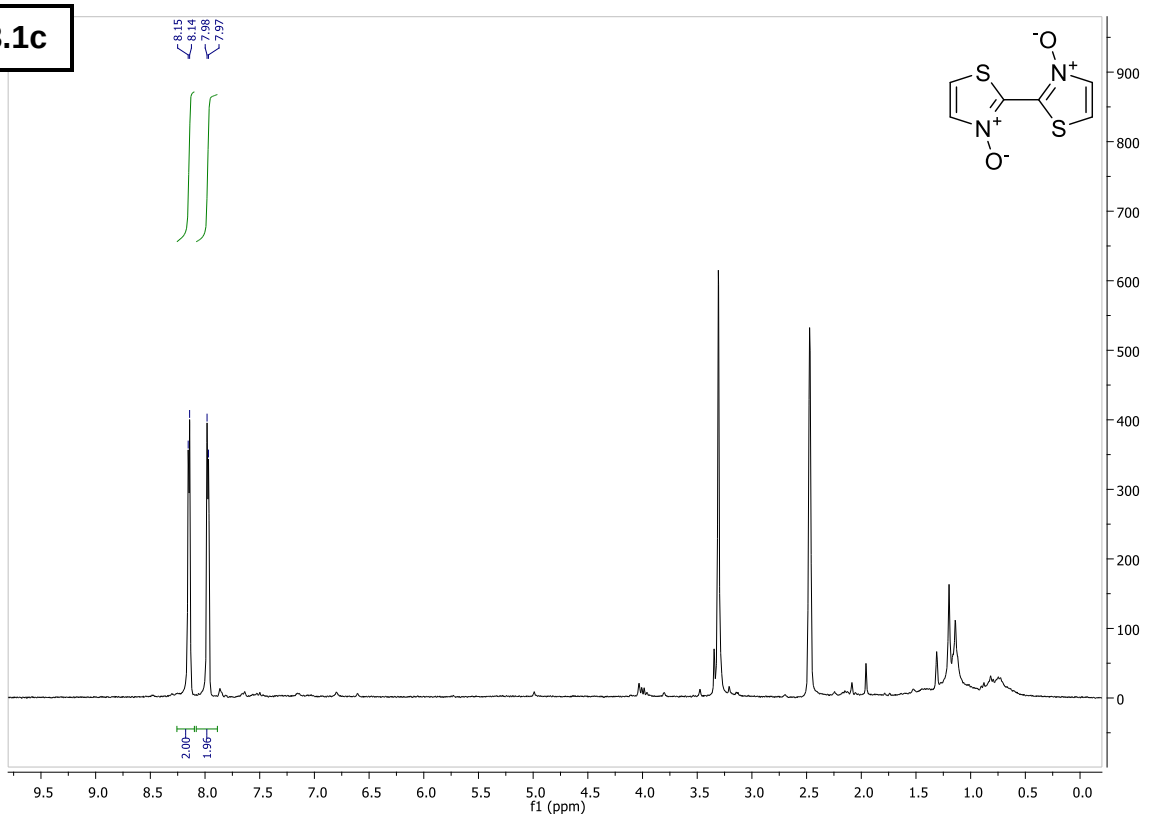

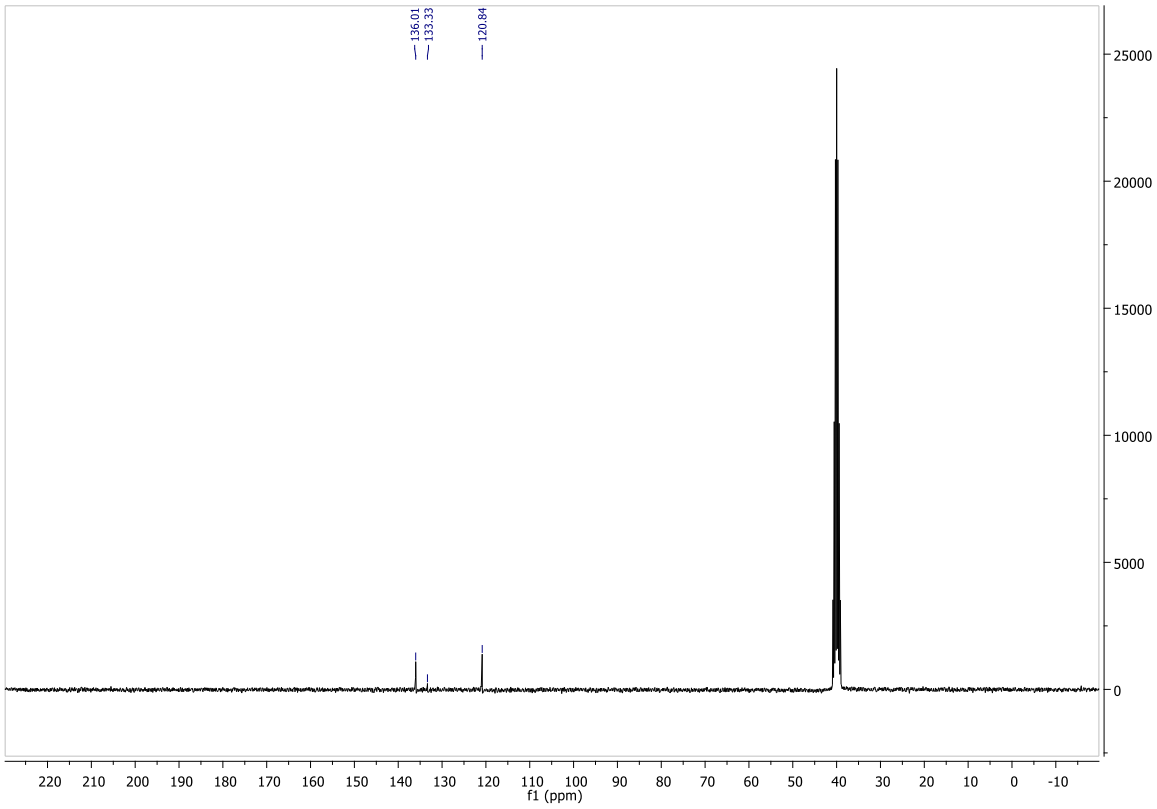

3.2a

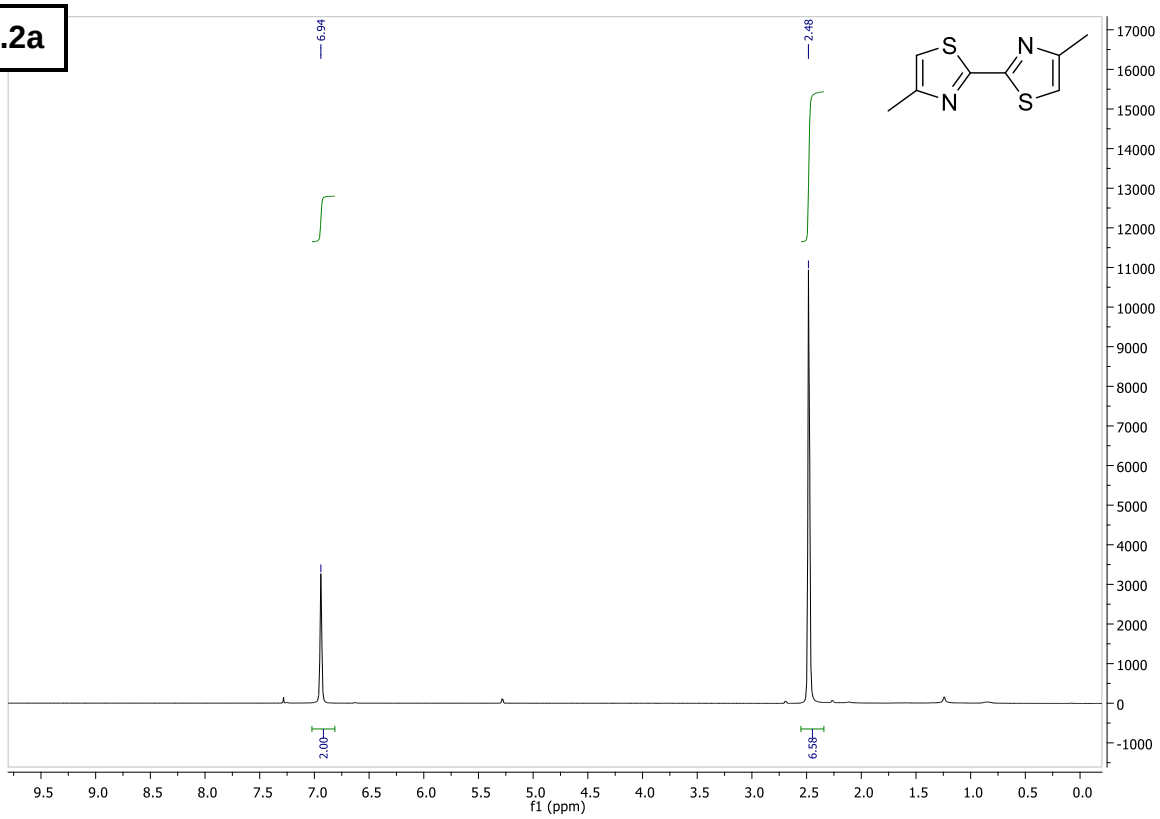

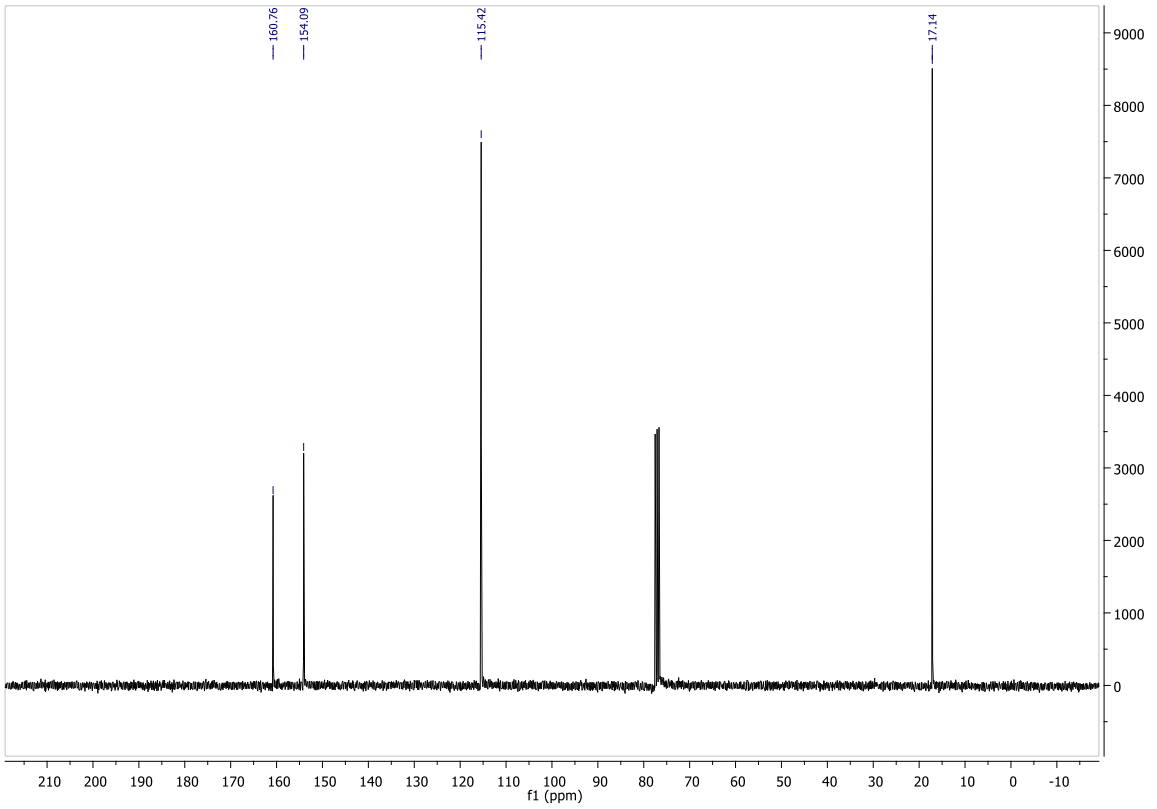

3.2b

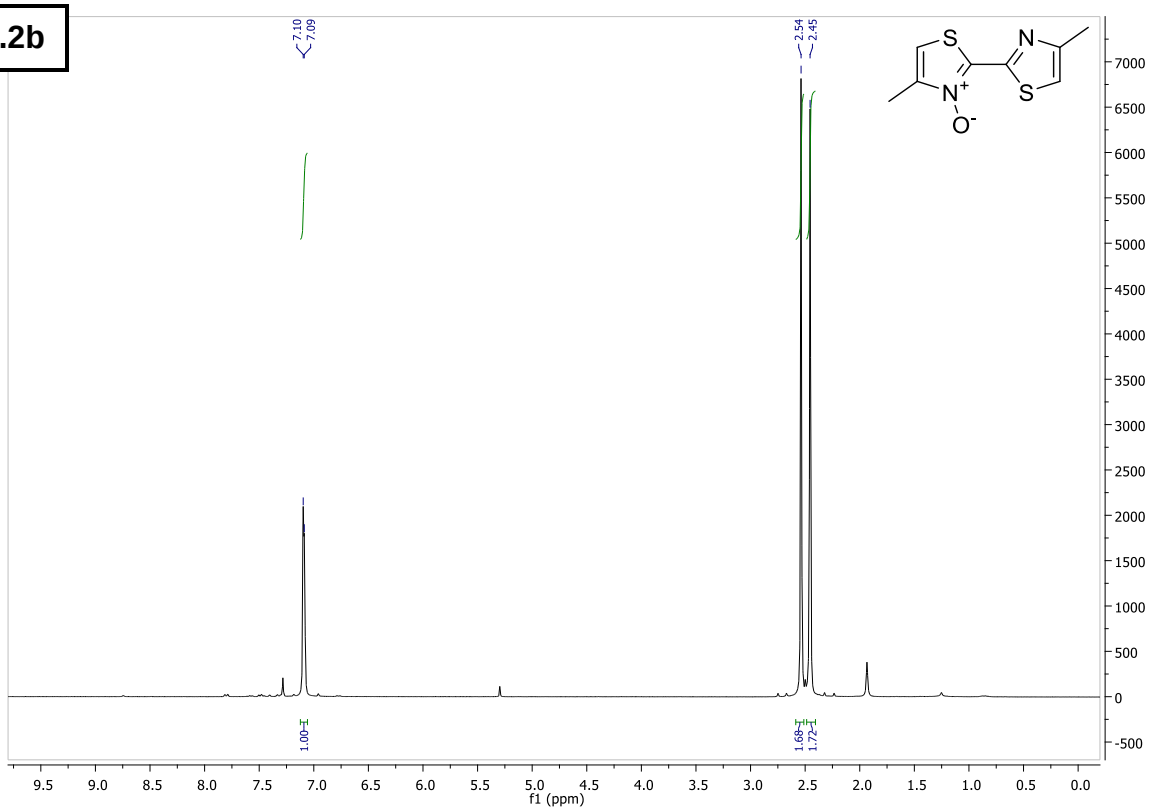
7.10
7.09
2.54
2.45
1.00
1.68
1.72
f1 (ppm)

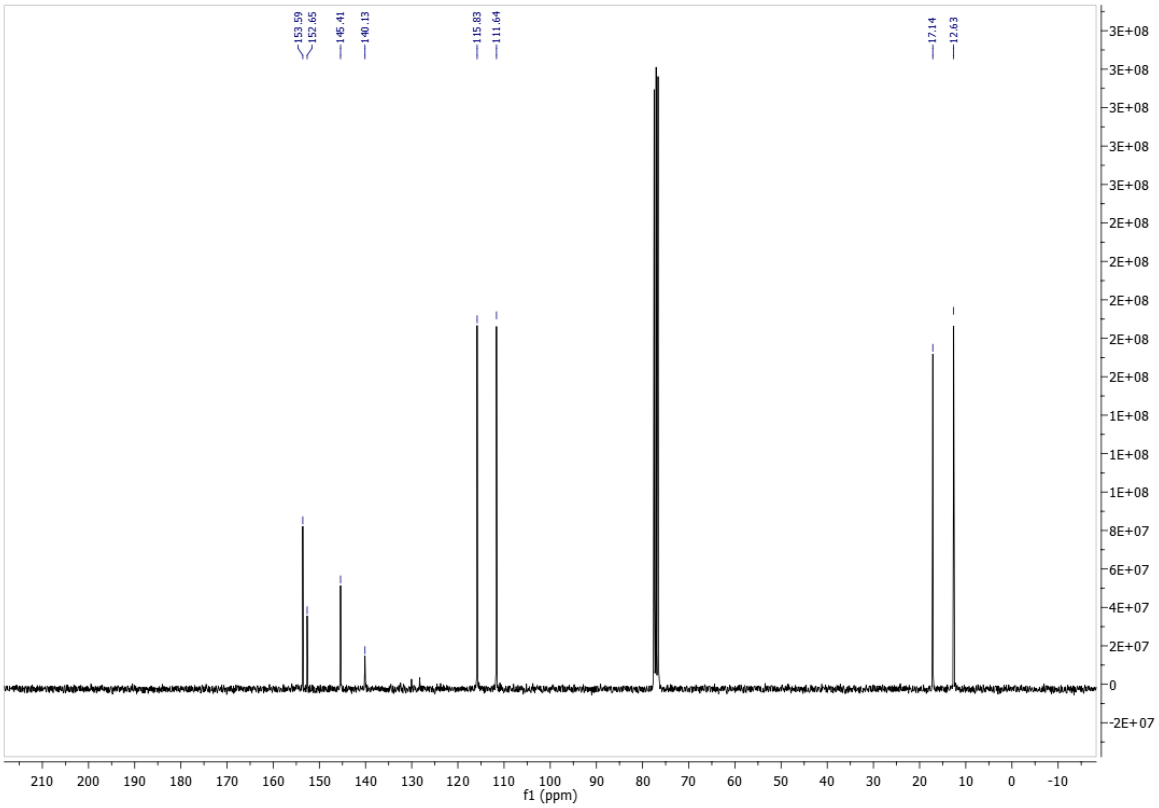
153.59
152.65
145.41
140.13
115.83
111.64
17.14
12.63
f1 (ppm)

3.2c

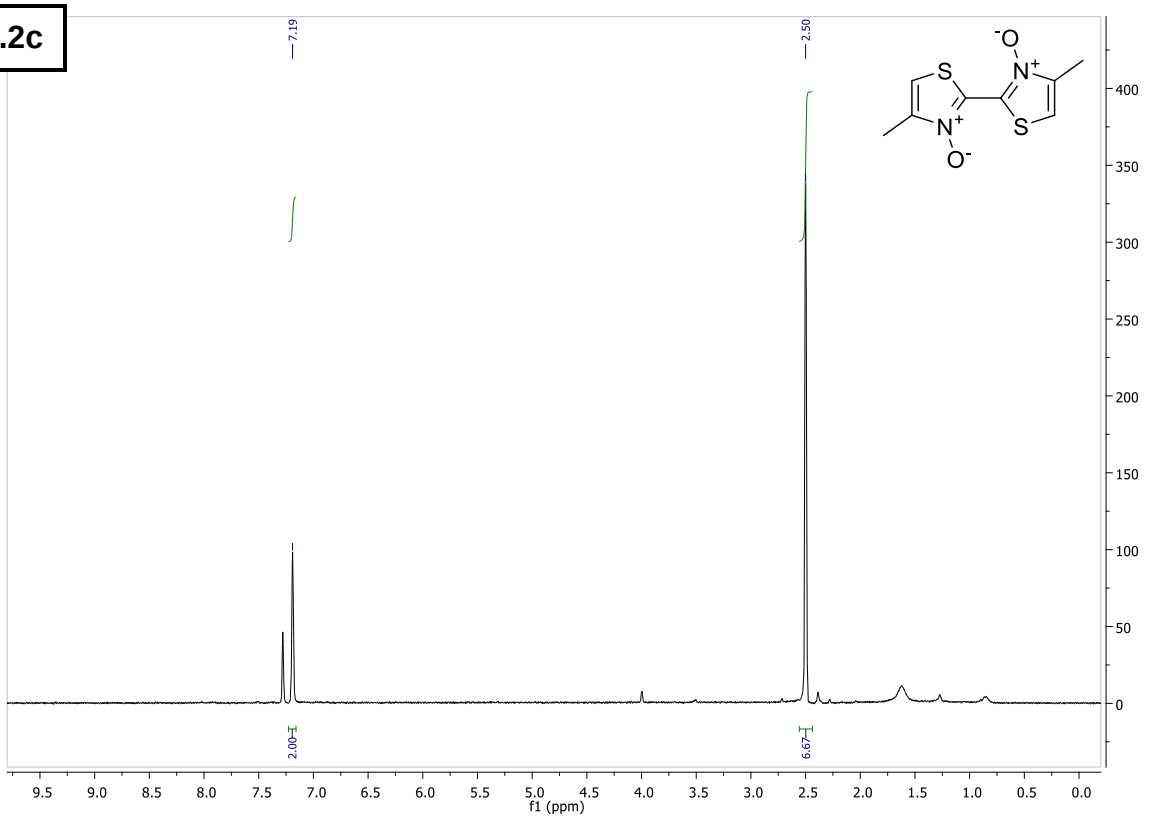
7.19
2.50
2.00
6.67
f1 (ppm)

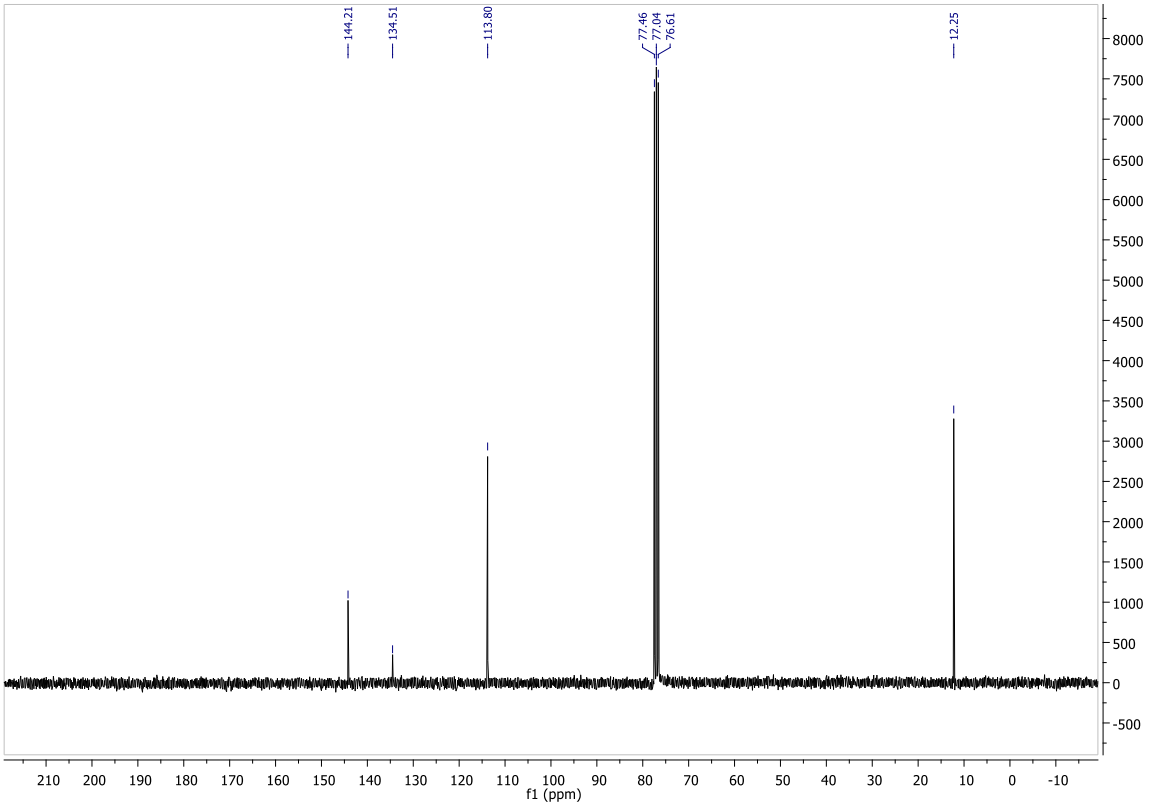
144.21
134.51
113.80
77.46
77.04
76.61
12.25
f1 (ppm)

3.3a

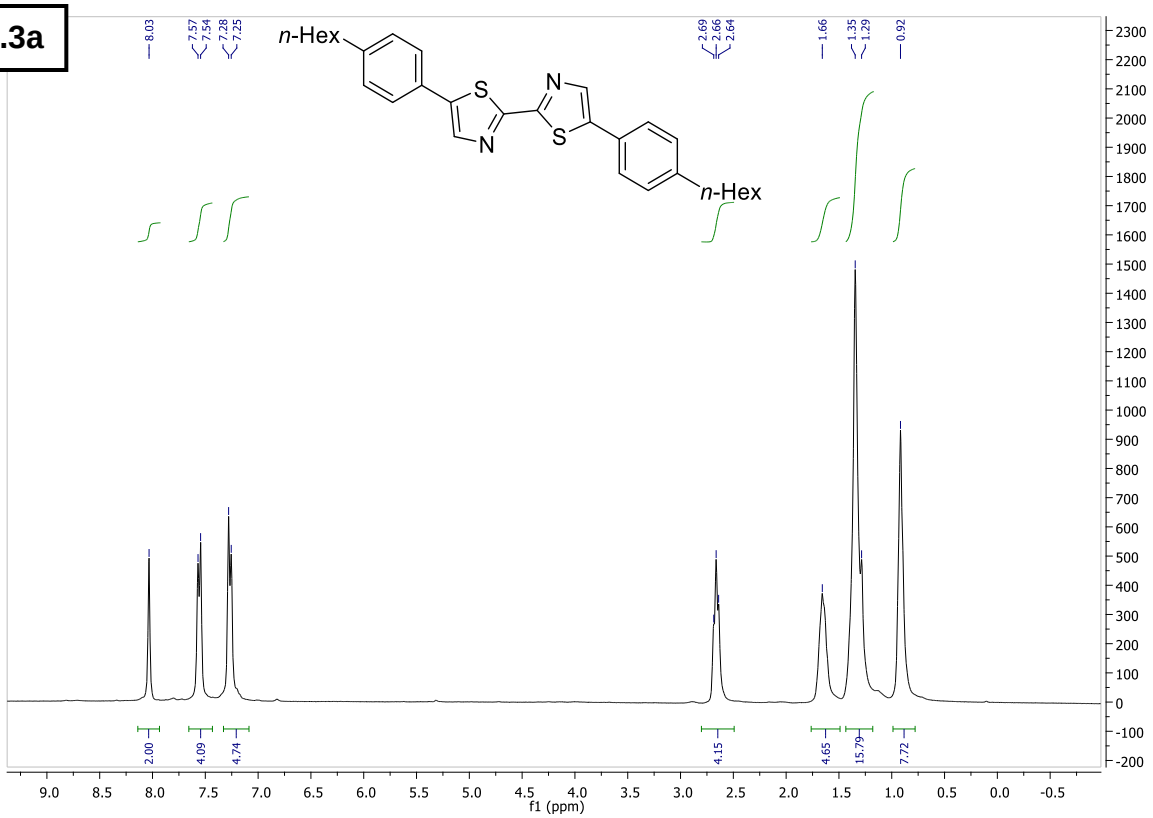
8.03
7.57
7.54
7.28
7.25
n-Hex
S
N
N
S
n-Hex
2.69
2.66
2.64
1.66
1.35
1.29
0.92
2.00
4.09
4.74
4.15
4.65
15.79
7.72
f1 (ppm)

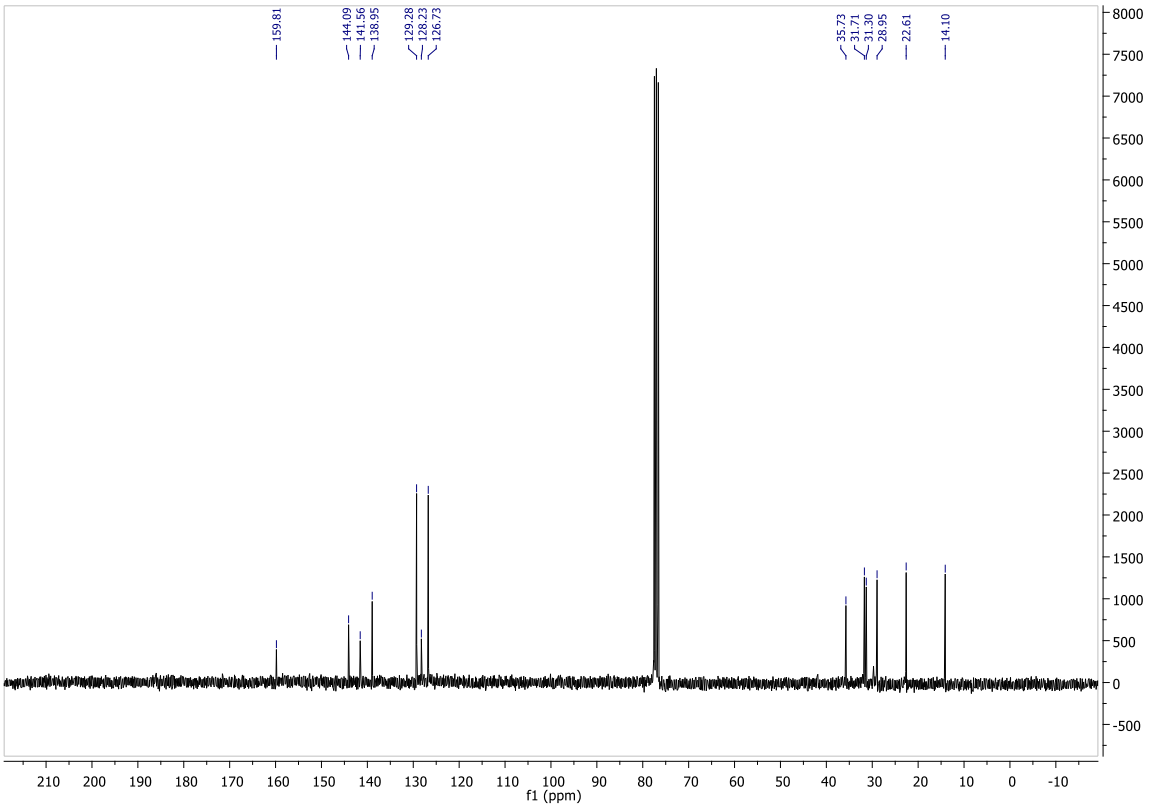
159.81
144.09
141.56
138.95
129.28
128.23
126.73
35.73
31.71
31.30
28.95
22.61
14.10
f1 (ppm)

3.3c

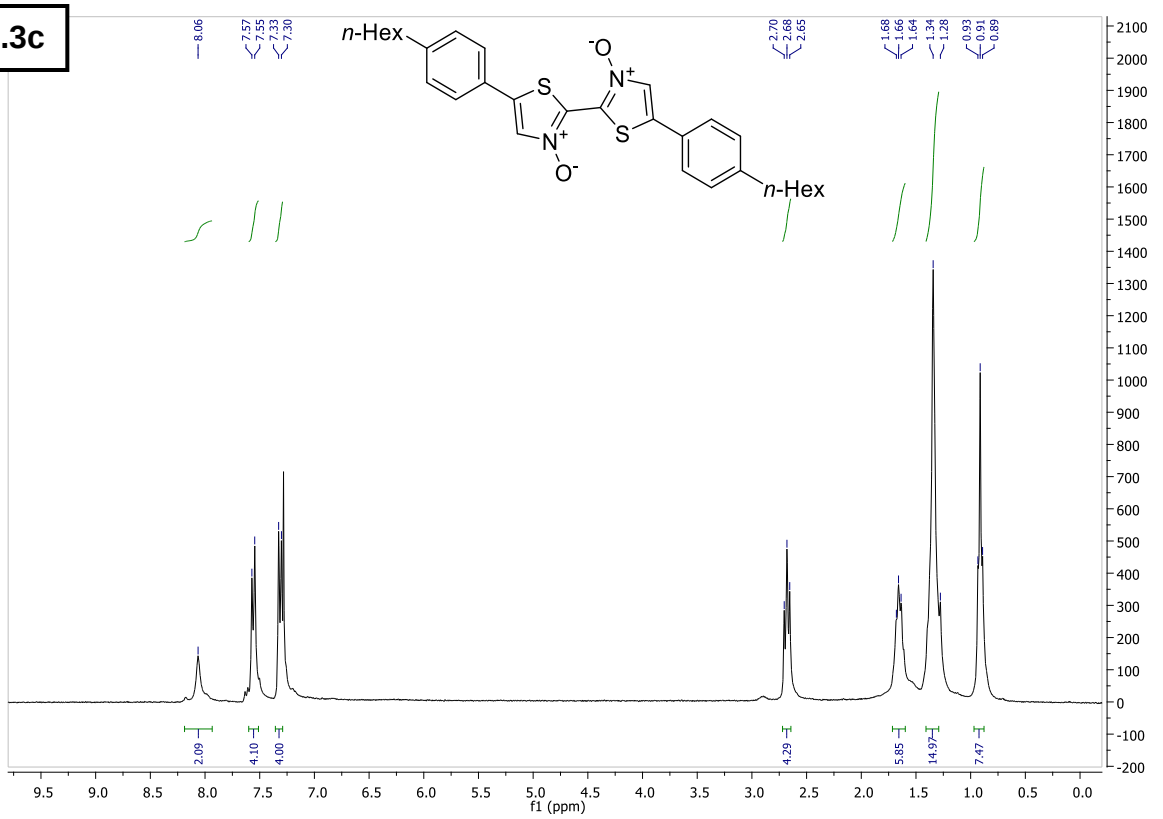
8.06
7.57
7.55
7.33
7.30
2.70
2.68
2.65
1.68
1.66
1.64
1.34
1.28
0.93
0.91
0.89
n-Hex
n-Hex
2.09
4.10
4.00
4.29
5.85
14.97
7.47
f1 (ppm)

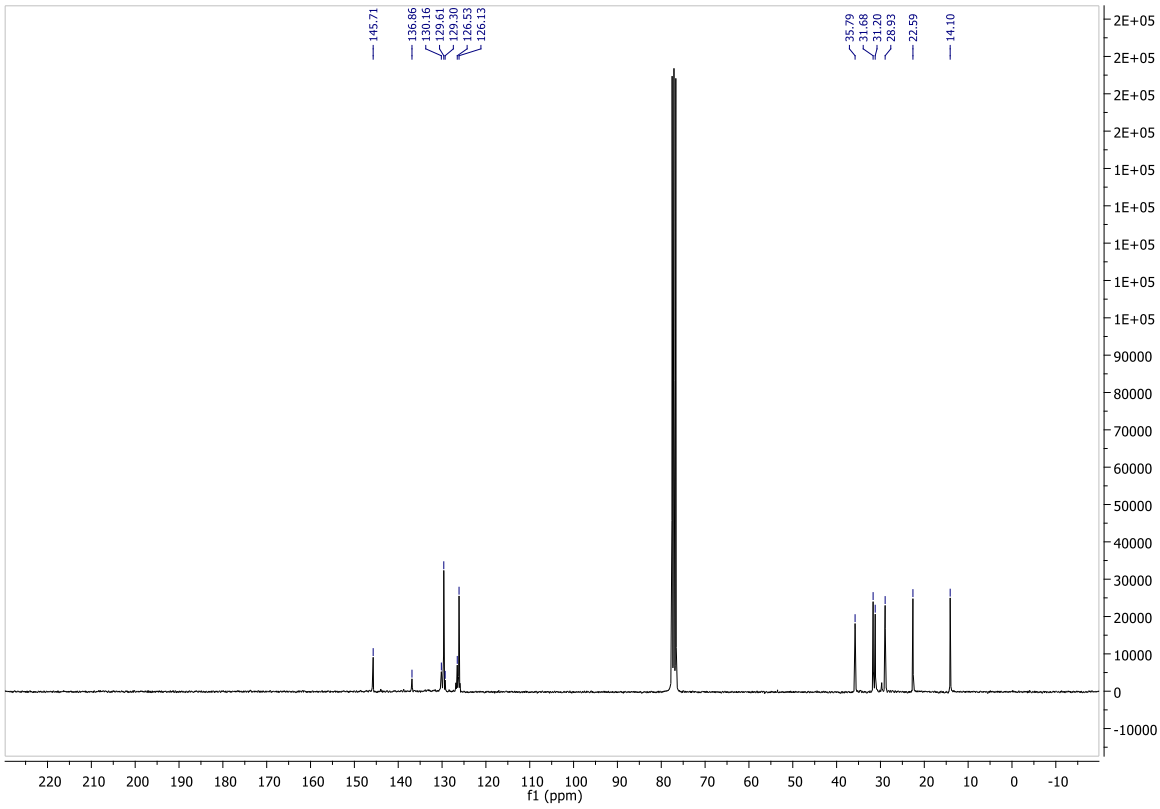
145.71
136.86
130.16
129.61
129.30
126.53
126.13
35.79
31.68
31.20
28.93
22.59
14.10
f1 (ppm)

3.5a

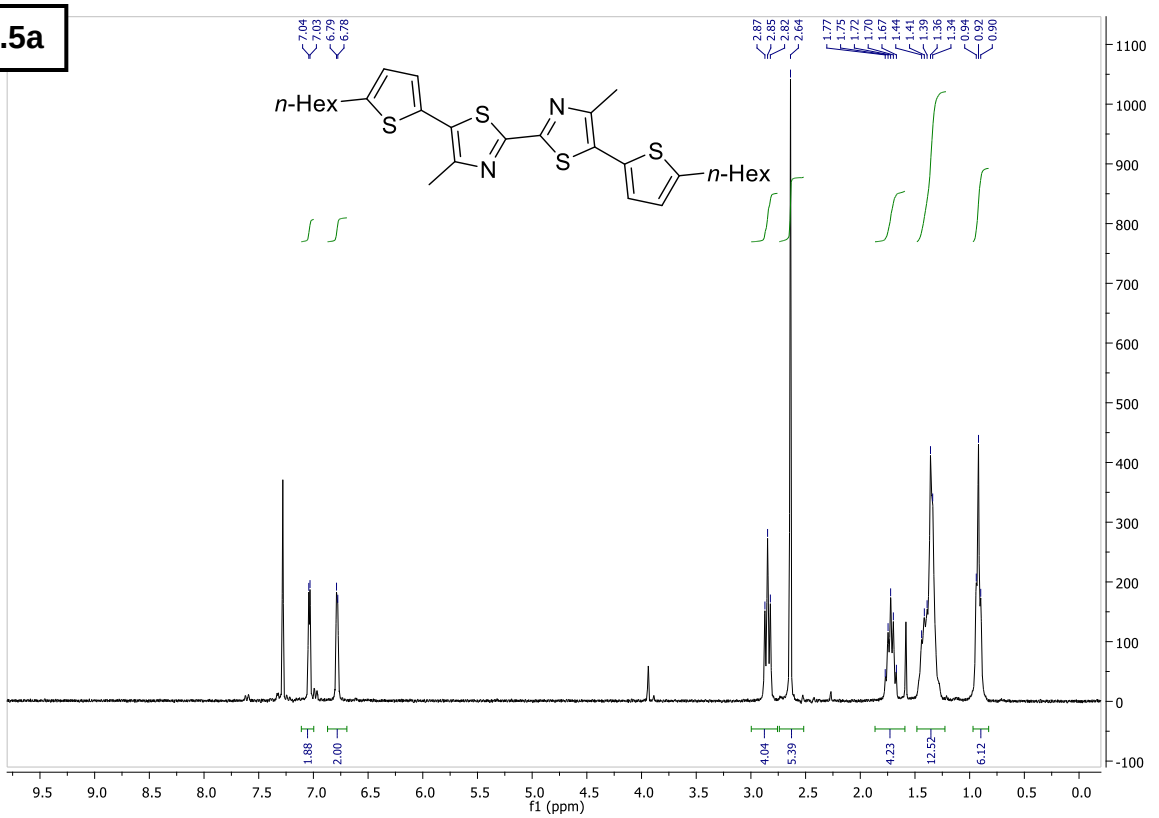
7.04
7.03
6.79
6.78
2.87
2.85
2.82
2.64
1.77
1.75
1.72
1.70
1.67
1.44
1.41
1.39
1.36
1.34
0.94
0.92
0.90
n-Hex
n-Hex
S
S
N
N
S
S
1.88
2.00
4.04
5.39
4.23
12.52
6.12
f1 (ppm)

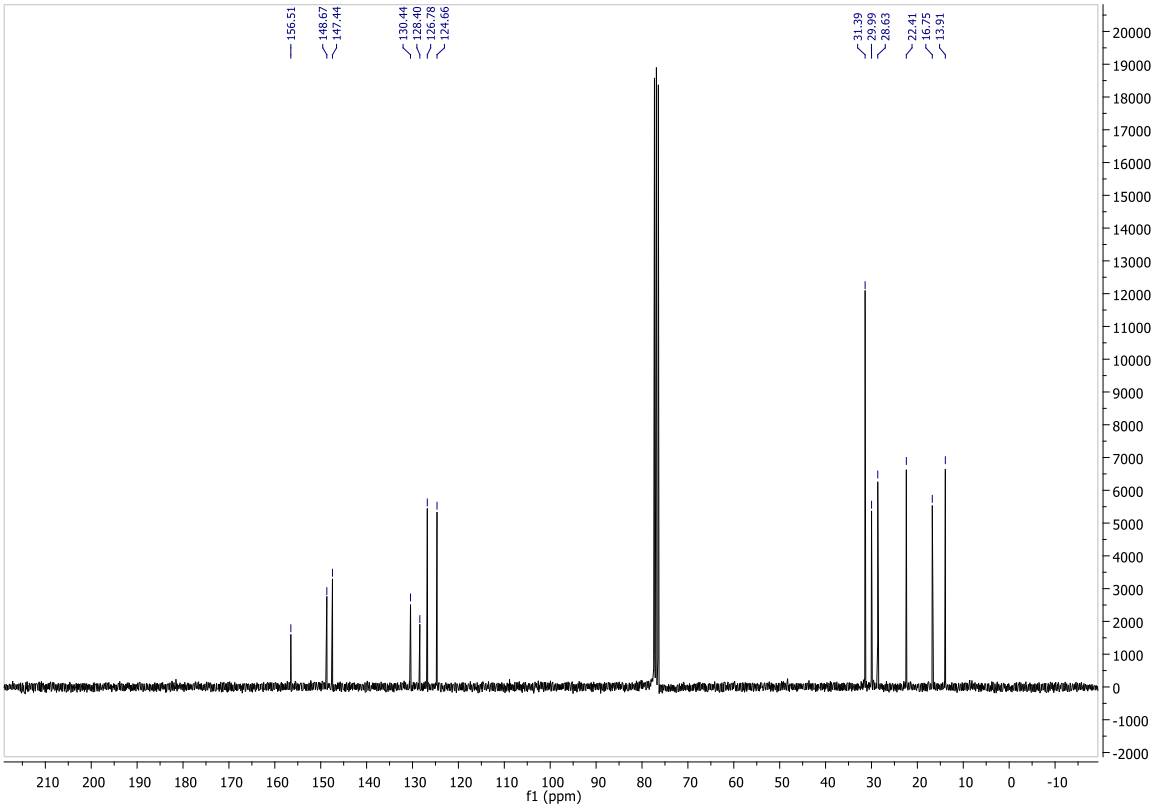
156.51
148.67
147.44
130.44
128.40
126.78
124.66
31.39
29.99
28.63
22.41
15.75
13.91
f1 (ppm)

3.5b

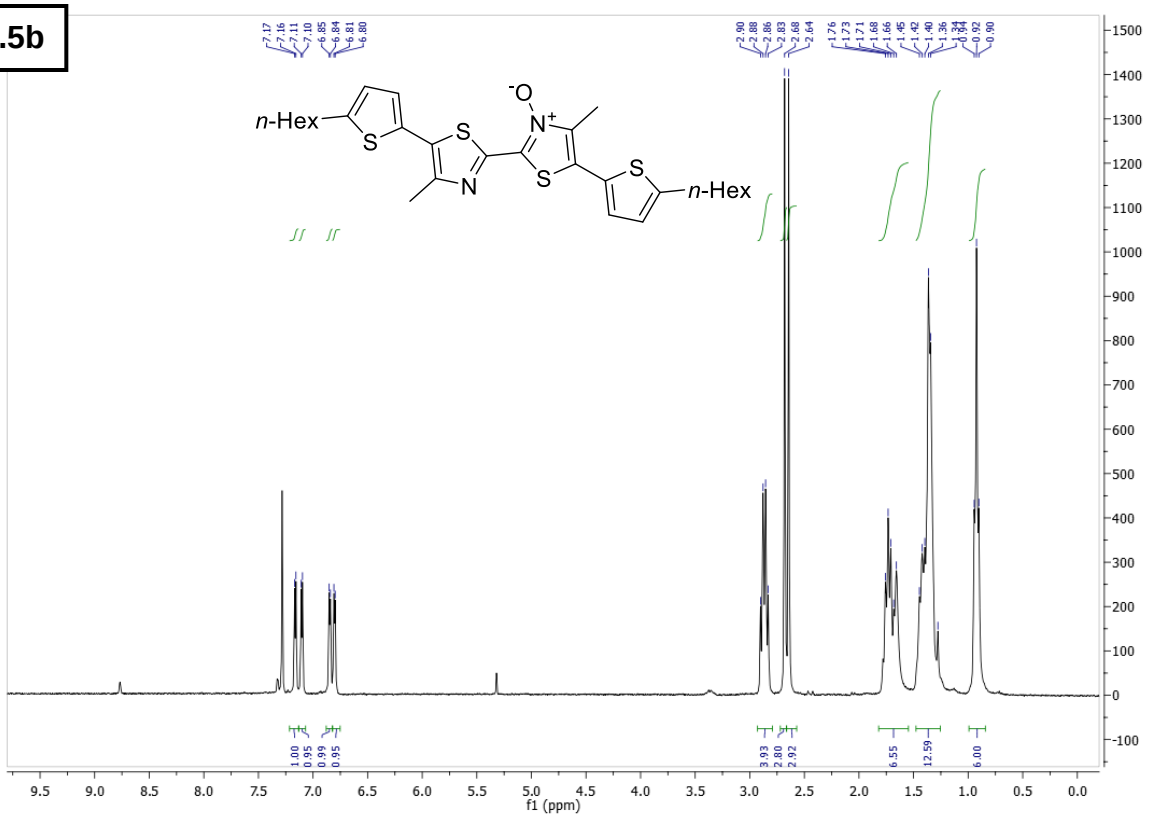

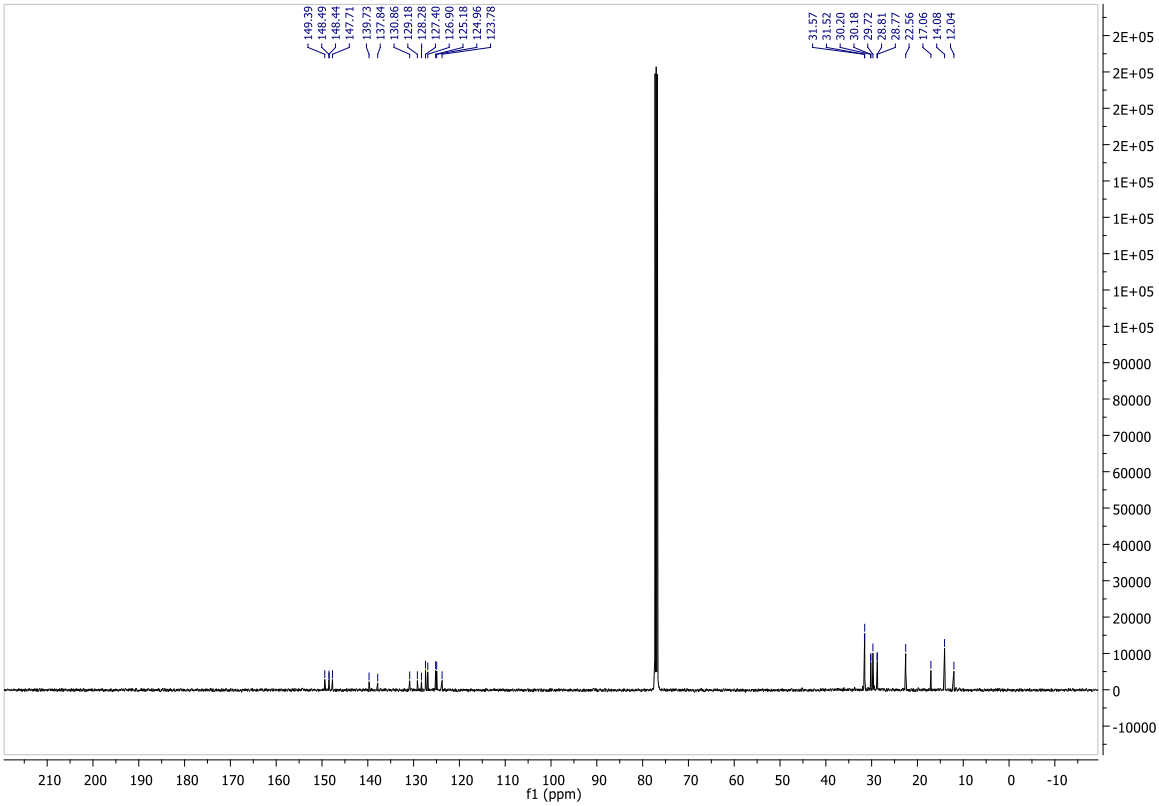

3.5c

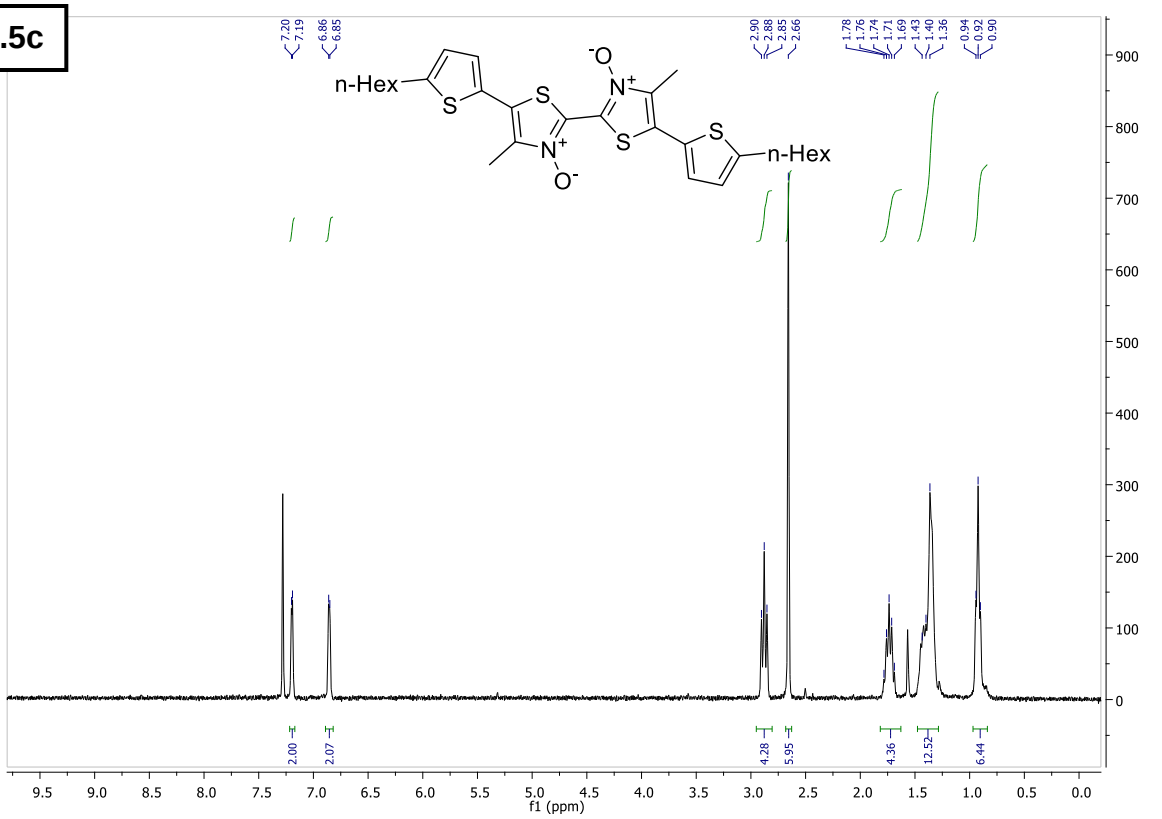
7.20
7.19
6.86
6.85
2.90
2.88
2.85
2.66
1.78
1.76
1.74
1.71
1.69
1.43
1.40
1.36
0.94
0.92
0.90
n-Hex
n-Hex
2.00
2.07
4.28
5.95
4.36
12.52
6.44
f1 (ppm)

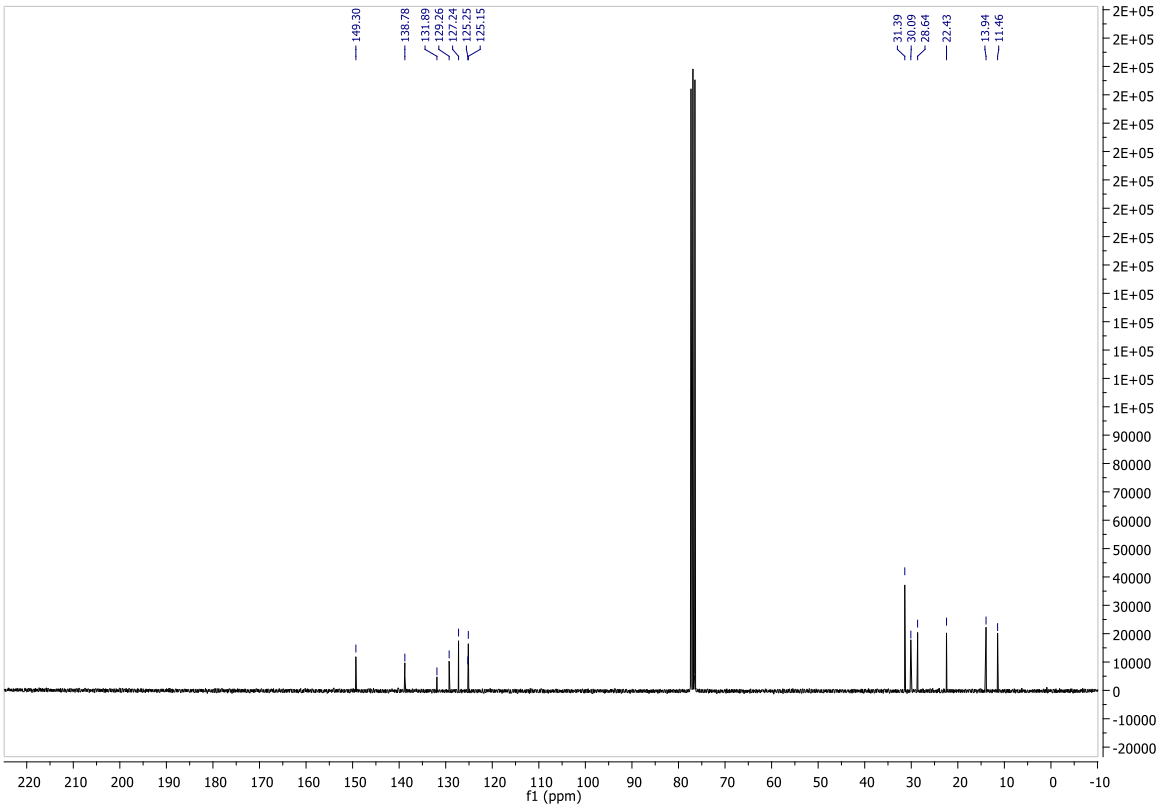
149.30
138.78
131.89
129.26
127.24
125.25
125.15
31.39
30.09
28.64
22.43
13.94
11.46
f1 (ppm)

3.6

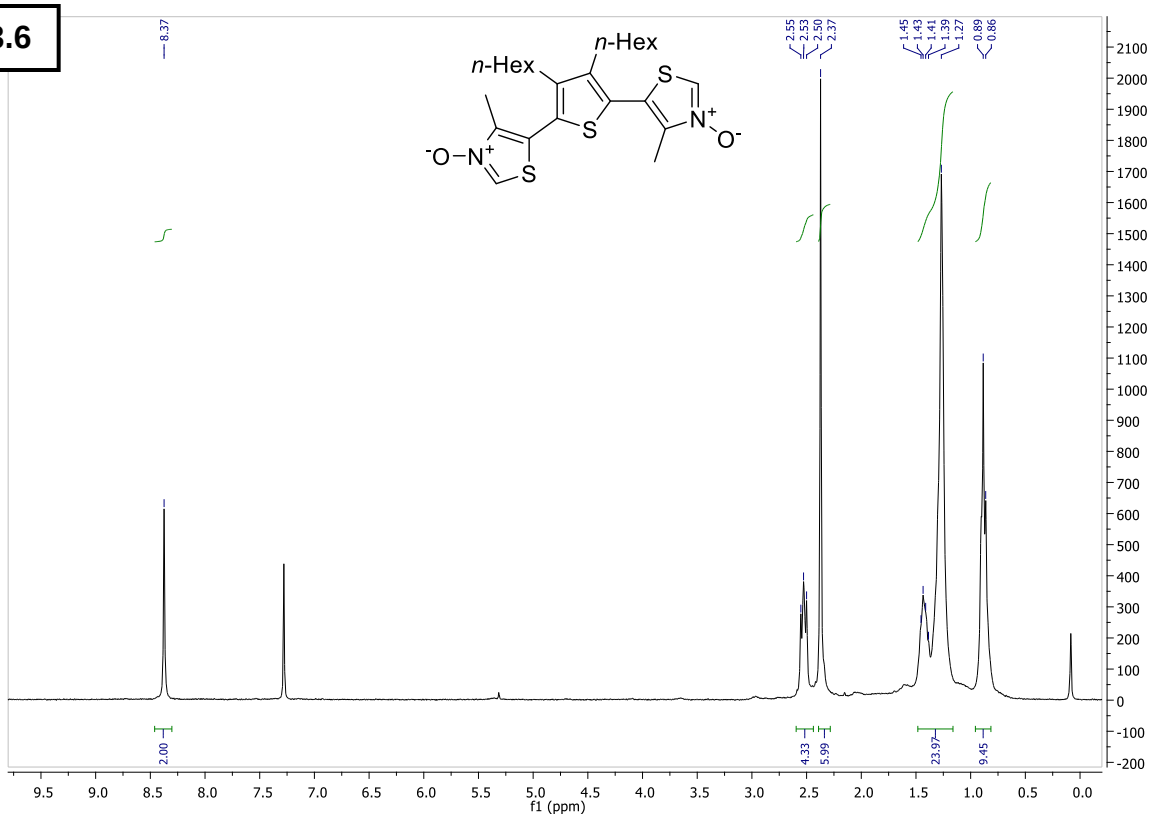
8.37
2.55
2.53
2.50
2.37
1.45
1.43
1.41
1.39
1.27
0.89
0.86
n-Hex
n-Hex
S
S
S
N+
O-
-O
N+
2.00
4.33
5.99
23.97
9.45
f1 (ppm)

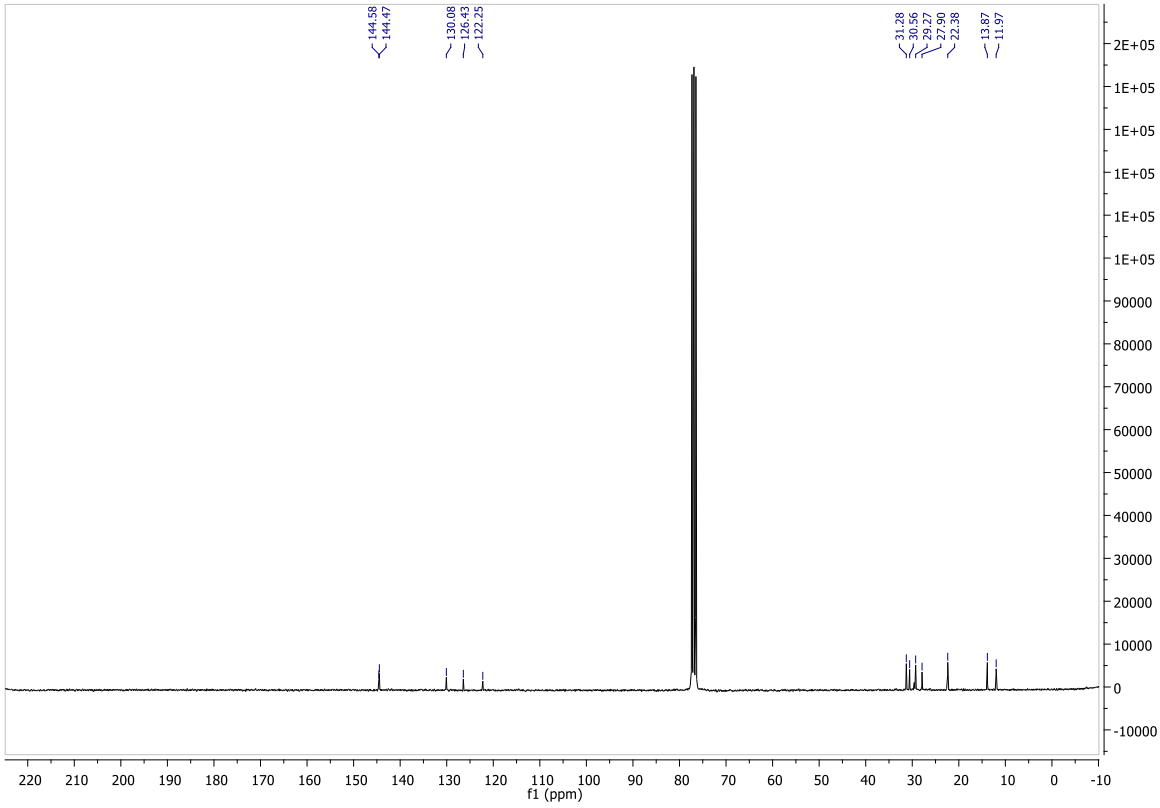
144.58
144.47
130.08
126.43
122.25
31.28
30.56
29.27
27.90
22.38
13.87
11.97
f1 (ppm)

3.7b

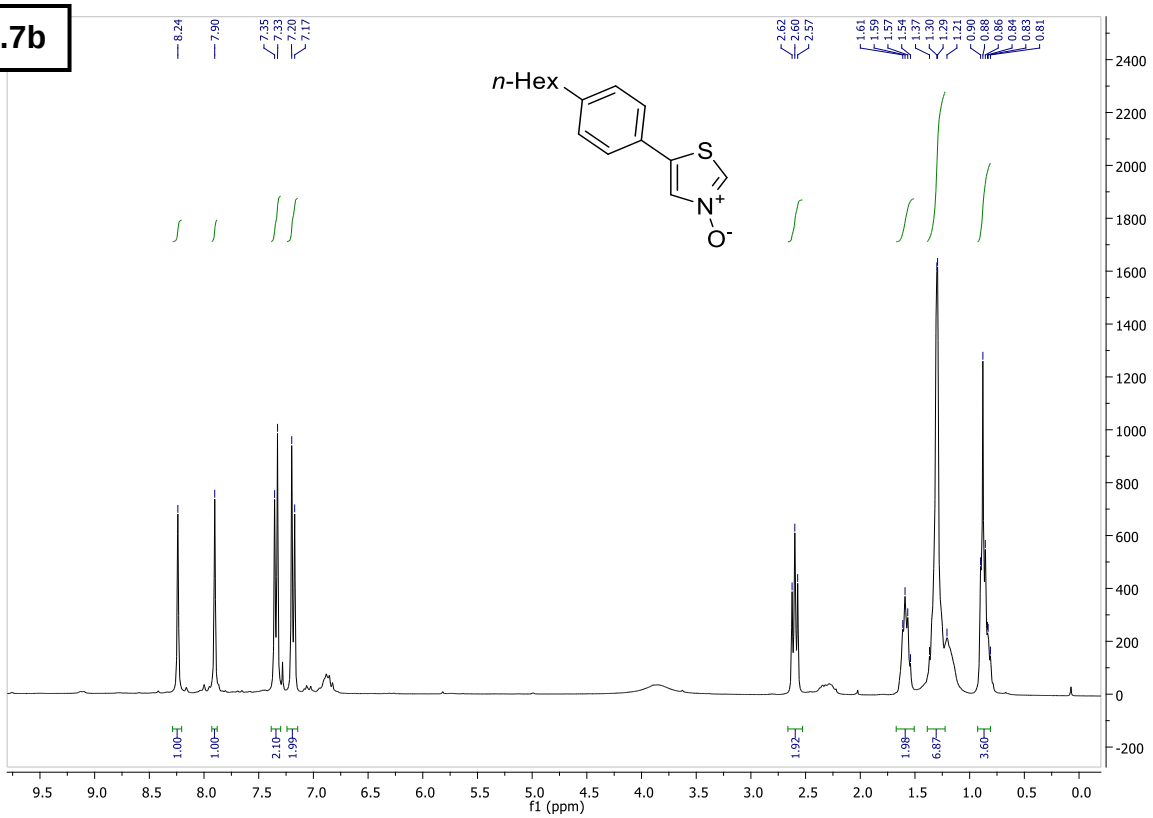
8.24
7.90
7.35
7.33
7.20
7.17
2.62
2.60
2.57
1.61
1.59
1.57
1.54
1.37
1.30
1.29
1.21
0.90
0.88
0.86
0.84
0.83
0.81
n-Hex
S
N+
O-
1.00
1.00
2.10
1.99
1.92
1.98
6.87
3.60
f1 (ppm)

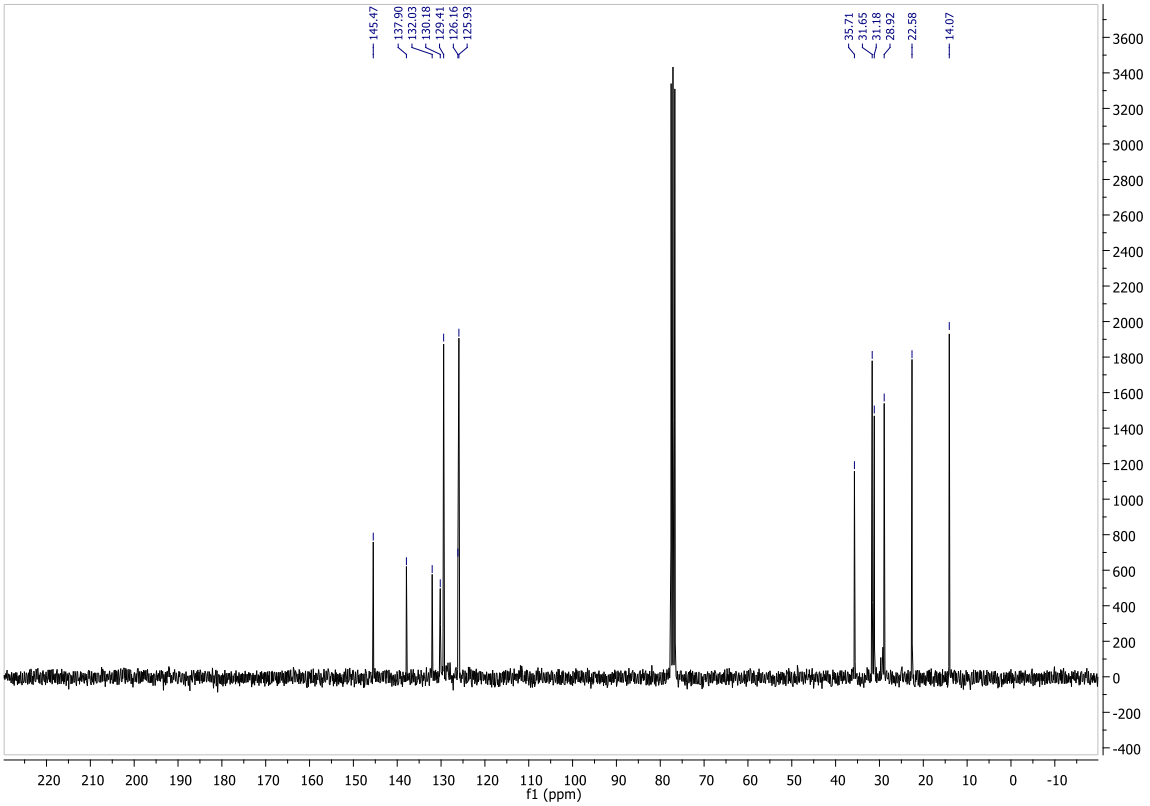
145.47
137.90
132.03
130.18
129.41
126.16
125.93
35.71
31.65
31.18
28.92
22.58
14.07
f1 (ppm)

3.8a

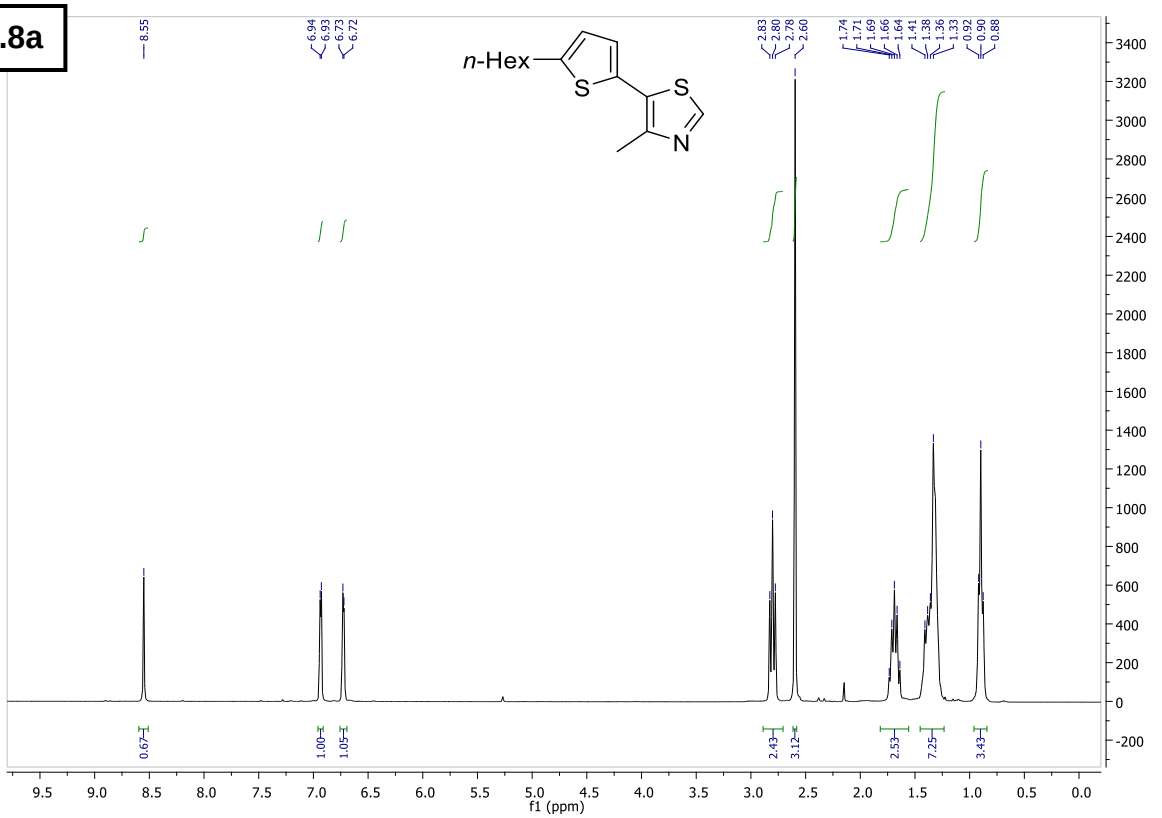
8.55
6.94
6.93
6.73
6.72
2.83
2.80
2.78
2.60
1.74
1.71
1.69
1.66
1.64
1.41
1.38
1.36
1.33
0.92
0.90
0.88
n-Hex
S
S
N
0.67
1.00
1.05
2.43
3.12
2.53
7.25
3.43
f1 (ppm)

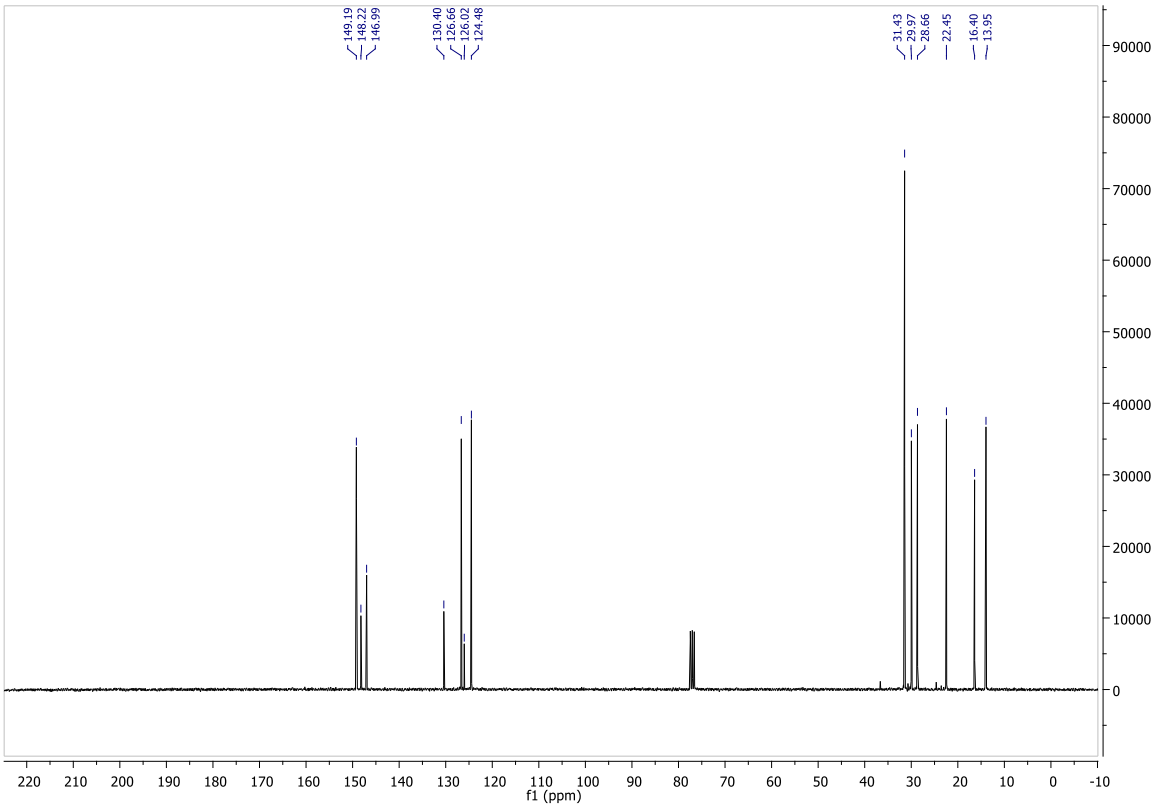
149.19
148.22
146.99
130.40
126.66
126.02
124.48
31.43
29.97
28.66
22.45
16.40
13.95
f1 (ppm)

3.8b

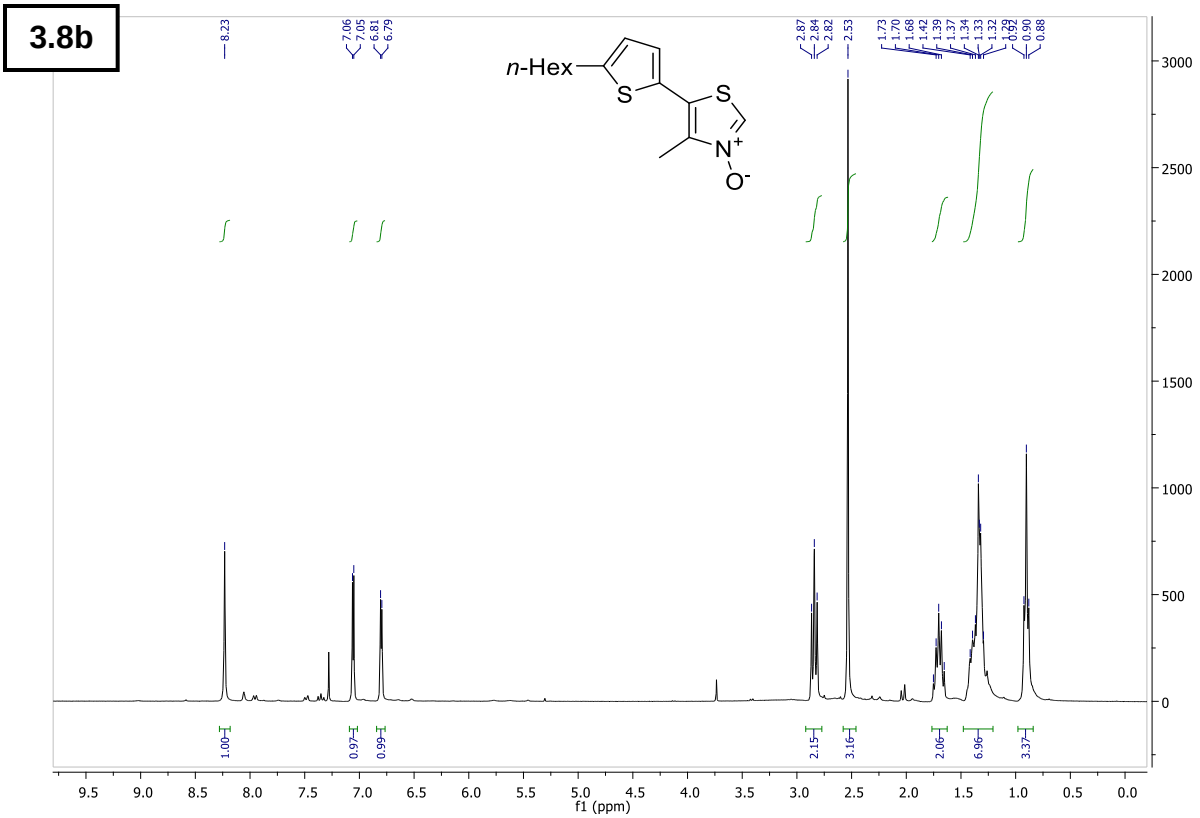
8.23
7.06
7.05
6.81
6.79
2.87
2.84
2.82
2.53
1.73
1.70
1.68
1.42
1.39
1.37
1.34
1.33
1.32
0.92
0.90
0.88
n-Hex
S
S
N+
O-
1.00
0.97
0.99
2.15
3.16
2.06
6.96
3.37
f1 (ppm)

4.1

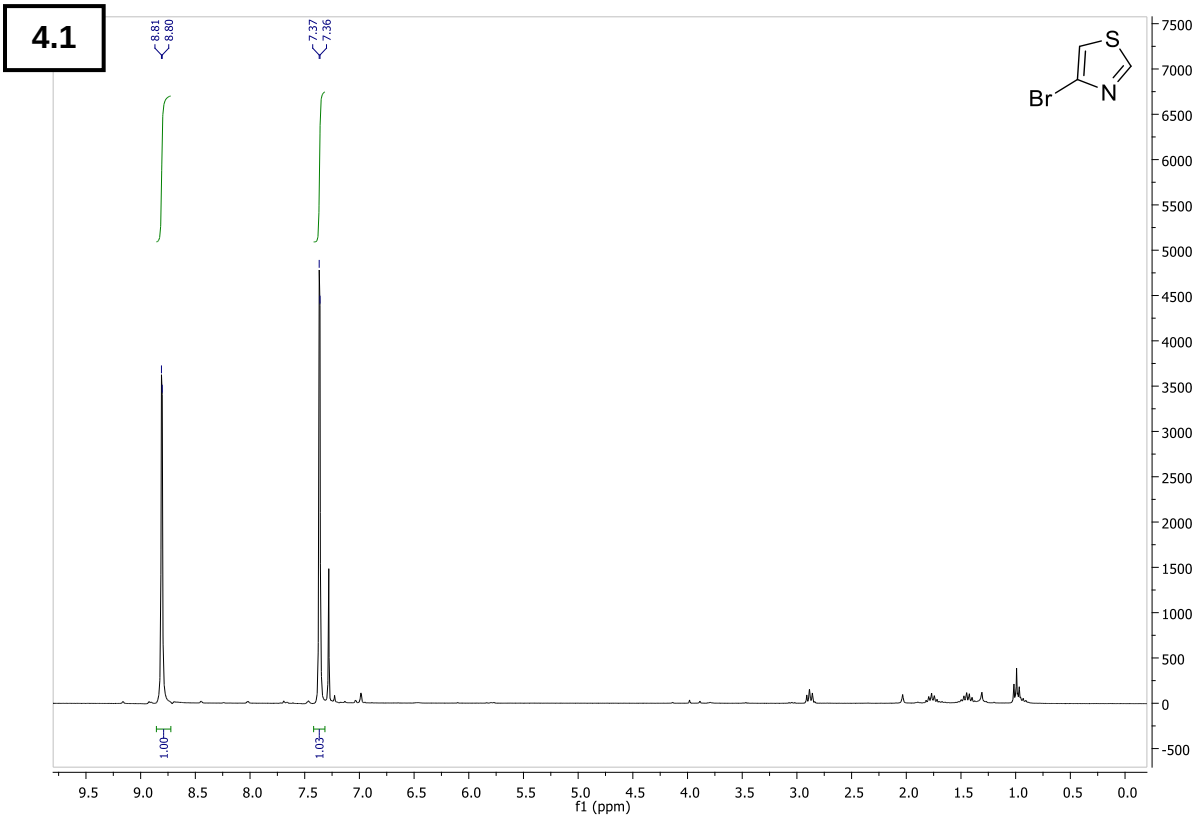
8.81
8.80
7.37
7.36
S
Br
N
1.00
1.03
f1 (ppm)

4.2

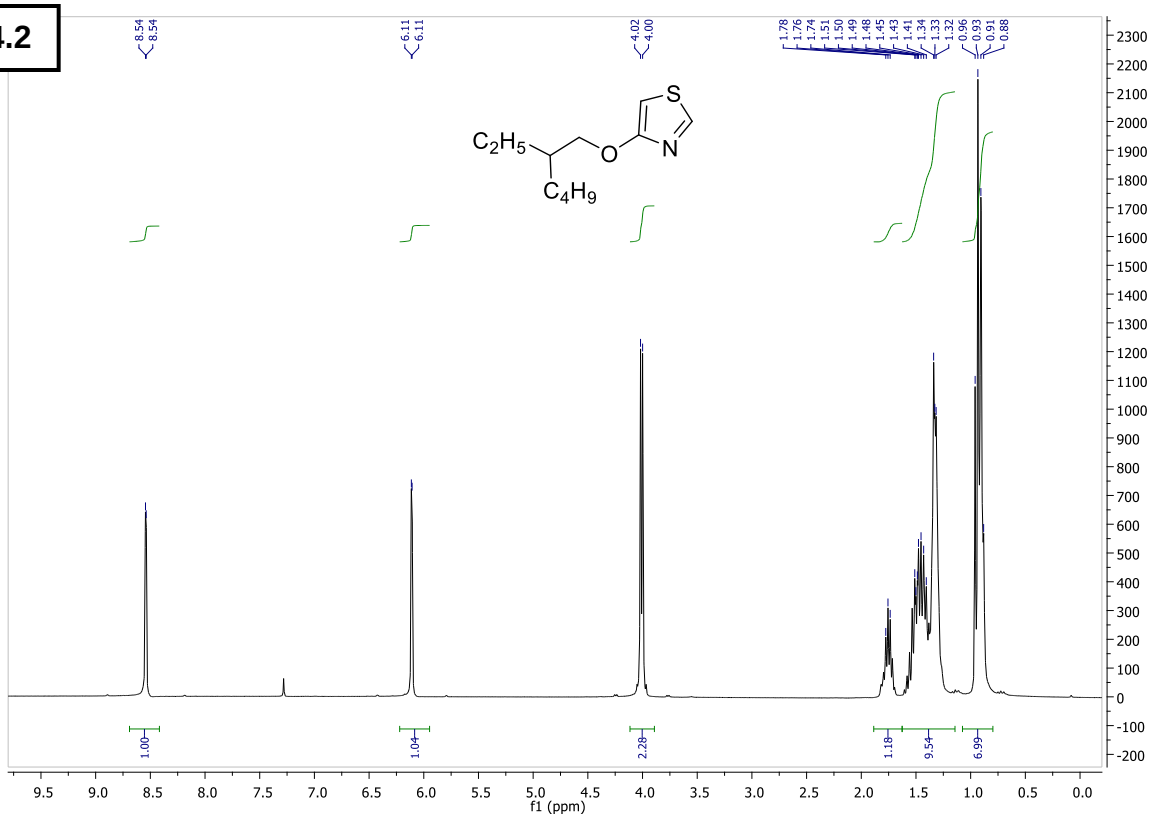
8.54
8.54
6.11
6.11
4.02
4.00
1.78
1.76
1.74
1.51
1.50
1.49
1.48
1.45
1.43
1.41
1.34
1.33
1.32
0.96
0.93
0.91
0.88
S
N
O
C_2H_5
C_4H_9
1.00
1.04
2.28
1.18
9.54
6.99
f1 (ppm)

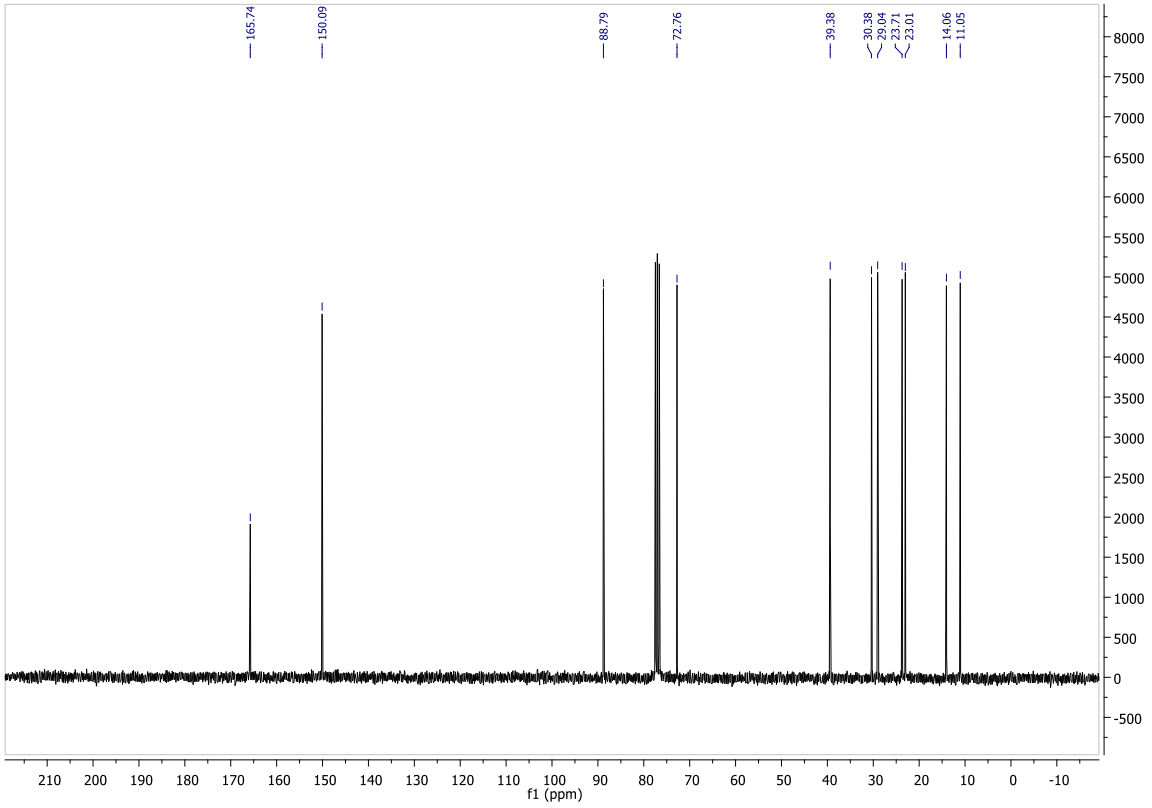
165.74
150.09
88.79
72.76
39.38
30.38
29.04
23.71
23.01
14.06
11.05
f1 (ppm)

4.3

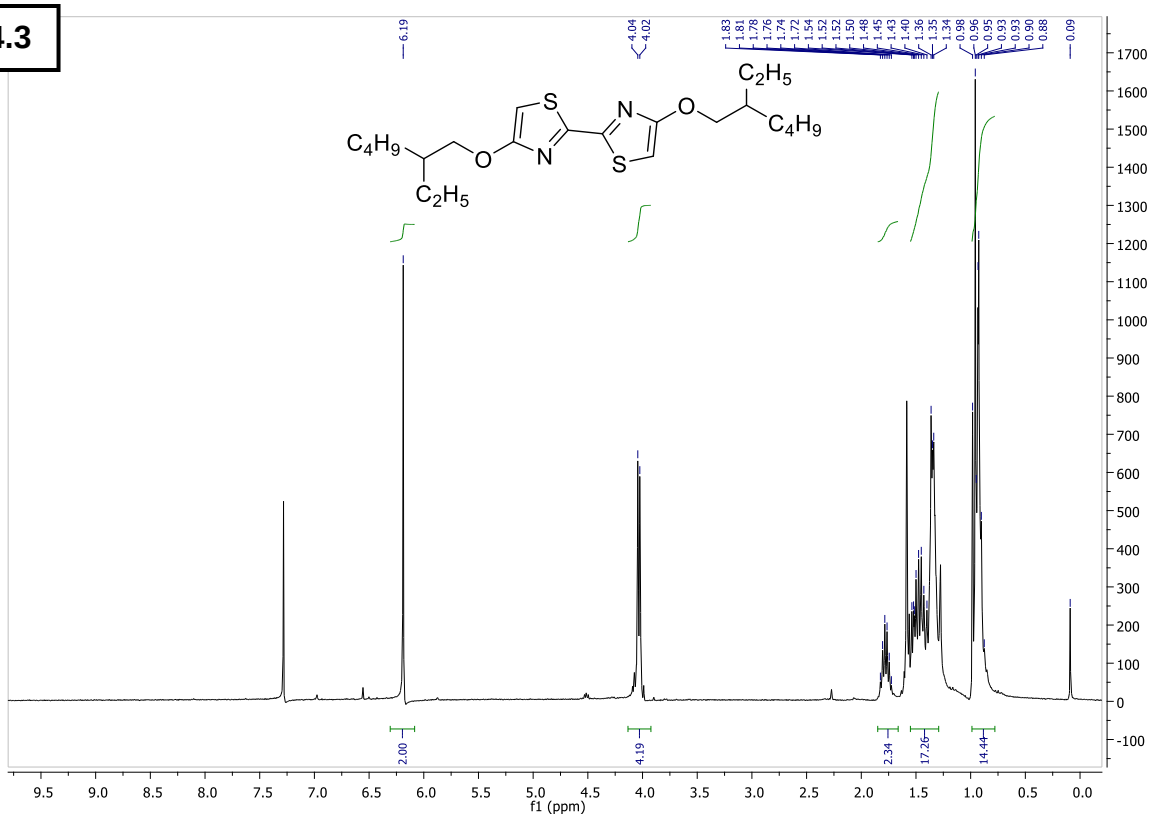
6.19
4.04
4.02
1.83
1.81
1.78
1.76
1.74
1.72
1.54
1.52
1.52
1.50
1.48
1.45
1.43
1.40
1.36
1.35
1.34
0.98
0.96
0.95
0.93
0.93
0.90
0.88
0.09
C2H5
C4H9
C4H9
C2H5
S
N
O
N
O
S
2.00
4.19
2.34
17.26
14.44
f1 (ppm)

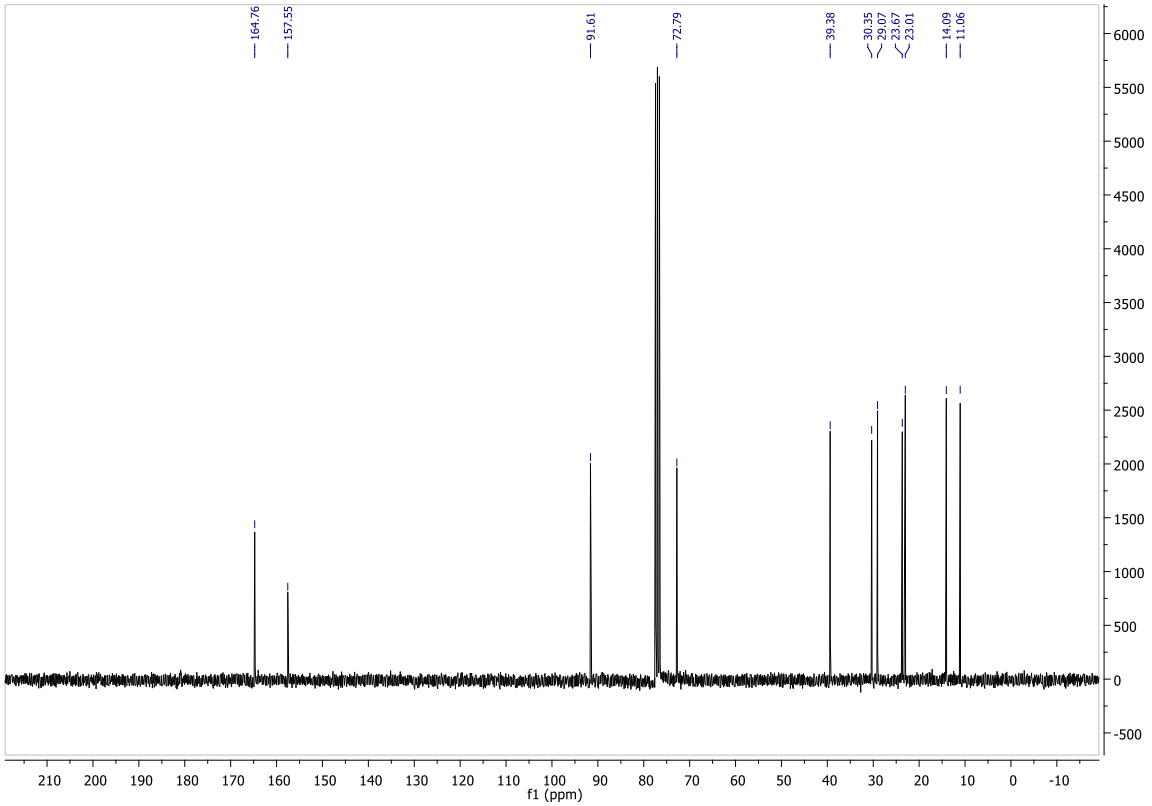
164.76
157.55
91.61
72.79
39.38
30.35
29.07
23.67
23.01
14.09
11.06
f1 (ppm)

5.1

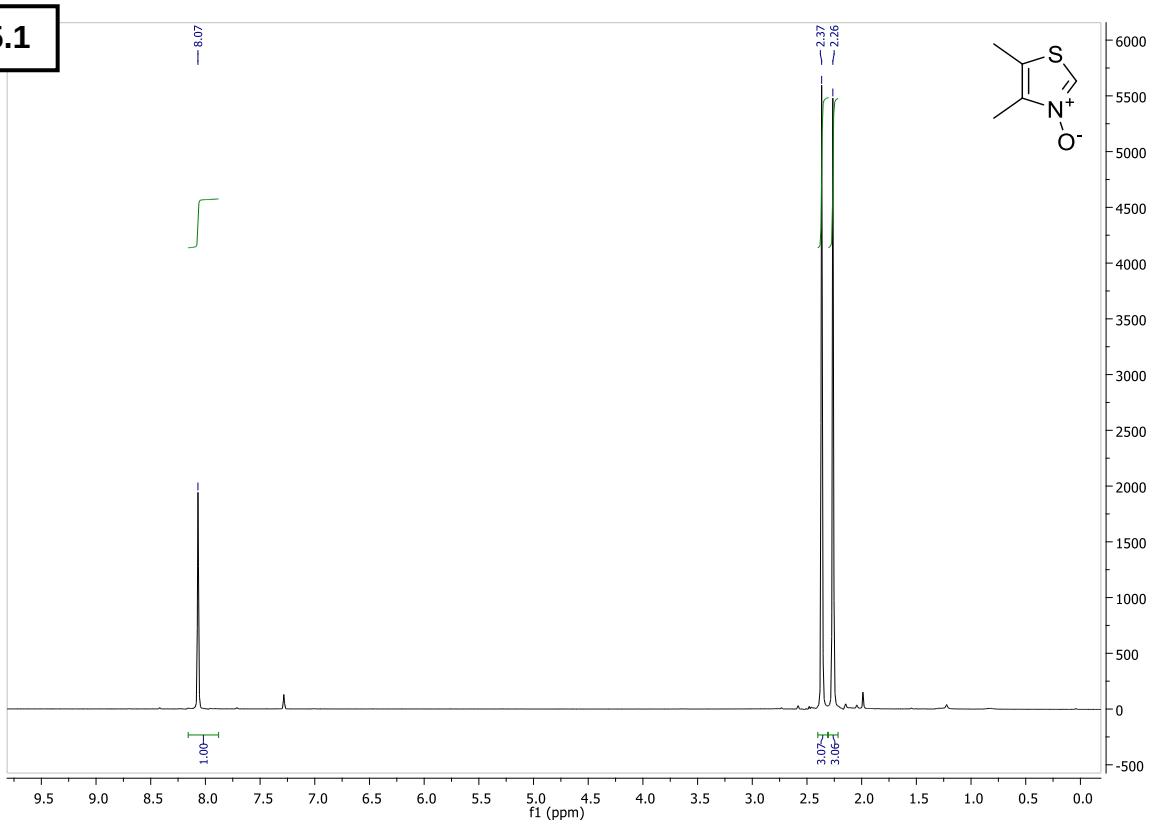

5.2

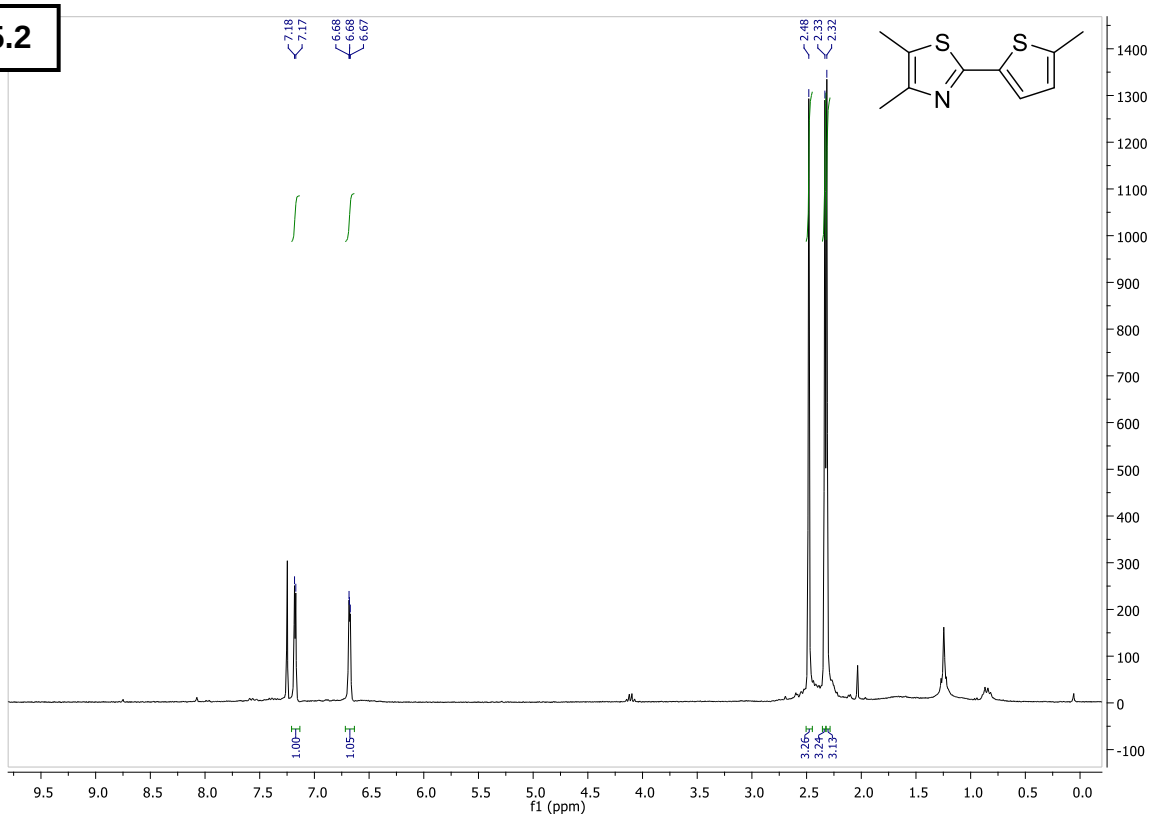
7.18
7.17
6.68
6.68
6.67
2.48
2.33
2.32
S
S
N
1.00
1.05
3.26
3.24
3.13
f1 (ppm)

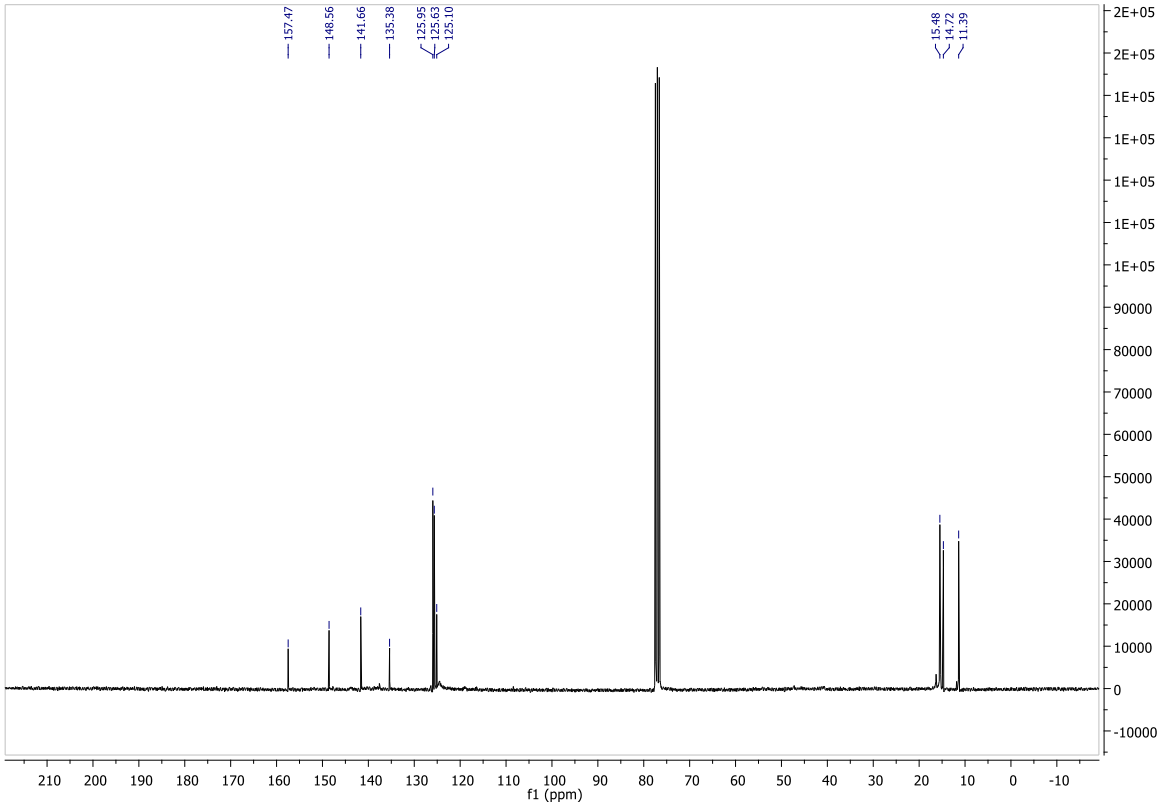
157.47
148.56
141.66
135.38
125.95
125.63
125.10
15.48
14.72
11.39
f1 (ppm)

5.4

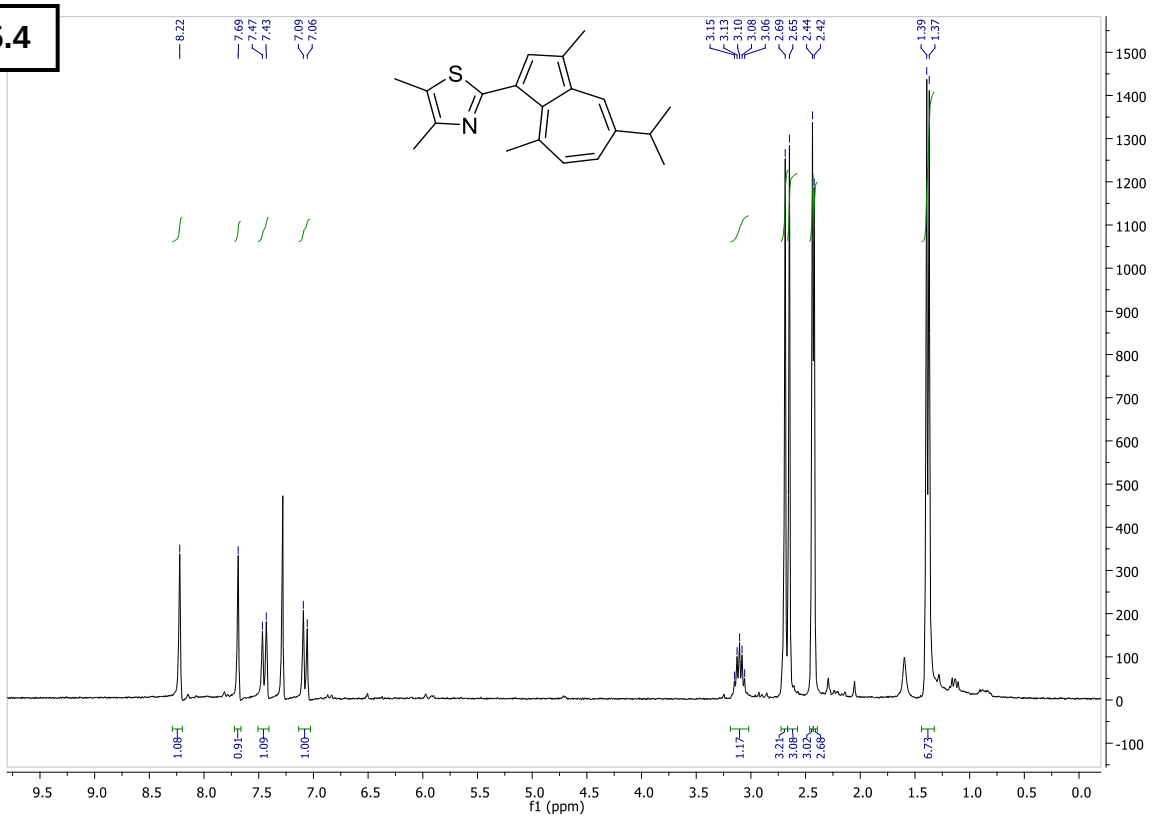
8.22
7.69
7.47
7.43
7.09
7.06
3.15
3.13
3.10
3.08
3.06
2.69
2.65
2.44
2.42
1.39
1.37
S
N
1.08
0.91
1.09
1.00
1.17
3.21
3.08
3.02
2.68
6.73
f1 (ppm)

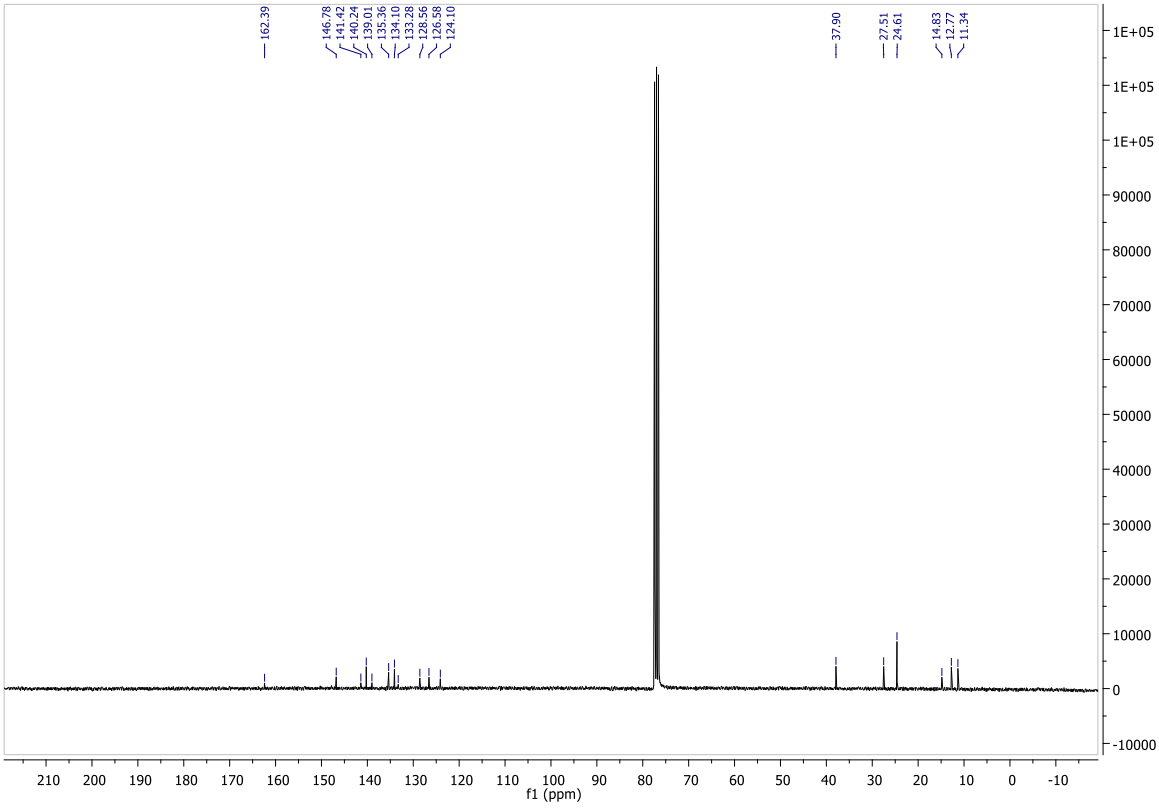
162.39
146.78
141.42
140.24
139.01
135.36
134.10
133.28
128.56
126.58
124.10
37.90
27.51
24.61
14.83
12.77
11.34
f1 (ppm)

5.5

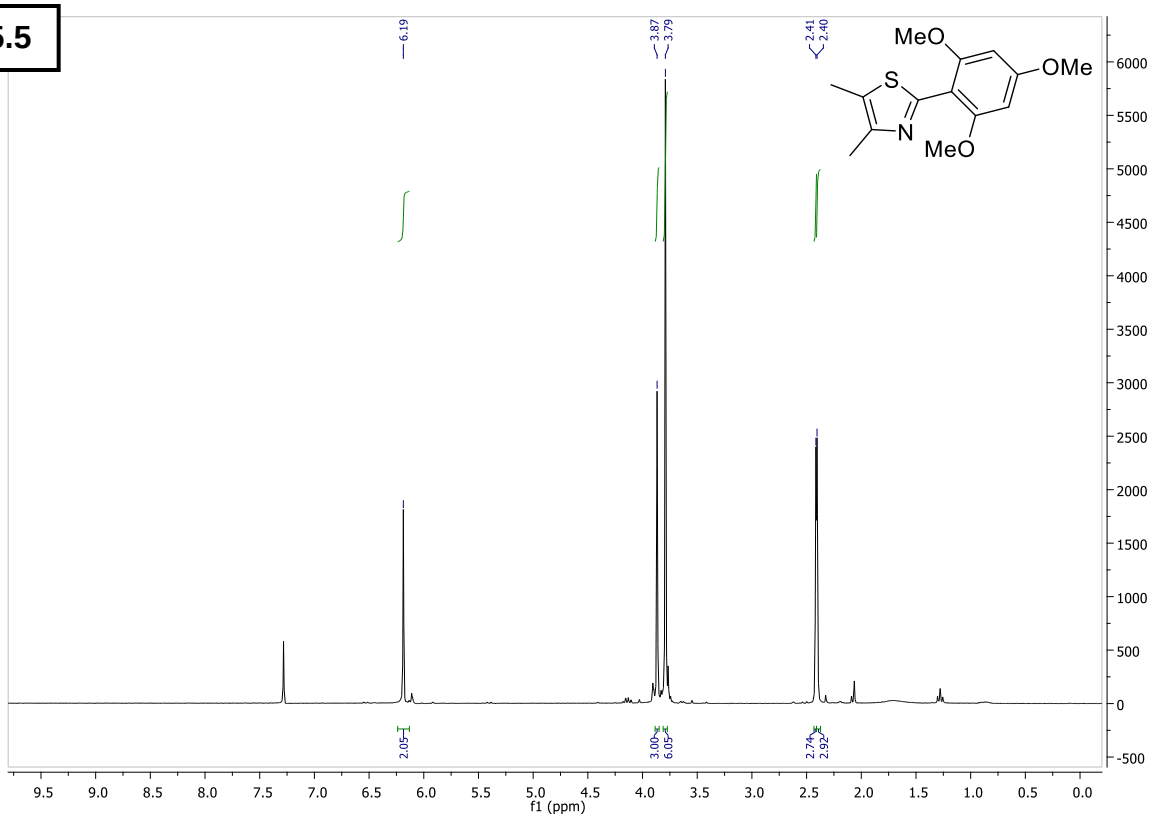
6.19
3.87
3.79
2.41
2.40
MeO
OMe
MeO
S
N
2.05
3.00
6.05
2.74
2.92
f1 (ppm)

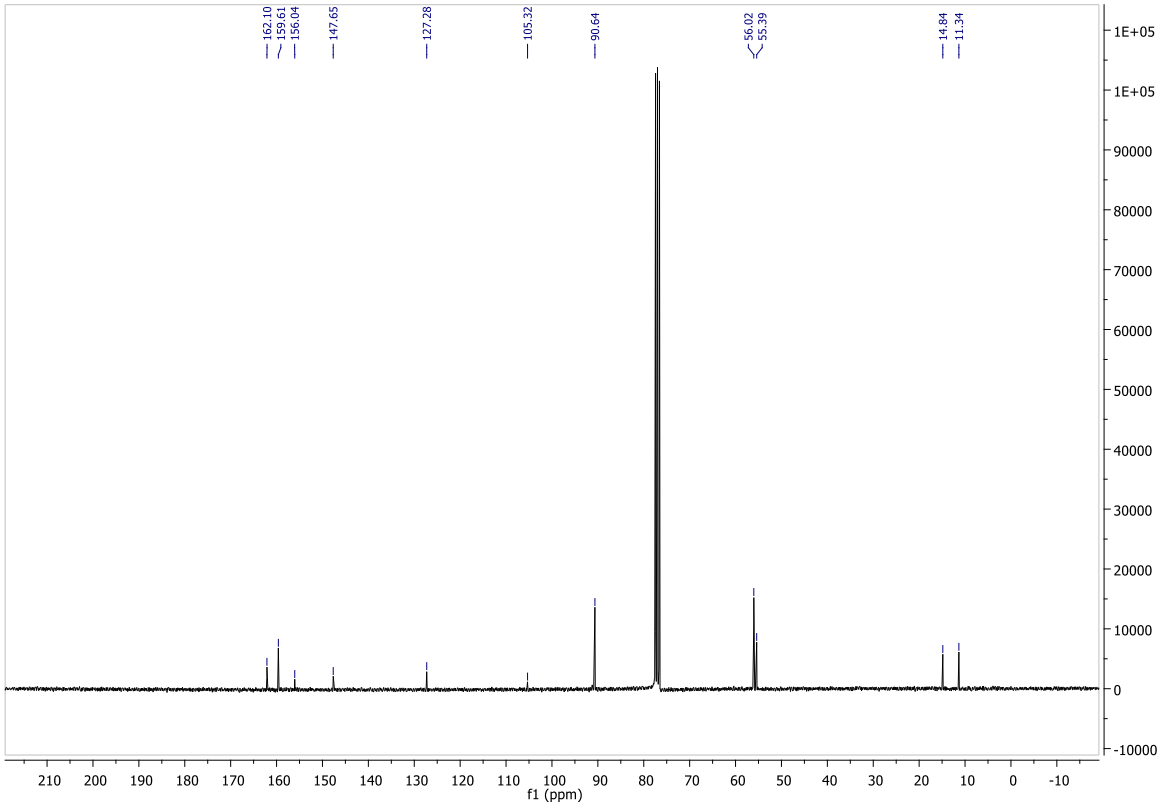
162.10
159.61
156.04
147.65
127.28
105.32
90.64
56.02
55.39
14.84
11.34
f1 (ppm)

5.6

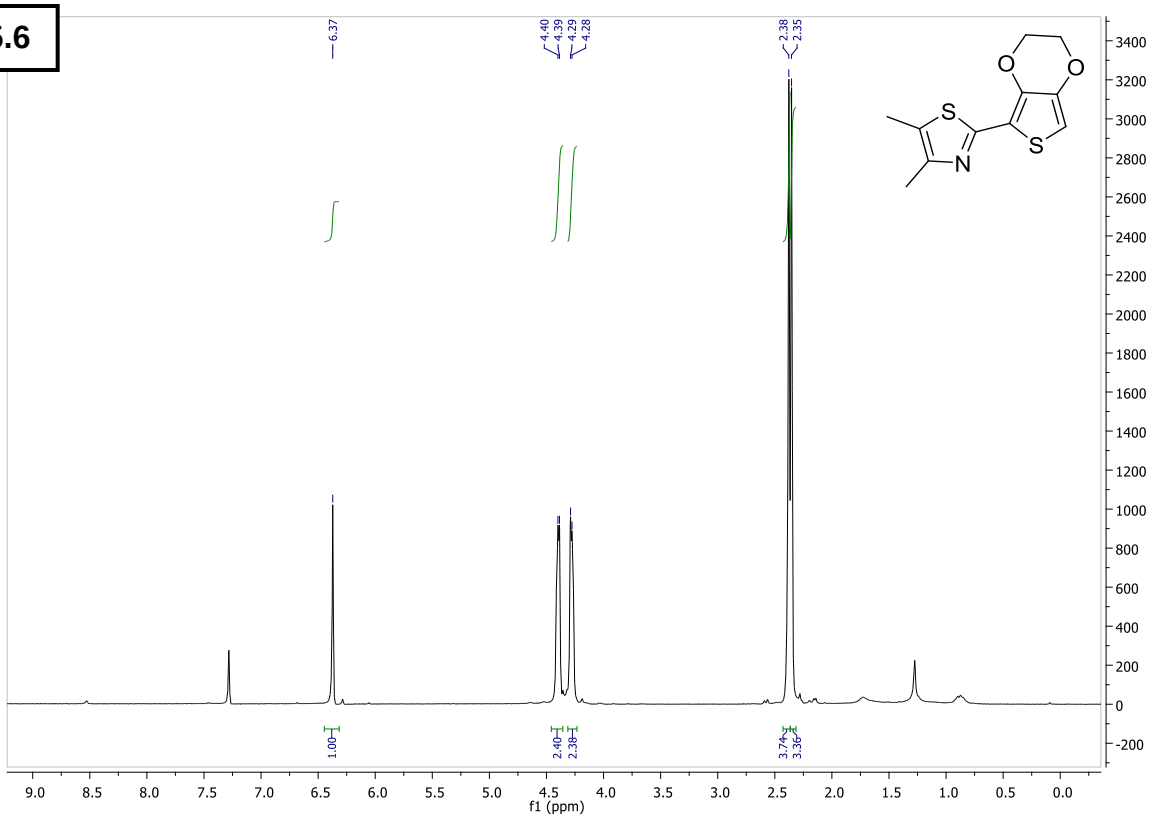
6.37
4.40
4.39
4.29
4.28
2.38
2.35
1.00
2.40
2.38
3.74
3.36
f1 (ppm)

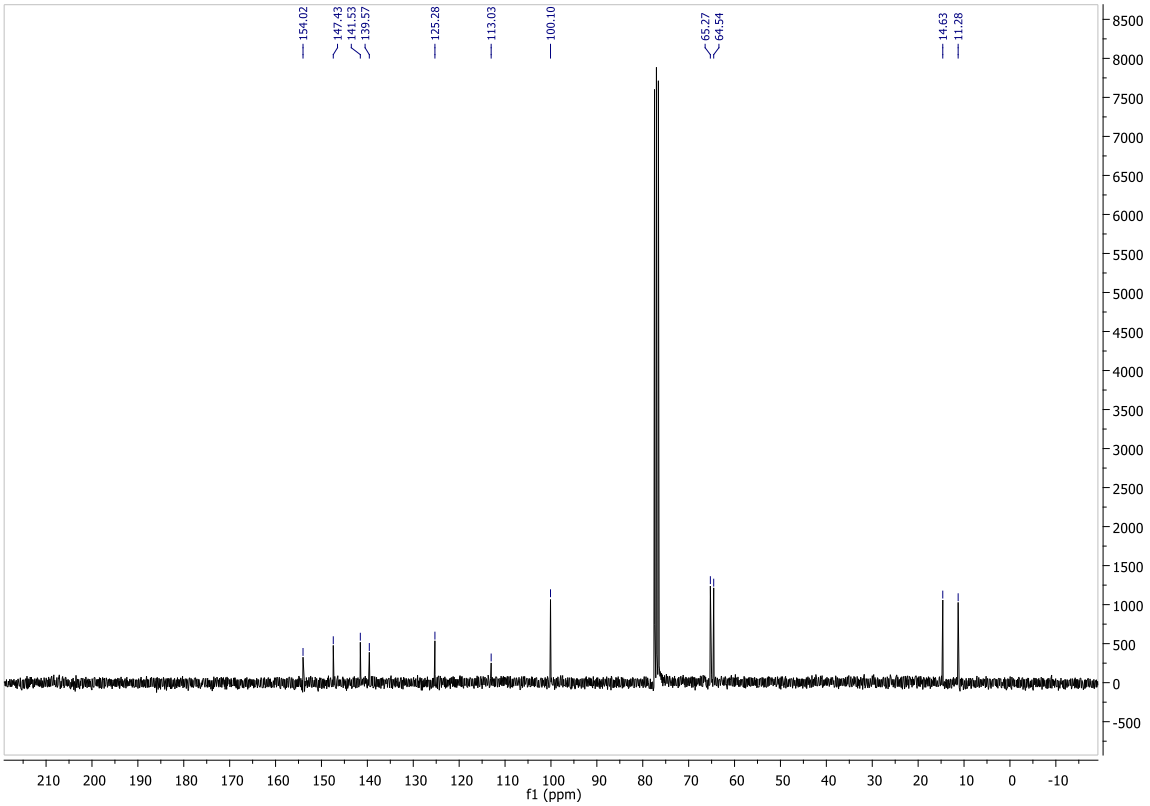
154.02
147.43
141.53
139.57
125.28
113.03
100.10
65.27
64.54
14.63
11.28
f1 (ppm)

P1

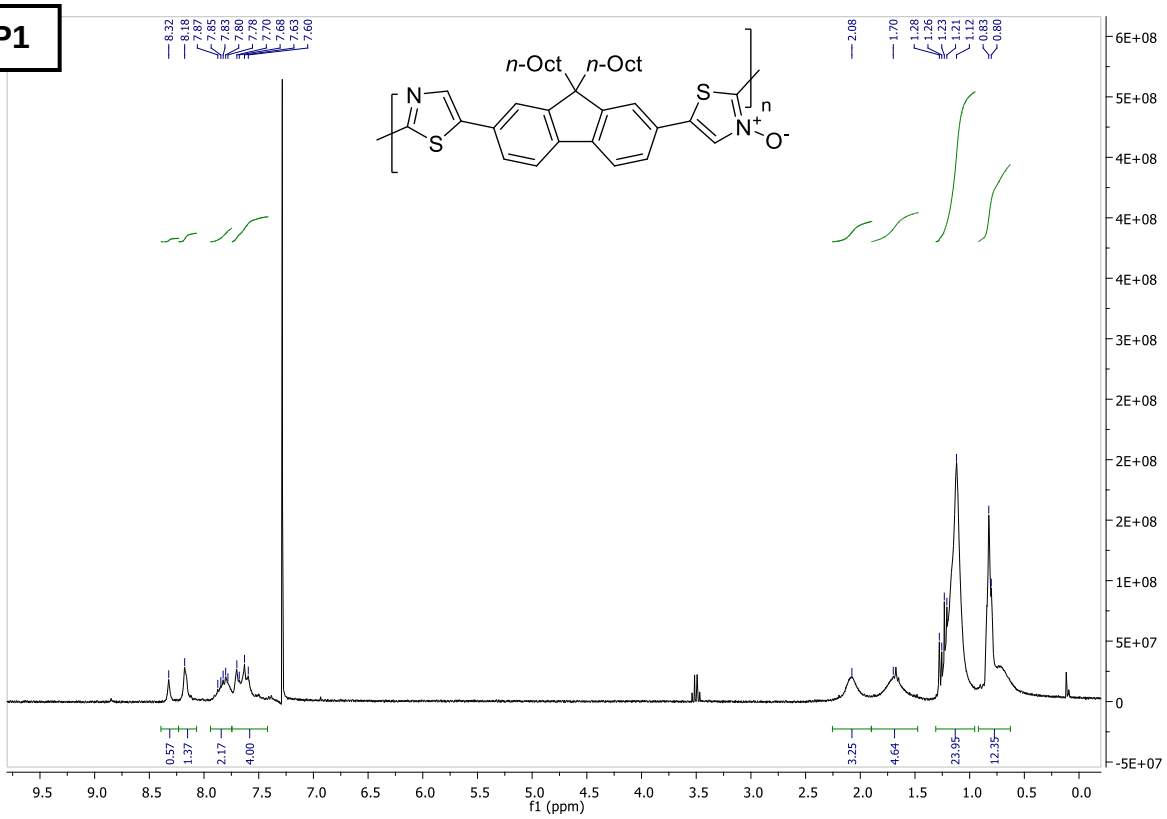

P2

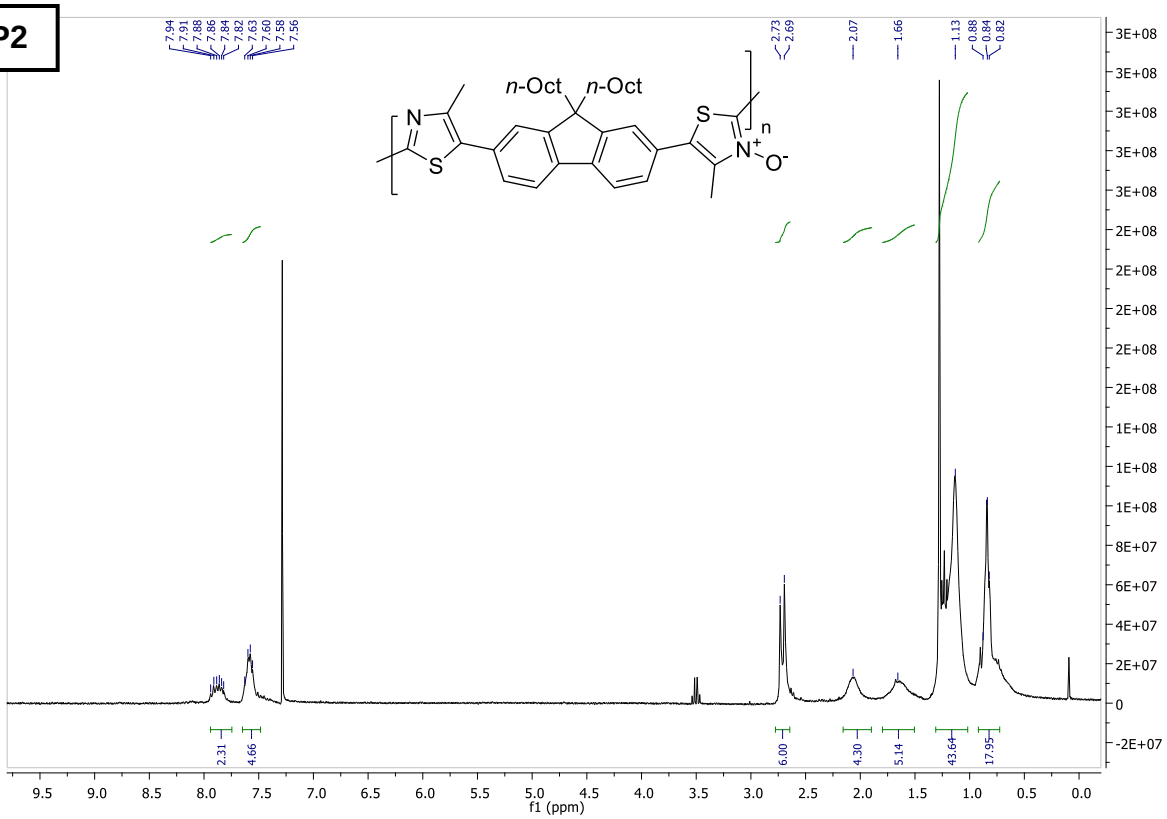

P3

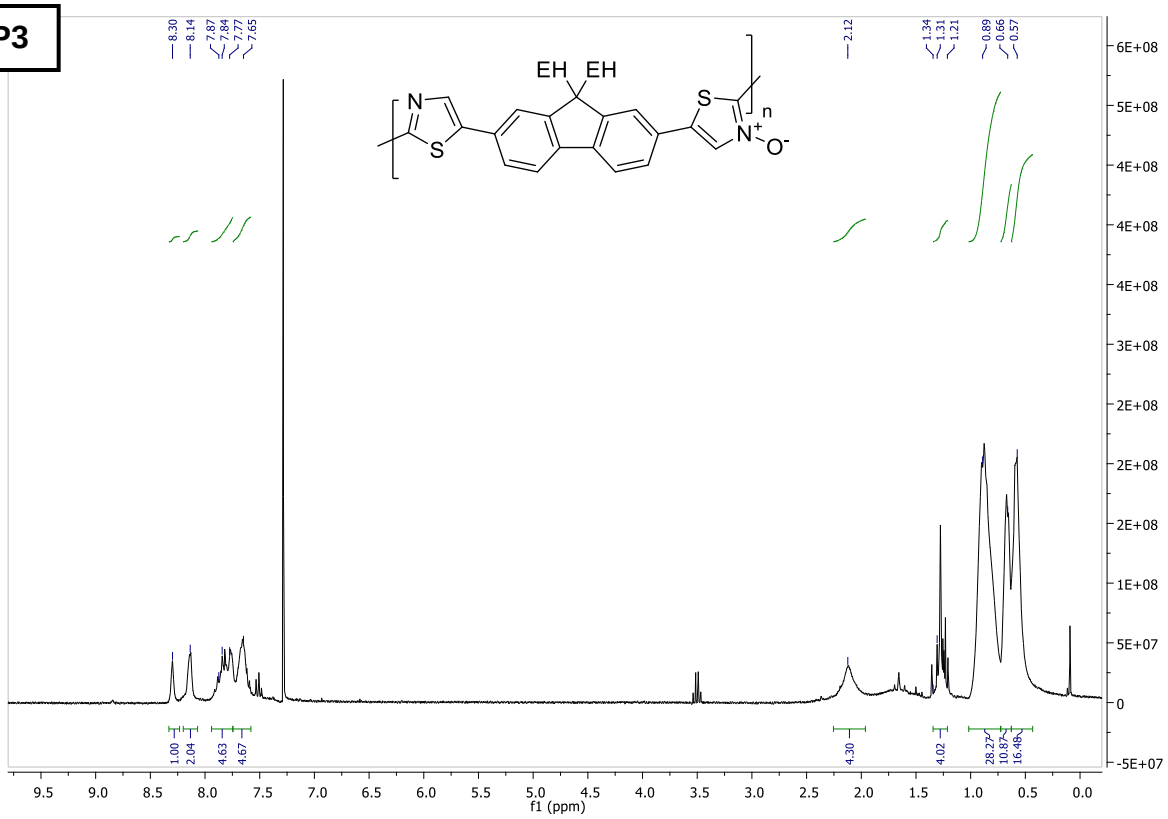
8.30
8.14
7.87
7.84
7.77
7.65
2.12
1.34
1.31
1.21
0.89
0.66
0.57
EH EH
N
S
S
N+
O-
n
1.00
2.04
4.63
4.67
4.30
4.02
28.27
10.87
16.48
f1 (ppm)

P4

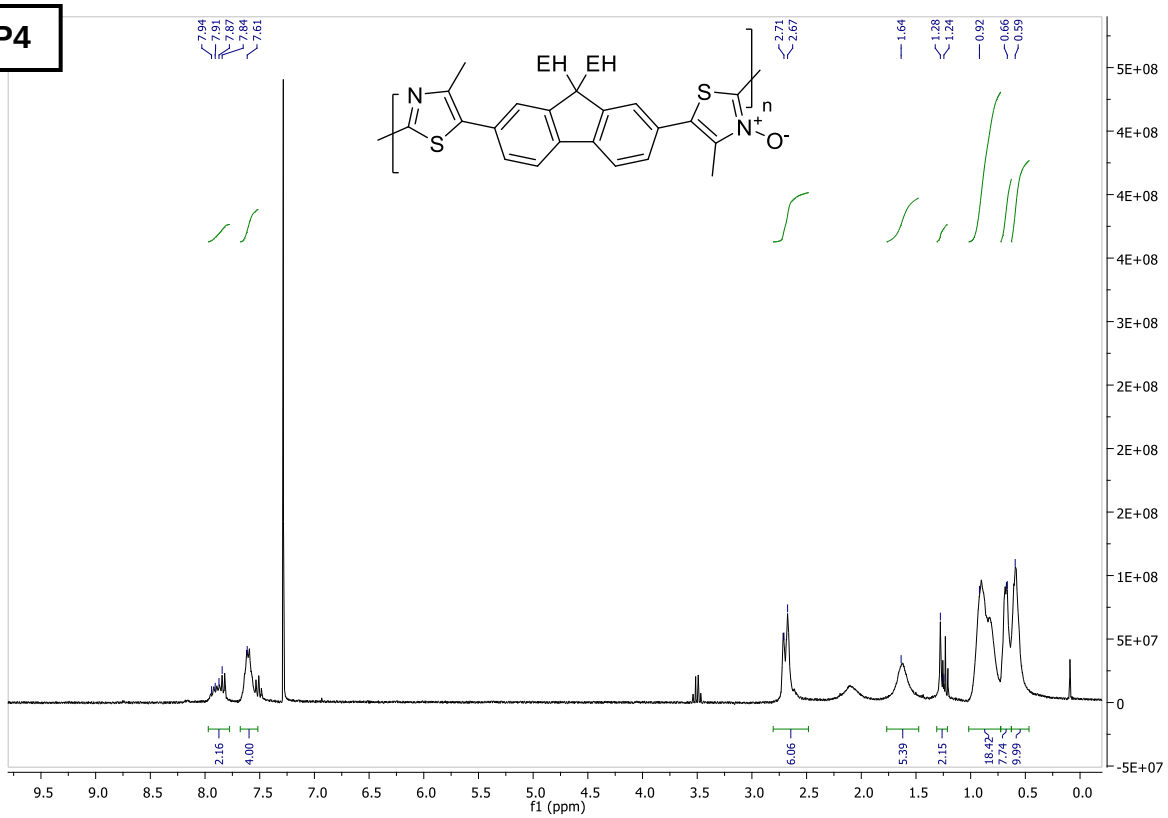
7.94
7.91
7.87
7.84
7.61
2.71
2.67
1.64
1.28
1.24
0.92
0.66
0.59
EH EH
N
S
S
N+
O-
n
2.16
4.00
6.06
5.39
2.15
18.42
7.74
9.99
f1 (ppm)

P6

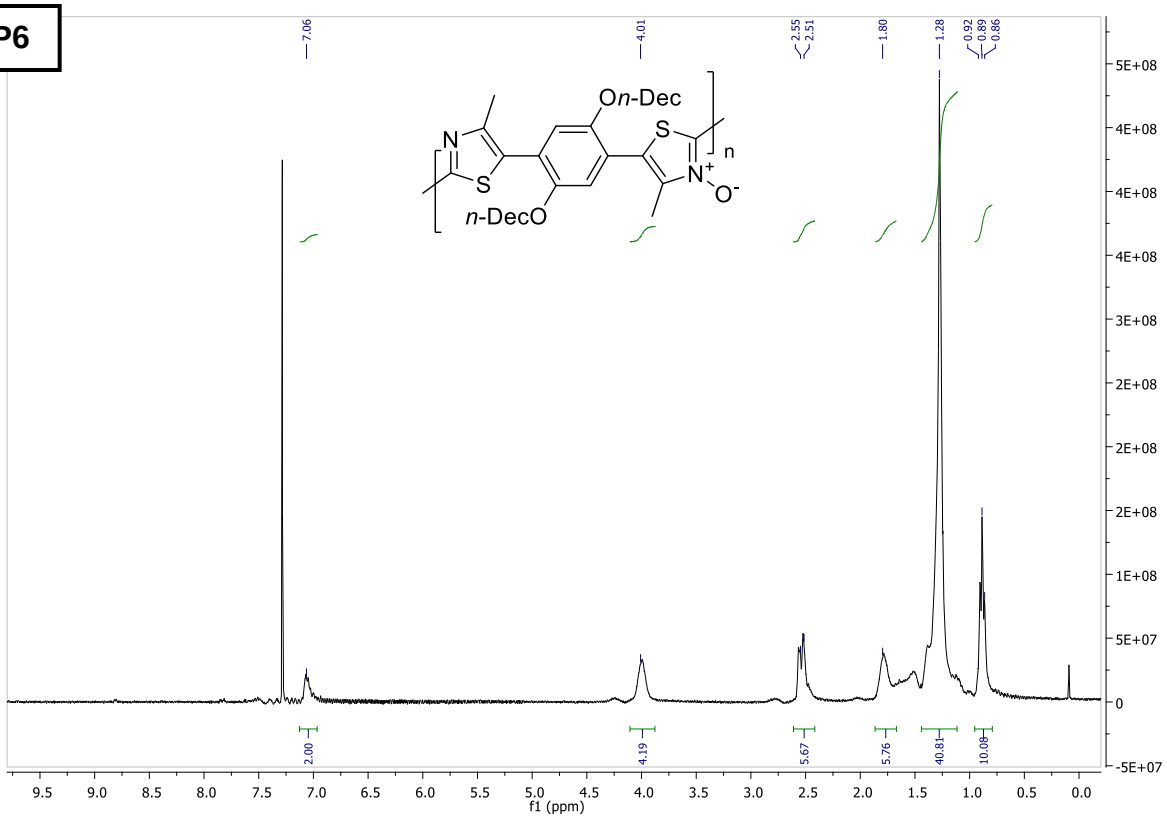
7.06
4.01
2.55
2.51
1.80
1.28
0.92
0.89
0.86
On-Dec
n-DecO
n
2.00
4.19
5.67
5.76
40.81
10.08
f1 (ppm)

P7a

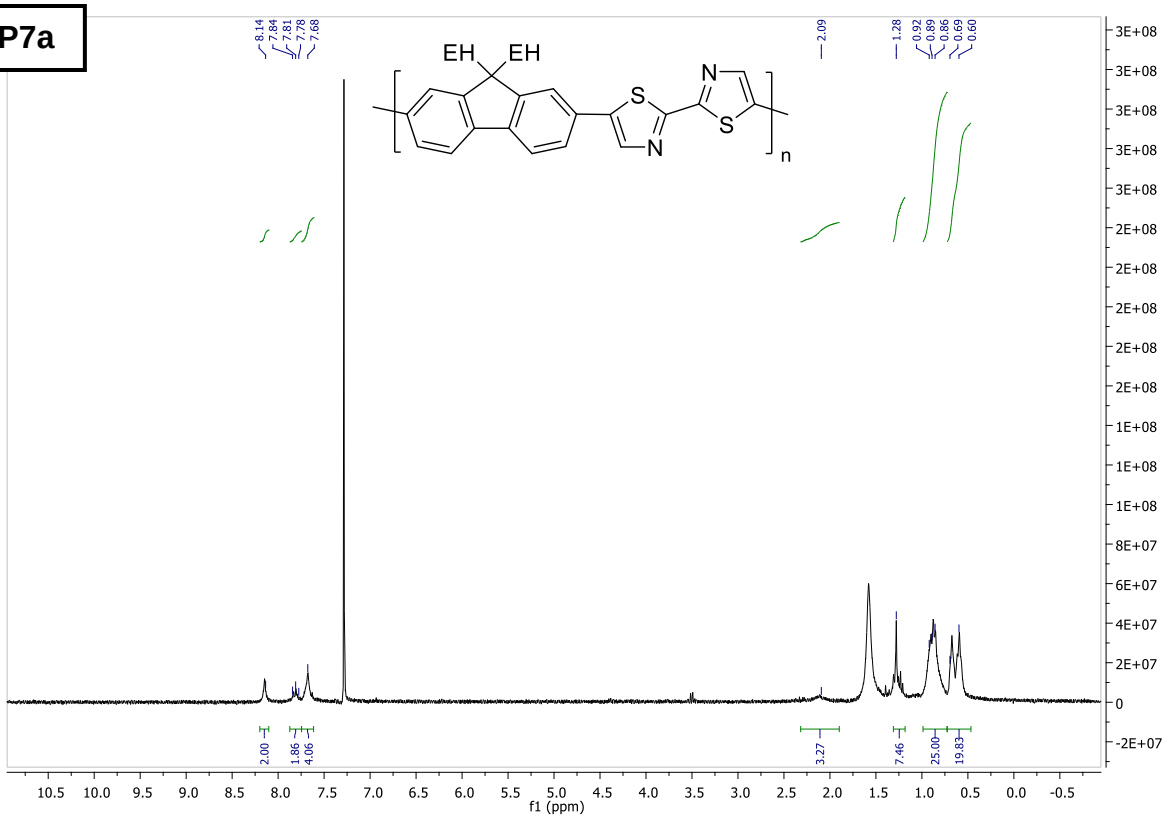
8.14
7.84
7.81
7.78
7.68
2.09
1.28
0.92
0.89
0.86
0.69
0.60
EH
EH
n
2.00
1.86
4.06
3.27
7.46
25.00
19.83
f1 (ppm)

P8a

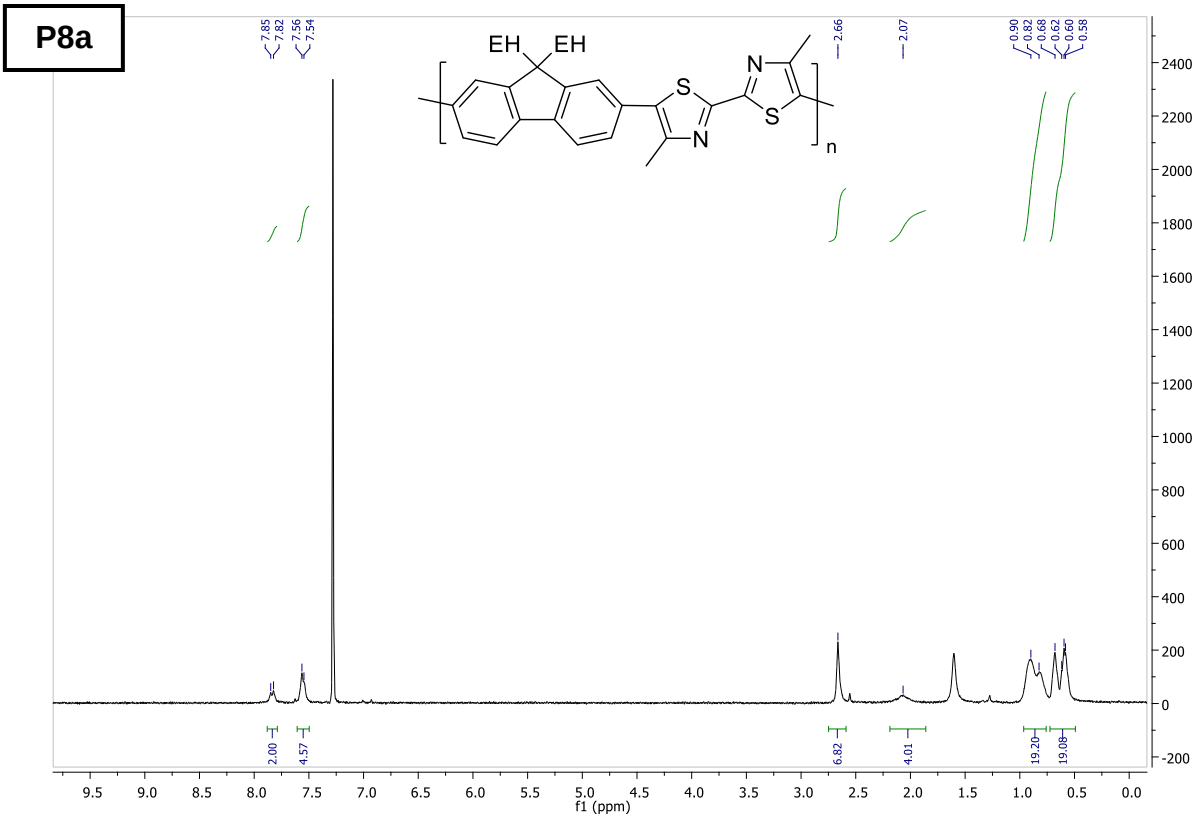
7.85
7.82
7.56
7.54
2.66
2.07
0.90
0.82
0.68
0.62
0.60
0.58
EH
EH
S
N
N
S
n
2.00
4.57
6.82
4.01
19.20
19.08
f1 (ppm)

P8c

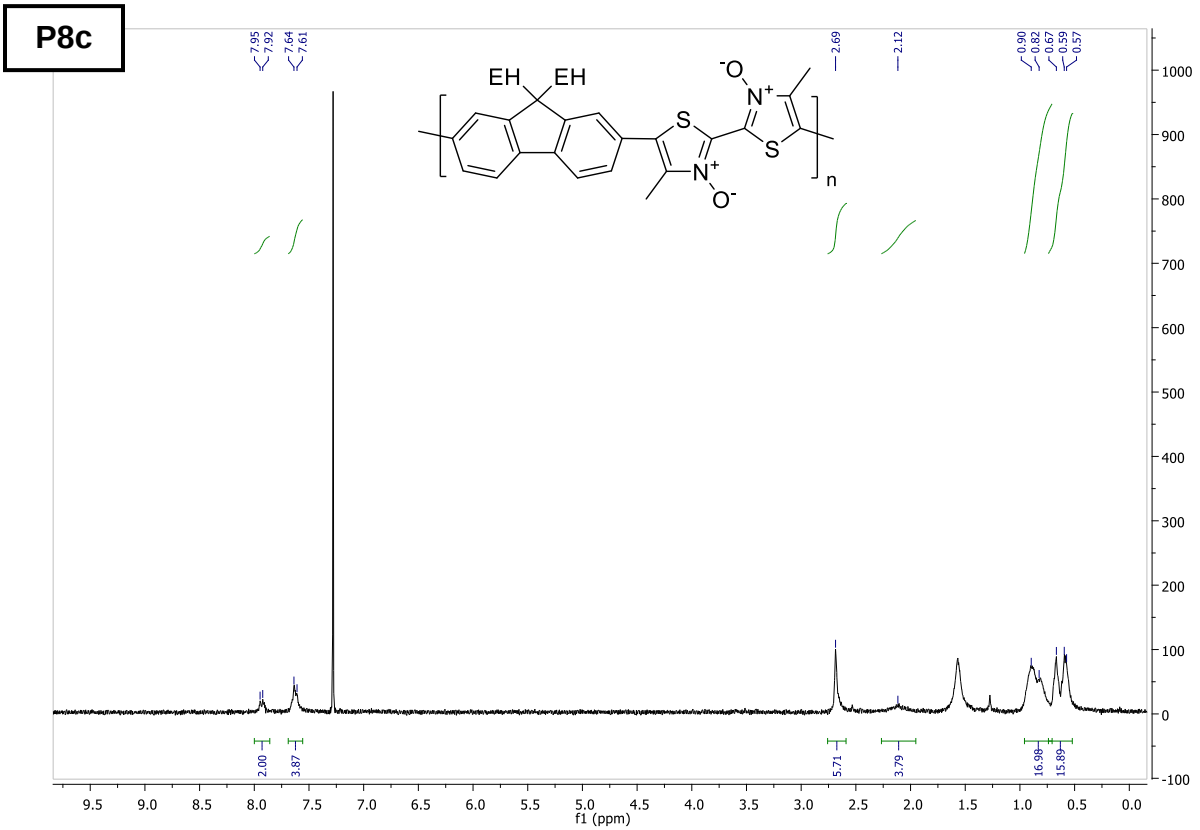
7.95
7.92
7.64
7.61
2.69
2.12
0.90
0.82
0.67
0.59
0.57
EH
EH
-O
N+
S
N+
O-
S
n
2.00
3.87
5.71
3.79
16.98
15.89
f1 (ppm)

P9a

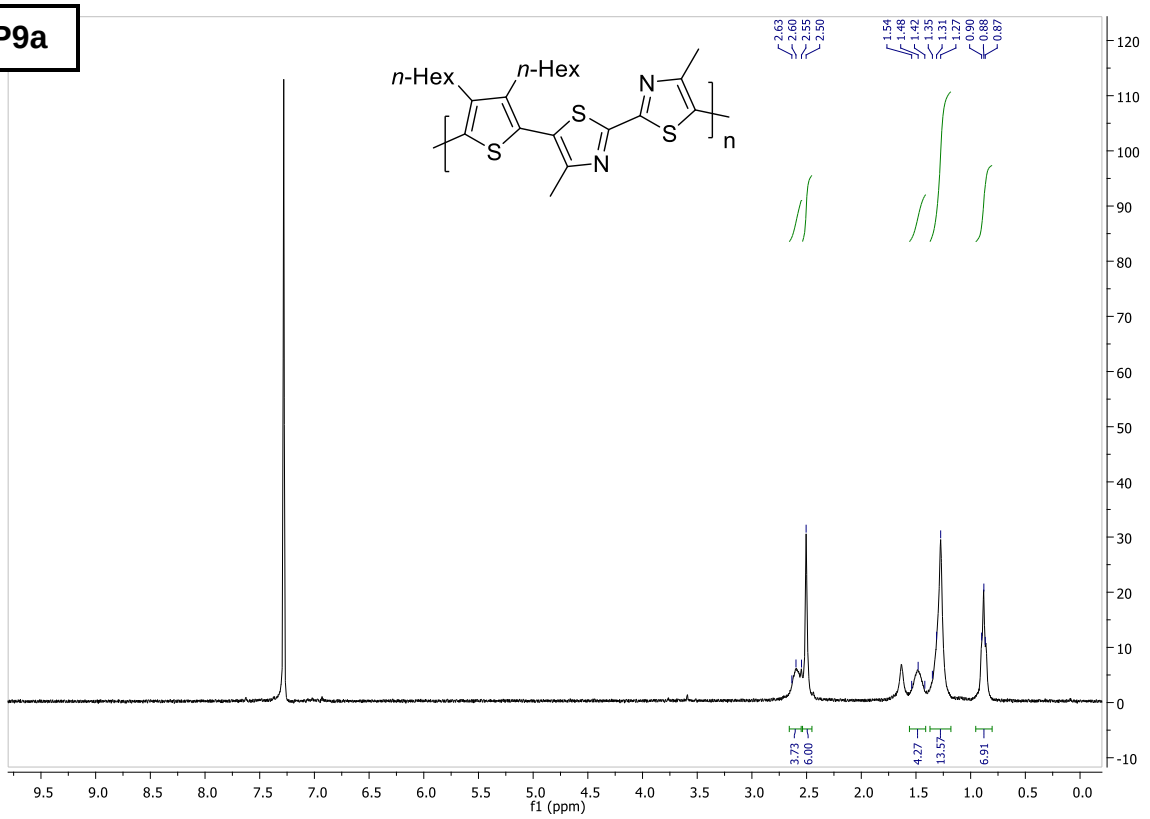
n-Hex
n-Hex
S
N
S
S
N
n
2.63
2.60
2.55
2.50
1.54
1.48
1.42
1.35
1.31
1.27
0.90
0.88
0.87
3.73
6.00
4.27
13.57
6.91
f1 (ppm)

P9b

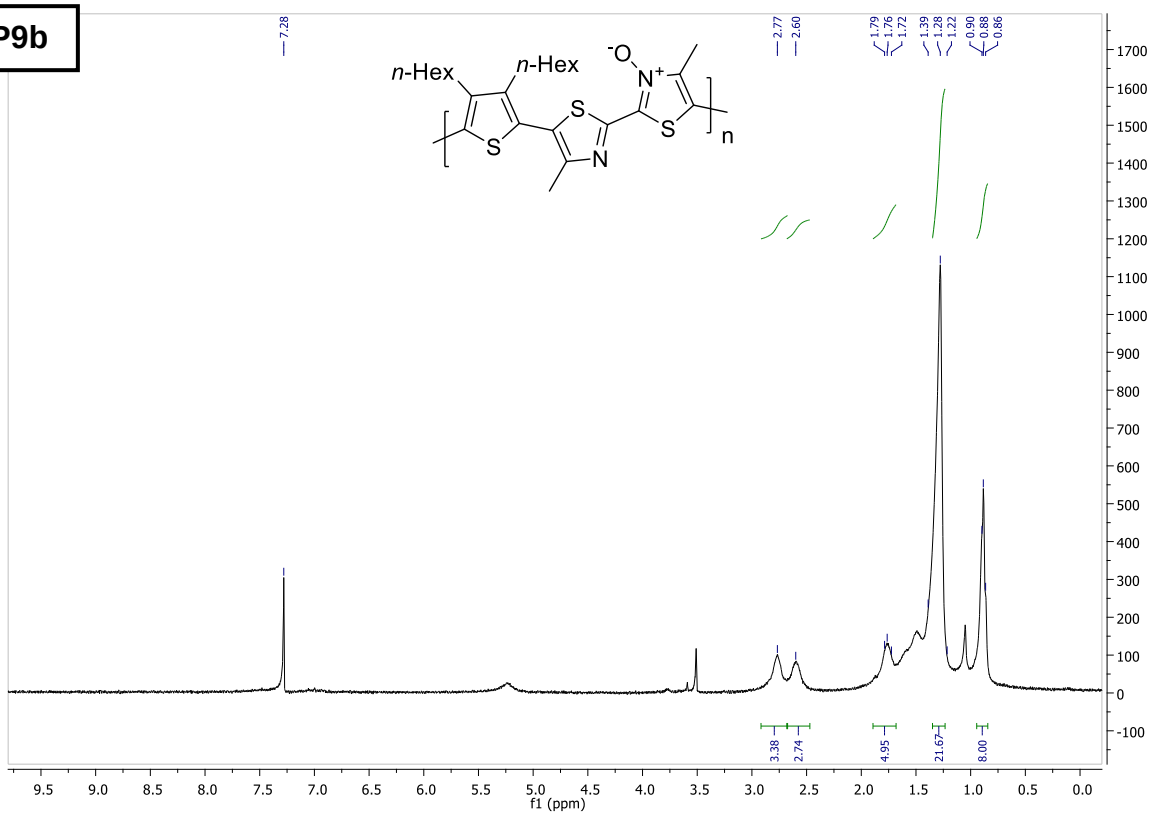
7.28
n-Hex
n-Hex
-O
N+
S
S
N
S
n
2.77
2.60
1.79
1.76
1.72
1.39
1.28
1.22
0.90
0.88
0.86
3.38
2.74
4.95
21.67
8.00
f1 (ppm)

P9c

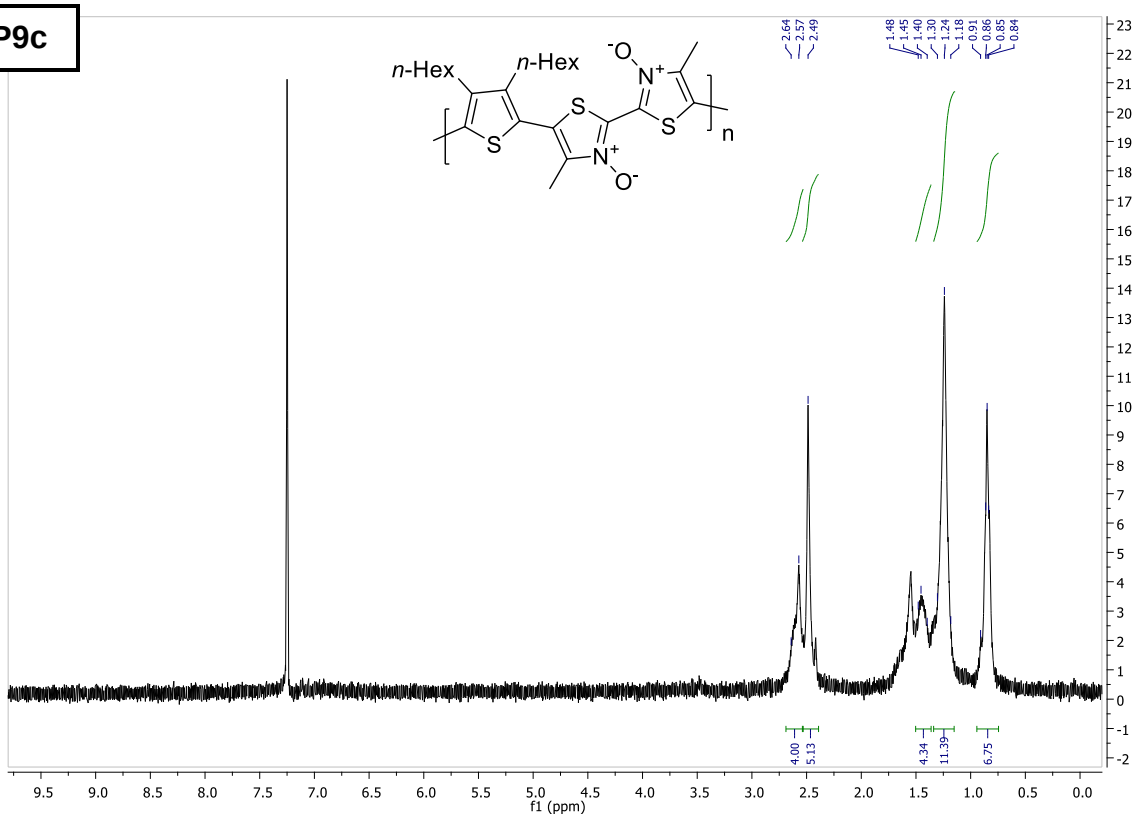
n-Hex
n-Hex
S
S
N+
O-
S
N+
O-
n
2.64
2.57
2.49
1.48
1.45
1.40
1.30
1.24
1.18
0.91
0.86
0.85
0.84
4.00
5.13
4.34
11.39
6.75
f1 (ppm)

P10

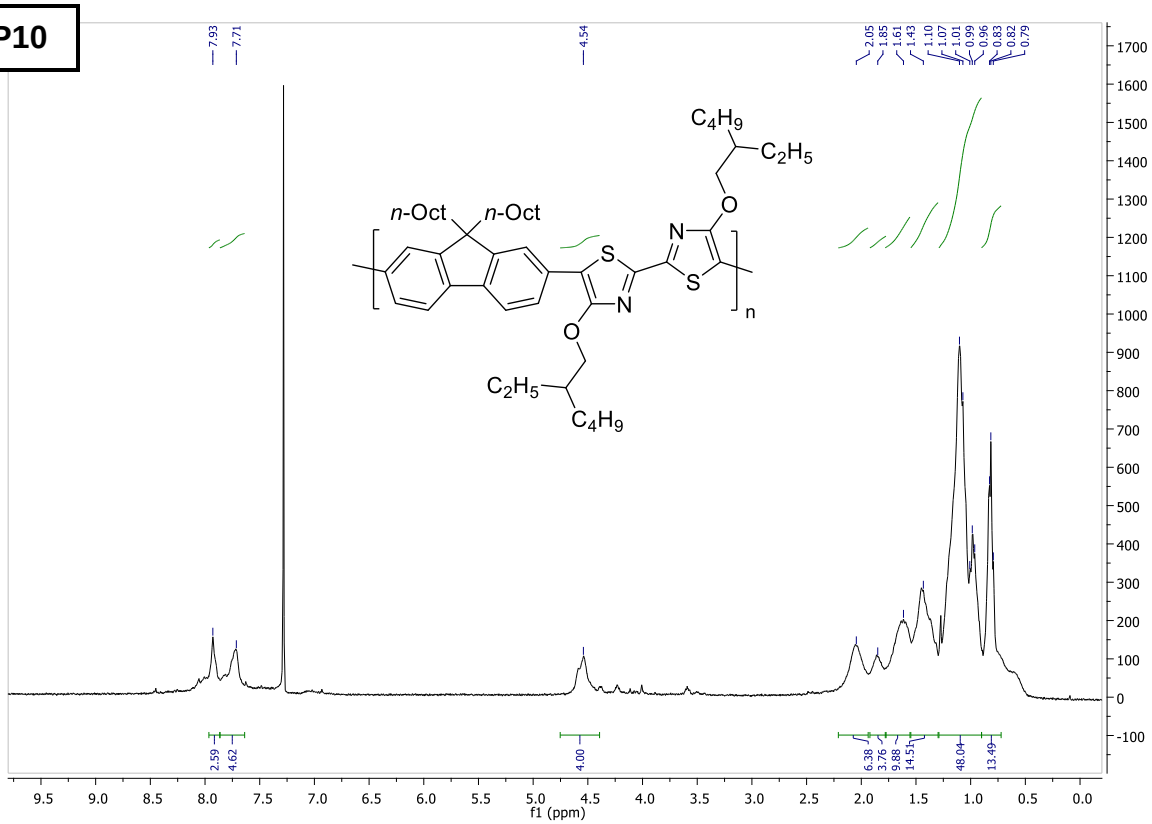
7.93
7.71
4.54
2.05
1.85
1.61
1.43
1.10
1.07
1.01
0.99
0.96
0.83
0.82
0.79
C4H9
C2H5
n-Oct
n-Oct
O
N
S
S
N
n
O
C2H5
C4H9
2.59
4.62
4.00
6.38
3.76
9.88
14.51
48.04
13.49
f1 (ppm)

P12

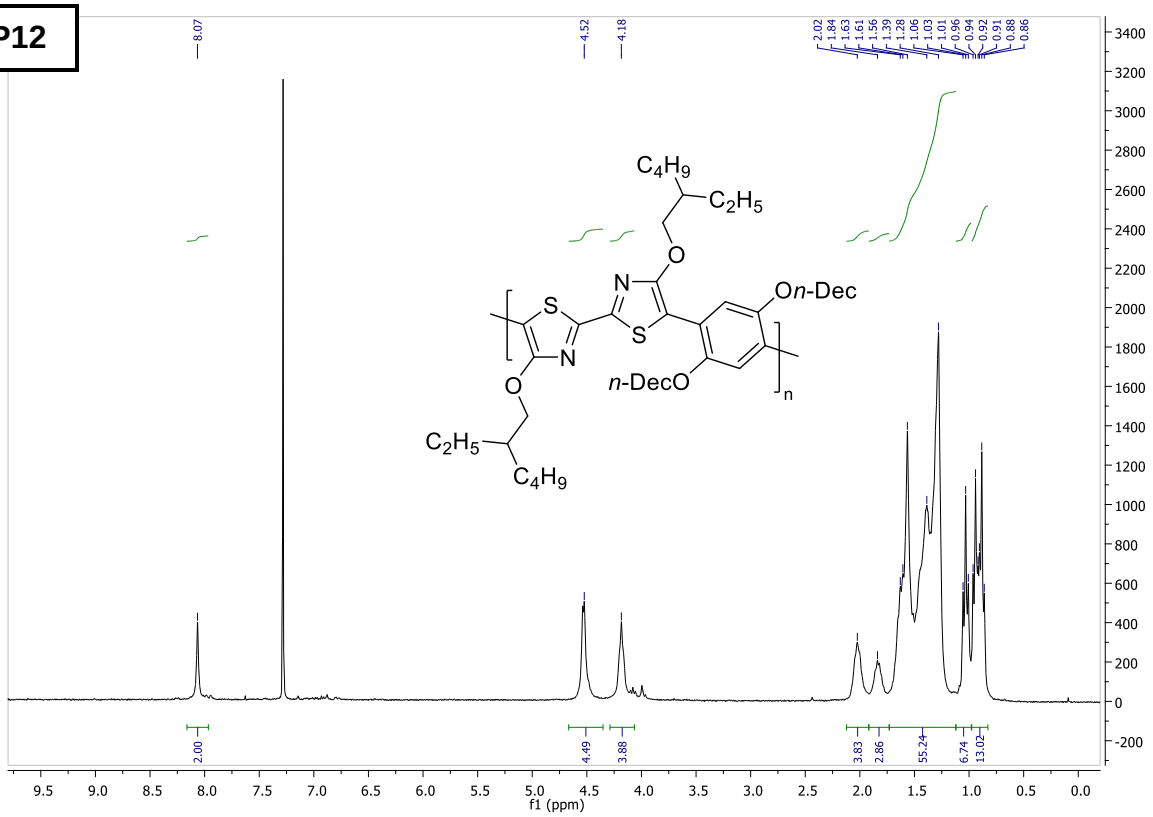
8.07
4.52
4.18
2.02
1.84
1.63
1.61
1.56
1.39
1.28
1.06
1.03
1.01
0.96
0.94
0.92
0.91
0.88
0.86
C4H9
C2H5
O
N
S
S
N
O
On-Dec
n-DecO
n
C2H5
C4H9
2.00
4.49
3.88
3.83
2.86
55.24
6.74
13.02
f1 (ppm)

P13

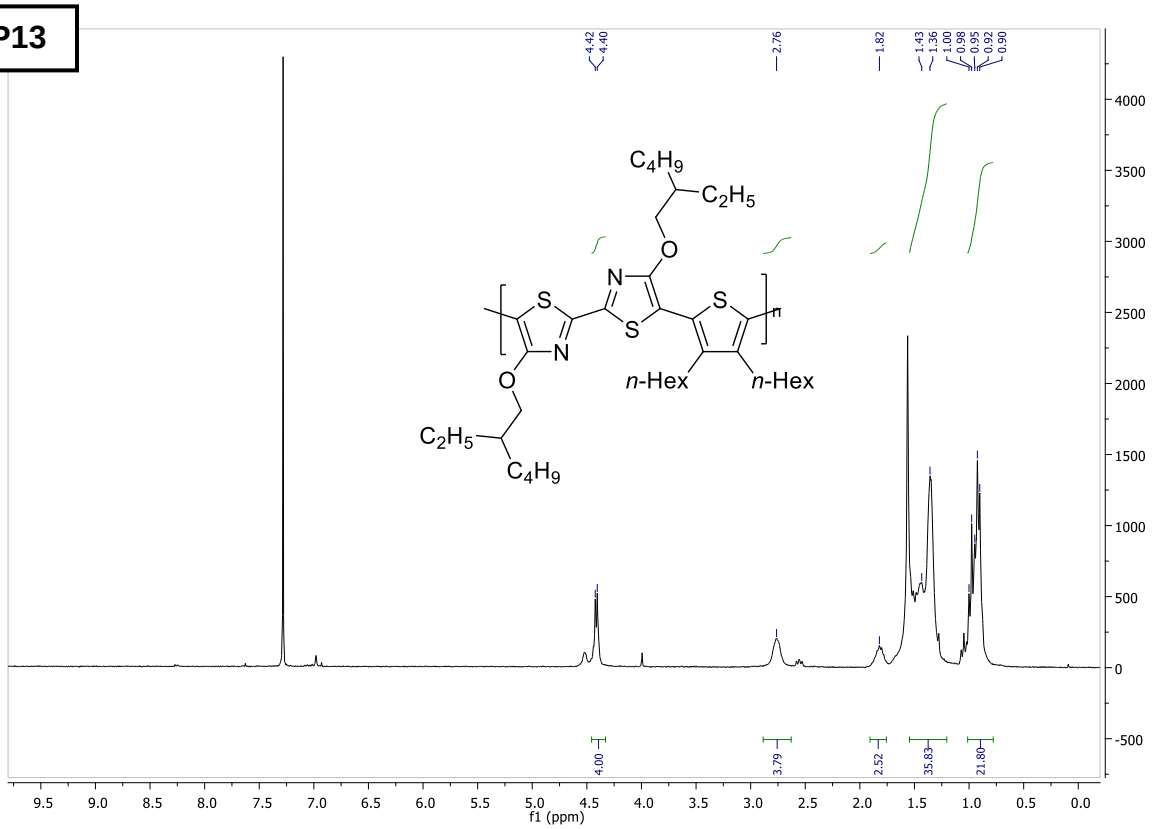
4.42
4.40
2.76
1.82
1.43
1.36
1.00
0.98
0.95
0.92
0.90
C4H9
C2H5
O
N
S
S
N
O
n
n-Hex
n-Hex
C2H5
C4H9
4.00
3.79
2.52
35.83
21.80
f1 (ppm)

P14

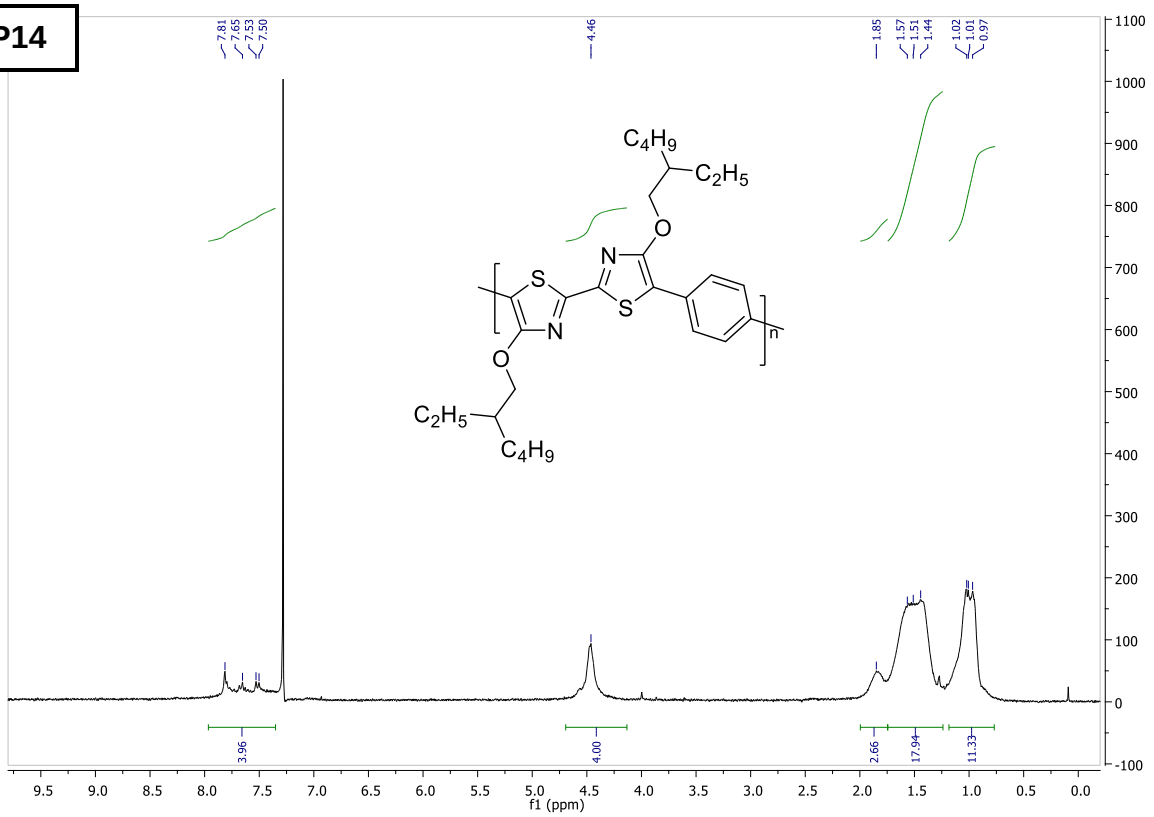
7.81
7.65
7.53
7.50
4.46
1.85
1.57
1.51
1.44
1.02
1.01
0.97
3.96
4.00
2.66
17.94
11.33
f1 (ppm)

P15

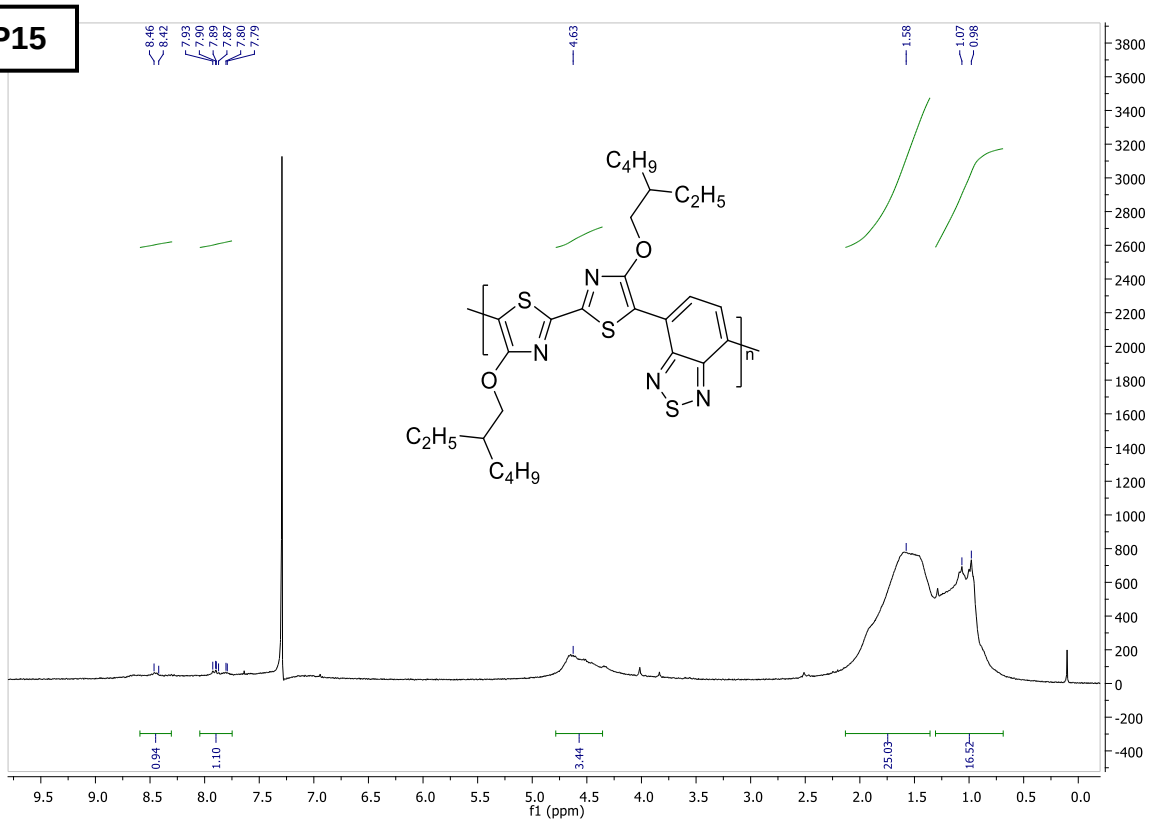
8.46
8.42
7.93
7.90
7.89
7.87
7.80
7.79
4.63
1.58
1.07
0.98
0.94
1.10
3.44
25.03
16.52
f1 (ppm)

P16

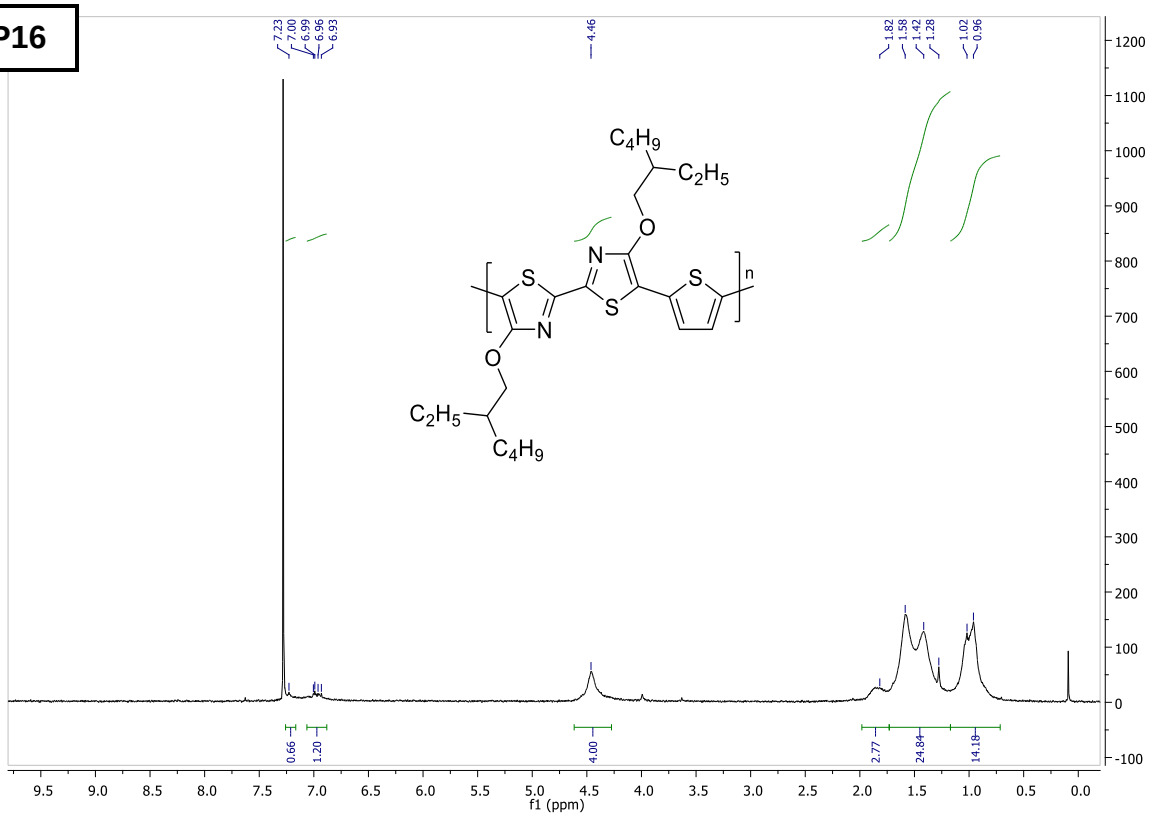
7.23
7.00
6.99
6.96
6.93
4.46
1.82
1.58
1.42
1.28
1.02
0.96
C4H9
C2H5
O
N
S
S
S
N
n
O
C2H5
C4H9
0.66
1.20
4.00
2.77
24.84
14.18
f1 (ppm)

6.1

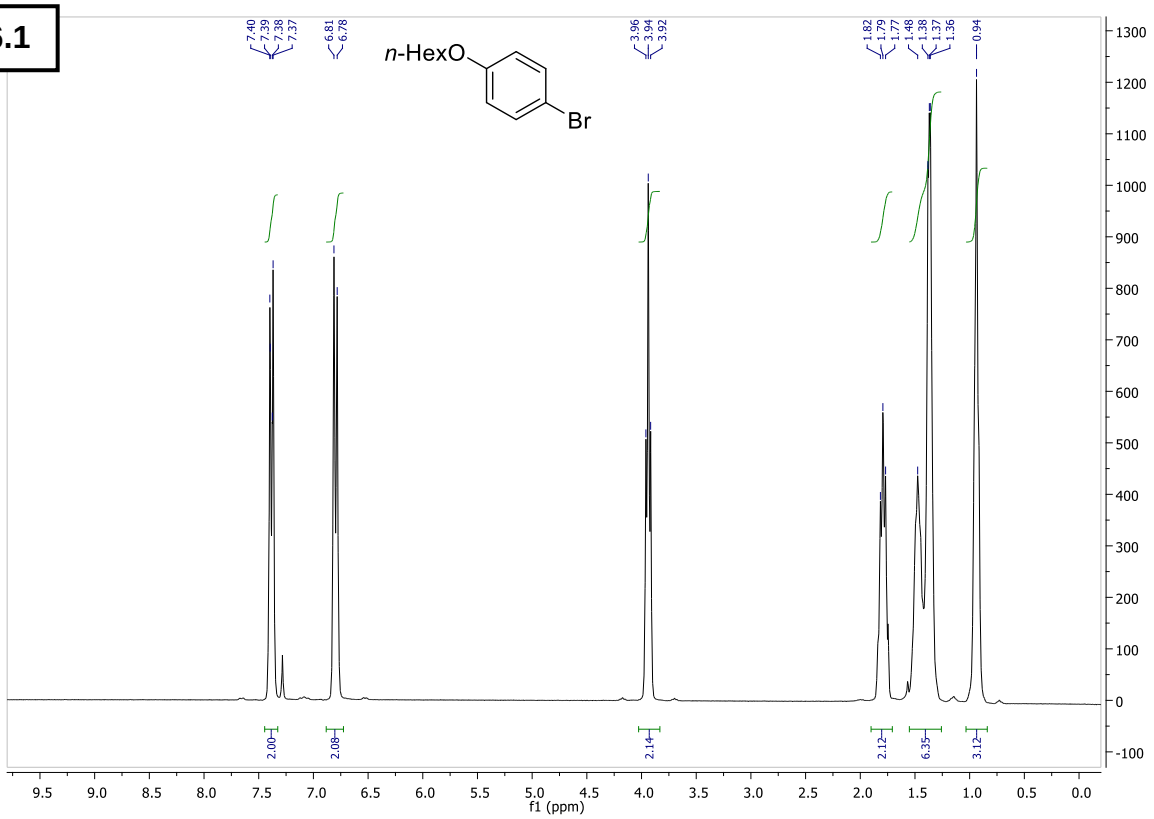
7.40
7.39
7.38
7.37
6.81
6.78
n-HexO
Br
3.96
3.94
3.92
1.82
1.79
1.77
1.48
1.38
1.37
1.36
0.94
2.00
2.08
2.14
2.12
6.35
3.12
f1 (ppm)

6.2

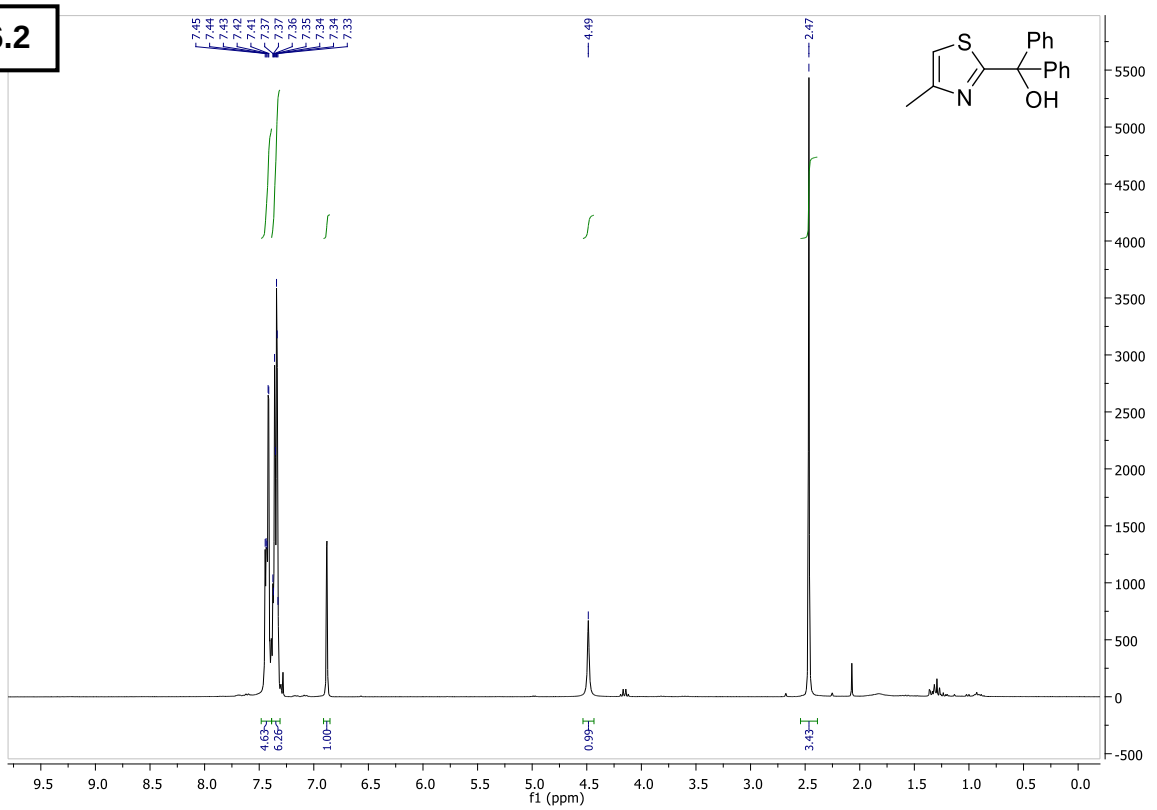
7.45
7.44
7.43
7.42
7.41
7.37
7.37
7.36
7.35
7.34
7.34
7.33
4.49
2.47
S
Ph
Ph
N
OH
4.63
6.26
1.00
0.99
3.43
f1 (ppm)

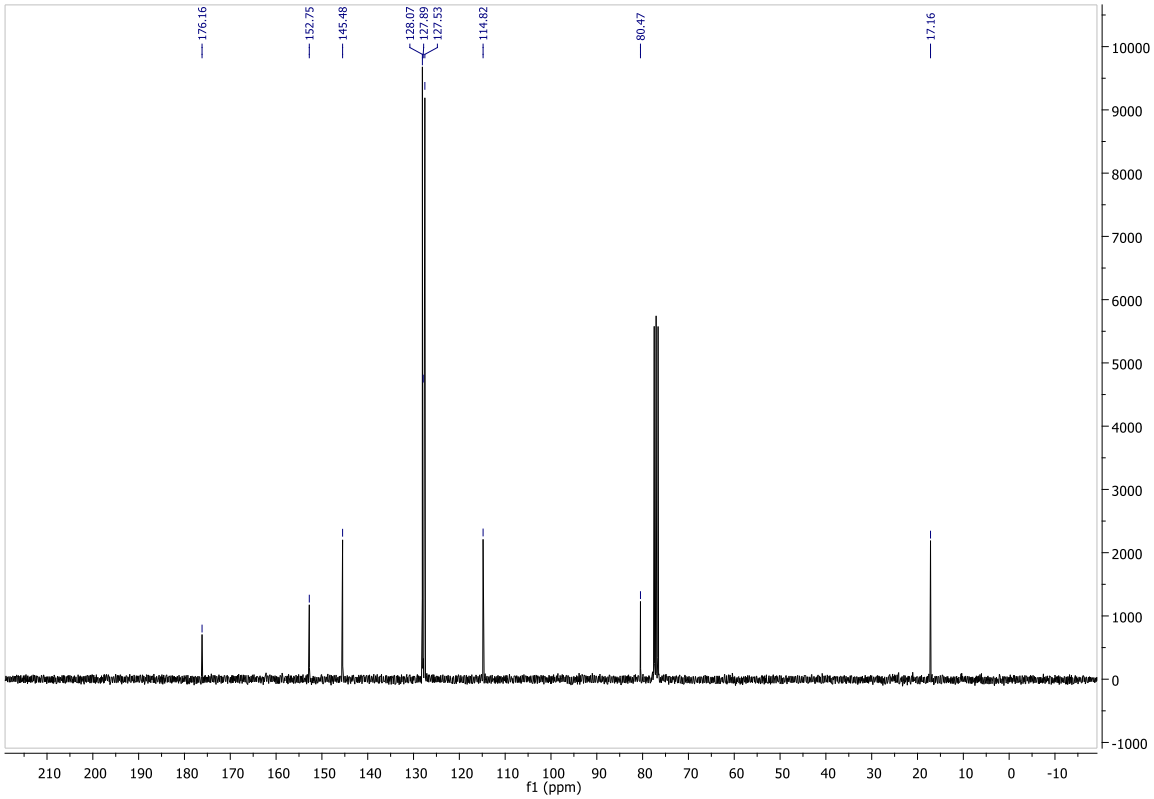
176.16
152.75
145.48
128.07
127.89
127.53
114.82
80.47
17.16
f1 (ppm)

6.3

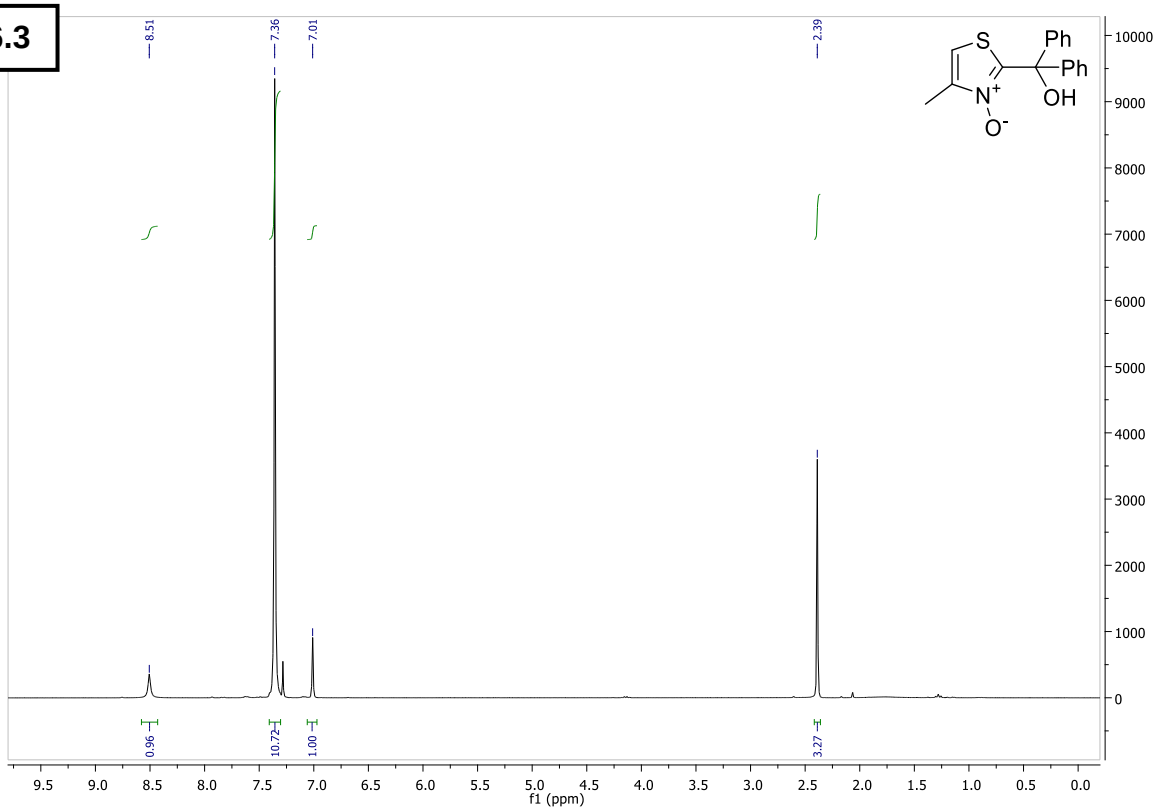
8.51
7.36
7.01
2.39
S
Ph
Ph
OH
N+
O-
0.96
10.72
1.00
3.27
f1 (ppm)

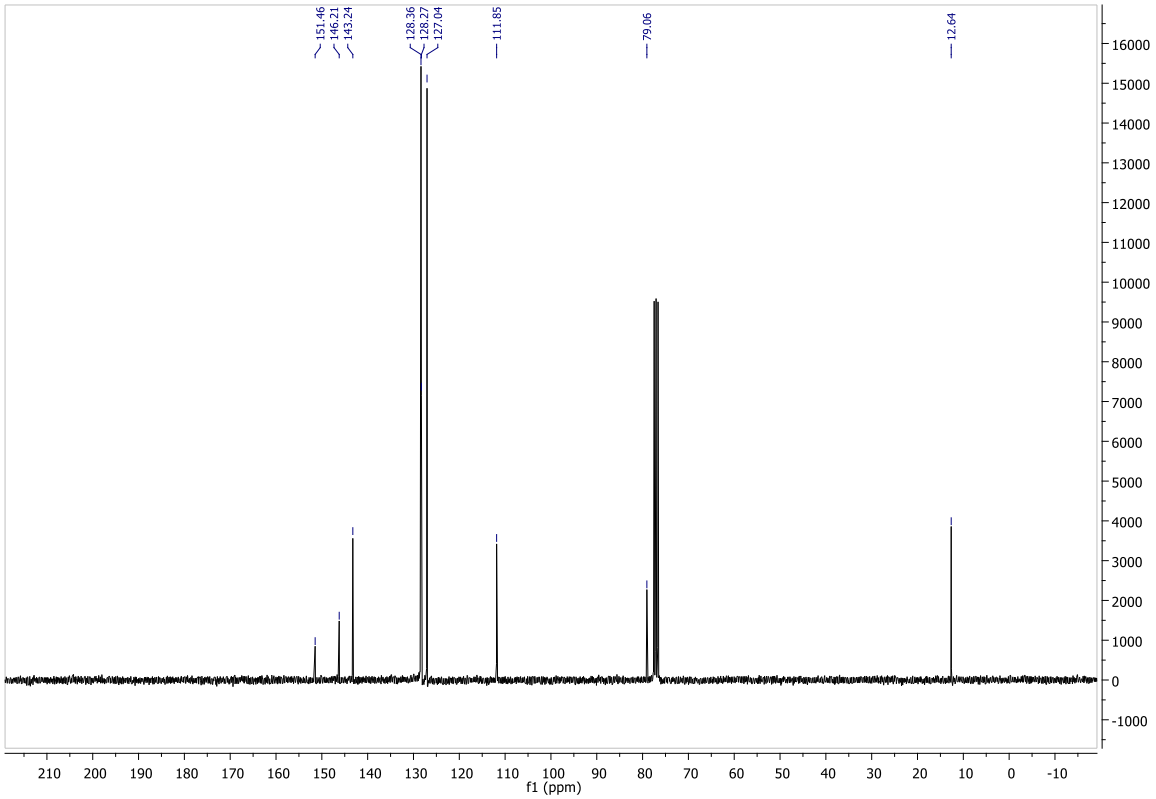
151.46
146.21
143.24
128.36
128.27
127.04
111.85
79.06
12.64
f1 (ppm)

6.4

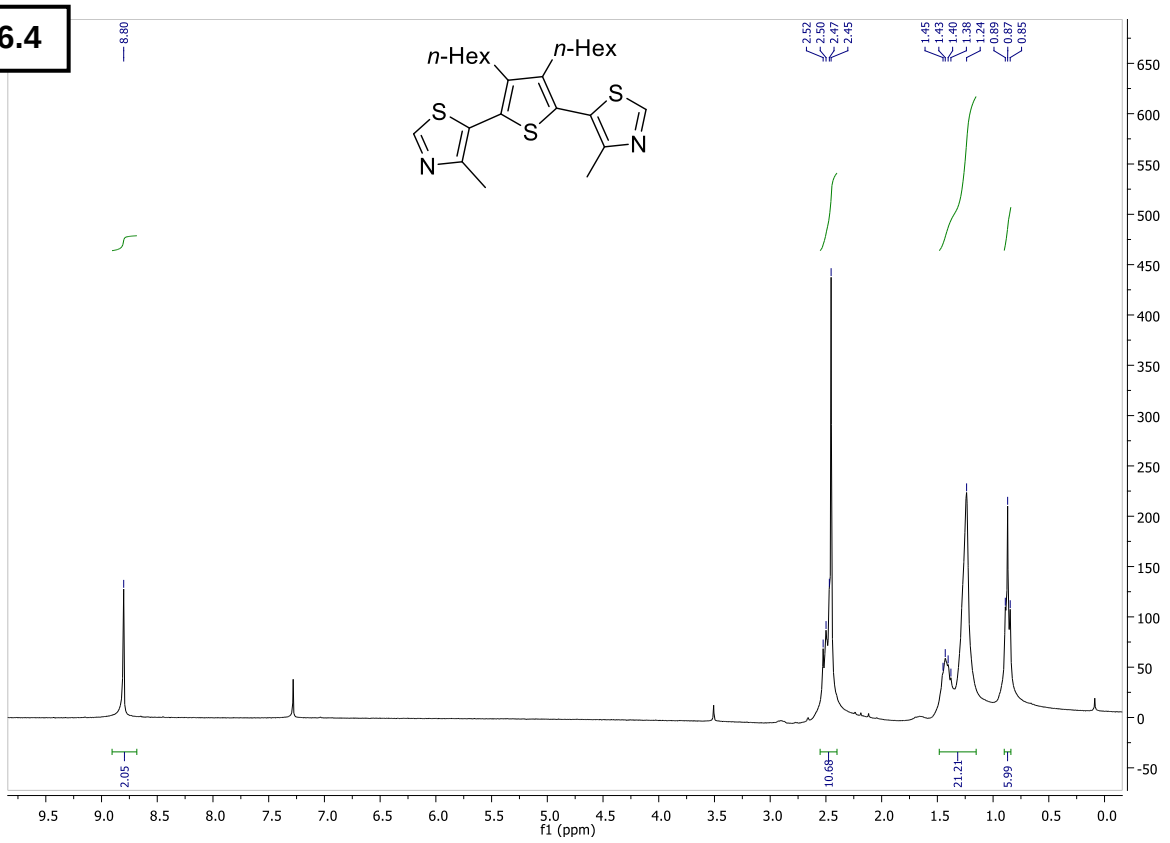
8.80
2.52
2.50
2.47
2.45
1.45
1.43
1.40
1.38
1.24
0.89
0.87
0.85
n-Hex
n-Hex
S
S
S
N
N
2.05
10.68
21.21
5.99
f1 (ppm)

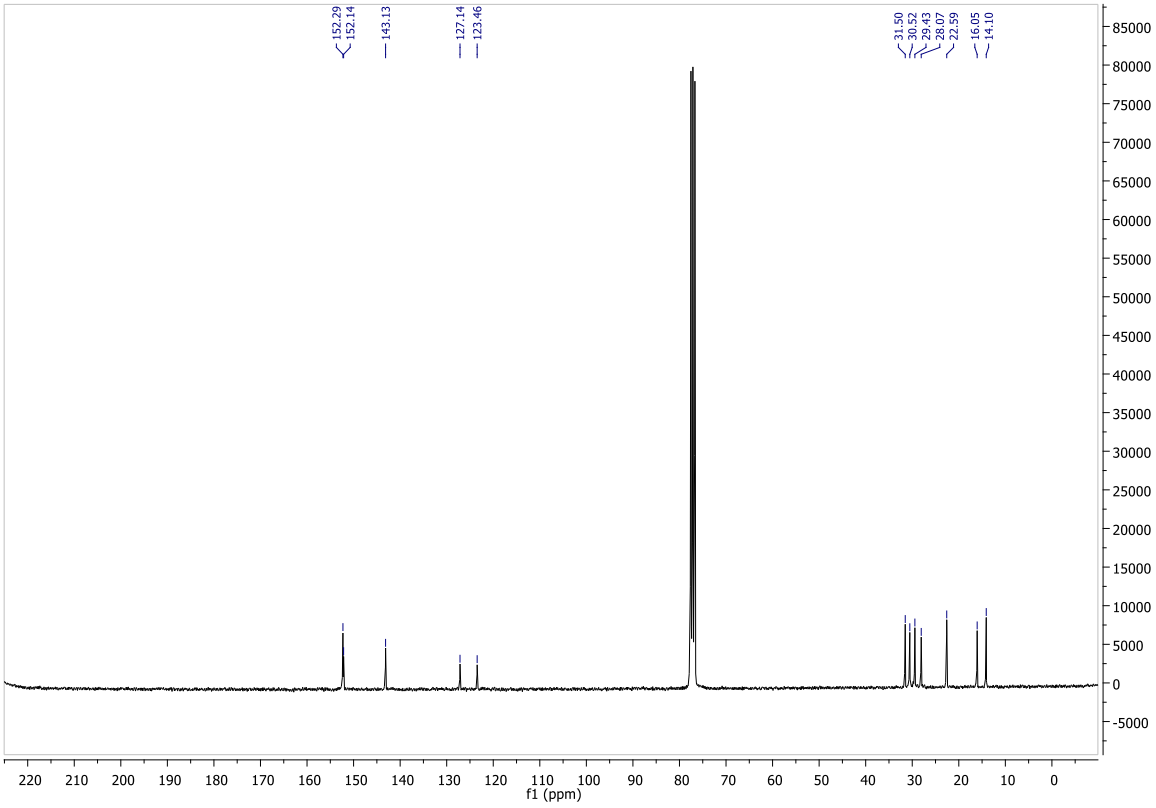
152.29
152.14
143.13
127.14
123.46
31.50
30.52
29.43
28.07
22.59
16.05
14.10
f1 (ppm)

References

1 J. Clayden, N. Greeves and S. Warren, *Organic Chemistry*, Oxford University Press, 2012.

2 H. Klauk, *Organic Electronics*, Wiley, 2006.

3 H. Shirakawa, E. J. Louis, A. G. MacDiarmid, C. K. Chiang and A. J. Heeger, *J. Chem. Soc. Chem. Commun.*, 1977, 578–580.

4 The Nobel Prize in Chemistry, https://www.nobelprize.org/prizes/chemistry/2000/summary/, (accessed 25 September 2020).

5 M. Muccini, *Nat. Mater.*, 2006, **5**, 605–613.

6 J. L. Brédas, D. Beljonne, V. Coropceanu and J. Cornil, *Chem. Rev.*, 2004, **104**, 4971–5003.

7 V. Coropceanu, J. Cornil, D. A. da Silva Filho, Y. Olivier, R. Silbey and J.-L. Brédas, *Chem. Rev.*, 2007, **107**, 926–952.

8 J. R. Reynolds, B. C. Thompson and T. A. Skotheim, *Conjugated Polymers Properties, Processing, and Applications*, CRC Press, 4th edn., 2019.

9 K. C. Nicolaou, *Proc. R. Soc. A Math. Phys. Eng. Sci.*, 2014, **470**, 20130690.

10 C. Kittel, *Introduction to Solid State Physics*, John Wiley & Sons, 8th edn., 2005.

11 A. Dolgonos, T. O. Mason and K. R. Poeppelmeier, *J. Solid State Chem.*, 2016, **240**, 43–48.

12 J. L. Bredas, *Mater. Horizons*, 2014, **1**, 17–19.

13 N. Elgrishi, K. J. Rountree, B. D. McCarthy, E. S. Rountree, T. T. Eisenhart and J. L. Dempsey, *J. Chem. Educ.*, 2018, **95**, 197–206.

14 D. J. Graham, *Standard Operating Procedures for Cyclic Voltammetry*, Daniel J. Graham, 2018, First., 2018.

15 D. S. Correa, E. S. Medeiros, J. E. Oliveira, L. G. Paterno and L. H. C. Mattoso, *J. Nanosci. Nanotechnol.*, 2014, **14**, 6509–6527.

16 S. Himmelberger, K. Vandewal, Z. Fei, M. Heeney and A. Salleo, *Macromolecules*, 2014, **47**, 7151–7157.

17 A. Facchetti, *Chem. Mater.*, 2011, **23**, 733–758.

18 J. Lawrence, E. Goto, J. M. Ren, B. McDearmon, D. S. Kim, Y. Ochiai, P. G. Clark, D. Laitar, T. Higashihara and C. J. Hawker, *J. Am. Chem. Soc.*, 2017, **139**, 13735–13739.

19 K. Müllen, J. R. Reynolds and T. Masuda, Eds., *Conjugated Polymers: A Practical Guide to Synthesis*, Royal Society of Chemistry, Cambridge, 2013.

20 X. H. Zhu, J. Peng, Y. Cao and J. Roncali, *Chem. Soc. Rev.*, 2011, **40**, 3509–3524.

21 Y. Lin, Y. Li and X. Zhan, *Chem. Soc. Rev.*, 2012, **41**, 4245–4272.

22 H. Meier, U. Stalmach and H. Kolshorn, *Acta Polym.*, 1997, **48**, 379–384.

23 J. Rissler, *Chem. Phys. Lett.*, 2004, **395**, 92–96.

24 A. Mishra and P. Bäuerle, *Angew. Chemie - Int. Ed.*, 2012, **51**, 2020–2067.

25 K. Okamoto, J. Zhang, J. B. Housekeeper, S. R. Marder and C. K. Luscombe, *Macromolecules*, 2013, **46**, 8059–8078.

26 B. Walker, C. Kim and T. Q. Nguyen, *Chem. Mater.*, 2011, **23**, 470–482.

27 M. T. Lloyd, J. E. Anthony and G. G. Malliaras, *Mater. Today*, 2007, **10**, 34–41.

28 S. R. Forrest, *Nature*, 2004, **428**, 911–918.

29 L. Dai, D. W. Chang, J. B. Baek and W. Lu, *Small*, 2012, **8**, 1130–1166.

30 D. Jariwala, V. K. Sangwan, L. J. Lauhon, T. J. Marks and M. C. Hersam, *Chem. Soc. Rev.*, 2013, **42**, 2824–2860.

31 H. W. Kroto, J. R. Heath, S. C. O'Brien, R. F. Curl and R. E. Smalley, *Nature*, 1985, **318**, 162–163.

32 V. Georgakilas, J. A. Perman, J. Tucek and R. Zboril, *Chem. Rev.*, 2015, **115**, 4744–4822.

33 S. Iijima, *Nature*, 1991, **354**, 56–58.

34 I. V. G. and A. A. F. K. S. Novoselov, A. K. Geim, S. V. Morozov, D. Jiang, Y. Zhang, S. V. Dubonos, *Science (80-.).*, 2004, **306**, 666–669.

35 C. R. Newman, C. D. Frisbie, D. A. Da Silva Filho, J. L. Brédas, P. C. Ewbank and K. R. Mann, *Chem. Mater.*, 2004, **16**, 4436–4451.

36 R. Li and G. Liu, *Flexible and Stretchable Electronics*, CRC Press, 2020.

37 C. Wang, H. Dong, W. Hu, Y. Liu and D. Zhu, *Chem. Rev.*, 2012, **112**, 2208–2267.

38 LG Display opens 8.5th generation OLED panel production plant in Guangzhou, China, http://www.lgdisplay.com/eng/prcenter/newsView, (accessed 25 March 2020).

39 R. P. Xu, Y. Q. Li and J. X. Tang, *J. Mater. Chem. C*, 2016, **4**, 9116–9142.

40 N. C. Greenham, *Nature*, 1995, 121–128.

41 S. Ogawa, Ed., *Organic Electronics Materials and Devices*, Springer Japan, Tokyo, 2015.

42 B. P. Rand, J. Genoe, P. Heremans and J. Poortmans, *Prog. Photovolt Res. Appl.*, 2007, **15**, 659–676.

43 C. J. Brabec, S. Gowrisanker, J. J. M. Halls, D. Laird, S. Jia and S. P. Williams, *Adv. Mater.*, 2010, **22**, 3839–3856.

44 J. E. Anthony, A. Facchetti, M. Heeney, S. R. Marder and X. Zhan, *Adv. Mater.*, 2010, **22**, 3876–3892.

45 A. W. Hains, Z. Liang, M. A. Woodhouse and B. A. Gregg, *Chem. Rev.*, 2010, **110**, 6689–6735.

46 Y. Cheng, S. Yang and C. Hsu, *Chem. Rev.*, 2009, **109**, 5868–5923.

47 J. Roncali, *Macromol. Rapid Commun.*, 2007, **28**, 1761–1775.

48 C. Liu, K. Wang, X. Gong and A. J. Heeger, *Chem. Soc. Rev.*, 2016, **45**, 4825–4846.

49 J. L. Brédas, *J. Chem. Phys.*, 1985, **82**, 3808–3811.

50 T. M. Swager, *Macromolecules*, 2017, **50**, 4867–4886.

51 K. Tanaka, S. Wang and T. Yamabe, *Synth. Met.*, 1989, **30**, 57–65.

52 E. J. Dell and L. M. Campos, *J. Mater. Chem.*, 2012, **22**, 12945–12952.

53 F. Wudl, N. Kobayashi and A. J. Heeger, *J. Org. Chem.*, 1984, **49**, 3382–3384.

54 L. Groenendaal, F. Jonas, D. Freitag, H. Pielartzik and J. R. Reynolds, *Adv. Mater.*, 2000, **12**, 481–494.

55 J. P. Ferraris and T. L. Lambert, *J. Chem. Soc. Chem. Commun.*, 1991, 1268–1270.

56 T. L. Lambert and J. P. Ferraris, *J. Chem. Soc., Chem. Commun.*, 1991, 752–754.

57 E. E. Havinga, W. ten Hoeve and H. Wynberg, *Synth. Met.*, 1993, **55**, 299–306.

58 H. Zhou, L. Yang, S. Stoneking and W. You, *ACS Appl. Mater. Interfaces*, 2010, **2**, 1377–1383.

59 H. Zhou, L. Yang and W. You, *Macromolecules*, 2012, **45**, 607–632.

60 J. Roncali and C. Thobie-Gautier, *Adv. Mater.*, 1994, **6**, 846–848.

61 J. Roncali, C. Thobie-Gautier, E. H. Elandaloussi and P. Frère, *J. Chem. Soc. Chem. Commun.*, 1994, 2249–2250.

62 H. Brisset, C. Thobie-Gautier, A. Gorgues, M. Jubault and J. Roncali, *J. Chem. Soc. Chem. Commun.*, 1994, 1305–1306.

63 H. Huang, L. Yang, A. Facchetti and T. J. Marks, *Chem. Rev.*, 2017, **117**, 10291–10318.

64 S. L. Cockroft, J. Perkins, C. Zonta, H. Adams, S. E. Spey, C. M. R. Low, J. G. Vinter, K. R. Lawson, C. J. Urch and C. A. Hunter, *Org. Biomol. Chem.*, 2007, **5**, 1062.

65 C. R. Martinez and B. L. Iverson, *Chem. Sci.*, 2012, **3**, 2191.

66 R. Steyrleuthner, M. Schubert, I. Howard, B. Klaumünzer, K. Schilling, Z. Chen, P. Saalfrank, F. Laquai, A. Facchetti and D. Neher, *J. Am. Chem. Soc.*, 2012, **134**, 18303–18317.

67 G. R. Hutchison, M. A. Ratner and T. J. Marks, *J. Am. Chem. Soc.*, 2005, **127**, 16866–16881.

68 G. C. Welch, R. C. Bakus, S. J. Teat and G. C. Bazan, *J. Am. Chem. Soc.*, 2013, **135**, 2298–2305.

69 C. Scharsich, R. H. Lohwasser, M. Sommer, U. Asawapirom, U. Scherf, M. Thelakkat, D. Neher and A. Köhler, *J. Polym. Sci. Part B Polym. Phys.*, 2012, **50**, 442–453.

70 R. Traiphol, N. Charoenthai, T. Srikhirin, T. Kerdcharoen, T. Osotchan and T. Maturos, *Polymer (Guildf).*, 2007, **48**, 813–826.

71 I. F. Perepichka, E. Levillain and J. Roncali, *J. Mater. Chem.*, 2004, **14**, 1679–1681.

72 J. Mei and Z. Bao, *Chem. Mater.*, 2014, **26**, 604–615.

73 F. Sugiyama, A. T. Kleinschmidt, L. V. Kayser, D. Rodriquez, M. Finn, M. A. Alkhadra, J. M. H. Wan, J. Ramírez, A. S. C. Chiang, S. E. Root, S. Savagatrup and D. J. Lipomi, *Polym. Chem.*, 2018, **9**, 4354–4363.

74 T. Lei, J. Y. Wang and J. Pei, *Chem. Mater.*, 2014, **26**, 594–603.

75 Z. Liu, G. Zhang and D. Zhang, *Acc. Chem. Res.*, 2018, **51**, 1422–1432.

76 J. Hassan, M. Sévignon, C. Gozzi, E. Schulz and M. Lemaire, *Chem. Rev.*, 2002, **102**, 1359–1469.

77 Z. Bao, Y. Chen, R. Cai and L. Yu, *Macromolecules*, 1993, **26**, 5281–5286.

78 R. N. McDonald and T. W. Campbell, *J. Am. Chem. Soc.*, 1960, **82**, 4669–4671.

79 N. C. Greenham, S. C. Moratti, D. D. C. Bradley, R. H. Friend and A. B. Holmes, *Nature*, 1993, **365**, 628–630.

80 D. J. Schipper, M. Hutchinson and K. Fagnou, *J. Am. Chem. Soc.*, 2010, **132**, 6910–6911.

81 S. Selmani, L. Vanderzwet, A. J. Kukor and D. J. Schipper, *Synlett*, 2018, **29**, 2552–2556.

82 R. J. Waltman and J. Bargon, *Can. J. Chem.*, 1986, **64**, 76–95.

83 S. Sadki, P. Schottland, N. Brodie and G. Sabouraud, *Chem. Soc. Rev.*, 2000, **29**, 283–293.

84 J. Roncali, *Chem. Rev.*, 1992, **92**, 711–738.

85 N. Toshima and S. Hara, *Prog. Polym. Sci.*, 1995, **20**, 155–183.

86 V. M. Niemi, P. Knuuttila, J.-E. Österholm and J. Korvola, *Polymer (Guildf).*, 1992, **33**, 1559–1562.

87 A. de Meijere and F. Diederich, *Metal-Catalyzed Cross-Coupling Reactions*, Wiley-VCH, Second., 2004.

88 J. K. Stille, *Angew. Chemie Int. Ed. English*, 1986, **25**, 508–524.

89 C. Cordovilla, C. Bartolomé, J. M. Martínez-Ilarduya and P. Espinet, *ACS Catal.*, 2015, **5**, 3040–3053.

90 B. Carsten, F. He, H. J. Son, T. Xu and L. Yu, *Chem. Rev.*, 2011, **111**, 1493–1528.

91 I. J. Boyer, *Toxicology*, 1989, **55**, 253–298.

92 E. Le Grognec, J. M. Chrétien, F. Zammattio and J. P. Quintard, *Chem. Rev.*, 2015, **115**, 10207–10260.

93 S. P. Mishra, A. K. Palai, R. Srivastava, M. N. Kamalasanan and M. Patri, *J. Polym. Sci. Part A Polym. Chem.*, 2009, **47**, 6514–6525.

94 N. Miyaura and A. Suzuki, *Chem. Rev.*, 1995, **95**, 2457–2483.

95 J. Sakamoto, M. Rehahn, G. Wegner and A. D. Schlüter, *Macromol. Rapid Commun.*, 2009, **30**, 653–687.

96 N. Blouin, A. Michaud and M. Leclerc, *Adv. Mater.*, 2007, **19**, 2295–2300.

97 A. Yokoyama, R. Miyakoshi and T. Yokozawa, *Macromolecules*, 2004, **37**, 1169–1171.

98 J. Schmidt, M. Werner and A. Thomas, *Macromolecules*, 2009, **42**, 4426–4429.

99 A. Elangovan, Y. H. Wang and T. I. Ho, *Org. Lett.*, 2003, **5**, 1841–1844.

100 N. Camaioni, F. Tinti, L. Franco, M. Fabris, A. Toffoletti, M. Ruzzi, L. Montanari, L. Bonoldi, A. Pellegrino, A. Calabrese and R. Po, *Org. Electron.*, 2012, **13**, 550–559.

101 S. Y. Liu, H. Y. Li, M. M. Shi, H. Jiang, X. L. Hu, W. Q. Li, L. Fu and H. Z. Chen, *Macromolecules*, 2012, **45**, 9004–9009.

102 M. P. Nikiforov, B. Lai, W. Chen, S. Chen, R. D. Schaller, J. Strzalka, J. Maser and S. B. Darling, *Energy Environ. Sci.*, 2013, **6**, 1513–1520.

103 L.-C. Campeau and K. Fagnou, *Chem. Commun.*, 2006, **12**, 1253–1264.

104 G. P. McGlacken and L. M. Bateman, *Chem. Soc. Rev.*, 2009, **38**, 2447–2464.

105 D. J. Schipper and K. Fagnou, *Chem. Mater.*, 2011, **23**, 1594–1600.

106 D. Lapointe and K. Fagnou, *Chem. Lett.*, 2010, **39**, 1118–1126.

107 S. I. Gorelsky, D. Lapointe and K. Fagnou, *J. Am. Chem. Soc.*, 2008, **130**, 10848–10849.

108 S. I. Gorelsky, D. Lapointe and K. Fagnou, *J. Org. Chem.*, 2012, **77**, 658–668.

109 A. Bruneau, M. Roche, M. Alami and S. Messaoudi, *ACS Catal.*, 2015, **5**, 1386–1396.

110 P. Berrouard, A. Najari, A. Pron, D. Gendron, P. O. Morin, J. R. Pouliot, J. Veilleux and M. Leclerc, *Angew. Chemie - Int. Ed.*, 2012, **51**, 2068–2071.

111 M. Sévignon, J. Papillon, E. Schulz and M. Lemaire, *Tetrahedron Lett.*, 1999, **40**, 5873–5876.

112 L. G. Mercier and M. Leclerc, *Acc. Chem. Res.*, 2013, **46**, 1597–1605.

113 P. O. Morin, T. Bura, B. Sun, S. I. Gorelsky, Y. Li and M. Leclerc, *ACS Macro Lett.*, 2015, **4**, 21–24.

114 J. R. Pouliot, F. Grenier, J. T. Blaskovits, S. Beaupré and M. Leclerc, *Chem. Rev.*, 2016, **116**, 14225–14274.

115 K. Nakabayashi, *Polym. J.*, 2018, **50**, 475–483.

116 H. Bohra and M. Wang, *J. Mater. Chem. A*, 2017, **5**, 11550–11571.

117 S. Kowalski, S. Allard and U. Scherf, *Macromol. Rapid Commun.*, 2015, **36**, 1061–1068.

118 Y. Yang, J. Lan and J. You, *Chem. Rev.*, 2017, **117**, 8787–8863.

119 C. Liu, H. Zhang, W. Shi and A. Lei, *Chem. Rev.*, 2011, **111**, 1780–1824.

120 C. Liu, J. Yuan, M. Gao, S. Tang, W. Li, R. Shi and A. Lei, *Chem. Rev.*, 2015, **115**, 12138–12204.

121 Y. Wei and W. Su, *J. Am. Chem. Soc.*, 2010, **132**, 16377–16379.

122 D. R. Stuart and K. Fagnou, *Science (80-.).*, 2007, **316**, 1172–1175.

123 R. Geyer, J. R. Jambeck and K. L. Law, *Sci. Adv.*, 2017, **3**, 19–24.

124 A. T. Balaban, D. C. Oniciu and A. R. Katritzky, *Chem. Rev.*, 2004, **104**, 2777–2812.

125 Z. Li, J. Ding, N. Song, J. Lu and Y. Tao, *J. Am. Chem. Soc.*, 2010, **132**, 13160–13161.

126 H. H. Cho, T. E. Kang, K. H. Kim, H. Kang, H. J. Kim and B. J. Kim, *Macromolecules*, 2012, **45**, 6415–6423.

127 L. Ying, B. B. Y. Hsu, H. Zhan, G. C. Welch, P. Zalar, L. A. Perez, E. J. Kramer, T. Q. Nguyen, A. J. Heeger, W. Y. Wong and G. C. Bazan, *J. Am. Chem. Soc.*, 2011, **133**,

18538–18541.

128 T. Yamamoto, H. Suganuma, T. Maruyama and K. Kubota, *J. Chem. Soc., Chem. Commun.*, 1995, 1613–1614.

129 T. Yamamoto, A. Morita, Y. Miyazaki, T. Maruyama, H. Wakayama, Z. hua Zhou, Y. Nakamura, T. Kanbara, S. Sasaki and K. Kubota, *Macromolecules*, 1992, **25**, 1214–1223.

130 T. Yamamoto, H. Suganuma, T. Maruyama, T. Inoue, Y. Muramatsu, M. Arai, D. Komarudin, N. Ooba, S. Tomaru, S. Sasaki and K. Kubota, *Chem. Mater.*, 1997, **9**, 1217–1225.

131 J. K. Politis, M. D. Curtis, L. Gonzalez, D. C. Martin, Y. He and J. Kanicki, *Chem. Mater.*, 1998, **10**, 1713–1719.

132 T. Yamamoto, H. Kokubo, M. Kobashi and Y. Sakai, *Chem. Mater.*, 2004, **16**, 4616–4618.

133 D. H. Kim, B. L. Lee, H. Moon, H. M. Kang, E. J. Jeong, J. Il Park, K. M. Han, S. Lee, B. W. Yoo, B. W. Koo, J. Y. Kim, W. H. Lee, K. Cho, H. A. Becerril and Z. Bao, *J. Am. Chem. Soc.*, 2009, **131**, 6124–6132.

134 R. P. Ortiz, H. Yan, A. Facchetti and T. J. Marks, *Materials (Basel).*, 2010, **3**, 1533–1558.

135 I. Osaka, R. Zhang, J. Liu, D. M. Smilgies, T. Kowalewski and R. D. McCullough, *Chem. Mater.*, 2010, **22**, 4191–4196.

136 F. Pammer, J. Jager, B. Rudolf and Y. Sun, *Macromolecules*, 2014, **47**, 5904–5912.

137 H. L. Su, D. N. Sredojevic, H. Bronstein, T. J. Marks, B. C. Schroeder and M. Al-Hashimi, *Macromol. Rapid Commun.*, 2017, **38**, 1–24.

138 Y. Lin, H. Fan, Y. Li and X. Zhan, *Adv. Mater.*, 2012, **24**, 3087–3106.

139 J. Lee, B. J. Jung, S. K. Lee, J. I. Lee, H. J. Cho and H. K. Shim, *J. Polym. Sci. Part A Polym. Chem.*, 2005, **43**, 1845–1857.

140 M. Kuramochi, J. Kuwabara, W. Lu and T. Kanbara, *Macromolecules*, 2014, **47**, 7378–7385.

141 J. Kuwabara, M. Kuramochi, S. Liu, T. Yasuda and T. Kanbara, *Polym. J.*, 2017, **49**, 123–131.

142 R. Matsidik, M. Giorgio, A. Luzio, M. Caironi, H. Komber and M. Sommer, *European J. Org. Chem.*, 2018, **2018**, 6121–6126.

143 Q. Guo, D. Wu and J. You, *ChemSusChem*, 2016, **9**, 2765–2768.

144 A. Faradhiyani, Q. Zhang, K. Maruyama, J. Kuwabara, T. Yasuda and T. Kanbara, *Mater. Chem. Front.*, 2018, **2**, 1306–1309.

145 R. A. Mirabal, L. Vanderzwet, S. Abuadas, M. R. Emmett and D. Schipper, *Chem. - A Eur. J.*, 2018, **24**, 12231–12235.

146 C. C. A. Voll and T. M. Swager, *J. Am. Chem. Soc.*, 2018, **140**, 17962–17967.

147 Y. Terao, H. Wakui, T. Satoh, M. Miura and M. Nomura, *J. Am. Chem. Soc.*, 2001, **123**, 10407–10408.

148 Y. Terao, H. Wakui, M. Nomoto, T. Satoh, M. Miura and M. Nomura, *J. Org. Chem.*, 2003, **68**, 5236–5243.

149 Y. Terao, M. Nomoto, T. Satoh, M. Miura and M. Nomura, *J. Org. Chem.*, 2004, **69**, 6942–6944.

150 A. B. Bíró and A. Kotschy, *European J. Org. Chem.*, 2007, 1364–1368.

151 J. R. Bour, J. C. Green, V. J. Winton and J. B. Johnson, *J. Org. Chem.*, 2013, **78**, 1665–1669.

152 L. J. Gooßen, G. Deng and L. M. Levy, *Science (80-.).*, 2006, **313**, 662–664.

153 L. J. Goossen, N. Rodríguez, B. Melzer, C. Linder, G. Deng and L. M. Levy, *J. Am. Chem. Soc.*, 2007, **129**, 4824–4833.

154 P. Forgione, M. C. Brochu, M. St.-Onge, K. H. Thesen, M. D. Bailey and F. Bilodeau, *J. Am. Chem. Soc.*, 2006, **128**, 11350–11351.

155 K. Fagnou and M. Lautens, *Angew. Chemie Int. Ed.*, 2002, **41**, 26–47.

156 M. Nakano, H. Tsurugi, T. Satoh and M. Miura, *Org. Lett.*, 2008, **10**, 1851–1854.

157 N. Rodríguez and L. J. Goossen, *Chem. Soc. Rev.*, 2011, **40**, 5030–5048.

158 Y. S. Park, T. S. Kale, C. Y. Nam, D. Choi and R. B. Grubbs, *Chem. Commun.*, 2014, **50**, 7964–7967.

159 Y. S. Park, Q. Wu, C. Y. Nam and R. B. Grubbs, *Angew. Chemie - Int. Ed.*, 2014, **53**, 10691–10695.

160 F. Y. Shih, S. Tian, N. Gallagher, Y. S. Park and R. B. Grubbs, *Polym. Chem.*, 2018, **9**, 3223–3231.

161 G. S. Sinclair, A. J. Kukor, K. K. G. Imperial and D. J. Schipper, *Macromolecules*, 2020, **53**, 5169–5176.

162 E. Amir and S. Rozen, *Chem. Commun.*, 2006, 2262–2264.

163 R. E. Moreira, G. S. Sinclair and D. J. Schipper, *Can. J. Chem.*, 2019, **97**, 360–365.

164 L. C. Campeau, M. Bertrand-Laperle, J. P. Leclerc, E. Villemure, S. Gorelsky and K. Fagnou, *J. Am. Chem. Soc.*, 2008, **130**, 3276–3277.

165 E. Perspicace, L. Cozzoli, E. M. Gargano, N. Hanke, A. Carotti, R. W. Hartmann and S. Marchais-Oberwinkler, *Eur. J. Med. Chem.*, 2014, **83**, 317–337.

166 D. J. Pascoe, K. B. Ling and S. L. Cockroft, *J. Am. Chem. Soc.*, 2017, **139**, 15160–15167.

167 B. R. Beno, K. S. Yeung, M. D. Bartberger, L. D. Pennington and N. A. Meanwell, *J. Med. Chem.*, 2015, **58**, 4383–4438.

168 M. Iwaoka, S. Takemoto and S. Tomoda, *J. Am. Chem. Soc.*, 2002, **124**, 10613–10620.

169 J. Roncali, P. Blanchard and P. Frère, *J. Mater. Chem.*, 2005, **15**, 1589–1610.

170 M. Turbiez, P. Frère, M. Allain, C. Videlot, J. Ackermann and J. Roncali, *Chem. - A Eur. J.*, 2005, **11**, 3742–3752.

171 Y.-Z. Dai, N. Ai, Y. Lu, Y.-Q. Zheng, J.-H. Dou, K. Shi, T. Lei, J.-Y. Wang and J. Pei, *Chem. Sci.*, 2016, **7**, 5753–5757.

172 Z. B. Henson, G. C. Welch, T. van der Poll and G. C. Bazan, *J. Am. Chem. Soc.*, 2012, **134**, 3766–3779.

173 J. E. Coughlin, A. Zhugayevych, R. C. Bakus, T. S. Van Der Poll, G. C. Welch, S. J. Teat, G. C. Bazan and S. Tretiak, *J. Phys. Chem. C*, 2014, **118**, 15610–15623.

174 Y. Cheng, Y. Qi, Y. Tang, C. Zheng, Y. Wan, W. Huang and R. Chen, *J. Phys. Chem. Lett.*, 2016, **7**, 3609–3615.

175 S. Zhang, Y. Qin, M. A. Uddin, B. Jang, W. Zhao, D. Liu, H. Y. Woo and J. Hou, *Macromolecules*, 2016, **49**, 2993–3000.

176 E. D. Głowacki, M. Irimia-Vladu, S. Bauer and N. S. Sariciftci, *J. Mater. Chem. B*, 2013, **1**, 3742–3753.

177 Y. Gu, T. Kar and S. Scheiner, *J. Am. Chem. Soc.*, 1999, **121**, 9411–9422.

178 J. Liu, B. Walker, A. Tamayo, Y. Zhang and T.-Q. Nguyen, *Adv. Funct. Mater.*, 2013, **23**, 47–56.

179 A. B. Tamayo, B. Walker and T. Q. Nguyen, *J. Phys. Chem. C*, 2008, **112**, 11545–11551.

180 Y. Qiao, Y. Guo, C. Yu, F. Zhang, W. Xu, Y. Liu and D. Zhu, *J. Am. Chem. Soc.*, 2012, **134**, 4084–4087.

181 N. E. Jackson, B. M. Savoie, K. L. Kohlstedt, M. Olvera De La Cruz, G. C. Schatz, L. X. Chen and M. A. Ratner, *J. Am. Chem. Soc.*, 2013, **135**, 10475–10483.

182 J. C. Sancho-García and J. Cornil, *J. Chem. Phys.*, 2004, **121**, 3096–3101.

183 F. Weinhold and C. R. Landis, *Discovering Chemistry with Natural Bond Orbitals*, John Wiley & Sons, Inc., Hoboken, NJ, USA, 2012.

184 R. F. W. Bader, *Chem. Rev.*, 1991, **91**, 893–928.

185 T. A. Keith, 2017. AIMALL (Version 17.11.14) (TK Gristmill Software, Overland Parks KS, USA, 2017).

186 M. H. Kolář and P. Hobza, *Chem. Rev.*, 2016, **116**, 5155–5187.

187 G. S. Sinclair, R. C. M. Claridge, A. J. Kukor, W. S. Hopkins and D. J. Schipper, Chem. Sci. Submitted.188 Y. Li, J. Jin, W. Qian and W. Bao, *Org. Biomol. Chem.*, 2010, **8**, 326–330.

189 S. Tretiak, A. Saxena, R. L. Martin and A. R. Bishop, *Phys. Rev. Lett.*, 2002, **89**, 1–4.

190 E. D. Głowacki, G. Voss, L. Leonat, M. Irimia-Vladu, S. Bauer and N. S. Sariciftci, *Isr. J. Chem.*, 2012, **52**, 540–551.

191 P. J. J. Carr, J. Warneke, J. Featherstone, C. Jenne, E. Loire and W. S. Hopkins, *Mol. Phys.*, 2019, **117**, 2972–2979.

192 C. Shi, Y. Yao, Yang and Q. Pei, *J. Am. Chem. Soc.*, 2006, **128**, 8980–8986.

193 E. Täuscher, L. Calderón-Ortiz, D. Weiß, R. Beckert and H. Görls, *Synthesis (Stuttg).*, 2011, 2334–2339.

194 X. Guo, J. Quinn, Z. Chen, H. Usta, Y. Zheng, Y. Xia, J. W. Hennek, R. P. Ortiz, T. J. Marks and A. Facchetti, *J. Am. Chem. Soc.*, 2013, **135**, 1986–1996.

195 Q. Wei, S. Miyanishi, E. Zhou, K. Hashimoto and K. Tajima, *Synth. Met.*, 2014, **196**, 139–144.

196 S. I. Gorelsky, *Coord. Chem. Rev.*, 2013, **257**, 153–164.

197 S. Pivsa-Art, T. Satoh, Y. Kawamura, M. Miura and M. Nomura, *Bull. Chem. Soc. Jpn.*, 1998, 71, 467–473.

198 A. Yokooji, T. Okazawa, T. Satoh, M. Miura and M. Nomura, *Tetrahedron*, 2003, **59**, 5685–5689.

199 G. S. Sinclair, J. A. Buratynski, J. M. Oates and D. J. Schipper, Manuscr. in Prep.

200 G. Conboy, R. G. D. Taylor, N. J. Findlay, A. L. Kanibolotsky, A. R. Inigo, S. S. Ghosh, B. Ebenhoch, L. Krishnan Jagadamma, G. K. V. V. Thalluri, M. T. Sajjad, I. D. W. Samuel and P. J. Skabara, *J. Mater. Chem. C*, 2017, **5**, 11927–11936.

201 T. Nußbaumer and R. Neidlein, *Heterocycles*, 2000, **52**, 349–364.

202 A. Hantzsch and J. H. Weber, *Berichte der Dtsch. Chem. Gesellschaft*, 1887, **20**, 3118–3132.

203 L.-F. Lai, C.-L. Ho, Y.-C. Chen, W.-J. Wu, F.-R. Dai, C.-H. Chui, S.-P. Huang, K.-P. Guo, J.-T. Lin, H. Tian, S.-H. Yang and W.-Y. Wong, *Dye. Pigment.*, 2013, **96**, 516–524.

204 W. Lu, J. Kuwabara and T. Kanbara, *Polym. Chem.*, 2012, **3**, 3217.

205 M. T. Chhabria, S. Patel, P. Modi and P. S. Brahmkshatriya, *Curr. Top. Med. Chem.*, 2016, **16**, 2841–2862.

206 E. Vitaku, D. T. Smith and J. T. Njardarson, *J. Med. Chem.*, 2014, **57**, 10257–10274.

207 A. Reissert, *Berichte der Dtsch. Chem. Gesellschaft*, 1905, **38**, 1603–1614.

208 J. A. Bull, J. J. Mousseau, G. Pelletier and A. B. Charette, *Chem. Rev.*, 2012, **112**, 2642–2713.

209 W. E. Feely and E. M. Beavers, *J. Am. Chem. Soc.*, 1959, **81**, 4004–4007.

210 T. Kato and H. Yamanaka, *J. Org. Chem.*, 1965, **30**, 910–913.

211 R. M. Kellogg and T. J. Van Bergen, *J. Org. Chem.*, 1971, **36**, 1705–1708.

212 H. Andersson, F. Almqvist and R. Olsson, *Org. Lett.*, 2007, **9**, 1335–1337.

213 M. Begtrup, L. B. L. Hansen, S. Grundvig, Y. Stenstrøm, A. Z.-Q. Khan, J. Sandström and P. Krogsgaard-Larsen, *Acta Chem. Scand.*, 1992, 46, 372–383.

214 H. Mayr and A. R. Ofial, *J. Phys. Org. Chem.*, 2008, **21**, 584–595.

215 H. Mayr, Ofial, A. R. Mayr's Database of Reactivity Parameters; https://www.cup.lmu.de/oc/mayr/reaktionsdatenbank.

216 T. Truong, J. Alvarado, L. D. Tran and O. Daugulis, *Org. Lett.*, 2010, **12**, 1200–1203.

217 Z. Liang, J. Zhao and Y. Zhang, *J. Org. Chem.*, 2010, **75**, 170–177.

218 T. Wöhrle, R. Gündemir, W. Frey, F. Knecht, A. Köhn and S. Laschat, *Chem. - A Eur. J.*, 2017, **23**, 4149–4159.